

NGUYEN Thi Minh Ngoc

Recent geochemical and mineralogical
alteration processes in tropical coastal
sediments of Vietnam



Ernst-Moritz-Arndt-University Greifswald
Germany 2006

Recent geochemical and mineralogical alteration processes in tropical coastal sediments of Vietnam

Dissertation

in fulfilment of the academic grade
doctor rerum naturalium (Dr. rer. nat.)

at the Faculty of Mathematics and Natural Sciences
Ernst-Moritz-Arndt-University Greifswald



NGUYEN Thi Minh Ngoc
born on 17.7.1979 in Phu Tho, Vietnam

Greifswald, Germany 2006

Dekan: Prof. Dr. rer. nat. **Klaus FESSER**

1. Gutachter 1: Ass. Prof. Dr. Habil **Jörn KASBOHM**

2. Gutachter 2: Prof. Dr. **Georg IRION**

Tag der Promotion: 17.11.2006

Luận án, con dành tặng gia đình
& các cháu Bổng, Nhím, cu Tít, cu Mít thương yêu
- nơi luôn cho con tình yêu và nghị lực

TABLE OF CONTENT

INDEX OF FIGURES	iii
INDEX OF TABLES	viii
ABBREVIATIONS	x
ACKNOWLEDGEMENTS	xi
1 INTRODUCTION	1
1.1 Motivation	1
1.1.1 Meaning of coastal zone for regional development & problems	1
1.1.2 Coastal sediments in the view of a real complex of geological process	2
1.2 Aims of this Ph.D. work	3
2 COASTAL SEDIMENTS IN TROPICAL CONDITIONS	5
2.1 Environmental setting of coastal sediments	5
2.1.1 Climate and Oceanography	5
2.1.2 Geological and geographical setting	7
2.2 Sources of coastal sediments and yields	8
2.3 Transport to the sea	9
2.4 Morphology and driving forces	10
2.4.1 Vegetation	11
2.4.2 Anthropogenic effects	14
2.5 Maturation process in coastal sediments	15
2.5.1 Difference between soil profile and coastal sediment profile	15
2.5.2 Nutrients, geochemistry and mineralogy of coastal sediment profiles	17
2.5.3 Expected models of driving forces	23
3 MATERIALS & METHODS	24
3.1 Sampling and Materials	24
3.1.1 Sampling sites in Red River Delta	25
3.1.2 Sampling site in Dam Mon	26
3.1.3 Sampling site in Nha Phu	27
3.2 Methods	29
3.2.1 Grain size analysis	29
3.2.2 Chemical analysis	31
3.2.3 Nutrients	32
3.2.4 Mineralogical analysis	33
3.2.5 Mathematical methods	52
4 RESULTS	54
4.1 Grain size analysis	54
4.1.1 Red River Delta	54
4.1.2 South Central Coast	59
4.2 Nutrients	66
4.2.1 Red River Delta	66
4.2.2 South Central Coast	67
4.3 Geochemistry	69
4.3.1 Physico-chemical condition (pH, Eh)	69
4.3.2 Major elements	70
4.3.3 Minor chemical elements	80
4.4 Mineralogy	91
4.4.1 Red River Delta	91
4.4.2 South Central Coastline	107
5 DISCUSSION	124
5.1 Coastal sedimentary environment – an interface between terrigenous and marine sedimentation, biota as well as human activities	124
5.1.1 Sedimentological meaning of grain size distribution data	124
5.1.2 Reconstruction of paleogeographical situation	130
5.2. Syn-sedimentary processes - mirroring in elemental distribution and mineral matter	134
5.2.1. Hydrodynamic – mirroring in elemental distribution and mineral matter	134
5.2.2. Physico-chemical processes	144
5.2.3. Clarification of coastal sediments	149

5.2.4.	Summary on syn-sedimentary processes	153
5.3.	Post-sedimentary processes - mirroring in elemental distribution and mineral matters.....	154
5.3.1.	Geochemical mirror of post-sedimentary processes	154
5.3.2.	Mineralogical mirror of post-sedimentation	157
5.3.3.	Dissolution of clay minerals in saline water	160
5.3.4.	Smectitization.....	165
5.3.5.	Kaolinitization	169
5.3.6.	Meta-stable neoformed phases during post-sedimentary processes.....	175
5.3.7.	Summary on post-sedimentary processes	176
5.4.	Post-sedimentary processes with involvement of mangrove biota – mirroring by elemental distribution and mineral matter	179
5.4.1.	Diagenetic process of nutrients.....	179
5.4.2.	pH/Eh zoning along depth profile in MF sediments.....	180
5.4.3.	Trapping processes in mangrove forest	183
5.4.4.	Intensification of dissolution process under effects of root system	184
5.4.5.	Intensification of smectitization under effects of root system	184
5.4.6.	Intensification of kaolinitization under effects of root system.....	186
5.4.7.	Summary on biota-induced post-sedimentary processes.....	187
5.3.	Post-sedimentary processes influenced by human activities (e.g. shrimp pond cultivation).....	188
5.5.1.	Dispersion in surface sediments.....	189
5.5.2.	Removal of mangroves and effects from remains of decaying roots.....	190
5.5.3.	Summary of human-induced effects on post-sedimentary processes.....	191
6	CONCLUSION & SUMMARY	192
7	REFERENCES	196
8	APPENDICES	209

INDEX OF FIGURES

Figure 2.1. Variation in area of wetland types along coastline of Vietnam	11
Figure 2.2. Low tidal mudflats, mangrove forests and shrimp ponds in the Red River estuary	13
Figure 2.3. Low tidal mudflats, mangrove forests and shrimp ponds in the south central coast	13
Figure 2.4. Distribution of population density in provinces of Vietnam	14
Figure 2.5. Equation for sequence of ion uptake by plants from a soil/ wetland system	16
Figure 2.6. Conceptual model of oxygen flux and zoning of oxidation potential in mangrove sediment profile.....	18
Figure 2.7. Thermodynamic concept by Lippmann (1979) describing main pathways of mineral alteration.....	20
Figure 2.8. Expected models for driving-forces of mineral alteration	23
Figure 3.1 Locations of case study areas in Vietnam	24
Figure 3.2. The sampling sites in coastal zone of Red River Delta - coring in intertidal mudflat and grabbing surface sediments along tidal creeks	25
Figure 3.3. Sampling sites in Dam Mon (with old mangrove forest area) and Nha Phu (with young mangrove forest area).....	26
Figure 3.4. GSD patterns of replica measurements for sample with and without organic matters.....	29
Figure 3.5. Visualisation of GSD patterns by GSD maps	30
Figure 3.6 Data of pH/Eh were extracted when stable values of balance states were reached	31
Figure 3.7. XRD pattern of powder, randomly oriented mount specimen	36
Figure 3.8. Example on an XRD pattern for oriented mount specimen.....	36
Figure 3.9. Deconvolution of the 7 Å	37
Figure 3.10. TEM micrographs of kaolinite and halloysite	38
Figure 3.11. Deconvolution of (060) reflections.....	39
Figure 3.12. TEM micrographs of Chlorite, Saponite, Illite, dioctahedral Vermiculite, Montmorillonite and Beidellite.....	40
Figure 3.13. Deconvolution of 2θ range (Cu beam) from 27.3 - 33.3.....	41
Figure 3.14. Identification of smectites and diVS-ml based on deconvoluted background XRD patterns	42
Figure 3.15. TEM graphs of mixed layer structures	46
Figure 3.16. Identification of KE-ml structures with different proportion of expandable layers	49
Figure 4.1. PCA-biplots on correlation among sedimentological parameters (arrows) and sampling locations (xy-dots)	54
Figure 4.2. Variation of grain size composition and sedimentological parameters along tidal creeks in the Red River Delta.....	55
Figure 4.3. Composition of grain size fractions and sedimentological parameter (So, Sk) of coastal sediment profiles in the Red River Delta	55
Figure 4.4. Grain Size Distribution (GSD) maps of sediment profiles in estuary of the Red River Delta, North Vietnam.....	56
Figure 4.5. Deconvolution of GSD pattern	57
Figure 4.6. Modelled end-members of GSD patterns in coastal sediments of Red River Delta	57
Figure 4.7. Computed contribution of end-members in sediment profiles in estuary of the Red River Delta.....	58
Figure 4.8. Composition of grain size fractions (background) and sedimentological parameter (So, Sk, Ku) (line) of coastal sediment profiles in Dam Mon and Nha Phu	59
Figure 4.9. PCA Biplots of correlation among sedimentology parameters and sampling sites	60
Figure 4.10. Grain Size Distribution (GSD) maps of sediment profiles in Dam Mon and Nha Phu, Central coast of Vietnam	62
Figure 4.11. Modelled end-members of GSDs in coastal sediments of South Central Coast, central coast of Vietnam	64

Figure 4.12. Contribution of end members in sediments at depth intervals in profiles of Dam Mon and Nha Phu, central coast of Vietnam	65
Figure 4.13. Distribution of nutrients according to depth profiles in coastal sediments of Red River Delta, Dam Mon and Nha Phu	66
Figure 4.14. Net ecosystem stoichiometry of sediments in the Red River Delta estuary.....	67
Figure 4.15. Net ecosystem stoichiometry of coastline muddy sediments of Dam Mon (dark diamond) and Nha Phu (empty square), central Vietnam	68
Figure 4.16. Scatter diagrams of selected elements for RRD sediments.....	72
Figure 4.17. PCA biplots of chemical parameters for grain sizes fractions in the Red River Delta	73
Figure 4.18. Chemical variation according to the depth in profiles of LM (a), MF (b), SP (c) in estuary of the Red River Delta	73
Figure 4.19. PCA biplots on major chemical elements in sediment samples in Dam Mon (a) and Nha Phu (b)	76
Figure 4.20. Scatter diagrams of selected elements for muddy sediments in the Dam Mon.	77
Figure 4.21. Scatter diagrams of selected elements for muddy sediments in the Nha Phu...	77
Figure 4.22. Variation of major elements according to depth in sediment profile of Dam Mon	79
Figure 4.23. Variation of major elements according to depth in sediment profile of Nha Phu	80
Figure 4.24. Chemical variation according to the depth in profiles of LM (a). MF (b). SP (c) in the Red River estuary	85
Figure 4.25. PCA biplots on minor chemical elements of sediment samples in Dam Mon (a) and Nha Phu (b)	87
Figure 4.26. Variation of trace elements according to depth in sediment profile of Dam Mon coastline.....	89
Figure 4.27. Variation of trace elements according to depth in sediment profile of Nha Phu coastline.....	90
Figure 4.28. Variation in crystallite parameters (d-value, peak intensity, FWHM) of clay minerals according to the depth	91
Figure 4.29. Variation in crystallite parameters (shifting of peak position, peak intensity, FWHM) of clay minerals according to grain size separation.....	93
Figure 4.30. TEM images of particles in diVS-ml series in Red River Delta sediments.....	95
Figure 4.31. Frequency distribution of diVS-ml series in sediment profiles of Red River Delta	97
Figure 4.32. Octahedral occupation of diVS-ml series.....	99
Figure 4.33. TEM images of KE-ml particles in sediments of the RRD.....	100
Figure 4.34. Frequency distribution of KE-ml series in sediment profiles of RRD.....	102
Figure 4.35. TEM images of particles in IS-ml series in coastal sediment sample of RRD..	104
Figure 4.36. TEM images of Chlorite and CS-ml particles in RRD sediments	106
Figure 4.37. TEM images of diVS-ml particles and their end-members in coastal sediments of South Central Coast	109
Figure 4.38. Frequency distribution of diVS-ml series in sediment profiles of Dam Mon ...	111
Figure 4.39. Frequency distribution of diVS-ml series in sediment profiles of Nha Phu.....	112
Figure 4.40. Octahedral occupations of diVS-ml structures in Dam Mon (a) and Nha Phu (b)	115
Figure 4.41. TEM images of particles in KE-ml series in sediments of the South Central Coast.....	115
Figure 4.42. Frequency distribution of KE-ml series in sediment profiles of Dam Mon.....	117
Figure 4.43. Frequency distribution of KE-ml series in sediment profiles of Nha Phu	118
Figure 4.44. TEM images of CS-ml particles and their end-members in coastal sediments of South Central Coast	121
Figure 4.45. TEM images of particles in IS-ml series in sediments of the South Central Coast	122
Figure 5.1. Modelled end-members are compared with mean size and full pattern of GSD in RRD profiles	126
Figure 5.2. Modelled end-members are compared with mean size and full pattern of GSD in Dam Mon profiles (a) and Nha Phu profiles (b)	128

Figure 5.3. Normalization of age of syn-sedimentary matters in RRD profiles (in 2001).....	132
Figure 5.4. Normalization of distance between syn-sedimentary coastline and coastline in 2001.....	133
Figure 5.5. Enrichment behaviours of major chemical elements in grain size fractions in comparison to the bulk.....	134
Figure 5.6. Enrichment behaviours of minor chemical elements in grain size fractions in comparison to the bulk, on example of 0 – 3 cm surface sediments in MF profile, RRD	136
Figure 5.7. Influences of accumulation factor on elemental distribution (a, b) and XRD peak of quartz (1.82 Å) in three profiles of Nha Phu	137
Figure 5.8. Influences of accumulation factor on elemental distribution in low tidal mudflat profiles of coastal sedimentary sites along Vietnam	138
Figure 5.9. Influences of accumulation factor on distribution of Pb concentration in coastal sediments of Vietnam	140
Figure 5.10. Influences of erosion factor on distribution of Al in coastal sediments	141
Figure 5.11 Distributions of erosion factor and chemical elements in SP profile of RRD....	142
Figure 5.12. Influences of erosion factor on enrichment of heavy metal – Pb in coastal sediments.....	143
Figure 5.13. Influences of aeolian factor on distribution of Silicon and quartz	143
Figure 5.14. Comparison distribution of total organic carbon in the studied MF profiles and Avicenia mangrove profile in French Guiana, Amazon delta (Marchand et al. 2003).....	145
Figure 5.15. Differentiation in grain sizes, clay mineralogy, major and minor chemical elements between Red River Delta, Dam Mon and Nha Phu, as mirrors of sediment source	150
Figure 5.16. Correlation between enrichment of K and feldspar in bulk samples of LM profile in Dam Mon	155
Figure 5.17. Correlation between enrichment of K (a), Fe (b) and Mg (c) and relative quantity of expandable phase in fractions < 2 µm.....	156
Figure 5.18. Correlation between enrichment of heavy metals (a, b, c) and the minor element – Rb and relative quantity of expandable phase in fractions < 2 µm	156
Figure 5.19. Mineralogical features as mirror of interactions among post-sedimentary processes in coastal environment	158
Figure 5.20. Decrease of DCM and DCM/Q indicating dissolution of clay phases in the older sediments.....	160
Figure 5.21. Dissolution resistance of diVS-ml structures, based on half-time-dissolution coefficient $t_{0.5}$	163
Figure 5.22. Typical modification in frequency spectra of diVS-ml during the dissolution process.....	164
Figure 5.23. XRD evidences for smectitization (example of LM profile in Dam Mon, XRD for oriented mount, EG specimens).....	165
Figure 5.24. Abundance of smectitic diVS-ml in the deeper part of the core.....	166
Figure 5.25. Schematic representation of the distribution of charges in a diVS-ml crystal (half unit-cell, Mac Evan crystallites)	167
Figure 5.26. Charge behaviour of diVS-ml series (on example of sample DM-LM, 10 – 20 cm depth).....	168
Figure 5.27. Model of step-wise arrangement in charges of IV- (green stepped line), VI- (grey gauss-like curve) and interlayer K (red solid bar)	168
Figure 5.28. Typical modification in frequency spectra of KE-ml during the dissolution with preferential leaching of smectitic layer	170
Figure 5.29. Sketch of a smectite 2:1 layer during kaolinitization	172
Figure 5.30. Percentage of OH-groups of the octahedral sheet vs. %K in KE-ml	172
Figure 5.31. Interlayer charge of KE-ml series as a function of kaolinitic layer percentage	174
Figure 5.32. Tetrahedral Si of KE-ml series as a function of kaolinitic layer percentage	174
Figure 5.33. Octahedral Mg in KE-ml series as a function of kaolinitic layer percentage ...	175
Figure 5.34. Octahedral Fe in KE-ml series as a function of kaolinitic layer percentage	175

Figure 5.35. Continuous adaptation of interlayer charge during the development from structures with lower SiIV to structures with higher SiIV values in the determined mixed layer series	178
Figure 5.36. Zoning of pH/Eh system along mangrove forest sediment profiles in Dam Mon (a) and Nha Phu (b).....	181
Figure 5.37. SAEDs shows the conversion from 2M1 structure to turbostratic order when diVS 90 (with 90% of smectitic layers) was smectitized to diVS50 (with 50% of smectitic layers).....	185
Figure 5.38. Layer charge behaviours of diVerm, K-leached diVerm and diVS10 in diVS-ml series in rhizosphere layer, MF profile in Red River Delta.....	186
Figure 8.1. Simulation of original dataset and products of PCA –score and loading matrixes	210
Figure 8.2. PCA score plot (a) and loading plot (b) projected on the two main principal components.....	210
Figure 8.3. Concentrative contribution of major elements from grain size fractions to the bulk of mudflat sediments in the Red River Delta	214
Figure 8.4. Concentrative enrichments major elements in grain size fractions in comparison to the bulk of mudflat sediments in RRD	214
Figure 8.5. Concentrative enrichments minor elements in grain size fractions in comparison to the bulk of mudflat sediments in RRD	214
Figure 8.6. XRD patterns of powder, random oriented mount specimen of bulk sample from muddy sediment profiles in the estuary of the Red River Delta	215
Figure 8.7. XRD- powder, random oriented mount patterns of grain-size fractions separated from bulk, surface sediment (0-3cm) in mangrove forest of the Red River Delta	216
Figure 8.8. XRD patterns of powder, random oriented mount specimen of clay fractions (<2µm) dispersed from muddy sediment profiles in the estuary of the Red River Delta	217
Figure 8.9. XRD patterns of oriented mount specimens of clay fractions (<2µm) dispersed from muddy sediment profiles in estuary of the Red River Delta	218
Figure 8.10. XRD patterns of powder, random oriented mount specimen of clay fractions (<2µm) dispersed from muddy sediment in low tidal mudflat profile in Dam Mon	219
Figure 8.11. XRD patterns of powder, random oriented mount specimen of clay fractions (<2µm) dispersed from muddy sediment in mangrove forest profile in Dam Mon	220
Figure 8.12. XRD patterns of powder, random oriented mount specimen of clay fractions (<2µm) dispersed from muddy sediment in shrimp pond profile in Dam Mon ..	221
Figure 8.13. XRD patterns of powder, random oriented mount specimen of clay fractions (<2µm) dispersed from muddy sediment in low tidal mudflat profile in Nha Phu	222
Figure 8.14. XRD patterns of powder, random oriented mount specimen of clay fractions (<2µm) dispersed from muddy sediment in mangrove forest profile in Nha Phu	223
Figure 8.15. XRD patterns of powder, random oriented mount specimen of clay fractions (<2µm) dispersed from muddy sediment in shrimp pond profile in Nha Phu...	224
Figure 8.16. XRD pattern of oriented mount specimens for sediment samples in low tidal mudflat profile of Dam Mon.....	225
Figure 8.17. XRD pattern of oriented mount specimens for sediment samples in mangrove forest profile of Dam Mon	226
Figure 8.18. XRD pattern of oriented mount specimens for sediment samples in shrimp pond profile of Dam Mon.....	227
Figure 8.19. XRD pattern of oriented mount specimens for sediment samples in low tidal mudflat profile of Nha Phu.....	228
Figure 8.20. XRD pattern of oriented mount specimens for sediment samples in mangrove forest profile of Nha Phu	229
Figure 8.21. XRD pattern of oriented mount specimens for sediment samples in shrimp pond profile of Nha Phu.....	230

Figure 8.22. Haft time of dissolution ($t_{0.5}$) of dioctahedral vermiculite/smectite mixed layer series (diVS-ml series) of clay fractions ($<2\mu\text{m}$) dispersed from sediment profiles in estuary of the Red River Delta	231
Figure 8.23. Haft time of dissolution ($t_{0.5}$) of dioctahedral vermiculite/smectite mixed layer series of clay fractions ($<2\mu\text{m}$) dispersed from sediment profiles in estuary of the Dam Mon	232
Figure 8.24. Haft time of dissolution ($t_{0.5}$) of dioctahedral vermiculite/smectite mixed layer series of clay fractions ($<2\mu\text{m}$) dispersed from sediment profiles in estuary of the Nha Phu	233
Figure 8.25. Frequency distribution of IS-ml series in sediment profiles of Red River delta	234
Figure 8.26. Interlayer charge versus tetrahedral Si in mixed layer series of clay fractions ($<2\mu\text{m}$) dispersed from sediment profiles in estuary of the Red River Delta.....	241
Figure 8.27. Interlayer charge versus tetrahedral Si in mixed layer series of clay fractions ($<2\mu\text{m}$) dispersed from sediment profiles in estuary of the Red River Delta.....	242
Figure 8.28. Interlayer charge versus tetrahedral Si in mixed layer series of clay fractions ($<2\mu\text{m}$) dispersed from sediment profiles in estuary of the Red River Delta.....	243
Figure 8.29. XRD peak area of calcite (2.13 \AA) and ratios to quartz peak (1.82 \AA) indicates the abundance of calcite in coarse and medium sizes	244
Figure 8.30. Influences of accumulation factor on distribution of heavy metals in RRD	245
Figure 8.31. Influences of accumulation factor on major elemental distribution in coastal sedimentary sites along Vietnam	245
Figure 8.32. Influences of hydrodynamic factors on clay mineral composition in fractions $< 2\mu\text{m}$	246
Figure 8.33. Influences of accumulation factor on distribution of heavy metals and minor elements in Dam Mon and Nha Phu	247
Figure 8.34. Influences of accumulation factor on distribution of heavy metals and minor elements in Dam Mon and Nha Phu	247
Figure 8.35. Mineralogical features as mirror of interactions among post-sedimentary processes in coastal environment of Red River Delta.....	248
Figure 8.36. Variation of XRD peak area along profiles in RRD in connection with TOC, and hydraulic permeability.....	249
Figure 8.37. Variation of XRD peak area along profiles in Dam Mon in connection with TOC, pH, Eh and hydraulic permeability	251
Figure 8.38. Mineralogical features as mirror of interactions among post-sedimentary processes in coastal environment of Nha Phu	252
Figure 8.39. Variation of XRD peak area along profiles in Nha Phu in connection with TOC, pH, Eh and hydraulic permeability	253

INDEX OF TABLES

Table 2.1. Basic factors in formation and maturing of coastal sediments.....	6
Table 3.1. Location and setting of study sites	28
Table 3.2. Equipment and technical parameters of XRD measurements	33
Table 4.1. The deconvoluted Gaussian modes	63
Table 4.2. pH and Eh along depth profiles in low tidal mudflat (LM), mangrove forest (MF) and shrimp pond (SP) of coastal sediments in Dam Mon and Nha Phu	69
Table 4.3. Concentrations (%) of chemical elements in coastal sediments of Vietnam	70
Table 4.4. Average, standard deviations, minimum and maximum concentration of the studied major chemical elements in the estuarine muddy sediments of the Red River Delta	71
Table 4.5. Distribution of major elements (wt. %) in grain size fractions of sediment samples in RRD	74
Table 4.6. Average, standard deviations, minimum and maximum concentrations of major elements in the coastline muddy sediments of Dam Mon and Nha Phu	76
Table 4.7. Minor elements in the coastal sediments of Red River Delta, Dam Mon & Nha Phu	81
Table 4.8. Average, standard deviations, minimum and maximum concentration of the studied heavy metals in the estuarine muddy sediments of the Red River Delta ..	82
Table 4.9. Average, standard deviation and concentration range of the studied minor elements in muddy sediments of Vietnam coastline.....	83
Table 4.10. Distribution of minor elements in grain size fractions of RRD sediments	84
Table 4.11. Frequency (%) of mixed layer series in sediment profiles in Red River estuary ..	94
Table 4.12. Crystallite parameters of diVerm structures in fraction < 2 µm of sediments in RRD based on ~10 Å and 10.2 Å reflections	96
Table 4.13. Mineral formulae [O10(OH)2] of diVS-ml series from fraction < 2 µm, dispersed from sediment profiles in estuary of Red River Delta	99
Table 4.14. Crystallite parameters of kaolinite & KE-ml structures based on 7 Å and 7.4 Å	101
Table 4.15. Mineral formulae [O10(OH)n]* of clay minerals from fractions < 2 µm, RRD sediments	103
Table 4.16. Frequency (%) of mixed layer series in sediment profiles in the coastal zone in Dam Mon – South Central Coast.....	108
Table 4.17. Frequency (%) of mixed layer series in sediment profiles in the coastal zone in Nha Phu.....	108
Table 4.18. Crystallite parameters of diVS-ml and/or IS-ml structures in SCC sediments ..	110
Table 4.19. Mineral formulae [O10(OH)2] of clay minerals from fractions < 2 µm, dispersed from sediment profiles in Nha Phu	114
Table 4.20. Crystallite parameters of kaolinite and KE-ml structures in SCC sediments...	116
Table 4.21. Mineral formulae [O10(OH)2] of KE-ml series from fractions < 2 µm, dispersed from sediment profiles in Dam Mon	119
Table 4.22. Mineral formulae [O10(OH)2] of KE-ml series from fractions < 2 µm, dispersed from sediment profiles in Nha Phu	120
Table 5.1. Input data for constructing age normalization model and distance normalization model.....	131
Table 5.2. Estimation on chemical contribution of hydrodynamic accumulation factor	139
Table 5.3. Correlation between heavy metals and possible proxies.....	146
Table 5.4. Enrichment ratios of heavy metals in coastal sediments of Vietnam	152
Table 5.5. Principal mineral modification during post-sedimentation and assumed processes	159
Table 5.6. Comparison between the % Kaol estimated by linear system & non-linear system of %(OH) vs. (% Kaol.).....	172
Table 5.7. Main chemical variations along sedimentary profiles and assumed driving processes	177
Table 5.8. Ratios of key parameters between surface layer and the nearby subsurface layer	189

Table 8.1. Results obtained for the reference material Miramichi River Estuary Sediment (MESS-1) and Baie des Chalerus (BCSS-1) and real samples in coastline of Vietnam	209
Table 8.2. Summary on protocol and established commands of PCA and EMMA	211
Table 8.3. Rotated principal component matrix – reveals from PCA for chemical parameters of sediments in Dam Mon and Nha Phu	212
Table 8.4. Rotated principal component matrix – reveals from PCA for chemical parameters of sediments in Dam Mon and Nha Phu	212
Table 8.5. Correlation matrix of the major and minor elements in the coastline of Vietnam	213
Table 8.6. Mineral formulae [O10(OH)2] of clay minerals from fraction < 2 µm, dispersed from sediment profiles in estuary of Red River Delta.....	235
Table 8.7. Crystallite parameters of chlorite & CS-ml structures of RRD sediments based on 7 Å, 14 Å and 14.2 Å reflection.....	236
Table 8.8. Crystallite parameters of CS-ml structures in SCC sediments	236
Table 8.9. Mineral formulae [O10(OH)n] of clay minerals from fraction < 2 µm, dispersed from sediment profiles in estuary of Red River Delta	237
Table 8.10. Mineral formulae [O10(OH)2] of CS-ml series from fractions < 2 µm,	238
Table 8.11. Mineral formulae [O10(OH)2] of IS-ml series from fractions < 2 µm, dispersed from sediment profiles in South Central Coast	239
Table 8.12. Mineral formulae [O10(OH)2] of clay minerals from fractions < 2 µm, dispersed from sediment profiles in Nha Phu	240
Table 8.13. Principal mineral modification during post-sedimentation and assumed processes in Red River Delta	250
Table 8.14. Principal mineral modification during post-sedimentary processes in Nha Phu	254
Table 8.15. Ratios of key parameters between surface layer and the nearby subsurface layer in sediments of Dam Mon and Nha Phu	255

ABBREVIATIONS

General		Name of Clay Minerals	
ABBR.	FULL NAMES	ABBR.	FULL NAMES
550°C	Thermal treatment to 550°C	di-	Diocahedral
AD	Air dried	tri-	Triocahedral
CSD	Coherent scattering domain size	-ml	mixed layer
DM	Dam Mon	diCM	Diocahedral clay mineral
e.g.	for example	diVerm	Diocahedral Vermiculite
E.M.A	Ernst-Moritz-Arndt	triVerm	Triocahedral Vermiculite
EDX	Energy Dispersive X-ray	Kaol.	Kaolinite
EG	Ethylene Glycolation	Chl	Chlorite
Eh	Redox potential	Q	Quartz
EMMA	end member model approach	Feld.	Feldspar
et al.	et al.ii	Py	Pyrite
etc.	et cetera	IS	Illite/Smectite mixed layer structure
FA	factor analysis	diVS	Diocahedral clay mineral/Smectite mixed layer structure
FWHM	Full width at haft maximum	KE	Kaolinite/Expandable mixed layer
GSD	Grain size distribution	CS	Chlorite/Saponite mixed layer
i.e.	that is	CV	Chlorite/ Triocahedral Vermiculite mixed layer
Infl.	Influence	CSV	Chlorite/Saponite/ Triocahedral Vermiculite mixed layer
LD	laser diffraction	XII	Interlayer
LM	low tidal mudflat	IV	Octahedral layer
max	Maximal	VI	Tetrahedral
MF	mangrove forest	n ^{IV}	number of octahedral cations
min	Minimal	Si ^{IV}	Tetrahedral Si
NP	Nha Phu		
PA	Peak area		
PC	principal component		
PCA	principal component analysis		
pH	ponds Hydrogenium		
PSD	Particle size distribution		
RRD	Red River Delta		
SAED	Selected Area Electron Diffraction		
SP	shrimp pond		
STA	Sedimentation Trend Analysis		
TEM	Transmission Electron Microscopy		
VN	Vietnam		
vs.	versus		
XRD	X-ray diffraction		
XRF	X-ray Fluorescence Analysis		

ACKNOWLEDGEMENTS

First of all, I would like to show deep gratitude to my supervisor, PD. Dr. habil. Jörn Kasbohm, for his excellent guidance and ideas for my study. Without his patience in answering all my questions and encouragement, I would have not made it. Thanks are to his continuous support, facilitating me to gather fruitful discussions from international conferences. His kindly favour to my field works and sampling in Vietnam (2004) is also highly appreciated.

Next, I would like to thank my vice supervisors, Prof. Mai Trong Nhuan (Hanoi National University, Vietnam) and Prof. Dr. Harm Wulff (Department of Biochemistry, University of Greifswald). Their discussions and kindly supports motivated my progress.

Financial support from the Ministry of Education and Training of Vietnam (MOET), German Academic Exchange Service (DAAD) and German Federal Ministry of Education and Research (BMBF), funds for participation in international conferences are acknowledged.

I would appreciate highly the organization for my Ph.D. work of Joint Educational Training Center” (JETC), especially Prof. Dr. Maria-Theresia Schafmeister, Dr. Jörn Kasbohm, Dr. Le Thi Lai, Prof. Le Tran Binh, Dr. Luu Lan Huong and Dr. Henry Witt.

I am especially thankful for feeling welcome and facilitated by colleagues in the Institute of Geology and Geography, University of Greifswald: Manfred Zander, Monika Schäfer, Marianne Siebrand, Gisela Liebenow. I thank them for kindly help on getting the TEM-EDX, XRD, XRF analyses done.

Thanks go to Prof. Reinhard Lampe, Prof. Jan Harff, Dr. Hinrich Meyer for guidance and facilitation for my field works in Vietnam 2004. Their facilitation in analyses of C-S, LD and scientific documents are also acknowledged.

I appreciate all members of the Geology Faculty, Hanoi University of Sciences for their generous help throughout my work. A special gratitude is dedicated to Prof. Nguyen Van Nhan for his warm care and encouragement.

Special thanks are due to Thao, Huan and Grothe Steffen for sharing ups and downs, and cares every day. The fruitful discussions, generous helps with language, volume formatting and much as unnameable assistances, I acknowledge.

I thank my dearest friends in Vietnam: Que, Tuan, Duong^A, Duong^B and every member of my honey groups, who shared with me thoughts, feelings and granted me heartfelt wishes.

For the unforgettable time together in Greifswald, I acknowledge my Geschwister-Scholl friends and my roommates for sharing homesick and daily joys. Their kindly helps to solve computer troubles are also appreciated.

Being my home in Germany, my cousins - Ninh H.D., Chinh P.T., my nephew - Linh and the cozy time together with warm-cares are precious presents to me. I would like to thank them for these real motivations.

Finally, I am indebted to my grand-mother, dad, mum, sisters, brothers and kids, who are always beside me, love and care, regardless of geographical distance.

1 INTRODUCTION

1.1 Motivation

1.1.1 Meaning of coastal zone for regional development & problems

Coastal areas are developed and intensive exploited regions on the one side, but on the other side these areas are very sensitive ecological zones. Its individual contribution to the regional development can be measured in terms of availability of productive ecosystems (e.g. mangroves, fish-stock), fertile agricultural land, clean water coherence with marine resources (GESAMP et al. 1997). Statistic data showed that coastal resource supply approximately 90% of world fish catch (Pernetta & Milliman 1995). Because of the presence of rich natural resources and other favorable natural conditions, the coast is a zone of active development.

Considering geographical features with 3.200 km coastline, the meaning of coastal zone is very impressive for Vietnam. Intensive exploitation of aquaproducts and shrimp farming in the coastal environment, which grows 10-15% annually during the last few years (Vietnamese GSO 2004) are, to a large extent, based on the large diversity of marine species, mangroves and their associated ecological processes (Hong & San 1993, Thanh et al. 2003). Rapid growth of tourism is linked with favourable geographical, historical context and also biodiversity of the reserved mangrove ecosystem (Adger et al. 2001, Hoi et al. 1997). Spectacular development of infrastructures, water transportation and agriculture are facilitated by fertile alluvia land as well as hydrodynamic potential (Adger et al. 2001). In fact, the coastal zone is a place where different interests meet and conflicts arise between various stakeholders (Sekhar 2005).

Coastal zone, for these significant benefits, supports the majority of the planet's human population (World Bank 1996). Vietnam is a typical example where one can observe population shift from the hinterlands to coastal areas, up to a quarter of the total population in recent time (Sekhar 2005).

In recent decades, rapid urbanization and coastal human activities looking for economic development like shrimp aquaculture, mangrove exploitation, overfishing etc. has led to irreversibly deterioration of fish stocks and other valuable ecosystem and resources (Thornton et al. 2003). Degradation in quality of sediments and water environment due to uncontrolled land-using, and additionally by heavy metals (Tuan et al. 2003; Tuyen et al. 2001; Quyen et al. 2000) and organic pollutants (Nhuan et al. 2003) brought by rivers has depleted the long-term potential benefits of coastal regions (Sekhar 2005) and affected millions of people who depend on the coastal living resources for their livelihood (UNEP 1999).

This makes it necessary to understand the geographical, geological background and context of the diverse coastal regions before initiating any new management approaches and socio-economic planning.

1.1.2 Coastal sediments in the view of a real complex of geological process

Coastal zone is a dynamic region, where terrigenous sediments and sea meet together, results in complex of geological processes. Natural coastal processes are influenced by mangrove biota (Padmala et al. 1997; Wassermann 2001) and also more intensively by human activities for recent decades (Thornton 2003).

Hydrodynamic processes are mirrored in morphological features and grain size distribution (Phai 1998; van Maren 2004), whereas geochemical processes and environmental variations are more likely to leave imprints on clay minerals - the most sensitive matters to mineralogical and geochemical modifications (Velde 1995; Chamley 1989).

For the important meaning of coastal zone in regional development, several studies have laid interest on geological processes (e.g. Tam 1992, Tanabe et al. 2003), geochemical processes (Cu 1993-1998; Nhuan et al. 2003), biota influence (Hong & San 1993; Tri et al. 1998) and impacts from human activities (Li et al. 2006; Ninh et al. 1992; Thanh et al. 2003) related to land-use changing. However, multidiscipline studies on net-system of sediment – biota – human activities are rarely in Vietnam. It is also to notice that imprints of environmental variations those recorded by clay matters are missing until now.

Clay minerals in coastal sediments are widely reported to compose of chlorite, kaolinite, smectite and illite as main composition (Chamley 1989). Recently, with development of analytical techniques (e.g. TEM-EDX, XRD for oriented specimens), abundance of mixed layer structure instead of pure clay minerals have been determined for weathering products and soil materials over the world (Srodon 1999) and also in Vietnam (Thanh et al. 2000; Tra et al. 2000). Although the abundance of mixed layer phases can also be expected for coastal sediments, literatures for presence of mixed layer structures as well as their origin, pathway there are rare (Srodon 1999).

Observed differentiations of clay mineral distribution in several estuaries and coastal bay (Chamley 1989) suggest for occurrence of coastal processes as driving force. However, explanations for these differentiations are in controversy (Chamley 1989): whether the imprints mirror influences of short-term alteration processes or the imprints are only results of hydrodynamic mixing? In fact, some chemical processes like desorption/adsorption of heavy metals in estuaries (e.g. van der Weijden et al. 1977; Hatje et al. 2003) have been widely published. And recently, field measurement and experimental studies have also determined mineral modifications of clay minerals in contact with saline water like formation of illitic layer on montmorillonite structure (Herbert et al. 2004). These results

are thus to expect possible mineralogical processes that govern distribution and characteristics of clay size materials. It is likely that variations in salinity, hydrochemistry or maturing time, buried conditions in early diagenetic processes are key driving forces. In review of Srodon (1999) the most convincing evidence, so far, for short-term mineral alteration of coastal sediment was provided by Righi et al. (1995) who detected progressive illitization in 350 year old polder of Atlantic coast of France. Hence, geochemical and mineralogical processes in recently coastal sediments remain a big unsolved problem.

Influences of biota in motivating weathering processes and alteration processes were well reported, with notices on nutrient supply functions and activities of rhizosphere (e.g. cation uptake, oxygen diffusion (Fried & Shapiro 1961; Gabet et al. 2003; Yang et al. 2004). In coastal sediments, presences of mangroves were determined to modify morphological features, sediment distribution patterns (Gabet et al. 2003), facilitate trapping of muddy sediments, organic matters, heavy metals (Lacedar et al. 1993, Marius & Lucas 1991), mobilization of chemical elements via cation uptakes (Rains & Epstein 1967b; Machado et al. 2002) and to modify redox profile of sediment (Clark 1997). Chemically, organic matters from mangroves can enable the formation of sulfur layers and also sulphatization processes (Clark 1997; Cu 1993, 1996). However, roles of mangroves on desorption/absorption processes of chemical elements as well as on mineralogical processes of the underlying sediments are up to now unclear.

Also in involvement with coastal processes, human-induced activities are known commonly for changing of land-using picture, morphological and hydrodynamic variation, pollutant supply (Thanh et al. 2003). However, influences of human activities, specifically on geochemistry and mineralogy of sediments, are difficult to be distinguished from natural processes (Wassermann 2001).

Taken together, although coastal zone register significant meaning in regional development and being interesting white field for geological processes, geochemical as well as mineralogical processes there in recent decades, in interaction with biota-induced and human activities induced variabilities, are until now inadequately understood.

1.2 Aims of this Ph.D. work

The aim of this work is to give contribution to solve the above mentioned questions. In detail, the following sub-questions are concerned:

- To reveal principal features of coastal sediments in various coastline types of Vietnam, based on granulometric, nutrients, geochemical and mineralogical data. Characterization of crystal structures and chemical formulae of clay minerals in fractions $< 2 \mu\text{m}$ are to carry out based on TEM-EDX investigation for single particle.

- To address the principal synsedimentary hydrodynamic processes in coastal sedimentation of Vietnam, based on End Member Modelling Algorithm (EMMA) and reconstruct the historical development.
- To address features of elemental distribution and mineral matter as mirroring of principal synsedimentary hydrodynamic processes.
- To address geochemical and mineralogical alterations as mirroring of short-term post-sedimentary diagenesis.
- To address geochemical and mineralogical alterations as mirroring of biota-induced post sedimentation.
- To address geochemical and mineralogical alterations as mirroring of human-induced processes

Studies were based on three case environments with different features on coastline types, source rock, distance between river mouth and location of sedimentation, sedimentation rate, mangrove maturity, and intensity of human activities as well: Red River Delta in North Vietnam and Dam Mon, Nha Phu in the South Central Coast. For all studied region it should be investigated for the upper 1 m only to recognize especially processes in the youngest past. The background for this limitation of sampling is to get a better knowledge, what is happened during the sedimentation and in the early diagenesis to consider better these processes better also for investigations in deeper horizons of a basin development.

2 COASTAL SEDIMENTS IN TROPICAL CONDITIONS

2.1 Environmental setting of coastal sediments

Vietnam is characterized by a 3,260 km long coastline, along which coastal sediments are transported, accumulated, eroded and become mature. These processes are running under a tropical climate in the setting of interactions among terrestrial currents, sea dynamics, coastal vegetation and human activities.

2.1.1 Climate and Oceanography

The climate of Vietnam varies from humid tropical in the southern lowlands to temperate in the northern highlands. Coastal zone is characterized by a *tropical moist monsoonal climate with a pronounced maritime influence* (Pfeiffer 1984). High temperature, humidity and rainfall (Table 2.1) *promote intensity and speed of chemical and biological processes, as well as formation of kaolinitic weathering crusts* (Thang 2000, Righi & Meunier 1995).

The seasonal changes (Table 2.1) are generally marked with much more vertical sedimentation in the water column during winter than summer (Allen 2000). In the Red River Delta, the *hot wet summer* (April to October) brings greater amount of weathering materials to the estuary, *causing intensive seaward progradation* whereas the *cold winter* (November to March) *favors vertical sedimentation*. In the South Central Coast, the rainy summer (August to December) collects 80% of total rainfall, *causing intensive leaching on the coastal mountainous areas and contributing most of materials for coastal sedimentation*.

In Red River Delta estuary and South Central Coast, tide variability follows regular and irregular diurnal regimes respectively (Table 2.1), allowing the *daily alternative dry and wetting cycles to occur on surface layer of coastal tidal mudflats*. *Youthful mudflats like low tidal mudflats are submerged by tide during most of the day, whereas mature ones like high tidal mudflat or mangrove forest may be drowned on few hours*. When tide level is much higher than the bed (e.g. in high tide), mud tends to settle over the whole submerged tidal area regardless of height in the tidal frame. But when the bed surface is near the tide level (e.g. in neap tide), sedimentation of muds is subjected to *rework processes by turbulence currents* (Allen 2000). *Wave and tide dynamic are considered as essential factor that can induce syn-sedimentary erosion* (van Maren & Hoekstra 2004, van den Bergh et al. 2006, van Maren 2006).

Table 2.1. Basic factors in formation and maturing of coastal sediments*(World Conservation Monitoring Center (1992))*

<i>Parameters</i>	Red River Delta	South Central coast (Dam Mon and Nha Phu)
I. Climate	Tropical moist monsoonal climate with a pronounced maritime influence ^[1]	
Rain falls	1300 – 1800 mm/year	1285 mm/year
Temperature (° C)	Summer: 27 – 29°C Winter: 16 – 21°C	24 – 29°C
Humidity	80 %	80 %
Seasonal regime	Hot, wet summer/cold winter	Rainy summer/dry winter
II. Oceanography		
Tide	Diurnal Mean tide: 1.9–2.6 m High tide: 3.2–4 m	Irregular diurnal Mean tide: 0.5 m High tide: 1.5 – 2 m
Wave	At the river mouth: ^[2] Mean height: 0.73 m Maximum height: 5.6 m In storms: 7 – 8 m	Along the coast: ^[3] Mean height: 1.0 m Maximum height: 3.5 m In storms: 7 – 12 m
Prevailing winds	north and east in winter, and east and southeast in summer	north – northeast (3.8 m/s) and west–southwest (2.6 m/s)
pH of sea-water	8.0 to 8.4	
III. Hydrology		
River	Long, high loaded Red River system (1126 km long, 114 k tons/ year) ^[3]	Short, slope rivers and drainages (< 15 km long) ^[3]
IV. Geological setting		
Geological structure	Inherited fill-up on basin with Neogene and Quaternary sediments ^[4, 5]	Alternative distribution of Jura – Kreta magmatic rocks, sediments and Quaternary sediments ^[6]
Coastline type	Deltaic estuary	Cliffy coastline separated by peninsulas, embayments and estuaries
Seaward extension rate	80 m/ year ^[3]	Nearly unchanged ^[3]
Vertical sedimentation rate	1 – 7 cm/y in coastal mudflats ^[7] ~ 5 cm/y in LM ~ 3 cm/y in MF ~ 1 cm/y in SP	0.05 – 0.1 cm / year in coastal shelf ^[3] ~ 0.03 cm/y in MF ~ 0.02 cm/y in LM ~ 0.02 cm/y in SP
Duration of post-sedimentary	< 100 years for upper 1 m	> 400 years for upper 1 m
Sea-level-change circle	Modern transgression	Modern transgression
V. Vegetation	Young mangrove forest (< 30 years old) (Avicenia dominated)	Century age mangrove forest (~ few hundreds years old) (Avicenia dominated)
Duration of biota	< 30 year	~ few hundreds year
VI. Anthropogenic influences	Dominantly by mangrove cutting and aquaculture	

^[1]: Pfeiffer (1984)^[2]: Hori et al. (2004)^[3]: Schimanski & Stattegger (2005)^[4]: Mathers and Zalasiewicz (1999)^[5]: Nghi (1989), Lam & Boyd (2003), Mathers et al. (1996),

Tanabe et al. (2003a)

^[6]: Nhuan et al. (2002)^[7]: Nhuan et al. (2003)

2.1.2 Geological and geographical setting

Geological and geographical setting of Vietnam coherent with development of two mega delta: Red River Delta in the northern part, Mekong delta in the southern part and the coastal mountain system in middle of the country. Development course of the Red River Delta is controlled by the Neogene Red River fault system, which stretches NW-SE (Ngoi et al. 2000). The sedimentary basin, approximately 500 km long and 50–60 km wide, is filled with Neogene and Quaternary sediments with a thickness of more than 3 km. The Quaternary sediments, which unconformable overlie the Neogene deposits, comprise three formations, the Vinh Phuc, Hai Hung, and Thai Binh formations, in ascending order. Sediments are composed mainly of sands and gravels with subordinate lenses of silt and clay, deposited since the last glacial maximum (Nghì et al. 1989; Mathers et al. 1996; Mathers & Zalasiewicz 1999; Tanabe et al. 2003a). *Grain-size composition and characteristics of fine sediments (silt, clay) can record highlighted events along long-term history of the deltaic development* (Nghì 1989; Tanabe et al. 2006). *The present-day sedimentation takes place as a continuous inheritance of sedimentary cycle on the base of the sediment basin structure.* In modern coastal fine sediments as well as in peat swamp and lagoonal facies of Holocene formation, *clay minerals were recognized with interlayer-deficient micas¹, kaolinite and montmorillonite* (Bieu & Nghì 1998; Nhuan et al. 2002).

In South Central Vietnam, the elongation of Truong Son Mountain range along the coast constructs the *zigzag coastline with alternative peninsulas* (e.g. Hon Gom), *embayments* (Nha Phu, Van Phong), and *small estuaries* (e.g. Can river, Cai river in Nha Phu embayment). The cliffs developed on intrusive *magmatic formations* ($\gamma\delta J_3$ dq, $\gamma\zeta K$ dc, γK_2 cn), *terrigenous sediments, igneous sedimentary rocks* (J_2 ln, K nt) of Kreta and Jura ages and are *covered by Quaternary sandy unconsolidated sediments*. The muddy sediments dominate at small estuaries, cover bottoms of embayments (e.g. Nha Phu, Van Phong) and distribute as wide, continuous fields at the shelf of > 35 m water depth.

Due to influences of the large river systems, Holocene deposits from the delta in Northern coast and Southern coast of Vietnam are similar in preference of seaward progradation to vertical sedimentation (Table 2.1) (Schimanski & Stattegger 2005). In contrast, the South Central coast developed vertical thickness during Holocene due to the proximity of mountainous rivers draining directly into the SCS nearby. The effect of *sediment starvation* accompanying the rapid sea level rise was neutralized due to the narrowness of the shelf *in the South Central Coast area, keeping a position close to the shoreline* (Schimanski & Stattegger 2005).

¹ in former times called as hydromica

2.2 Sources of coastal sediments and yields

Alluvia materials from Red River system were determined as the main source for sedimentation in coastal zone and sea shelf (Bach & Phuc 1999; Schimanski et al. 2006). These materials have diverse, poly-source, with lithoclasts from Precambrian crystalline rocks and Palaeozoic to Mesozoic sedimentary rocks surrounding mountainous catchment (Mathers et al. 1996; Mathers & Zalasiewicz 1999), weathered materials (Thang 2000), limestone cliffs on both sides of the lower reaches of the river (van Maren 2005; Tanabe et al. 2003), Neogen and Quaternary sediment covering river basin (Phai et al. 1998), soils from deltaic catchment (Bach & Phuc 1998). And also various altered materials from the Red River metamorphic zone along the fault fill the Red River delta can be combined. Due to such high variability in rock source, a rather complex geochemistry and mineralogy of the coastal sediment, as well as alteration levels, is expected.

Investigations by Bach & Phuc (1999) on alluvia at the Red River estuary revealed the dominance of sand and mud. The sand consists of medium-grain quartz (80 - 98%), followed by feldspars (~1%), mica (~1%), electro-magnetic minerals (chlorite, amphibole, ilmenite and magnetite) and heavy minerals (i.e. zircon, rutile and anatase). In muddy sediment, *kaolinite, chlorite, montmorillonite and interlayer-deficient mica were detected in coastal sediments of both Red River and Mekong River Delta* (Schimanski 2005; Nghi et al. 1991).

In south central coast of Vietnam, coastal sediments are mainly *sourced from rock fragments, weathering crust and soils which develop on Deo Ca granite complex, Nha Trang anderit formation and Quaternary sediments from surrounding coastal mountains of Truong Son range*. Schimanski et al. (2006) and Jagodziński (2005) described material in the central shelf of Vietnam mainly made up of *sand to clay and contained various amount of foraminifera, shell fragments, lithoclasts and plant fragments in the coarse fraction*. In fine fractions, *illite, kaolinite, chlorite and smectite* were determined as main clay mineral compositions (Schimanski 2002; Jagodziński 2005).

Soil matter is a significant contribution to the budget of rivers, especially to the fine fractions, on their way to the sea. *Clay mineralogy of soils composition varied with relief, parent rocks and locations all over Vietnam* (Tra et al. 2000). Soils derived from limestone show a heavy-clay texture, with kaolinite as predominant mineral in clay fraction. Soils derived from basalt have also a heavy-clay texture, but the clay mineralogical composition was different with relief. The clay fraction of ferralsols on the hillside is composed of kaolinite, whereas that of luvisols on the terrace comprises smectite and 7 Å halloysite.

The soils distributed in the mountainous regions and north midlands are characterized by the intergraded vermiculite-chlorite whereas the fluvisols in agro-economic zones of the Red River Delta and the Mekong River Delta contain kaolinite as main composition of the

clay fractions, “mica” (mentioned for 10 Å phase in XRD patterns of clay fractions) and partially with *chlorite* (Kasbohm et al. 2003; Thanh et al. 2000; Tra et al. 2000). The mentioned “mica” is suggested to include *dioctahedral vermiculite* as main component, rarely also *illite*, *biotite* or *muscovite* (Kasbohm et al. 2003). *Smectite* and *vermiculite* were also detected in the Red River Delta (Kasbohm et al. 2003; Thanh et al. 2000; Tra et al. 2000). Kasbohm et al. (2003) described composition of smectite characterizing mainly for montmorillonite but rarely for beidellite and saponite. Also, *soil vermiculites* were suggested to have *dioctahedral structures* (Douglas 1989). And the *trioctahedral types* remains mainly in coarser fractions and become rare in fines.

Mixed layer structures were also detected as *vermiculite/smectite mixed-layer* (Kasbohm et al. 2003; Thanh et al. 2000; Tra et al. 2000), *illite-smectite mixed-layer* (Kasbohm et al. 2003) and *mica/vermiculite/smectite* mixed-layer particles (Thanh et al. 2000; Tra et al. 2000) in the Red River Delta, *vermiculite/smectite* and *chlorite-vermiculite mixed-layer* particles in the Mekong River Delta (Tra et al. 2000).

Non-clay minerals included in the clay fractions are quartz, feldspar, different Fe-hydroxides and hematite and traces of apatite, rutile, and gibbsite.

2.3 Transport to the sea

Transported by rivers, detrital sediments drain into the South China Sea (SCS), are reworked and distributed in geomorphologic formations along the Vietnamese coast.

In North Vietnam, sediments are transported to the sea mostly by the Red River system. The Red River has its sources in the Tibetan Plateau, *elongating 1,126 km and discharged average 130,106 tons of sediments annually* (Phai et al. 1998). This *huge sediment load gives rise to a fast progradating deltaic development*. Because the dominant sediment type transported by the Red River is fine silt, most sediment can be assumed to be *transported in suspension* (van Maren 2004). As the Red River is seasonal dynamic, during summer monsoon season (June - October), 85% of annual water and 96% of the total annual sediment load are discharged to the sea, resulting in huge deposit (Phai et al. 1998; Pruszk et al. 2002; van Maren 2005). This seasonal variation is an important factor on morphological evolution of coastal sediments.

In contrast, the proximity of small mountainous rivers draining the Truong Son chain are flowing into the SCS along the south central coast, and causes a high abundance of lithoclasts in the Holocene sediments (Schimanski & Stattegger 2005). Length of the rivers ranges from 10 – 15 km. *Sediment yield by small mountainous rivers is generally underestimated* (Milliman & Syvitski 1992). River currents become much more intensive in storm season (August - December), discharging 80% of their water to the sea.

2.4 Morphology and driving forces

Geomorphologic formations in the coastal zone result from dynamic interactions among river sediments, sea, climatic events, development of vegetation as well as human activities (Schimanski & Stattegger 2005).

In Red River estuary, *sedimentation and erosion have been recognized as the major geomorphologic processes under wave-dominated condition and abundant suspended loads carried by the Red River* (Nghie et al. 1988; Phai 1998; van Maren 2005; Tanabe et al. 2006).

Observations and investigations (e.g. van Maren & Hoekstra 2003; van Maren. 2004; Phai 1998) documented the dominant *sequences of present-time expanding sedimentation in the Red River mouth as follows*: delta-front sedimentation - formation and growth of sandy barrier-spits in front of the river mouth - subsequent attachment to the mainland by lagoon infilling (lagoon processes) – development of mangrove forest - formation of human-made geomorphologic features – breach of the mouth bars and creation of a new river outlet. The present barrier-spit system has formed only recently in the 1970s, but inactive barriers on the delta plain show that this barrier formation occurs repetitively (Tanabe et al. 2003; van Maren 2004). Such bar-built mechanism observed in the Red River estuary is comparable to Mekong river estuary and *typically found in tropical areas with strong seasonal variation in discharge and active coastal deposition* (van Maren 2004 and references therein). According to Thanh & Huy (2000), *the progradating sedimentation rate is averagely 50 m/ year during the last 50 years*.

Lagoon processes start with *deposition of fine-grained suspended matter in lagoon by out-flowing river water and alternating effect of ebb- and flood-direct currents, forming low tidal mudflats*. Currently tidal mudflats in the Red River Delta estuary occur mostly between low tide level (0 m) and high tide level (+ 4 m) in comparison to mean tide (2 m) (Cu 1993). Infilling up the lagoon is dominant in rainy season, when the supplied fine sediments can settle in a low energy environment (van Maren 2004). *As deposition increases to raise the background higher than medium sea level (Cu 1993), the environment may favour the settlement of mangrove trees in front of a former barrier, located at the landward of the lagoon*. Determination of vertical sedimentation rate in mangrove forest by Nhuan et al. (2003), based on biomarkers, obtain values of 4.5 – 5.5 cm/y. Infilling of the lagoon reduces its width and in its final stage, the lagoon may appear as a tidal creek. If the former barrier is high enough and the associated beach is wide enough, the barrier will be subjected to eolian processes. Once the width of the lagoon were narrowed by infilling, the great blocked discharge from river has been forming a significant stress on the mouth barrier, tending to breach it out.

Significant insert in the natural formation sequence of barrier-lagoon system are land-using processes, which produce typical human-made morphological units, such as aquaculture ponds and dyke systems. Dykes have been created right on the area of mangrove forest, and also on the unstable ground of low tidal mudflats inside lagoon to take advance in extension. Aquaculture ponds are developed on the area of mangrove forest, after the mangrove trees has been cut and removed. The formation of such human-made geomorphologic features during the land-using processes occurs parallel to the next step in natural formation sequence of barrier-lagoon system.

Different from coastal morphological processes in deltaic estuary, *sediments in the mountainous central coast of Vietnam undergo reworking and deposit under strong influence of marine factors (i.e. wave, tide, long-shore currents) and aeolian deposition (Schimanski 2002). Whereas in deltaic areas, abundances of sediment supply facilitate expansion of the land seaward dramatically, high slope of the coastal shelf in mountainous central coast of Vietnam favors rapid sedimentation to form thick layer of Holocene sediments (Schimanski & Stattegger 2005). Muddy sediments in estuaries are supplied by short rivers and originate from surrounding mountainous rocks, weathering crust and soils. Studies of Nhuan et al. (2003) on deposition of biomarkers in estuaries of Can river and Giang river of the south central coast revealed vertical sedimentation rate less than 1 - 1.5 cm/y. It thus suggests a lower sedimentation in mangrove forest area of Dam Mon, where river source is much depleted.*

In a sedimentological study of the Langebaan lagoon and coastal embayment located south of Cape Town, South Africa, Flemming (1988) stated that *coastal and lagoon sediments tend to present bi- or multimodal grain size distributions which are produced by the mixing of two or more hydraulic grain-size populations.*

2.4.1 Vegetation

Vietnam is located in the tropical semi-evergreen seasonal rain forest and moist rain forest zones. *The principal land use throughout the delta is the cultivation of rice (Gramineae).*

Vegetations in coastal areas are dominated and characterized by mangrove forest ecosystems containing 36 species and covering 156,608 hectares of wetland (Vietnam Institute of Forest Inventory and Management 2002 – Statistic data in 1999).

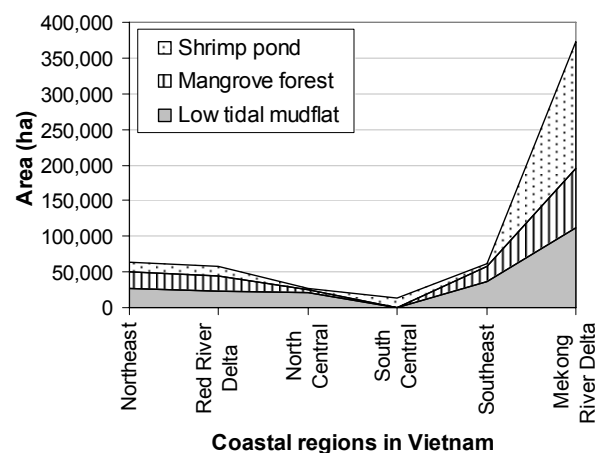


Figure 2.1. Variation in area of wetland types along coastline of Vietnam

(Statistic investigation 1999 -2000 of Vietnam Ministry of Fishery and Institute of Forest Inventory and Management)

Covering area as well as number of mangrove species decrease intensively from Mekong River Delta via Red River Delta to the south central coast (Hong and San 1993), due to deficiency of sediment in shallow-water wetland and strong storms (Figure 2.1).

In the Red River Delta appears 33 % of total mangrove area in Vietnam. Principal natural mangrove vegetations are diverse, including *Sonneratia caseolaris*, *Kandelia candel*, *Aegiceras corniculatum*, *Avicennia spp.*, *Rhizophora stylosa*, *Bruguiera gymnorhiza*, *Acanthus ebracteatus*, and *Derris trifoliata*. Recent decades, the natural mangrove forests have been replaced by a much simpler planted community dominated by *S. caseolaris*, *B. gymnorhiza*, and *A. corniculatum*. (World Conservation Monitoring Center 1992; Hong & San 1993). *Due to the cold winter in North Vietnam, mangroves in the Red River mouth are more stunted in comparison to mangroves in central Vietnam and in Mekong river delta (Figure 2.2).*

The area of mangrove forest in Central Vietnam (Figure 2.3) *accounts for only 2 % total mangrove wetland of Vietnam*, covering 30 – 40 % of 6,500 ha narrow tidal mudflat (Vietnam Institute of Forest Inventory and Management 2002). *There are located the oldest mangroves remained in Vietnam in current time (Hong & San 1993), besides young replanted mangroves in Nha Phu lagoon.* The old mangrove forest in Dam Mon until now remains 15 hectares, thinly fringing 2.5 km coastline. This ecosystem is diverse with 14 species of true mangroves, dominated by *Sonneratia alba*, followed by *Avicennia spp.* and *Rhizophora mucronata* (Hoa 2001, unpublished data). In Nha Phu lagoon, there is young, replanted mangrove forest with 14 true mangrove species and 6 species of mangrove associates, dominated by *Avicenniaceae* and *Rhizophoraceae*.

Mangrove habitats favored a high biodiversity of algae, seagrass, benthos, marine shrimps, cephalopods and fishes. Many species of which (e.g. Metanacus Enris, Scylla Serata, Lutianus, Epinephelus, Nemipterus, Grasilaria Verrucosco) are of significant commercial values (Tang 1994; Hong 1993). Being not only the source of natural source of larva shrimps, mangrove forest is also the nursery ground for brackish water aquaculture, which is of great economic benefits (Hong & San 1993). Additionally, mangrove forests play a vital role in stabilizing shorelines and providing coastline protection against erosion, cyclones as well as other extreme weather events (Hong & San 1993). However, mangrove forest cover in Vietnam decreased from 400,000 – 500,000 ha in 1943 to 180,000 – 200,000 ha in 1995 and continues to decrease until now. This process was caused by the war and by domestic use, and is favoured recently by cutting for shrimp farming (Hong & San. 1993; Tri et al. 1998). Vietnam has lost more than 80% of its mangrove forests over the last 50 years (Hong & San 1993). Today, shrimp aquaculture is thought to be the single greatest threat to the mangroves that remain (Hong & San 1993, Thornton et al. 2003).

a) Low tidal mudflat and mangrove forest in Red River estuary



d) Shrimp pond



b) Mangrove forest during neap tide



c) Mangrove forest during spring tide



Figure 2.2. Low tidal mudflats, mangrove forests and shrimp ponds in the Red River estuary

a) Century-old mangrove forest in Dam Mon



b) Shrimp pond in Dam Mon



d) Living by the coastal zone (Nha Phu)



c) Mangrove forest and shrimp pond in Nha Phu



Figure 2.3. Low tidal mudflats, mangrove forests and shrimp ponds in the south central coast
Notes: Mangroves are marked by arrows.

2.4.2 Anthropogenic effects

The sudden increase of herbs dominated by the *Gramineae* (rice) in contrast to decrease of arboreal taxa to become most obviously in the late Holocene (8540 cal. year BP) in palynological records of the *Red River Delta* are considered to reflect the *widespread and intensifying of human impacts on the coastal natural vegetation* (Li et al. 2006).

Human impacts however vary with the regions due to irregular population distribution of Vietnam. Population density in Vietnam is 249 inhabitants per km², diversely with high concentration in big cities and coastal provinces and low concentration in mountainous provinces (Figure 2.4). *Population density in the RRD (1204 person/ km²) is much more than in Mekong delta (420 person/ km²) and the south central coast (211 person/ km²).*

High population brings intensive reclamation in along rivers and coastal area, with rapid growth of big cities, ‘economic zones’, major ‘economic corridors’, centralized industrial zones and the aqua-farms. *Pollutants from industrial wastes (i.e. Cu, Pb, Zn), agriculture (i.e. pesticides, herbicides) and living waste cause an environmental stress in the delta areas* (Wetland National Report of Vietnam 2003; Thornton et al. 2003).

Resembling in other tropical developing countries, *shrimp farming in coastal zone of Vietnam has experienced spectacular growth over recent decades*, mostly for export to the West (Thornton et al. 2003). The main raised products are tiger shrimps, crabs, red algae (*Gracilaria*) and natural shrimps. Percentage of aquaculture in structure of agriculture – forestry – fishery increased from 16.01% (in 2001) to 17.45% (in 2003) (General Statistics Office of Vietnam 2004). Each hectare of aqua-farm, averagely brings 25 – 30 millions VND (Vietnam Ministry of fishery 2001), corresponding to about 1,570 – 1,880 USD at current exchange ratios (Feb. 2006).

In 2000, 13,852 ha of brackish wetland had been used for shrimp farming over the coastal area of the Red River Delta (Vietnam Ministry of Fishery 2000), comparably to the south central coast (14,873 ha). Areas of wetland used for aquaculture in Mekong River Delta (179,045 ha) was much higher (Figure 2.1). Due to *low longevity of aquaculture productivity caused by uncontrolled coherent environmental problems* (Hong 1998, Cu 1998), currently, most of shrimp farms have been changed from extensive farming

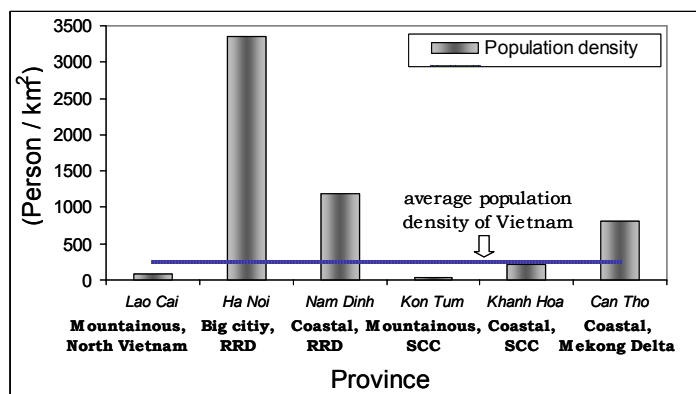


Figure 2.4. Distribution of population density in provinces of Vietnam

(General Statistics Office of Vietnam 2004)

(popularly in 1980s - 1999) to improved extensive and intensive (industrial) farming methods (~10 – 40 hectare/pond) in the north and central Vietnam and integrated mangrove – shrimp farms (~100 hectare/field) in Mekong River Delta. *Cu (1993) reported presence of sulphur accumulating layers in tidal mudflats and sulphatization in the Red River mouth and some other estuaries in North Vietnam, which probably caused depletion in quality and productivities of shrimp farms.* Low quality of pond water, environmental pollution and epidemics were also reported in shrimp farms in China (1991-1993), Indonesia (1991 – 1998), and Taiwan (1987 – 1990) (ACIAR 1999). Also along the coastline of Vietnam this was the main reason for loss of shrimp harvests and degradation of pond quality (Hong & San 1993). *Conflicts are clear between the need for a healthy ecological support system and the environmental effects of shrimp farming.* In the Gulf of Thailand, effluent from shrimp farms has led to serious sea grass losses and sequently affecting vulnerable *Dugong dugon* populations in these habitats (Thornton et al. 2003).

2.5 Maturation process in coastal sediments

2.5.1 Difference between soil profile and coastal sediment profile

Coastal modern sediments, or wetland, are referred as hydric soils (Soil Survey Staff 1993). According to Ramsar Wetland Classification (1996), the natural coastal wetlands such as *intertidal mudflat (i.e. low tidal mudflat, mangrove forest on high tidal mudflat, salt marshes)* belong to “*estuarine wetland*” group whereas *aquaculture ponds in estuary and coastal zone* belong to “*man-made wetland*” group.

Development of coastal sediment profiles and soil profiles all occur in *surface conditions, which facilitate the tropical weathering processes.* However, in comparison to soil profile which is originated mostly from the weathered materials of underlying parent rocks (Allen & Hajek 1989), *coastal sediments can be linked with poly-source attributes.* Due to water saturated environment, matters of coastal sediment profiles have a *development which depends significantly on interaction with chemical substances and elements in brackish water* (Chamley 1989). Therefore, together with the mineral assemblages induced from parent soils, *altered minerals can be expected to present in coastal sediments.*

The mature processes of soil and coastal sediment profile *can be facilitated by vegetation and animal living in the habitats,* with the invasion of rhizosphere and organic matters decomposed from trees. *Uptakes of cations (i.e. K, Na, Mg) nutrients (i.e. N, P) by vegetation developed on soils have been mentioned in several researches on soil/plant system (e.g. Fried & Shapiro 1961; Rains & Epstein 1967a, Yang et al. 2004).* Concerning coastal wetland/plants interactions, Rains & Epstein (1967b) also documented the potassium uptake by the mangrove *Avicennia Marina* as well as by high saline barley plants. Equation for sequence of ion uptake by plants from a soil/ wetland system (Figure

2.5) was also developed by Fried & Shapiro (1961) where minerals, organic matter, or surface adsorbed ions are the source of the uptaken ions. Vegetation uptakes cations (i.e. K, Mg) and nutrients (i.e. N, P) (Yang et al. 2004) from soils/ wetland sediments but supplies S, C_{organic} to them (Cu 1996).

Natural soil profile as well as natural coastal wetland profiles (e.g. low tidal mudflat, mangrove forest) are under no or low influences by human. Soils under cultivation are affected by human to make them more suitable for plant growth through the addition of organic materials and natural or synthetic fertilizer, by regulation of pH/ salinity or water-retaining capacity, and by irrigation. Coastal man-made wetland types (e.g. aquaculture pond), are modified from natural types by water circulation due to closed system and the cutting of natural vegetation. Sediments in ponds are adjusted to favour survival and development of shrimps, by means of *pH regulation (addition of powdered limestone, dolomite)*, *by water exchange through sluice gates, oxygen invasion, addition of shrimp foods, anti-biotic medicine*.

The influences of water and oxygen on development of soil profile and coastal wetland profiles are different. Water occupies the spaces between soil particles and is held by surface tension on particle surfaces, interacts with primary mineral through dissolution process. The dissolution is facilitated by leaching of cation by rain or surface water going through the profile. Therefore, chemistry and mineral phases in the topsoil tend to be more simple than those under surface. Air occupies the remaining void space in soil profile, promote the oxidation. In natural coastal wetland, sediments are rarely exposed to the air or only exposed for few hours during the neap tide. Water-saturated condition limits interaction between wetland sediment and air oxygen, except for small dissolved oxygen in sea water and oxygen obtained from reduction of oxides (e.g. $\text{Fe}(\text{OH})_3 \rightarrow \text{Fe}_2\text{S}_3$).

The mature process thus is governed by wet-dry cycles, sea water dynamic and hydro-chemistry during the early diagenesis. *And, the deeper along depth profile, the more mature the material becomes.* In addition, the *reductive environment is possibly formed* due to oxygen limitation, especially in case of high decaying organic matter received.

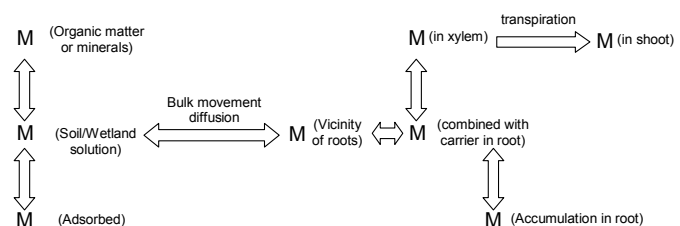


Figure 2.5. Equation for sequence of ion uptake by plants from a soil/ wetland system

(Fried & Shapiro 1961). *M* is the ion studied.

2.5.2 Nutrients, geochemistry and mineralogy of coastal sediment profiles

Nutrients

Organic matters in coastal mudflat are sourced from coastal ecosystems (Woesten et al. 2003), and/or from products of biological processes occurring in the drainage basin and in the river (organic Carbon and organic Nitrogen) (Moreira-Turcq et al. 2004 and references therein). Sorption of dissolved organic matter on surfaces of clay mineral particles represents one of the most important geochemical processes and seems to be responsible for the preservation of organic matters in coastal marine sediment and aquatic system (Moreira-Turcq et al. 2004). Out of the components in the nutrient cycles, species of C, N, P and S play important roles and have been most extensively investigated and documented in literatures. Studies of Cu (1998); Alongi (2000) revealed the variation of concentrations of organic carbon ($C_{org} = 0.5 - 3.5 \%$) for coastal sediments of Vietnam, with higher amounts in deltaic estuaries but lower amount in mountainous coastline (Cu 1998). Similar values of C_{org} contents were also documented for estuaries in Amazon by Marchand et al. (2004). Studies of Cu (1993 1996 1998) documented also the extensive sulphur accumulation in subsurface layers of some tidal mudflat in North Vietnam. The author claimed that the *reductive conditions and production of sulphurs, H_2S were facilitated with the reduction of SO_4^- from sea water by organic matters from mangroves*. In bottom sediments of shrimp ponds which contain mangrove remains in the Red River estuary, iron pyrite (FeS_2) has been detected and H_2S measured is from 0.03 – 1.23 mg/l.

In coastal muddy sediments, with high amount of sulphur, the formation of pyrite is in favor. According to Goldhaber (2005), pyrite can be formed by direct precipitation from homogenous polysulfide solution or interaction of precursor iron monosulfide with oxidized aqueous sulphur species (e.g. polysulphur), H_2S or simply oxidation of iron monosulfide. The pathway which forms pyrite from oxidation of iron monosulfide appropriates in the upper portion of coastal wetland sediments, where oxidants as O_2 or Mn/Fe oxides are abundant. Environment in deeper portions of wetland profile is more favorable for the formation of pyrite by progressive transformation from precursor iron monosulfide reacts via intermediate unstable species: mackinawite (FeS) and greigite (Fe_3S_4). In the presence of H_2S , the two intermediate species are metastable. Microbial produced H_2S is known as the dominant pathway of diagenetic organosulphur compounds formation. In most environments, authigenic organosulphur compounds are second only to pyrite as product of sulphur diagenesis. In Fe-poor sediments, the formation of organosulphur may be dominant.

Geochemistry of coastal sediment profiles

Reviewing in literatures by Marchand et al. (2004) revealed few investigations on influences of mangroves on pH, Eh values as well as behaviours of pH and Eh along the depth profiles in coastal muddy sediments. Typically were the studies of Clark et al. (1998), Marchand et al. (2004) for depth profiles and Marchand et al. (2004), Larceda et al. (1998) for influences of mangroves on pH, Eh of sediments.

Based on data on pore water geochemistry (salinity, pH, redox potential and solid phase of sulphides) in French Guiana mangrove forest, Marchand et al. (2004) determined that zoning of mangrove species was independent from soil salinity. Beneath *Rhizophora* stands, sediment properties reflect anaerobic and sulphidic conditions close to the sediment surface. In contrast, beneath *Avicennia* stands, sediment geochemistry mostly depends on the stages in forest development, on contents in sedimentary organic matter and on seasonal changes. In the early stage of *Avicennia* settlement, the sediment at the level of radial, pneumatophore-bearing cable roots, displays permanent suboxic conditions with high Eh values reaching 400 mV as an effect of the oxidation produced by the cable root system. The development of mature *Avicennia* stands results in accumulation of sedimentary organic matter and promotes low Eh-values and the reduction of pore-water sulphate. As a result, suboxic processes dominate in the upper, 20-cm-thick layer; organic matter decomposition and sulphur oxidation strongly acidify the sediment. Below 20 cm, the sediment is anaerobic and sulphidic.

Investigation by Marchand (2004) in French Guiana revealed that sediments in young or mature mangrove forests performed pH-values of 6.0 - 7.0 that were stable with depth. Whereas sediments in senescent or dead mangrove forests performed pH-values of 4.0 - 5.0 in surface layer that increased gradually to 6.7 at 40 cm depth and then became stable with depth.

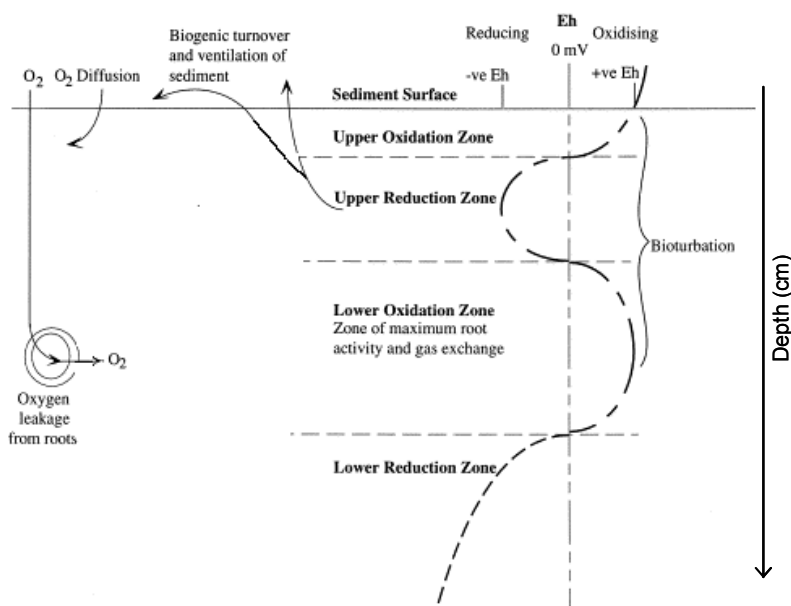


Figure 2.6. Conceptual model of oxygen flux and zoning of oxidation potential in mangrove sediment profile

(Clark 1997)

The tendencies that Eh increased with depth in all profiles can be interpreted considering the redox model described by Clark et al. (1998). According to this research, sediments under *Avicenia*-dominated mangrove forest contain generally four main layers of redox patterns: (1) upper oxidation zone (UOZ) resulted from oxygen diffusion from the surface; (2) upper reduction zone (URZ) (interval of ~5 - 20 cm depth) appeared due to absence of oxygen supply; (3) lower oxidation zone (LOZ) (interval of 20 – 30 cm depth) that received oxygen from flush of root biomass and (4) lower reductive zone (LRZ). Marchand et al. (2006) discussed that the URZ (see the interval of 0 – 25 cm in Figure 2.6) reflects a sulphate reduction zone. The presence of LOZ underlying URZ makes the sedimentary profile different from general soil profile in terms of redox condition, where the surface layer is more oxidized than the deeper parts. This specific feature in the mangrove sediment profile is resulted growth of cable root systems that release oxygen to the reducing ambient sediment and the deficiency of reactive organic matters (Thibodeau & Nickerson 1986; Marchand et al. 2003; Marchand et al. 2004).

In Vietnam, studies on pH and Eh values of coastal sediments concentrated mostly on the average values. According to Cu (1998), surface sediments (0 - 20cm) in low tidal mudflats have pH of 7.8 – 8.0, more alkaline than those in high tidal mudflats (pH = 7.4-7.8). The pH measured in sediments in shrimp ponds are in range of 6.0 – 8.2, decreasing in the later months of shrimp crops (June - September) (Dao 2004). Eh values of surface sediments (0 - 20 cm) are averagely -19 mV in low tidal mudflat and -43 mV in mangrove forest (Cu 1998).

Muddy sediments in coastal wetland are differentiated in redox conditions and highly accumulation of organic matter, clay minerals. Therefore, they can act as a sink or source of heavy metals (Marchand et al. 2006). Clays have high specific surface area and can directly trap heavy metals, but they also may act as a substrate for organic matter flocculation (Keil et al. 1994) that in turn adsorbs metals.

Study by Cu (1998) indicated also high concentrations of heavy metals in coastal tidal mudflats of the Red River, especially in surface layer. However, no connection with clay matters has been addressed. Studies of Nhuan et al. (2003) documented also the accumulation of toxic organic compounds (i.e. OCPs, PCBs), which sourced from detritus.

Variation of chemical elements during the maturing processes is coherent with mineral composition. Progressing weathering and alteration lead to a shift towards an aluminum rich composition that can be approximated by the Chemical Index of Alteration (CIA) of Nesbitt and Young (1984): $CIA = 100 (Al_2O_3 / (Al_2O_3 + CaO^* + Na_2O + K_2O))$ with CaO^* is the silicate bound concentration only. The thermodynamic concept of Lippmann (1979) offers generally conclusions to the main weathering pathways depended from the Si, K and pH-activities (Figure 2.7).

Mineralogy of coastal sediment profiles

Maturing processes of clay minerals have been well studied with focus on soil matters in weathering conditions or sediment matters of deep cores (Srodon 1999). According to review of Srodon (1999), there were *quite few studies on maturing processes of clay minerals in coastal sediments. The most convincing evidence (Srodon 1999), so far, for short-term mineral alteration of coastal sediment* was provided by Righi et al. (1995) who detected *progressive illitization in 350 year old polder of Atlantic coast of France, where the sediments were K-rich and also subjected to alternative drying – wetting circle.*

Because coastal wetlands are known as deposit basin of detritus surface-formed matters (Chamley 1989; Velde 1995), geochemical and mineralogical processes in these environments could have connection with maturing clay matters in the parent soil materials. Also, the alteration processes in weathering condition should be referenced when studying coastal sediments, considering the near-surface positions and short-term maturing period of recent materials (Figure 2.8).

Researches on *coarse fractions* showed that the mineral suites in deltaic estuaries and along the coastline of Vietnam composed of *quartz, feldspars*, lithoclasts and heavy minerals. Jagodziński (2005) determined the composition of detritus minerals in coarse fractions in central coastal shelf of Vietnam including major amounts of quartz, feldspars, micas, amphibole, tourmaline, epidotes, chlorite, and pyroxene, with minor amounts of olivine, silimanite, biotite, zircon, garnets and traces of glauconite, andalusite, kyanite, apatite and rutile.

Fine sediments are composed mainly of clay minerals, which are the most sensitive components to environmental variability. In the coastal sediments near the Red River estuary (Nghì 1988, Bach et al. 1998) and along the central coastlin *smectite and chlorite are determined as* typically for clay mineralogy of sedi (Chamley 1989; Marchand et al. 2004, Par

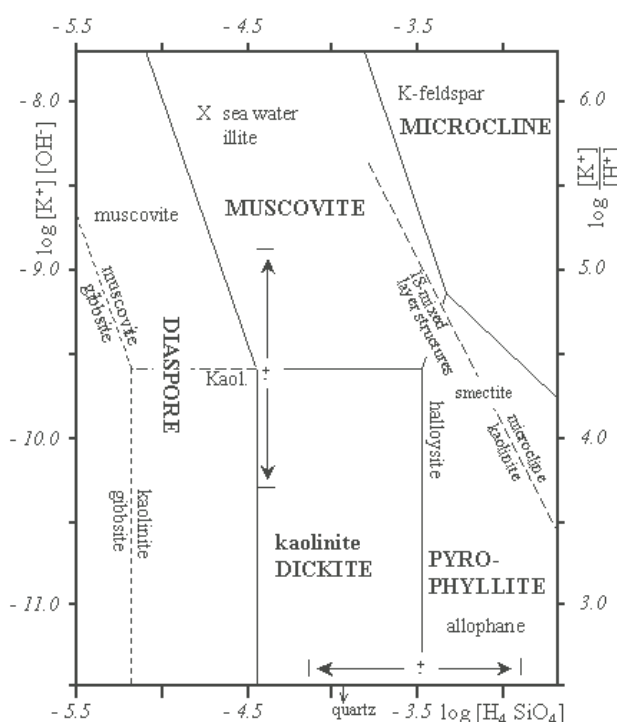


Figure 2.7. Thermodynamic concept by Lippmann (1979) describing main pathways of mineral alteration

(for Al_2O_3 is a constant)

illite-kaolinite-smectite-chlorite assemblage have different proportions and chemical composition depending on the investigated locations (Chamley 1989 and references therein). Some researches suggested that these four *clay minerals may also include their modified products and mixed layer structures* (Jagodźiński 2005) *occurring in parent materials* (Thanh et al. 2000; Tra et al. 2000, Kasbohm et al. 1998) *or as their transformed intermediates* (Velde 1995). There is general correspondence between the composition of estuarine and coastal clay assemblage and mineral composition of suspended matter in rivers (Bach & Phuc 1999; Owen et al. 1974), and of rocks and soils in the hinterland (Chamley 1989).

Due to their surface negative charge, clay minerals tend to be more or less balanced by hydrated ions in river water during the transportation and in sea water during the deposition and diagenesis. *When the clays in fresh water currents come to the saline sea water, particles undergo changes in salinity, pH and hydrochemical conditions. Some surface charge disturbances and even sheet reorganization are therefore expected* (Chamley 1989). However, *behaviours of adaptation as well as alteration of clay during the settlement and profile developing are in controversy interpretations.*

On experiments with clay minerals immersed in sea water in laboratory condition, Carroll & Starkey (1958) and Herbert et al. (2004) determined that *layer reorganisation and some alterations of smectite could happen in only few days on exposure to saline water.*

Most of the studies performed on estuarine clay assemblage consider the transition of clay minerals from fresh water to saline water environments as the first step of diagenetic evolutions (Chamley 1989). *Tendencies how clays adjust in real context of changing from fresh water to saline water environments, however, were mentioned in various controversy viewpoints and different interpretations as following.*

The transformation happening when clays started to deposit in sea-water environments and altered during mature course of coastal wetland profiles may be *degradative or aggradative* (Millot 1970). General geochemical process in surface environment (Figure 2.6) follows the feldspar – alteration series with direction from micaceous clay minerals – illite – vermiculite – smectite – kaolinite (Righi and Meunier 1995). Weaver (1989) has brought evidence for aggradation of soil vermiculites back to more micaceous or illitic nature during the development of wetland profile in marine environment. Potassium fixation of soil vermiculites (Douglas 1989) from sea water should be responsible for this observation.

Some researches stated about *instability of clay minerals in such changing conditions with possible transformations* of from illitic clay minerals towards chloritic (Power 1954, 1957, 1959; Hillier 1993), chloritic and IS-ml towards illitic (Chamley 1964), vermiculitic and chloritic towards illitic (Grim & Loughnan 1962), smectitic towards chloritic and illitic (Grim & Johns 1954; Whitehouse & McCarter 1958) and smectitic to illitic only (Power 1957). *Neoformation of chlorite* is favoured in saline water environment due to tendencies that Mg from sea water moved into the exchange positions in preference to Ca and Na

(Carroll & Starkey 1958). Carroll & Starkey (1958), Roberson (1974) and Dilli & Rao (1982) also stated that *alteration involves interlayer exchange rather than octahedral or tetrahedral substitutions*. However, reveals from X-ray diffraction and K-Ar age dating (Hoffman 1979) showed that only 0.2- 0.3% of K₂O may enter the illite network. Mackenzie & Garrels (1966a) observed *release of silicon from smectite and other clay minerals in their experiments under laboratory conditions, showing crystal instabilities in transformation processes. The dissolved Si increased downcore in slightly buried marine sediments, parallel to higher crystallinity and slightly formation of smectite* (Arrhenius 1963; Gieskes 1983).

However, *illitization of smectite* and illite-smectite mixed layer minerals in sediments is probably the most documented process of *clay diagenesis in the depth of sedimentary basins* (reviewed by Środoń 1999), which involves *with influences of increasing temperature and pressure in buried environment*.

In addition, Jean (1971) has suggested that *clay minerals in estuaries could be also authigenic formed as precipitation from hydroxide gels*. Markin & Aller (1984) and Mackin (1986) found a release of Al and Si out of clay minerals to sea water, parallel to small amount of chlorite precipitated in slightly buried sediments in China Sea and New-England coastline. Nontronite was also observed to precipitate from dissolved Si and Fe in recent sediments from Nares abyssal plain by De Lange & Rispen (1986). *Different viewpoint was stated by Arrhenius (1963), based on his synthesis experiments, that precipitation of aluminium species in marine environment tended to form zeolite rather than phyllosilicates* and clay minerals were generally stable in shallow-buried common sediments. Based on theoretical calculations, Machenzie & Garrels (1966a) stated that in order to maintain steady state conditions in the sea, about 7 % of clay minerals in marine sediments need to be formed authigenically. Berner (1971) recalculated and stated the same tendency but with the number of only 4 %.

However, *some authors mentioned that chlorite and other clay minerals present in the coastal zones are detritus* (Morton 1972; Owen et al. 1974) and that *transformation could happen only in case of sufficient long residence time or until the deposited depth of sufficient P/T influences (~ 100 – 150 m)* (Hoffmann 1979; Larsen & Chilingar 1979 1983; Berner 1980). The interpretations were based on correspondence between the composition of coastal sediment and suspended matters in river, and the lack of chlorite in some in regions (which were described to be favourable for its neoformation).

Notable is that many of the above *controversy interpretations* on origin of clay minerals (neo-formed or detritus sourced) *were mentioned for the same investigated coastal regions*, for example: Grim & Johns (1954) and Morton (1972) in Guadalupe deltaic estuary and San Antonio bay, Power (1954, 1957, 1959) and Owen et al. (1974) in Chesapeake bay).

Agreement of most researches is that clay minerals in coastal sediments are detritus in origin. When they are transported to the sea, clays may be stable in inherited form of parent materials or exchange some cations with sea water and thus experienced partly or completely transformation toward other forms or authigenic precipitated from solution or amorphous gels (Velde 1995). However, if there may happen some transformations, clay mineral modifications appear to occur close to the sediment - sea water interface, in limited variation extent and hardly to come to the end point: end-members (reviewed by Price 1976; Kastner 1981; Chamley 1989 and Srodon 1992). Velde (1995) also emphasized that clays of transformed origin are characterized by an intermediate character.

2.5.3 Expected models of driving forces

Based on characteristics of the coastal sediment profiles as revealed above, expected models of driving forces for geochemical and mineralogical processes can be developed (Figure 2.8). The models were constructed on data of depths and positions of profiles, vertical sedimentation rates, progradating rates, availability of mangroves and root layers. Detail calculations are presented in Table 5.1.

It is to expect the higher maturing of material in lateral direction: LM < MF < SP and also from top to down: upper parts < lower parts. Very high influence of biota can be expected in upper part of mangrove forest profiles and slighter influence is possible in the subsurface part of shrimp pond profiles, inferring to mangrove remains.

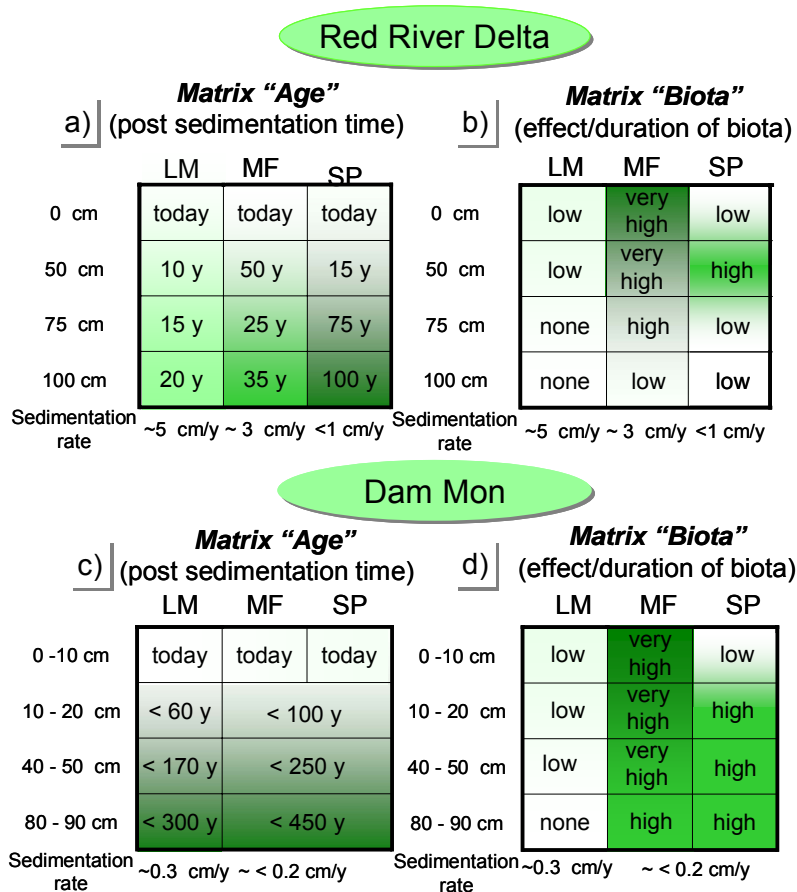


Figure 2.8. Expected models for driving-forces of mineral alteration

(i) duration of diagenesis and (ii) duration of biota activities in sedimentary profiles of investigated sites in Red River Delta (North Vietnam) and Dam Mon (South Central Vietnam).

The highest influence of biota in the 50 cm upper refers to rhizosphere layer in MF profile

3 MATERIALS AND METHODS

3.1 Sampling and Materials

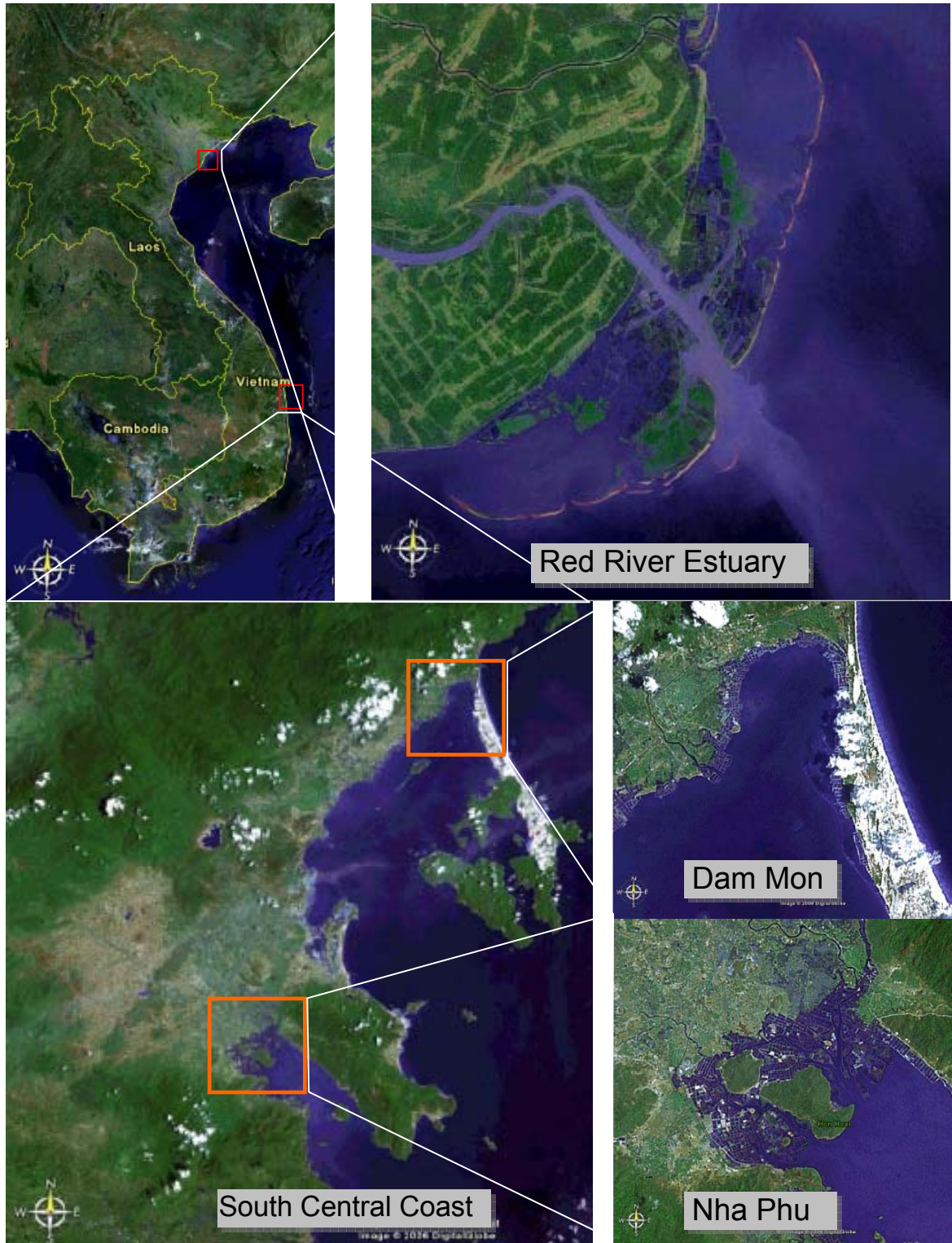


Figure 3.1 Locations of case study areas in Vietnam

Map sources: MDA EarthSat 2006.

3.1.1 Sampling sites in Red River Delta

In order to investigate geochemical and mineralogical characteristics of the sediments in deltaic estuary, one case study was chosen in southern bank of Ba Lat mouth, the main branch at the Red River estuary, belong to Nam Dinh province. Coastal sediments in the estuary were influenced by the huge Red River delta and the long river system as transportation means (Figure 3.1).

The differentiation of muddy sediments in the estuary area of Red River Delta was based on an exhaustive surface sampling made with a hand-drill equipment down to 150 cm depth, across the transect via low tidal mudflats (LM), mangrove forests (MF) and shrimp ponds (SP) (KT-sample, see Figure 3.2). Additionally, nine surface sediment cores had been taken by grab equipment along two creeks, one crossing mangrove area and the other crossing shrimp farming area (BL-sample, see Figure 3.2).

All the collected sediments in the Red River estuary were brown in colour, fairly soft, sticky to hand and could be easily squeezed through the fingers. Following the description by Pons (1965), these materials correspond to practically unripe to haft-ripe degree.

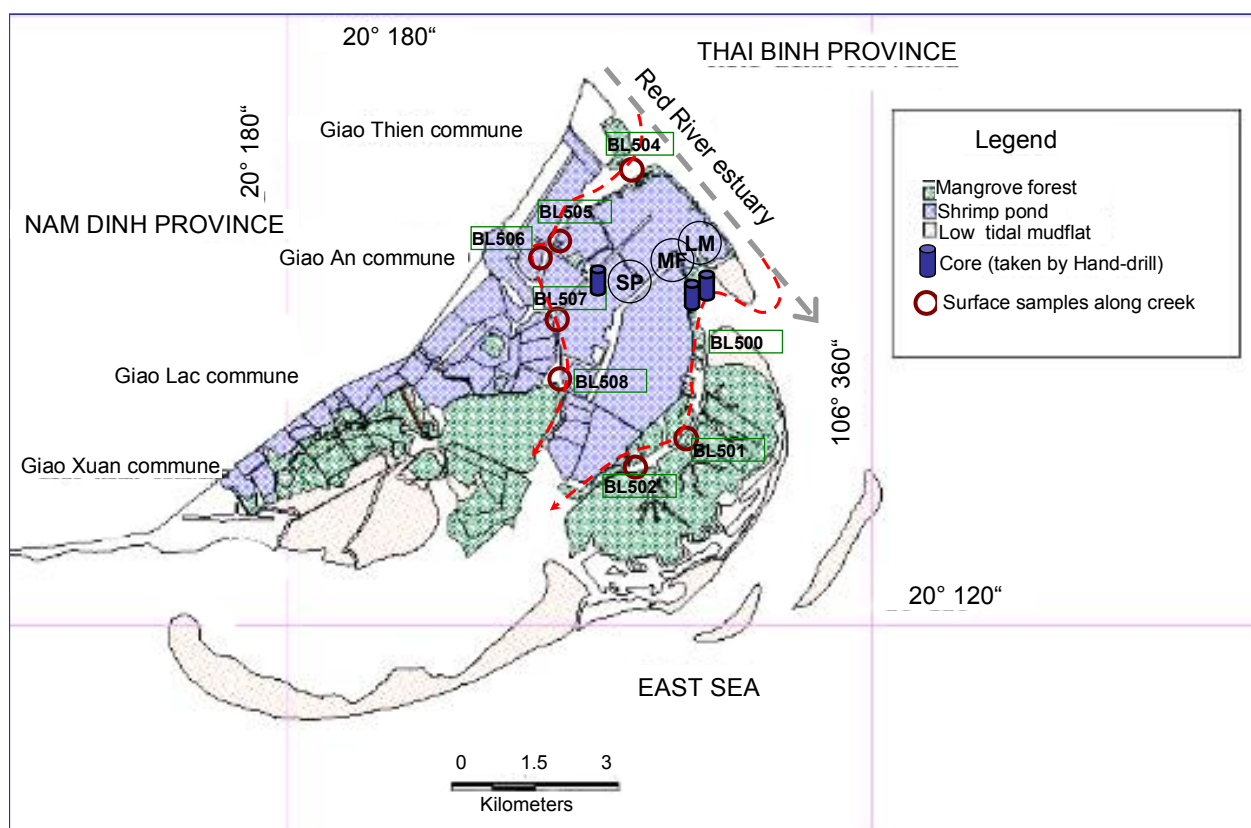


Figure 3.2. The sampling sites in coastal zone of Red River Delta - coring in intertidal mudflat and grabbing surface sediments along tidal creeks

LM = core in Low tidal mudflat, MF = core in Mangrove forest, SP = core in Shrimp pond

Source of map: Dao 2004

The sediment profiles (LM, MF, SP) showed rather homogenous grain size composition and colour along the depth. Sediments in LM profile were characterized by the most practically unripe, especially in 40 – 50 cm surface layer. The deeper part were slightly riper, however displayed the homogenous colour as upper part. Surface layer of MF profile was in chestnut brown colour of 3 – 5cm thick, thinner than that in LM profile. Subsurface horizon to the depth of 50 – 60 cm was recognized as rhizosphere layer with rather high density of roots, leaves, plant fragments with fibre undergoing decomposition. The bottom, where fibrous matters depleted considerably, occurred at a depth of 60 – 140 cm. Bottom horizon and subsurface horizon showed the darker brown colour with higher ripe degree relatively to the thin surface layer. Profile in SP displayed practically ripe, brown sediments in surface layer (0 – 20 cm), the subsurface part contained decomposing roots, haft ripe with dark brown colour.

In addition to data revealed from the collected samples, chemical data from grab alluvia samples in estuary, taken in 2000 by WOTRO project, were used for comparison. The sampling took place during the coastal investigation in Phase 1 of WOTRO project (2000 - 2001). The details on undertaken research activities are presented in WOTRO 2001 report.

3.1.2 Sampling site in Dam Mon

Together with deltaic coastline type (RRD), the coastal mountainous coastline in South Central Coast (Khanh Hoa province) is principal coastline type, constructing the coastal zone along Vietnam. Hand-drill cores of the upper 100 cm sedimentary column had been taken in LM, MF and SP in Nha Phu bay (young mangrove forest area) and in Dam Mon, that belongs to Hon Gom peninsular (old mangrove forest area). These wetland types distributes on muddy field of South Central Coast.



Figure 3.3. Sampling sites in Dam Mon (with old mangrove forest area) and Nha Phu (with young mangrove forest area)
(Vietnamese National geographic directorate, 1998)

In Dam Mon, coastal sediments are under intensive influences of sand-formations covering Hon Gom peninsular. Sands were observed to contain mainly of quartz, feldspar and ilmenite. The sampling locations in LM, MF and SP were influenced mainly by sea and alongshore current but hardly affected of river (Can river) due to far distance (Figure 3.3). During neap tide, the low tide was observed with width of about 100 m, slowly slopping seaward. The sediments in low tidal mudflat core were olive grey in colour, and appeared to be homogenous admixture of fine sand and clay.

The mangrove forest in Dam Mon is century-old, with the oldest mangrove trees aging up to more than 100 years. According to Hong (2000), these mangroves are the oldest ones that remained in Vietnam. Mangroves include 14 species, dominated by *Sonneratia alba*, followed by *Avicennia spp.* and *Rhizophora mucronata*, etc. (Hoa 2001). Since 20th century, area of mangrove forest has been reducing rapidly due to uncontrolled exploitation of wood, bare land for aquaculture and building construction. Nowadays, the area of mangrove forest that is in conservation accounts to 15 ha elongating 2.5 km of the coastline (Hoa 2001).

Sediments in mangrove forest were also olive grey in colour and contained more silty particles than the LM core. Surface layer (0 - 10 cm) was light brownish olive grey in colour and finer in grain size distribution whereas the deeper parts were darker in colour and contain aggregations of decayed matters. During the drilling, strong smell which is typical for sulphide from sediments of upper 1 m was observed. Nearby the mangrove forests are several shrimp ponds.

Shrimp ponds in South Central Coast were mostly farmed on an extensive or advanced extensive basis. Shrimp pond sediments are below water level during the shrimp cultivation season, also in the sampling time. Sediments were sandy, with light brownish olive grey colour and rather homogenous in colour and grain size. With increasing depth, the sediments were slightly finer. When taking the samples, upper 30 cm of the core were disturbed and contaminated by shrimp pond water, therefore, these upper parts from this core material were excluded, but the 10 cm surface sediments were taken separately by grab equipment. Data for the lacking intervals (10 - 30 cm depth) in some calculation was lineal interpolated from data of surface samples (0-10 cm) and deeper part of the core (30 – 40 cm).

3.1.3 Sampling site in Nha Phu

The third sampling region for case study was Nha Phu embayment (Figure 3.3). This region observed is connected with small delta and surrounding coastal mountains. Hydrodynamic setup involved two small mountainous rivers: Cai river and Giang river and alongshore current inside the Nha Phu embayment. Coastal sediments were originated from the rivers and also from weathering products of surrounding mountains. In the last 10 - 20 years, mangrove forest in this area was diverse with 14 true mangrove species, and dominated by *Avicenniaceae* and *Rhizophoraceae*. Mangrove area was gradually replaced by shrimp pond and re-planted

surrounding the ponds. The nowadays mangrove forest is young (< 20 years) and dominated by *Rhizophoraceae*. Sediment samples were also taken across three transects through low tidal mudflats, mangrove forests and shrimp ponds of Nha Phu embayment (Figure 3.3).

In sediment profile of mangrove forests, there is a hard layer of shell fractions at the depth of about 50 cm, which limited the length of core in mangrove forest to only 50 cm. This hard shell layer may corresponded to wave influence of former low tidal mudflat, where hydrodynamic was high, facilitating accumulation of shell fragments in storm. The collected samples showed also coarser materials in the upper 30 cm of low tidal mudflat profile, which was admixture with approximately 5 % of shell fragments in size of few millimetres. Sediments in this layer were sandy silt, greyish brown in colour. Deeper parts (30 – 100 cm) were finer, with grain size composition of silty mud, darker brown in colour and of practically unripe to half ripe degree.

Surface sediments (0-10 cm) in core of mangrove forest profile were light greyish brown in colour, silty and coarser in comparison to deeper parts (10 – 50 cm). The subsurface sediments (10 – 50 cm) had darker grey brown colour, contain massive amount of roots and fibrous matter in decomposition. Slight smell of sulphide was detected. The whole core in mangrove forest profile was practically unripe in mature degree.

The shrimp ponds close to the mangrove forests, were sampled after drowning out of water due to fail of aquaculture cultivation caused by an epidemic. Sediment core in shrimp pond was rather homogenous in brown colour, practically unripe in surface layer (0- 10 cm) and half ripe in lower parts (10 – 100 cm). No organic matter was detected.

Table 3.1. Location and setting of study sites

Core sediments (taken by hand-drill)						
Location	Site	Sample name	Depth (cm)	Latitude	Longitude	Date
RRD, North Vietnam	LM	RRD-LM	0 - 140	20°15.2'N	106°34.3'E	Jul-2001
	MF (young age)	RRD-MF	0 - 75	20°15.2'N	106°34.3'E	Jul-2001
	SP	RRD-SP	0 - 90	20°15.3'N	106°33.3'E	Jul-2001
Dam Mon, South Central Vietnam	LM	DM-LM	0 - 100	12°37.5'N	109°21.2'E	Jul-2004
	MF (century age)	DM-MF	0 - 100	12°45.3'N	109°21.2'E	Jul-2004
	SP	DM-SP	0 - 100	12°43.5'N	109°21.2'E	Jul-2004
Nha Phu, South Central Vietnam	LM	NP-LM	0 - 100	12°25.6'N	109°09.2'E	Jul-2004
	MF (young age)	NP-MF	0 - 60	12°25.7'N	109°09.1'E	Jul-2004
	SP	NP-SP	0 - 100	12°34.7'N	109°35.9'E	Jul-2004
Surface sediments (taken by grab)						
Red River Delta, North Vietnam	Creek passing mangrove area	BL500	0 - 10	20°14.9'N	106°34.5'E	Jul-2004
		BL501	0 - 10	20°13.8'N	106°34.2'E	Jul-2004
		BL502	0 - 10	20°13.5'N	106°33.5'E	Jul-2004
	Creek passing shrimp farm area	BL504	0 - 10	20°16.3'N	106°33.6'E	Jul-2004
		BL505	0 - 10	20°15.7'N	106°32.8'E	Jul-2004
		BL506	0 - 10	20°15.7'N	106°32.8'E	Jul-2004
		BL507	0 - 10	20°15.5'N	106°32.5'E	Jul-2004
		BL508	0 - 10	20°14.4'N	106°32.6'E	Jul-2004

3.2 Methods

3.2.1 Grain size analysis

Sample Analysis

For particle size analyses approximately 1 g of material was dry-sieved with a sieve of 1 mm mesh width. Fine-grained material was analysed using laser diffraction technology after destruction of mineral aggregates in an ultrasonic bath for 3 minutes (Laser Particle Sizer Analysette 22 by Fritsch). With 62 channels of measurement, the device covers a range from 0.18 to 940 μm of particle diameters, giving patterns of Grain Size Distribution (GSD) curves (grain sizes in μm versus % class weight). Grain size measurements have been made on natural samples without removing fine-grained organic matters. This was chosen, because comparison between measurement with and without organic matters for the same samples (removed by low temperature ashing by plasma beam for 2 hours) showed very small differences on GSD patterns (Figure 3.4). The results also indicated rather good reproducibility of measurement.

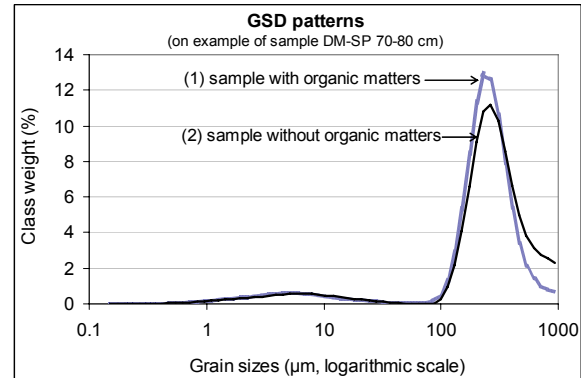


Figure 3.4. GSD patterns of replica measurements for sample with and without organic matters

Only small differences (< 2% of class weight) detected in sandy sizes ($\sim 100 - 1000 \mu\text{m}$) reflected rather good reproducibility.

Computation and Visualisation

In order to use international accepted units of particle sizes cited in mineralogical data, data of grain sizes were displayed in μm (not in phi-scale as suggested by Folk & Walk, (1957)). The Grain Size Distribution (GSD) patterns and Sediment Trend Analysis (STA) used the log of grain size instead of the absolute size. In the studied purposes, the log-distribution appears to work well, possibly because it highlights various important features of naturally occurring sediments like polymodal grain size distribution, variation in moments of sediment during transport process, etc. On the other hand, the log-distribution deemphasizes other features like noises of grain size distribution which were caused by temporal fluctuation, sampling errors, analytic noise, etc. (McLaren and Bowles 1985).

Percentage composition of grain size fractions ($< 2 \mu\text{m}$, $2 - 6.3 \mu\text{m}$, $6.3 - 20 \mu\text{m}$, $20 - 63 \mu\text{m}$, $63 - 200 \mu\text{m}$, $200 - 630 \mu\text{m}$ and $> 630 \mu\text{m}$) were calculated based on cumulative GSD curves. Statistical granulometric parameters (mean, sorting, skewness and kurtosis) were calculated using the graphic formula documented by Folk & Ward (1957). Grain size compositions and granulometric parameters were visualized according to depth profiles.

In order to maintain the whole original information of Grain Size Distribution (GSD) patterns, GSD maps were developed from orthographic projection of grain size distribution curve on the plane between depth axis and grain size axes (Figure 3.5) (Beierle et al. 2002) and were used to reveal sedimentary faces distribution in the investigated sediment profiles.

A Principal Component Analysis (PCA) and factorial multivariate analysis (see Chapter 3.2.5) from the granulometric parameters and composition of grain size fractions were carried out, using the MATLAB and SPSS statistical software packages to reveal correlation among the variables. The PCA method was additionally applied for GSD curves of each sediment profiles using non-negative normalisation approach to reveal principal modal of sedimentations.

Polymodal character was further investigated with deconvolution method using multi-gauss-log (x) as fitting function. The procedures were carried out on ORIGIN 7.1 and WINFIT 2.6 program.

An End-Member Modeling Algorithm (EMMA) (see Chapter 3.2.5) was conducted to support reveals from polymodal analysis of GSD patterns and to estimate contribution of modes in each investigated sub-environment.

And finally, a classification of the GSDs was based on properties and composition of the deconvoluted and computed EMMA modes characterising different environments numerically.

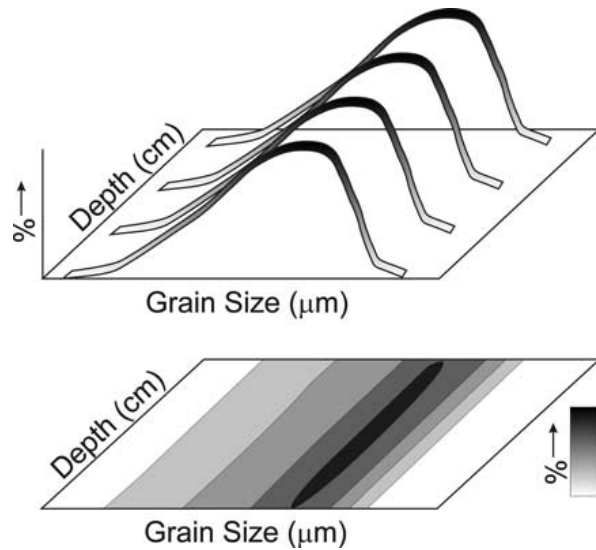


Figure 3.5. Visualisation of GSD patterns by GSD maps

According to Beierle et al. 2002.

3.2.2 Chemical analysis

pH and Eh

pH and Eh values of sediment samples were measured by pH96 Microprocessor pH-Meter, WTW in field work. For each measurement, about 20 m g of fresh samples were diluted by distil water to 20 ml and homogenously stirred. The redox electrode was periodically checked using a 0.43 V standard solution and demineralised water. Electrodes were inserted for several minutes in the muddy sample until stable values were reached, then were thoroughly washed. Redox data were reported for the balance state (Figure 3.6), relative to a standard hydrogen electrode. Error of < 10% for both pH and Eh values was determined based on repeat measurements of three samples.

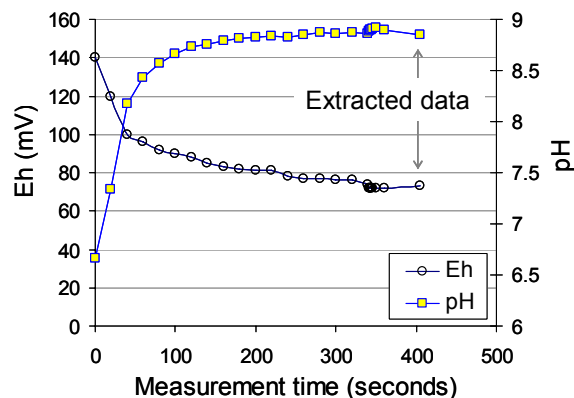


Figure 3.6 Data of pH/Eh were extracted when stable values of balance states were reached

On example of sample DM-LM (0-10 cm)

XRF

The analytical technique X-Ray Fluorescence (XRF) has been carried out for all the collected sediment samples to determine concentrations of major elements SiO_2 , TiO_2 , Al_2O_3 , Fe_2O_3 , MnO , MgO , CaO , Na_2O , K_2O , P_2O_5 , adsorbed H_2O , LOI (loss of ignition) and minor elements (Ba, Ce, Co, Cr, Cs, Cu, Ga, Hf, La, Nb, Ni, Pb, Rb, Sc, Sn, Sr, Th, V, Y, Zn and Zr). Bulk samples and grain size fractions were freezing dried, homogenously milled to < 63 μm powder, accurately weighted to 0.800 gram. Loss of weight after routinely heating to 150° C and 1050° C allowed determination of adsorbed H_2O amount and LOI, respectively. The remained sample after ignition were prepared in a flux mixture with 2.000 mg of lithium tetraborate ($\text{Li}_2\text{B}_4\text{O}_7$) (melting point 920° C) and 1.932 mg of lithium metaborate (LiBO_2) (melting point 845° C) were anhydrous dense molten fluxed in platin cup on flame of 1000 – 1200° C to assure homogeneity. Each sample was prepared for Plasma Quad analysis by adding about 0.02 gram Indium (I_2O_5). These extracted samples were then analyzed for major silica elements, metal concentrations and REE, based on a Philips PW 2404 X-ray spectrometer with current of 10 mA and voltage of 20 kV.

The accuracy and precision of the result were verified by analysis of certified reference materials *Miramichi River Estuary Sediment* (MESS-1), *Baie des Chalerus Marine sediment* (BCSS-1), (NRC 1990) from the National Research Council, Canada. The reproducibility of the method was tested by replicate analyses of one example of real

samples in estuary of the Red River, Northern Vietnam (RRD) and in coastline of South Central Coast, central Vietnam (KH).

The certified values of these standard reference materials, as well as results obtained from measurement on our XRF equipments are presented in the Table 8.1 (Appendix). Results agree with certified values, showing relative error between 0 – 20 % for almost all elements, and good precision (relative deviations < 12 %). Results obtained for Co (DL = 5), Ni (DL = 5) and La (DL = 20) in case of low concentration are unreliable due to high values for detection limits.

To distinguish influences between syn- and post-sedimentary processes, hydrodynamic governing or chemical/mineralogical modification, natural and anthropogenic driving factors on behaviour of minor elements, sediment enrichment factors were tested parallel to concentrative assessment. Traditionally, enrichment of elements was to consider with background values, granulometry variation and their commonly conservative hosts (Hirst 1962; Kemp 1976; Padmalal et al. 1997; Wassermann 2001). Enrichment factor can be determined based on normalizing element concentration to background values, percentages of grain size fractions, or a recognized conservative element (Al, Mn). For the diversity in factors those governing behaviours of major and minor elements in coastal sedimentary environments (Padmalal et al. 1997), well correlation between elemental distributions with any conservative factor can be indicative for a driving force.

In this study, ratios of minor elements ratios against hydrodynamic factors (EMMA results from grain size data) were used to reveal to role of the corresponding syn-sedimentary processes on elemental distribution. Enrichment of chemical elements to the world near-shore mud (Wedepohl 1960) was used for comparison and estimation of material maturity. Enrichment to Al was used to determine variation with total clay content (Hirst 1962) and to Mn to determine partly variation with oxides/ hydroxides of Mn host (Larceda et al. 1988b). Ratios of elements versus C_{organic} were used to address correlation and possibility of hosting by organic matter (Larceda et al. 1988b), the conservative element is also possible chosen as C_{organic} . A non-conservative behaviour may exist because of water-sediment interactions or as a result of anthropogenic impacts.

3.2.3 Nutrients

Concentrations of the nutrient carbon and sulphur were simultaneously fractional analyzed based on CS-500 CS analyser which featured a high temperature resistance furnace upto 1550°C (230 V AC+ 10% 50/60 Hz, 0.33A/75 W). Before measurement of sample, calibration has been conducted based on 4 times measuring of standard agents: EDTA and coal. The freezing dried sample was exactly weighted by 200 mg into a ceramic combustion boat on an electronic balance which was interfaced to the CS-500. The ceramic

boat with the sample was placed on the furnace platform and the thermal analysis cycle begins. At the end of the cycle, the analysis results and thermal patterns were extracted from the built-in display and external PC. Concentration of free carbon and sulphur were determined for the phase in lower temperature range and carbides and sulphide were determined by the phase of several seconds later in the thermal patterns. Accuracy was 0.002 % for carbon and 0.0004 % for sulphur.

3.2.4 Mineralogical analysis

XRD

In laboratory, X-ray diffraction (XRD) was the primary method used to determine mineral composition and to characterize clay minerals of the sediment samples. XRD investigations were carried out in terms of single phase minerals, coherent scattering domain size, expandable properties as well as responses to thermal treatment. For identification, XRD patterns of bulk sample and grain size fractions were tested by Rietveld refinement approach based on Autoquan 2.6.1.

Samples were prepared as randomly oriented powder of bulk and grain size fractions and as oriented mount specimens of fractions $< 2 \mu\text{m}$. The bulk samples were milled and sieved to particle size of smaller than $63 \mu\text{m}$ before measurements. For comparison in effect of grinding on XRD patterns and for quantification by Rietveld refinement, some samples have been milled to smaller than $32 \mu\text{m}$.

For XRD measurements of randomly oriented powder specimens, a SIEMENS D5000 diffractometer equipped with a Cu tube, $\text{K}\alpha_{1,2}$ radiation (operated at 40 kV, 30 mA; variable slits: 20 mm, soller: 0.5/25, step and time: $0.02^\circ 2\theta$ for 3s) (0) and secondary curved graphite monochromator was adopted. The data, obtained for the range from 4 to $68^\circ 2\theta$, reflect all hkl-spacing diffractions of the measured material. Based on search-match system with reference from JCPDS database (1978, 1979) and indicative peaks

Table 3.2. Equipment and technical parameters of XRD measurements

<i>Equipment</i>	<i>Siemens D5000 X-ray diffractometer</i>	<i>Praezitronic Freiberg HZG 4 / Seifert C3000</i>
X-ray tube	<i>CuKα</i>	<i>CoKα</i>
Wavelength	1.54 Å	1.79 Å
Voltage	40 kV	30 kV
Current	30 mA	30 mA
Step	$0.02^\circ 2\theta/3\text{s}$	$0.03^\circ 2\theta/2\text{s}$
2 Soller-slits	0.5/25	0.5/25
Divergence-slit	20 mm	1.09 mm
Scatter-slit	2.0 mm	6.0 mm
Detector-slit	0.06 mm	0.35 mm
Counter	Scintillation counter	Proportional Counter
Other	Graphite secondary-monochromator	Fe-filter

documented by Moore & Reynolds (1997), clay minerals and other clay-size crystals were identified.

XRD patterns were obtained also by oriented specimens after air-drying (AD), ethylene-glycol-saturation (EG) and heating (550°C for 4 hours) procedures. For these investigations, a Freiberg Praezitronic HZG 4A-2 diffractometer equipped with a Co tube, $K\alpha_{1,2}$ -radiation (operated at 30 kV, 30 mA) was used. The goniometer was linked with a Seifert C3000 controlling unit with fixed slits (1.09 mm/ 6.0 mm) with detector slit of 0.35 mm and soller at 0.5/25 (Table 3.2). The XRD diagrams were recorded using a counting time of 2 seconds per step of $0.02^\circ 2\theta$ from $4^\circ 2\theta$ to $34^\circ 2\theta$, displayed all reflection of 00l spacing for the investigated clay particles.

Commonly, ethylene glycol (EG) is used to stabilize a swelling state under room humidity. The 17 Å peak of basal spacing was used as reference state for swelling clays in the laboratory mineralogical determination (Moore & Reynolds 1997). Based on response of 00l-spacing with EG saturation and thermal behaviour of the clay (Starkey et al. 1984), the minerals were identified and characterized, supportively for the phase identification in the powder XRD patterns.

In the XRD patterns of randomly oriented powder, the (060) reflection allow distinction between dioctahedral and trioctahedral type because the b cell dimension is sensitive to the size of the cations and to site occupancy in the octahedral sheet and is unaffected by the monoclinic angle β . Dioctahedral clay minerals are common in soils and surface sediments and have d(060) XRD peak near 1.50 Å, whereas trioctahedral clay minerals have d(060) peak closer to 1.54 Å (Borchardt 1989). The d(060) near 1.52 Å is indication for saponite or nontronite. More detail was described by Moore & Reynolds (1997) and references therein.

XRD patterns were decomposed into symmetric elementary Gaussian curves using Winfit program to consider also coinciding peaks (Krumm 1994). Reveals from the refined profiles included peak positions, d-values, intensity, FWHM and area. Furthermore, Fourier transformation implement (Winfit) was adopted for the determination and characterization of coherent scattering domain size (CSD).

TEM – EDX

The preparation of suspensions was standardized as follows: First, the fraction $< 2 \mu\text{m}$ was extracted from clay sample by sedimentation method, subsequently, 1mg of this fraction was diluted in distilled water (5 times for illitic sample and progressively upto 10 times for smectitic sample) and placed for 15 min in an ultrasonic bath for dispersion, then dropped on carbon-coated Cu-grids by air drying. In cases of sea water-contaminated sediment samples, dialysis treatment was adopted using QuixSep 2 ml dialysers for bulk sample to

remove adsorbed salt before the extraction of $< 2 \mu\text{m}$ fraction. Fe-removal by Na-dithionite treatment (Mehra et al. 1960) was also adopted for Fe-contaminated samples.

To observe morphology and measure chemical composition of individual particles in specimens of the $< 2 \mu\text{m}$ fraction, the transmission electronic microscope JEOL JEM1210 (LaB6-cathode at 120 kV) equipped with an Energy Dispersive X-ray (EDX) spectrometer (OXFORD-LINK) was used. Individual particles were identified and characterized based on morphological description (Henning & Stoerr 1986) and mineral formula calculated from EDX point analysis (according to Koester 1977). Besides, the electron diffraction allows an evaluation of the stack order. Ring-like structures of the electron spots indicate for clay minerals a turbostratical order of the layers. Based upon the comparison of the intensities of (020)- and (110)- interferences in a convergent beam-system, Zoller (1993) has demonstrated the possibility to distinguish between a 2M- or 1M-order for 2:1 sheet silicates:

2M-polytype: $|110|/|020| > 1$

1M-polytype: $|110|/|020| < 1$

In order to evaluate the mineral formula of the individual particles the photons of each analyzed particle were detected for 20 sec. The excited XRF-area of each particle is less than 100 nm in a diameter. The EDX-measurements were carried out standardless and by using of k-factors following the procedures of Cliff and Lorimer (1975).

The procedure of Köster (1997) for the conversion the EDX-analyse to a mineral formula was adopted. The measured data-set have been evaluated in relation to the total charge.

For each sample, about 200 particles of various morphologies have been identified based on calculation of mineral formula to ensure representation by appearance frequency. These analyses were made in the laboratories of E-M-A-University of Greifswald.

Identification of clay minerals

In the investigated samples, the following specific clay minerals were involved: chlorite, kaolinite, illite, dioctahedral vermiculite, smectites, and various mixed layer series. Mineral composition of bulk sample was identified by diagnostic reflections in XRD patterns of powder randomly oriented mount specimen. Clay matters in fractions $< 2 \mu\text{m}$ were determined and characterized based on 00l reflections in XRD patterns of oriented mount specimens. Deconvolution of overlapping peaks was based on Winfit 2.6.1. Example illustrations were given in the Figure 3.7 and Figure 3.8 for XRD patterns of powder specimen and oriented mount specimen, respectively. Morphology, polytype and chemical formulae of particles in fractions $< 2 \mu\text{m}$ which were further investigated by TEM-EDX, were used for confirmation of the identified phases and characterization.

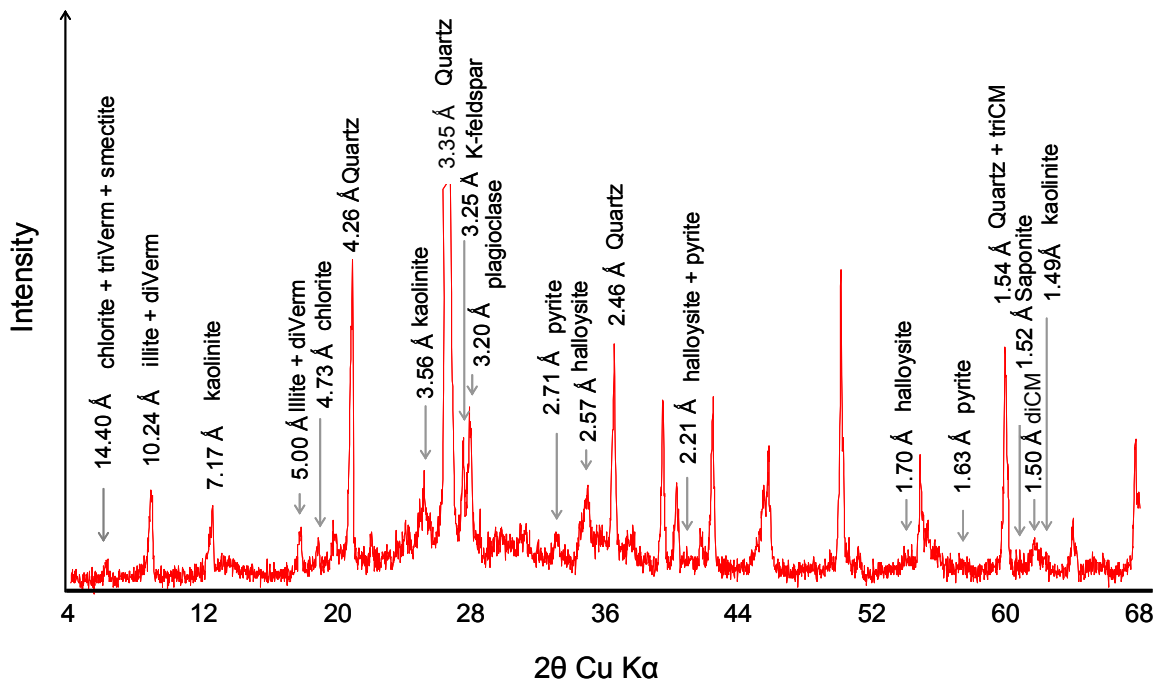


Figure 3.7. XRD pattern of powder, randomly oriented mount specimen

Example of sample RRD-MF, 71 – 73 cm depth; d-values (in Å) are placed on top of the depicted peaks

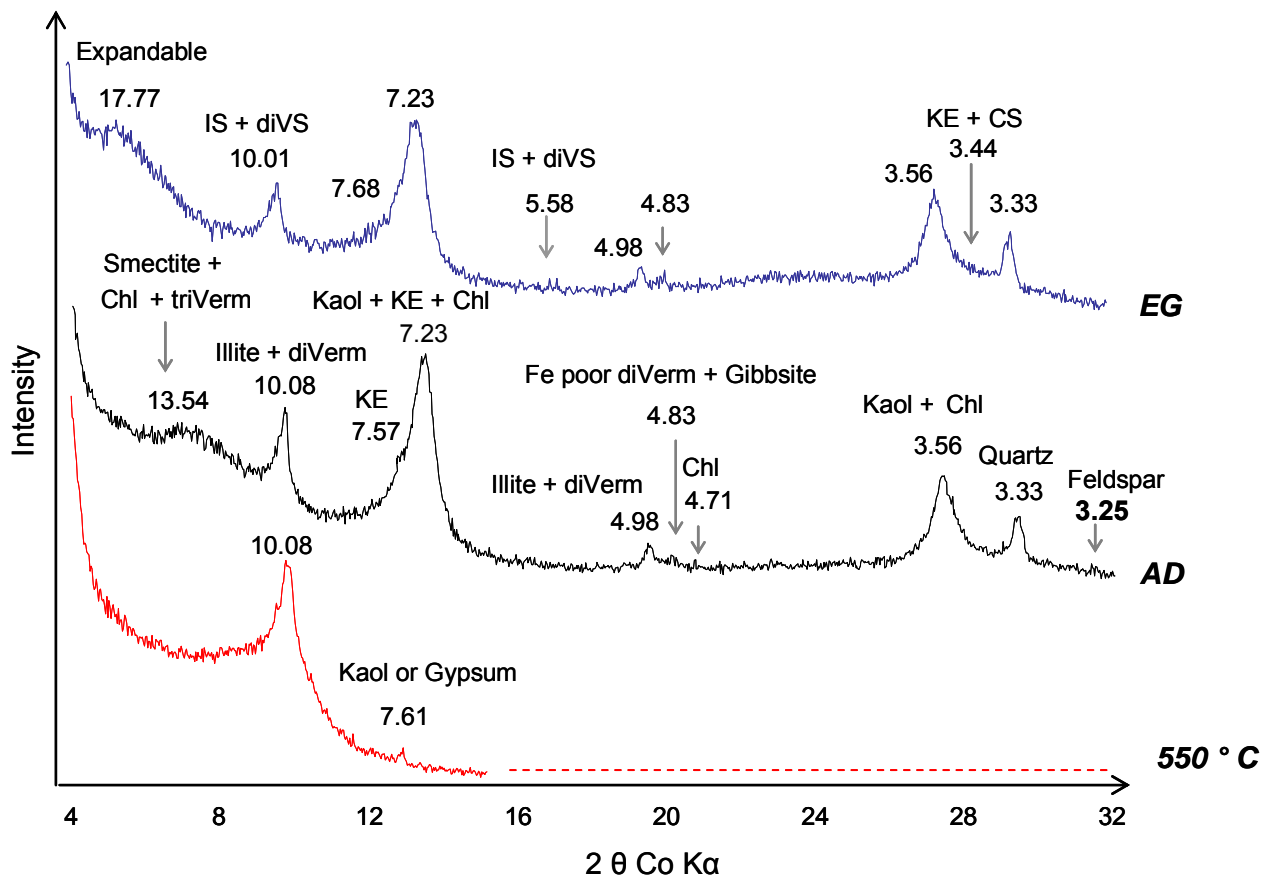


Figure 3.8. Example on an XRD pattern for oriented mount specimen

Example of sample: NP-MF, 0-10 cm; d-values (in Å) were placed on top of the depicted peaks

The identification of micaceous clay species is based on the mica nomenclature worked out by Rieder et al. (1998). Simulation of theoretical variability of mineral formula for individual clay minerals in the calculation model was based on literatures (e.g. Newman 1980; Srodon et al. 1992) with the key parameters: layer charges, interlayer fixed cations (i.e. K), octahedral occupations and content of Si in tetrahedral layer.

Kaolin minerals (*Kaolinite and halloysite*)

Kaolinite and 7 Å dehydrated halloysite have single-layer structures and the same chemical formula ($\text{Al}_4\text{SiO}_{10}(\text{OH})_8$). They are recognized by the 001-reflection near 7 Å.

In bulk powder samples, reflections of kaolinite were determined, however occasionally in very low intensity due to predominance by sharp, intensive peaks of quartz (Figure 3.7). In these cases, detection of (060) reflection surrounding 1.490 Å (Figure 3.11) was additionally diagnostic signal of kaolinite. Reflections near the diagnostic peaks at 2.57 Å, 1.69 Å and 2.22 Å (Figure 3.7) implied that halloysite was included in the kaolin phases (Bailey, 1980). In XRD patterns of < 2µm fractions (oriented mount specimen), reflections of 7.2- Å 001-spacing and 3.57 Å 002-spacing peaks characterized kaolinite. The 7.4 Å 001-spacing and 3.63 Å 002-spacing peaks is more typically for halloysite due to small amount of hydrated cations absorbed in interlayer (Bailey 1989) which formerly full hydrated moist condition of wetland and latterly slightly dehydrated by air dried preparation (Figure 3.16a). Diffractions of kaolinite keep unchanged under ethylene glycolation solvation but kaolinite is destroyed after heating to 550°C (Figure 3.8).

The 7 Å peak with asymmetric manner, which decrease in intensity after EG treatment suggested overlapping admixture with reflections of other minerals. Deconvolution of the asymmetric 7 Å peak (Figure 3.9) allowed distinguishing well ordered kaolinite (7.1 – 7.2 Å) which remained unchanged in intensity and FWHM under treatment by EG from other minerals such as kaolinite expandable (KE-ml) (7.59 Å), halloysite (7.31 Å), chlorite (7.09 Å).

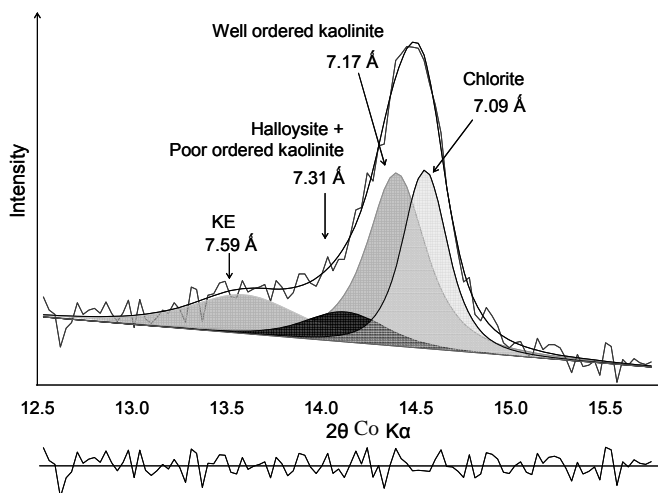


Figure 3.9. Deconvolution of the 7 Å

Example of XRD pattern (powder specimen of sample RRD-SP (0 – 3 cm)

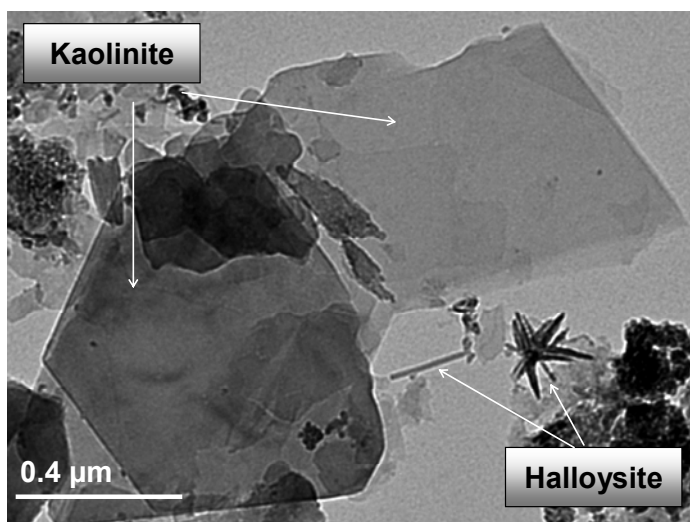


Figure 3.10. TEM micrographs of kaolinite and halloysite

Notes: Measured using Jeol JEM 1210 1210 linked with ISIS LINK-OXFORD EDX-system and a GATAN MULTISCAN camera.

Samples: RRD-MF (80-90 cm)

Poor ordered kaolinite referred to the reflection surrounding 7.3 \AA and might be confused by slightly dehydrated halloysite or KE-ml reflections.

Under TEM observations of fraction $< 2 \text{ }\mu\text{m}$, kaolinite particles were diagnosed as platy crystals with pseudo-hexagonal borders (Figure 3.10). Beside occurrence of particles in large sizes ($1 - 2 \text{ }\mu\text{m}$) which characterized detritus euhedral origin, exhibition of fine particles ($< 0.5 \text{ }\mu\text{m}$) posed to a sedimentary anhedral origin (Henning & Stoerr 1986). In few cases, kaolinite occurred in slat shapes with pseudo-hexagonal contours. Halloysite particles were identified with tubular shapes (Figure 3.10), commonly with the length smaller than a half of micrometer.

TEM-EDX analysis determined the similar formulae for kaolinite and halloysite, with commonly detected Fe in octahedral occupations. The Fe-bearing kaolinite was also mentioned by Schroeder and Pruett (1996).

Chlorite

In bulk samples, chlorite was indicated by (001) reflection surrounding 14.2 \AA (Figure 3.7) and the (060) reflection near $1.544 - 1.549 \text{ \AA}$ of trioctahedral polytype (Moore & Reynolds 1997) (Figure 3.11). This 060 peak was obvious when deconvoluting the 1.54 \AA peak from interference with (121) reflection of quartz. The 1.545 \AA sharp peak with $\text{FWHM} = 0.25$ was typically for quartz and the 1.546 \AA referred to chlorite.

In oriented mount patterns, presence of chlorite was noticed by the peaks surrounding 14.2 \AA , remained (in 2θ positions) after ethylene glycolation or 550° heating, and peaks near 4.71 and 3.53 \AA (Figure 3.8). The (002) reflection of chlorite, because of interference by presence of kaolinite in sample, could be determined by $7.02 - 7.09$ peaks in the deconvoluted patterns (Figure 3.9). Weakening of the 001, 003 and 005 reflections relatively to the 002 and 004 reflections inferred that chlorite contain high amount of Fe (Brown and Brindley 1980).

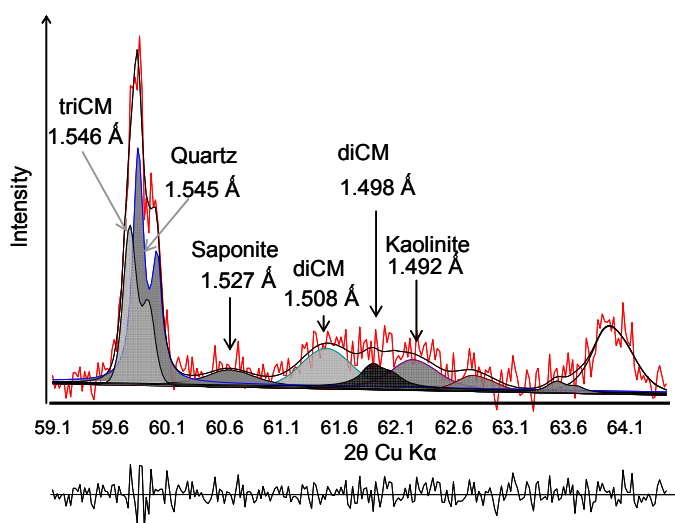


Figure 3.11. Deconvolution of (060) reflections

*Example of XRD pattern for powder specimen, sample NP-MF (0 – 10 cm)
diCM = dioctahedral clay minerals*

Decrease in intensity of 14.2 Å after glycolation and 550° C heated (Figure 3.8) suggested an overlap by other expandable phases like vermiculite, smectite or mixed layer structures which have also reflections near 14 Å in air-dried condition.

In transmission electron micrographs (Figure 3.12a), chlorites were depicted as large xenomorphic platelets (~ 1 µm), aggregates and parallel intergrowths of these platelets. There were only few cases that chlorite particles exhibited medium sizes, as broken fragment of the large ones or aggregation of highly exfoliating stacks. Ragged edges were commonly observed.

All the detected chlorite particles were determined as Fe-rich chlorite species. In chemical formula, the number of cations in octahedral layer ranged from 4.95 (dioctahedral species - donbassite-like) to 6.05 (trioctahedral Mg-rich species - clinochlore or Fe-rich species: chamosite). The value of tetrahedral Si is from 2.3 to 3.0. The empirical formula as average values was:



Illite

Illite is defined as a series name for dioctahedral interlayer deficient micas, according to IMA report on the nomenclature of micas (Rieder et al. 1998). Illite term in this sense is, in many cases, comparable to the cited mica or hydromica terms in literatures which referred to the diagnostic XRD peaks near 10 Å, 5 Å. In stricto sensu, in this report illite term is handled as a real end-member mineral of the illite – smectite mixed layer series according to Srodon et al. (1992), instead of as a group name. This mineral has two tetrahedral and one octahedral layer with an interlayer ion population (potassium) holding the layers firmly together give a near 10 Å unit layer, which produced peaks near 10 Å.

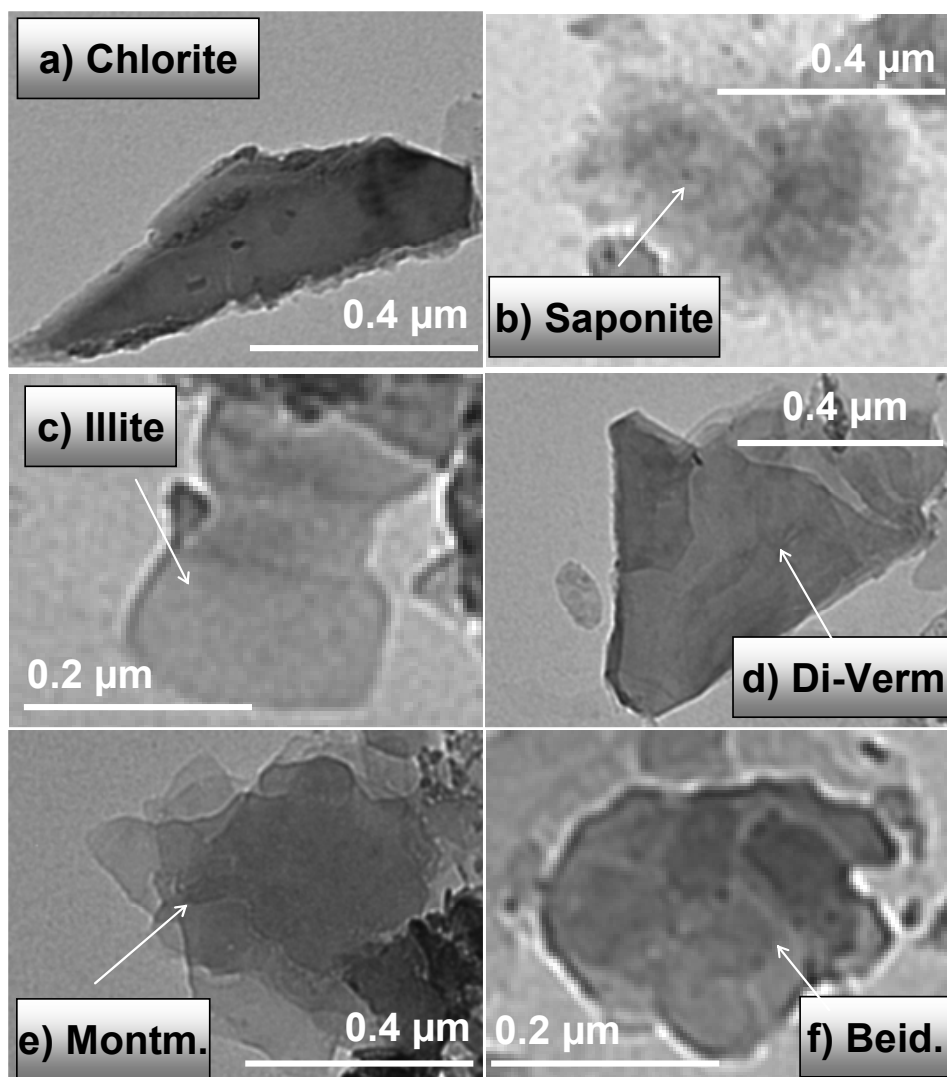


Figure 3.12. TEM micrographs of Chlorite, Saponite, Illite, dioctahedral Vermiculite, Montmorillonite and Beidellite

Notes: Measured using Jeol JEM 1210 1210 linked with ISIS LINK-OXFORD EDX-system and a GATAN MULTISCAN camera.

Samples: a + d: RRD-LMs; b: DM-MF (80-90 cm), c+e: RRD-MF(80-90), f: RRD-MF (0-3 cm)

In XRD patterns, the phase of illite (in stricto sensu, used throughout the dissertation) was detected based on the peaks near 10 Å and 5 Å (Figure 3.7, Figure 3.8). These peaks, when displayed asymmetric manner, might include not only illite but also IS-ml, dioctahedral vermiculite, diVS-ml – the structures with slightly higher basal spacing (Figure 3.14). Dioctahedral structures of these clay minerals corresponded to 060 reflections at 1.50 Å (Figure 3.11). Illite, however, can be distinguished by its substantially nonexpanding-lattice characteristic: unchanged intensity after EG treatment.

Illite phases were recognized not only in polytype 2M₁ (with peaks near 3.74 Å, 3.47 Å comparably to the diagnostic reflections of 2M₁ at 3.72 Å, 3.49 Å, respectively) but also in 1M (with peaks near 3.65 Å, 3.10 Å comparably to the diagnostic reflections at 3.66 Å, 3.07 Å, respectively) (Bailey 1980) in oriented mount patterns (Figure 3.13).

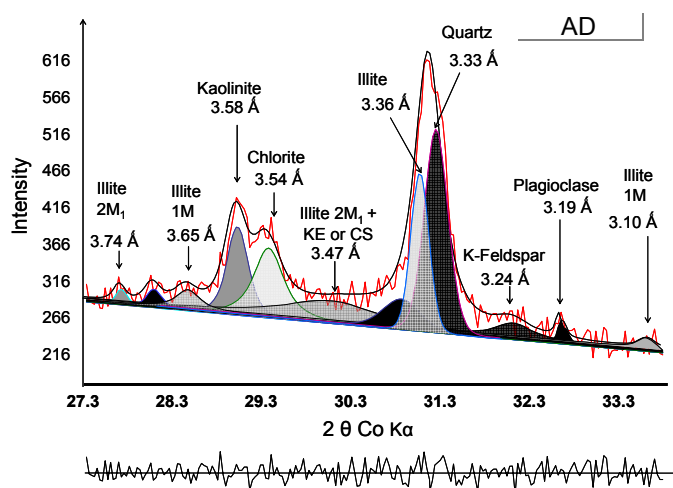
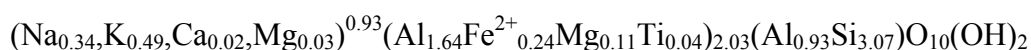


Figure 3.13. Deconvolution of 2θ range (Co beam) from 27.3 - 33.3

Chlorite was noticed with 3.54 Å peak; Illite with 3.36 Å peak; Illite 2M1 with 3.74 Å and 3.47 Å and illite 1 M with 3.65 Å and 3.10 Å. Example of XRD pattern for oriented mount, EG specimen, sample RRD-MF (53 – 56 cm depth).

Pure illite particles (100% illitic percentage) were detected in traces by TEM. Illite particles occurred in xenomorphic platelets and aggregates of platelets and rarely in slat-shaped morphology (Figure 3.12c). These particles exhibited platy xenomorphic platelets in small sizes (0.2 - 0.3 μm). Some other particles had been detected with ragged edges and rough surface. A recognition and evaluation of illite based solely on morphological data are difficult, because of no clear-cut differentiation between illite and IS-mixed layer structures and association of several other clay minerals possibly also in xenomorphic shape, specifically in case of admixture.

Chemically, illite (in stricto sensu) is referred as end-member in I/S series which has interlayer charge up to 0.9 per $O_{10}(OH)_2$ as revealed from analyses on different techniques (Meunier and Velde 1989; Lanson and Champion 1991; Srodon et al. 1992). For determination based on EDX-data, illite was named for particles with interlayer charge ranging between 0.85 and 1.0, tetrahedral Si between 2.8 and 3.22, number of octahedral cations between 1.9 and 2.0, and interlayer K is higher than Na. The idealized mineral formula is: $FIX_{0.89}Al_{1.85}Fe_{0.05}Mg_{0.10}[(OH)_2Si_{3.2}Al_{0.8}O_{10}]$ (Srodon et al. 1992) and the average empirical formula of illite in the investigated samples was:



Vermiculite

Whereas, trioctahedral vermiculite may form by the weathering of biotite or hydrothermal alteration, dioctahedral vermiculite is proposed a result of muscovite degradation and its alteration via illite. The structure of dioctahedral vermiculite is not as well understood due to it is too small for single-crystal x-ray examination as well as due to its tendency of forming mixture with other minerals (Douglas 1989). Its structure and composition thus were assumed extrapolatedly based on its similarity to its precursor minerals: illite or muscovite (Douglas 1989, Moore & Reynolds 1997).

Trioctahedral Vermiculite

Presence of trioctahedral vermiculite in the investigated sediments were suggested by a reflection surrounding 14.2 Å that was commonly observed in XRD patterns of air-dried, oriented mount specimens (Figure 3.8) along with low intensity reflections at 4.76 Å, 2.52 Å in XRD patterns of powder specimens (Figure 3.7). In case of sample containing chlorite and smectite, identification of trioctahedral vermiculite based on 14.2 Å in XRD patterns might be confused (Douglas 1989). It needed further confirmation based on morphology and chemical formulae of single particle.

In soils, trioctahedral vermiculite occurred commonly as rather large platy xenomorphic crystals or lath shaped particles and rarely in sizes $< 2 \mu\text{m}$ (Douglas 1989). TEM investigations revealed the presence only in trace of trioctahedral vermiculite in fraction $< 2 \mu\text{m}$ of some samples in Red River Delta and Nha Phu, which shaped in xenomorphic platelet. The observed irregular edges as well as moiré patterns of these platelets were typically for weathering imprints (Henning & Stoerr 1986).

Diocetahedral Vermiculite

Diocetahedral vermiculite, in according to international mica classification (IMA 1998) defined as a K-deficient illite species, was expected to have similar behaviour to illite (in stricto sensu) in XRD patterns with reflections surrounding 10 Å. Because interlayer structures of diocetahedral vermiculite contained some hydrated cations which substituted for potassium, d-spacing value of this mineral were slightly higher than non-expanding illite in air-dried condition. After ethylene glycolation (EG), diocetahedral vermiculite, those having interlayer charge < 0.72 , could expand slightly to 14 - 16 Å (Moore & Reynolds 1997). Thus, an asymmetric manner of 10 Å toward lower 2θ angle in air dried patterns which became symmetric in EG patterns of XRD, oriented mount specimens (Figure 3.8) should be noticed as indication for diocetahedral vermiculite in the investigated sediments.

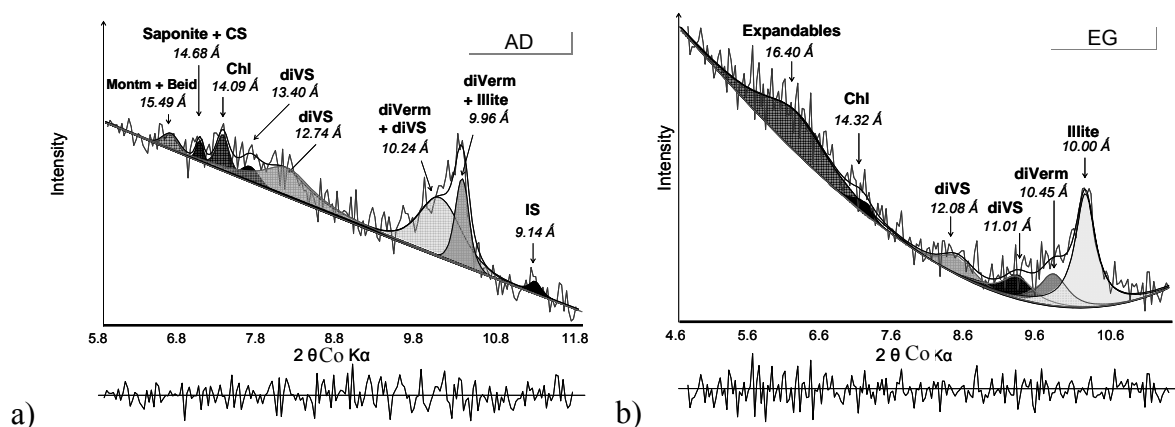


Figure 3.14. Identification of smectites and diVS-mI based on deconvoluted background XRD patterns

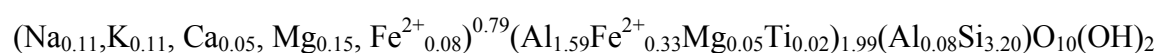
Example from sample NP-SP (0-10 cm);

a) air-dried specimen (AD); b) ethylene glycol saturated specimen (EG)

Figure 3.14 shows an example of deconvolution for 10 Å, where dioctahedral vermiculite could be distinguished from illite (a) and slightly expanding of this mineral after ethylene glycol solvation (b). Exhibition of the (003) peak near 4.83 Å (Figure 3.8) was also indicative for Fe-poor type of dioctahedral vermiculite (Moore & Reynolds 1997). This reflection might be confused from (001) reflection of gibbsite or (003) from chlorite, which were also detected in the samples.

Dioctahedral vermiculite tended to occur in very fine grain fractions (Douglas 1989). Under TEM observations, the dioctahedral vermiculite grains of coastal sediments appeared as rather large platy crystals (0.7-1.0µm) and in small particles of only a few nanometres in the maximum dimension. Dominant habit of the dioctahedral vermiculites is xenomorphic platelets (Figure 3.12d) or conspicuous parallel intergrowths of these platelets. In addition, few particles occurred in lath shapes. Some thin platelets which showed moiré patterns (Figure 3.12d) or irregular, ragged edges characterizing for modification of precursors by weathering process (Henning & Stoerr 1986).

Chemically, dioctahedral vermiculite displayed rather similar formula to illite, with substitution in the interlayer of K by (hydrated) Na⁺, Ca²⁺, Mg²⁺ and Fe²⁺ in some cases. The interlayer charge is between 0.7 and 0.99 with average content of K less than 0.8 per half unit cell, tetrahedral Si between 2.8 and 3.3 and number of octahedral cations between 1.95 and 2.03. The idealized formula: M⁺_{0.75}(Al_{1.8}(Mg, Fe)_{0.2})_{2.0}[(OH)₂Si_{3.0}Al_{1.0}O₁₀], was also mentioned by Vicente et al. (1997). The empirical formula of dioctahedral vermiculite, averagely calculated for all detected particles in coastal sediments of Vietnam were:



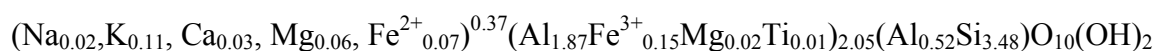
Smectite

Montmorillonite, beidellite and nontronite were known as dioctahedral 10 Å structures and saponite as trioctahedral 14 Å structures. Dioctahedral and trioctahedral smectite species – presented in the samples, were indicated by 060 reflections near 1.50 Å and 1.52 – 1.53 Å, respectively (Figure 3.11). The usual for dioctahedral smectites under air dried conditions was greater than the 10 Å layer units due to the presence of hydrated cations absorbed in interlayers. The normal basal spacings are 12.5 Å for monohydration state (one water layer) and 15.2-15.4 Å for two water layers which could be observed in powder XRD patterns (Figure 3.14a). However, composition of these smectite phases should not be estimated based on peak positions from air-dried pattern due to the high sensitivity of basal spacing to ambient humidity (Moore and Reynolds 1997).

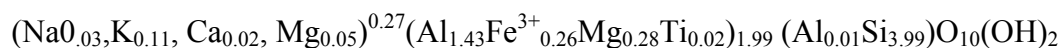
Diocahedral smectite responded with a peak near 17 Å in EG pattern (Figure 3.14b), parallel to depletion in intensity of 14 Å and 10 Å in AD patterns (Figure 3.8). The broad manner of these 17 Å inferred to admixture of mixed layer series with different percentage of smectitic proportion or also low charge (< 0.72) diocahedral vermiculite (Malla and Douglas 1987).

For distinguishing beidellite from montmorillonite based on XRD patterns, Klopogge et al. (1990) proposed the so-called Greene-Kelly method using Li saturation. However in this contribution, with purpose to reveal sensitive chemical alterations caused by differentiation between environments, the method mentioned above was avoided due to possibility of chemical interference. Additionally, the amounts of beidellite as well as montmorillonite were estimated to be rather low, sequently reduce the accuracy of the method in case of adoption. Other obstacles in determining beidellite from montmorillonite based on XRD patterns alone were mentioned in detail by Malla & Douglas (1987).

This dissertation distinguished these two minerals based on agreement between particle morphology in TEM image and chemical formulae calculated from TEM-EDX analysis. Beidellite particles occurred commonly in small xenomorphic platelets of few nanometres (Figure 3.12f), with rough surface or well developed platy crystals. Occasionally, particles developed in pseudo-hexagonal shapes which were similar to kaolinite. Chemically, beidellite was named for a diocahedral smectite species with most of the interlayer charge originated from tetrahedral substitution. The beidellite particles have interlayer charge between 0.3 and 0.5, tetrahedral Si between 3.4 and 3.6, and number of octahedral cations between 1.95 and 2.03. Also, the content of K in interlayer is lower than 0.1 and Al in octahedral layer is higher than 1.85. The idealized formula is: $M^{+}_{0.35}Al_2Si_{3.5}Al_{0.3}O_{10}(OH)_2$ and the average formula of beidellite structures which were determined was give bellows:

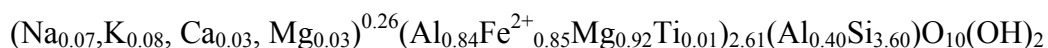


Different from beidellite in xenomorphic shapes, montmorillonite was recognized in typical shapes of thin-film platelets (Figure 3.12e). Xenomorphic shapes were occasionally depicted. In chemical structure, montmorillonite particles were tetrasilic with layer charge derived from octahedral sheet. The interlayer charge of montmorillonite varied from 0.15 to 0.45. The tetrahedral Si of from 3.93 to 4.0, and number of octahedral cations from 1.98 to 2.02 were considered as boundary chemical value of this mineral. The average formula was:



Saponite was also detected in some samples of Dam Mon and Nha Phu by TEM-EDX, in shapes of poor ordered particles with diffuse edges (Figure 3.12b), containing high Mg in

structure. In comparison to the idealized formula: $M^{+}_{0.33}(Mg_{2.67}Fe^{+3}_{0.33})Si_{3.33}Al_{0.67}O_{10}(OH)_2$ (Newman 1990), saponite particles determined had a lower tetrahedral charge and higher occupations of Al and Fe in octahedral layer. The average formula of saponite in samples of Dam Mon and Nha Phu was:



Saponite particles have the interlayer charge vary between 0.3 and 0.4, tetrahedral Si between 3.4 and 3.7 and number of octahedral cations is in range of 2.65 and 3.05.

In the sediment samples of Dam Mon, it was occasionally detected one mineral species, which generally resembled saponite, but had rather high Al in the octahedral occupation. The average formula was followed:



This so-called Al-saponite needed further investigation for confirmation.

Mixed layer series

In the investigated samples, four main series of mixed layer structures were determined: illite/smectite, dioctahedral vermiculite/smectite, kaolinite/expandable and chlorite/saponite.

Illite/Smectite mixed layer (IS-ml)

In air-dried XRD patterns, presences of mixed layer structures illite/smectite and dioctahedral vermiculite/smectite were suggested by reflections in the ranges between 10 - 14 Å (Figure 3.14a). The diffraction patterns of air dried illite/smectite were altered significantly by solvation with EG and such behaviour leads to the provisional identification of illite/smectite. Smectitic mixed layer structures were expanded to the broad peak surrounding 17 Å after ethylene glycolation (Figure 3.14b), overlapping with smectite phases. Meanwhile, mica- like mixed layer structures (e.g. diVS) responded to reflections in the range of 10 – 14 Å (Figure 3.14b).

Association of several reflections in this range suggested a spread variety of mixed layer structures with different smectite layers percentage.

According to Moore and Reynolds (1997), presence of IS-ml series were also recognized by I(001)/S(002) peaks in range of 8.58 – 9.82 Å and I(002)/S(003) peaks in range of 5.1 – 5.61 Å (Figure 3.8). However reflections in the range of 7 – 10 Å and 5 – 7 Å appeared in most of XRD graphs, the corresponding reflections were not always determined. This thus suggested that IS-ml particles might occur in series of wide range of smectitic proportions, rather than single dominated phase.

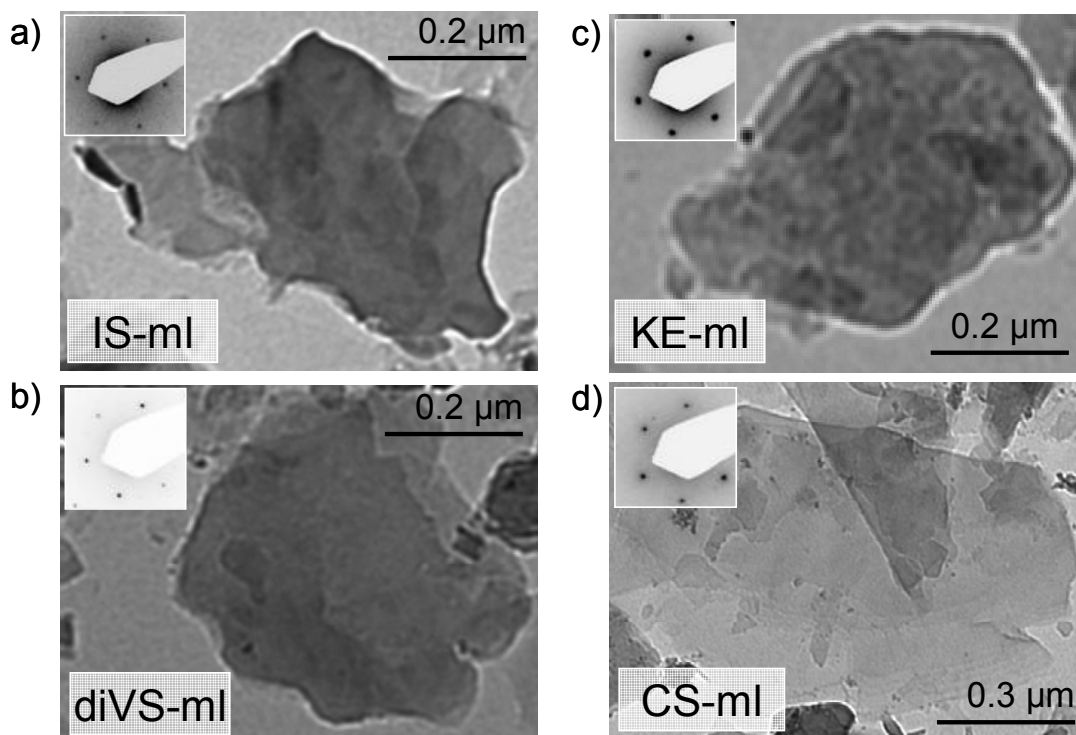


Figure 3.15. TEM graphs of mixed layer structures

Examples in sample RRD-LM (0-3 cm). Inserts were SAEDs.

Based on TEM, structures of IS-ml series were chemically distinguished from diVS-ml series. In TEM micrographs, IS-ml occurred as pseudomorphic shapes of both illite and montmorillonite, with platy xenomorphic particles of small to medium sizes (few nanometres) (Figure 3.15a). Curled edges were commonly. IS-ml particles displayed not only turbostratic order but also $2M_1$ polytype (see the insert picture in Figure 3.15a). Velde & Brusewitz (1986), Meunier & Velde (1990) and Srodon et al. (1992) demonstrated that the chemical composition of I/S changes continuously from one end point of montmorillonite smectite to the another point of illite, but the path line is different for various geological origins because of the precursor illite and smectite have different layer charges.

Sato et al. (1990) indicated, using the Greene-Kelly test of IS-ml for diagenetic shale and sandstone that the smectitisation did not proceed directly from precursor montmorillonite to ordered IS, until the precursor montmorillonite was altered to beidellitic composition. Then the beidellite component was converted to ordered IS-ml. In addition, Meunier et al. (2000) proposed that the growth of IS-ml proceed via development of vermiculitic layer in interface or inner structure of montmorillonite, then precipitated to form illite of fixed chemical composition. Therefore, it was reasonable to expect the vermiculitic or/and beidellitic layers included in chemical composition of IS-ml series. Also, beidellitic layers were expected in chemical composition of diVS-ml series.

According to Srodon et al. (1992), in illite-smectite mixed layer structures (IS-ml), the end members are characterized by a typical total charge - 0.4 for montmorillonite and 0.89 for illite. The share of smectite in illite/smectite-mixed layer structure could be estimated according to Srodon et al. (1992). Because the layer content of smectite correlates with content of Al in tetrahedral layer and shows a linear connection with the “fixed” interlayer cations (K, Na) from the illitic components of the structure.

The smectite or illite ratio can be estimated from Al content in the tetrahedral layer [1 & 2].

$$S\% = 100.4x^2 - 213x + 109 \quad [1]$$

$$MLXX = 100 - S\% \quad [2]$$

S% - smectite ratio in the mixed layer, *x* - Al content in the tetrahedral layer, *MLXX* – illite ratio in the mixed layer

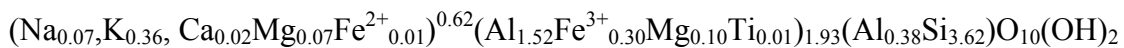
Based on theoretical values of the end members, the actual interlayer charge (XII_{soll}) [3] and furthermore the minimum content of “fixed” cations (K, Na) in the interlayer [4] were calculated, to verify IS-ml plausibility.

$$XII_{soll} = (0.89 * MLXX + 0.4 * S\%)/100 \quad [3]$$

$$FIX_{min} = 0.89 * MLXX \quad [4]$$

The I/S mixed layer have been subdivided by the amount of illite ratio in the mixed layer structure.

In the investigated samples, IS-ml structures were revealed to show an average formula as given bellows:



correspondingly to IS-ml with 40 – 50 % montmorillonitic proportion.

Diocahedral Vermiculite/Smectite mixed layer (diVS-ml)

Behaviours of diVS-ml series in XRD pattern resembled IS-ml in many aspects. However, diVS-ml structure is expected to expand more intensively due to slightly higher expandability of vermiculite relatively to illite. Malla and Douglas (1987), working with soil clay minerals, described some vermiculite structures with two different layer charges, those producing spacings of both 14 and 18 Å after ethylene glycol solvation. The described species by these authors can be comparable with our defined diVS-ml structure with the low layer charge relevant to our defined diVerm and the other, high layer charge relevant to smectite).

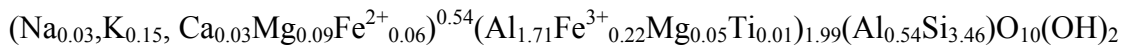
Figure 3.14a showed the indicative reflection of diVS structures in the range of 10 – 14 Å of air-dried XRD pattern. After EG treatment, these mixed layer structures expanded to the

broad reflection near 17 Å (Figure 3.14a), overlapping with smectite and other mixed layer structure. The new reflections in the range of 10 – 14 Å, then indicated weakly expandable diVS-ml structure corresponding to low smectitic proportion. However, it was difficult to distinguish continuous series of diVS from IS-ml based on the crystallite parameters due to overlapping reflection in the 10 – 14 Å range of XRD patterns. This series, thus were further determined and characterized based on TEM-EDX.

In fractions < 2 µm, diVS-ml shaped well with in xenomorphic platelets (Figure 3.15b) and rarely in pseudo-hexagonal shape. Few particles were observed with rough surface or ragged edges. Sizes of particles ranged from few nanometres to approximately one micrometer.

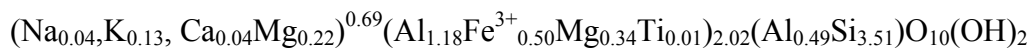
For the estimation of share proportions in diVS-ml structure, the formulae described above for IS-ml structures have been adapted. The diVS-ml series had been subdivided by the equivalent calculation of proportional mixing between theoretical values of Si in the tetrahedral layer, number of octahedral cations, interlayer charge and fix cations of the two end members: dioctahedral vermiculite and montmorillonite. Modelled tetrahedral Si value of 3.1 was for 100% di-vermiculite and of 3.95 was for 100 % smectite in the structure. Limits of the calculation were a postulation by the distribution of own measured values and limits for theoretical values of the end members

Based on TEM-EDX data, a series in wide chemical range of diVS-ml were determined with the average formula given as bellows:



correspondingly to diVS-ml structure with 30 – 40 % montmorillonitic proportion.

Besides, in sediments of Dam Mon, a species of high charge diVS-ml was detected with the following formula:



Particles were Fe-enriched, occurred in xenomorphic shape occasionally as observed under TEM graphs.

Kaolinite/Expandable mixed layer (KE-ml)

In soil, kaolinite can be involved as one end member in the mixed layer series: kaolinite/expandable (KE) (Hughes et al. 1993). The 2:1 layer in this structure can vary from a low charge expandable (smectite) to high charge expandable (dioctahedral vermiculite). Detection of kaolinite/expandable was readily made by XRD studies of < 2 µm fraction sample after air drying, ethylene glycol solvation and a heating routine

(Hughes et al. 1993). In air-dried XRD pattern, presence of KE-ml was suggested with the broad asymmetric 7 Å where KE structures were deconvoluted from mixture with kaolinite, halloysite and chlorite (Figure 3.9). This 7 Å reduced intensity when saturated with ethylene glycol solvation (~ 1.3 times on example in Figure 3.8), parallel to appearance of 17 Å reflection. The 17 Å peak of expandable-rich KE ($001_{\text{kaol}}/001_{\text{exp}}$) with ethylene glycol solvation was extremely broad even at low percentages of 7 Å interlayering, distinguishingly from kaolinite-rich KE, smectite and other mixed layer structures.

According to calculation by NEWMOD (Hughes 1993), broad (001/002) peak or smear between the range of $d = 7.43$ Å and 8.46 Å (Figure 3.16a) and (002/005) peak or smear between the range of $d = 3.39$ Å and 3.54 Å (Figure 3.16b) suggested the presence of expandable kaolinite or kaolinite-expandable mixed layer series. Composition of randomly interstratified kaolinite/smectite could be determined based on $\Delta 2\theta$ parameter (Moore & Reynolds 1997). Example in Figure 3.16a showed the corresponding reflection between (001/002) at 8.32 and (002/005) at 3.39 Å, reflecting KE structures containing 70 – 80 % of smectitic proportion were the dominant phase in KE-ml series of the sample. In case of mixture of KE structures with none typical dominant phase, reflections occurred without corresponding couple (Cuadros & Dudek 2006).

In admixture with CS-ml, this determination of end-member proportion was difficult due to overlap diagnostic range of 002/002 CS with 001/002 KE and diagnostic range of 004/005 CS with 002/005 KE.

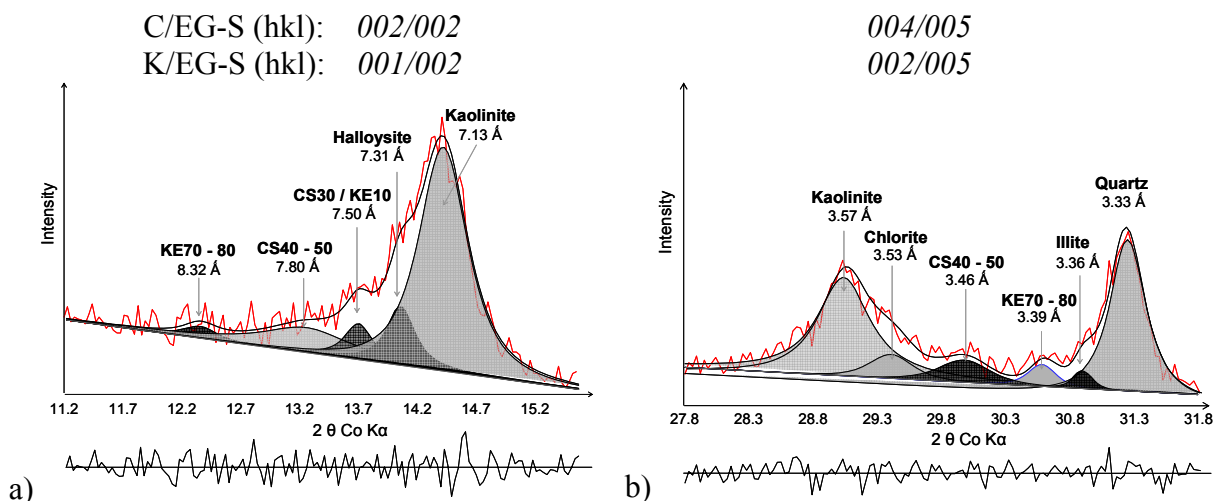
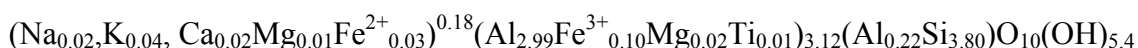


Figure 3.16. Identification of KE-ml structures with different proportion of expandable layers
Example on sample DM-LM (80 – 90 cm)

TEM experiments showed KE-ml structures in pseudomorphic shapes of not only kaolin minerals (Figure 3.15c) (i.e. hexagonal, lath or tubular) but also beidellite particles (xenomorphic platelets) as end-member minerals (Henning and Stoerr 1986). In fractions < 2 μm , KE-ml particles ranged widely in sizes, from large, single particles of 1-2 μm to tiny particles of only few nanometres in aggregation. Particles were commonly observed with rough surface, indicating alteration processes. Polytypes of 2M₁, 1M and turbostratic order were depicted. In the calculation system, empirical formulae were calculated for admixture between full unit cell of kaolinite (with total charge of 28) and half unit cell of smectite (with total charge of 22). Average formula was:



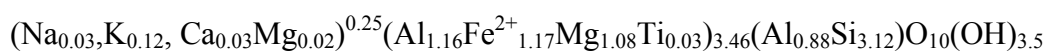
Number of OH group varies from 2 to 8, corresponding to ratio of smectitic proportion, from 100% smectite (n = 22) to 100% kaolinite (n = 8).

Chlorite/Saponite mixed layer (CS-ml)

Ethylene glycol solvated and air dried preparation yielded little information on mixtures versus mixed layering in the chlorite/saponite series because of severe peak interferences (Moore & Reynolds 1997). Only tracing from heated preparation showed promise of definite analysis. Structures in CS-ml series were indicated by 002/002 peaks in range of 7.18 – 8.39 Å and 004/005 peaks in range of 3.39 – 3.53 Å (Figure 3.14). Similarly to KE-ml, the composition of CS-ml structure could be determined based on corresponding Chlorite/ ethylene glycolated Smectite (C/EG-S) reflection couple between 002/002 and 004/ 005 (Moore & Reynolds 1997) as shown in the Figure 3.14.

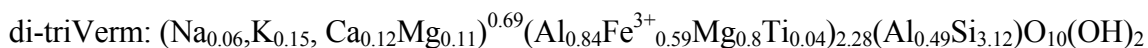
In TEM observations, Chlorite/Saponite mixed layer particles displayed similar morphology as chlorites, with platy xenomorphic shapes (Figure 3.15d), generally in large crystals (0.8 – 1 μm). Determination of formulae and layer proportion of CS-ml particles were based on the similar systems for Modeling IS-ml and diVS-ml. Chemical formula of the mixed layer structure is defined by synchronously proportional contributions of end-members in terms of total charge (28 for chlorite, 22 for saponite and tri-vermiculite), theoretical values of interlayer charge (0 for chlorite, 0.35 for saponite and 0.75 for tri-vermiculite), tetrahedral Si and number of octahedral cations.

The determined mixed layer structures had both Fe^{2+} and Mg occupations in octahedral layers. Potassium was generally main cations in the interlayers as shown in the calculated formula following:



correspondingly to CS-ml with 50-60 % saponitic proportion.

Beside the four principal mixed layer series, trace of mixed layer structures between trioctahedral and dioctahedral vermiculites (di-triVerm), kaolinite/vermiculite (KV-ml), chlorite/trioctahedral vermiculite (CV-ml), chlorite/trioctahedral vermiculite/saponite (CSV) were depicted in traces.



Non-clay minerals

In XRD patterns, the most obvious determined non-clay minerals were quartz, feldspar and pyrite. Besides, hydroxides of Al and Fe occurred under TEM images as precipitated aggregations of tiny amorphous particles or coating over other minerals. Gypsum, ilmenite and hematite were observed in well crystallite.

Particles of quartz dominated in bulk samples with intensive, sharp reflections at 3.35 Å (001-spacing), 4.28 Å (002 - spacing), 2.46 Å (003 spacing) in XRD patterns (Figure 3.7). Other reflections of quartz in the sample caused interference with indicative reflections of clay minerals (e.g. interference with (001) reflection of illite at 3.36 Å – see Figure 3.16b, with 060 reflection of triCMs at 1.544 Å – see Figure 3.11). Quartz were detected also in fractions < 2 µm, based on reflections at 3.34 Å, 4.25 Å (Figure 3.8) and chemical composition as SiO₂ in TEM-EDX calculation.

K-feldspars were noticed with diagnostic 002- reflections surrounding 3.25 Å and plagioclase with diagnostic reflections surrounding 3.18 – 3.21 Å (Figure 3.7, Figure 3.8). Pyrite was detected by the diagnostic peaks at 2.71 Å (200), 1.63 Å (113), 2.21 Å (112), appearing commonly in fractions of coarse grain size (Figure 3.7). Gypsum exhibited in trace with the sharp reflection surrounding 7.6 Å in XRD patterns of oriented mount specimens and with the well crystallite hexagonal shapes and chemical formula under TEM-observation. Other reflections of gypsum at 2.87-2.89 Å, 4.27 Å were also detected (Figure 3.7).

Hematite was indicated with reflections at 1.69 Å and 2.52 Å in XRD patterns of powder samples (Figure 3.7). In fractions < 2 µm, hematite occurred in rare frequency, with Fe-rich, typical non-transparent, well crystallite hexagonal shapes.

Gibbsite was indicated with reflections surrounding 4.8 Å and 1.67 Å in XRD patterns (Figure 3.8). In TEM images for fractions < 2 µm, gibbsite was rare detected. Particles aggregated in small sizes. The Ti-bearing minerals referring to ilmenite and anatase were also determined in traces based on TEM-EDX investigations.

Other non-clay minerals were observed in low intensity, platokurtic reflections at 6.11 Å, 3.11 Å and 2.35 Å (Boehmite), 3.01 Å, 2.13 Å and 2.29 Å (Mg-bearing Calcite), 2.81 Å, 2.00 Å and 1.64 Å (Halite) (Figure 3.7).

3.2.5 Mathematical methods

Principal component analysis (PCA)

Compositional variation among a series of geological specimens (e.g. sediment samples) may be attributed to physical mixing or mathematically analogous processes (Weltje 1997), such as appearance of some hydrodynamic mode or a new sedimentary source (in cases of granulometry data) or fractional transformation into new phases (in cases of geochemical and mineralogical data). When using the original data matrix to search and identify these underlying trends or processes, it faced some general difficulties due to large amount of parameters to consider. The variation of trace elements was dimmed by the variation of major elements. Therefore, Principal Components Analysis (PCA) and Factor analysis (FA) were used as tools in attempts to reduce a large set of variables to achieve a more meaningful, smaller set of variables. Each subset or factor that is relatively independent of one another, are composed of most strongly correlated parameters. Factors which are generated are thought to be representative of the underlying processes that have created the correlations among variables, which played a principle role in the development of the geological formation. This version of PCA is named Q-factor analysis (Davis 1973).

With our muddy sediments sampled from different types of coastal wetlands of Vietnam, PCA and FA tools were used (Table 8.2a) in two ways. Firstly, PCA and FA tools were used for single dataset of each region (the same sedimentary source) to search for most highlighted process/ group of processes those happened during the development of the sediment profile. Information can be extracted from high correlations in the rotated principal component matrix (see Table 8.3 or Table 8.4 in Appendix for example). Results of these analyses were presented with number of principal presenting in the dataset, characteristics or composition of each factor and influence percentage of factors on total variance of dataset.

Secondly, PCA and FA tools were applied on the dataset which was combined from datasets of different wetland types, sediment sources, levels of influence by mangrove forest and aquaculture to determine differentiation in influences of the recognized driving processes during the morphological transformation as well as the short-term alterations related to specific events. Results of these analyses were presented in PCA biplots, a combination between score plot (xy-dots - projection of analyzed samples on the two principal factors with highest influences) and loading plot (arrows - projection of analyzed parameters on the two principal factors with highest influences) (see notations and illustration in Figure 8.2, Appendix).

End-member Modeling algorithm (EMMA)

The detail algorithm was described by Weltje (1997, 2001). The EMMA approach was developed on basis of PCA. End members are obtained by ordinary least square non-negative matrix factorization of principal components. Therefore, datasets which conform to a linear mixing model can be expressed as mixtures of a fixed number of end members. The end members represent a series of fixed compositions which can be regarded as distinct subpopulations within the dataset being analyzed. The resulting mixing model is subject to strict non-negativity and constant-sum constraints on EM compositions and mixing coefficients to ensure physical interpretability of the model parameters. According to Weltje (1997), variation among a series of chemical bulk compositions of samples, derived from a single muddy body of the coastal wetland, may reflect differing proportional contributions of fixed number of minerals and their chemical compositions. And if the number of end-members and their chemical composition are known accurately, the mineralogical composition of each sediment sample can be estimated using standard least-squares techniques.

With muddy sediments collected from coastal wetlands of Vietnam, this EMMA tool was used for datasets of particle size distribution, summarizing variations among these granulometric populations in terms of proportional contributions of (theoretical) end members. The end members were expected to be hydrodynamic modes in cases of granule data. The compositional variation of the end members in each depth interval of sediment profiles were expected to assigned to some underlying processes or specific events.

The calculations of EMMA were performed by MATLAB version. The established commands for EMMA Modeling of these datasets were summarized in Table 8.2b (Appendix).

4 RESULTS

4.1 Grain size analysis

4.1.1 Red River Delta

STA approach based on parameterized data

The PCA-biplot (Figure 4.1) offer a clear differentiation of the investigated sedimentary areas in three groups: (i) tidal creek: bottom materials along the creek which passing shrimp ponds areas, (ii) tidal creek: bottom materials along the creek passing mangrove forest areas, and (iii) core materials in low tidal mudflat (LM), mangrove forest (MF) and shrimp pond (SP). In terms of granulometric attributes, sediments in tidal creeks (groups I + II) showed a linear correlation whereas sediments in LM+MF+SP concentrated in a cloud (group III).

Samples from all three groups are classified as silt, mud, sandy silt and sandy mud tidal flat facies of upper Thai Binh formation ($Q_{IV}^3tb_3$ amb, mb). Dominating in all samples silt fraction was ranging from 50.7 – 67.5 %, followed by clay fraction (14.8 – 37.5 %) and the remains were fine sand fractions. The creek sediments (groups I + II) had generally higher portions for sandy fractions than the core sediments in LM+MF+SP (group III). Of the two creeks, sediments in the creek passing mangrove area (group II) showed sandy portions approximately 2 times higher than sediments in the creek passing shrimp ponds areas (groups I) (Figure 4.2).

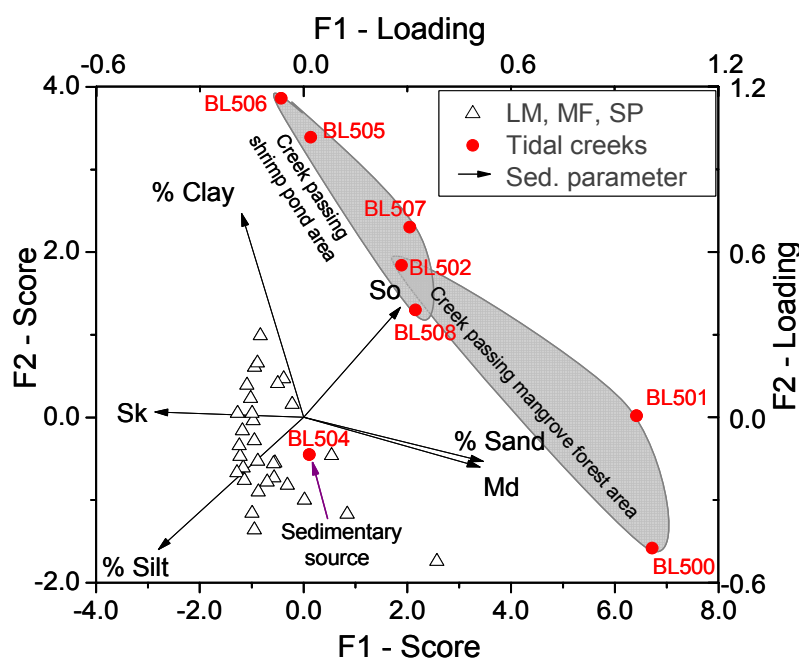


Figure 4.1. PCA-biplots on correlation among sedimentological parameters (arrows) and sampling locations (xy-dots)

Total variance explained 79.7 % tendency.

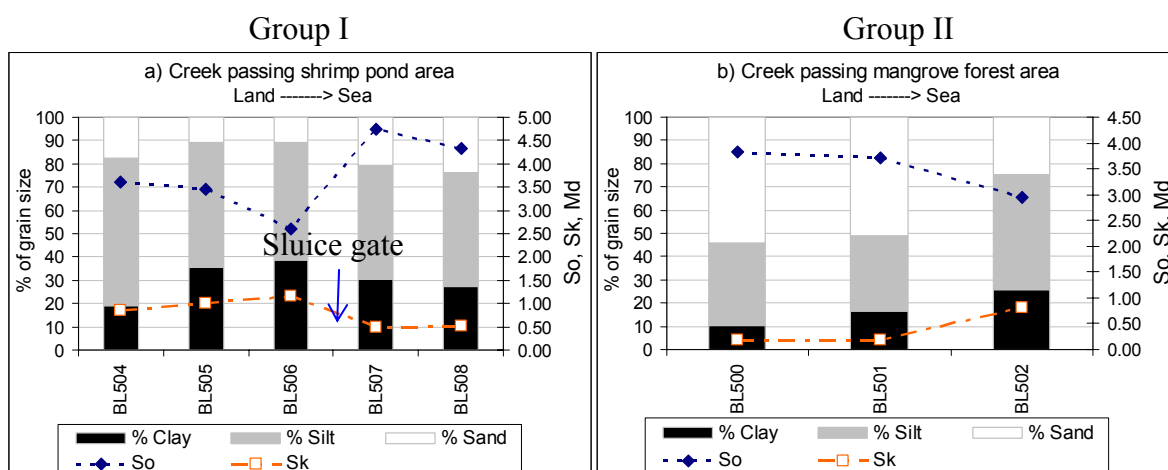


Figure 4.2. Variation of grain size composition and sedimentological parameters along tidal creeks in the Red River Delta

Dash lines express sorting So and Sk; Solid line expresses mean size (Md) in mm; In background, dark tone expresses sand percentage; grey tone expresses silt percentage and light tone expresses clay percentage.

The sediments of all three groups were very poorly sorted with So ranging from 2.7 – 3.7. Along the creek passing mangrove forest (Figure 4.2b, left), the sediments become finer, better sorted and more positively skew from land to sea. Similar tendency was seen for the fragment before sluice gate in the creek passing shrimp pond area (samples BL504, BL505, BL506 in Figure 4.2a, right). It was notable that, sediments in the fragment from the sluice gate for water exchange in shrimp pond to the sea of the creek passing shrimp pond area (samples BL507 and BL508 in Figure 4.2a, right) showed a sudden increase in amount of sand. This creek fragment came along with a slightly increase of sorting (poorer sorting degree) and a decreasing of skewness.

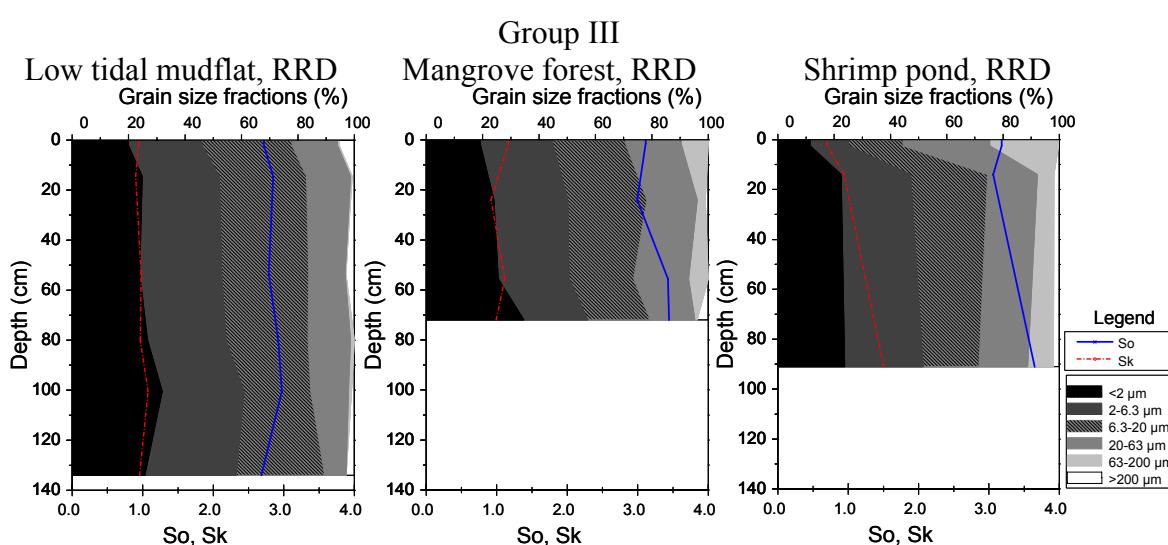


Figure 4.3. Composition of grain size fractions and sedimentological parameter (So, Sk) of coastal sediment profiles in the Red River Delta

Within the cloudy concentrated group of core sediments in LM+MF+SP (group III), granulometric attributes showed a strong correlation among each other samples but no specific correlation to any sedimentological parameter. Grain size composition of sediments in profiles of low tidal mudflat, mangrove forest and shrimp pond displayed a regular contribution of fractions $< 2 \mu\text{m}$, $2 - 6.3 \mu\text{m}$, $6.3 - 20 \mu\text{m}$ (Figure 4.3). Each of these three fractions accounted for approximately 20 – 30 % of total grain sizes. Amounts of $20 - 63 \mu\text{m}$ fractions were in range of 7.6 – 19.6 %. An exceptionally high value of 30.7 % of $20 - 63 \mu\text{m}$ fractions was to consider in the 0 – 3 cm surface layer of shrimp pond profile, where occurred sudden decrease in composition of all fractions $< 20 \mu\text{m}$. Fractions of $63 - 200 \mu\text{m}$ were observed in profiles of mangrove forest and shrimp pond with amount of 0 – 25 %, but absent to rare in profile of low tidal mudflat. Coarser grains ($> 200 \mu\text{m}$) had concentration less than 4 % (Figure 4.3). Along all the profiles, fine fractions increased slightly with increasing depth, parallel to increase of skewness and sorting parameters of grain size distribution (GSD) patterns.

EMMA approach based on full GSD patterns

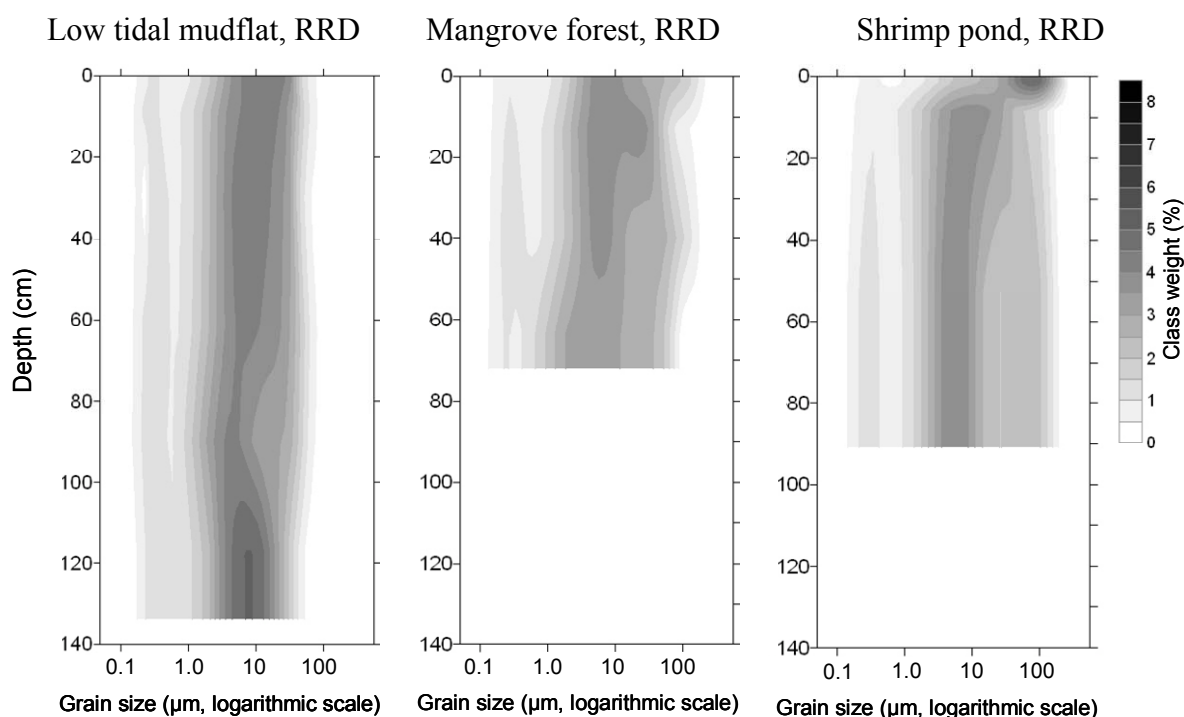


Figure 4.4. Grain Size Distribution (GSD) maps of sediment profiles in estuary of the Red River Delta, North Vietnam

Visualisation of GSD maps according to Beierle et al. 2002. Darker tone of colour expresses higher percentage of class weight in GSD curves

The multimodal character of sedimentations was shown in Grain Size Distribution (GSD) maps (Figure 4.4). Similar constant sequence of a silty fraction as principal mode (sizes of 6 – 10 μm), and additionally small modes at fine sand (sizes of 70 – 80 μm) and clay fractions (sizes of 0.2 – 0.6 μm) were recognized. With class weight < 5%, all GSD maps showed a platokurtic distribution. GSD in surface sediments of low tidal mudflat and mangrove forest profiles were more platokurtic in shape and slightly broader toward coarser range.

Along the low tidal mudflat profile, sedimentation modals were fairly symmetric, and shifted slightly toward range of finer particles within upper layers. Whereas, surface layer (0-3 cm uppermost) in shrimp pond profile showed a sudden depletion of fine particles and change into sandy mode (Figure 4.4, right).

Mangrove forest had changed its kurtosis to more platokurtic distribution from the depth of 10 - 20 cm to lower part. This is a different behaviour to the profiles of low tidal mudflat and shrimp pond, where the kurtosis remained along the depth.

Deconvolution of GSD patterns in mudflat sediments of the Red River Delta (Figure 4.5) revealed that their component modes (at sizes of fine sand, silt and clay) were well described by ideal log-Gauss function. Of all intervals, GSD patterns were determined to comprise three component Gaussian modes, in different contribution ratios. The silty clay mode located at the range of 0.4 μm . Fine silt mode was surrounding 9 – 10 μm and the very fine sand mode was surrounding 80 - 100 μm sizes. Degree of sorting (relevant to lower value of S_o) increased from sediment profiles of low tidal mudflat (2.7 – 3.0), via mangrove forest (3.0 - 3.4) to shrimp pond (3.1 – 3.7). In all profiles, sorting in surface sediments is slightly better than that in the deeper intervals.

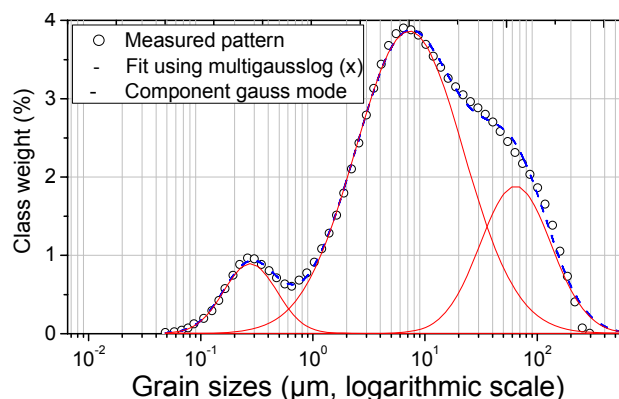


Figure 4.5. Deconvolution of GSD pattern
(Fit using 4-multigausslog(x) function)

(on example of surface sediment samples in mangrove forest of the Red River Delta)

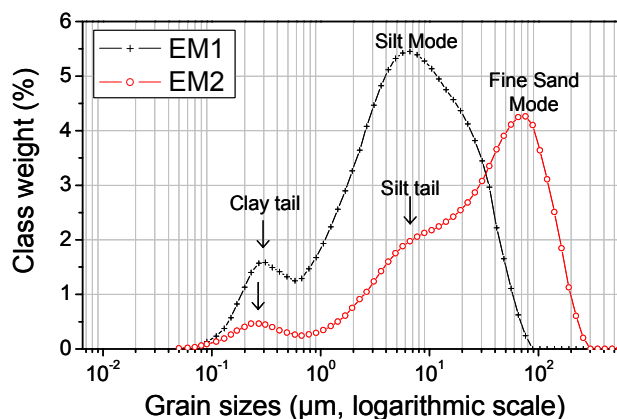


Figure 4.6. Modelled end-members of GSD patterns in coastal sediments of Red River Delta

EMMA approach for 2 principal components;
Total variance explained = 96.9%;
Convergence at 1346 steps

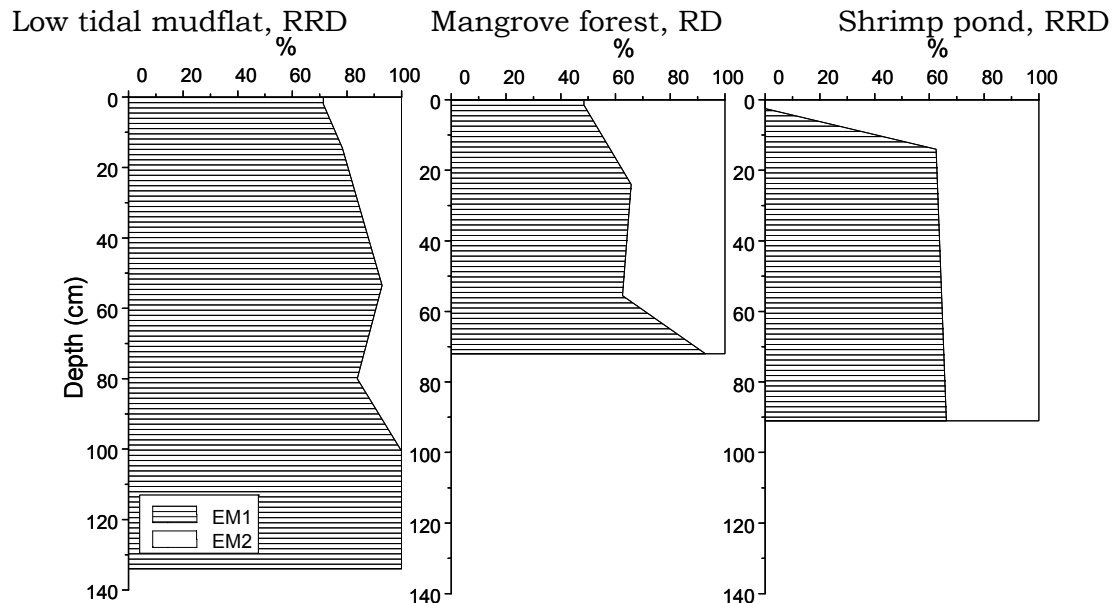


Figure 4.7. Computed contribution of end-members in sediment profiles in estuary of the Red River Delta

EMMA approach for 2 principal components. Total variance explained = 96.9%; EM1 correlates to silty mode and EM2 correlates to sandy mode

However, multimodal GSD patterns of the investigated silty sediments prevent reliable interpretation of the grain size moment statistics in terms of sediment transport mechanism or sediment source. End-members were calculated by End-Member Modeling Algorithm (EMMA) using GSDs of 30 samples in order to interpret the observed grain size data in terms of such underlying processes.

PCA of the whole dataset of measuring steps in GSD patterns of coastal mudflat sediments in the Red River Delta revealed that the distribution of grain sizes at each investigated sampling location was governed by two

principal underlying factors, which could explain 96.9 % total variance. EMMA of the mixing processes between these two factors allowed recognition of two compositional factors: (i) a silt mode with a clay tail [EM1] and (ii) a fine sand mode with silt and clay tails [EM2] (Figure 4.6). Each compositional factor is rather a mixture of Gaussian modes than an ideal unimodal distribution.

Quantification of end-members contribution in the investigated sediments was based on score dataset obtained by EMMA. From low tidal mudflat, via mangrove forest to shrimp pond profiles, contribution of EM1 (silt mode) increased and contribution of EM2 (fine sand mode) decreased. The same behaviour is to recognize with the depth in all three profiles: fine sand mode (EM2) decreased with the depth, compensated by the increase of silt mode (EM1) (Figure 4.7).

4.1.2 South Central Coast

STA approach based on parameterized data

From the calculated grain size parameters, the main sediment types in South Central Coast – South Central Coast of Vietnam were revealed to range from very fine silt to fine sand with mean particle sizes of 7.0 – 228 μm . In intertidal mudflat, dominant composition is fine sand with average value of 58 % (ranging from 0 – 92 %), followed by silt (6 – 86 %) and clay (3 – 30 %). Mean sizes varied with depth intervals and locations, but reflected no recognizable specific tendencies along the investigated sediment profiles. Figure 4.8 illustrated grain size composition and sedimentological parameters along coastal sediment profiles in the Dam Mon, the peninsular area and Nha Phu lagoon, Central coast of Vietnam.

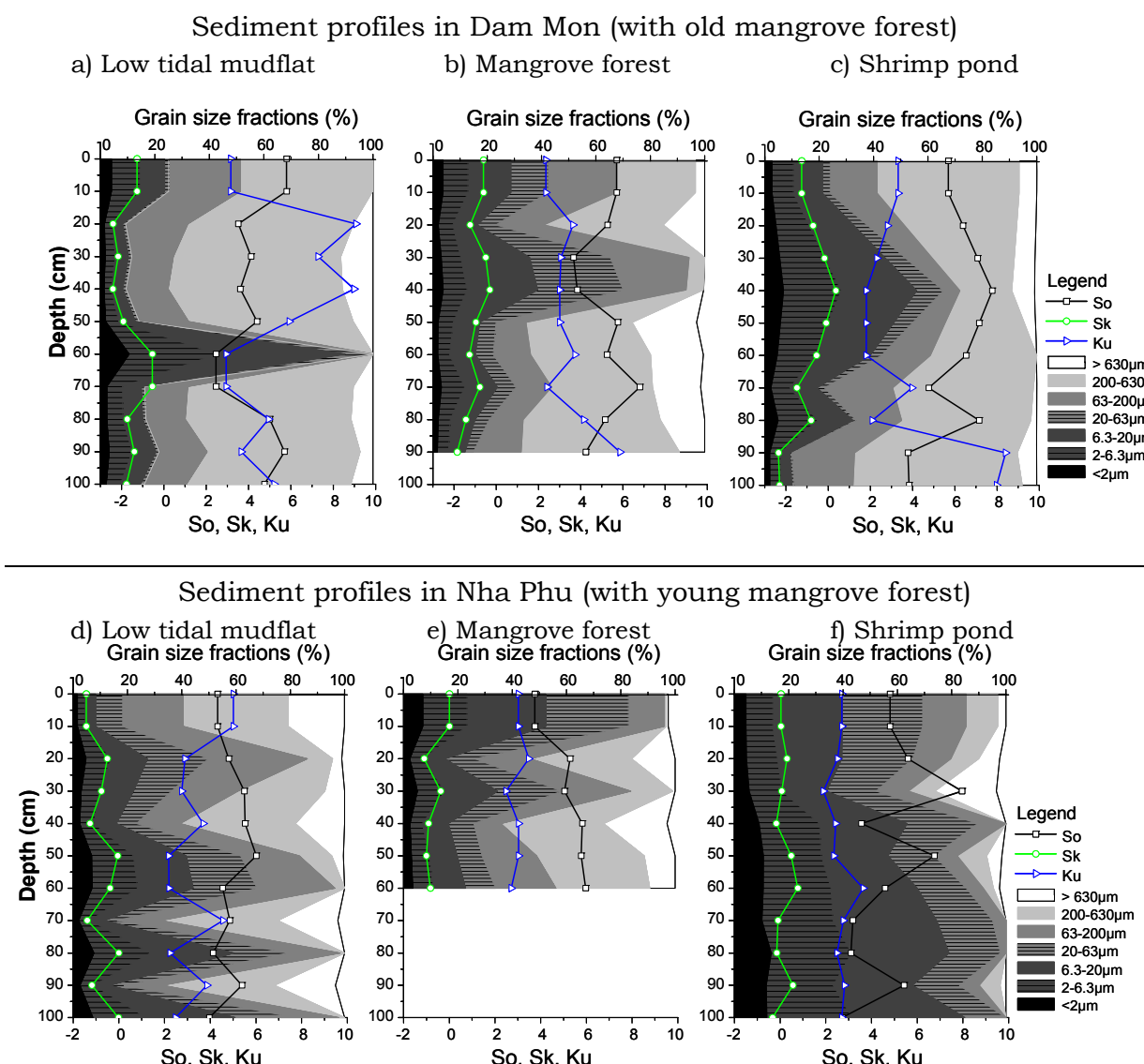


Figure 4.8. Composition of grain size fractions (background) and sedimentological parameter (So, Sk, Ku) (line) of coastal sediment profiles in Dam Mon and Nha Phu

Sediments in Dam Mon were generally coarser than those in Nha Phu. Dominantly in profiles of Dam Mon were fractions of 200 – 630 μm while in Nha Phu, compositions of grain size fractions were regularly distributed (Figure 4.8). Fractions < 2 μm in most of the intervals of sediment profiles accounted for less than 4 %, only few had up to 10 %. In both areas, from profiles of low tidal mudflats via mangrove forests to shrimp ponds, the amount of fine fractions increased continuously, with emphasis on surface layers. However, the profile structures generally remained.

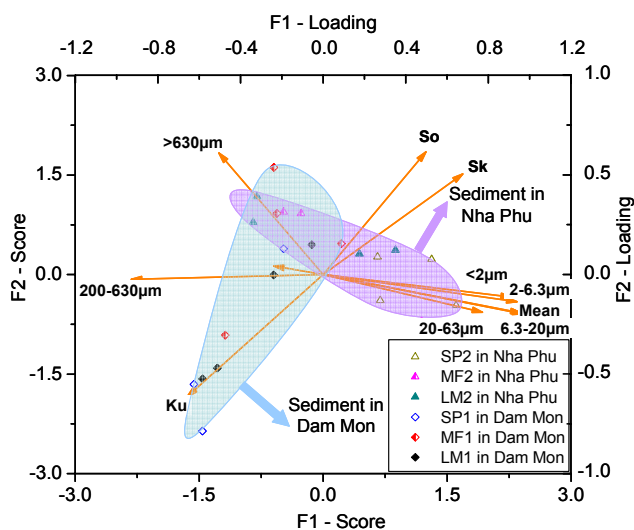


Figure 4.9. PCA Biplots of correlation among sedimentology parameters and sampling sites

Xy-dots expresses scores of sediments in low tidal flat (LM), mangrove forest (MF) and shrimp pond (SP) of Nha Phu (triangles) and Dam Mon (diamonds). Arrow expresses loadings of grain-size fraction percentage and parameters: So, Sk, Ku and Mean size

These sediments were very poorly sorted with the sorting (So) ranging from 3.0 to 7.0. It is probably caused by big sampling interval (10 cm) but also by polymodal grain size distributions. Sorting is rather stable with depth profiles (Figure 4.8). Different from sediments in the Red River estuary, coastal sediments in South Central Coast had negative skewness values (-2 to 0). The kurtosis ranging between 3 to 9 in Dam Mon and between 2 to 5 in Nha Phu sediments, characterised by a normal to leptokurtic distribution in Dam Mon with a dominance of coarse particles but platykurtic – to normal distribution in Nha Phu with a dominance of fine particles. The increase of Kurtosis in upper part of low tidal mudflat profile and lower part of shrimp pond in Dam Mon corresponds to high concentration of sandy facies showing the leptokurtic distribution caused by this coarse sizes range.

Correlations among grain size composition and sedimentological parameters were also revealed from PCA biplots (Figure 4.9), which allowed distinguishing group of Dam Mon sediments from group of Nha Phu sediments.

Nha Phu sediments:

In consideration together with values of grain-size parameters, sediments in Nha Phu were found to differentiate from each other mainly in Md and grain size distribution, reflected by linear distribution between size fractions and Md. While sediments in mangrove forest and low tidal mudflat correlated rather strongly with fractions 63-20 μm and > 63 μm and did not

show clearly differences in correlation with different grain size fractions. The sediments in shrimp pond had completely different behaviour in terms of these sedimentological parameters. In addition to higher accumulation of these fine fractions in shrimp pond, the stronger correlation with muddy sizes (vectors of Md, fractions $< 2 \mu\text{m}$, $2-63 \mu\text{m}$, $6.3-20 \mu\text{m}$ and $20-63 \mu\text{m}$) inferred that fines were the most stable size fraction in all GSD patterns.

Dam Mon sediments:

Different from mostly silty sediments in Nha Phu, all profiles of Dam Mon had fine sand dominantly in composition as stable size fractions, which was reflected by strongly correlation among sediment samples and coarse fractions.

The differentiation of each sedimentary environment/depth intervals from others in Dam Mon are mainly laid on sedimentological parameters (So, Sk, Ku) and coarse grain size fractions ($63-200 \mu\text{m}$, $200-630 \mu\text{m}$ and $>630 \mu\text{m}$), corresponding to linear distribution of samples along these vectors. Sediments in shrimp pond and low tidal mudflat correlate strongly to kurtosis and also have more leptokurtic distribution than sediments in mangrove forest.

EMMA approach based on full GSD patterns

Polymodal manners were recognized in GSD maps (Figure 4.10), varying in wide range along depth profiles. Sediment profiles in Dam Mon were characterized by sandy facies as the main mode, which are rather stable during the development of profiles, whereas profiles in Nha Phu showed the interlayer mixture of sandy and silty facies, corresponding to the cross structure of sediments in river mouth. Correspondingly, in sediments of Dam Mon, fraction sizes of $200 - 630 \mu\text{m}$ were dominantly in grain size composition, stable distributed along the profile whereas in profiles of Nha Phu, proportion of grain sizes showed a wide variation but no preference of dominance. Comparable tendencies were found in the sediment structures of mangrove forests of the two sampling sites, which had fine particles accumulating at surfaces layer, became coarser at the depth of $10-20 \text{ cm}$, then starting the bimodal distribution between sand and silt facies (Figure 4.10). In shrimp ponds of these sampling sites, there was the tendency of fine silty facies gradually transforming to silty facies from bottom to surfaces.

The presence of sandy facies in profiles of Dam Mon explained for different grain size composition from that in Nha Phu shrimp pond. Also South Central Coast sediments show a polymodal manner of particle size distributions (Figure 4.10). For the GSD dataset of coastal sediments in South Central Coast, the higher goodness of fit has been obtained using multigausslog(x) fitting function for deconvolution (Purkait 2002), in comparison to hyperbolic function (Christiansen and Hartman 1991).

Six typical peak modes had been determined (Table 4.1) and described below.

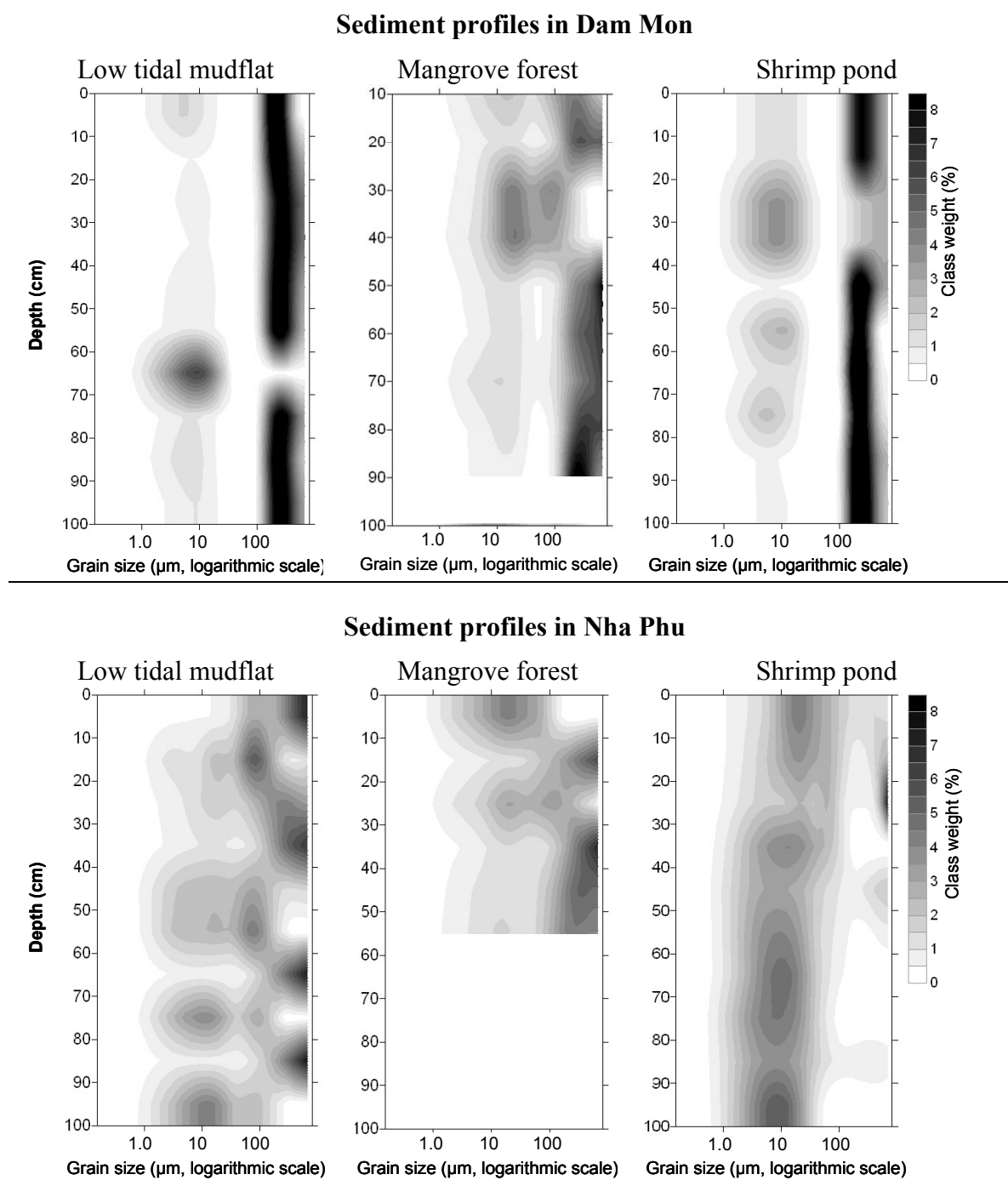


Figure 4.10. Grain Size Distribution (GSD) maps of sediment profiles in Dam Mon and Nha Phu, Central coast of Vietnam

Visualisation of GSD maps according to Beierle et al. 2002; Darker tone of colour expresses higher percentage of class weight in PSD curves.

Table 4.1. The deconvoluted Gaussian modes
(on examples of mangrove forest profile in Dam Mon)

Profile/ depth interval		Mode position* (μm , logarithmic scale)					
Sample	Depth (cm)	Mode 1	Mode 2	Mode 3	Mode 4	Mode 5	Mode 6
MF1/1	0 - 10	$10^{0.35}$	-	$10^{1.2}$	-	$10^{2.3}$	-
MF1/2	10 - 20	$10^{0.35}$	-	$10^{1.2}$	-	$10^{2.4}$	$10^{2.85}$
MF1/3	20 - 30	-	$10^{0.85}$	$10^{1.3}$	$10^{2.0}$	-	-
MF1/4	30 - 40	-	$10^{0.85}$	$10^{1.2}$	$10^{1.9}$	-	-
MF1/5	40 - 50	-	-	$10^{1.2}$	-	$10^{2.4}$	$10^{3.0}$
MF1/6	50 - 60	-	$10^{0.85}$	$10^{1.2}$	-	$10^{2.4}$	$10^{3.0}$
MF1/7	60 - 70	$10^{0.5}$	-	$10^{1.2}$	-	$10^{2.4}$	$10^{3.2}$
MF1/8	70 - 80	-	$10^{0.85}$	$10^{1.2}$	-	$10^{2.45}$	$10^{3.0}$
MF1/9	80 - 90	$10^{0.35}$	-	$10^{1.2}$	-	$10^{2.4}$	-
MF1/10	90 - 100	-	$10^{0.85}$	-	$10^{2.1}$	-	-
Summary as typical peaks		$10^{0.35-0.5}$	$10^{0.85}$	$10^{1.2-1.3}$	$10^{2.0}$	$10^{2.4}$	$10^{2.8-3.2}$

*: Mode position refers to the highest point on its distribution curve, corresponds to the most frequently-occurring particle diameter

Clay mode (1): was determined in the range of mud-clay (100.35 to $100.5 \mu\text{m}$: $\sim 2 - 3 \mu\text{m}$). Shape of the mode is rather platokurtic. This mode appeared in low intensity scattered in low tidal mudflat and mangrove profiles of Dam Mon and Nha Phu. In shrimp pond profiles of the both regions, the peak of this mode appears all along the profile, and also in low intensity. Very fine silt mode (2): covers the range of mud ($100.85 \mu\text{m}$: $\sim 7 \mu\text{m}$), with distribution shape differs from platokurtic to normal. This mode appeared in all intervals of profiles in Dam Mon and South Central Coast. In comparison to sediments in Dam Mon, sediments in South Central Coast have higher intensity of mud mode.

Medium silt mode (3): shapes in platokurtic or normal distribution in range of $10^{1.2} - 10^{1.3} \mu\text{m}$ ($\sim 16 - 20 \mu\text{m}$). Rather popularly occurred in profiles of Nha Phu, however, this mode was generally absent in profiles of low tidal mudflat and shrimp pond of Dam Mon. Sandy silt mode (4): or coarse silt/very fine sand mode has peak position around $10^{2.0} \mu\text{m}$ ($\sim 100 \mu\text{m}$) with rather leptokurtic to normal distribution.

Similarly to the medium silt mode 3, the absence of sandy silt mode along the whole low tidal mudflat and shrimp pond profiles of Dam Mon, in opposite to Nha Phu profiles, was observed. Fine/medium sand mode: (5): located at the position of $10^{2.4} \mu\text{m}$ ($\sim 250 \mu\text{m}$), at the range of fine to medium sand. Leptokurtic is characteristic for the shape of these mode peaks. In Dam Mon, this fine sand mode has the highest intensity in the whole sediment profiles of low tidal mudflat and shrimp pond. In the upper parts of sediments in Dam Mon mangrove forest, intensity of this mode decreases. In vice versa, the presence of this mode in Nha Phu lagoon is only of low intensity for all profiles. The decrease of intensity in the surfaces layer of mangrove forest was also observed.

Coarse sand mode (6): is in range of $10^{2.8}$ - $10^{3.0}$ μm (~ 630 - 1000 μm), rather leptokurtic distributed. This mode appears in almost all intervals along Dam Mon and Nha Phu profiles.

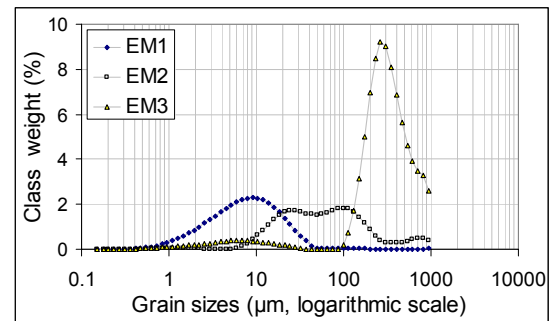
In order to address behaviour and to quantify influence of the determined modes in terms of real underlying principal processes, computation of principal end-members by EMMA approach were adopted for the whole measurement steps of GSD dataset. For dataset of the both regions: Dam Mon and Nha Phu, it was revealed that the sedimentation there was governed by 3 principal factors. Using 3 principal factors (representatively for the entire datasets) could be explained for 92.4 % and 88.9 % total variance of the underlying processes in sediments of Dam Mon and Nha Phu, respectively.

EMMA approach demonstrated contribution of 3 end-members as main modes to the GSD patterns of each investigated interval. Positions of end-member sets in Dam Mon and Nha Phu were comparable (Figure 4.11). The end-member EM 1 correlated to mode of fine silt size (~ 10 μm), and tended to shape in Gaussian unimode, comparably to mode 1 as revealed by deconvolution approach. The end-member EM 2 was not a real Gaussian unimode but rather a combination of a fine silt (~ 1.4 μm) mode and a silt (~ 100 μm) mode. In addition, a small tail in the range of clay was recognized in EM 2. EM 2 corresponded to mode 3 and 4 and the tail corresponded to mode 1.

The end-member EM 3 were a combination of two sand modes (one at size of ~ 50 μm and the other at size of $250 - 300$ μm) and a clay-fine silt tail, corresponding to modes 5, 6 and 1. The sandy silt mode end-member (EM 2) of Nha Phu sediments is comparable to EM 2 of Dam Mon, but contains greater amount of coarse particles. In vice versa, the sand mode end-member (EM 3) in Dam Mon is generally coarser than EM 3 in Nha Phu.

Based on the most highlighted feature of the determined end-members, EM 1, EM2 and EM3 were referred as fine silt mode, sandy silt mode and sand mode, respectively.

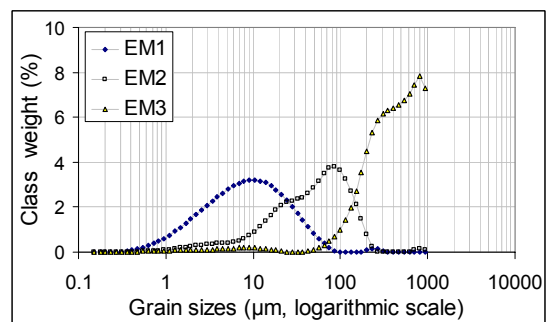
a) End-members of Dam Mon sediments



Total variance explained = 92.4%

Convergence at 921 steps.

b) End-member of Nha Phu sediments



Total variance explained = 88.9%

Convergence at 1610 steps

Figure 4.11. Modelled end-members of GSDs in coastal sediments of South Central Coast, central coast of Vietnam

EMMA approach for 3 components.

In the EMMA approach, contributions of the end-member along the sediment profiles were based on normalisation of score matrix to total of 100 %. The obtained results were displayed in Figure 4.12. The six sedimentary environments showed different behaviours in contribution of the end-member modes. EM 2 [fine silty - silty] were nearly lacked in LM and SP sediments of Dam Mon but showed fairly high contribution in MF profile of Dam Mon as well as all profiles of Nha Phu. In the both regions, from LM via MF to SP, it was revealed an increasing tendency of the end-member EM 1 [fine silty], with emphasis in higher part in profiles. However, layer of 10 cm upper in shrimp pond profiles of the both region showed a sudden depletion in contribution of EM 1, whereas contribution of EM 2 remained stable.

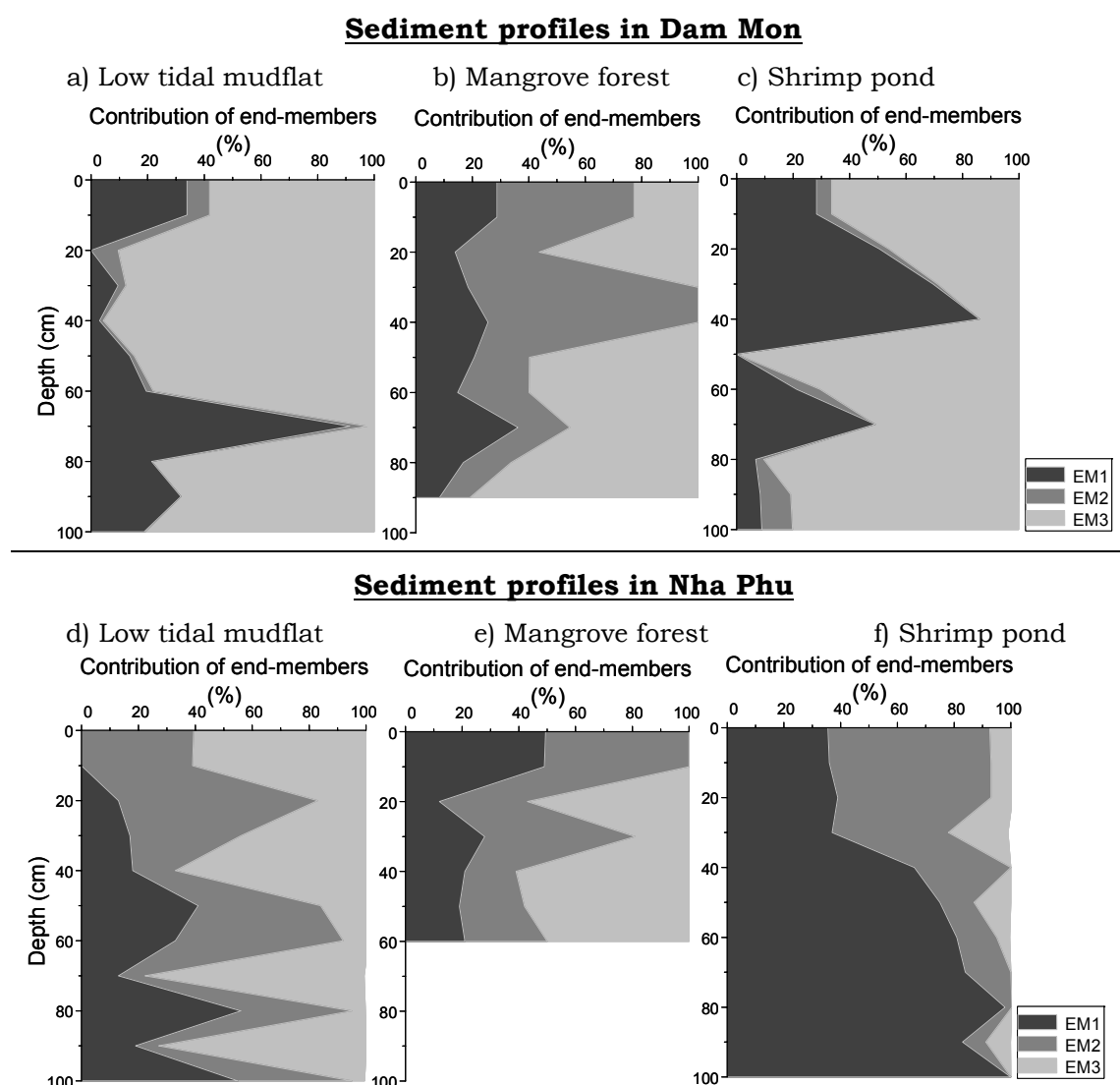


Figure 4.12. Contribution of end members in sediments at depth intervals in profiles of Dam Mon and Nha Phu, central coast of Vietnam

EMMA approach for 3 end-members.

EM 1 correlates to fine silt mode, EM2 to sandy silt mode and EM3 to sand mode

4.2 Nutrients

4.2.1 Red River Delta

Content of organic carbon (C_{org}), phosphate (P) and sulphurs (S) have been investigated, in order to determine how these principal nutrients behaved and distributed in granulometry - geochemistry- mineralogy network of environmental variation. In deltaic estuarine sediments of the Red River Delta, contents of C_{org} ranged from 0.4 – 1.0 %, total S from 0.11 to 0.28 % and total P from 0.15 to 0.22 % (Figure 4.13). Contents of C_{org} and P were high in surface sediments of MF profile (Figure 4.13a, c), whereas content of S depleted. In opposite, a high accumulation of sulphur was seen in surface layer of SP profile (Figure 4.13b).

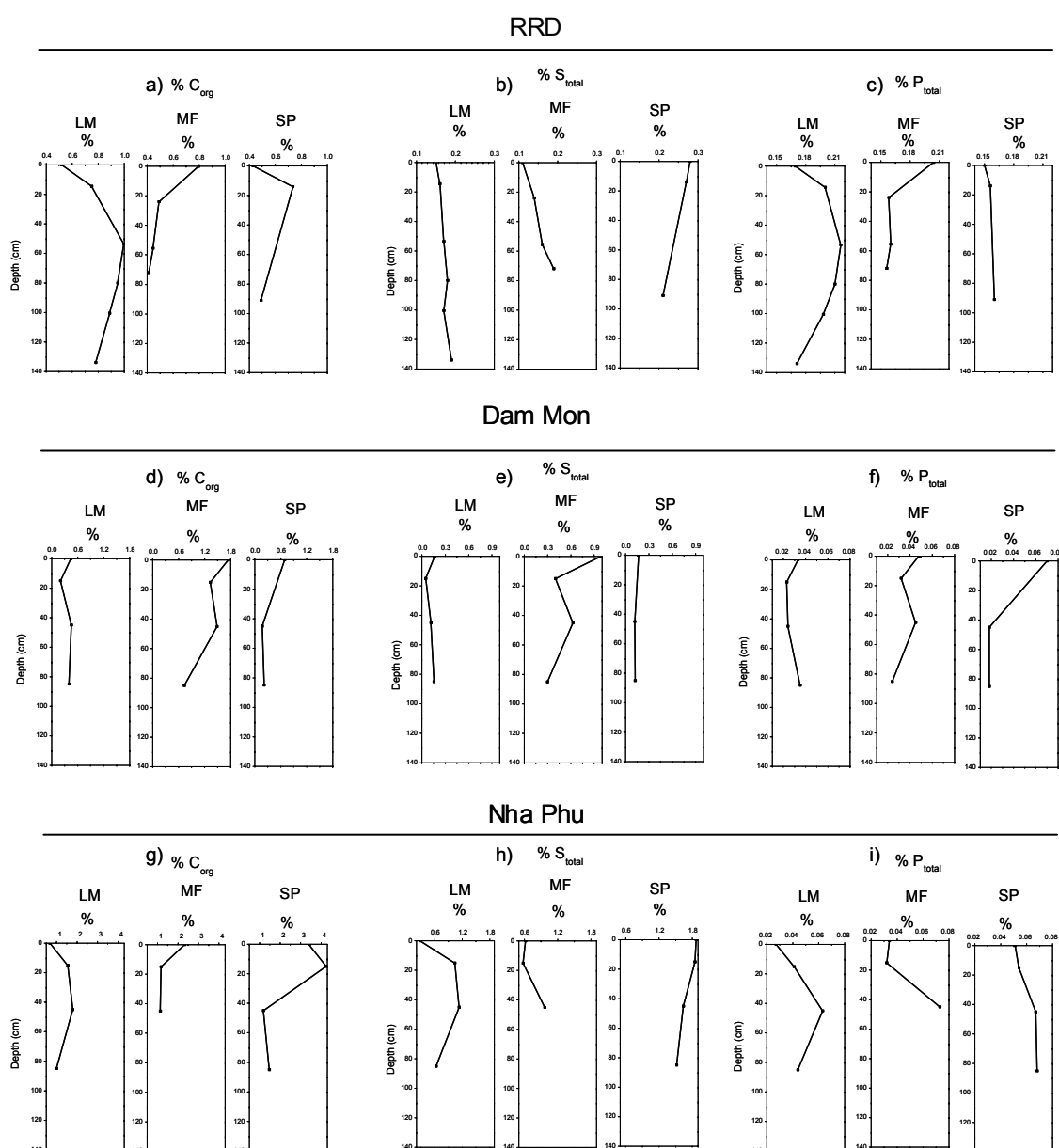


Figure 4.13. Distribution of nutrients according to depth profiles in coastal sediments of Red River Delta, Dam Mon and Nha Phu

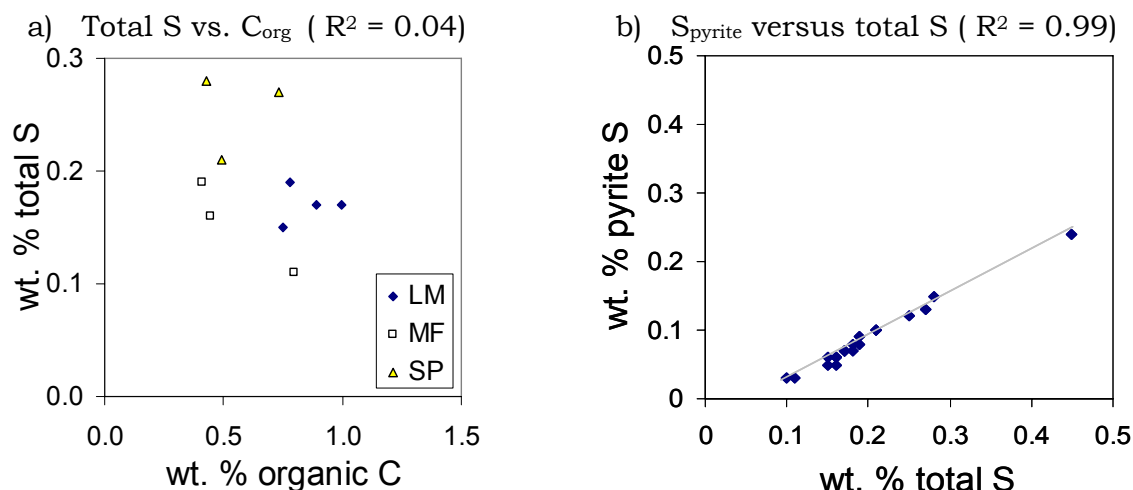


Figure 4.14. Net ecosystem stoichiometry of sediments in the Red River Delta estuary
a) total S versus $C_{organic}$; ; b) S_{pyrite} versus total S

In sediments of RRD, total sulphur exhibited no correlation with content of C_{org} (Figure 4.14a). In all intervals, approximately a half of sulphurs were detected to be in pyrite form (Figure 4.14b). The S_{pyrite}/S_{total} ratios remained unchanged among profiles of LM, MF and SP. The C/S ratios varied in wide range, from 1.5 – 7.2, generally high in tidal mudflats, and low in SP and lower part of MF profiles.

According to the depth, distributions of the nutrients C, S, P were different among the profiles LM, MF and SP. In LM profile, contents of C_{org} and P tended to accumulate at 60 cm depth layer. In surface layer occurred a slightly nutrient depletion (Figure 4.13a, c). Content of sulphur remained stable with depth (Figure 4.13b). In MF profiles, contents of C_{org} and P increased from the lower parts to upper parts in all profiles, especially intensive in surface layer (Figure 4.13a, c). Content of sulphur was high at 40 – 60 cm depth, but decreased significantly in surface layer (Figure 4.13b). In SP profile, the subsurface sediments had similar distribution of C_{org} and P as observed in MF profile. However, the surface sediments showed a completely different behaviour (Figure 4.13a, c). Therein, contents of C_{org} and P decreased suddenly and significantly. The distribution curves thus had the highest accumulation at near-surface layer (~20 cm depth). It is to remark in this profile that the sulphur content tended to accumulate highly, especially in surface layer.

4.2.2 South Central Coast

In sediments of South Central coast, contents of organic carbon and sulphur were much higher than those in sediments of the Red River Delta, but the content of phosphor was much lower. Contents of C_{org} ranged from 0.2 – 1.7 % in Dam Mon and 0.7 – 4.2 % in Nha Phu. Contents of sulphur ranged from 0.05 – 1 % in Dam Mon and 0.3 – 1.9 % in Nha Phu. Contents of total P in both areas were less than 0.1 %.

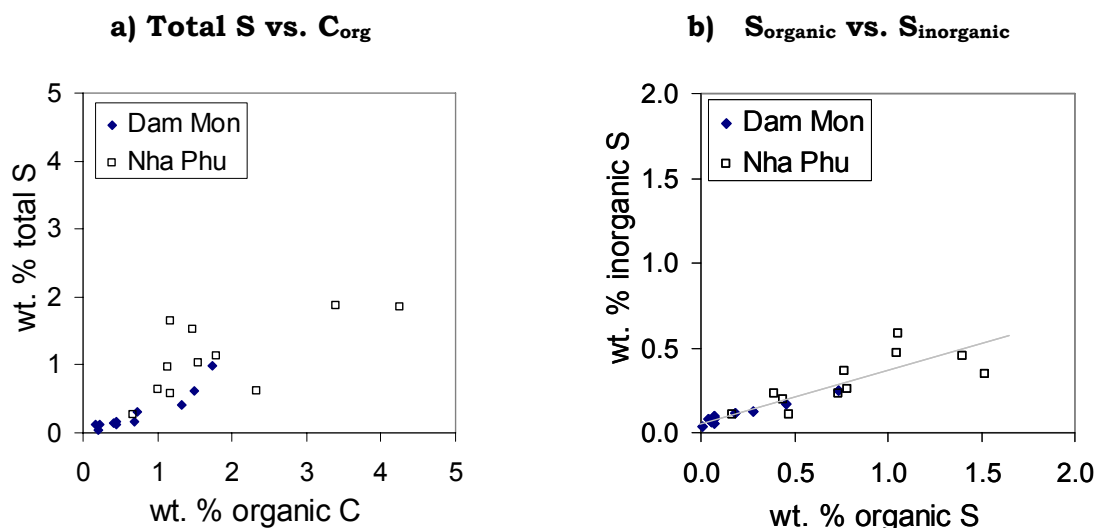


Figure 4.15. Net ecosystem stoichiometry of coastline muddy sediments of Dam Mon (dark diamond) and Nha Phu (empty square), central Vietnam

a) total S versus C_{org}; b) total P versus C_{org}

In Dam Mon, the nutrients C_{org}, S and P tended to accumulate highly in MF profiles but in Nha Phu, these matters in SP sediments were generally higher than in MF sediments (Figure 4.13d, e, f, g, h, i). In Dam Mon sediments, correlation between C_{org} and S (Figure 4.15a), S_{organic} and S_{inorganic} (Figure 4.15b) were relatively high. Distributions according to the depth of these nutrients were similar and co-varied from profile to profile (Figure 4.13d, e, f). Differently, in Nha Phu sediments, correlation between C_{org}, S, and P was low. Similar behaviours of these nutrients along the depth profiles were only observed in LM profile. In MF and SP, each nutrient behaved a distinctive behaviour.

Comparing to content of total sulphur, organic carbon was higher accumulated (C/S = 0.7 – 4.7). The C/S ratios in Nha Phu were generally higher than sediments in Dam Mon (Figure 4.15b). Of the total sulphur, the inorganic species accounted for approximately 30 %. Ratios of S_{inorganic} / S_{organic} were approximately 1: 3 and stable in all samples (Figure 4.15). The detected inorganic sulphur phases referred to high valent oxidized sulphur such as sulphonate and sulphate (Jokic et al. 2003).

According to the depth, distribution behaviours of C, S, P varies from profile to profile. In low tidal mudflat sediment, content of C_{org} was almost stable in the profile of Dam Mon but accumulation at 60 cm depth in the profile of Nha Phu. S and P showed the similar behaviours to C_{org}. In mangrove forest profiles of both regions, all nutrients tended to accumulate at 40 – 60 cm depth intervals (Figure 4.13d, e, f, g, h, i). Nutrients were also enriched in surface sediment in MF profile of Dam Mon. In shrimp pond sediments, sulphur was slightly accumulated in surface layer of profiles in both regions. Also, C_{org} increases from lower parts to upper part, and intensively concentrated in surface layer. Content of P was high in surface sediment of SP profile in Dam Mon but low in surface sediment of SP profile in Nha Phu.

4.3 Geochemistry

4.3.1 Physico-chemical condition (pH, Eh)

Red River Delta

Coastal tidal mudflats in the Red River estuary had pH ranging from 7.64 – 7.93 in 0 - 20 cm surface layer, and from 7.63 – 8.99 at deeper layers (20 – 100 cm), reflecting a chemical environment of neutral to slightly alkaline (WOTRO report, phase 1). Values of Eh of sediments in intertidal mudflats ranged from – 43 mV to 268 mV, reflecting conditions of weakly reductive to weakly oxidized potentials (WOTRO report, phase 1).

South Central Coast

Table 4.2. pH and Eh along depth profiles in low tidal mudflat (LM), mangrove forest (MF) and shrimp pond (SP) of coastal sediments in Dam Mon and Nha Phu

Depth (cm)	a) pH						b) Eh					
	Dam Mon			Nha Phu			Dam Mon			Nha Phu		
	old mangrove forest LM	MF	SP	young mangrove forest LM	MF	SP	old mangrove forest LM	MF	SP	young mangrove forest LM	MF	SP
0 - 10	8.87	8.4	8.37	8.41	8.37	8.18	87	7	27	25	27	-145
10 - 20	8.40	7.85	-	8.45	8.09	7.10	43	130	-	37	24	75
20 - 30	8.62	7.13	-	8.45	7.86	8.31	49	147	-	57	100	120
30 - 40	8.62	7.40	8.52	8.57	7.46	8.22	83	130	121	57	137	125
40 - 50	8.66	8.01	8.39	8.69	7.71	8.25	90	125	129	50	142	120
50 - 60	8.64	8.05	8.78	8.47	7.72	8.05	100	143	155	70	150	157
60 - 70	8.73	8.39	8.71	8.51	-	8.12	132	142	125	134	-	127
70 - 80	8.76	8.27	8.61	8.39	-	8.15	128	147	127	147	-	115
80 - 90	8.72	8.35	8.82	8.41	-	8.23	130	142	124	149	-	137
90 - 100	8.70	8.03	8.85	8.48	-	8.20	133	147	121	147	-	165

- : lack of sample; LM: low tidal mudflat; MF: mangrove forest; SP: shrimp pond

Sediments along the central coast of Vietnam had pH ranging from 7.13 – 8.87 (Table 4.2a), reflected *weakly alkaline environments*. pH of sediment profiles in Nha Phu embayment were generally lower than pH of sediment profiles in Dam Mon peninsular (Table 4.2a). *pH in sediments of low tidal mudflat (LM) profile were higher than those in shrimp pond (SP) profile and lowest in mangrove forest (MF) profile.*

Along the depth of LM and SP profiles, pH was rather stable (Table 4.2a). *Only in surface sediments (0 - 10 cm layer) of all profiles, pH increased, reflecting a higher alkaline condition. Exception in SP profile in Nha Phu was the lower pH value at the interval of 10 – 20 cm (see highlighted bars in Table 4.2a). In MF profiles, the intervals of 10 – 40 cm depth in Dam Mon and 20 – 60 cm depth in Nha Phu showed depletion in pH values (see highlighted bars in Table 4.2a), implying presence of a slightly acidification in these zones.*

Table 4.2b presents values of Eh along depth profiles of Dam Mon and Nha Phu. Eh ranged from -145 mV to 165 mV, reflecting *reductive to weakly oxidized redox potentials*, in both regions. Redox potentials of sediments in MF and SP profiles were generally higher than those in LM profiles, but showed an intensive depletion in 0 – 30 cm surface layers (see highlighted bars with italic manner in Table 4.2b). *In the intervals that had lower pH values* (i.e. 10 – 40 cm depth in DM-MF, 10 – 60 cm depth in NP-MF and 10 – 20 cm depth in NP-SP), redox conditions were distinctively with *higher Eh values than surface parts but slightly lower Eh values than the deeper parts* (see highlighted bars in Table 4.2b).

4.3.2 Major elements

The Table 4.3 presents concentrations of the major elements: Si, Ti, Al, Fe, Mg, Mn, Ca, Na, K, and P (traditionally as oxides) in coastline muddy sediments in case studies of RRD (North VN) and Dam Mon, Nha Phu (South Central Coast). A differentiation in chemical composition among sediments of three regions is noticed. Sediments in Dam Mon were characterized by high SiO₂ (86.91%) whereas Red River Delta and Nha Phu sediments showed lower SiO₂ concentration. RRD sediments contained the high amount of Al, Mg, Fe, Mn while Nha Phu sediments contained high amount of Ca, Na.

The high correlations among clay forming elements group (Al, Fe, Mg, Mn, Ti) were addressed based on correlation matrix (Table 8.5, Appendix). Furthermore, chemical correlations among major elements and samples as showed in PCA biplots (Figure 5.15b) allowed distinguishing clearly three zones corresponding to sample groups of RRD, DM, NP.

Table 4.3. Concentrations (%) of chemical elements in coastal sediments of Vietnam

		SiO ₂	TiO ₂	Al ₂ O ₃	Fe ₂ O ₃	MgO	MnO	CaO	Na ₂ O	K ₂ O	P ₂ O ₅	LOI	H ₂ O-	Sum
Red River Delta	Mean	67.5	0.8	13.2	4.5	1.7	0.10	1.2	1.0	2.1	0.1	4.9	0.6	98.73
	Min	60.9	0.8	11.1	0.7	1.5	0.06	0.6	0.9	1.8	0.1	4.4	0.5	
	Max	72.9	0.9	15.6	6.0	2.0	0.15	1.6	1.2	2.9	0.2	6.1	0.6	
	STDV	<i>4.0</i>	<i>0.0</i>	<i>1.7</i>	<i>1.4</i>	<i>0.2</i>	<i>0.00</i>	<i>0.2</i>	<i>0.1</i>	<i>0.3</i>	<i>0.0</i>	<i>0.7</i>	<i>0.0</i>	
Dam Mon	Mean	86.9	0.4	4.5	1.1	0.5	0.02	0.5	0.8	1.7	0.0	2.7	0.3	99.40
	Min	71.7	0.1	3.0	0.4	0.3	0.01	0.1	0.4	1.5	0.0	1.1	0.1	
	Max	92.4	0.7	11.2	2.7	0.8	0.04	1.6	2.1	3.1	0.1	6.2	0.8	
	STDV	<i>4.2</i>	<i>0.1</i>	<i>1.5</i>	<i>0.5</i>	<i>0.2</i>	<i>0.00</i>	<i>0.4</i>	<i>0.4</i>	<i>0.3</i>	<i>0.0</i>	<i>1.5</i>	<i>0.2</i>	
Nha Phu	Mean	69.4	0.5	11.3	3.4	0.8	0.05	1.3	1.7	2.5	0.1	6.6	1.5	99.12
	Min	51.3	0.3	7.4	1.1	0.3	0.03	0.6	1.2	2.2	0.0	2.3	0.3	
	Max	81.8	0.7	17.1	5.2	1.6	0.08	2.7	2.6	3.1	0.1	10.0	8.7	
	STDV	<i>7.6</i>	<i>0.1</i>	<i>3.0</i>	<i>1.2</i>	<i>0.4</i>	<i>0.00</i>	<i>0.5</i>	<i>0.3</i>	<i>0.2</i>	<i>0.0</i>	<i>2.1</i>	<i>1.9</i>	
Near shore muds*		58.9	0.78	16.7	6.9	2.6	0.09	2.2	1.6	3.6				

*: Average the world near-shore mud, after different authors from Wedepohl (1965)

Red River Delta

Bulk chemistry

Table 4.4. Average, standard deviations, minimum and maximum concentration of the studied major chemical elements in the estuarine muddy sediments of the Red River Delta

Environment		MAJOR ELEMENTS (%)										Total
		SiO ₂	TiO ₂	Al ₂ O ₃	Fe ₂ O ₃	MgO	MnO	CaO	Na ₂ O	K ₂ O	LOI	
Low tidal mudflat	Mean	63.5	0.8	14.5	5.6	1.9	0.12	1.4	1.1	2.2	6.9	98.76
	Min	60.9	0.8	12.3	4.9	1.6	0.08	1.2	1.0	2.0	5.6	
	Max	68.3	0.9	15.6	6.0	2.0	0.15	1.6	1.2	2.4	7.7	
	STDV	2.6	0.0	1.2	0.4	0.1	0.02	0.1	0.1	0.2	0.7	
Mangrove forest	Mean	70.4	0.8	12.4	4.3	1.6	0.08	0.9	0.9	1.9	5.0	98.94
	Min	65.7	0.8	11.1	4.1	1.5	0.06	0.8	0.9	1.8	4.3	
	Max	72.9	0.9	14.6	4.6	1.9	0.11	1.0	1.0	2.2	6.3	
	STDV	2.9	0.0	1.4	0.2	0.1	0.02	0.1	0.0	0.2	0.8	
Shrimp pond	Mean	70.6	0.8	12.0	4.5	1.6	0.06	1.0	1.2	1.8	5.0	98.84
	Min	70.0	0.8	11.3	4.2	1.5	0.06	0.6	1.1	1.8	4.7	
	Max	71.1	0.8	12.4	4.7	1.6	0.07	1.3	1.2	1.9	5.6	
	STDV	0.5	0.0	0.5	0.2	0.0	0.00	0.3	0.1	0.1	0.4	
Estuarine alluvia		57.97	0.91	16.92	6.41	2.15	0.10	1.25	1.38	2.84	9.02	98.96
Near shore muds*		58.90	0.78	16.70	6.90	2.60	0.09	2.20	1.60	3.6		

*: Average world near-shore muds, after different authors from Wedepohl (1960)

In Table 4.4, the average values as well as of concentration ranges of LM, MF, SP and estuarine alluvia (i.e. the bottom alluvia sediments deposited in front of the Red River estuary) are shown. Sediments exhibited *low variation among sedimentary environments*. Concentrations of clay-forming elements (i.e. Al, Fe, Mg, Mn, K) in sediments of low tidal mudflat profile were higher than those in sediments of mangrove forest and shrimp pond. Concentration of Na was high in low tidal mudflat and concentration of Ca was high in shrimp pond.

In sediments, SiO₂ presents mostly as quartz and rationally contributions in silicate minerals. Therefore, increase or decrease of SiO₂ in bulk samples points to variation of quartz content. The Fe₂O₃ concentrations determined included both trivalent Fe and divalent Fe, as some amount of divalent Fe can be oxidized when samples were exposed to the air oxygen. K₂O was related to K-Feldspar in coarse fractions (i.e. sand, silt) and to K bearing micaceous clay minerals in fine fractions. LOI was a function of calcium carbonate, structural water (from clay minerals), organic matter and other volatiles released during the ignition (Manjunatha & Shankar 1997).

Correlations among major chemical elements

As shown in the xy-plots for some selected key elements of all sediments samples in RRD, Al₂O₃ and Si₂O were highly linear anti-correlated. Al₂O₃ showed high correlations with MgO, Fe₂O₃ and MnO, but low correlations with K (Figure 4.16). Although concentrations of Fe, Mg, K in SP were lower than in LM and MF, the enrichment ratios to Al were similar.

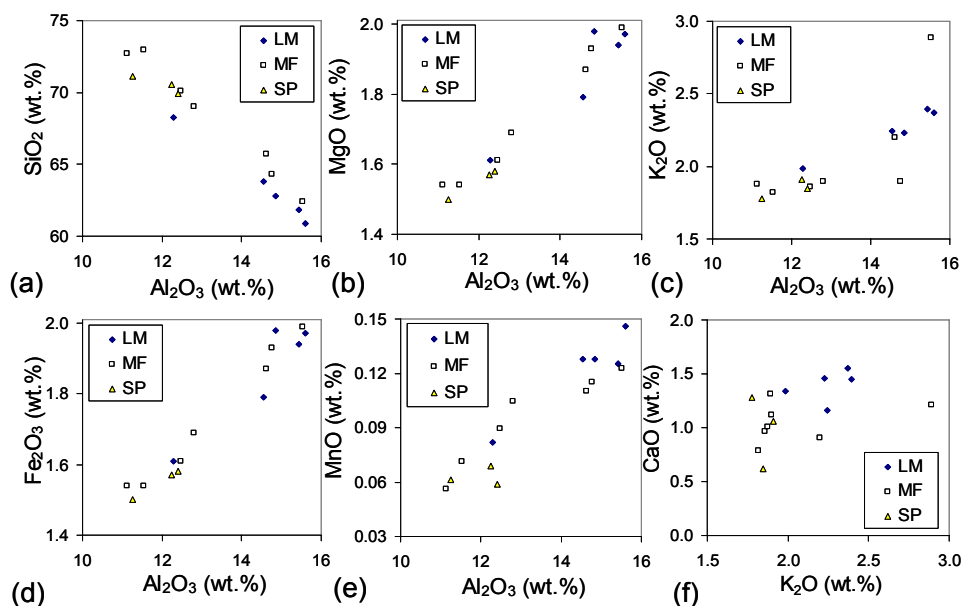


Figure 4.16. Scatter diagrams of selected elements for RRD sediments

LM: low tidal mudflat; MF: mangrove forest; SP: shrimp pond

Distribution of chemical elements in grain size fractions

The distribution of major elements with grain size distribution are presented in Table 4.5 for five sediment samples in LM, MF and SP profiles of RRD. *In all samples, except for Si, Ca and Na, all the elements showed increase in concentration continuously from the coarsest fractions ($> 63 \mu\text{m}$) to finest fractions ($< 2 \mu\text{m}$).* Concentrations of Al_2O_3 in fractions $< 2 \mu\text{m}$ were 2.3 to 6.6 times higher than those in fractions $> 63 \mu\text{m}$. In similar manner, concentrations of other clay-forming elements (i.e. Mg, Fe, Ti, Mn, K) had concentrations in fractions $< 2 \mu\text{m}$ of 1.5 to 3.8 times higher than their concentrations in fractions $> 63 \mu\text{m}$.

In opposite to clay-forming elements, *Si shows clear decreasing concentrations with decreasing grain sizes.* Concentrations of SiO_2 in the fractions $< 2 \mu\text{m}$ were 1.4 to 1.8 times lower than those in the fractions $> 63 \mu\text{m}$. Different from other elements, *Ca and Na showed the highest concentrations at 6.3 - $63 \mu\text{m}$ range, and slightly depleted in finer fractions.* Variation of LOI and adsorbed H_2O exhibits similar tendency as clay-forming elements, which *accumulate more intensively in finer fractions.*

Factor analysis (Figure 4.17) indicated that these chemical variances could be represented by 3 principal factors: F1 (Al_2O_3 , MgO, K_2O , Fe_2O_3 , MnO) and negative F1 (SiO_2), F2 (TiO_2) and F3 (Na_2O and CaO). Therefore distribution behaviour according to grain sizes of the following groups of elements was determined:

- i) Si (-F1) occurred dominantly in fraction $> 63 \mu\text{m}$ and decreased gradually with finer sizes.

ii) Al, Mg, K, Fe, Mn (F1) (clay forming elements group) showed similar distribution, highly concentrating in fraction $< 2\mu\text{m}$ and than decreasing in coarser sizes, an opposite behaviour to Si. The concentration of absorbed water was similar to this group.

iii) Ti (F2) had low concentration in fraction $> 63\mu\text{m}$ with rather stable concentration in finer fractions. Slightly accumulation in the fractions $< 6.3\mu\text{m}$ could be seen.

iv) Ca and Na (F3) appeared dominantly in fractions of $20 - 63\mu\text{m}$, and decreased with finer sizes.

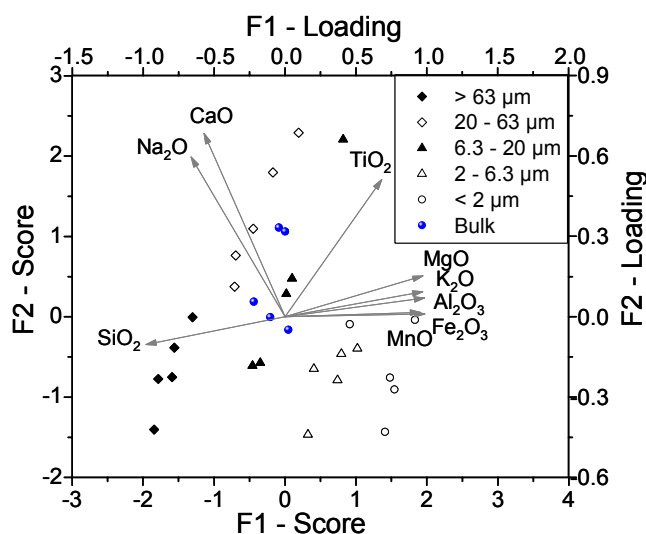


Figure 4.17. PCA biplots of chemical parameters for grain sizes fractions in the Red River Delta

On example of sample RRD-MF (0 -3 cm)

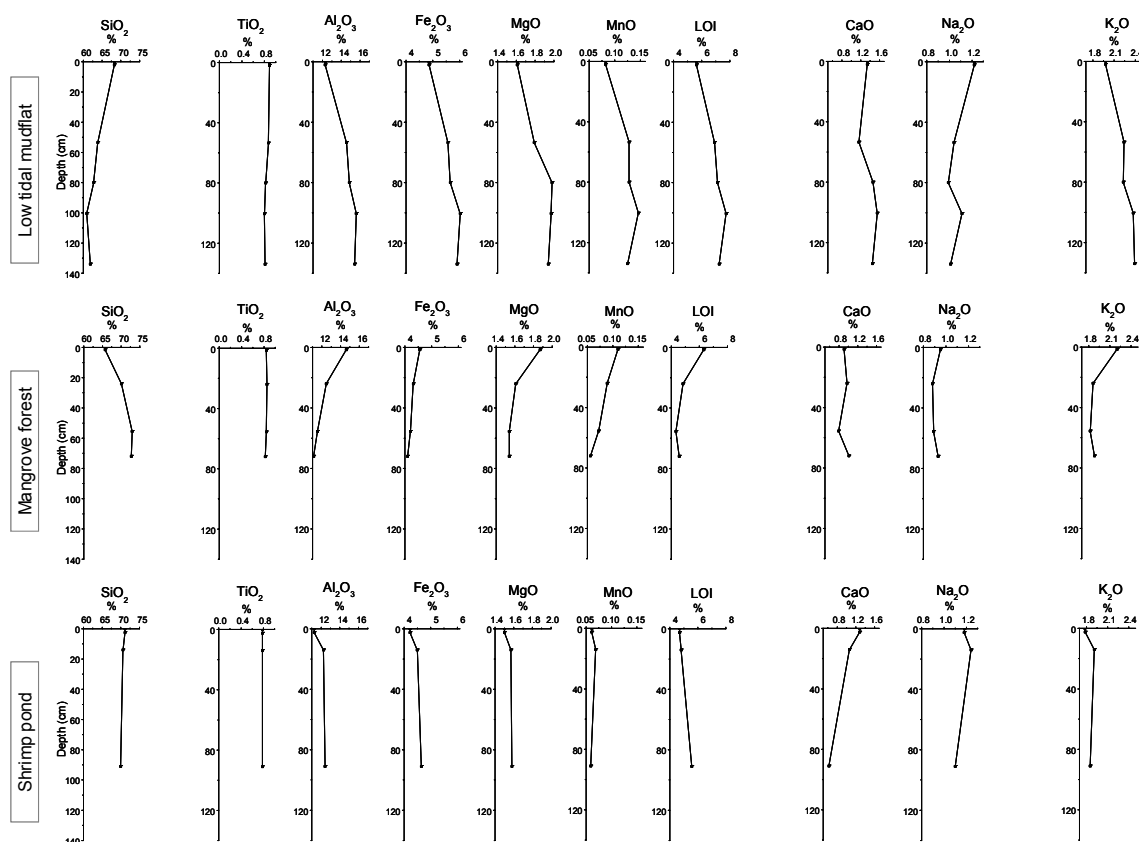


Figure 4.18. Chemical variation according to the depth in profiles of LM (a), MF (b), SP (c) in estuary of the Red River Delta

Table 4.5. Distribution of major elements (wt. %) in grain size fractions of sediment samples in RRD

Profile	Depth		wt. %	SiO ₂	Al ₂ O ₃	Fe ₂ O ₃	MnO	MgO	CaO	Na ₂ O	K ₂ O	P ₂ O ₅	GV1000°C	H ₂ O	Sum (%)
LM	0 - 3 cm	BULK	in bulk	68.34	12.45	4.97	0.08	1.55	1.20	1.00	2.02	0.12	4.49	0.43	96.6
		> 63 µm	48%	78.91	9.19	3.53	0.06	1.19	1.20	0.88	1.70	0.08	2.97	0.16	99.9
		20 - 63 µm	16%	74.45	10.62	4.24	0.06	1.49	1.51	1.19	1.72	0.14	3.20	0.24	98.9
		6.3 - 20 µm	16%	67.32	14.46	5.47	0.10	1.96	1.30	1.65	2.35	0.13	5.18	0.48	100.4
		2 - 6.3 µm	10%	56.94	19.22	7.86	0.15	2.30	1.06	0.67	2.85	0.16	7.65	0.75	99.6
		< 2 µm	10%	43.65	25.28	11.08	0.14	2.48	1.09	0.90	3.31	0.23	11.05	1.77	101.0
SP	0 - 3 cm	BULK		69.49	10.72	3.99	0.08	1.41	0.60	0.90	1.68	0.12	3.77	0.55	93.3
		> 63 µm	29%	85.58	4.17	2.82	0.04	1.09	0.68	1.00	1.40	0.08	2.74	0.25	99.8
		20 - 63 µm	22%	83.44	6.73	3.00	0.04	1.18	0.69	1.14	1.33	0.12	2.32	0.24	100.2
		6.3 - 20 µm	18%	76.24	9.00	4.04	0.08	1.55	0.59	1.06	1.74	0.13	3.56	0.43	98.4
		2 - 6.3 µm	14%	65.93	17.32	5.08	0.12	1.86	0.51	0.73	2.20	0.13	4.93	0.71	99.5
		< 2 µm	17%	49.98	27.59	7.47	0.16	2.12	0.59	0.62	2.60	0.21	7.70	1.60	100.6
MF	0 - 3 cm	BULK		65.14	12.85	4.63	0.11	1.90	1.00	1.01	2.26	0.13	5.06	0.62	94.7
		> 63 µm	24%	81.91	5.58	3.09	0.06	1.44	0.93	0.97	1.87	0.08	3.70	0.29	99.9
		20 - 63 µm	20%	80.84	4.86	3.26	0.06	1.68	1.27	1.61	1.87	0.13	2.90	0.26	98.7
		6.3 - 20 µm	20%	71.31	12.07	4.20	0.11	2.13	1.13	1.23	2.34	0.13	4.64	0.46	99.7
		2 - 6.3 µm	13%	63.40	14.91	5.76	0.20	2.45	1.05	0.80	2.84	0.15	6.36	0.80	98.7
		< 2 µm	23%	49.85	22.44	8.48	0.20	2.61	0.99	0.77	3.28	0.22	9.41	1.48	99.7
MF	53 - 56 cm	BULK		69.88	11.92	4.32	0.07	1.60	0.87	0.91	1.94	0.11	4.29	0.39	96.3
		> 63 µm	45%	82.26	7.01	3.04	0.05	1.26	0.91	0.91	1.66	0.08	2.85	0.19	100.2
		20 - 63 µm	19%	79.52	8.44	3.62	0.05	1.46	1.01	1.17	1.63	0.13	2.91	0.19	100.1
		6.3 - 20 µm	16%	70.11	12.82	4.82	0.09	1.96	0.87	1.15	2.18	0.12	4.95	0.48	99.5
		2 - 6.3 µm	10%	59.71	18.14	6.65	0.14	2.36	0.76	0.74	2.74	0.15	7.25	0.62	99.3
		< 2 µm	11%	47.07	25.07	9.33	0.17	2.55	0.83	0.62	3.19	0.22	10.28	1.37	100.7
MF	71 - 73 cm	BULK		70.81	11.27	4.14	0.06	1.51	0.80	0.89	1.81	0.11	4.14	0.34	95.9
		> 63 µm	43%	79.96	8.47	3.16	0.05	1.31	0.88	1.05	1.70	0.07	3.12	0.15	99.9
		20 - 63 µm	19%	78.80	8.69	3.42	0.04	1.30	0.91	0.99	1.45	0.12	2.91	0.17	98.8
		6.3 - 20 µm	11%	72.03	12.89	4.63	0.06	1.73	0.66	0.93	1.95	0.12	4.46	0.38	99.8
		2 - 6.3 µm	9%	64.65	16.95	6.03	0.10	2.09	0.69	0.73	2.37	0.14	6.25	0.50	100.5
		< 2 µm	17%	58.77	19.71	7.05	0.10	2.12	0.84	0.67	2.48	0.18	7.68	0.95	100.6

Variation of major elements with depth

Concentrations and variations of major elements according to the depth are presented in Figure 4.18. Along all sediment profiles, behaviours of major chemical elements followed five main groups: (i) Si, (ii) Ti, (iii) clay forming elements - Al, Fe, Mg, Mn, (iv) Ca, Na and (v) K.

In low tidal mudflat profile, SiO₂ decreased with depth, Ti remained stable, clay forming elements increased with depth as compensation for the decrease of Si, Ca and Na concentrated highly in surface layer and K increased with depth.

In mangrove forest profile, the tendencies were different from LM profile. SiO₂ increased with depth, Ti remained stable, clay forming elements accumulated highly in surface layer, Ca and Na were mostly stable with lightly accumulation in surface layer, K was also accumulated in surface layer.

In shrimp pond profile, concentrations of all major elements were fairly stable with depth. Readable variation was only in thin surface layer (0 - 3 cm), where SiO₂ increased suddenly and leaching of Al₂O₃, Fe₂O₃, TiO₂, MgO, MnO and K₂O as reverse. Concentrations of CaO and Na₂O were high in surface sediments, similarly to their behaviours in LM and MF profiles.

South Central Coast

Concentrations of major chemical elements of sediments in coastal tidal environments (LM, MF, SP) of Dam Mon and Nha Phu are presented in the Table 4.6. Sediments in Dam Mon were enriched with SiO₂ (71.72 – 92.42 %), followed by Al₂O₃ and K₂O. Sediments in Nha Phu contained less SiO₂ but more Al₂O₃, Fe₂O₃, K₂O, CaO and Na₂O. In Dam Mon, sediments in MF contained higher concentrations of clay-forming elements and also LOI, in comparison to LM and SP sediments. Concentration of Ca was high in LM profile. In Nha Phu, concentration of clay-forming elements and LOI were also high in MF and SP, relatively to sediments in LM. Concentration of Ca was high in LM and SP profiles.

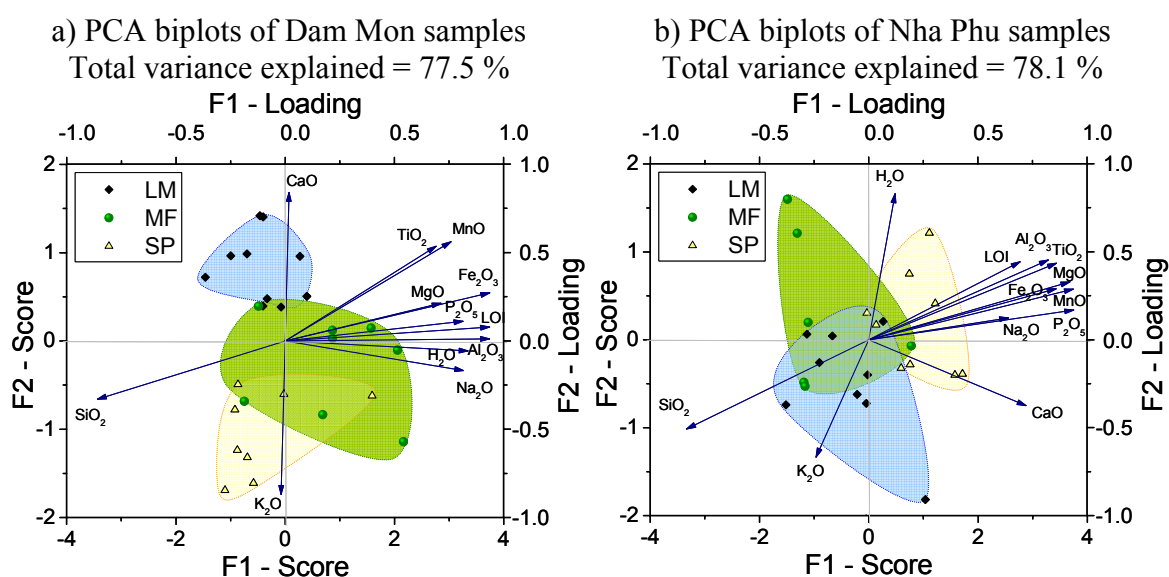
Correlations among major chemical elements

Factor analysis for dataset of samples in Dam Mon indicated the chemical grouping of major elements according to 4 principal components: F1 (Al₂O₃, Fe₂O₃, TiO₂, MnO, LOI and H₂O) and negative F1 (SiO₂), F2 (Al₂O₃, Fe₂O₃, MgO, P₂O₅), F3 (CaO) and negative F3 (K₂O) and F4 (Na₂O), as reflected by groups of high correlation coefficients in Table 8.3 (Appendix). The potential of total explaining variance of F1, F2, F3 and F4 were 61.7, 15.8, 9.4 and 4.1 %, respectively. Considering the influence of the two first factors F1 and F2 on the samples (see PCA biplots in Figure 4.19a), *three groups of samples corresponding to every investigated environment (LM or MF or SP) were well distinguished*. Chemical values of samples distributed along Ca – K correlation line. *Sediments in LM profile correlated to variance of calcium and sediments in SP profile correlated with variance of potassium. MF sediments acted as intermediate and also higher influenced by clay forming elements group.*

Table 4.6. Average, standard deviations, minimum and maximum concentrations of major elements in the coastline muddy sediments of Dam Mon and Nha Phu

Environment		MAJOR ELEMENTS (%)										
		SiO ₂	TiO ₂	Al ₂ O ₃	Fe ₂ O ₃	MgO	MnO	CaO	Na ₂ O	K ₂ O	LOI	total
Dam Mon sediments												
Low tidal mudflat	Mean	87.9	0.4	4.0	0.9	0.5	0.02	0.7	0.7	1.5	2.2	98.79
	Min	86.3	0.3	3.0	0.5	0.3	0.01	0.4	0.5	1.5	1.4	
	Max	91.8	0.5	5.1	1.3	0.8	0.03	1.0	1.2	1.6	3.1	
	STDV	1.66	0.08	0.64	0.25	0.17	0.00	0.23	0.20	0.03	0.48	
Mangrove forest	Mean	83.7	0.5	5.4	1.4	0.5	0.03	0.5	1.1	1.8	4.7	99.67
	Min	71.7	0.3	3.7	0.7	0.3	0.01	0.1	0.5	1.6	2.0	
	Max	91.5	0.7	11.2	2.7	0.7	0.04	1.6	2.1	3.1	7.0	
	STDV	4.77	0.14	2.04	0.51	0.10	0.01	0.49	0.44	0.44	1.45	
Shrimp pond	Mean	89.1	0.3	4.2	0.8	0.5	0.01	0.4	0.9	1.8	2.0	99.90
	Min	84.1	0.1	3.4	0.4	0.3	0.01	0.1	0.4	1.7	1.2	
	Max	92.4	0.3	5.3	1.4	0.8	0.02	0.7	1.4	1.9	3.5	
	STDV	2.44	0.06	0.60	0.31	0.18	0.00	0.21	0.33	0.06	0.76	
Nha Phu sediments												
Low tidal mudflat	Mean	74.4	0.4	9.4	2.9	0.7	0.04	1.4	1.6	2.6	5.8	99.20
	Min	67.1	0.3	7.4	1.1	0.3	0.03	0.9	1.2	2.2	2.6	
	Max	81.8	0.5	12.6	4.1	1.1	0.05	2.7	1.9	3.1	8.7	
	STDV	4.49	0.06	1.54	0.86	0.21	0.01	0.49	0.22	0.25	1.84	
Mangrove forest	Mean	72.9	0.4	9.8	2.4	0.5	0.03	0.7	1.7	2.6	7.9	98.94
	Min	64.3	0.3	8.1	1.6	0.4	0.03	0.6	1.3	2.5	4.5	
	Max	78.1	0.5	13.6	3.9	1.0	0.04	0.8	2.6	2.8	14.3	
	STDV	4.77	0.07	1.75	0.70	0.21	0.01	0.12	0.44	0.11	3.72	
Shrimp pond	Mean	62.2	0.6	14.2	4.5	1.2	0.06	1.5	1.9	2.4	10.6	99.14
	Min	51.3	0.5	10.9	3.6	0.7	0.04	0.9	1.7	2.2	7.4	
	Max	68.4	0.7	17.1	5.2	1.6	0.08	2.2	2.2	2.4	18.7	
	STDV	5.17	0.08	2.25	0.54	0.30	0.01	0.38	0.21	0.07	3.28	
Near-shore muds*		58.9	0.78	16.7	6.9	2.6	0.09	2.2	1.6	3.6		

*: Average world near-shore muds, after different authors from Wedepohl (1965)

**Figure 4.19. PCA biplots on major chemical elements in sediment samples in Dam Mon (a) and Nha Phu (b)**

Extraction Method: PCA with varimax rotation and Kaiser normalization

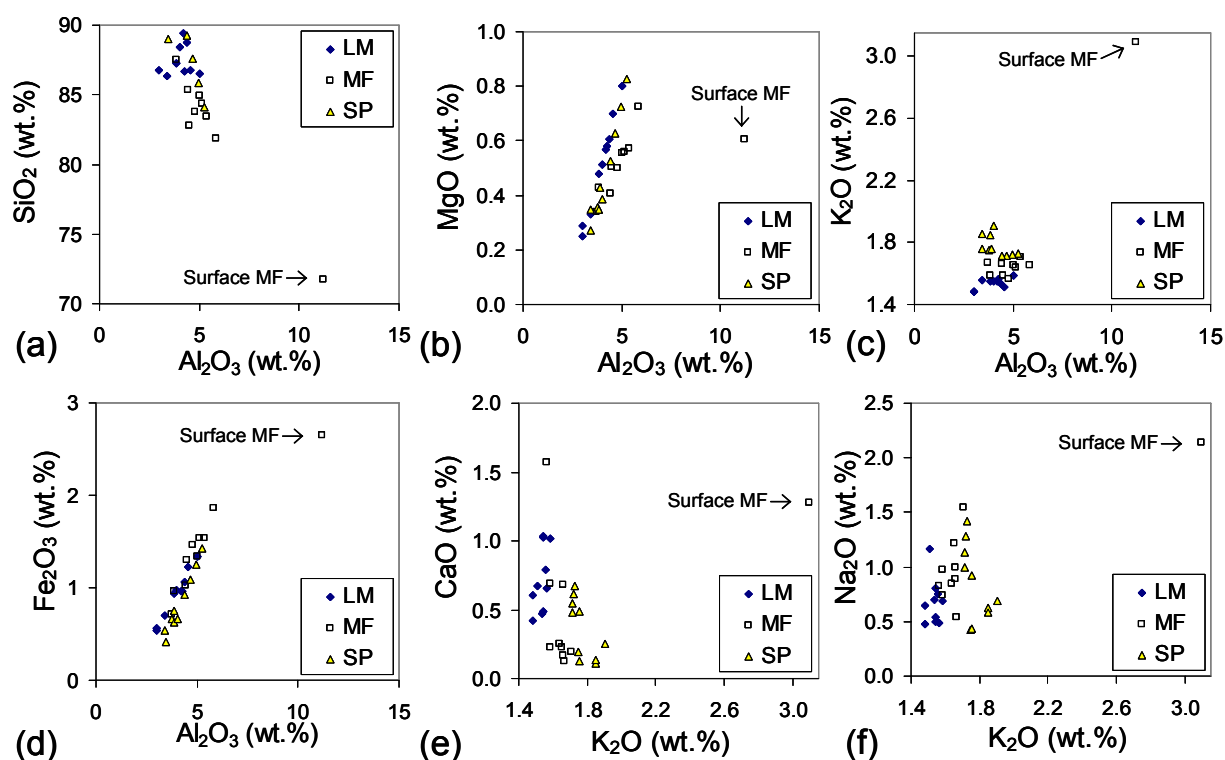


Figure 4.20. Scatter diagrams of selected elements for muddy sediments in the Dam Mon
 LM: low tidal mudflat; MF: mangrove forest; SP: shrimp pond

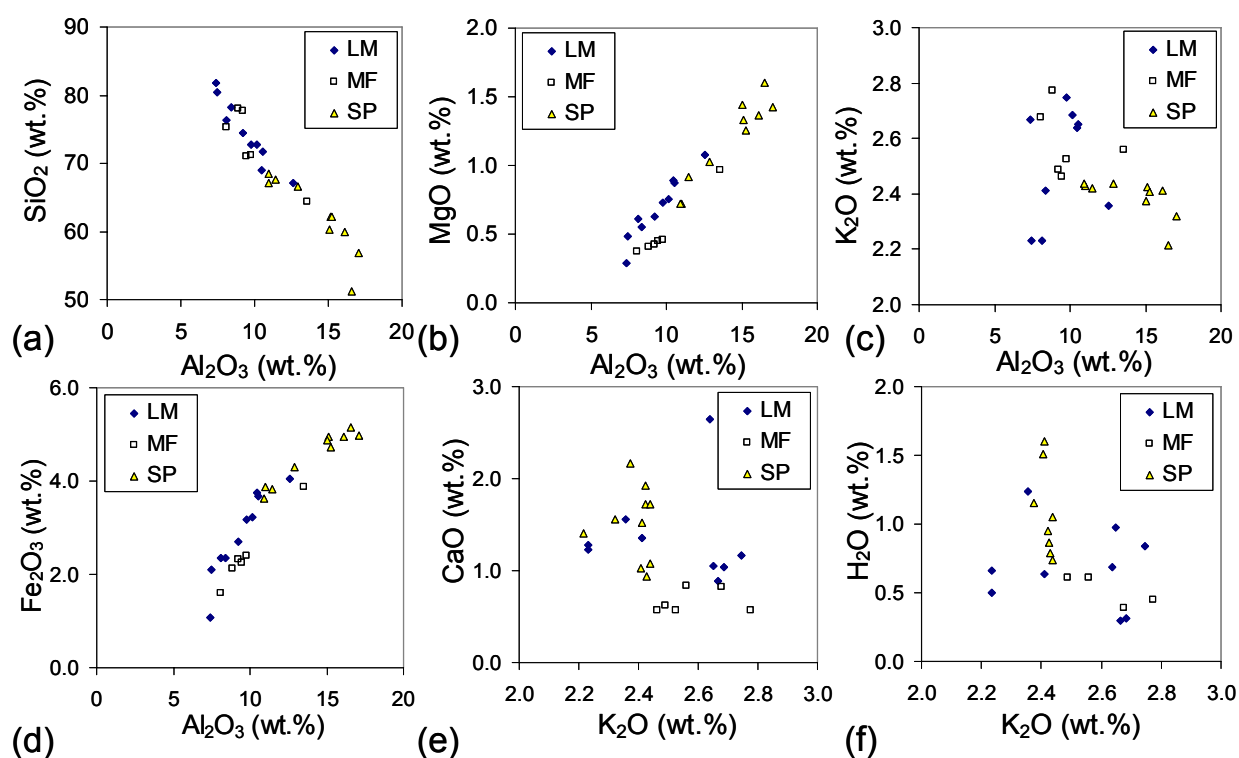


Figure 4.21. Scatter diagrams of selected elements for muddy sediments in the Nha Phu
 LM: low tidal mudflat; MF: mangrove forest; SP: shrimp pond

Chemical variances in samples of Nha Phu were also highlighted by 4 principal factors (Table 8.3, Appendix): F1 (Al_2O_3 , Fe_2O_3 , MgO , Na_2O , P_2O_5 , *LOI*) and negative F1 (SiO_2), F2 (Al_2O_3 , Fe_2O_3 , MgO , MnO , CaO , TiO_2 , P_2O_5), negative F3 (K_2O) and F4 (H_2O). The components F1, F2, F3 and F4 could explain for 67.2, 10.9, 10.0 and 5.2 % of total variance, respectively. *Differentiations according to sediment profiles in Nha Phu were observed, however not so typically, in PCA biplots (Figure 4.19b). Sediments in SP profile correlated to groups of clay-forming elements, and were influenced of both CaO and H₂O parameters. Sediments of LM were highly influenced by variation in potassium concentration whereas sediments in MF profile were coherent with changing of adsorbed water content.*

In order to investigate chemical behaviours of sediments in relation to principal variations, scatter diagrams of some selected elements were developed (Figure 4.20). Selection of plotted elements was based on the above results from factor analysis, including Si, Al, Mg, Fe, Ca, K and Na. SiO_2 . SiO_2 (negative F1 factor) showed a fairly high inverse correlation with Al (representative for both F1 and F2) in both regions Dam Mon and Nha Phu. Mg and Fe showed high correlation with Al, whereas the correlations among Ca, K, Na and Al were low.

In coastal sediments of Dam Mon, the sample of surface sediment in MF profile were separately examined as it was anomaly from the others (Figure 4.20). Sediments in Dam Mon showed narrow ranges of samples at the high Si concentration and low Al, K, Na, Ca. Concentrations of Fe were fairly stable with only slight enrichment in MF relative to those in LM and SP profiles. At a given Al concentration, Mg concentrations were slightly higher in LM sediments relatively to MF and SP sediments. At a given Al concentration, from LM via MF to SP profiles, concentrations of K, Na increased when Ca decreased.

Sediments in Nha Phu showed scatter values in wide range of all elements: Si, Al, K, Ca, and Na (Figure 4.20). At a given Al concentration, MF sediments had slightly lower concentrations of Fe and Mg. Whereas Al, Fe, Mg, Ca and adsorbed water were highest accumulated in SP profile, these elements were reversely depleted in MF sediments.

Variation of major elements with depth

Behaviour of major elements according to the depth followed four main groups: (i) Si, (ii) clay forming elements (Al, Ti, Fe, Mg, Mn) and *LOI*, (iii) Ca and Na and (iv) K. These groups were corresponding to principal factors which were obtained by PCA treatment.

In coastal sediments of Dam Mon, concentrations of SiO_2 were high and relatively stable along the depth of all profiles (Figure 4.22). In surface sediments of MF, SiO_2 decreased

slightly in surface layer whereas concentrations of clay-forming elements, LOI and Na, Ca, K were enhanced. Along this MF profile, concentrations of clay-forming elements decreased slightly with increasing depth but K had stable concentration. Ca and Na showed some anomaly increase in some intervals might be resulted from contamination with shell fragments and sea salt. The irregular behaviours of Ca were also clear to see in low tidal mudflat profile, with anomaly increase in some intervals. In shrimp pond, concentrations of clay-forming elements and Na, Ca decreased slightly with increasing depth, but K remained stable.

In sediments of Nha Phu (Figure 4.23), concentrations of SiO_2 and clay-forming elements were irregular with depth, interlayering between intervals with high SiO_2 and intervals with low SiO_2 . This irregular trend was most obvious in low tidal mudflat profile and also in mangrove forest profile. It is to notice the corresponding behaviour of LOI, clay-forming elements, Na versus irregular variations of SiO_2 . Similarly to their behaviours in Dam Mon, concentrations of Ca in Nha Phu exhibited high values in some intervals irregularly. Meanwhile, concentrations of K remained stable with depth. Slightly accumulation of clay-forming elements was to observe in surface layer (10 – 20 cm) of mangrove forest, together with LOI and Na concentration (Figure 4.23). In shrimp pond profile, SiO_2 decreased with depth and clay –forming elements increased as compensation. However concentration of K was still unchanged.

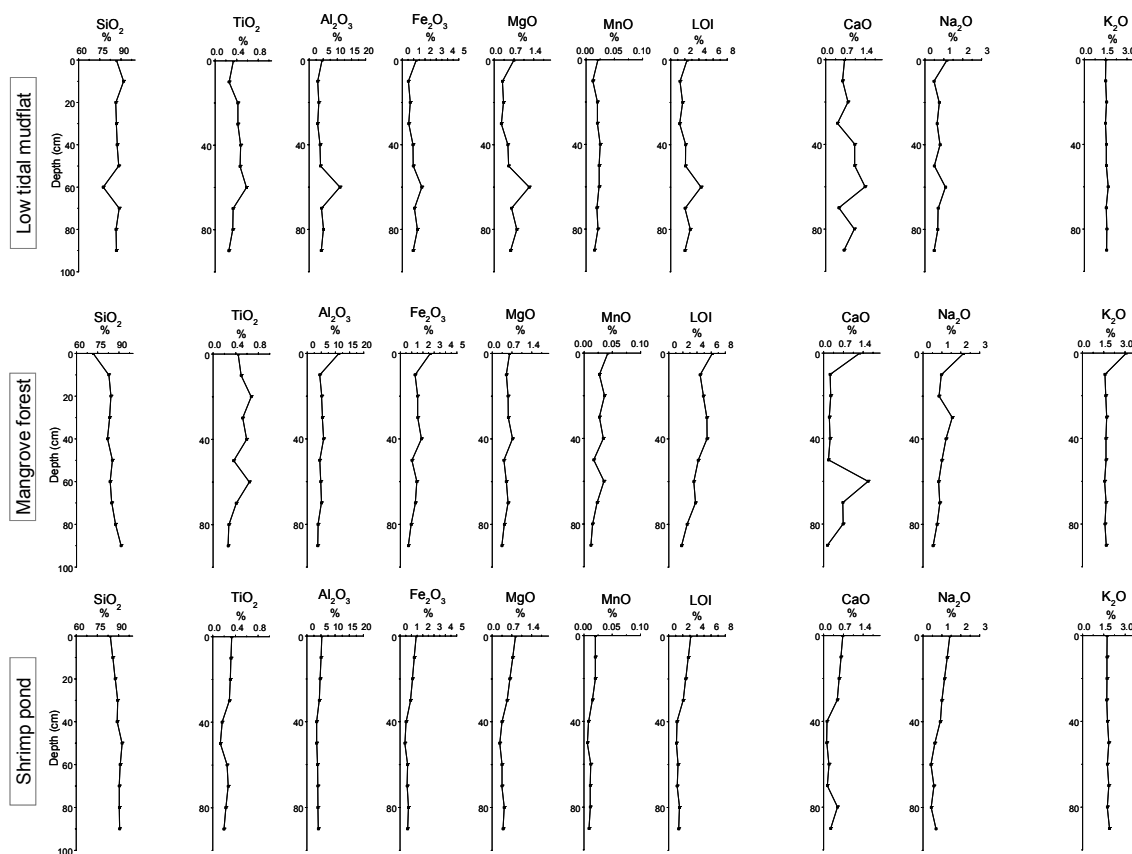


Figure 4.22. Variation of major elements according to depth in sediment profile of Dam Mon

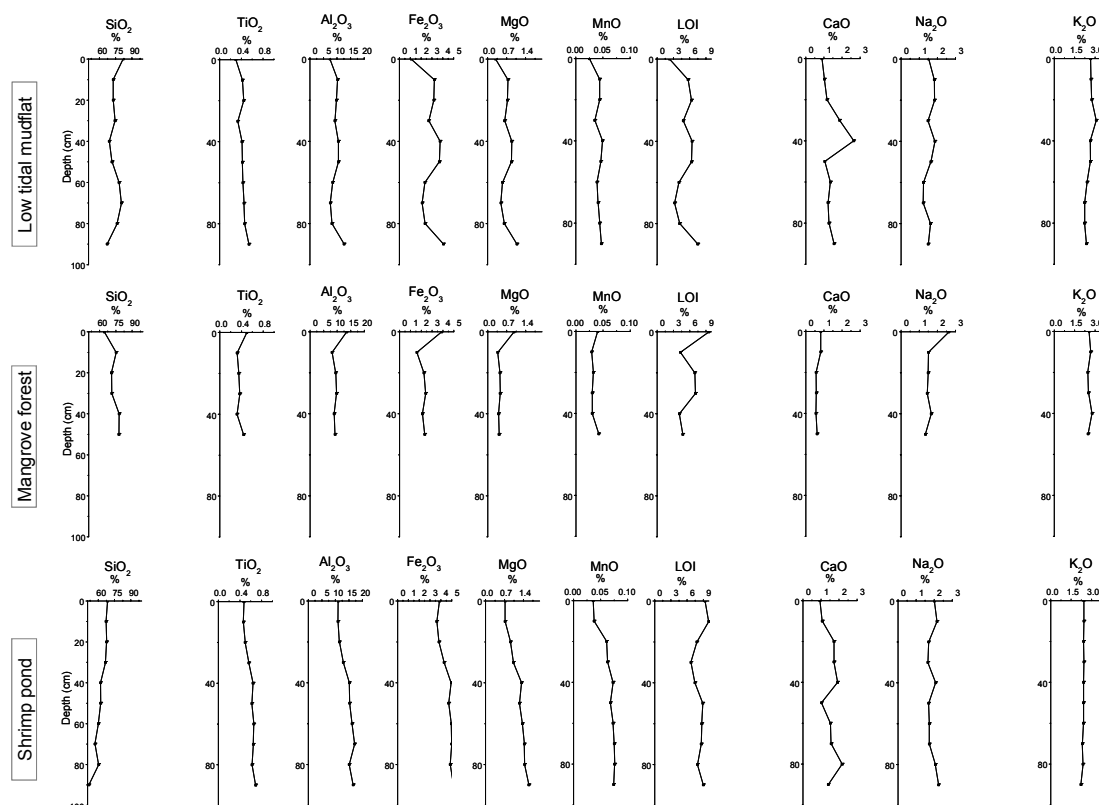


Figure 4.23. Variation of major elements according to depth in sediment profile of Nha Phu

4.3.3 Minor chemical elements

Table 4.7 displays concentrations of minor elements in coastal sediments of Red River Delta, Dam Mon and Nha Phu and the reference data for average world near-shore mud (Wedepohl 1960). The highest accumulation of all minor elements was clear to see in sediments of the Red River Delta. Concentrations of these elements in Nha Phu were slightly higher than those in Dam Mon.

The correlation matrix (Table 8.5, Appendix) revealed strong correlations among heavy metals (i.e. Cu, Pb, Zn), minor transition elements (i.e. Y, Nb, V, Ga, Ce) with clay forming elements (Al, Fe, Mg, Mn, Ti). Additionally, Sr showed high correlation with Ca whereas Rb showed high correlation with K, reflecting the association due to chemical similarity.

Table 4.7. Minor elements in the coastal sediments of Red River Delta, Dam Mon & Nha Phu

Element	Red River Delta				Dam Mon				Nha Phu				Near-shore mud*
	Mean	Min	Max	STDV	Mean	Min	Max	STDV	Mean	Min	Max	STDV	
Pb	103	31	144	36.4	15	8	22	3.4	29	14	46	8.7	20
Cu	116	36	181	42.5									48
Zn	119	32	178	41.3	18	7	50	8.8	53	25	86	19.3	95
Co	25	4	32	7.2					7	5	10	1.9	13
Cr	88	11	108	24.8	16	8	27	5.2	25	10	58	11.0	100
Ni	47	37	59	5.1	8	5	11	2.4	11	6	25	4.8	55
Rb	121	109	136	10.1	64	48	141	15.8	107	84	121	8.4	13
Ce	83	70	96	10.0	39	22	61	11.1	63	33	92	15.3	
Sr	103	88	109	8.4	67	42	142	22.1	136	100	194	22.0	< 250
Ba	356	338	392	21.7	250	209	330	29.8	254	193	287	21.6	750
Y	33	30	35	2.0	12	4	21	3.8	26	14	46	8.2	27
Zr	307	252	382	56.0	307	100	672	167.0	355	184	514	95.4	160
Nb	19	18	19	0.4	8	3	17	2.8	13	8	19	2.8	
V	96	89	110	8.5	19	12	35	5.6	38	16	65	13.5	130
Hf					11	5	21	5.0	11	6	19	3.4	
Ga	17	15	19	1.5	5	3	13	2.6	13	7	20	3.7	19
La					28	21	40	7.6	35	21	49	8.4	92
U	7	5	9	1.5	7	4	11	2.1	8	4	12	2.0	
Th	15	14	16	1.1	12	6	21	4.2	21	10	66	10.4	

* Average the world near-shore mud, after different authors from Wedepohl (1965)

Red River Delta

Table 4.8 shows concentrations of pollutant metals (Cu, Pb, Zn, Co, Ni, Cd) and Table 4.9 shows concentrations of other minor elements for three profiles in RRD: LM, MF and SP.

Heavy metals: Muddy sediments in the Red River estuary showed rather highly accumulation of heavy metals. Some heavy metals (i.e. Pb, Cu, Zn, Ni) showed even higher concentration than Canadian standards: TEL and PEL (Table 4.8). Concentrations of Zn, Cr, Ni, Co and Cd were lower than their concentrations in estuarine alluvia, but higher than in average concentrations in suspended matters along Red river (data by Lai 1995).

Other minor elements: These other minor elements including transition metals (Sc, V, Y, Zr, Nb, Mo, Hf, Ta, W, Bo), alkali metals (Rb, Cs), alkaline earth metals (Sr, Ba), other metals (Ga), rare earth (La, Ce, Nd) and actinides (Th, U) were detected in the sediments of the Red River Delta (Table 4.9). Zr showed highly accumulation in estuarine mudflats. Barium tended to be much depleted whereas the other minor elements had comparable concentrations. Almost of minor elements accumulated highly in MF sediment, especially in surface layer. Exception was the Zr that was highly accumulated in LM sediments.

Table 4.8. Average, standard deviations, minimum and maximum concentration of the studied heavy metals in the estuarine muddy sediments of the Red River Delta

Sediment profile		Heavy metals (mg/kg)						
		Pb	Cu	Zn	Cr	Ni	Co	Cd
Low tidal mudflat	Mean	119	144	138	97	53	29	0.29
	Min	69	83	86	85	41	25	0.26
	Max	139	181	174	108	59	32	0.31
	St.Dev	25.8	33.8	29.3	9	6	2.5	0.02
Mangrove forest	Mean	97	102	114	82	44	24	0.22
	Min	61	68	85	76	37	20	0.16
	Max	120	144	162	95	52	27	0.29
	St.Dev	24.5	29	29.6	7.7	5.8	2.6	0.05
Shrimp pond	Mean	87	89	94	82	42	20	0.23
	Min	61	88	87	72	40	18	0.21
	Max	108	91	99	87	46	22	0.26
	St.Dev	19.5	1.4	4.9	6.9	2.7	1.9	0.02
RRD estuarine alluvia	Mean	103.6	127.2	254.3	103.6	68.1	37.1	0.62
Total RRD estuarine muds	Mean	103.4	115.9	118.9	88.2	47.0	25.0	0.25
Intertidal mudflats in RRD estuary ^{(1)*}	0 – 5 cm	255.6	237.1	326.0	115.0	68.1		0.14
	40 – 60 cm	151.4	127.6	212.2	92.0	56.0		0.07
RR average ^{(2)*}		89	33	160	103	49	14	
Near-shore muds ^{(3)*}		20	48	95	100	55	13	
TEL ^{(4)*}		30.2	18.7	124	52.3	15.9		0.676
PEL ^{(4)*}		112	108	271	160	42.8		4.21

* : Referenced data

⁽¹⁾ : Investigation by Cu (1998) on 60 cm depth profiles.⁽²⁾ : Average suspended sediments of 15 sites along the Red River (Lai. 1995)⁽³⁾ : Average world near-shore muds. from different authors in Wedepohl (1965)⁽⁴⁾ : TEL: threshold effect level; PEL: probable effect level CCME (2002) Canadian Standards for marine sediment quality (dry weight); **Values** > Probable effect level (PEL) are displayed in **Bold**; PEL > **Values** > TEL are displayed in **Italic Bold**.

Table 4.9. Average, standard deviation and concentration range of the studied minor elements in muddy sediments of Vietnam coastline

		Pb	Zn	Cr	Ni	Rb	Ce	Sr	Ba	Y	Zr	Nb	V	Hf	Ga	La	U	Th
Red River Delta																		
Low tidal mudflat	Mean	119	138	97	53	103	68	82	340	38	373	17	84		12		6	21
	Min	69	86	85	41	97	59	81	318	30	363	16	76		11		6	20
	Max	139	174	108	59	109	78	83	361	45	382	19	93		13		6	23
	STDV	25.8	29.3	9	6	5.7	9.7	0.8	21.5	7.2	9.6	1.4	8.8		1.0		0.4	1.5
Mangrove forest	Mean	97	114	82	44	124	80	92	364	33	276	19	95		17		7	23
	Min	61	85	76	37	116	70	82	338	32	203	18	91		16		6	14
	Max	120	162	95	52	135	92	106	403	34	350	19	103		17		7	42
	STDV	24.5	29.6	7.7	5.8	8.1	9.3	10.1	28.4	0.8	60.0	0.4	5.6		0.5		0.5	13.4
Shrimp pond	Mean	87	94	82	42	115	80	86	349	41	269	15	89		14		6	21
	Min	61	87	72	40	107	79	83	336	41	260	14	81		13		5	20
	Max	108	99	87	46	123	81	89	362	42	278	17	97		16		7	22
	STDV	19.5	4.9	6.9	2.7	8.0	1.0	3.1	13.3	0.4	9.0	1.5	7.7		1.3		0.9	0.7
Dam Mon																		
Low tidal mudflat	Mean	17	23	20	6	71	45	68	251	14	432	11	21	14	5		6	16
	Min	13	11	13	5	59	24	42	223	7	168	7	12	9	3		4	10
	Max	22	50	27	11	141	61	142	330	21	672	17	35	21	13		11	21
	STDV	2.9	10.7	4.3	2.0	23.7	11.3	27.4	29.3	4.1	170.1	2.7	6.6	5.1	2.8		2.3	3.6
Mangrove forest	Mean	15	16	13	6	65	27	59	268	10	174	6	16	6	4		6	11
	Min	11	7	8	5	60	22	44	231	3	100	3	12	2	3		4	6
	Max	19	29	20	9	71	36	79	311	13	260	8	21	11	7		9	14
	STDV	2.9	6.5	3.8	1.4	3.2	4.3	11.6	25.0	2.5	49.5	1.5	3.9	2.9	1.4		1.5	2.6
Shrimp pond	Mean	13	15	14	5	58	30	75	231	10	298	8	16	10	4		5	10
	Min	8	7	9	5	48	21	48	209	4	170	6	10	5	3		4	6
	Max	17	24	20	6	66	37	103	257	14	499	10	20	17	6		9	14
	STDV	3.0	5.0	3.6	0.3	4.5	5.2	17.3	15.6	2.6	109.5	1.3	3.5	3.9	1.3		2.0	2.8
Nha Phu																		
Low tidal mudflat	Mean	25	42	19	7	105	57	143	249	23	438	11	29	14	10	31	6	21
	Min	14	25	10	5	84	33	119	193	14	300	8	16	10	7	20	4	10
	Max	37	58	31	11	119	69	194	287	30	514	13	42	19	14	49	9	66
	STDV	6.5	10.9	6.3	2.1	9.4	10.9	20.7	24.6	4.5	62.7	1.7	7.2	3.0	2.3	9.8	1.7	15.2
Mangrove forest	Mean	26	43	19	7	107	54	108	238	21	299	11	31	10	11	24	8	16
	Min	17	30	13	5	100	41	100	224	17	246	10	19	9	9	20	6	12
	Max	36	77	29	13	121	81	122	247	32	425	15	53	13	17	28	9	23
	STDV	5.9	15.6	5.0	2.9	7.7	13.4	7.5	7.9	5.2	63.2	1.8	10.9	1.8	2.7	3.3	0.9	3.8
Shrimp pond	Mean	35	71	35	12	109	75	146	269	33	306	15	50	8	16	39	9	23
	Min	22	52	23	6	100	54	125	246	23	184	12	39	5	13	32	6	15
	Max	46	86	58	25	116	92	162	280	46	411	19	65	12	20	47	12	28
	STDV	7.9	13.1	9.6	5.3	6.5	11.3	11.8	11.6	6.9	73.0	2.2	8.5	2.4	2.5	5.0	1.9	3.7
Near-shore muds*		20	95	100	55	13		< 250	750	27	160		130		19	92		

*: Wedepohl (1965)

Table 4.10. Distribution of minor elements in grain size fractions of RRD sediments

Env.	Depth		wt. %	Pb	Zn	Co	Cr	Ni	Rb	Sr	Ba	Y	Zr	Nb	V	Ga	Ce	U	Th
LM	0 - 3 cm	BULK	in bulk	111	136	31	97	53	115	113	358	31	343	18	83	16	83	7	17
		> 63 μm	48%	95	56	27	72	36	88	107	311	25	240	15	57	11	64	6	12
		20 - 63 μm	16%	52	115	29	120	43	88	112	308	44	1086	22	69	12	109	7	23
		6.3 - 20 μm	16%	97	146	32	97	58	128	112	414	35	229	21	90	18	75	7	15
		2 - 6.3 μm	10%	174	266	42	137	99	170	138	498	40	156	26	140	26	126	14	26
		< 2 μm	10%	282	452	53	170	116	248	154	558	38	148	20	190	34	136	12	28
SP	0 - 3 cm	BULK		61	87	32	72	40	126	96	386	33	251	18	91	18	78	6	16
		> 63 μm	29%	45	41	24	54	25	97	91	350	23	178	15	62	14	61	5	11
		20 - 63 μm	22%	29	56	27	67	28	90	94	351	33	553	20	67	13	73	6	16
		6.3 - 20 μm	18%	48	79	32	65	41	124	97	400	32	205	20	86	18	73	8	14
		2 - 6.3 μm	14%	73	102	40	80	55	164	99	469	42	173	22	120	23	93	5	17
		< 2 μm	17%	152	225	58	130	79	227	104	519	54	177	19	180	31	129	6	28
MF	0 - 3 cm	BULK		120	164	31	92	52	137	111	395	31	239	20	102	19	82	8	20
		> 63 μm	24%	120	80	24	78	39	98	104	338	23	163	14	66	12	63	5	10
		20 - 63 μm	20%	47	91	21	92	34	94	111	335	35	639	21	66	13	81	5	17
		6.3 - 20 μm	20%	73	124	32	79	48	127	104	406	33	192	21	95	19	71	6	26
		2 - 6.3 μm	13%	137	218	42	106	66	178	122	462	34	140	24	128	24	108	14	24
		< 2 μm	23%	247	367	48	136	90	240	152	574	40	150	28	190	32	120	16	32
MF	53 - 56 cm	BULK		100	115	23	80	43	120	112	346	29	296	18	84	16	77	9	19
		> 63 μm	45%	44	53	20	58	25	92	108	303	21	177	14	58	12	53	7	12
		20 - 63 μm	19%	49	74	18	92	33	90	106	300	39	861	22	69	14	87	9	19
		6.3 - 20 μm	16%	104	130	27	77	49	127	109	389	33	209	21	94	17	80	5	23
		2 - 6.3 μm	10%	188	192	27	122	83	178	148	468	38	154	26	132	24	118	14	38
		< 2 μm	11%	355	379	45	142	97	260	146	548	38	174	22	184	32	138	18	28
MF	71 - 73 cm	BULK		62	85	20	76	38	116	108	359	30	244	18	83	15	76	6	14
		> 63 μm	43%	38	41	17	58	24	101	108	345	22	153	13	62	11	51	5	10
		20 - 63 μm	19%	36	52	15	77	28	87	97	290	34	561	20	66	13	73	8	15
		6.3 - 20 μm	11%	60	86	17	75	41	121	91	376	34	228	20	94	16	86	5	15
		2 - 6.3 μm	9%	104	134	30	96	48	162	130	438	42	202	24	122	22	112	14	18
		< 2 μm	17%	144	221	34	126	88	184	144	502	46	222	26	148	28	134	5	26

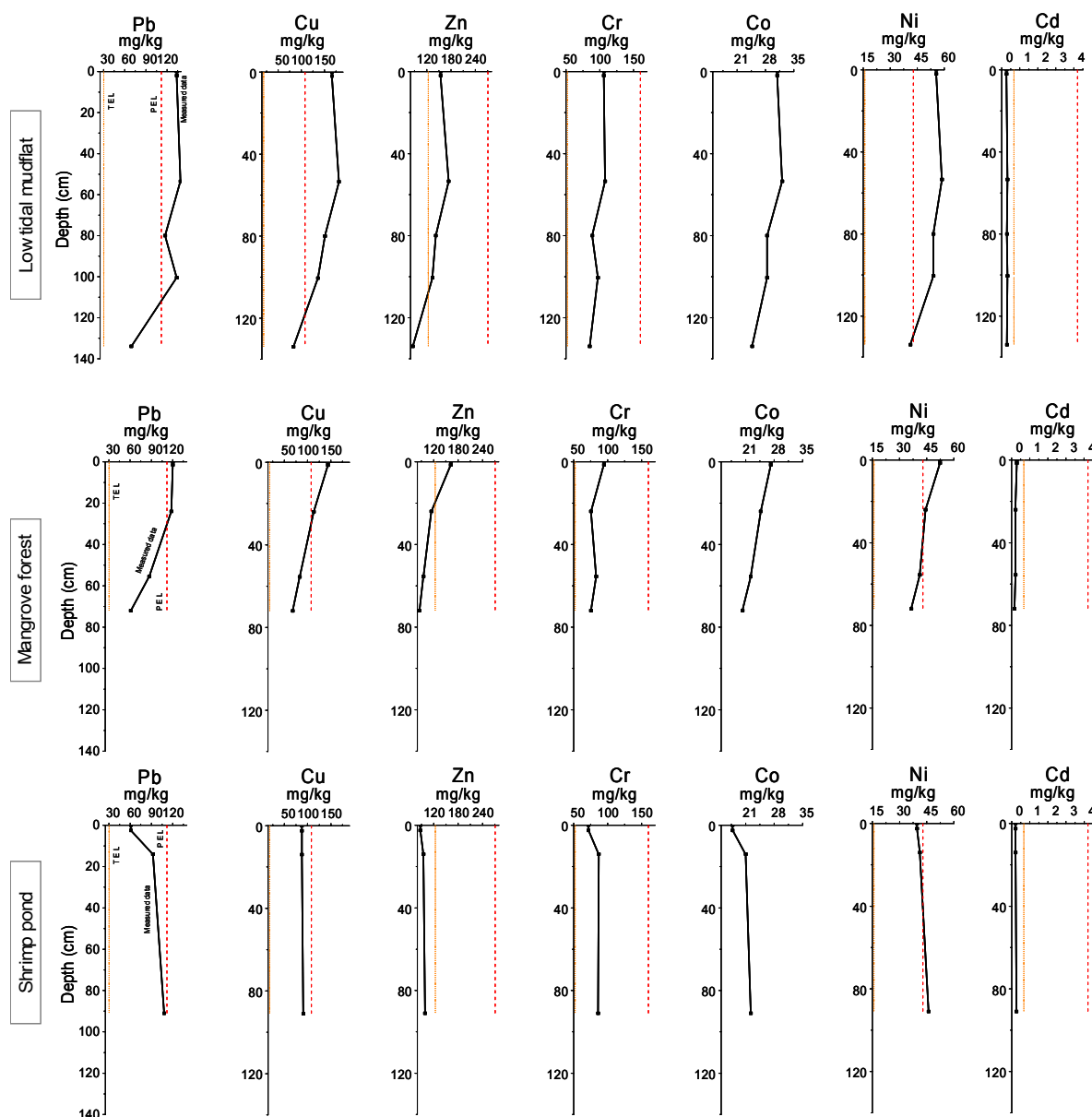


Figure 4.24. Chemical variation according to the depth in profiles of LM (a). MF (b). SP (c) in the Red River estuary

Solid line: measured data; dash line: TEL; dot line: PEL (Canadian Standards for marine sediment quality (dry weight), CCME 2002)

Distribution of minor elements in grain size fractions

Table 4.10 presents the concentrations of minor elements in the five grain-size fractions of five samples in LM, MF and SP sediments of RRD. In all samples, distribution of *all most minor elements*, except for Zr, showed a *clear increasing trend continuously from coarse fraction to fine fraction*. The most intensive variations were observed with heavy metal elements, with their concentrations in the fractions $< 2 \mu\text{m}$ of 1.7 to 8.1 times higher than theirs in the fractions $> 63 \mu\text{m}$. Concentration of other minor elements in the fractions $< 2 \mu\text{m}$ were 1.1 to 3.2 times higher than theirs in the fractions $> 63 \mu\text{m}$.

The exceptional case, *element Zr showed a very high concentration in 20 – 63 μm fractions*, of 3.1 to 4.9 times higher than the fractions $> 63 \mu\text{m}$. Concentrations of Zr decreasing continuously from these 20 – 63 μm sizes to finer sizes. Fractions $< 2 \mu\text{m}$ have Zr concentrations of 2.5 to 7.3 times lower than the 20 – 63 μm fractions.

Variation of minor elements with depth

Concentrations of minor elements in intervals along profiles of LM, MF and SP were presented in the Figure 4.24. *In profiles of MF and LM, concentrations of all heavy metals increased from the deeper to upper layers* (Figure 4.24). The highest accumulations of these pollutants were at the depth of 40 – 60 cm in LM profile but at surface layer in MF profile. *Distinctively, concentrations of all heavy metals decreased dramatically in upper layers in SP profile* (Figure 4.24), suggested a leaching process. The concentrative depletions were most obviously with of Pb, Zn, Co and Cr. The distribution tendencies of minor elements developed in the similar manner to Al_2O_3 concentration (Figure 4.18).

South Central Coast

Heavy metal: In sediments of Dam Mon and Nha Phu, *concentrations of pollutant heavy metals: Pb, Zn, Cr were relatively low* (Table 4.9). The highest concentrations were found in sediments of low tidal mudflat. Sediments of Nha Phu had slightly higher concentration of heavy metals, which accumulated dominantly in SP sediments.

Other minor elements: Minor elements in Dam Mon exhibited in *low values and showed the similar behaviours to heavy metals*, which concentrated most highly in low tidal mudflat profile. In MF and SP sediments, their concentrations were comparable.

In Nha Phu, except for Mo, Rb, Sr and Zr, *most of minor elements had low concentration* (Table 4.9). *Resembling behaviours of heavy metals*, minor elements were most highly accumulated in SP sediments.

Factor analysis and PCA biplots: Factor analysis on minor elements of the sediments in Dam Mon (Table 8.3, Appendix) revealed *three major components*: F1 (explained 62.6 % of total variance) included *heavy metals (Pb, Zn, Cr, Ni) and Ba, Y, Nb, V*. F1 had also high correlation with Ga and Ce. The second component F2 (explained 15.4 % of total variance) included *Rb, Sr, Ga and U* whereas the third component F3 could explain for 6.9 % total variance and responded to *Zr only*. Orthographical projection of the whole dataset on the first two principal factors (see PCA biplots in Figure 4.25a) shows the correlation distribution of these three components relatively to samples of different profiles: low tidal mudflat (LM,) mangrove forest (MF) and shrimp pond (SP). Sediments of different profiles in *Dam Mon showed a low level differentiation* in terms of minor chemistry. Obviously was the similarity between sediment samples in low tidal mudflat and shrimp pond. However, *sediment samples in mangrove forest presented a bias toward high correlation with most of minor elements* (i.e. Zn, Ni, Cr, Nb, Zr, V and Ce) (Figure 4.25a).

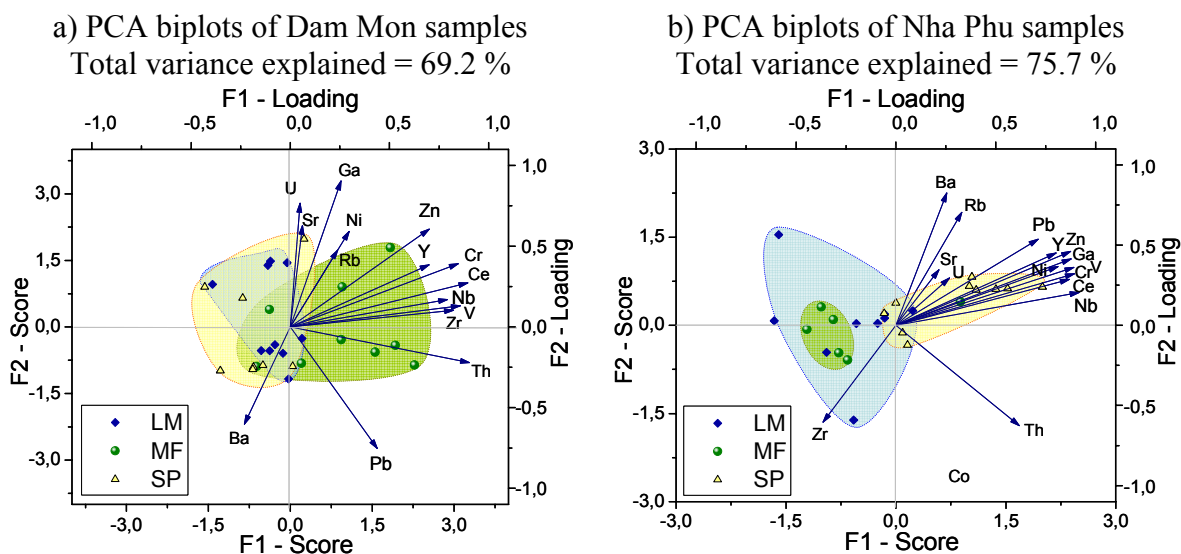


Figure 4.25. PCA biplots on minor chemical elements of sediment samples in Dam Mon (a) and Nha Phu (b)

Extraction Method: PCA with varimax rotation and Kaiser normalization.

In Nha Phu, behaviours of minor elements were governed by *three principal factors* (Table 8.4, Appendix): F1 (explained 61.5 % total variance) included *heavy metals* (Pb, Zn, Cr, Ni) and Y, Nb, V, Ga, Ce; F2 (10.8 %) included Ba and F3 (8.6 %) included Zr only. Even though Ba was the second factor governing minor chemistry of sediments in Nha Phu, this element presented none specific correlation with the other alkali earth element like Rb, Sr. Actinides (U, Th) showed no specific correlation with any of the other elements, either. Specific behaviour of Zr in sediments of Nha Phu was similar to that observed in Dam Mon.

PCA biplots of Nha Phu sediments on the first two principal components F1 and F2 is displayed in Figure 4.25b. *Group of sediments in mangrove forest showed high correlations among each others.* However, *this group was bearred also by the group of sediments in low tidal mudflat profile in terms of chemical correlation.* Both environments correlated highly with Zr. Differently, sediments in shrimp pond profile showed a readily bias toward most of the other minor elements (i.e. Pb, Zn, Cr, V, Ga, Nb, Ce, Sr and U).

Variation of minor elements with depth

In Dam Mon (Figure 4.26), the three profiles: LM, MF and SP showed *different behaviours of minor elements with depth.* In LM profile, concentrations of minor elements were rather stable with increasing depth. Irregular increase of some Sr, Ba, Zr and U were to observe in some intervals. Zr accumulated highly at 30 - 60 cm depth interval.

In MF profile, the high accumulation of all most minor elements in upper part and especially in 0 - 10 cm surface layern was to notice. Exceptions were also Zr, U and Th, the elements showing irregular increase in some intervals.

In shrimp pond profile, concentrations of heavy metals and minor elements were almost stable, with slightly higher concentration in upper part versus the deeper part. Concentration of Pb decreased slightly in surface layer. Concentrations of Ba and U varied irregularly with depth but Zr exhibited similar depth behaviour to heavy metals and other minor elements.

In Nha Phu sediments (Figure 4.27), *minor elements showed also specific behaviours with depth for every profile*. In the profile of low tidal mudflat, three groups of minor elements with specific behaviours could be distinguished. Firstly was group of minor elements that decreased in upper part of profile, including heavy metals (Pb, Zn, Cr, Ni) and V, Nb, Ga, Ce. The second group included alkaline earth elements (Rb, Sr, Ba) and actinide element Th those remained stable in concentration with depth. The third group containing only Zr that concentrated highly in upper part of profile. Uranium showed undefined tendency of distribution.

In mangrove forest profile, *except for alkaline earth elements (Rb, Sr, Ba), Zr and U which remained stable in concentration with the depth, most of the minor elements were highly accumulated in surface sediments*. In reverse to tendencies observed in mangrove profile, *depletion in concentrations of minor elements was readily observed in surface layer shrimp pond sedimentary profile*.

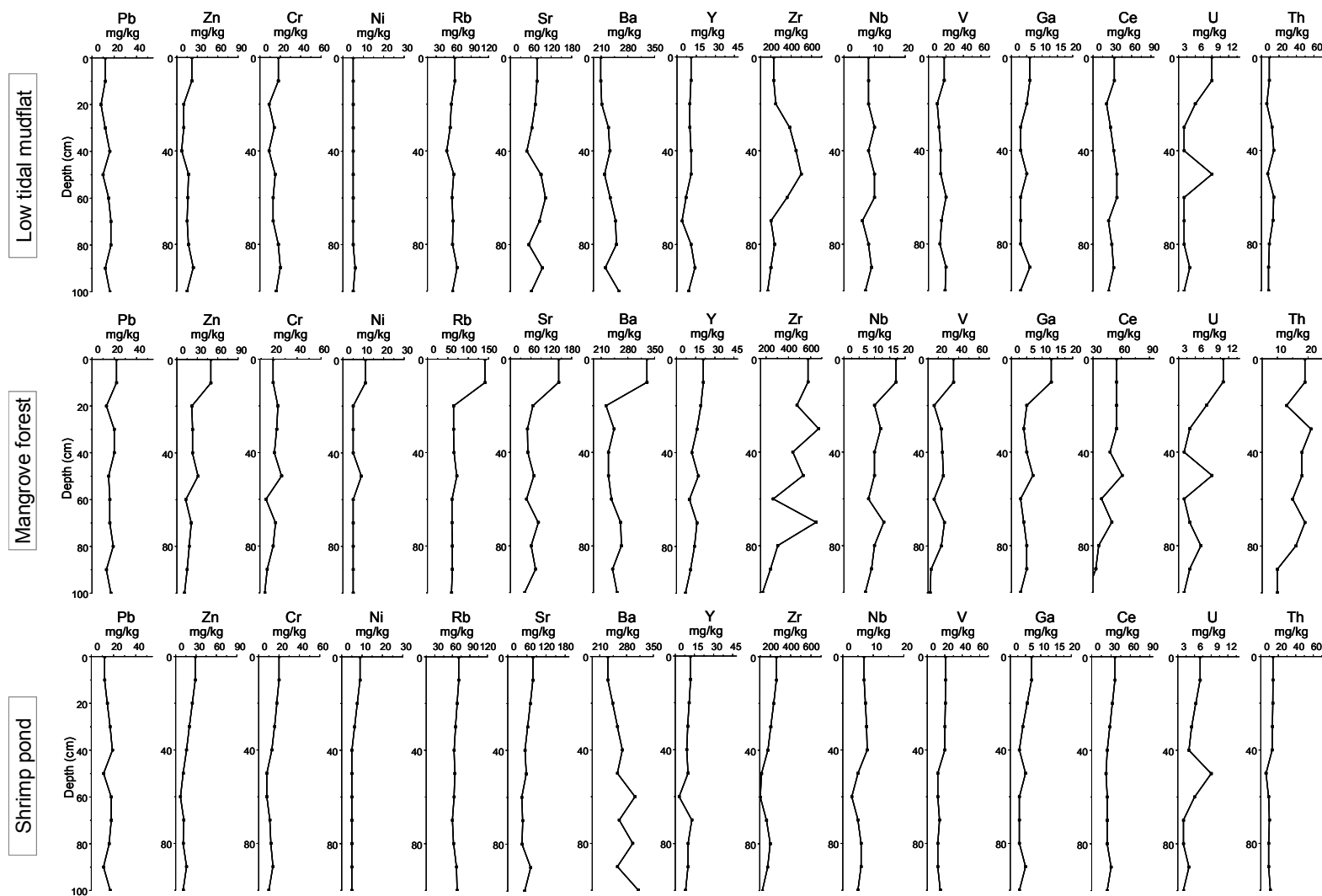


Figure 4.26. Variation of trace elements according to depth in sediment profile of Dam Mon coastline

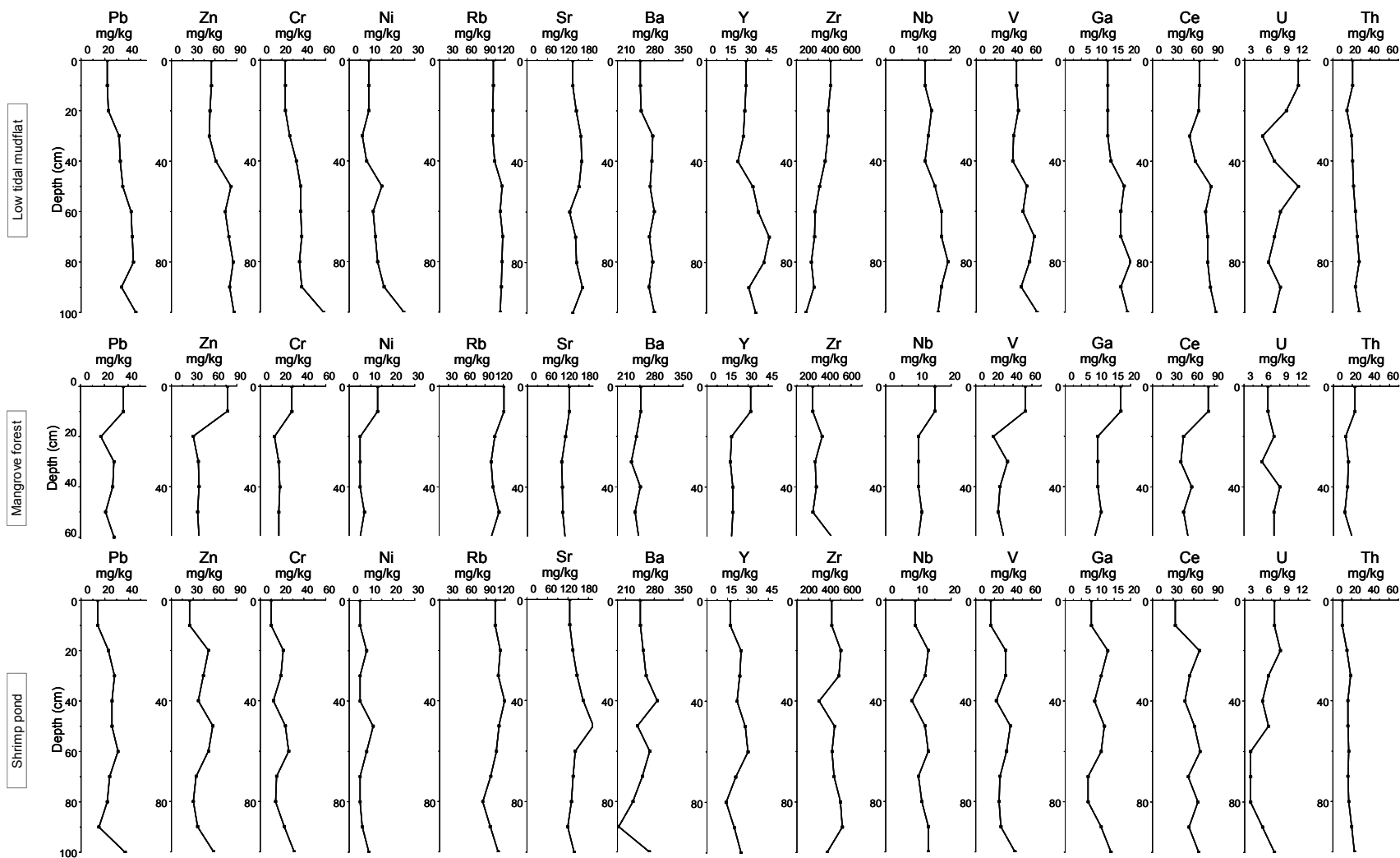


Figure 4.27. Variation of trace elements according to depth in sediment profile of Nha Phu coastline

4.4 Mineralogy

4.4.1 Red River Delta

Bulk mineralogy

In Red River Delta (RRD), coastal sediments were characterized by remarkable bulk mineralogical homogeneity, as revealed by similar XRD patterns for randomly oriented mount specimens (Figure 8.6 – Appendix). The mineral suite consisted essentially of quartz, K-feldspar, plagioclase, pyrite and clay minerals. The clay mineral assemblage contained kaolinite, chlorite, illite, dioctahedral vermiculite, smectite structures and mixed layer series as revealed in fine fractions. Hematite, gypsum, gibbsite, calcite, anatase, and ilmenite were detected in traces.

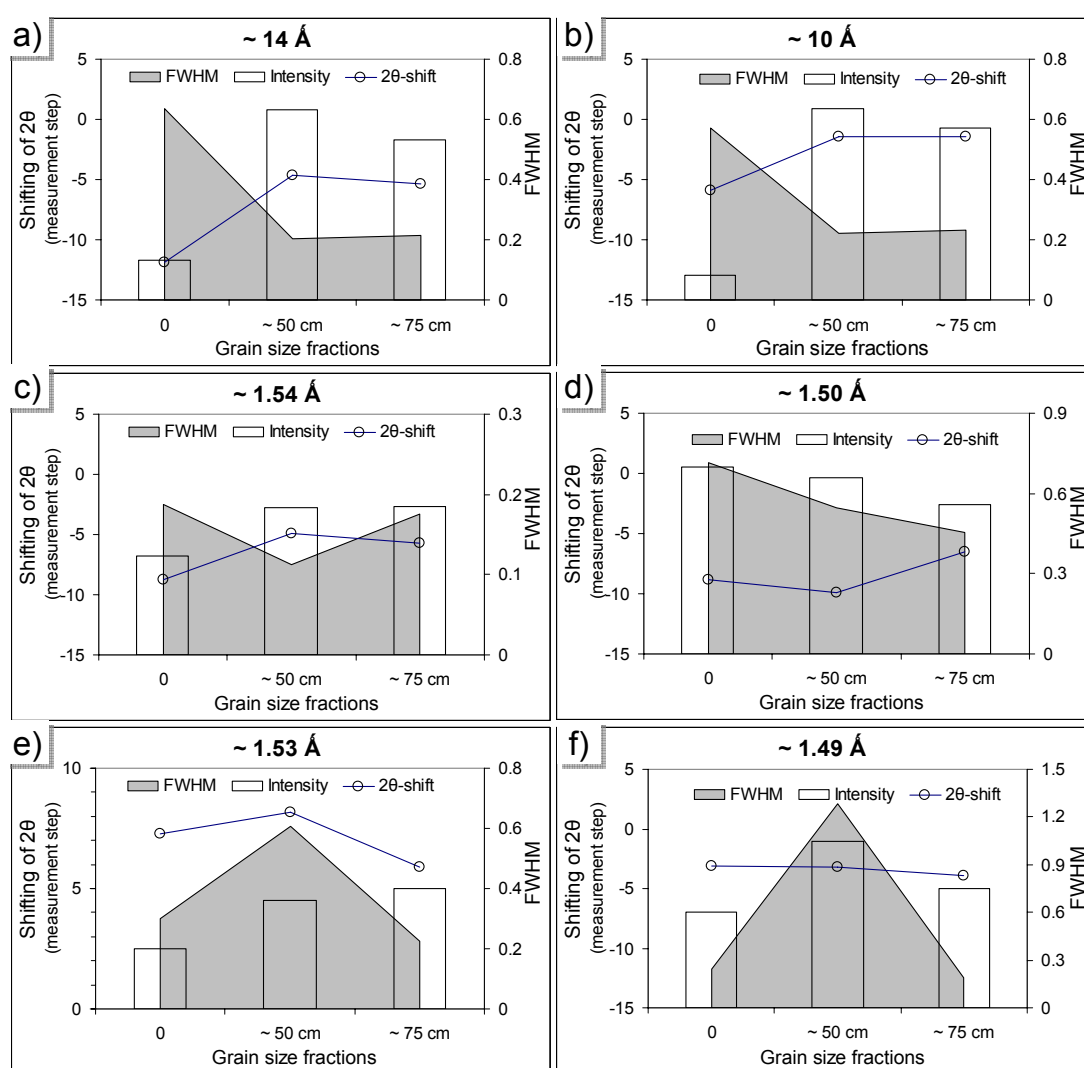


Figure 4.28. Variation in crystallite parameters (d-value, peak intensity, FWHM) of clay minerals according to the depth

On example of mangrove forest profile in RRD; Data extracted from powder XRD patterns based on WinFit; Negative values of 2θ-shift (left axis) indicate shifting of peak position to lower 2θ angle and vice versa.

Surface sediment samples (Figure 8.6a, c, f – Appendix) of low tidal mudflat (LM), mangrove forest (MF) and shrimp pond (SP) profiles showed no significant differences in terms of new mineral phases but slightly differences in intensity of reflections from some clay phases: 14 Å phase (chloritic, smectitic or trioctahedral vermiculitic minerals), 7 Å phase (kaolinitic minerals) and 10 Å phase (illitic or dioctahedral vermiculitic minerals). *The 7 Å and 10 Å reflections were most intensive in sediments of MF.*

From surface layer to deeper parts in all profiles (Figure 8.6 a-b, c-d-e, f-g, Appendix), intensity of clay phases reflections increased whereas intensity of quartz reflections were comparable among patterns of the intervals. An illustration was given in the Figure 4.28, with example of mangrove forest profile. *It was to notice an increase in intensity of the 14 Å and 10 Å reflections with increasing depth (see bar), parallel to decrease in full width at half maximum (FWHM) of these peaks (see grey area).* However the variation in intensity of the 1.54 Å reflections, which represent quartz, was regardless. *Intensity of 1.50 Å, that characterizes dioctahedral clay minerals decreased with depth but intensity of 1.49 Å characterizing kaolinite, tended to increase at the ~ 50 cm depth interval.* In sediment of MF profile, K-feldspar with reflection about 3.25 Å was more commonly than in LM and SP profiles. With increasing depth, intensities of feldspar (3.25 Å) and plagioclase (3.20 Å) reflections increased whereas intensities of pyrite (i.e. 1.63 Å, 2.71 Å, 2.21 Å) decreased.

Distribution of mineralogy according to grain size

Mineral composition showed a clear differentiation according to grain size distribution (Figure 8.7 – Appendix). With decreasing grain sizes, intensity of quartz and feldspars decreased but intensity of clay minerals increased. *Intensity of clay minerals, characterized by reflections surrounding 14 Å, 10 Å, 7 Å and 5 Å increased significantly in fractions < 6.3 µm. The highest intensity of dioctahedral clay species was reached in fractions < 2 µm, considering the most intensive reflection of 1.50 Å in these fractions.*

On example of surface sediment in mangrove forest profile (Figure 4.29), it was revealed that trioctahedral vermiculite and chlorite particles occurred mainly in fractions > 6.3 µm, characterized by intensive reflections of trioctahedral structures (1.53 Å). In the fractions < 2 µm, depletion of quartz was impressed by decreasing intensity of the 1.54 Å peak (see bar, Figure 4.29). *Also in these fine sizes, increase in d-value and FWHM of the 14 Å, 1.50 Å reflections referred to smectite particles of poorer order.*

Kaolinitic structures increased in intensity but decrease in FWHM in fractions < 2 µm (see bar for intensity, grey area for FWHM of 1.49 Å, Figure 4.29). The different behaviour of intensity was indicating the *existence of two kaolinite types: (i) well ordered kaolinite in fractions > 2 µm and (ii) poor ordered kaolinite and/or halloysite in fraction < 2 µm.*

In addition to the increase in intensity, slightly expansion of FWHM of 1.50 Å reflection in fractions < 2 µm suggested a presence of poor order dioctahedral smectitic species. Saponitic phase was revealed to appear in all fractions < 63 µm.

Whereas trioctahedral structures (chlorite, trioctahedral vermiculite) occurred mainly in coarser fractions, *di*octahedral structures (1.50 \AA) displayed a gradual increase with the finer sizes. Intensity of the illitic structures (10 \AA) also increased with finer sizes.

The fractions $< 2 \mu\text{m}$, thus were characterized by high accumulation of clay minerals of poor orders, including kaolinite, smectitic and vermiculitic structures. Meanwhile, chlorite and trioctahedral vermiculite occurred mainly in the coarser grain sizes, typically for soil and surface sedimentary matters (Douglas 1989).

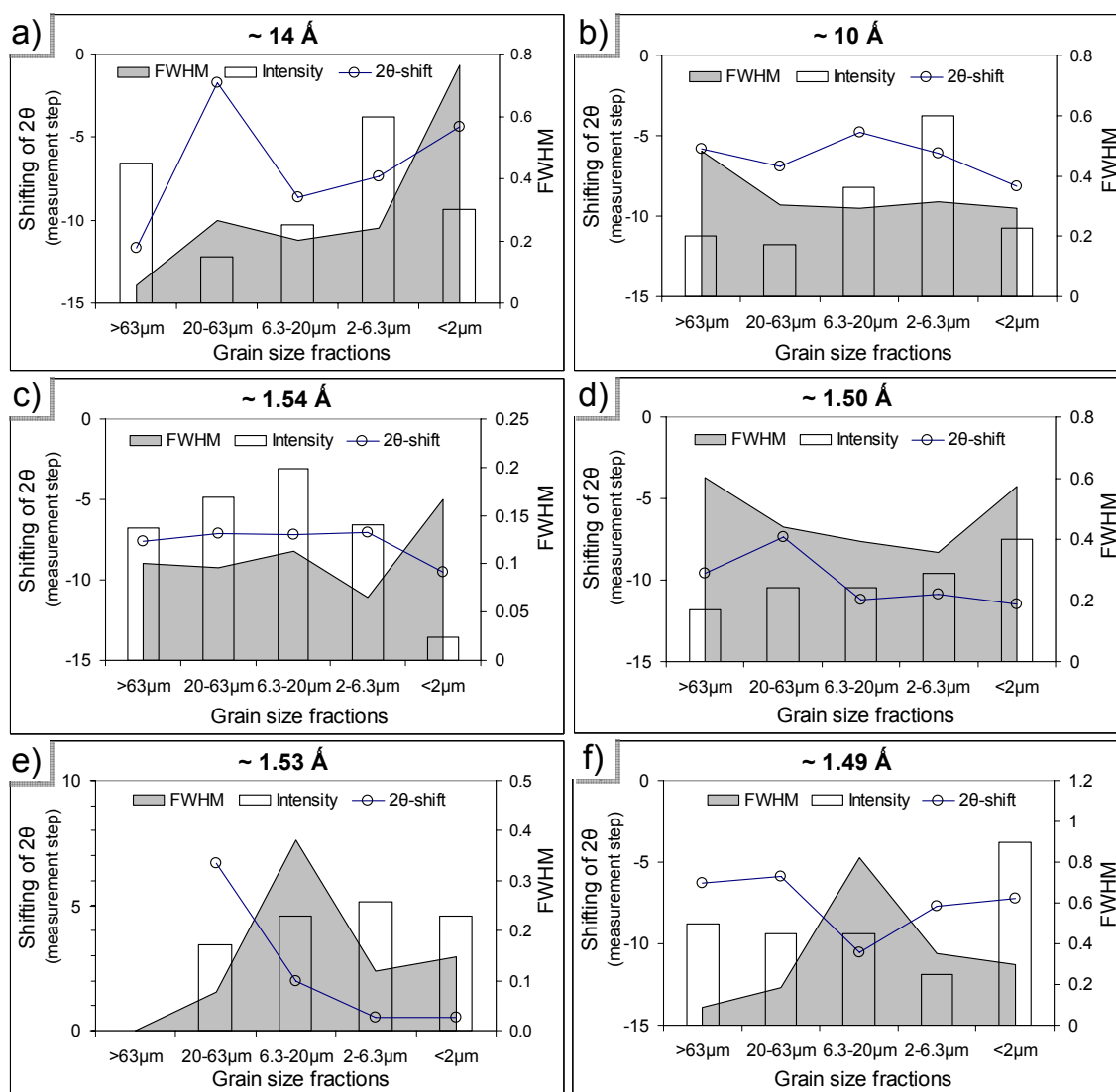


Figure 4.29. Variation in crystallite parameters (shifting of peak position, peak intensity, FWHM) of clay minerals according to grain size separation

On example of sample “Mangrove forest, RRD” (0-3 cm). Data extracted from powder XRD patterns based on Winfit; Negative values of 2θ -shift (left axis) indicate shifting of peak position to lower 2θ angle and vice versa.

Mineralogy of fractions $< 2 \mu\text{m}$

In fine sediment matters of the Red River Delta, four mixed layer series and their end-members have been determined to represent for clay mineralogy. These were IS-ml, diVS-ml, KE-ml and

CS-ml (Table 4.11). Dominant in all environments, at all depth intervals of profiles were diVS-ml (64 - 79 %), followed by KE (5 - 22 %), IS-ml (6 – 14 %) and CS (1 - 9 %). The associated non-clay minerals appeared in trace, including quartz, feldspars and pyrite.

Under TEM observations, particles occurred in a wide range of morphological varieties. Dominantly were xenomorphic platelets of varying sizes, together with pseudo-hexagonal, laths, slats and tubular. Beside particles with sharp edges, abundance of flakes and *particles with curled edges, folds at edges or ragged edges were observed, suggesting dissolution or alteration of precursor materials*. Large platy crystals (~ 1.0 µm) were also depicted for kaolinite, chlorite and CS-ml particles. Medium sizes of few nanometres in the maximum dimension were most common with particles of dioctahedral vermiculite, illite, beidellite, montmorillonite, kaolinite and mixed layer structures. Kaolinite, KE and diVS-ml occurred also in very small sizes (~ 0.1 - 0.2 µm). Generally, *particle sizes became finer with increasing depths in all profiles*.

Results on particle morphology, crystal structure and chemical composition of clay phases in the determined mixed layer series are shown in more detail followingly.

Table 4.11. Frequency (%) of mixed layer series² in sediment profiles in Red River estuary
Reveals from TEM-EDX analyses (Jeol JEM-1210)

	Depth (cm)	total diVS-ml	di Verm	di VS	lc Mont	total KE-ml	Kaol	KE	Beid	total IS-ml	Illite	IS	Mont	total CS-ml	Chl	CS	Sap
Low tidal mudflat	0-3	71%	27	40	4	12%	0	8	4	9%	0	5	4	7%	3	4	0
	53-56	77%	38	38	1	9%	1	7	1	7%	1	6	1	8%	1	7	0
Mangrove forest	0-3	64%	22	41	1	22%	5	12	5	11%	0	10	1	4%	0	4	0
	53-56	70%	11	58	1	14%	5	7	2	8%	0	7	1	9%	1	7	0
	71-73	70%	19	46	5	13%	5	5	3	14%	1	8	5	6%	1	5	0
Shrimp pond	0-3	79%	21	58	0	14%	2	8	4	6%	0	6	0	1%	0	1	0
	53-56	71%	38	32	1	5%	0	4	2	15%	1	13	1	9%	2	7	0

² KE-ml: Kaol: Kaolinite; Beid: Beidellite; KE: mixed layer structures; Kaolinite/Beidellite mixed layer series including end members; diVerm.: dioctahedral vermiculite; Mont: Montmorillonite; diVS: dioctahedral vermiculite/smectite mixed layer structures; diVS-ml: dioctahedral vermiculite/smectite mixed layer series including end members; IS-ml: illite/smectite mixed-layer series including end members; IS: illite/smectite mixed layer structures; Chl: Chlorite; Sap: Saponite; CS: chlorite/saponite mixed layer structures; CS-ml: chlorite/saponite mixed layer series including end members.
* These abbreviations were used through out this chapter

diVS-ml series and end members: diVerm and MontmorilloniteMorphology

The grains of dioctahedral vermiculite and diVS mixed layer structures in the fraction $< 2 \mu\text{m}$ were observed frequently under transmission electron microscope (TEM) (Figure 4.30). Dioctahedral vermiculite (diVerm) particles occurred in xenomorphic platelets and conspicuous parallel intergrowths of these platelets (Figure 4.30). *The observed moiré patterns were typical for modification by weathering process (Henning & Stoerr 1986). Signals of alteration processes were more obvious in the diVS mixed layer particles, which showed commonly curled edges, rough surface and tendency to flake along the base planes.* Lath shapes were also occasionally observed. The vermiculites occurred either as rather large platy crystals or in very small particles of only few nanometres in maximum dimension. The platelets of diVerm were well commonly ordered in polytypes of $2M_1$ (Figure 4.30a) and $1M$ (Figure 4.30c) and corresponding polytypes were observed for diVS-ml structures (Figure 4.30b, d).

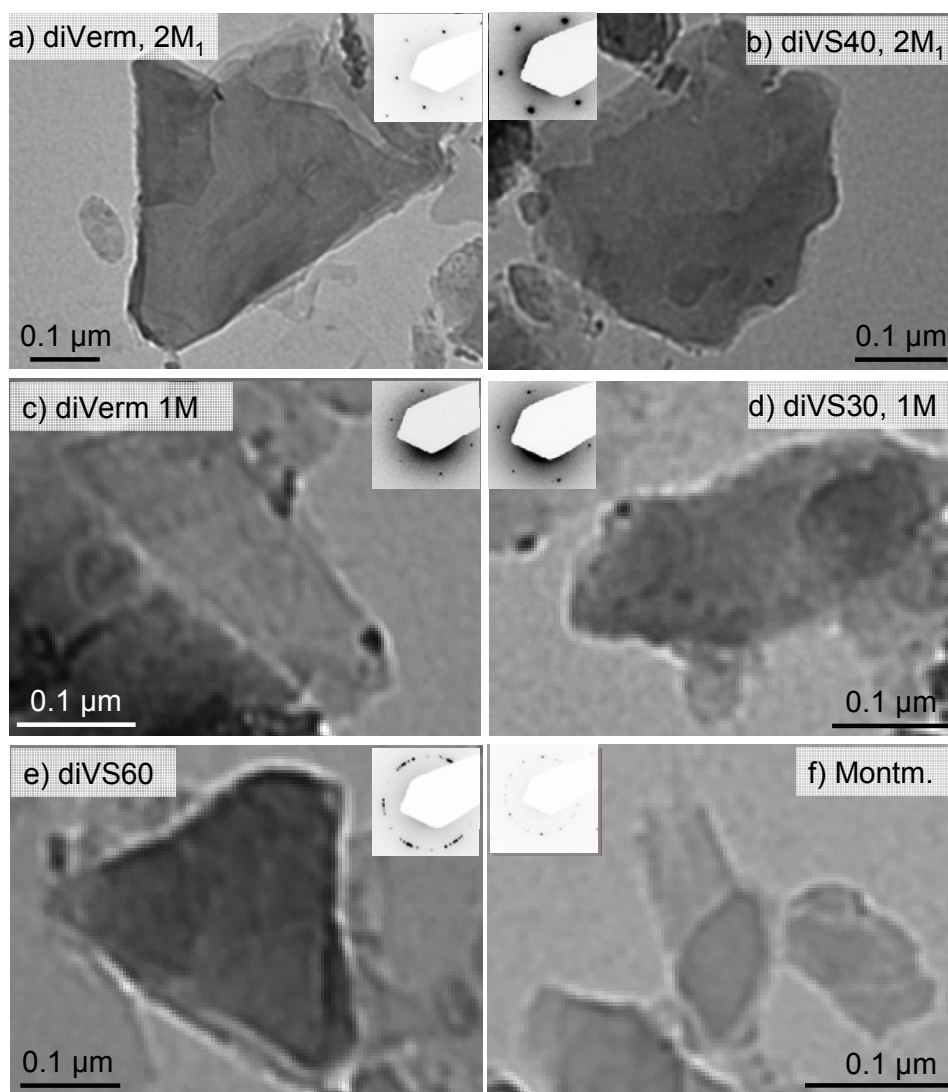


Figure 4.30. TEM images of particles in diVS-ml series in Red River Delta sediments
Reveals from TEM-EDX analyses (Jeol JEM-1210)

Particles of diVS-ml in *turbostratic order* (Figure 4.30e) were also quite commonly.

Although montmorillonite had been mentioned as an essential constituent of subtropical to tropical soils (Borchardt 1989; Henning & Stoerr 1986), only few montmorillonite particles were detected in the fraction $< 2\mu\text{m}$ of sediments in the Red River estuary. Particles displayed not only thin-film platelets, similarly to description to the Wyoming type, but also platy, xenomorphic forms with a beginning orientation of the layers in the stack (Figure 4.30f).

Crystallite structure

Table 4.12 shows crystallite parameters of particles in diVS-ml series, revealed from the deconvoluted 10 \AA reflections in XRD patterns of air-dried and ethylene glycolated specimens.

In fraction $< 2\text{ }\mu\text{m}$, the detected particles of illite were in very low frequency (Table 4.11). It was reasonable to assume that *the 10 \AA reflection was responsible dominantly for structures of dioctahedral vermiculite particles*, which had much higher appearance frequency. However, it was to note that the 10 \AA reflection in EG pattern should contain also the collapsed structure of IS-ml particles, as reflected by increase of coherent scattering domain size (CSD) after EG treatment (Table 4.12a). The diVerm particles were quite well ordered with relatively high CSD.

Table 4.12. Crystallite parameters of diVerm structures in fraction $< 2\text{ }\mu\text{m}$ of sediments in RRD based on $\sim 10\text{ \AA}$ and 10.2 \AA reflections

Data extraction by WinFit, from XRD patterns of oriented mount specimen

Profile	Depth (cm)	Air-dried				Ethylene Glycolation			
		d-value (Å)	CSD (Å)	Int.max	FWHM (Å)	d-value (Å)	CSD (Å)	Int.max	FWHM (Å)
a) diVerm structure									
LM	0 – 3	9.96	300 – 330	621	0.179	9.96	> 400	214	0.131
LM	53 – 56	9.99	220 - 230	144	0.266	9.94	310 – 380	109	0.148
MF	0 - 3	9.92	250 – 260	548	0.252	9.94	> 400	210	0.132
MF	53 – 56	9.96	240 - 250	473	0.212	9.98	170 - 190	315	0.215
MF	71 – 73	9.98	250 - 260	499	0.222	9.93	370 - 440	270	0.146
SP	0 – 3	10.00	260 – 270	435	0.238	9.96	340 – 410	256	0.146
SP	53 – 56	9.96	270 - 280	285	0.224	9.97	350 - 390	165	0.165
b) diVS-ml structures									
LM	0 – 3	10.18	80 – 90	134	0.635	10.03	~ 70	218	0.540
LM	53 – 56	10.29	70 - 80	58	0.765	10.02	70 – 80	140	0.483
MF	0 - 3	10.17	60 – 70	196	0.662	10.07	~ 80	34	0.719
MF	53 – 56	10.20	50 - 60	186	0.694	10.00	~ 80	140	0.456
MF	71 – 73	10.27	~ 50	158	0.836	10.08	70 – 80	74	0.763
SP	0 – 3	10.25	60 – 70	219	0.754	10.00	60 - 70	165	0.548
SP	53 – 56	10.21	~ 60	114	0.634	10.12	50 - 60	70	0.781

In air-dried states, the d-spacing of diVS-ml structures increased with depth in LM and MF profiles, showing the *increase in their expandability*. CSD of diVS-ml structures decreased with increasing depth in all profiles, *reflecting generally higher disorder degree*.

The *mixed layer structures* showed broad reflection ($\text{FWHM} = 0.634 - 0.836 \text{ \AA}$), corresponding to *smaller CSD* ($50 - 90 \text{ \AA}$) (Table 4.12b), in comparison to diVerm end-member. CSD of diVS-ml structures in MF sediments were lower than those in LM and SP sediments, *mirroring a higher disorder level*.

After ethylene glycolation, the expansion of mixed layer structures to 17 \AA gave rise to depletion of the 10.2 \AA reflection (or asymmetric part in 10 \AA reflection). The remains at 10 \AA , which were observed with $\text{CSD} = 50 - 80 \text{ \AA}$, thus referred to crystallite structures of pure illite or high charge dioctahedral vermiculite ($\text{XII} > 0.72$), which were nearly not expandable (Moore & Reynolds 1997).

Occurrence and distribution along depth profile

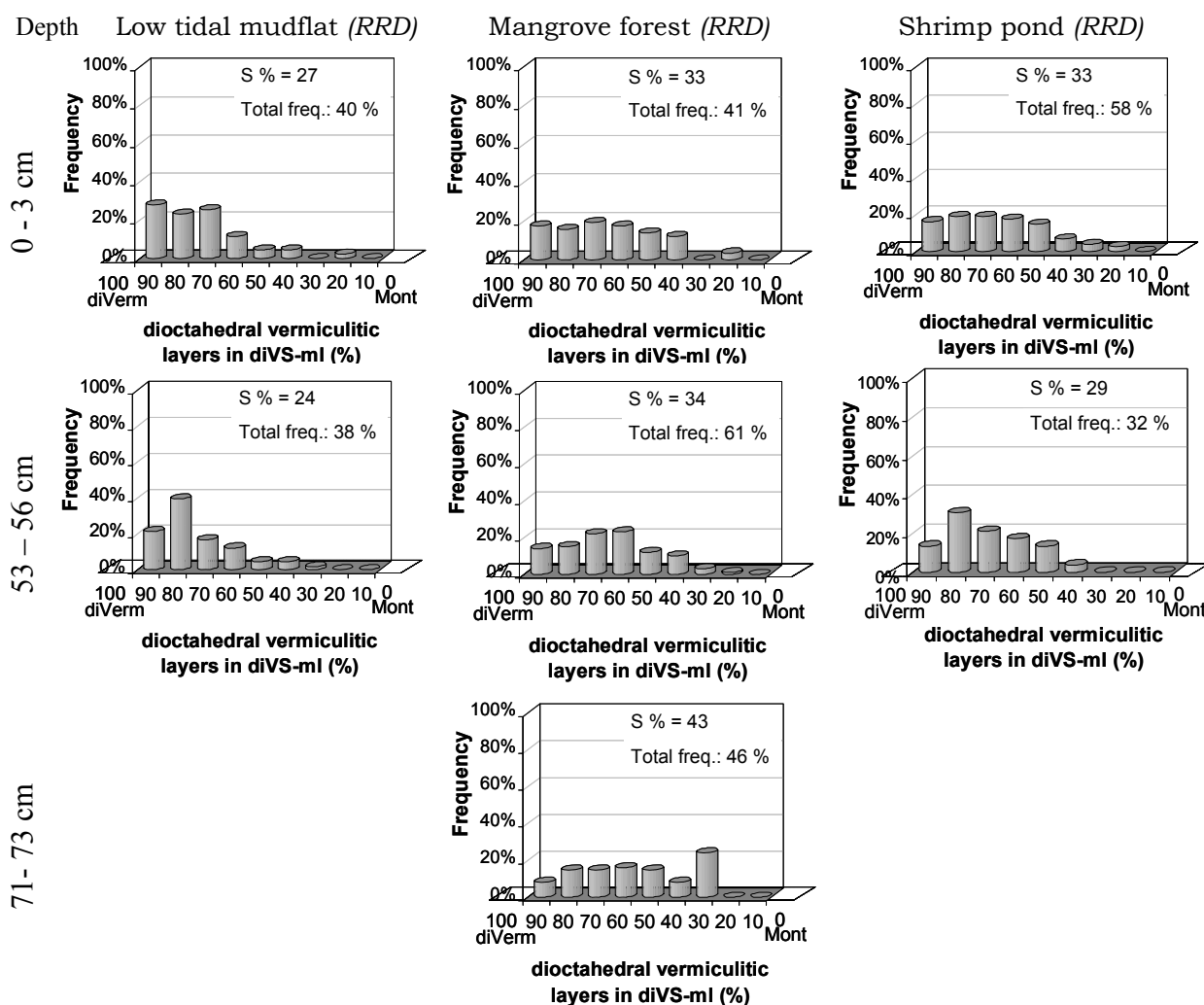


Figure 4.31. Frequency distribution of diVS-ml series in sediment profiles of Red River Delta

Reveals from TEM-EDX analyses (Jeol JEM-1210); diVerm: dioctahedral vermiculite; Mont: Montmorillonite; S% displayed weighted average proportion of montmorillonitic layers in all particles

Presence of diVS-ml in some soil pedons over catchment of the RRD was documented by Kasbohm (2005), Thanh et al. (2000) and Tra et al. (2000). As mentioned above for Table 4.11, in the investigated samples in estuary of the RRD, occurrence of diVS-ml series accounted for 64 – 77 % total appearance frequency of mineral particles in fractions $< 2 \mu\text{m}$, dominated by pure dioctahedral vermiculite and diVS mixed layer structures. *In surface sediments (0-3 cm), frequency of diVS mixed layer particles increased from LM via MF to SP profile in reverse to the decrease of diVerm.* It reflected a higher abundance of smectitic layers in the total composition. Similarly, the *smectite ratio S% in surface layer (Figure 4.31) increased from LM via MF to SP.* Frequency distribution of diVS-ml structures with different percentage of smectitic layers (Figure 4.31) showed asymmetric gauss-like distribution bias vermiculitic end-member for all investigated profiles, with mean values (see S% in top positions) relevant to structures with surrounding 70 – 80 % of vermiculitic proportions.

From top to down in all three profiles, a gradual moving of the gauss-like distributions toward montmorillonite end-member was to observe. Particularly in MF profile, *the layer of 53 – 56 cm depth had higher frequency of diVS mixed layer particles than the deeper portion.* However average smectite ratio S% in this layer (34 %) was much lower than that in 71 – 73 cm depth layer (43 %). Sediment layer of 53 – 56 cm depth in shrimp pond profile had relative low frequency and smectite ratio.

Chemical variation

Table 4.13 displays average chemical composition of diVS-ml particles and their end-members: dioctahedral vermiculite and montmorillonite. Formula of dioctahedral vermiculite particles showed mainly Mg and K in the interlayers. *The octahedral layer is dominated by Al together with Fe^{3+} .* That means, the mica that altered to diVerm is a Mg^{VI} -poor phase.

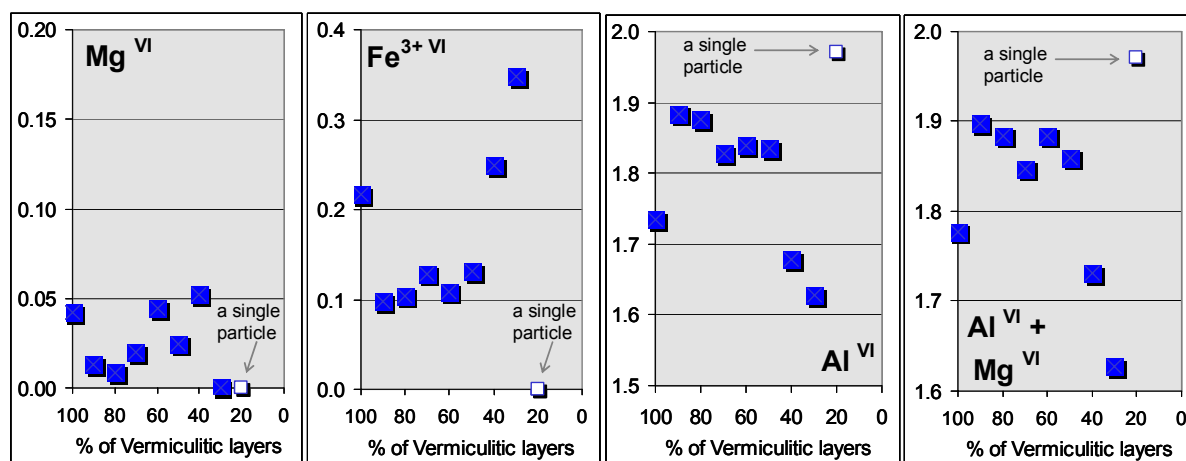
Only few particles of montmorillonite were detected by TEM-EDX. These montmorillonite particles were observed to be low charged (XII: ~ 0.20). In surface sediments, montmorillonite particles had higher content of Mg and Fe^{3+} in the octahedral layer than those in the deeper parts. Similarly to diVerm, *diVS-ml structures had substitution in octahedral layer mainly by Fe^{3+} , with amount of 0.12 – 0.19 out of 2 occupations.* *Contents of K in interlayers were low (XII < 0.35).* *DiVS-ml particles in MF were more smectitic than in the other profiles ($\text{Si}^{\text{IV}} = 3.50 - 3.57$ in comparison to 3.44 – 3.49).* Also, *interlayer K of diVS-ml of MF sediments is lower than in LM sediments.* In MF, particles became more smectitic with depth (Si^{IV} increased from 3.50 to 3.52 to 3.57; interlayer charge decreased from 0.48 to 0.47 to 0.44). In LM and SP profiles, these tendencies were not to observe.

Octahedral occupation

Behaviour of octahedral occupations in diVS-ml series was illustrated in Figure 4.32, on example of MF sediment (53 – 56 cm depth). It was obviously for the tendency that the diVS-ml particles containing *higher smectitic proportion were also the structures with higher octahedral sites were occupied by Fe.* With increasing depth along all three profiles, octahedral substitution by Mg increased whereas substitution by Fe remained stable (Table 4.13).

Table 4.13. Mineral formulae $[O_{10}(OH)_2]$ of diVS-ml series from fraction $< 2 \mu m$, dispersed from sediment profiles in estuary of Red River Delta*Average values calculated based on TEM-EDX analyses (Jeol JEM-1210)*

Sediment profile	Depth (cm)	No of particles	Interlayer				Octahedral layer				Tetrahedral layer					n^{VI}
			Ca	Mg	Na	K	Fe ²⁺	Al	Fe ³⁺	Fe ²⁺	Mg	Ti	Al	Si	XII	
Dioc. Vermiculite		275	0.03	0.15	0.07	0.26	0.07	1.70	0.23	0.00	0.05	0.02	0.84	3.16	0.82	1.99
LM	0-3	30	0.01	0.13	0.01	0.31	0.09	1.74	0.20	0.00	0.04	0.02	0.82	3.18	0.78	1.98
LM	53-56	69	0.04	0.16	0.05	0.30	0.05	1.69	0.23	0.00	0.07	0.02	0.84	3.16	0.85	1.98
MF	0-3	35	0.04	0.09	0.01	0.27	0.11	1.71	0.25	0.00	0.03	0.02	0.84	3.16	0.78	1.98
MF	53-56	19	0.02	0.15	0.01	0.20	0.13	1.73	0.22	0.00	0.04	0.01	0.83	3.17	0.80	1.99
MF	71-73	31	0.02	0.17	0.07	0.24	0.08	1.68	0.25	0.00	0.07	0.02	0.82	3.18	0.86	1.99
SP	0-3	28	0.01	0.17	0.03	0.23	0.09	1.74	0.22	0.00	0.03	0.02	0.83	3.17	0.80	1.99
SP	53-56	63	0.02	0.15	0.18	0.23	0.05	1.70	0.23	0.00	0.06	0.02	0.85	3.15	0.84	1.99
Montmorillonite		12	0.00	0.02	0.01	0.12	0.01	1.62	0.16	0.04	0.15	0.01	0.02	3.98	0.19	1.97
LM	0-3	3	0.01	0.07	0.00	0.06	0.00	1.36	0.33	0.00	0.29	0.03	0.02	3.98	0.22	1.98
LM	53-56	1	0.00	0.07	0.00	0.09	0.00	1.54	0.25	0.00	0.21	0.00	0.00	4.00	0.22	2.00
MF	0-3	2	0.00	0.00	0.05	0.11	0.00	1.50	0.25	0.00	0.17	0.03	0.03	3.97	0.17	1.91
MF	71-73	5	0.00	0.00	0.00	0.13	0.01	1.86	0.03	0.09	0.00	0.01	0.02	3.98	0.16	1.97
SP	53-56	1	0.00	0.00	0.00	0.30	0.00	1.59	0.08	0.00	0.33	0.00	0.00	4.00	0.30	2.00
diVS-ml		477	0.02	0.05	0.01	0.27	0.04	1.80	0.15	0.00	0.03	0.02	0.50	3.50	0.50	1.98
LM	0-3	45	0.01	0.05	0.00	0.33	0.03	1.76	0.19	0.00	0.04	0.02	0.54	3.46	0.52	1.99
LM	53-56	68	0.03	0.06	0.02	0.31	0.03	1.74	0.19	0.00	0.06	0.02	0.56	3.44	0.58	1.98
MF	0-3	60	0.02	0.03	0.00	0.26	0.06	1.85	0.13	0.00	0.01	0.01	0.50	3.50	0.48	1.99
MF	53-56	100	0.01	0.03	0.00	0.26	0.04	1.83	0.13	0.00	0.03	0.01	0.48	3.52	0.47	1.99
MF	71-73	76	0.01	0.04	0.00	0.22	0.06	1.84	0.12	0.00	0.02	0.01	0.43	3.57	0.44	1.98
SP	0-3	76	0.01	0.04	0.01	0.27	0.05	1.78	0.17	0.00	0.03	0.02	0.51	3.49	0.49	1.97
SP	53-56	52	0.02	0.08	0.09	0.25	0.01	1.76	0.15	0.00	0.08	0.01	0.53	3.47	0.56	2.00

**Figure 4.32. Octahedral occupation of diVS-ml series**

Reveals from TEM-EDX analyses (Jeol JEM-1210); Example of sample RRD-MF (53 – 56 cm); dark square with shadow indicates average values of particles with the same smectitic proportion; The empty square indicates value of only one particle

To summary, diVS-ml series – the dominant clay mineral group in sediments of RRD was corresponding mostly for the 10 Å clay phase. In earlier literatures (e.g. Chamley 1989, Thanh et al. 2000; Tra et al. 2000, Nghi 1998), the 10 Å clay phase were generally quoted as mica, hydromica or illite. In RRD sediments, diVS-ml was combined from K-poor, Mg^{VI} -poor diVerm phase and low charge montmorillonite phase. DiVS-ml retained imprints of chemical weathering process, such as curled edges, rough surface, and moiré patterns on surface morphology. Also, diVS-ml structures showed higher disorder level (smaller CSD, diffused edges, popular turbostratic ordering, higher Fe^{3+} substitution in octahedral layer), relatively to diVerm end-member.

DiVS-ml series in mangrove forest profile exhibited higher disorder level than the other profiles (i.e. LM and SP), higher average smectitic proportion, Fe^{3+} substitution in octahedral layer, especially in the interval of 50 cm depth. In this interval and also in the deeper part of sediment profiles, a movement of frequency distribution spectra toward montmorillonitic end-member was to see (in comparison to diVS-ml series in surface layer).

KE-ml series and end-members: Kaolinite and beidellite

Morphology

In addition to idiomorphic, pseudo-hexagonal kaolinite plates in medium to large sizes (0.7 – 1.5 μm), occurrence of aggregation by small, poor ordered particles was observed, characterizing sedimentary origin. Kaolinite particles showed their typical 1M polytype in SAED patterns (monocline).

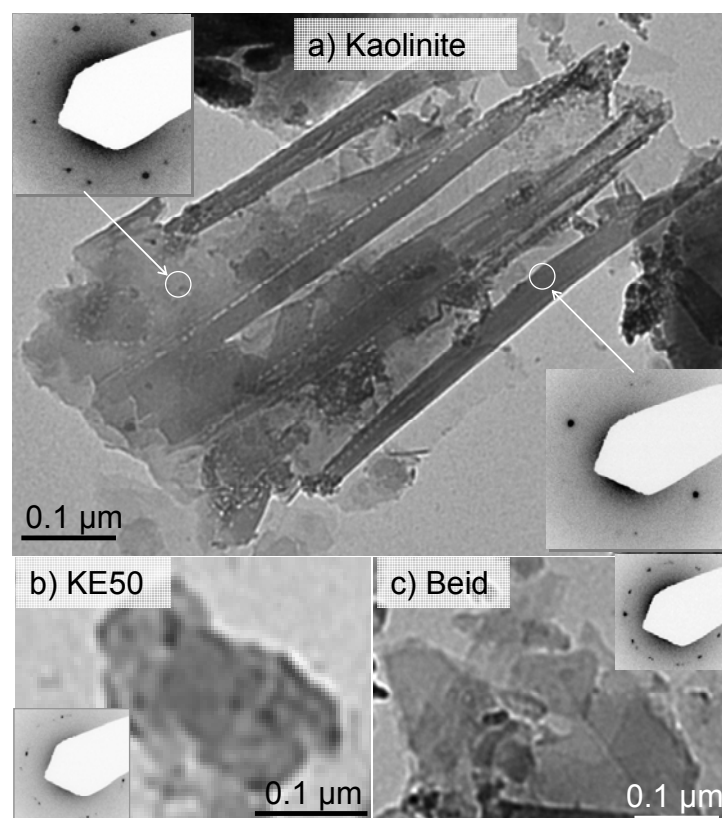


Figure 4.33. TEM images of KE-ml particles in sediments of the RRD

Reveals from TEM-EDX analyses (Jeol JEM-1210); Inserts are SAED image of the particles

Kaolinite particles were distinguished from halloysite particles, which also presented in the samples with small but typical tubular forms (0.1 – 0.3 μm). Elongated kaolinites in slat form (Figure 4.33a) had also been found, however only in occasional frequency.

Beidellite occurred as xenomorphic platelets in small sizes (few nanometres) and tended to form aggregation (Figure 4.33c). SAED of beidellite in Figure 4.33c showed the intergrowth of two particles with 1M polytype. *The irregular kaolinite/expandable mixed layer exhibited not only morphological features of beidellite (i.e. xenomorphic forms) but also of kaolinite (pseudo-hexagonal forms) (Figure 4.33b). Folds and curled edges were also detected.* KE-ml structures were detected in well order with 1M polytype and also in turbostratic order.

Crystallite structure

In the investigated sedimentary environments, KE-ml series exhibited a variety in proportional contribution of end members. Kaolinite particles in sediments of the RRD estuary were quite disordered with CSD < 200 Å and large FWHM (0.30 – 0.88) (Table 4.14). *The highest disorder degree was observed for kaolinite particles in MF profile, relatively to LM and SP profiles.* Generally, the mixed layer structures KE had smaller domain sizes than pure kaolinite. Along the profiles of low tidal mudflat and mangrove forest, *CSD of kaolinites decreased obviously from top to down (Table 4.14a), mirroring a higher degree of disorder.* However, the opposite trend was to observe for KE mixed layer structures: *with increasing depth, CSD increased (Table 4.14b). Exception was the 53 – 56 cm depth interval in mangrove forest, where CSD value of KE-ml was quite high.*

Table 4.14. Crystallite parameters of kaolinite & KE-ml structures based on 7 Å and 7.4 Å

Data extraction by WinFit, from XRD patterns of oriented mount specimen

Profile	Depth (cm)	D-value (Å)	Air-dried			D-value (Å)	Ethylene Glycolation		
			CSD (Å)	Int.max	FWHM (Å)		CSD (Å)	Int.max	FWHM (Å)
a) Kaolinite									
LM	0 – 3	7.13	190 – 200	219	0.3	7.15	170 - 220	106	0.144
LM	53 – 56	7.15	80 - 90	64	0.472	7.11	> 400	19	0.138
MF	0 - 3	7.26	~ 100	67	0.614	7.12	200 - 210	110	0.322
MF	53 – 56	7.20	70 – 80	82	0.774	7.14	190 – 200	164	0.325
MF	71 – 73	7.22	60 - 70	57	0.882	7.13	190 - 240	167	0.15
SP	0 – 3	7.17	140 – 150	125	0.413	7.17	90 – 100	137	0.423
SP	53 – 56	7.12	170 - 180	139	0.347	7.15	130 - 140	79	0.433
b) KE – ml structures									
LM	0 – 3	7.33	50 – 60	39	1.121	7.24	80 – 90	39	0.614
LM	53 – 56	7.61	~ 90	30	0.388	7.29	90 - 100	13	0.692
MF	0 - 3	7.59	50 – 60	23	1.223	7.28	30 – 40	40	1.722
MF	53 – 56	7.63	120 - 130	39	0.417	7.28	50 – 60	45	1.015
MF	71 – 73	7.58	70 – 80	11	0.481	7.18	~ 80	56	0.785
SP	0 – 3	7.49	30 - 40	46	1.456	7.57	60 – 70	13	0.6
SP	53 – 56	7.32	70 - 80	29	0.881	7.41	~ 50	15	1.35

Occurrence and distribution along depth profile

KE-ml series accounted for 4 – 12 % of total particle frequency in fractions $< 2 \mu\text{m}$ (Table 4.11). Frequency distribution of particles with different kaolinitic proportion was scatter, with more commonly particles of 70 – 80 %, 50 %, 30 % of smectitic percentage ($S\% = 33 - 58 \%$), in agreement to reveals from XRD patterns. *In all profiles, frequency of KE-ml decreased from the upper sediments to deeper parts* (Figure 4.34).

Chemical variation

The Al-rich octahedral structures of beidellites were revealed from Table 4.15. *Octahedral substitutions by Fe and Mg were more intensive in sediments of MF and SP profiles*. The Fe enrichment of in chemical structures was also found in the interlayer, where presence of Fe dominated over other cations (i.e. K, Na, Mg). *Along the sedimentary core in MF profile, Al substitution in tetrahedral layer in particles decreased with depth to the direction of more smectitic compound*.

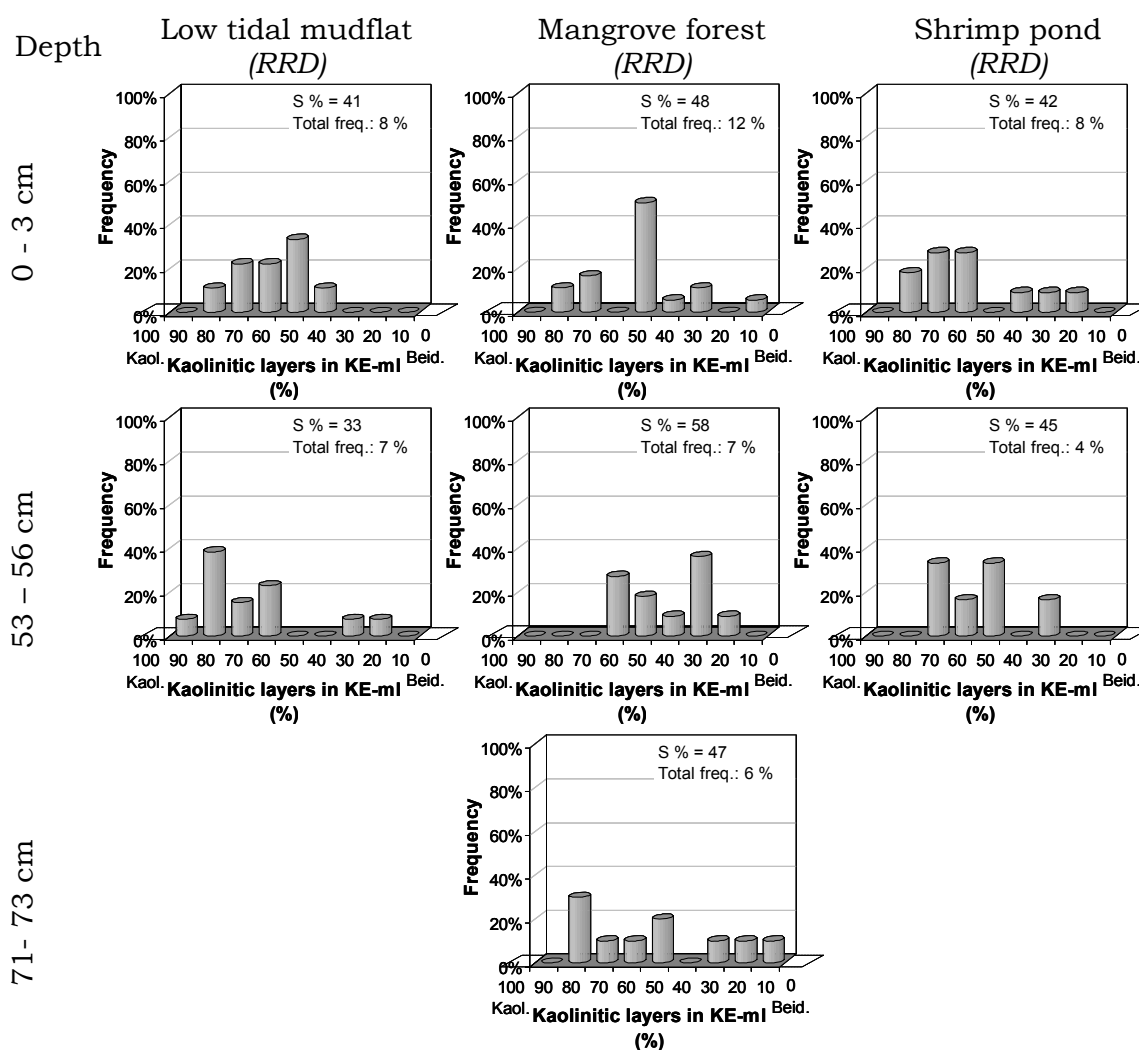


Figure 4.34. Frequency distribution of KE-ml series in sediment profiles of RRD

Reveals from TEM-EDX analyses (Jeol JEM-1210); Beid.: Beidellite; Kaol.: Kaolinite; S% displayed weighted average proportion of beidellitic layers in all particles

Table 4.15. Mineral formulae $[\text{O}_{10}(\text{OH})_n]^*$ of clay minerals from fractions $< 2 \mu\text{m}$, RRD sediments
Average values calculated based on TEM-EDX analyses (Jeol JEM-1210)

Sediment profile	Depth (cm)	No of particles	Interlayer					Octahedral layer					Tetrahedral layer			n^{VI}
			Ca	Mg	Na	K	Fe^{2+}	Al	Fe^{3+}	Fe^{2+}	Mg	Ti	Al	Si	XII	
Beidellite		29	0.02	0.04	0.01	0.06	0.08	1.96	0.07	0.00	0.00	0.02	0.52	3.48	0.35	2.03
LM	0-3	4	0.02	0.06	0.00	0.05	0.12	1.96	0.04	0.00	0.00	0.02	0.53	3.47	0.44	2.01
LM	53-56	2	0.06	0.12	0.00	0.05	0.00	1.48	0.47	0.00	0.00	0.07	0.55	3.45	0.39	1.96
MF	0-3	7	0.03	0.03	0.00	0.04	0.06	2.00	0.04	0.00	0.00	0.01	0.51	3.49	0.30	2.04
MF	53-56	3	0.02	0.06	0.00	0.06	0.08	1.98	0.04	0.00	0.01	0.01	0.52	3.48	0.40	2.03
MF	71-73	5	0.01	0.03	0.00	0.09	0.09	1.97	0.05	0.00	0.00	0.02	0.49	3.51	0.34	2.02
SP	0-3	5	0.03	0.02	0.01	0.06	0.09	2.05	0.00	0.00	0.00	0.01	0.53	3.47	0.33	2.05
SP	53-56	3	0.03	0.03	0.05	0.03	0.07	2.02	0.05	0.00	0.00	0.00	0.57	3.43	0.34	2.07
Kaolinite		21	0.00	0.00	0.00	0.02	0.00	3.73	0.18	0.01	0.03	0.04	0.03	3.97	0.03	3.96
LM	0-3	2	0.01	0.00	0.00	0.00	0.00	3.78	0.20	0.00	0.00	0.05	0.14	3.86	0.02	3.97
LM	53-56	1	0.01	0.00	0.00	0.00	0.00	3.82	0.17	0.00	0.00	0.01	0.04	3.96	0.03	3.99
MF	0-3	7	0.00	0.00	0.00	0.02	0.00	3.68	0.21	0.04	0.03	0.03	0.02	3.98	0.02	3.96
MF	53-56	1	0.00	0.00	0.00	0.05	0.00	3.46	0.32	0.00	0.11	0.06	0.00	4.03	0.05	3.93
MF	71-73	8	0.00	0.00	0.01	0.02	0.00	3.81	0.13	0.00	0.02	0.03	0.01	3.99	0.02	3.97
SP	0-3	2	0.00	0.02	0.00	0.00	0.00	3.62	0.23	0.00	0.05	0.08	0.08	3.92	0.03	3.91
SP	53-56	2	0.01	0.00	0.00	0.00	0.00	3.78	0.20	0.00	0.00	0.05	0.14	3.86	0.02	3.97
KE-ml		92	0.01	0.00	0.02	0.06	0.03	3.05	0.09	0.00	0.01	0.01	0.22	3.78	0.17	3.15
LM	0-3	14	0.02	0.01	0.01	0.08	0.02	3.21	0.11	0.00	0.00	0.01	0.17	3.83	0.15	3.33
LM	53-56	22	0.01	0.00	0.05	0.07	0.01	3.17	0.12	0.00	0.00	0.02	0.20	3.80	0.17	3.28
MF	0-3	18	0.01	0.00	0.01	0.03	0.04	2.99	0.06	0.00	0.00	0.01	0.23	3.77	0.14	3.05
MF	53-56	12	0.01	0.00	0.00	0.06	0.08	2.81	0.03	0.00	0.00	0.01	0.28	3.72	0.24	2.84
MF	71-73	10	0.01	0.01	0.01	0.09	0.03	2.96	0.05	0.00	0.07	0.01	0.23	3.77	0.19	3.07
SP	0-3	10	0.01	0.00	0.00	0.05	0.02	3.11	0.11	0.00	0.00	0.02	0.20	3.80	0.13	3.23
SP	53-56	6	0.00	0.01	0.09	0.07	0.00	2.93	0.11	0.00	0.04	0.03	0.23	3.77	0.19	3.08

*: $n_{(\text{beidellite})} = 2$; $n_{(\text{kaolinite})} = 8$; and $n_{(\text{KE})}$ were assumed to be *linearly* proportional intermediate

Kaolinite particles were Fe-rich with 5-7 % of octahedral occupations by Fe^{3+} (Table 4.15). In mixed layer structures, layer charge due to tetrahedral substitution of Si^{4+} by Al^{3+} was balanced by K^{+} and Fe^{2+} in interlayer. Isomorphic substitution of Fe^{3+} in the octahedral layer of kaolinite was reported by Jefferson et al. (1975) based on Mössbauer spectroscopic data.

All together, some variations in KE-ml series could be detected for frequency, particle morphology, CSD as well as chemical structure when comparing three environments (LM, MF, SP), the top with the down as well the mixed layer structures with end-members. From top to down, frequency of KE-ml decreased for full spectra. Kaolinite showed higher degree of disorder but KE-ml showed larger CSD sizes. Highest CSD was reached in the interval of 53 – 56 cm depth in mangrove forest profile. The average concentration of tetrahedral Al decreased also in deeper parts, which is obvious in MF profile. For lateral comparison, KE-ml in MF profiles exhibited the highest degree of disorder, octahedral substitution by Fe^{3+} and Mg^{2+} . Comparing to end-members, KE-ml contained morphological features of both kaolinite and beidellite, but more commonly in turbostratic ordering.

IS-ml mixed layer series and end-members: illite and montmorillonite

The illite/smectite mixed layer structures (IS-ml) occurred as intermediate products in transformation sequence between illite and montmorillonite.

Morphology

Although illite was documented to be very commonly in weathered matters, only few particles of pure illite in the fraction $< 2\mu\text{m}$ had been found in estuarine sediments of the Red River Delta (Table 4.11). Illite particles were characterized by xenomorphic shape (Figure 4.35), distinguishingly from thin-film platelets of montmorillonite particles, which had been described above. IS-ml particles were more commonly observed with curled edge, which were typically for expandable properties (Henning & Stoerr 1986). The xenomorphic platelets became smaller in size with increasing percentage of smectitic layers in the mixed layer structure (Figure 4.35).

Crystallite structure

Crystal parameters of IS could be referred also from the 10 \AA as description above for diVS-ml structure. But interference between these two series IS-ml and diVS-ml, and the predominance of diVS-ml series in samples should be considered.

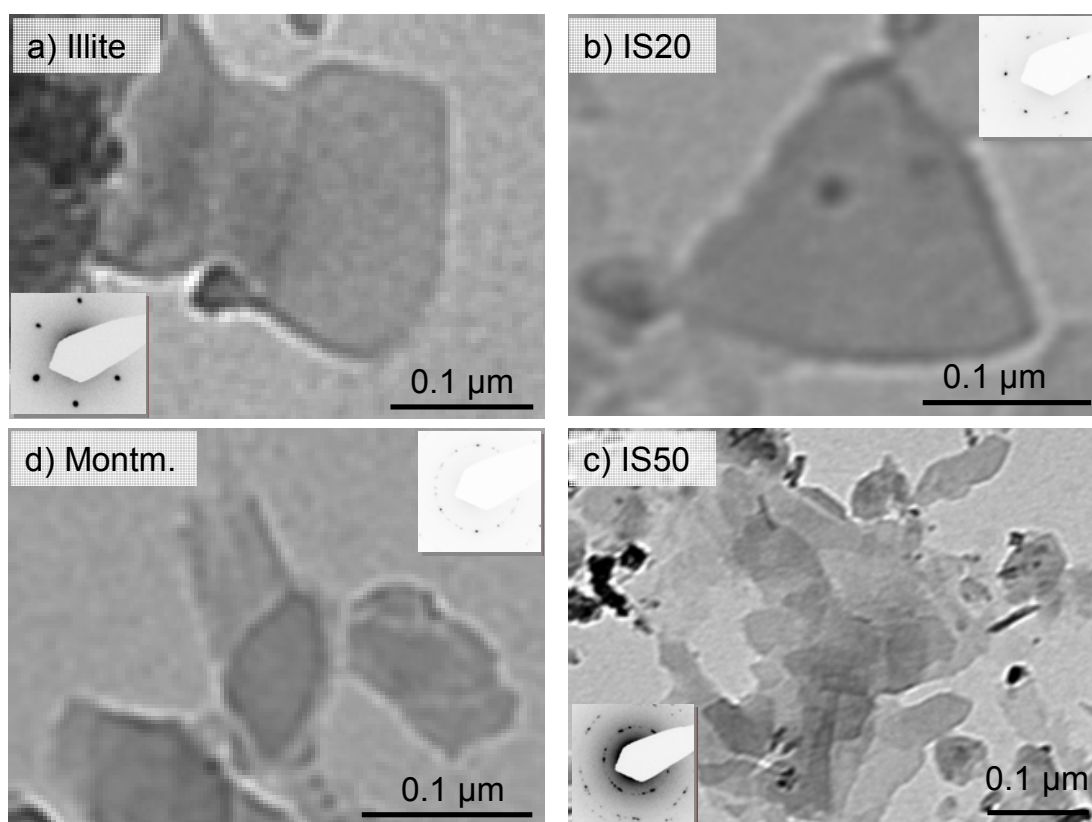


Figure 4.35. TEM images of particles in IS-ml series in coastal sediment sample of RRD

Reveals from TEM-EDX analyses (Jeol JEM-1210); Inserts are SAED image of the particles. Examples in samples RRD-MF 71-73 cm.; a) illite; b) IS-ml with 20 % smectitic percentage; c) IS-ml with 50 % smectitic percentage; d) montmorillonite. Scale bar = $0.1\mu\text{m}$.

In Figure 4.35, the end-member pure illite particle showed clearly order of $2M_1$ polytype structure. The $2M_1$ polytype was also to observe for some IS-ml particles, however, the most commonly polytype of these mixed layer structures was turbostratic ordering.

Occurrence and distribution along depth profile (Figure 8.25, Appendix)

IS-ml series accounted for low frequency in total particle frequency occurring in fractions $< 2 \mu\text{m}$ (6 – 15 %) dominated by mixed layer structures (Table 4.11). Particles of pure illite and montmorillonite occurred occasionally.

The distribution spectra was scatter in LM profile but tended to follow gauss functions in MF and SP profiles (Figure 8.25, Appendix). *In surface sediments, average percentage of smectitic proportion in the whole mixed layer series (S%) increased from LM via MF to SP profiles.* From the top to the deeper parts, a gradual moving of frequency distribution toward montmorillonitic particles was generally observed in profiles of low tidal mudflat and mangrove forest, corresponding to the increase of S%. Exception was the deeper part of shrimp pond profile (53 – 56 cm), where IS-ml series were abundant and illitic.

Chemical variation (Table 8.6, Appendix)

In the IS-ml series from the investigated sediments, average composition of the illite end-member exhibited a higher charge characteristic. The interlayer charge of 0.96 was dominated by K, but a relative high amount of Na was to consider.

CS-ml series and end members: chlorite and saponite

Morphology

In electron micrographs, chlorites were depicted as xenomorphic platelets or parallel intergrowths of these platelets (Figure 4.36). Particles occurred with large crystallite platelets and were abundant with ragged or bending edges. SAED pattern showed $1M$ polytype of this mineral in the investigated sediments. CS-ml particles had similar morphology to chlorites, but occurred more commonly in smaller sizes. It was also to detect CS composition on edges of chlorite structure (Figure 4.36). Mixed layer structures showed a polytype in the direction of turbostratic order formation with typical conspicuous stacks of platelets.

Crystallite structure (Table 8.7, Appendix)

The mixed layer structures were determined including types with 40 – 50 % of saponitic layers in all samples and 70 – 90 % of chloritic layers, with agreement between TEM and XRD data.

Table 8.7 (Appendix) presents crystallite parameters of chlorite, revealed for the 7 \AA reflection of chlorite (deconvoluted from overlapping with reflections of kaolinite and KE-ml) and the 14 \AA reflection. Low values of FWHM, intensity as well as high values of CSD revealed that chlorite particles in the sample were well ordered, and occurred in low quantity in the samples. CS-ml structures were also well ordered, however in lower degree relatively to pure chlorite particles. CS-ml showed slightly expansion under EG saturation with increase of d-spacing and CSD.

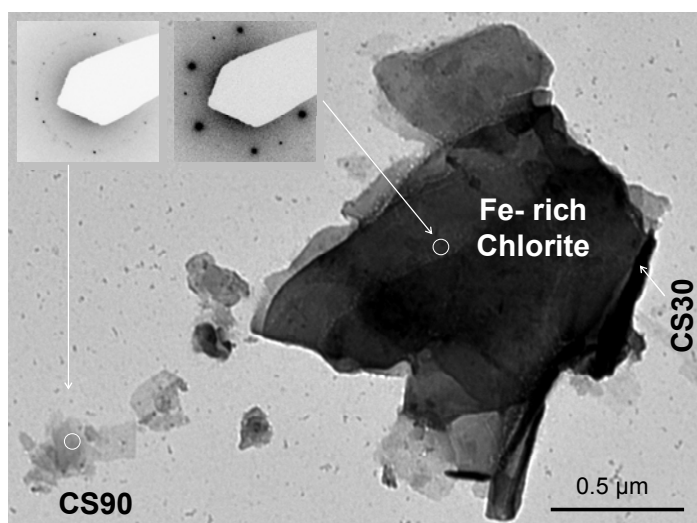


Figure 4.36. TEM images of Chlorite and CS-ml particles in RRD sediments

Reveals from TEM-EDX analyses (Jeol JEM-1210); Inserts are SAED image of the particles

Occurrence and distribution along depth profile

CS-ml structures appeared in the fractions $< 2 \mu\text{m}$ with frequency varying from 1 – 7 % of total observed particles. The highest frequencies were observed at the depth of 51 – 53 cm in all profiles.

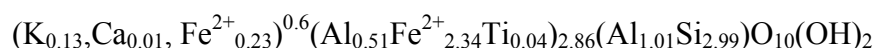
Mixed layer structures with 40 – 60 % of saponitic proportion were dominated in the whole series, corresponding to reveals from XRD data. CS-ml structures with 70 – 80 % of saponitic proportion were also detected in sediments of LM profile as well as in subsurface sediments in MF and SP profile.

Chemical variation

The detected Fe- rich chlorites (Table 8.9, Appendix) appeared mostly in large crystallite platelets.

Associated minerals in fractions $< 2 \mu\text{m}$

Beside the principal four mixed layer series mentioned above for clay matters, the clay mineral - trioctahedral vermiculite was also detected in traces, in deeper parts of sediments in MF and SP profiles. In MF, the triVerm had higher Fe substitution in octahedral layer and interlayer than the triVerm in SP profile. Average formula of triVerm in MF was:



The associated non-clay minerals included quartz, feldspar, pyrite and hydroxides of Fe and Al, also in trace. Pyrite appeared in a wide range of sizes, from fractions $> 63 \mu\text{m}$ to fractions $< 2 \mu\text{m}$. Single line analysis for these reflections determined that pyrite was poor ordered with average CSD of 230 \AA .

In conclusion, muddy sediments in estuary of the RRD were dominated by clay minerals, with association of quartz, feldspars, pyrite and hydroxides of Al, Fe. Clay matters concentrated in fraction $< 2 \mu\text{m}$, comprising essentially of four mixed layer series: diVS-ml, KE-ml, IS-ml and CS-ml. DiVS-ml series and KE-ml were dominantly. In comparison to end-members, mixed layer structures exhibited more popularly diffused edges on crystals, turbostratic ordering, smaller CSD and octahedral substitution by Fe^{3+} .

Comparison between samples of different environments (LM, MF, SP) as well as of different depth intervals have revealed variation tendencies in relative quantity (XRD-data), total frequency, frequency spectra, ordering degree, chemical structures. Exceptions were commonly detected in the 53 – 56 cm depth interval of MF profile.

4.4.2 South Central Coastline

Bulk mineralogy

In South Central Coast - the South Central Coast of Vietnam, the mineralogical suit of muddy sediments (sampled in Dam Mon and Nha Phu) had been determined to contain clay minerals (kaolinite, illite, vermiculites, smectites, chlorite, mixed layer series) and associated non-clay minerals (quartz, feldspar, calcite, pyrite, hematite, gypsum). In each coastal region, a qualitative seen homogenous distribution of mineral assemblage was revealed in patterns among different profiles as well as along the depth (Figure 8.10, Figure 8.11).

Mineralogy of fraction $< 2 \mu\text{m}$

In fractions $< 2 \mu\text{m}$, clay minerals were determined with association of non-clay minerals like quartz, feldspar, hematite, gypsum and pyrite. Similarly to clay matters of the RRD sediments, the clay suit in the south central coast contained kaolin groups (incl. kaolinite and halloysite), chlorite, illite, vermiculite (di- and tri-octahedral species), smectites (beidellite, montmorillonite, saponite) and mixed layers, relevant to *four principal series of mixed layers* (Table 4.16, Table 4.17). These series were dioctahedral vermiculite/smectite mixed layers (diVS-ml), and kaolinite/expandable mixed layers (KE-ml), chlorite/saponite mixed layers (CS-ml) and illite/smectite mixed layers (IS-ml). DiVS-ml was the dominant series in total particle frequency, followed by KE-ml. CS-ml in Dam Mon was more popular than in Nha Phu but IS-ml in both regions was detected only in very low frequency.

Additionally, traces of other mixed layer species such as chlorite/trioctahedral vermiculite, trioctahedral vermiculite/ dioctahedral vermiculite, kaolinite/ dioctahedral vermiculite were detected.

Dioctahedral Vermiculite/Smectite mixed layer series (diVS-ml)

Morphology

TEM images showed typical xenomorphic shapes with moiré patterns of dioctahedral vermiculite particles in sediments of the south central coast of Vietnam (Figure 4.37a, c). DiVerm particles occurred commonly in both 1M and 2M_1 polytypes. Acting as intermediate

in the transformation series between diVerm and montmorillonite, diVS-ml structures exhibited corresponding polytypes and also *turbostratic order* (Figure 4.37b, d, e). These mixed layer platelets were readily observed with *diffuse outlines*, characterizing modification by the ambient.

“Low charge” montmorillonite particles occurred in a wide range of morphological variety, from thin-film platelets (Figure 4.37f) to xenomorphic particles (Figure 4.45e) and nepheloids (Figure 4.45d) with sizes of few nanometres (Figure 4.45d, e). The polytype 1M was determined.

Table 4.16. Frequency (%) of mixed layer series³ in sediment profiles in the coastal zone in Dam Mon – South Central Coast

Reveals from TEM-EDX analyses (Jeol JEM-1210), counting > 100 particles per sample

Sediment profile	Depth (cm)	total diVS-ml	diVerm	diVS	hc diVS	Mont	total KE-ml	Kaol	KE	Beid	total CS-ml	Chl	CS	Sap	total IS-ml	Illite	IS	Mont
Low tidal mudflat (LM)	0-10	62 %	21	30	11	<1	19 %	4	12	3	15 %	<1	9	6	<1 %	<1	<1	<1
	10-20	68 %	39	22	6	<1	17 %	1	11	4	9 %	<1	4	5	1 %	<1	1	<1
	40-50	71 %	34	25	11	1	10 %	1	3	5	9 %	<1	5	4	1 %	<1	<1	1
	80-90	67 %	27	29	11	<1	10 %	3	4	3	17 %	<1	7	10	1 %	<1	1	<1
Mangrove forest (MF)	0-10	54 %	28	26	<1	<1	40 %	2	28	11	1 %	<1	<1	1	1 %	<1	1	<1
	10-20	64 %	17	37	10	<1	29 %	4	12	13	4 %	<1	2	2	2 %	<1	2	<1
	40-50	70 %	33	36	1	<1	18 %	3	11	4	8 %	<1	1	7	1 %	<1	1	<1
	80-90	65 %	34	27	4	<1	13 %	1	7	5	14 %	<1	4	10	3 %	<1	3	<1
Shrimp pond (SP)	0-10	71 %	35	36	<1	<1	14 %	1	8	6	13 %	<1	8	5	1 %	<1	1	<1
	40-50	54 %	29	18	6	1	16 %	4	8	3	19 %	<1	13	6	1 %	<1	1	1
	80-90	63 %	11	49	<1	3	16 %	<1	6	10	11 %	<1	3	8	10 %	<1	7	3

Table 4.17. Frequency (%) of mixed layer series⁴ in sediment profiles in the coastal zone in Nha Phu

Reveals from TEM-EDX analyses (Jeol JEM-1210), counting > 100 particles per sample

Sediment profile	Depth (cm)	total diVS-ml	diVerm	diVS	Mont	total KE-ml	Kaol	KE	Beid	total CS-ml	Chl	CS	Sap	total IS-ml	Illite	IS	Mont
Low tidal mudflat (LM)	0-10	62 %	23	40	<1	32 %	1	20	12	<1 %	<1	<1	<1	<1 %	<1	<1	<1
	10-20	62 %	22	39	<1	32 %	5	17	10	5 %	<1	5	<1	1 %	<1	<1	<1
	40-50	41 %	24	17	<1	54 %	6	44	5	2 %	<1	2	<1	2 %	1	1	<1
	80-90	58 %	30	28	<1	37 %	3	19	15	3 %	<1	2	2	1 %	<1	1	<1
Mangrove forest (MF)	0-10	64 %	29	35	<1	28 %	1	7	20	1 %	<1	1	<1	5 %	<1	5	<1
	10-20	58 %	27	30	1	41 %	3	30	7	<1 %	<1	<1	<1	1 %	<1	1	1
	40-50	28 %	15	13	<1	71 %	1	56	14	1 %	<1	1	<1	1 %	<1	1	<1
Shrimp pond (SP)	0-10	73 %	33	40	<1	23 %	1	12	10	<1 %	<1	<1	<1	3 %	1	2	<1
	10-20	50 %	9	40	<1	49 %	3	22	23	1 %	<1	1	1	<1 %	<1	<1	<1
	40-50	41 %	5	33	3	57 %	3	37	17	2 %	<1	2	<1	5 %	<1	2	3
	80-90	62 %	25	36	<1	29 %	2	12	15	6 %	<1	6	<1	2 %	<1	1	<1

³ Abbreviations of mineral name: see Table 4.11

⁴ Abbreviations of mineral name: see Table 4.11

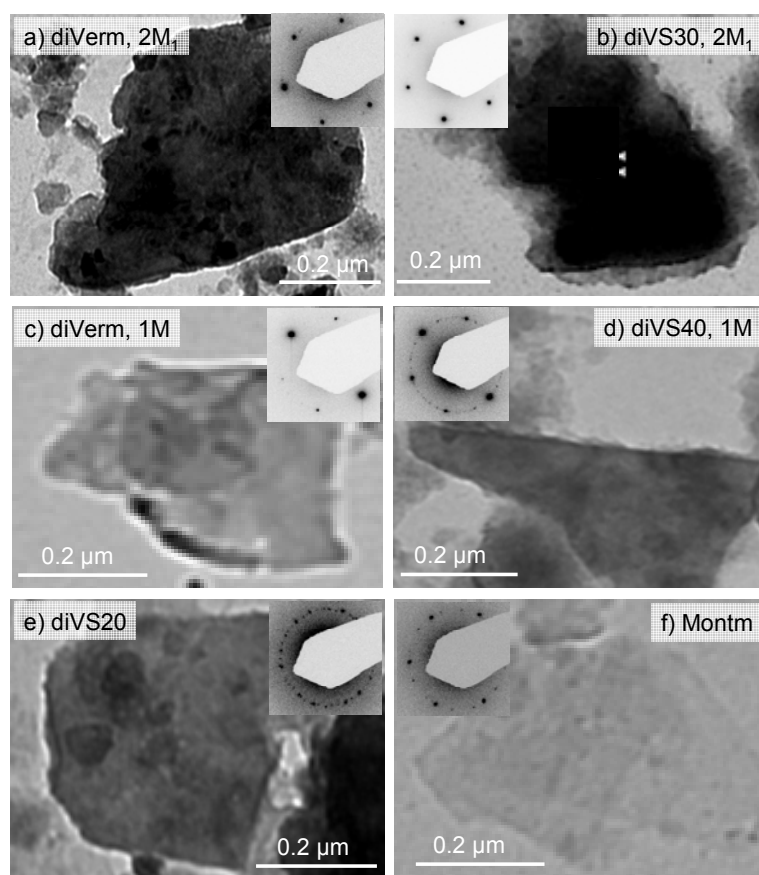


Figure 4.37. TEM images of diVS-ml particles and their end-members in coastal sediments of South Central Coast

Reveals from TEM-EDX analyses (Jeol JEM-1210); Inserts are SAEDs of particle. Values behind diVS structure indicate smectitic percentage

Crystallite structure

Deconvolution of the 10 Å reflection in XRD-diffractogram allowed distinguishing of dioctahedral vermiculite from reflections of pure illite. These diVerd particles were revealed to be rather well ordered, with FWHM ranging from 0.16 – 0.30, corresponding to coherent scattering domain sizes (CSD) from 130 – 470 Å (Table 4.18). From top to down in all profiles, *d-values of diVerd structures increased generally and CSD became smaller*, reflecting intensification of disorder levels or alteration to diVS-ml structures in deeper sediments.

In comparison to the end-members, diVS-ml structures showed higher degree of disorder, as reflected by smaller CSD values. The end-member mineral diVerd and also diVS mixed layer structures had increasing *d-values* and decreasing CSD with depth.

Along mangrove forest profiles in both regions Dam Mon and Nha Phu, *CSD of diVS-ml was slightly intensified at intervals of 50 cm but CSD of diVerd decreased.*

Occurrence and distribution along depth profile

The mixed layer series diVS accounted for the main composition in clay matters of the fractions < 2 μm, with 41 – 70 % of total particle frequency. Approximately a half of the series were determined as pure dioctahedral vermiculite (with 100% diVerd layers). The end-member montmorillonite was detected in trace.

Frequency of diVS-ml structures with different smectitic proportion followed asymmetric Gaussian distribution, unimodal bias vermiculite or bimodal in manner (Figure 4.38).

Table 4.18. Crystallite parameters of diVS-ml and/or IS-ml structures in SCC sediments

based on XRD reflections in 10 – 14 Å ranges

Data extraction by WinFit; XRD patterns of oriented mount, air-dried (AD) specimens

Dam Mon						Nha Phu					
Profile	Depth (cm)	d-value (Å)	CSD (Å)	Int.Max	FWHM (Å)	Profile	Depth (cm)	d-value (Å)	CSD (Å)	Int.Max	FWHM (Å)
diVerm and/or Illite											
LM	0 - 10	9.96	290 - 300	133	0.252	LM	0 - 10	9.97	320 – 340	52	0.226
LM	10 - 20	9.96	330 - 350	101	0.21	LM	10 - 20	9.96	> 400	136	0.135
LM	40 - 50	9.97	200 - 280	292	0.128	LM	40 - 50	10.01	200 – 260	143	0.37
LM	80 - 90	9.99	130 – 140	101	0.296	LM	80 - 90	10.00	> 400	223	0.154
MF	0 - 10	9.97	> 400	145	0.16	MF	0 - 10	9.96	> 400	567	0.112
MF	10 - 20	9.96	340 - 390	221	0.181	MF	10 - 20	9.97	> 400	151	0.146
MF	40 - 50	9.98	240 – 250	112	0.284	MF	40 - 50	9.98	280 – 300	69	0.246
MF	80 - 90	10.00	290 - 300	78	0.249						
SP	0 - 10	9.97	260 - 270	132	0.254	SP	0 - 10	9.94	> 400	78	0.154
						SP	10 - 20	9.93	280 – 290	138	0.258
SP	40 - 50	9.97	160 - 180	77	0.214	SP	40 - 50	9.95	360 – 400	259	0.184
SP	80 - 90	9.99	> 400	149	0.164	SP	80 - 90	9.95	330 – 360	229	0.198
diVerm / diVS-ml and/or IS-ml structure											
LM	0 - 10	10.25	180 - 190	41	0.276	LM	0 - 10	10.12	40 – 50	40	1.209
LM	10 - 20					LM	10 - 20				
LM	40 - 50	10.45	~ 80	17	1.133	LM	40 - 50	10.32	190 – 240	49	0.59
LM	80 - 90					LM	80 - 90				
MF	0 - 10	10.18	~ 120	47	0.505	MF	0 - 10				
MF	10 - 20	10.15	60 - 70	44	1.183	MF	10 - 20				
MF	40 - 50	10.29	90 – 100	44	0.732	MF	40 - 50	10.16	200 – 210	55	0.682
MF	80 - 90	10.08	70 - 80	35	0.524						
SP	0 - 10	10.16	90 – 100	58	0.692	SP	0 - 10	10.16	160 – 170	78	0.440
						SP	10 - 20	10.13	160 – 170	55	0.474
SP	40 - 50	10.21	~ 50	20	0.972	SP	40 - 50	10.22	100 – 110	60	0.648
SP	80 - 90	10.18	50 – 60	67	1.532	SP	80 - 90	10.12	150 – 160	88	0.448
diVS-ml and/or IS-ml structure											
LM	0 - 10	12.41	80 - 90	12	0.916	LM	0 - 10	12.24	60 – 70	25	0.944
LM	10 - 20	nd				LM	10 - 20	13.23	50 – 60	9	1.187
LM	40 - 50	13.30	50 - 60	27	1.006	LM	40 - 50	nd			
LM	80 - 90	13.00	60 - 65	19	0.952	LM	80 - 90	12.73	100 – 110	19	0.646
MF	0 - 10	12.35	120 - 125	16	0.569	MF	0 - 10	13.01	50 – 60	67	1.555
MF	10 - 20	12.36	80 – 90	27	0.907	MF	10 - 20	nd			
MF	40 - 50	13.50	40 - 60	22	0.946	MF	40 - 50	12.93	40 – 50	25	1.294
MF	80 - 90	13.25	60 - 70	46	1.123						
SP	0 - 10	nd				SP	0 - 10	13.18	40 – 50	27	1.414
						SP	10 - 20	nd			
SP	40 - 50	12.48	110 - 120	5	0.648	SP	40 - 50	12.57	30 – 40	54	1.62
SP	80 - 90	nd				SP	80 - 90	13.15	~ 40	92	1.52

LM: Low tidal mudflat; MF: Mangrove forest; SP: Shrimp pond

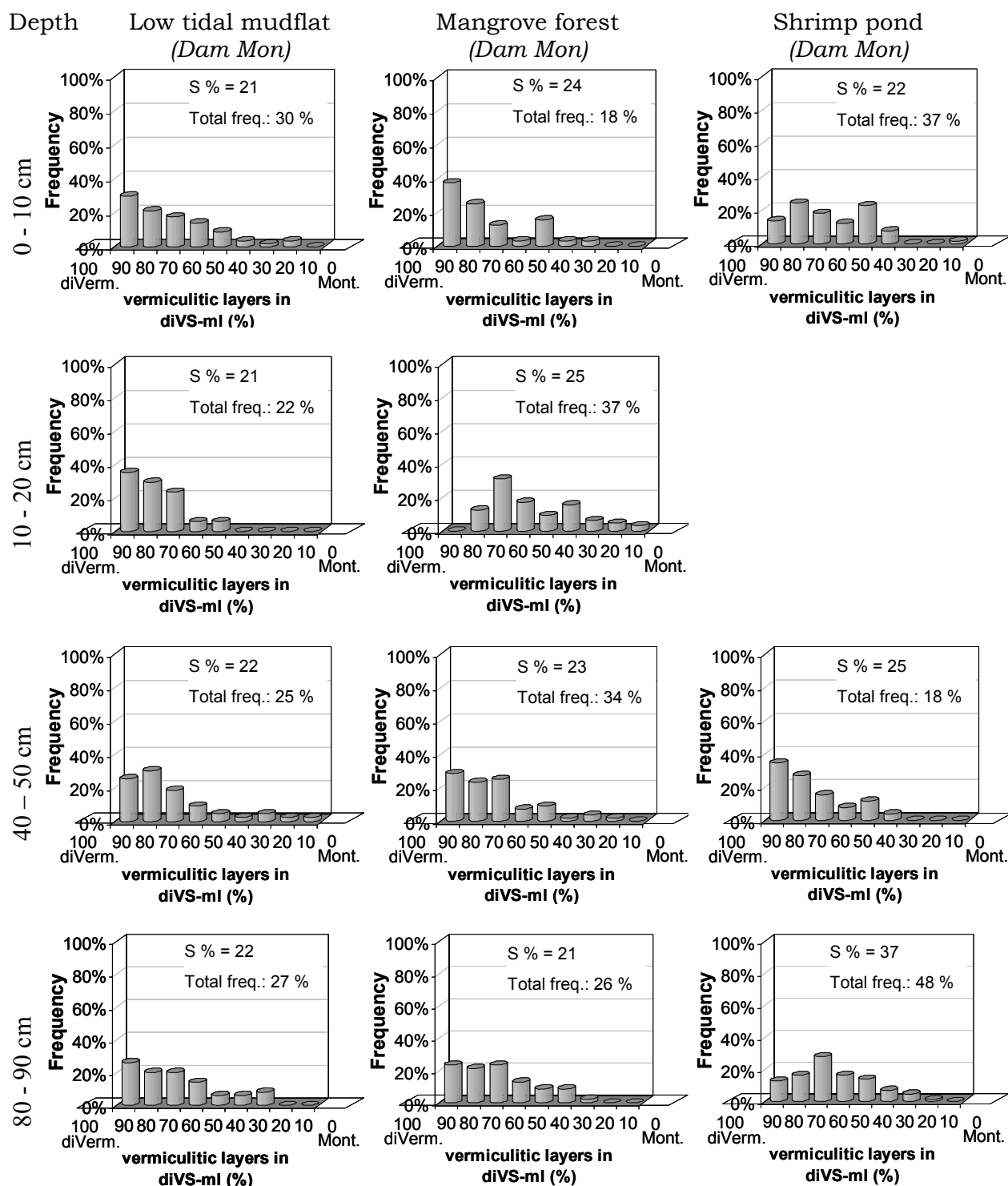


Figure 4.38. Frequency distribution of diVS-ml series in sediment profiles of Dam Mon

Reveals from TEM-EDX analyses (Jeol JEM-1210); Mont: Montmorillonite; diVerm: dioctahedral vermiculite; S% displayed average percentage of montmorillonitic layers in the whole diVS-ml series

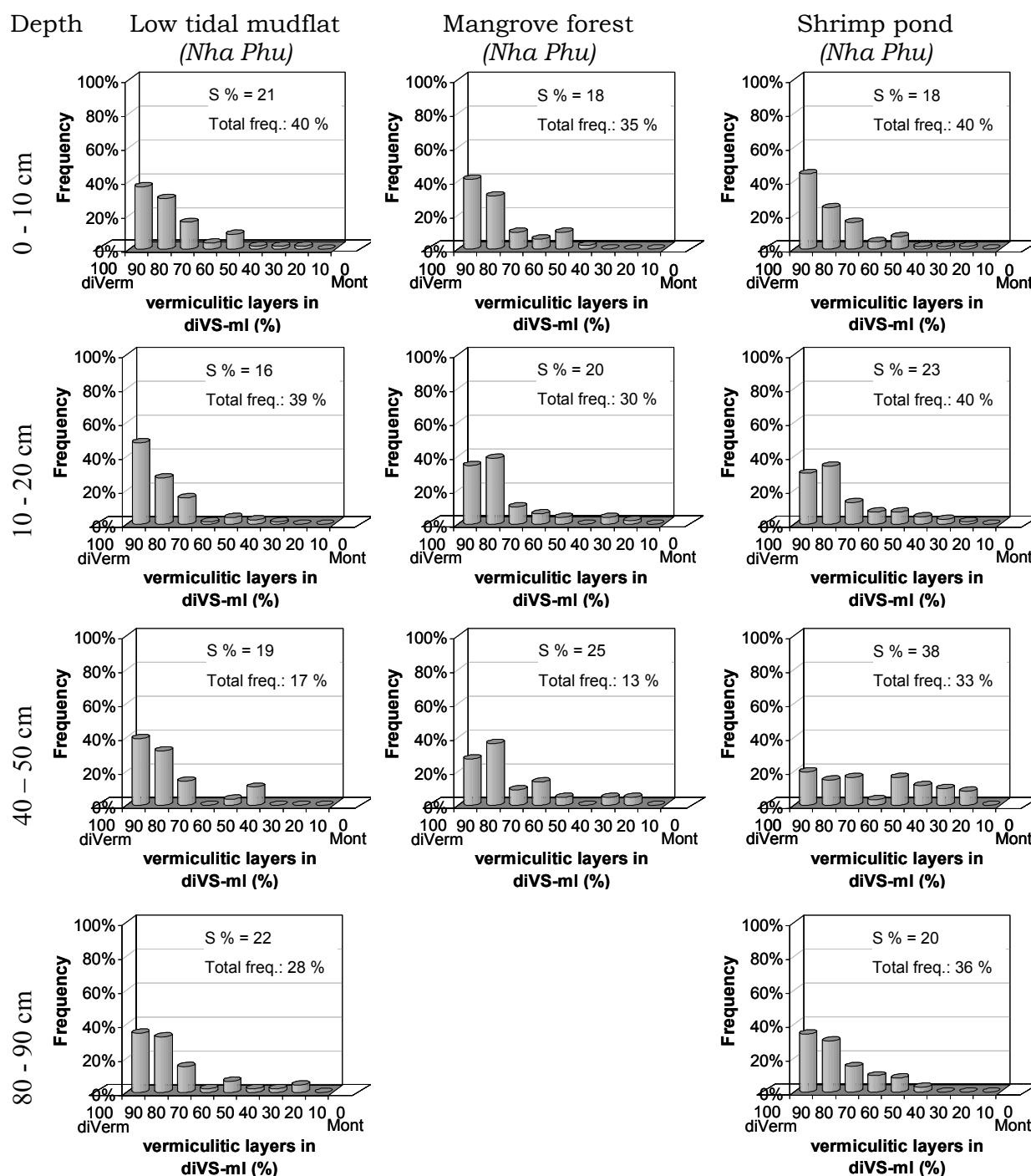


Figure 4.39. Frequency distribution of diVS-ml series in sediment profiles of Nha Phu

Reveals from TEM-EDX analyses (Jeol JEM-1210); Mont: Montmorillonite; diVerm: dioctahedral vermiculite; S% displayed average percentage of montmorillonitic layers in the whole diVS-ml series

Comparing the sequence of sediments from LM via MF to SP profiles, a stepwise formation of new distribution mode toward montmorillonitic was obviously, parallel to the gradual increase of S%. From top to down, the frequency distribution also moved gradually toward montmorillonitic structures. Exception of these tendencies was the intervals of 10 – 20 cm depth in MF profiles of Dam Mon (Figure 4.38) and 40 – 50 cm depth in Nha Phu (Figure 4.39), where frequency of diVS was rather high in smectitic ranges, so do the values of S%. S% values of diVS-ml structures in the subsurface sediments were generally higher than those

in surface sediments. At deepest part of SP profile, formation of a complete new mode with top position near diVS-ml structures with 70% vermiculitic layers was quite clear to see.

Similar trends were observed for profiles in Nha Phu sediments (Figure 4.39): a gradual moving toward montmorillonitic structures in mixed layer series from LM, via MF to SP as well as from top to down. In both localities, the deep horizon at 80 – 90 cm was not continuing the trends described from the top to the deeper section's parts.

Chemical variation

Particles of diVerm and diVS-ml, though accounted for high frequency in clay matters, displayed a rather homogenous chemical composition among different layers in sedimentary profiles. *Octahedral substitution for Al was mainly by Fe^{3+} up to averagely 0.3 of the 2 sites (Table 4.18). Mg and K were the main cations in interlayer, but slightly replaced by Na in surface sediments.* Different from the abundance of diVerm and diVS-ml, montmorillonite appeared occasionally in the samples of Dam Mon, and showed a relative high charge ($XII = 0.29 - 0.43$), resulted from octahedral substitution by Mg and Fe.

In mangrove forest profiles of both regions Dam Mon and Nha Phu, the contribution of potassium in the interlayer of mixed layer structures depleted clearly in the upper parts of profiles. However, octahedral substitutions were more intensified with increasing depth.

In SP sediments, diVerm and diVS-ml particles showed higher octahedral substitutions by Fe^{3+} than those in LM and MF sediments (Table 4.18). Along SP profile, both end-members and mixed layer structures of diVS-ml series exhibited increase in Si occupations in tetrahedral layers with increasing depth. Whereas, tetrahedral occupations in diVS-ml structures of LM and MF profiles were quite stable.

Octahedral occupations

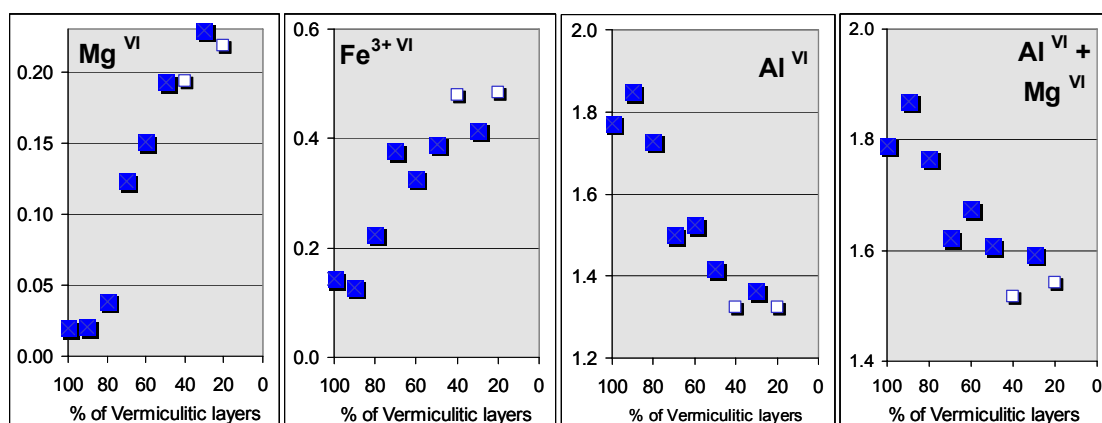
A generally tendency was to observe for octahedral occupations: from particles with higher vermiculitic proportion to particles with higher smectitic proportion (Figure 4.40a, left to right), octahedral Mg^{2+} increased, Fe^{3+} increased whereas Al^{3+} and the total $Al^{3+} + Mg^{2+}$ decreased. This was to show *higher substitution by both Mg^{2+} and Fe^{3+} into the octahedral layer occurred in the more smectitic diVS-ml structures.* This tendency was determined in both areas: Dam Mon and Nha Phu, similarly to the determined tendency in diVS-ml series of the Red River Delta.

Conclusively, some variation tendencies in appearance frequency, morphological features, crystal structures and chemical composition of diVS-ml series – the dominant clay phases in fractions $< 2\mu m$, can be determined. Comparing between end-members and mixed layer structures, diVS-ml had higher *degree of disorder, mirrored by smaller CSD, turbostratic ordering, diffused edges.* Comparing three profiles: LM, MF and SP, diVS-ml in characteristics of diVS-ml. Comparing from top to down, diVS-ml series exhibits higher degree of disorder, higher octahedral substitution by Fe^{3+} and moving of frequency spectra toward montmorillonitic end-member. Only two exceptions of these tendencies was *high frequency of smectitic diVS-ml in the intervals of 10 – 20 cm depth in MF profiles of Dam Mon (and 40 – 50 cm depth in Nha Phu).*

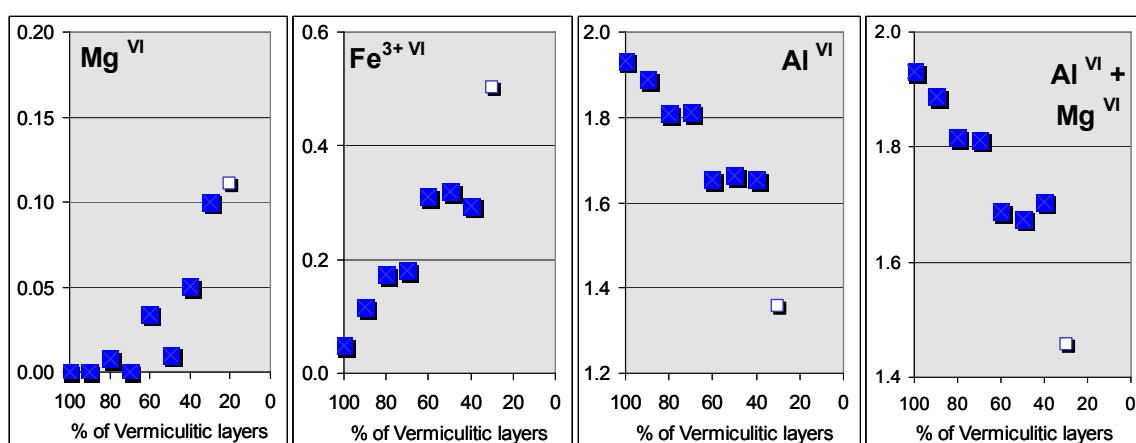
Table 4.19. Mineral formulae [O₁₀(OH)₂] of clay minerals from fractions < 2 µm, dispersed from sediment profiles in Nha Phu*Average values calculated based on TEM-EDX analyses (Jeol JEM-1210)*

Average values calculated based on TEM-EDX analyses (see SEM-EDX)															
Profile	Depth (cm)	Interlayer				Octahedral layer				Tetrahedral layer					n ^{VI}
		Ca	Mg	Na	K	Fe ²⁺	Al	Fe ³⁺	Fe ²⁺	Mg	Ti	Al	Si	XII	
Profiles in Dam Mon															
Dioc. Vermiculite		0.08	0.22	0.05	0.10	0.04	1.55	0.32	0.00	0.12	0.02	0.78	3.22	0.82	1.99
LM	0 – 10	0.05	0.26	0.05	0.06	0.04	1.53	0.33	0.00	0.13	0.02	0.77	3.23	0.82	1.99
LM	10 – 20	0.06	0.23	0.09	0.10	0.04	1.47	0.38	0.00	0.13	0.02	0.78	3.22	0.83	1.99
LM	40 – 50	0.22	0.13	0.02	0.07	0.02	1.63	0.25	0.00	0.11	0.01	0.78	3.22	0.83	1.99
LM	80 – 90	0.04	0.28	0.03	0.10	0.03	1.54	0.32	0.00	0.13	0.02	0.77	3.23	0.81	1.99
MF	0 – 10	0.11	0.10	0.04	0.08	0.11	1.76	0.21	0.00	0.03	0.01	0.79	3.21	0.77	1.99
MF	10 – 20	0.02	0.22	0.02	0.11	0.07	1.68	0.25	0.00	0.03	0.04	0.80	3.20	0.74	1.96
MF	40 - 50	0.14	0.17	0.04	0.10	0.04	1.50	0.35	0.00	0.13	0.03	0.78	3.22	0.83	1.98
MF	80 - 90	0.06	0.24	0.12	0.11	0.02	1.48	0.36	0.00	0.15	0.02	0.79	3.21	0.87	1.99
SP	0 - 10	0.02	0.29	0.01	0.10	0.05	1.52	0.36	0.00	0.10	0.02	0.81	3.19	0.84	1.99
SP	40 - 50	0.04	0.27	0.02	0.10	0.04	1.61	0.27	0.00	0.10	0.02	0.78	3.22	0.81	1.98
SP	80 - 90	0.03	0.28	0.07	0.17	0.01	1.41	0.36	0.00	0.21	0.03	0.73	3.27	0.87	1.98
Montmorillonite		0.05	0.04	0.07	0.06	0.00	1.34	0.32	0.00	0.33	0.01	0.02	3.98	0.32	1.99
LM	40 - 50	0.08	0.00	0.12	0.06	0.00	1.29	0.33	0.00	0.38	0.01	0.01	3.99	0.33	2.00
SP	40 - 50	0.00	0.19	0.00	0.04	0.00	0.88	0.53	0.00	0.55	0.06	0.01	3.99	0.43	1.96
SP	80 - 90	0.05	0.03	0.06	0.06	0.00	1.44	0.28	0.00	0.28	0.00	0.02	3.98	0.29	1.99
diVS-ml		0.04	0.13	0.02	0.11	0.04	1.63	0.27	0.00	0.10	0.02	0.53	3.47	0.55	2.00
LM	0 - 10	0.03	0.16	0.03	0.10	0.04	1.61	0.27	0.00	0.11	0.02	0.54	3.46	0.57	1.99
LM	10 - 20	0.03	0.13	0.03	0.14	0.04	1.66	0.27	0.00	0.07	0.02	0.59	3.41	0.57	2.00
LM	40 - 50	0.14	0.07	0.01	0.10	0.02	1.71	0.20	0.00	0.09	0.01	0.54	3.46	0.56	2.00
LM	80 - 90	0.02	0.15	0.01	0.10	0.03	1.66	0.25	0.00	0.09	0.01	0.53	3.47	0.53	2.00
MF	0 - 10	0.08	0.03	0.00	0.07	0.13	1.76	0.21	0.00	0.02	0.01	0.59	3.41	0.56	1.99
MF	10 - 20	0.02	0.15	0.01	0.11	0.04	1.63	0.27	0.00	0.09	0.01	0.50	3.50	0.52	1.99
MF	40 - 50	0.08	0.08	0.02	0.12	0.05	1.64	0.27	0.00	0.08	0.02	0.56	3.44	0.56	1.99
MF	80 - 90	0.03	0.14	0.06	0.12	0.02	1.61	0.28	0.00	0.10	0.02	0.54	3.46	0.56	1.99
SP	0 - 10	0.02	0.18	0.00	0.10	0.02	1.51	0.34	0.01	0.14	0.01	0.50	3.50	0.54	2.01
SP	40 - 50	0.03	0.16	0.00	0.15	0.03	1.64	0.27	0.00	0.08	0.02	0.57	3.43	0.57	1.99
SP	80 - 90	0.02	0.14	0.04	0.15	0.02	1.58	0.29	0.00	0.14	0.01	0.50	3.50	0.54	2.00
Profiles in Nha Phu															
Dioc. Vermiculite		0.05	0.15	0.12	0.11	0.08	1.60	0.33	0.00	0.05	0.02	0.80	3.20	0.79	1.98
LM	0 - 10	0.09	0.10	0.11	0.14	0.08	1.65	0.29	0.00	0.04	0.02	0.80	3.20	0.78	1.98
LM	10 - 20	0.02	0.18	0.04	0.10	0.11	1.53	0.40	0.00	0.04	0.03	0.80	3.20	0.77	1.97
LM	40 - 50	0.06	0.10	0.23	0.12	0.05	1.66	0.28	0.00	0.03	0.03	0.85	3.15	0.78	1.97
LM	80 - 90	0.05	0.15	0.06	0.15	0.08	1.60	0.33	0.00	0.05	0.02	0.79	3.21	0.77	1.98
MF	0 - 10	0.07	0.14	0.26	0.06	0.04	1.66	0.25	0.00	0.08	0.02	0.80	3.20	0.81	1.99
MF	10 - 20	0.04	0.12	0.13	0.07	0.13	1.72	0.25	0.00	0.02	0.01	0.83	3.17	0.78	1.99
MF	40 - 50	0.03	0.21	0.00	0.16	0.08	1.44	0.46	0.00	0.06	0.04	0.82	3.18	0.79	1.96
SP	0 - 10	0.05	0.10	0.19	0.13	0.08	1.63	0.32	0.00	0.04	0.01	0.80	3.20	0.79	1.99
SP	10 - 20	0.02	0.15	0.04	0.16	0.11	1.67	0.26	0.00	0.05	0.03	0.79	3.21	0.77	1.97
SP	40 - 50	0.07	0.18	0.07	0.10	0.07	1.50	0.39	0.00	0.09	0.03	0.79	3.21	0.81	1.98
SP	80 - 90	0.04	0.24	0.05	0.07	0.06	1.47	0.42	0.00	0.09	0.02	0.78	3.22	0.79	1.98
Montmorillonite	Low frequency														
diVS-ml		0.03	0.08	0.05	0.09	0.09	1.74	0.22	0.00	0.03	0.01	0.57	3.43	0.54	2.00
LM	0 - 10	0.06	0.04	0.03	0.09	0.11	1.78	0.19	0.00	0.02	0.01	0.58	3.42	0.56	1.99
LM	10 - 20	0.02	0.07	0.03	0.09	0.13	1.78	0.19	0.00	0.01	0.01	0.60	3.40	0.57	1.99
LM	40 - 50	0.04	0.06	0.15	0.10	0.07	1.71	0.25	0.00	0.04	0.01	0.59	3.41	0.57	2.00
LM	80 - 90	0.03	0.09	0.02	0.10	0.10	1.74	0.24	0.00	0.04	0.01	0.57	3.43	0.55	2.02
MF	0 - 10	0.05	0.11	0.18	0.06	0.02	1.68	0.27	0.00	0.05	0.01	0.58	3.42	0.59	2.01
MF	10 - 20	0.02	0.05	0.05	0.07	0.14	1.84	0.14	0.00	0.01	0.01	0.59	3.41	0.53	2.00
MF	40 - 50	0.01	0.07	0.01	0.21	0.06	1.73	0.23	0.00	0.01	0.03	0.55	3.45	0.50	1.97
SP	0 - 10	0.02	0.05	0.11	0.12	0.10	1.77	0.20	0.00	0.02	0.01	0.59	3.41	0.56	2.00
SP	10 - 20	0.01	0.08	0.01	0.10	0.12	1.78	0.20	0.00	0.01	0.01	0.57	3.43	0.52	1.99
SP	40 - 50	0.04	0.09	0.02	0.08	0.04	1.58	0.34	0.00	0.07	0.02	0.46	3.54	0.46	1.99
SP	80 - 90	0.03	0.12	0.03	0.05	0.08	1.73	0.23	0.00	0.03	0.01	0.58	3.42	0.55	1.99

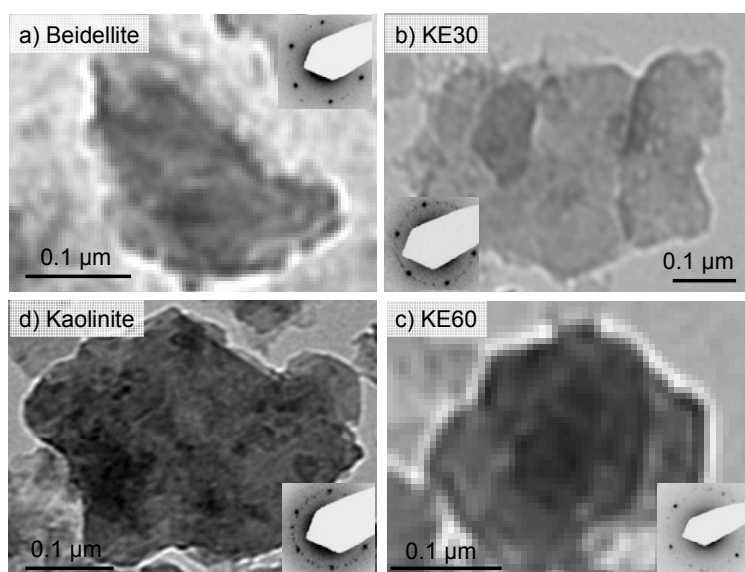
a) Dam Mon, example with sample DM-MF (40 - 50 cm)



b) Nha Phu, , example with sample NP-SP (10 - 20 cm)

**Figure 4.40. Octahedral occupations of diVS-ml structures in Dam Mon (a) and Nha Phu (b)**

Reveals from TEM-EDX analyses (Jeol JEM-1210); dark square with shadow indicates average values of particles with the same smectitic proportion; The empty square indicates value of only one particle

**Figure 4.41. TEM images of particles in KE-ml series in sediments of the South Central Coast**

Jeol JEM 1210. Inserts were SAED patterns

Table 4.20. Crystallite parameters of kaolinite and KE-ml structures in SCC sediments based on 7 Å XRD reflections

Data extraction by WinFit; XRD patterns of oriented mount, air-dried (AD) specimens

Dam Mon						Nha Phu					
Profile	Depth (cm)	d-value (Å)	CSD (Å)	Int.Max	FWHM (Å)	Profile	Depth (cm)	d-value (Å)	CSD (Å)	Int.Max	FWHM (Å)
Kaolinite											
LM	0 - 10	7.18	110 – 120	237	0.582	LM	0 - 10	7.18	120 - 130	123	0.563
LM	10 - 20	7.15	160 - 170	68	0.467	LM	10 - 20	7.17	~ 130	155	0.514
LM	40 - 50	7.17	140 - 150	123	0.517	LM	40 - 50	7.21	100 – 110	461	0.648
LM	80 - 90	7.14	130 – 140	193	0.438	LM	80 - 90	7.16	120 - 130	188	0.566
MF	0 - 10	7.18	110 - 120	240	0.605	MF	0 - 10	7.20	110 – 120	405	0.612
MF	10 - 20	7.14	140 - 150	140	0.519	MF	10 - 20	7.14	160	114	0.447
MF	40 - 50	7.17	130 - 140	196	0.57	MF	40 - 50	7.18	120 – 130	237	0.552
MF	80 - 90	7.15	130 - 140	91	0.526						
SP	0 - 10	7.17	130 – 140	285	0.523	SP	0 - 10	7.19	110	277	0.608
						SP	10 - 20	7.15	110 – 120	152	0.636
SP	40 - 50	7.16	~ 150	105	0.483	SP	40 - 50	7.18	130	299	0.579
SP	80 - 90	7.14	~ 170	104	0.408	SP	80 - 90	7.18	140	326	0.53
KE-ml structure (< 10 % of smectitic layers)											
LM	0 - 10	7.39	350 - 400	42	0.148	LM	0 - 10	7.44	~ 40	61	1.556
LM	10 - 20	7.34	~ 40	32	1.551	LM	10 - 20	7.36	60 – 70	79	1.15
LM	40 - 50	7.40	40 – 50	65	1.404	LM	40 - 50	7.54	30 - 40	167	1.671
LM	80 - 90	7.32	100 - 110	53	0.359	LM	80 - 90	7.44	~ 50	64	1.314
MF	0 - 10	7.47	~ 60	95	1.179	MF	0 - 10	7.46	30 - 40	215	1.499
MF	10 - 20	7.39	50 – 60	52	1.214	MF	10 - 20	7.33	50 - 60	38	1.223
MF	40 - 50	7.46	~ 40	79	1.32	MF	40 - 50	7.44	40 – 50	104	1.122
MF	80 - 90	7.37	40 – 50	30	1.531						
SP	0 - 10	7.43	50 – 60	113	1.29	SP	0 - 10	7.37	> 400	49	0.128
						SP	10 - 20	7.44	~ 60	62	1.12
SP	40 - 50	7.39	~ 40	60	1.572	SP	40 - 50	7.39	40 - 50	171	1.44
SP	80 - 90	7.33	50 – 60	50	1.434	SP	80 - 90	7.35	50 – 60	242	1.397
KE-ml structure (40 – 50 % of smectitic layers)											
LM	0 - 10	7.60	80 - 90	110	0.486	LM	0 - 10	7.57	> 400	105	0.128
LM	10 - 20	7.63	300 – 310	30	0.175	LM	10 - 20	nd			
LM	40 - 50	7.59	> 400	81	0.154	LM	40 - 50	7.61	280 – 350	94	0.164
LM	80 - 90	7.59	100 – 110	51	0.562	LM	80 - 90	nd			
MF	0 - 10	7.57	> 400	138	0.138	MF	0 - 10	7.62	> 400	47	0.192
MF	10 - 20	7.59	380 – 520	73	0.134	MF	10 - 20	7.35	230 – 670	38	0.054
MF	40 - 50	7.57	370 - 390	57	0.201	MF	40 - 50	nd			
MF	80 - 90	nd									
SP	0 - 10	7.59	> 400	74	0.137	SP	0 - 10	7.57	~ 70	124	0.613
						SP	10 - 20	nd			
SP	40 - 50	7.59	> 400	125	0.144	SP	40 - 50	7.58	> 400	71	0.134
SP	80 - 90	7.60	> 400	27	0.155	SP	80 - 90	7.57	390 - 400	17	0.19

nd : not detected

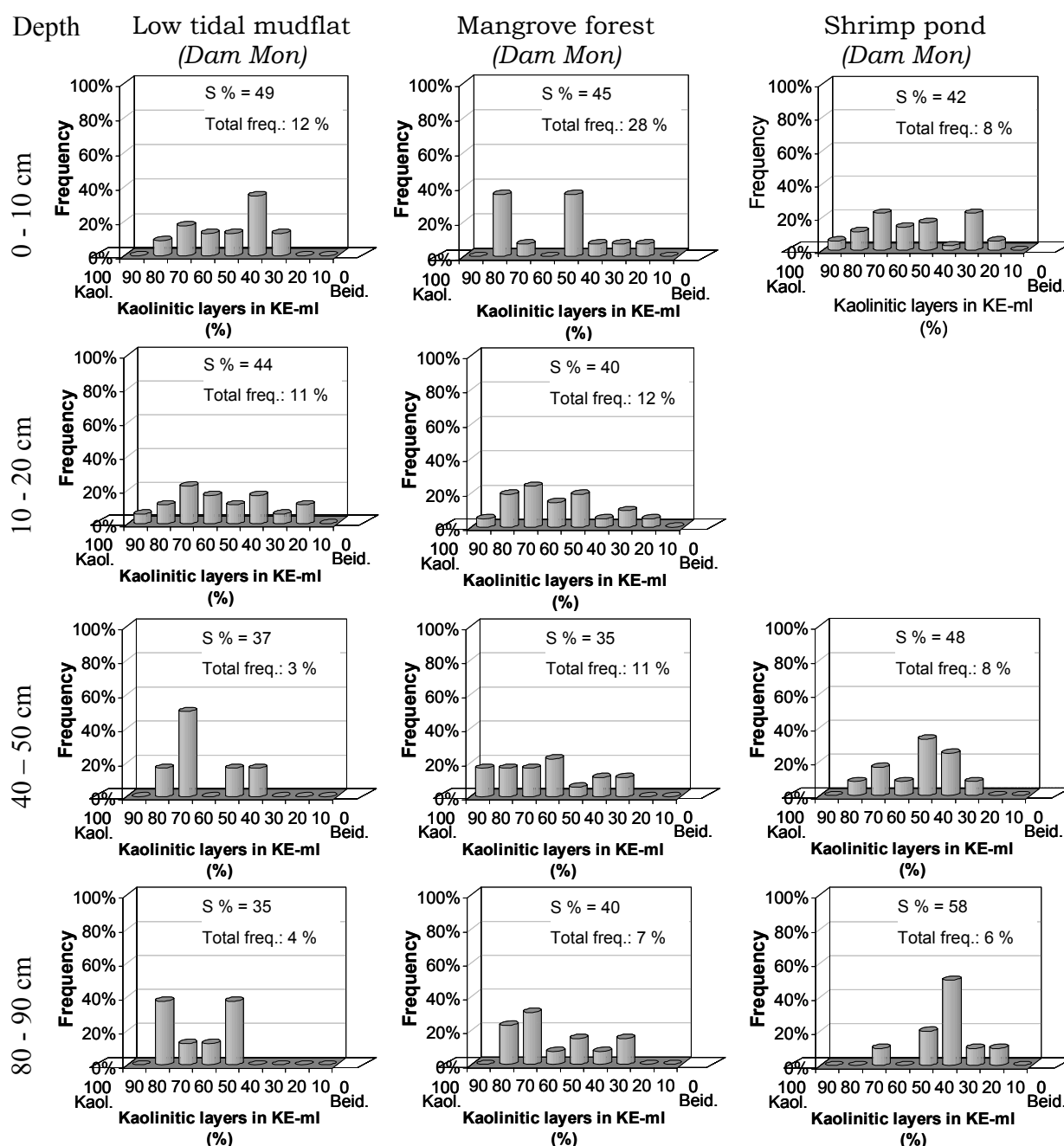


Figure 4.42. Frequency distribution of KE-ml series in sediment profiles of Dam Mon

Reveals from TEM-EDX analyses (Jeol JEM-1210); Beid.: Beidellite; Kaol.: Kaolinite; S% displayed weighted average proportion of beidellitic layers in all particles

Kaolinite/expandable mixed layer series (KE-ml)

Morphology

Particles of KE-ml series were rather commonly in fractions $< 2\mu\text{m}$ of the investigated sediments. Kaolinite particles were found not only in typical pseudohexagonal shapes of medium to large sizes (few nanometres to about $1\mu\text{m}$) with 1M polytype but also in aggregation of xenomorphic platelets in very small sizes ($\sim 1\text{-}2\text{ nm}$). Beidellites occurred also in small sizes and showed a destructive morphology of xenomorphic platelets, with folds and diffuse outlines. They were commonly in 1M polytype. The intermediate phase – KE-ml

particles – presented in both pseudo-hexagonal shapes from kaolinite and xenomorphic shapes from beidellite end-members. The 1M polytype was dominated in this mixed layer series.

Crystallite structure: Structures of kaolinite particles in surface layer of all profiles showed higher disorder degree than in subsurface parts, reflected by obvious decrease in sizes of coherent scattering domain (CSD) (Table 4.20).

Whereas, the CSD sizes of KE-ml structures exhibited intensively high values in surface sediments, and gradually increasing from the subsurface to deeper parts. Exceptions were the slightly higher values of CSD in the 10 -20 cm depth interval in mangrove forest profile of Dam Mon and 10 – 50 cm depth interval in mangrove forest profile of Nha Phu.

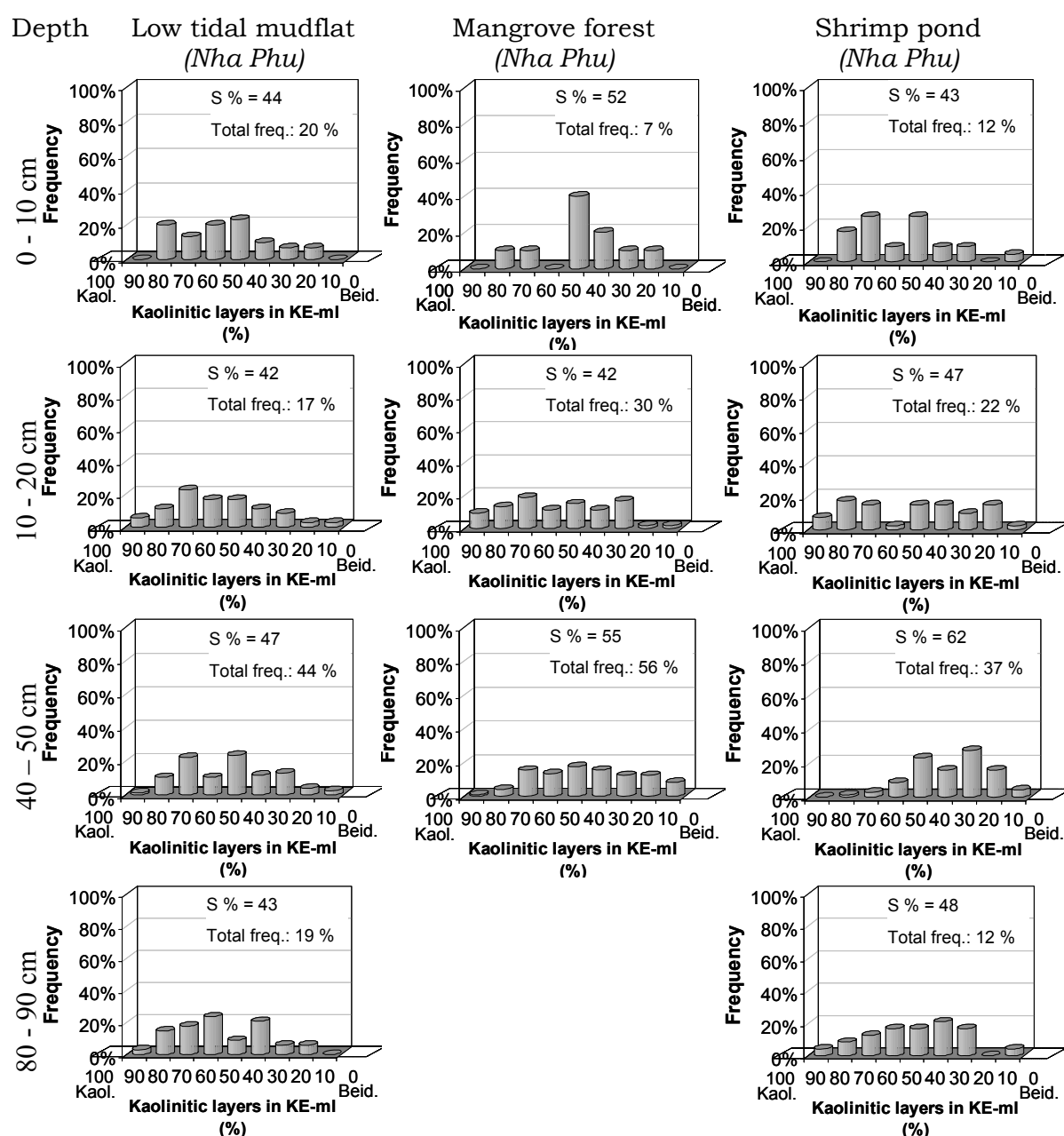


Figure 4.43. Frequency distribution of KE-ml series in sediment profiles of Nha Phu

Reveals from TEM-EDX analyses (Jeol JEM-1210); Beid.: Beidellite; Kaol: Kaolinite; S% displayed weighted average proportion of beidellitic layers in all particles

Table 4.21. Mineral formulae [O₁₀(OH)₂] of KE-ml series from fractions < 2 µm, dispersed from sediment profiles in Dam Mon*Average values calculated based on TEM-EDX analyses (Jeol JEM-1210)*

Sediment profile	Depth (cm)	Interlayer				Octahedral layer					Tetrahedral layer				n ^{VI}
		Ca	Mg	Na	K	Fe ²⁺	Al	Fe ³⁺	Fe ²⁺	Mg	Ti	Al	Si	XII	
Profiles in Dam Mon															
Beidellite		0.04	0.07	0.02	0.02	0.06	1.86	0.15	0.00	0.02	0.01	0.52	3.48	0.38	2.03
LM	0 - 10	0.01	0.06	0.00	0.01	0.09	1.94	0.11	0.00	0.00	0.01	0.52	3.48	0.33	2.05
LM	10 - 20	0.03	0.06	0.03	0.04	0.06	1.94	0.09	0.00	0.00	0.01	0.52	3.48	0.39	2.03
LM	40 - 50	0.11	0.04	0.00	0.03	0.02	1.84	0.17	0.00	0.03	0.01	0.52	3.48	0.38	2.04
LM	80 - 90	0.01	0.10	0.01	0.02	0.08	1.84	0.15	0.00	0.05	0.00	0.51	3.49	0.42	2.04
MF	0 - 10	0.07	0.06	0.01	0.03	0.05	1.73	0.27	0.00	0.05	0.01	0.52	3.48	0.42	2.05
MF	10 - 20	0.01	0.08	0.01	0.01	0.08	1.94	0.09	0.00	0.00	0.02	0.52	3.48	0.37	2.03
MF	40 - 50	0.07	0.06	0.00	0.01	0.08	1.81	0.18	0.00	0.03	0.02	0.55	3.45	0.42	2.02
MF	80 - 90	0.03	0.08	0.07	0.04	0.04	1.82	0.15	0.00	0.07	0.01	0.53	3.47	0.39	2.04
SP	0 - 10	0.01	0.06	0.02	0.03	0.07	1.94	0.09	0.00	0.00	0.01	0.51	3.49	0.33	2.03
SP	40 - 50	0.02	0.13	0.01	0.03	0.03	1.90	0.15	0.00	0.00	0.01	0.56	3.44	0.37	2.05
SP	80 - 90	0.04	0.08	0.03	0.03	0.03	1.82	0.19	0.00	0.01	0.02	0.52	3.48	0.38	2.02
KE-ml		0.03	0.01	0.01	0.03	0.02	3.03	0.08	0.00	0.02	0.01	0.21	3.81	0.16	1.70
LM	0 - 10	0.03	0.01	0.01	0.02	0.02	2.90	0.07	0.00	0.01	0.01	0.25	3.75	0.17	2.98
LM	10 - 20	0.03	0.00	0.02	0.02	0.03	2.98	0.08	0.00	0.02	0.01	0.23	3.77	0.18	3.09
LM	40 - 50	0.07	0.00	0.00	0.02	0.00	3.82	0.09	0.00	0.06	0.01	0.10	4.57	0.13	3.96
LM	80 - 90	0.00	0.01	0.02	0.02	0.03	3.30	0.13	0.00	0.03	0.01	0.13	3.87	0.12	3.46
MF	0 - 10	0.04	0.01	0.00	0.02	0.03	2.94	0.11	0.00	0.02	0.01	0.23	3.77	0.18	3.06
MF	10 - 20	0.01	0.02	0.01	0.01	0.03	3.04	0.08	0.00	0.03	0.01	0.21	3.79	0.12	3.15
MF	40 - 50	0.04	0.00	0.01	0.04	0.01	3.15	0.10	0.00	0.02	0.01	0.18	3.82	0.16	3.27
MF	80 - 90	0.03	0.00	0.02	0.02	0.02	3.10	0.07	0.00	0.02	0.02	0.20	3.80	0.14	3.19
SP	0 - 10	0.01	0.01	0.01	0.02	0.02	3.09	0.07	0.00	0.05	0.01	0.20	3.80	0.11	3.22
SP	40 - 50	0.03	0.01	0.00	0.05	0.03	2.95	0.08	0.00	0.01	0.01	0.24	3.76	0.19	3.04
SP	80 - 90	0.01	0.03	0.03	0.03	0.03	2.84	0.05	0.00	0.02	0.00	0.26	3.74	0.21	2.91

LM: Low tidal mudflat; MF: Mangrove forest; SP: Shrimp pond; XII: interlayer charge; n^{IV}: number of octahedral cations

Chemical variation

The end-member beidellite of KE-ml series showed homogenous chemical composition among particles, with medium charge (XII = 0.33 – 0.42) and averagely 1.70 – 1.94 octahedral occupation by Al.

Occurrence and distribution along depth profile

Particles of KE-ml particles appeared rather commonly in fractions < 2 µm, and varied significantly with depth intervals. Occurrence of KE-ml in sediments of Dam Mon was lower than of Nha Phu. In Dam Mon, *the total frequency of KE-ml structures in upper parts of sediment profiles was higher than the lower parts* (Figure 4.42). *However, variations of total frequency of KE-ml were not regular in profiles of Nha Phu* (Figure 4.43).

A wide range of structures with different end-member proportion were determined, from 10 – 80 % of smectitic layers. Average smectitic percentage ranged from 35 – 58 % in Dam Mon and from 42 – 62% in Nha Phu sediments. The KE-ml series in Nha Phu was gauss-like

distributed with the highest frequency of particles with 50 % smectitic layers. In Dam Mon, the moving of particle frequency toward kaolinitic end-member in the full frequency spectra of KE-ml were obvious in LM and MF profiles. This tendency was also clear to see with corresponding decrease of S%. In SP of Dam Mon, frequency of kaolinitic KE-ml particles were depleted in the deeper part. In Nha Phu, this tendency was also obvious, with higher frequency of kaolinitic KE-ml in the deeper parts of profiles (Figure 4.43). Exceptions were the specific abundance of kaolinitic KE-ml particles in the 10 – 50 cm depth interval in MF profile and 10 – 20 cm in SP profile, corresponding to low S% value (Figure 4.43).

KE-ml structures in Sediments in mangrove forest profiles had higher octahedral substitution and higher interlayer charge, in comparison to those in LM and SP profiles. Along all profiles of both regions, octahedral substitution by Fe^{3+} increased generally with increasing depth. Similar to kaolinite particles in estuarine sediments of the RRD, kaolinites in SCC bearred Fe^{3+} in octahedral layer ($\text{Fe}^{\text{IV}} = 0.25$). Particles in LM and MF profiles were Fe-richier than particles in SP profile.

Table 4.22. Mineral formulae $[\text{O}_{10}(\text{OH})_2]$ of KE-ml series from fractions < 2 μm , dispersed from sediment profiles in Nha Phu

Average values calculated based on TEM-EDX analyses (Jeol JEM-1210)

Sediment profile	Depth (cm)	Interlayer				Octahedral layer					Tetrahedral layer				
		Ca	Mg	Na	K	Fe ²⁺	Al	Fe ³⁺	Fe ²⁺	Mg	Ti	Al	Si	XII	n ^{VI}
Beidellite		0.03	0.04	0.03	0.03	0.08	1.83	0.18	0.00	0.02	0.01	0.51	3.49	0.37	2.03
LM	0 - 10	0.06	0.02	0.01	0.03	0.08	1.86	0.17	0.00	0.01	0.01	0.50	3.50	0.36	2.03
LM	10 - 20	0.03	0.03	0.01	0.02	0.11	1.87	0.16	0.00	0.00	0.01	0.53	3.47	0.36	2.03
LM	40 - 50	0.03	0.04	0.04	0.06	0.05	1.88	0.23	0.00	0.03	0.02	0.46	3.54	0.33	2.14
LM	80 - 90	0.03	0.05	0.01	0.02	0.10	1.82	0.17	0.00	0.02	0.02	0.51	3.49	0.40	2.01
MF	0 - 10	0.04	0.06	0.16	0.03	0.01	1.70	0.27	0.00	0.08	0.01	0.54	3.46	0.41	2.05
MF	10 - 20	0.03	0.04	0.03	0.02	0.12	1.83	0.16	0.00	0.01	0.02	0.51	3.49	0.41	2.00
MF	40 - 50	0.03	0.04	0.01	0.03	0.08	1.86	0.18	0.00	0.01	0.01	0.53	3.47	0.34	2.04
SP	0 - 10	0.03	0.05	0.08	0.06	0.04	1.80	0.22	0.00	0.01	0.01	0.54	3.46	0.38	2.03
SP	10 - 20	0.01	0.03	0.00	0.03	0.13	1.86	0.15	0.00	0.00	0.02	0.50	3.50	0.38	2.02
SP	40 - 50	0.03	0.05	0.01	0.02	0.08	1.83	0.18	0.00	0.02	0.01	0.49	3.51	0.37	2.02
SP	80 - 90	0.02	0.06	0.01	0.02	0.08	1.88	0.14	0.00	0.01	0.01	0.52	3.48	0.36	2.04
KE-ml		0.02	0.01	0.02	0.04	0.04	2.81	0.15	0.00	0.02	0.02	0.24	3.76	0.21	2.98
LM	0 - 10	0.04	0.00	0.01	0.03	0.02	2.98	0.11	0.00	0.01	0.01	0.22	3.78	0.17	3.10
LM	10 - 20	0.02	0.01	0.01	0.03	0.05	2.90	0.14	0.00	0.02	0.04	0.22	3.78	0.19	3.06
LM	40 - 50	0.01	0.00	0.06	0.07	0.03	2.78	0.21	0.00	0.01	0.02	0.24	3.76	0.22	3.01
LM	80 - 90	0.02	0.01	0.01	0.04	0.03	2.96	0.14	0.00	0.02	0.01	0.21	3.79	0.18	3.12
MF	0 - 10	0.02	0.02	0.13	0.01	0.01	2.85	0.06	0.00	0.06	0.01	0.26	3.74	0.25	2.97
MF	10 - 20	0.01	0.01	0.02	0.02	0.04	2.99	0.13	0.00	0.01	0.01	0.21	3.79	0.17	3.12
MF	40 - 50	0.03	0.01	0.00	0.04	0.06	2.70	0.16	0.00	0.01	0.01	0.26	3.74	0.24	2.87
SP	0 - 10	0.01	0.00	0.02	0.04	0.03	3.07	0.05	0.00	0.01	0.01	0.22	3.78	0.16	3.13
SP	10 - 20	0.01	0.01	0.00	0.02	0.07	2.93	0.10	0.00	0.01	0.01	0.23	3.77	0.19	3.04
SP	40 - 50	0.04	0.03	0.01	0.04	0.05	2.52	0.20	0.00	0.02	0.01	0.29	3.71	0.27	2.74
SP	80 - 90	0.02	0.01	0.02	0.03	0.04	2.86	0.13	0.00	0.04	0.02	0.23	3.77	0.19	3.03

LM: Low tidal mudflat; MF: Mangrove forest; SP: Shrimp pond; XII: interlayer charge; n^{IV} : number of octahedral cations

In sum, tendencies in variation of KE-ml series, which were found for RRD profiles, could also be addressed for sediments in the South Central Coast. These included the higher disorder degree (i.e. diffused edges, turbostratic ordering, lower CSD) of mixed layer structure versus end-members; with increasing depth: KE-ml frequency decreased, CSD of kaolinite decreased versus CSD of KE-ml increased, moving of frequency spectra toward kaolinitic end-member, higher octahedral substitution by Fe^{3+} . The decrease of total KE-ml frequency with depth was obviously in Dam Mon profiles but not typically for Nha Phu. However, in profiles of Nha Phu, the moving of frequency spectra toward kaolinitic end-member was to observe.

Of three environment types (i.e. LM, MF, SP), mangrove forest profiles exhibited the highest disorder degree, KE-ml total frequency and Fe^{3+} as octahedral substitution. Also in these MF profiles, the intervals of 10 – 20 cm depth in Dam Mon and 10 – 50 cm depth in Nha Phu exhibited high frequency of kaolinitic KE-ml.

Chlorite/Saponite mixed layer series (CS-ml)

In muddy sediments of the south central coast, pure chlorite was rarely detected. Presence of this mineral involved mostly in mixed layer structures with the other end-member saponite or trioctahedral vermiculite in some cases, and usually in low frequency (1 – 19 %). The CS-ml particles with low percentage of saponite (Figure 4.44) resembled typical morphology of chlorite (Henning & Störr 1986). The 1M polytype showed elongation to the b-axis. CS-ml structures with higher smectitic component showed flake outlines with diffuse turbostratic or ring-like order. CS-ml particles were rather disordered, with CSD ranging from 30 - 280 Å.

In sediments of SCC, saponite and CS-ml were the most Mg-enriched structures. Mg and Fe^{2+} occupations in octahedral sheet are comparable to each other and to the number of Al cations.

The high Fe^{2+} occupation in octahedral layer was also indicated by exhibition of 4.74 Å in all XRD patterns of oriented mount specimens (Moore & Reynolds 1997). The saponite particles had generally low interlayer charged ($\text{XII} < 0.36$).

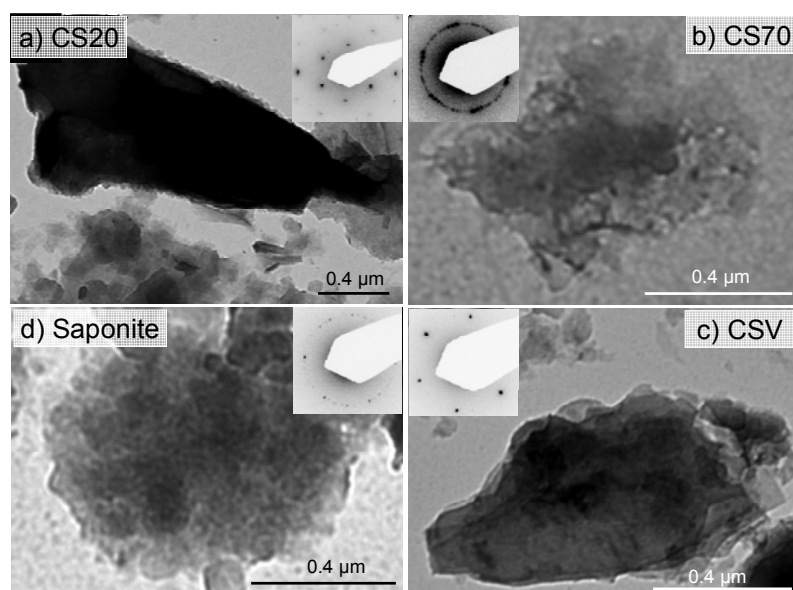


Figure 4.44. TEM images of CS-ml particles and their end-members in coastal sediments of South Central Coast

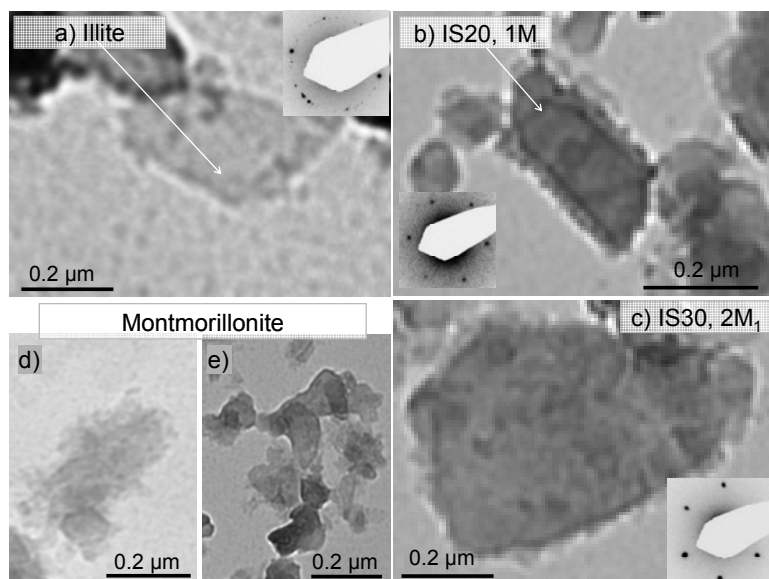


Figure 4.45. TEM images of particles in IS-ml series in sediments of the South Central Coast

Jeol JEM 1210. Inserts were SEAD patterns

Illite/ Smectite mixed layer series

Similarly to CS-ml series, the IS-ml structures were detected only in low frequency (). Under TEM investigations, IS-ml particles occurred in small sizes ($< 0.5 \mu\text{m}$) with ragged edges (Figure 4.45). Both 1M and $2M_1$ polytypes were detected. In comparison to IS-ml particles, montmorillonites had commonly smaller sizes, of only 1 – 2 nm that occurred in both nepheloid and xenomorphic forms.

Chemically, IS-ml particles were Na-rich and Fe-rich, dominating in octahedral substitution, especially in MF profiles. In MF profiles, octahedral Fe occupation was low in surface sediments and increased with increasing depth.

Associated minerals

Beside the four principal mixed layer series which were determined in sediments of SCC, some other clay and non-clay minerals were also detected in trace in sediments of Dam Mon profiles. Associated clay minerals included trioctahedral vermiculite, low-charge saponite, high-charge diVS-ml, and mixed layer structures between trioctahedral vermiculite and dioctahedral vermiculite (tri-diVerm). Behaviours and characteristics of these structures needed to consider with care due to their uncertainty in nomenclature and classification in comparison to literatures. Chemical formulae of these were displayed in the Table 8.12 (Appendix).

Trioctahedral vermiculite (triVerm) had one of the every four tetrahedral Si cations substituted by Al. In octahedral layer, Mg and Fe were dominantly occupied. Content of Mg were generally higher than Fe. Highest octahedral Mg and interlayer Mg were observed for trioctahedral vermiculite particles in shrimp pond. In LM profile, Na and K occupied as main cations in the interlayer of these triVerm.

The low-charge saponite was determined with lower interlayer charge and lower octahedral occupations than the saponite minerals which were defined and described in literatures (Newman 1987; Douglas 1989). The octahedral occupation in the detected low-charge saponite particles were about 2.45 to 2.57 with the dominance of Al in this layer.

The high charge species of diVS-ml corresponded to the end-member high charge diVerm occurred specifically in sediments of Dam Mon with frequency of 1 – 11%, more commonly in LM profile and surface sediment of the mangrove forest. The high charge species of diVS-ml were more smectitic than diVS-ml particles, with Si^{IV} ranging from 3.44 to 3.65.

The mixed layer structures tri-diVerm had high content of Mg in octahedral layer and interlayer, with higher number of octahedral occupations than dioctahedral clay minerals and S^{IV} of about 2.17 to 2.33. Octahedral occupations had averagely 0.6 -0.9 of Al cations.

The associated non-clay minerals such as quartz, feldspars, ilmenite, anatase, gypsum and hematite were also detected in trace under TEM investigation. The detected feldspars included both types: plagioclase and K-feldspar. Quartz and feldspars occurred in small to medium sizes, of 0.3 – 0.5 μm in dimension. Ilmenite and anatase occurred in very small sizes, of only 0.1 – 0.3 μm . Gypsum and hematite occurred also in small sizes, presenting clearly the hexagonal edges. These particles were morphologically similar to well order kaolinite particles, in electron micrographs. Although reflections of pyrite could be detected in XRD patterns of bulk samples, pyrite were not to find in the fractions < 2 μm .

Conclusively for mineralogy in the South Central Coast of Vietnam, a predominance of quartz, feldspar and clay phases were determined for bulk samples. The clay matters were composed also by four principal mixed layer series, those determined for RRD sediments. DiVS-ml registered for the predominant particle frequency in fractions < 2 μm , following by KE-ml. Although chlorites were not to detect, CS-ml were rather popular in Dam Mon sediments. In diVS-ml and KE-ml – the two dominant mixed layer series of samples, some variation tendencies could be revealed when comparing different environments, or the surface sediments to the lower parts. Mirroring signals included all morphological features, polytype, CSD, frequency spectra and chemical structures.

5 DISCUSSION

5.1 Coastal sedimentary environment – an interface between terrigenous and marine sedimentation, biota as well as human activities

5.1.1 Sedimentological meaning of grain size distribution data

Definition of data classes

There are two main different sedimentary systems that have been investigated: (i) tidal creek sediments in Red River Delta (RRD) and (ii) different sub-types of delta sediments like low tidal mudflat (LM), mangrove forest (MF) and shrimp ponds (SP) in the RRD and in two parts of South Central Coastline of Vietnam (SCC).

The statistical treatment (sediment trend analysis = STA) of the grain size distribution data from the first group (tidal creek sediments) revealed two data classes: data class I - creek passing shrimp farming area; and data class II - creek passing mangrove forest area.

Using EMMA-approach as statistical processing delta sediments of RRD were classified by two end members (EM1, EM2). Three end-members (EM1, EM2, EM3) were to consider for the tidal mudflat sediments in south central coastline. The polymodal GSD-pattern of the delta sediments were a not valid data set for the STA-approach.

Characterisation of data classes for tidal creek sedimentary environment (group I):

The creek passing shrimp farming area (data class I) is characterized by sand percentage < 25 %. From land to sea a continuous decreasing of grain size, sortness and increasing of skewness is to consider. This continuous changing of parameter is interrupted suddenly behind of a shrimp pond sluice gate. These gates are used to exchange the water in shrimp pond (~ 10 ha for each).

The creek passing mangrove forest (data class II) is characterized by sand percentage between 40 – 60 %. From land to sea, grain size and sortness decrease continuously and skewness increases comparable to data class I, but without any sudden interruption of this parameter's development.

Interpretation of data classes for tidal creek sedimentary environment (group I):

The different sand portion between the two data classes are to explain by different creek profile (see figure XX). The samples of data class I with a low sand portion are from a broad creek profile (with a lower transport energy of water) and samples from data class II were settled down in a narrow creek profile (with a higher transport energy of water). The situation that sampling site BL505 (data class I) is more than 100 m broad but sampling site BL501 (data class II) is a narrow creek (~30 – 40 m) is visualizing this discussion.

The mentioned continuous decreasing of grain size from land to the sea should be linked with a continuous loss of transport energy of the current from the Red River mouth (landside) to the

end of the creek (seaside). The loss of the transport energy is considered as only driving force for the mentioned grain size parameters development in data class II (passing mangrove forest). This tendency matches with the McLaren's case IIIa in STA approach (McLaren 1981): the sediment in transport undergoes selective deposition in direction from the land to the sea.

For the creek passing shrimp pond areas (data class I) a further influence is to consider explaining the sudden disruption of the parameter's development. For shrimp harvest, the farmers discharge suddenly the water out of the ponds. The water level in shrimp ponds is higher (~0.5 m) than the water level in the creek. The consequence during the harvest is higher transport energy in the creek. This higher energy is the reason that behind of this shrimp pond gate, only coarse sediment can be settled down now. This is expanding the grain size distribution spectrum (lower degree of sortness).

In summary, the different sand portion both data classes is representing only the different transport energy caused by the different creek profile, in the two data classes suspended matter undergoes selective deposition in direction from the land to the sea and the sudden interruption of grain size distribution behaviours is man-made in data class I (creek passing shrimp pond areas).

Characterisation of data classes for delta sedimentary environment in Red River Delta (group II):

Polymodal grain size distribution patterns are the basis for the two end-member EM1 and EM2 classified in the Red River Delta estuary. These two end-member EM1 and EM2 can explain 97 % total variance of all samples and grain size parameters concerning GSD distributions.

Two characteristics describe completely the two end-members:

RRD end-member:	EM 1	EM 2
Grain size distribution:	Silt with clay tail	Fine sand
Behaviour with increasing depth:	Increasing influence	Decreasing influence.

With increasing depth EM1 and EM2 show a vice versa behaviours. The result of this trend is a slight continuous decreasing of grain size with depth (see Figure 5.1).

Interpretation of data classes for delta sedimentary environment in Red River Delta (group II):

In the interaction between sedimentation of river freight and influence of the sea (wave, tide etc.), two main aspects should be to consider: accumulation and erosion processes. In studies of Andersen (1999) and van den Bergh et al. (2006) similar GSD-pattern like RRD's GSD-pattern (Figure 5.1) are linked with accumulation of sediments in such areas, mostly the fine fractions tend to be increased with the time. This accumulation process with the increasing of fine fractions is to accept with the lost of transport energy for the river mouth.

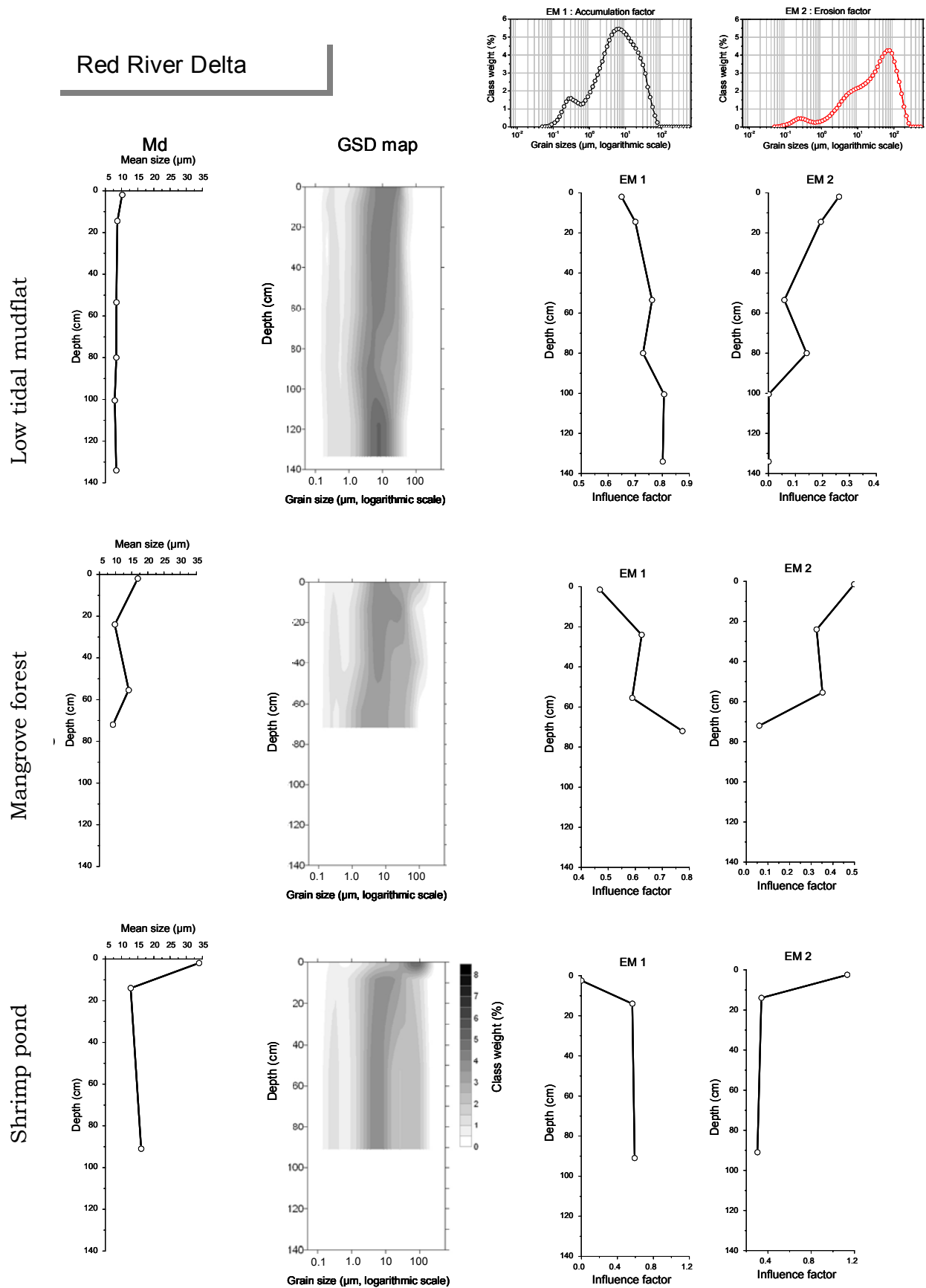


Figure 5.1. Modelled end-members are compared with mean size and full pattern of GSD in RRD profiles

The finer GSD-pattern and the increasing influence of EM1-parameter with the depth let conclude, that this end-member EM1 could represent this mentioned accumulation factor. The second end-member (EM2) is characterized by coarser material. This could reflect an erosion process of fine fractions e.g. by tide or wave energy, how it was described by Andersen (1999), too. Considering EM 1 as accumulation in the sense of grain size separation and EM 2 as erosion by tide or wave, the following trend is to expect: The influence of EM 1 (accumulation) should be increased with the longer distance from the river mouth. This higher influence with the distance to the river mouth is linked with a higher amount of fine materials. The influence of EM 2 (erosion) should be show near the coastline a maximum and should be reduced in larger distance from the coastline. Using this kind of interpretation for EM 1 and EM 2 their different behaviours in the depth of the sampled sediments is mirroring the distance from the river mouth to the sedimentation site in the time also for the Red River Delta. The same behaviours are obvious in all three environments (LM, MF, SP).

Van Maren & Hoekstra (2004), van den Bergh et al. (2006) and van Maren (2006) have investigated intensively the long-term sedimentary history of the Red river estuary since Pleistocene period. Additionally to the long-term parameter like bathymetry etc. they have mentioned that accumulation and erosion should have also in influence as driving forces for morphological evolution. When describing sedimentation and erosion processes in tidal mudflat of Danish Wadden Sea, Andersen (1999) explained that the variation of erosion threshold is mainly resulted from lateral variation in emersion time of the sedimentary environment. This indicate that determined influences of accumulation and erosion as the driving force for morphological evolution in the RRD are in agreement with other studies not only on the same areas but also the intertidal mudflat in other countries.

Characterisation of data classes for delta sedimentary environment in South Central Coast (group II):

Polymodal GSD patterns are also the basis for all three end-members EM 1, EM 2 and EM 3 classified in SCC. The three end-members represent for Nha Phu 89 % of total variance and for Dam Mon of 92 %. EM 1 is a unimodal silt distribution for Dam Mon and Nha Phu, too. EM 2 is a bimodal fine sand distribution for the two sampling sites but the coarser part of EM 2 in Nha Phu is higher than that in Dam Mon. EM 3 is also a bimodal distribution of coarse sand, but again in Nha Phu the coarser part of the bimodal distribution is increased. Behaviours in the depth are to analyse separately, because of the fast changing between coarse sand and fine overwhelm by other underlying trends:

Dam Mon	EM 1	EM 2	EM 3
GSD	unimodal silt	bimodal fine sand	bimodal coarse sand
Behaviour with increasing depth	Irregular	Irregular	Irregular
Nha Phu	EM 1	EM 2	EM 3
GSD	unimodal silt	bimodal fine sand	bimodal coarse sand
Behaviour with increasing depth	Irregular	Irregular	Irregular

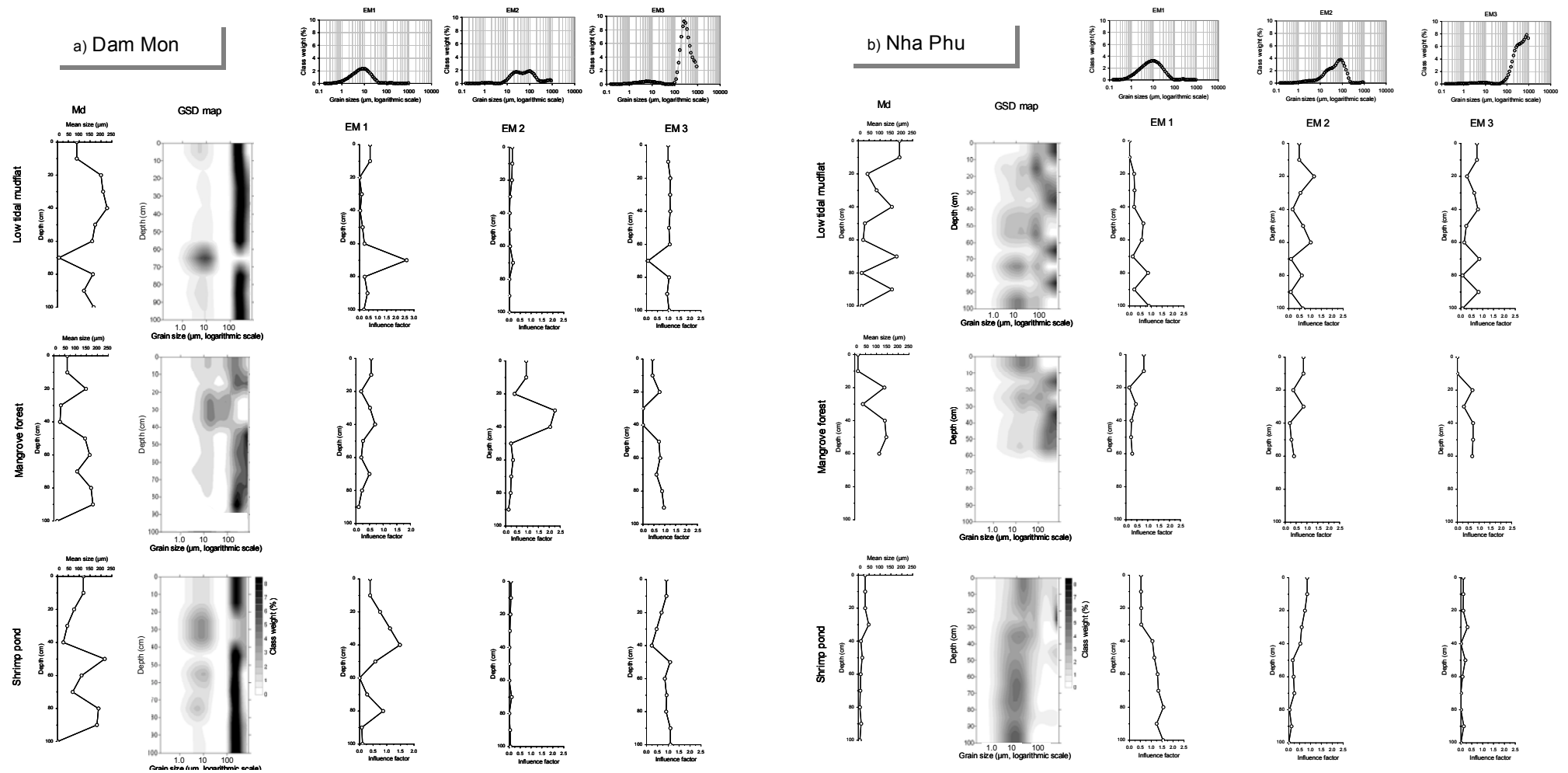


Figure 5.2. Modelled end-members are compared with mean size and full pattern of GSD in Dam Mon profiles (a) and Nha Phu profiles (b)

Interpretation of data classes for delta sedimentary environment in South Central Coast (group II):

The discussion to the meaning of the three end-members will start in comparison with the interpretation for RRD environments. The hypothesis is: EM 1 is comparable with accumulation of the terrigenous sediments and EM 2 could represent an erosion factor by tide or wave. Because of the low sedimentation rate in SCC, it would be possible to detect an aeolian influence, too. The surrounding material close to the coastline is linked mostly with moving sand dunes: that's why EM 3 should be interpreted as accumulation by wind in this first hypothesis in according to Prins et al. (2000b) and Weltje & Prins (2003). These authors described in the Arabia Sea an effect of wind as a principal end-member of terrigenous sediment supply.

It is to remember to the discussion in the RRD: a longer distance from the coastline should visualize a higher accumulation's influence of terrigenous sediments in finer fraction (EM 1). At the same case the influence of erosion by tide or wave should be decreased. This situation is clear to follow for Nha Phu in the shrimp pond environment (Figure 5.2b). Following the idea for EM 3 as wind factor under this situation, it is to expect a very low or ignorable effect by wind accumulation. EM 3 value in Nha Phu shrimp pond is nearby zero (Figure 5.2b).

The opposite behaviour should be to expect in the youngest sediments of Dam Mon in the low tidal mudflat. This site is isolated, surrounded by higher sand bar. Under these conditions activities of waves should be reduced drastically and the influence for accumulation of terrigenous materials should be very low. Only a more or less constant force of wind would be to consider. How to recognize in Figure 5.2a in Dam Mon low tidal mudflat the end-member EM 1 is very low, and only an event-like break is to seen. EM 2 is nearby zero and EM 3 is mostly constant with two inserted event-like breaks like in EM 1.

Dam Mon shrimp pond environment offers the same characterization: (i) EM 1 – low influence, disrupted only by two events; (ii) EM 2 – nearby zero and (iii) EM 3 – nearby constant, only disrupted by one event.

Also the mangrove forest environment in Dam Mon is following a similar characterization for the three end-members. The exception is EM 2 for the event-like disruption. Following the assumed meaning of EM 2 as erosion factor, it is to note that this area is known for its century aged mangrove forest. Some authors (Furukawa *et al.* 1997; Saad *et al.* 1999) have published that local erosion process can be generated by turbulence between mangroves prop roots. How is to explain the event-like disruption in all three environments of Dam Mon? Approaching the assumed meaning for EM 1, this disruption indicates a sudden higher influence of accumulated, terrigenous sediments. End-member EM 3 announces a sudden missing of the wind factor. A flooding of neighboured sand bar could explain the gap of the wind factor for this event-like break. In this time the general low influence of terrigenous sediments is to identify, because it is not overloaded now by the aeolian accumulation in this sampling site.

A further developing of the temporary flooding concept could help to interpret the GSD-pattern also in Nha Phu for its low tidal mudflat and mangrove forest environment. EM 1 and EM 2 show readily parallel behaviours, both in opposite to EM 3. The region of Nha Phu is known for its moving sand bars in the delta. The often changing of coarse and fine sand behaviours is typically for the sedimentation in Nha Phu. Additionally the core profile (fig. XX) is showing for the upper 50 cm two shell horizons. These aspects: moving sand bars, fast changing sediments and few shell horizons support the concept of temporary flooding.

EM 2 was discussed until now as erosion factor without to distinguish between tide or wave energy as possible driving force. The depth profile for Dam Mon (mangrove forest) shows high erosion activities for the time of temporary flooding of the neighbour sand bar. A possible tide effect should be to observe for the complete time, independent from the situation of the sand bar. The same precondition is not to expect for the effect of waves. The non-flooded sand bar protects the mangrove forest in the lagoon against the activities of waves. Temporary flooded this protection is not guaranteed and additional erosion effects caused by the turbidity between the mangrove roots (authors) are to assume. That means this event-like break of the sand bar indicates for EM 2 a preferred influence by waves instead of tide.

In sum, the six different depth profiles from SCC (Figure 5.2) can be explained now completely by the hypothesis:

EM 1: - accumulation of terrigenous sediments in the sense of grain size separation
(distance dependence)

EM 2: - erosion by wave activities

EM 3: - accumulation from neighbour sand bar by wind

A consequent approaching of these geological meanings for the three end-members indicates for the youngest sedimentation time in Nam Phu a steady change between temporary flooding and non-flooding of neighboured sand bars. The general low sedimentation rate with 1 - 2 cm/year (Nhuan et al. 2003) creates the chance to identify the aeolian influence. This mentioned low sedimentation rate let estimate the age of this time presenting the last 100 – 150 years.

The lagoon character has protected the sampling site in Dam Mon mostly. Only heavy events could distort this situation rarely. It is not possible to estimate the age of the sampled sediments in Dam Mon, because no data could be determined for the sedimentation rate in this gulf. But it could expect, that the 1 m cores from Dam Mon represent more than 100 – 150 years.

5.1.2 Reconstruction of paleogeographical situation

Using the geological meaning of the classified end-members, it would be interesting to reconstruct the paleogeographical situation, especially the changing distance between river mouth and sampling sites in the time. For paleogeographical reconstruction, the valid time intervals are requested to know, which is represented by the sampled 1 m cores.

Table 5.1. Input data for constructing age normalization model and distance normalization mode

Reference data & Field work measurements		
Parameter	Information	References
a) Vertical Sedimentation rate in LM and MF	~ 4.5 cm/y – 5.6 cm/y	Nhuan et al. (2003)
b) Average progradating rate during last 50 years (lateral sedimentation rate)	~ 50 m/y (irregularly)	Thanh & Huy (2000)
c) Sampling time	Summer 2001	
d) Sampling sites	Red River estuary, Giao Thuy district	
e) Location of LM core	~ 200 m seaward from the coastline in 2001	
f) Length of LM core	~ 135 cm	
g) Location of MF core	~ 100 m seaward from the coastline in 2001 ~ 100 m landward from the LM core	Field work measurement in 2001
h) Length of MF core	~ 70 cm	
i) Location of SP core	~ 1,800 m landward from the coastline in 2001	
k) Length of MF core	~ 90 cm	
Interpolated data		
(1) Averaged vertical sedimentation rate in LM = ~ 5 cm y ⁻¹ (see) (the same values were used for MF and SP with assumption those were formerly LM background)		
(2) Location of coastline in 2006 (estimated) = 250 m seaward from coastline in 2001		
(3) LM core in 2001		
Surface sediment (0 cm) aged 0 year old		
Bottom sediments (135 cm depth) of LM core aged 27 years old		* (=135 cm/5 cm y ⁻¹)
=> The 135 cm depth interval started deposit in ~ 1974/75		
Seaward distance of LM core from coastline in 1974/75 = ~ 1150 m		* (= 50m y ⁻¹ x 27y + 200 m)
(4) MF core in 2001		
Surface sediment (0 cm) aged ~ 0-2 year old		* (=100m/50 m y ⁻¹)
Bottom sediment (70 cm depth) ~ 16 year old		* (= 2 y + 70cm/5cm y ⁻¹)
=> The bottom (70 cm depth interval) started deposit in ~ 1985		
Seaward distance of MF core from coastline in 1985 = ~ 900 m		* (= 50m y ⁻¹ x 16y + 100 m)
(5) SP core in 2001		
Surface sediment (0 cm) aged ~ 40 year old		* (=1900m/50 m y ⁻¹)
Bottom sediment (90 cm depth) ~ 58 year old		* (= 40 y + 90cm/5cm y ⁻¹)
=> The bottom (90 cm depth interval) started deposit in ~ 1943		
Seaward distance of SP core from coastline in 1943 = ~ 1110 m		* (= 50m y ⁻¹ x 40y – 1800 m)

In estuary of the RRD, the estimation of vertical and lateral sedimentation rates is presented in the Table 5.1. Value of the vertical sedimentation is about 5 cm/ year and the value of lateral sedimentation (i.e. progradating) is averagely 50 m/ year during the last 50 years, based on the studies of Nhuan et al. (2003) and Thanh & Huy (2000), respectively. Approaching these estimations, it is possible to normalize the cores by age (Figure 5.3) and to reconstruct their environmental position in the time (Figure 5.4). The sketch of age normalization in Figure 5.3 visualize that the shrimp pond sediments is about 40 year older than the mangrove forest sediments and mangrove forest sediments is about 2 year older than the low tidal mudflat sediments. Besides, deeper parts of the cores are older than the upper parts. Summarizing, the sampled and investigated RRD-sediment is younger than 60 years.

Therefore, the highest degree of diagenetic effects on variation of mineralogy is to expect in the deepest part of SP. The deepest parts of all three profiles are determined to be deposited at a distance of about 1000 m far from the coastline than the top of each core (Figure 5.4).

For South Central Coast no data is available to conclude to the lateral sedimentation rates. Then the reconstruction was not conducted. Following the behaviour of the three end-members in shrimp pond profile of Nam Phu this sampling site was located also more far from the river mouth few hundred years ago.

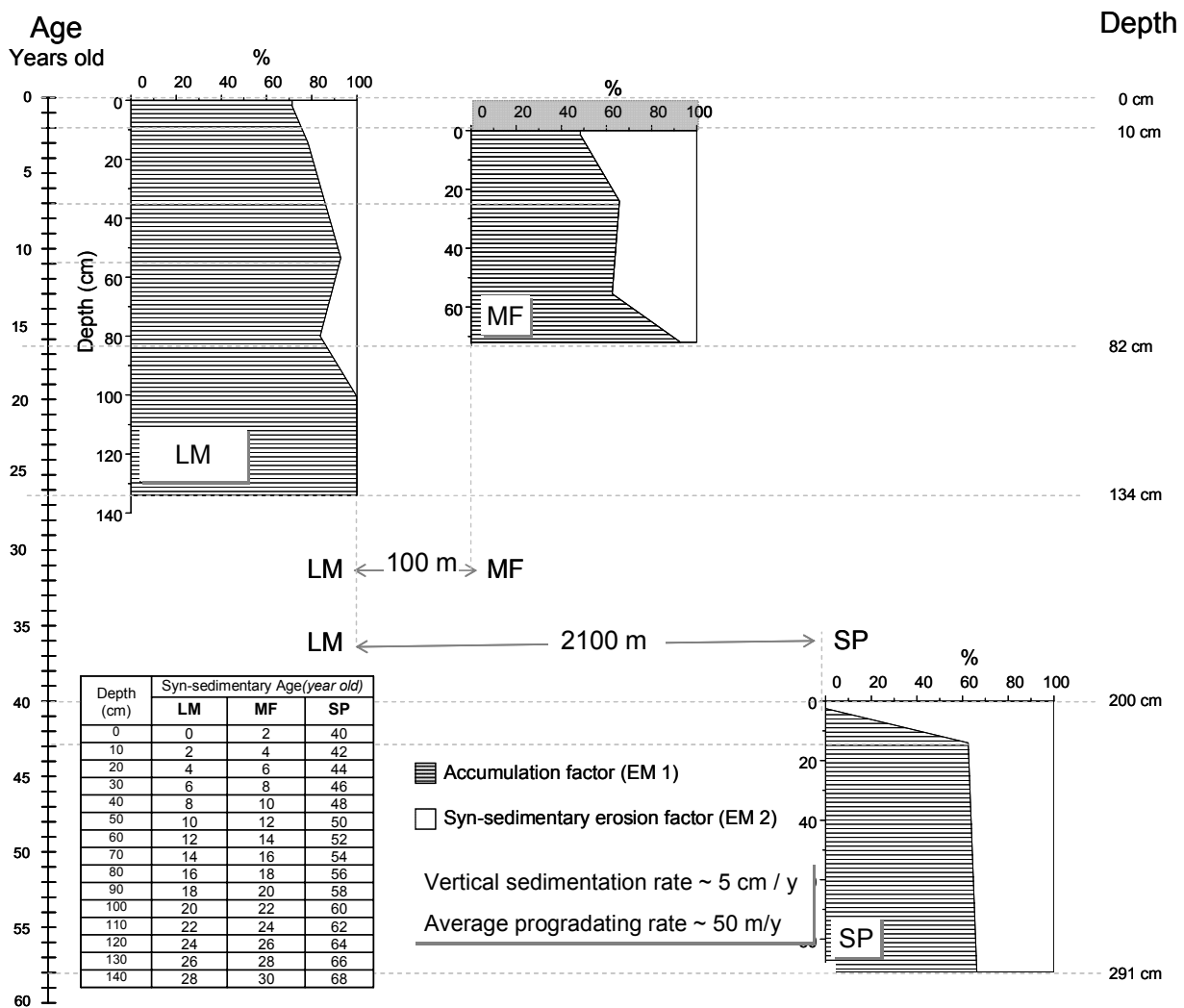


Figure 5.3. Normalization of age of syn-sedimentary matters in RRD profiles (in 2001)

The grey band in uppermost part of MF profile indicate mixture between surface sediments of the former LM environment (~ 2 years old) and of current MF environment (0-2 years old)

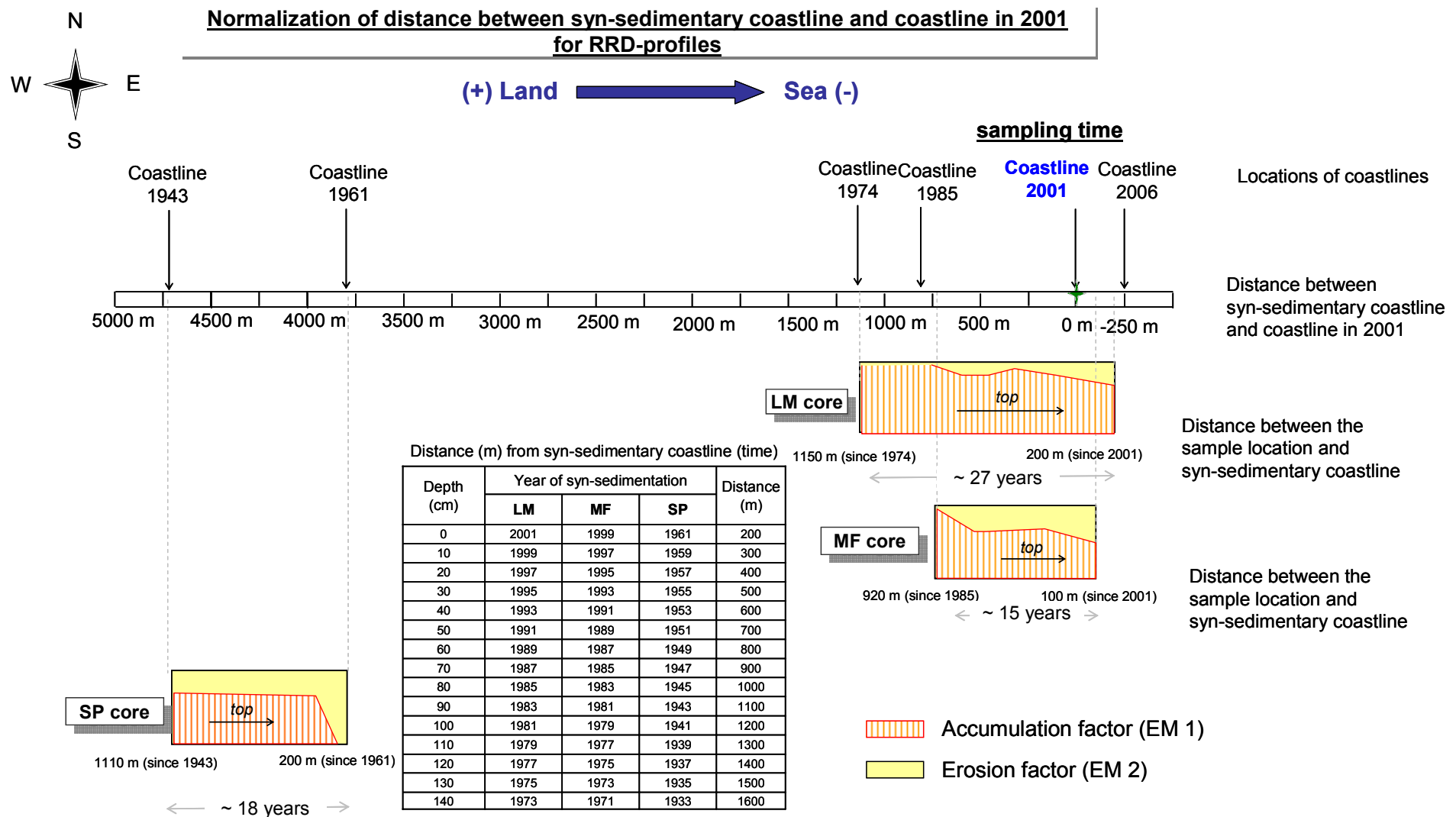


Figure 5.4. Normalization of distance between syn-sedimentary coastline and coastline in 2001

5.2. Syn-sedimentary processes - mirroring in elemental distribution and mineral matter

5.2.1. Hydrodynamic – mirroring in elemental distribution and mineral matter

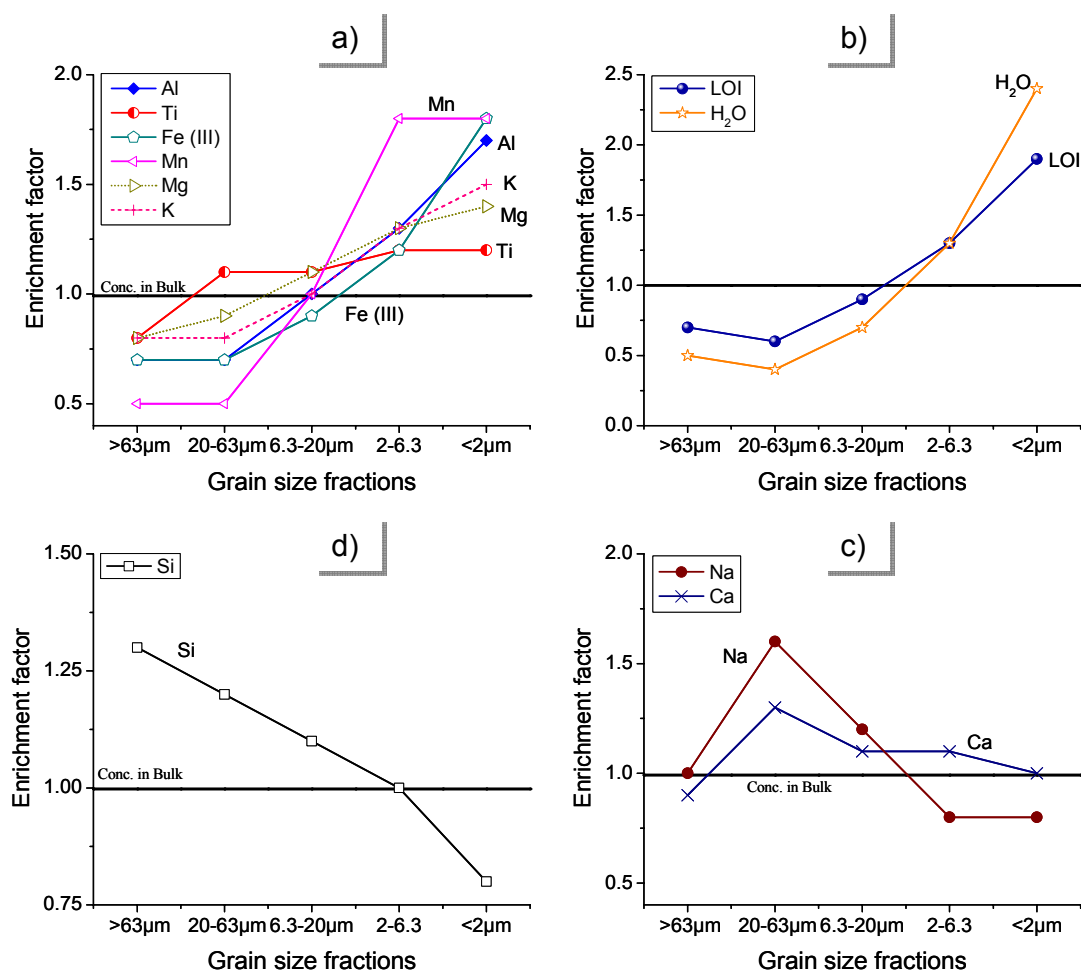


Figure 5.5. Enrichment behaviours of major chemical elements in grain size fractions in comparison to the bulk

Visualization for sample RRD-MF (0 - 3 cm); Similar enrichment behaviours are to observe also in the other samples of RRD (Figure 8.4)

Effect of grain size distribution

The granulometric studies on grain size fractions have affirmed the role of particle size in enriching the clay species and minor elements.

Clay matters

Mineral analysis of grain size fractions of sediments in the Red River estuary revealed the *enrichment of clay minerals in fine sediments*. It is indicated by increase in intensity of the 14 Å peak (smectitic and/or chloritic phases), 10 Å peaks (diVerm and/or illitic phases), and especially of the (060)-interference at 1.50 Å and 1.53 Å (see illustration in Figure 4.28). Exception is the kaolinitic phase that tends to remain unchanged in all fractions > 2 µm, but it increases suddenly in fractions < 2µm (see 1.49 Å reflections in Figure 4.28). The enrichment

of clay species in fine sediments is also demonstrated by the continuous increase of clay-forming elements (i.e. K, Al, Ti, Mg, Fe, Mn) in continuously from fractions $> 63 \mu\text{m}$ to fractions $< 2 \mu\text{m}$ (Figure 5.5a). Exceptions are slightly enrichment of Mn in the 2 - 6.3 μm fractions and Ti in the 20 – 63 μm fractions.

Non-clay matters

In opposite to clay matter, non-clay minerals tend to concentrate in the coarser fractions. The preferential accumulation of quartz in coarse sizes is indicated by the corresponding decrease from coarse to fine in intensity of the 1.54 \AA (Figure 4.28) and decrease in concentration of Si (Figure 5.5d). The decreasing tendency of concentration from coarse to fine characterizes also other non-clay minerals. However, while quartz is most commonly in the coarsest matters ($> 63 \mu\text{m}$), other non-clay minerals like feldspars, calcite, ilmenite, zircon are more commonly in the smaller sizes. The Ca, Na rich substances (e.g. feldspars or shell fragment) show the preferential accumulation in the 6.3 – 63 μm fractions with gradual decrease to fractions $< 2 \mu\text{m}$ (Figure 5.5c). XRD data revealed the highest ratios in peak area of the 2.13 \AA reflection of calcite versus 1.82 \AA reflection of quartz occurring in 6.3 – 20 μm fractions (Figure 8.29). Zircon occurs most commonly in fractions of 20 – 63 μm and also depletes in the finer fractions (Figure 5.6d). The slightly enrichment of Ti in the 20 – 63 μm fractions (Figure 5.5a) reflects a more commonly presence of Ti-bearing non-clay minerals (i.e. ilmenite or anatase) (Chapter 4.4) in these size, additionally to the Ti amount which isomorphically substitutes for Al in clay mineral structures. Whereas, the *enrichment of Mn in the 2 - 6.3 μm fractions (Figure 5.5a) indicates for an abundance of manganese hydroxides sol in these sizes.*

Adsorbed water and organic matters

Similarly to the distribution of clay forming elements, adsorbed H_2O and LOI tend to concentrate highly in the finer fractions (Figure 5.5b). The amount of lost on ignition (LOI) for coarse fractions is caused by carbonate mostly and for the fine fractions by dehydroxylation of 2:1 and 1:1 sheet silicates. In bulk sample of surface sediment (0-3 cm) in MF profile of RRD, about 1 – 2 % of calcium carbonate was identified by XRD but calcite is missing in the fine fractions (Figure 8.29).

Heavy metals and other minor elements

Figure 5.6 illustrates the different behaviours of minor chemical element groups according to grain size distribution. It is quite clear that *heavy metals are intensively enriched in the finer sediments* (Figure 5.6a). The enrichment ratios of minor elements in fractions $< 2 \mu\text{m}$ are 1.5 - 3.5 times in comparison to their concentration in bulk. According to Hirst (1962), in estuarine sediments, heavy metals can associate with clay minerals in both manners: cooperation in the degraded structures of clay minerals and absorbed in surface of clay particles.

Similarly to the heavy metals group, two elements: Ga and V accumulate highly in the finer fractions (Figure 5.6a). Because of similarity in cation diameters and chemical natures, Ga can substitute isomorphically for Al in clay mineral structures (Hirst 1962) and V tends to associate with Cr (Hirst 1962).

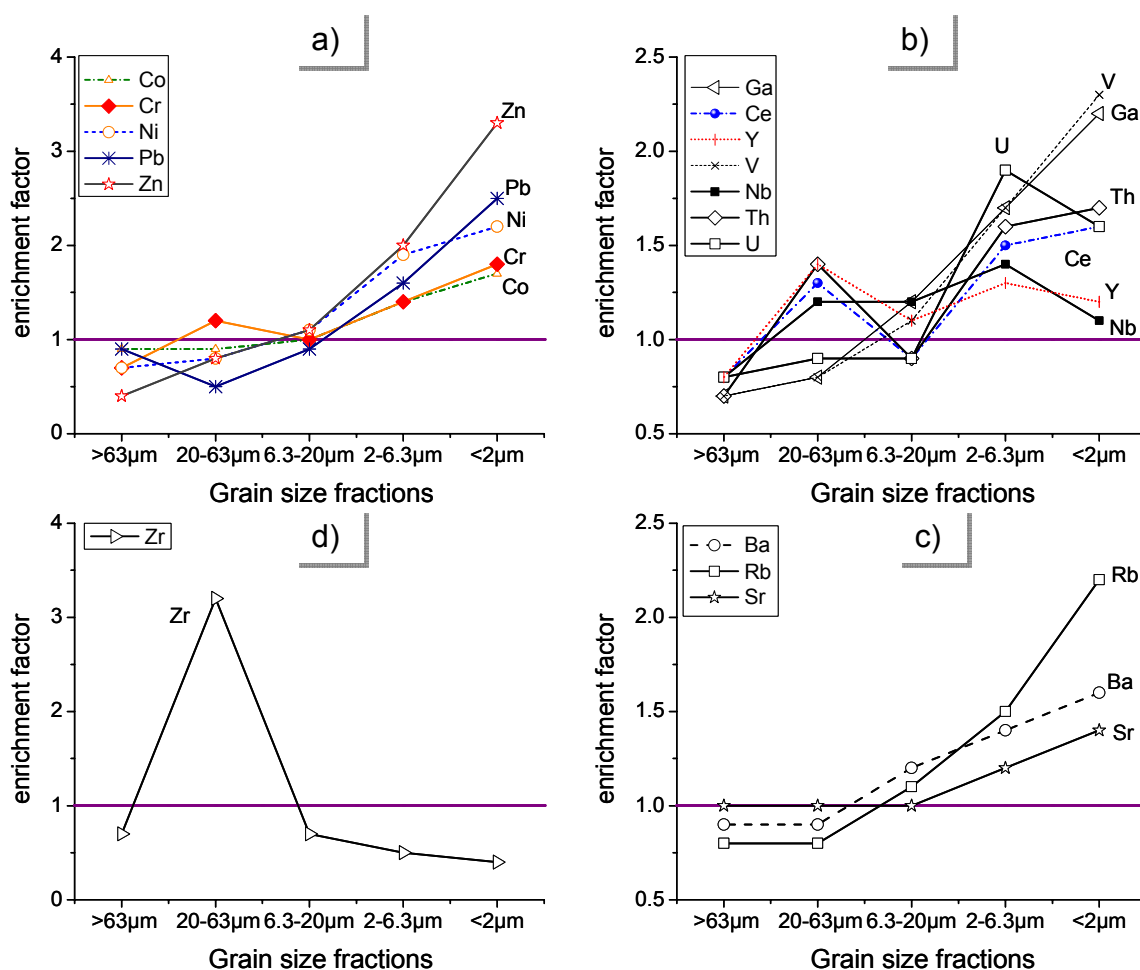


Figure 5.6. Enrichment behaviours of minor chemical elements in grain size fractions in comparison to the bulk, on example of 0 – 3 cm surface sediments in MF profile, RRD

Value of enrichment factor of trace element was calculated by dividing concentration of it in each grain size fraction to concentration of it in bulk

Hence, the pathway to estuary of Ga is to consider with transportation of clay minerals and pathway of V is comparable to mobilization of the heavy metal Cr. Generally, the other minor elements (U, Th, Ce, Y, Nb) show also enrichment in fine sizes. However, these elements are slightly enriched in the 20 – 63 µm fraction and 2 – 6.3 µm fractions which can be comparable to behaviours of major elements in non-clay minerals (represented mostly by Ca, Na and partly by Mn). These two tendencies suggest that minor elements associate with both clay matter group and non-clay group in suspended matters during the transportation to the estuary but with the preferential accumulation in clay minerals. Enrichment of heavy metals in fine grains was also documented by Gibb (1977) for sediments in Amazon and Yukon River and Padmala et al. (1997) in Vembanad estuary (India), referring to accumulation and high correlation between minor elements and silt, clay fractions.

With decreasing grain sizes, the alkaline minor elements such as Sr, Rb and Ba exhibit also the accumulation tendency, similarly to Ga and heavy metals, but completely different from behaviours of Ca and Na. It is to notice that the association in natural terrigenous soil/sediment

matters of element couples: Ca-Sr, K-Rb and Na-Ba, due to chemical similarity, is regularly (Hirst 1962, Alloway 1995). Therefore, it can be interpreted that the abundance of Ca and Na in coastal sediments is mostly linked with sea source (e.g. in forms of carbonate, shell fragment, halite, and absorbed dissolved Ca and Na), additionally to the Ca-Na amount in detritus minerals (e.g. feldspars, clay minerals).

In sum, the *distribution of mineral matter as well as chemical elements in the coastal shelf of Vietnam has been revealed to vary considerably with the textural characteristics of the sediments*. The finer sedimentary materials register higher concentration of clay species and minor elements than coarser sediments. Meanwhile, the coarser sediments contain more commonly non-clay matters like quartz, feldspars, zircon, ilmenite and/or anatase as well as shell-fragment.

With these strong dependences of elemental distribution on grain size separation, it is thus to expect also a significant influences of hydrodynamic factors on chemical distribution of coastal sediments. The discussion on hydrodynamic features of studied coastal environments in Chapter 5.1 has mentioned three principal dynamic grain size populations, which are accumulation, syn-sedimentary erosion and sediment deposition by aeolian forces.

Accumulation (factor concluded from EMMA-statistics concerning grain size data)

Mirror of accumulation influences by distribution of clay content and major elements

A comparison between Al_2O_3 , SiO_2 and hydrodynamic accumulation factor, which is originated by EMMA treatment, is visualized in Figure 5.7. The higher accumulation factor responds to higher amount of fine grain size fractions. A direct correlation of accumulation factor with Al_2O_3 and inverse correlation with SiO_2 is to explain with quartz amount (see XRD proofs in Figure 5.7c with inverse correlation between accumulation factor and peak area of 1.82 \AA for quartz). *Accumulation factor was discussed until now like a mirror for the distance of river mouth to sedimentation position*. The increasing clay matter amount, visualized by the mentioned behaviours of Al_2O_3 and SiO_2 as well as quartz, confirms this hypothesis.

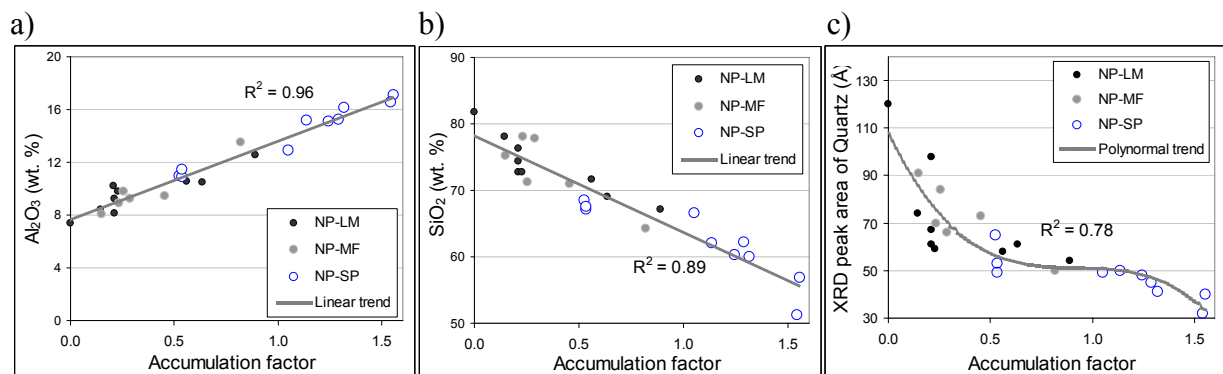


Figure 5.7. Influences of accumulation factor on elemental distribution (a, b) and XRD peak of quartz (1.82 \AA) in three profiles of Nha Phu

The higher values of factor correspond to higher Al_2O_3 but lower amount of SiO_2 and peak area of quartz reflection

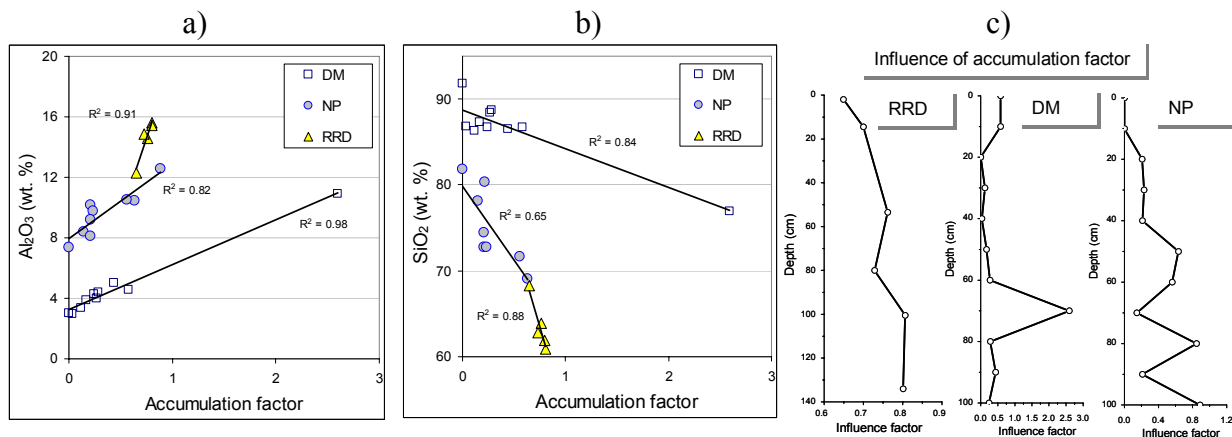


Figure 5.8. Influences of accumulation factor on elemental distribution in low tidal mudflat profiles of coastal sedimentary sites along Vietnam

The higher values of factor correspond to higher Al_2O_3 but lower amount of SiO_2 .

In addition, the zoning of SP samples versus LM and MF samples can also be seen (Figure 5.7). Recall that the three profiles have different ages ($\text{SP} > \text{MF} > \text{LM}$) (Figure 2.8). That's why this zoning of SP, with higher influence of accumulation factor, *refers that the older sediments in SP are affected mostly by river freight during synsedimentary processes, but the younger sediments (LM, MF) are more influenced by the other hydrodynamic factors like migration of sandbars* (aeolian factor corresponds to higher quartz content) (Chapter 5.1).

Figure 5.7 is expressing the correlation between accumulation factor and distribution of Al_2O_3 and SiO_2 in all the investigated low tidal mudflat profiles of Red River Delta, Dam Mon and Nha Phu. *The tilt angle infers to the sediment freight of river. Low angle responds to low sediment freight as seen for samples in Dam Mon and Nha Phu and high angle responds to high sediment freight as seen for samples in RRD.*

In SP- and MF-sediments of Red River Delta and Dam Mon, this situation does not present. Correlations between influence of accumulation factor and elemental concentration are low (Figure 8.30, Appendix). Additionally, correlation between relative quantity of clay phases in fractions $< 2 \mu\text{m}$ and accumulation factor (Figure 8.32a) showed also none-defined tendency. It thus suggests an interference of some processes during the syn- and post-sedimentary period on the original accumulation that occurring to the sediments.

In order to address if the accumulation process be interfered or not, the chemical contribution of accumulation end-member on bulk are examined. Chemical contribution of the accumulation factors can be relatively estimated based on chemical data of certain size fractions contributing the accumulation factor (Table 5.2). These parameters visualize the percentage of chemical elements in bulk chemistry, which is registered by hydrodynamic accumulation process.

Surface sediments exhibit similar chemical signals among three environments: LM, MF and SP, with comparable influence percentages for each chemical element (Table 5.2a). It

indicates that the source sediments to all three environments are similar. However, along the depth profile of mangrove forest (Table 5.2b), the accumulation factor in deeper sediments registers for lower percentage of total Al, Ca, Na concentrations than the surface sediment (see lower Al/Si ratios as well as lower influence percentage of Al, Ca and Na in Table 5.2). It demonstrates that original *chemical signals of accumulation factor in mangrove forest profile have been modified during the syn- and post-sedimentary period*. These tendencies explain also for the high enrichment of Al and other clay-forming elements in surface layer than the deeper sediments, although of lower accumulation influence.

Mirror of accumulation influences by distribution of minor elements

Distributions of minor elements along depth profiles have similar behaviours, as revealed from chemical results (Figure 4.24, Figure 4.26, Figure 4.27). It indicates that these elements have mostly the same transportation way to coastal environment. The statistical PCA data-treatment (Chapter 4.3.3) and correlation matrix (Table 8.5) indicated that most of minor elements are linked with heavy metals and clay-forming elements. Therefore, it is to suggest that influences of accumulation factor on distribution of these minor elements are comparable. The following discussion used Pb as an example element to highlight influence of accumulation factor. *Tendencies for other heavy metals (Cu, Zn, Cr, Cd) and minor elements (e.g. Rb, Sr, Ce) are comparable to the tendency of Pb*, as seen also in Figure 8.30 and Figure 8.33 (Appendix). Only Zr shows intensive enrichment in Dam Mon sediments, because of association tendency of zircon with sandy matter.

Table 5.2. Estimation on chemical contribution of hydrodynamic accumulation factor

(Values present percentage of the concentration of *M* – that respond to the grain-size fractions induced from hydrodynamic accumulation factor – on concentration of *M* in bulk; *M* is the studied chemical element or ratio of Al/Si)

a) Surface sediments in RRD										
Env.	% Infl ⁽¹⁾	Infl ratio ⁽²⁾	Influence percentage (in %)							
	Acc.Factor	Al/Si	SiO ₂	Al ₂ O ₃	Fe ₂ O ₃	MgO	CaO	Na ₂ O	K ₂ O	LOI
LM	70	0.16	45	31	30	34	36	44	31	29
MF	49	0.17	43	32	30	37	44	52	34	27
SP	10 ⁻⁴	0.16	43	33	33	36	41	47	34	29
b) Sediments along depth profile of MF (RRD)										
Depth	% Infl ⁽¹⁾	Infl ratio ⁽²⁾	Influence percentage (in %)							
	Acc.Factor	Al/Si	SiO ₂	Al ₂ O ₃	Fe ₂ O ₃	MgO	CaO	Na ₂ O	K ₂ O	LOI
~ 0 cm	49	0.17	43	32	30	37	44	52	34	27
~ 50 cm	63	0.16	35	32	32	35	36	42	32	30
~ 75 cm	93	0.15	31	27	27	28	29	31	26	25
⁽¹⁾ % Influence of accumulation factor in RRD (results from EMMA, Chapter 5.1.1) ⁽²⁾ Ratio between % influence on Al ₂ O ₃ versus % influences on SiO ₂ % <i>M</i> (accumulation) = $\sum a_i \cdot w a_i$ <i>M</i> : the investigated element <i>i</i> : index of the size fractions contributing accumulation end-member (in RRD cases: i.e. 6.3 – 20 μ m and 20 – 63 μ m); <i>a_i</i> = wt. % of size fraction <i>i</i> in bulk; <i>w a_i</i> = wt. % of the element <i>M</i> in the size fraction <i>i</i>										

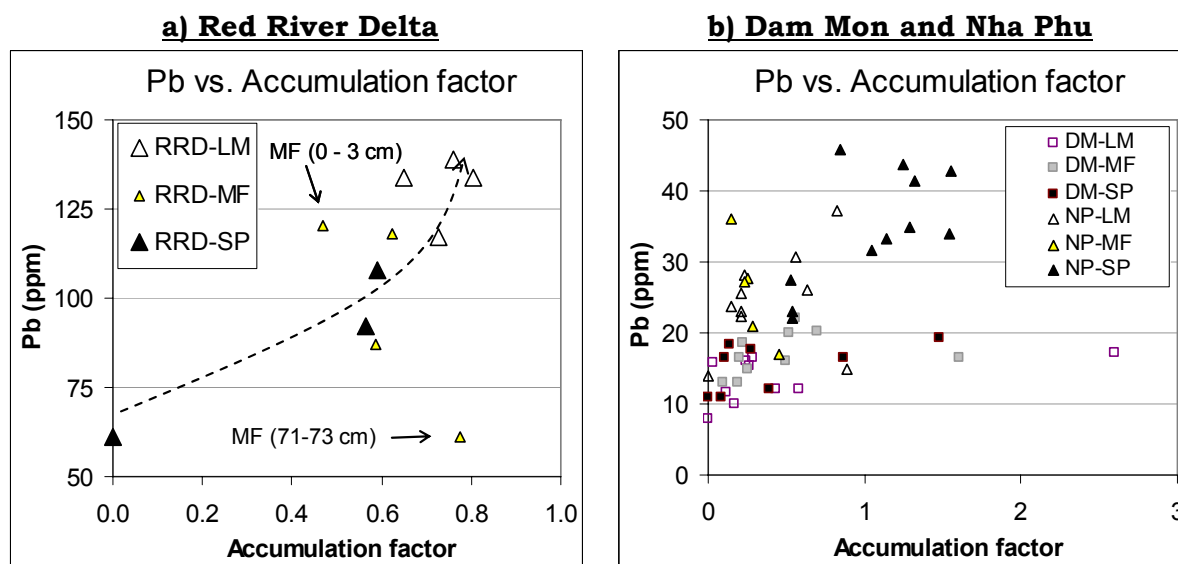


Figure 5.9. Influences of accumulation factor on distribution of Pb concentration in coastal sediments of Vietnam

The increase of accumulation influences results in concentrative increase of the heavy metal Pb as illustrated in Figure 5.9. In LM- and SP-sediments of Red River Delta (RRD), a *strong correlation between Pb-concentration and accumulation factor* is to identify (Figure 5.9a). Exception here is the samples in MF profiles of RRD, which exhibit very low concentration in the deepest part but high in surface layer (Figure 5.9a). This feature indicates less influence from accumulation and a *possible mobilization of heavy metals* induced from other processes in mangrove sediments. Accumulation of heavy metals and other minor elements in Dam Mon is generally lower than in Nha Phu. Both regions are much depleted in minor elements than the RRD sediments (see Figure 5.9 for Pb and see comparable tendencies for other minor elements in Figure 8.33 - Appendix). In comparison the LM and SP sediments, *the mangrove sediments* have higher tilt angle of elemental enrichment versus accumulation trend-line, inferring to a *higher capacity of heavy metal retention*. Because the higher accumulation influence means the higher concentration of fine materials, the increase of the heavy metal Pb is linked with the enrichment of clay matters in fine sizes. It is thus to impress the *significant influences of detrital accumulation factor on distribution of Pb as well as other minor elements in coastal sediments*.

Summarizingly, the accumulation factor defined by the grain size distribution is significantly mirrored by the elemental distribution in manner of allocating fine grain size, clay-rich materials and minor elements in coastal sea zones of longer distance from the syn-sedimentary coastline. Signals of accumulation factor on mineral and elemental distribution are obvious in Nha Phu profiles, where the hydrodynamic population is fundamentally governed by mountainous river and low tidal mudflats profiles of RRD and NP, where the interferences of biota and/or human activities are depleted. In MF and SP profiles of RRD and DM, signals of accumulation influence are overprinted by other processes.

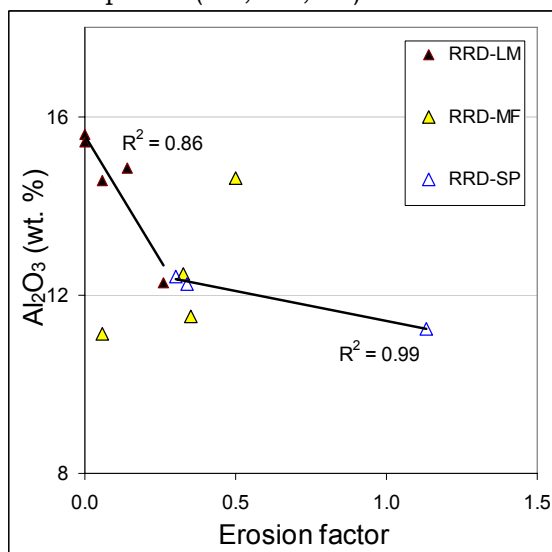
Syn-sedimentary erosion (by wave and tide)Mirror of erosion influences by distribution of clay-forming elements

In low tidal mudflat of RRD, influences of hydrodynamic accumulation factor on sediments are well mirrored by elemental distribution and clay matters (discussed in the above section). Because in RRD, erosion factor is the second principal dynamic that is oppositely to accumulation factor, the mirroring of erosion factor by elemental distribution and clay matters are thus indirectly correlation. The upper part of LM profile, where erosion influence is higher (Chapter 5.1.2), is mirrored by low Al, high Si and high quartz content, correspondingly.

Figure 5.10a offers visualization on relationships between influence of erosion factor and concentration of Al_2O_3 in bulk samples. Linear correlations with erosion processes are obvious for sediments in profile of low tidal mudflat and shrimp pond, but none correlation can be defined for sediments in mangrove forest. Figure 5.11 enables the comparison among depth distribution of Si, Al and Ca and depth behaviour of erosion factor in shrimp pond profile. The similar trend between Si and erosion factor and the opposite trend between Al and erosion are obvious. The similarity between depth distribution Al and other clay-forming elements (Mg, Fe, Mn, K) were revealed from results chapter, which mentioned for Figure 4.18, as well as from high correlations of these group (Table 8.5). Altogether, correlations and depth behaviours of elemental distribution and erosion factor are to impress the role of erosion on the depletion of clay-forming elements (represented by Al) in surface layer of LM and SP.

Exception is the distinctive behaviour of Ca, which concentrate highly in surface layer. It can be explained by anthropogenic addition of calcite and dolomite powder (Chapter 5.3), and remain of these chemicals specifically in surface layer.

a) Al_2O_3 (wt. %) vs. Erosion influences in three profile (LM, MF, SP) in RRD



b) Al_2O_3 (wt. %) vs. Erosion influences in shrimp pond profiles of RRD, DM and NP

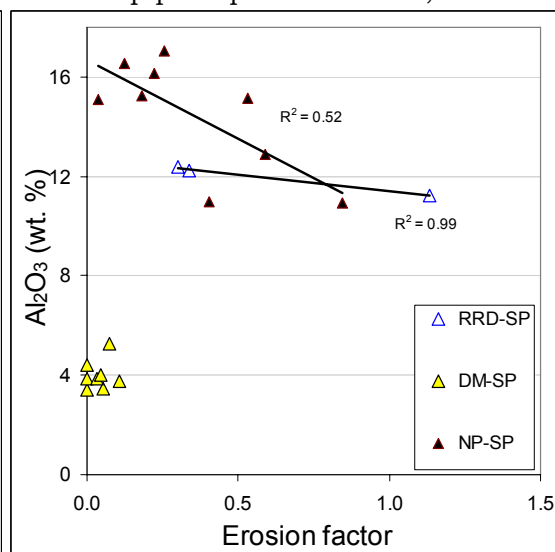


Figure 5.10. Influences of erosion factor on distribution of Al in coastal sediments

The tilt angle (Figure 5.10) mirrors intensity of Al (or clay species) leaching capacity of erosion factor. Higher tilt angle in samples of low tidal mudflat versus that in samples of shrimp pond can be seen in Figure 5.10a. It indicates that the leaching by wave and tide can remove Al more effectively than the leaching by water discharge in SP environment. However, the intensive erosion in SP (higher value of erosion factor, see Figure 5.10a) has resulted in very low amount of Al_2O_3 in all intervals of profile and especially in surface profile.

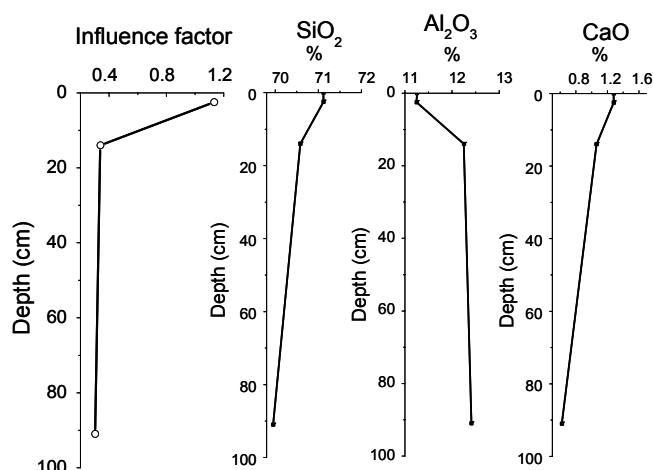


Figure 5.11 Distributions of erosion factor and chemical elements in SP profile of RRD

Higher influence of erosion factor responds to higher accumulation of Al but lower Si

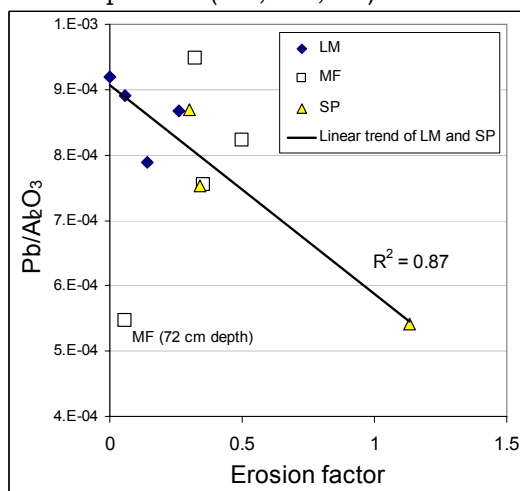
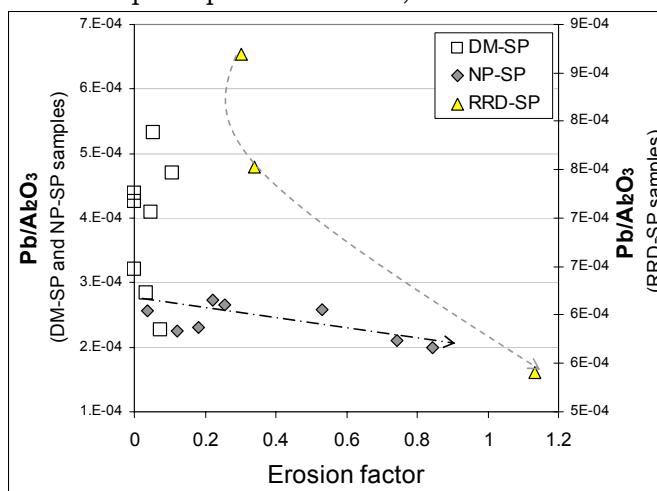
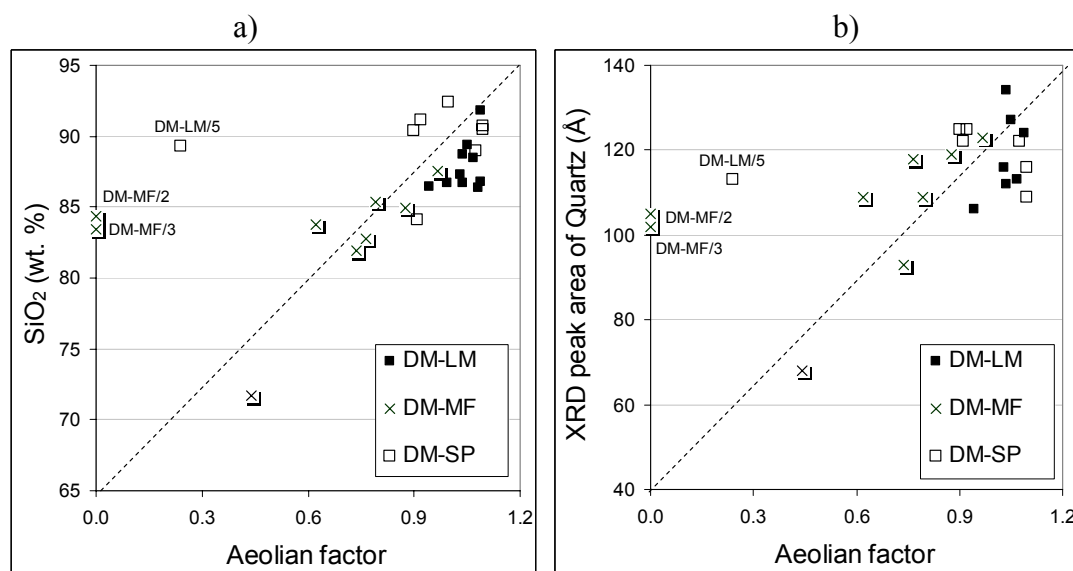
Besides, for RRD sediments, the principal syn-sedimentary hydrodynamic processes are defined to be accumulation and erosion. Therefore, behaviours of mangrove sediments profile, which shows no correlation with these both hydrodynamic factors, *indicate that the elemental distribution in mangrove forest profile is essentially driven by post-sedimentary process.*

Figure 5.10b visualizes the correlations between erosion factor and concentration of Al_2O_3 for all three shrimp pond profiles of Red River Delta, Dam Mon and Nha Phu. The direct correlations between erosion influences and Al_2O_3 concentration are obvious. However, none correlation can be defined for Dam Mon shrimp pond. These tendencies indicate readily that elemental distribution in shrimp ponds of Red River and Nha Phu is governed by erosion process. More detail discussion will be shown in Chapter 5.5.1.

Mirror of erosion influences by distribution of minor elements

Similar tendencies for Al versus erosion can be observed for heavy metals. For the reason that heavy metals behave similarly versus concentration of clay-forming elements (mirrored by high correlation coefficients in Table 8.5) or grain size distribution (Chapter 5.2.1), Pb was used as representative for this element group. Figure 5.12 shows the correlation between enrichment of Pb to clay matter (mirrored by $\text{Pb}/\text{Al}_2\text{O}_3$ ratio) and erosion factor. In RRD sediments, high correlations between Pb enrichment and erosion influenced can be addressed for LM and SP profiles (Figure 5.12a). Also, for shrimp pond sediments, high correlations between Pb enrichment and erosion are obvious only for Red River Delta and Nha Phu, but not for Dam Mon. These tendencies are comparable to tendencies for influences of erosion on distribution of Al_2O_3 concentration.

In sum, the effects of syn-sedimentary erosion are readily mirrored by elemental distribution in profiles of low tidal mudflat and shrimp pond. Higher influence of erosion factor responds to higher leaching of clay matters (mirrored by Al_2O_3 concentration) and decrease in capacity of heavy metals retention (mirrored by enrichment of Pb versus Al_2O_3).

a) Pb/Al_2O_3 vs. Erosion influences in three profiles (LM, MF, SP) in RRDb) Pb/Al_2O_3 (wt. %) vs. Erosion influences in shrimp pond profiles of RRD, DM and NP**Figure 5.12. Influences of erosion factor on enrichment of heavy metal – Pb in coastal sediments****Figure 5.13. Influences of aeolian factor on distribution of Silicon and quartz**

The higher values of factor correspond to higher amount of SiO_2 and peak area of quartz XRD reflection (1.82 \AA)

Deposition by aeolian matter

In addition to influences of accumulation factor and erosion factor, sediments in the central coast of Vietnam are driven principally by aeolian factor or deposition of aeolian matters. Figure 5.13 illustrates the enrichment of quartz and corresponding increase of Si content in Dam Mon sediments as a result of aeolian intensification. Sandy materials covering Hon Gom peninsular should be supplying source for this coastal region. Three exceptional samples correspond to dominant influences of accumulation factor (sample DM-LM/5) and erosion factor (samples DM-MF/2 and DM-MF/3).

The influence of aeolian factor on elemental distribution is not regularly due to dominantly interference by accumulation factor. Also, as mentioned in the chapter 5.1.1., due to high sedimentation rate, the aeolian influence on muddy sediments in the RRD is underestimated.

Therefore, whereas the aeolian factor makes high enrichment of sandy quartz in the coastal mud flats of Dam Mon, influences of this factor on sediments of Nha Phu is irregularly and in RRD is underestimated.

Summary

Consideration chemical distribution in connection with hydrodynamic variation has reveals that grain size distribution and corresponding hydrodynamic processes influences significantly on elemental distributions. Driving influences of accumulation is dominantly in Nha Phu profiles and LM profiles of RRD and Dam Mon, responding in higher clay species transported and deposited in lower sea zones. Erosion factor affects intensively sedimentary environments of RRD with different manner for different profiles in connection with abundance of suspended clay species. In LM and SP, erosion caused strongly resuspension and possibly also leaching of clay species in surface layer. Aeolian influences in Dam Mon is the dominant driving process of elemental distribution, causing abundance amount of quartz and corresponding Si concentration in this region. However, beside signals of syn-sedimentary hydrodynamic-driving processes, interferences of possible syn-sedimentary modification and post-sedimentary processes have been addressed, most obviously in MF and SP profiles of RRD and DM.

Effects of syn-sedimentary hydrodynamic processes on distribution of bulk mineralogy can be revealed from profiles of coastal sediments in Vietnam. In literature, it is well determined that the mineral distribution patterns reflects regional current pattern.

5.2.2. Physico-chemical processes

Nutrient supply by mangrove forest

In coastal sediments of Vietnam, concentration of total organic matter is comparable to that in sediment profile of *Avicenia* dominated mangrove forest in French Guiana of Amazon delta, which has been studied by Marchand et al. (2003) (Figure 5.14). The high accumulation in MF sediments than, especially in surface layer, indicates that organic matters present in coastal sediments are principally sourced from mangroves. Previous studies (e.g. Alongi et al. 1999; Marchand et al. 2003), based on the isotopic data, have also revealed that organic matters in sediments of several mangrove-fringed coasts are principally sourced from fragment mangrove species.

Contents of C_{org} in RRD (0.4 – 1.0 %) – the region with rapid sedimentation - are lower than in the south central coastline (Dam Mon, Nha Phu) (0.2 – 4.2 %) – the regions with much lower vertical sedimentation, suggesting a linkage between the rate of organic carbon burial rate of

sedimentation. This could be evidence to supports also for the assumption by Canfield et al. (1993) and Alongi et al. (2001) that the rate of organic carbon burial is a function of sedimentation rate. Additionally, the higher efficiency of organic carbon production from organic matters, responding to higher C_{org} concentration in Dam Mon, can links also with higher maturity of mangrove forest in comparison to younger mangroves in RRD. Higher aerobic mineralization and higher oxygen consumption during sulphate reduction should be the reason for that (Alongi et al. 2001).

Because shrimp ponds were constructed from former mangrove forest sediments, the organic matters presenting in these environments were also inherited and maintained in fine materials. The nutrients presented in LM are possibly obtained not only from river but also from leaching organic matters from MF by tide current. The roles of mangrove forest as not only a sedimentary sink for organic carbon but also a dominant source of organic carbon and other nutrients to adjacent coastal system were discussed by Alongi et al. (2001), based on isotopic data.

When delivered by creeks to intertidal mudflats, nutrients were trapped and stored in sediments. High correlations among C_{org} and size fractions of 2 - 6.3 μm and 6.3 – 20 μm in the Red River Delta sediments ($r^2 = 0.58 - 0.74$, $n = 12$) and all fractions < 63 μm in Dam Mon and Nha Phu ($r^2 = 0.5$, $n = 22$) sediments referred that these grain sizes were the main nutrient containers. Jokic et al. (2003) indicated that the preservation of the organic carbon compounds in wetland sediments was a result of their presence as surface adsorbed layers on the soil mineral particles. Sorption of dissolved organic matter on surfaces of clay mineral particles represents one of the most important geochemical processes and seems to be responsible for the preservation of organic matters in coastal marine sediment and aquatic system (Moreira-Turcq et al. 2004 and references therein).

Eh/pH system - a mixing condition between river-born sediments and sea water

In coastline muddy sediments of Vietnam, mixing between fresh water (river, drainage) and saline water (sea) gives rise to chemical environments in range of neutral to slightly alkaline and weakly reductive to weakly oxidized as revealed by $pH = 7.13$ to 8.87 , $Eh = -145$ to 268 mV in cases study of the Red River Delta in the North, Dam Mon and Nha Phu in the South Central Vietnam. The pH values are similar to those of French Guiana *Avicennia* forest, ranging from 5.2 to 7.2 (Marchand et al. 2004), African *Avicennia* forest, ranging from 6.2 to 8 (Middleburg et al. 1996), and of Australian *Avicennia* forest, ranging from 5.5 to 8 (Clark et al. 1998). The Eh-interval from weak reduction to weak oxidation (Eh ranging from -145 mV

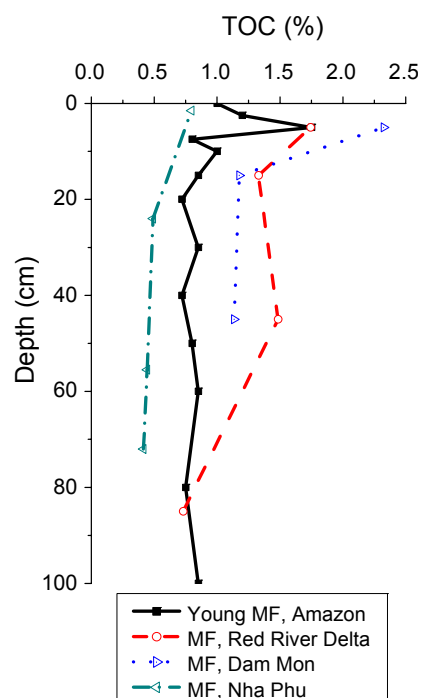


Figure 5.14. Comparison distribution of total organic carbon in the studied MF profiles and *Avicennia* mangrove profile in French Guiana, Amazon delta (Marchand et al. 2003)

to 165 mV) resembles conditions described for of various mangrove fringed coasts in several tropical countries (e.g. Clark et al. 1998; Middleburg et al. 1996; Marchand et al. 2004).

The role of sea water in terms of alkalisation are well reflected by more alkaline sediments in Dam Mon peninsular (Table 4.2a), where is dominated by influence of sea water, than in the Red River estuary and Nha Phu embayment (Table 4.2a), where is dominated by river influence. Furthermore, this role is imprinted by the sudden increase of pH in the 0 – 10 cm surface layer of all profiles (Table 4.2a). In shrimp pond sediments, the neutral pH of relates directly to the human-made regulation by adding dolomite/calcite powder in shrimp ponds in order to favour living and development of shrimps.

Though the problem of acidification caused by oxidation of H_2S has been documented in many mangrove fringed estuaries and related aquaculture ponds in Thailand, Indonesia (Thornton et al. 2003) and in Bach Dang estuary of Vietnam (Cu 1993), in none of the investigated sediment sample occurs the depletion of pH to less than 6. In RRD, although that the permeability is not so high, the maintain in balance state as mixing between river current and the sea of pH/Eh systems is promoted by rapid sedimentation, that prevent formation of organic-matter rich layers – the main factor to produce reductive, acidic agents. In Dam Mon and Nha Phu, the high permeable texture of sediments facilitating exchange and movement of pore water also limit pH/Eh from intensive changing.

Adsorption/ desorption of heavy metals and other minor elements

The above discussion on elemental distribution and accumulation factor has shown that heavy metals and minor elements are fundamentally detritus in origin and are transported by river to the coastal zones.

Table 5.3. Correlation between heavy metals and possible proxies

Red River Delta (n=12)							
	C_{org}	S_{Total}	SiO₂	Al₂O₃	MnO	Eh	pH
Cu	0.70	-0.62	-0.90	0.86	0.94	-	-
Pb	0.67	-0.22	-0.84	0.88	0.62	-	-
Zn	0.71	-0.61	-0.92	0.92	0.96	-	-
Cr	0.86	-0.25	-0.91	0.94	0.79	-	-
Ni	0.56	-0.60	-0.85	0.79	0.80	-	-
Cd	0.53	-0.53	-0.81	0.77	0.72	-	-
Dam Mon (n= 11 for C_{org}, S_{total} and n = 28 for major elements, Eh, pH)							
	C_{org}	S_{Total}	SiO₂	Al₂O₃	MnO	EH	PH
Pb	0.85	0.96	-0.95	0.95	0.81	-0.32	-0.26
Cr	0.77	0.58	-0.63	0.48	0.76	0.04	-0.44
Zn	0.81	0.87	-0.95	0.96	0.89	-0.52	-0.18
Ni	0.72	0.78	-0.84	0.86	0.74	-0.60	-0.28
Nha Phu (n= 11 for C_{org}, S_{total} and n = 27 for major elements, Eh, pH)							
	C_{org}	S_{Total}	SiO₂	Al₂O₃	MnO	EH	PH
Pb	0.18	0.43	-0.90	0.96	0.73	0.15	0.09
Cr	0.16	0.59	-0.92	0.95	0.92	0.28	0.08
Zn	0.27	0.56	-0.96	0.98	0.81	0.09	0.10
Ni	0.17	0.54	-0.93	0.98	0.86	0.19	0.12

When these elements, associating with suspended materials, meet the saline water, they are subjected not only to grain size distribution by hydrodynamic processes but also possibly to chemical variations (Harbison 1986). Any change in main proxies of heavy metals can basis for determination of desorption/re- adsorption process in coastal area. Table 5.3 presents correlation coefficients between heavy metals and representatives of possible proxies: Al for detrital clay minerals, C_{org} and S_{total} for mangrove-born organic matters and Mn partly for manganese oxides.

In Chapter 5.2.1, it has been revealed that minor elements, except for Zr, associates mostly with clay minerals during the transportation from source to sink, indicated by the high enrichments in fine sediments. These tendencies are confirmed by strong correlation of almost heavy metal elements with Al_2O_3 , as seen in the Table 5.3. Heavy metals show also high correlation with Mn ($R = 0.62 - 0.96$, Table 5.3), suggesting that manganese oxide is also a possible host. However, because Mn occurred only partly as manganese oxide in fractions of 2 -6.3 μm (Figure 5.5a, Chapter 5.2.1) but principally associate in structure of clay minerals, it is thus not clear for the possibility that manganese oxide acts as significant host for minor elements. Exception is the concentration of Cr in Dam Mon, which shows medium correlation with Al ($R = 0.48$) but higher correlation with Mn ($R = 0.76$). It can suggest that Cr in Dam Mon is preferably hosted by manganese oxides.

Besides high correlation with clay species, minor elements in Red River Delta and Dam Mon show also high correlation with C_{org} . It is to notice that the organic matters amount presenting in the coastal muddy sediment is mainly originated from mangrove ecosystems as demonstrated in the Chapter 5.2.2. High correlations between the detrital minor elements and mangrove originated organic carbon, thus indicates an occurrence of a partly desorption process of minor elements from surface of clay particles and re-adsorption by coastal organic matters during syn- and post-sedimentary periods. This desorption/ adsorption process allows minor elements to concentrate in organic-rich zone, additionally to the distribution tendency driven by accumulation factor (It is the tendency that minor elements tend to allocate in deeper part of core, corresponding to the zone of longer distance from syn-sedimentary coastline, where is more intensively influenced by accumulation factor, seen in LM profile, Chapter 5.2.1). In MF profiles, minor elements can be concentrated in surface layer, where surface material receives higher amount of organic matters. This tendency explains also for the distinguishing distribution tendency of minor element in MF profiles from LM profile, where influences by organic matters are lacked.

Only in Nha Phu, concentration of heavy metals shows low correlation with organic carbon but rather high with total sulphurs (S_{total}) ($R = 0.43 - 0.59$). Strong correlations of minor elements with S_{total} are most obviously in sediments under century-old mangrove forest in Dam Mon but no correlation or even negative correlation can be seen in Red River Delta. The

strong correlation between total sulphurs and sulphur in form of pyrite ($R = 0.99$) (Figure 4.14 in Chapter 4.2.1) indicates that sulphur content in coastal sediments involves mainly in form of sedimentary pyrite. Also in the Chapter 5.4.1, it is shown that sulphur tends to accumulate to form sulphur-rich layers in sediments of Dam Mon and Nha Phu, facilitated by continuous supply of organic matters by mangrove and low sedimentary rate. But the formation of sulphur-rich layer is not favourable in RRD due to high sedimentation rate. Therefore, the high correlation between minor elements and sulphur indicates also desorption from clay species and adsorption by sulphur-rich matters (e.g. sedimentary pyrite). The higher correlation or higher adsorption responds to lower sedimentation rate of the region and also to the longer time influenced by mangrove forest, as obviously in Dam Mon.

Thus, it is quite clear that when transported to estuary, some amount of heavy metals can be desorbed from clay minerals and re-adsorbed by organic matters in mangrove sediments.

Earlier studies reported two different explanations for the differentiation of heavy metals distribution in estuarine area. One explanation is linked with desorption mechanism of heavy metals out of detrital sediments, based on several laboratory experiments (e.g. Kharkar et al. 1968; Evans & Cutshall 1973) and field work investigations (e.g. Weijden et al. 1977; Li 1984; Padmalal 1993). Typical example is study of Padmalal (1993) that used the mechanism is used to explain for the decreasing trend of Cu and Co in muddy sediments from the near-shore to off-shore zones in Vembanad estuary. Additionally for this explanation is the study of Gier & Johns (2000) that worked out re-adsorption of heavy metals by organic carbon also in estuarine area. In contrast, the other explanation for rational concentrative distribution of major and minor elements is simply results from sedimentological and hydrological processes (e.g. Sholkovitz 1979a;b Nolting et al. 1990).

The evidences given in Chapter 5.2.1 (mirroring of hydrodynamic processes by elemental distribution) demonstrated that increase in accumulation factor can result in higher accumulation of heavy metals as well as other minor elements, typically in the condition that lacks of organic matters (i. e. LM profiles). However, correlations between concentrations of minor elements in sediments are revealed to demonstrate that the chemical modification does happen by means of adsorption/ desorption processes, parallel to hydrodynamic – induced distribution.

Significant roles of pH, Eh in driving mobilization and distribution of minor elements have been mentioned in several researches of estuarine regions (e.g. Clark et al. 1998; de Souza et al. 1986). However, the observed low correlations among heavy metal contents and pH/Eh values (Table 5.3) in these investigated regions refer that variation of these two physico-chemical factors have non-defined influences on elemental distribution. It could be resulted from high sedimentation rate in RRD and high permeability in DM and NP those limit pH/Eh state from intensive changing. The influences of pH/Eh on adsorption/ desorption should be questioned only when significant pH/Eh changing event could happen (e.g. intensive oxidation when the former MF sediments are exposed to construct shrimp pond).

Summary

When the river-born sediments reach saline water and temporary settle down, two main chemical processes occurring are determined (1) establishment of balance pH/Eh system as a mixture between river-born sediment and saline water and (2) desorption of heavy metals out of source clay minerals when the particle contact with sea water and re-adsorption by coastal – originated organic matters. The adsorption process, together with high concentration of heavy metals supplied by diversified industrial activities present in the RRD basin result in contamination of Cu, Pb, Cr and Ni in the coastal sediments. Although heavy metals are immobilized during the sedimentation (Wasserman 1991; Clark et al. 1998), these elements are possibly remobilized and become more harmful through plant uptake or entering the food chain (de Souza et al. 1986; Harbison et al. 1986) by the coastal biota (Bou-Olayan et al. 1995; de Mora et al. 2004).

5.2.3. Clarification of coastal sediments

Distribution of grain sizes, clay mineralogy, major and minor elements as mirroring of sediment supply

Discussion on influences of hydrodynamic factors on elemental distribution of clay matters, mirrored in sediment profiles (Chapter 5.1) have revealed the regional dependence, that correspond to specific sediment supply. Nha Phu profiles are more influenced by accumulation factor, with the meaning that fine grains, clay species and heavy metals as well can be transported to longer distance from the syn-sedimentary coastline. Meanwhile, profiles in Red River Delta are essentially driven by syn-sedimentary erosion process but profiles in Dam Mon are more obviously driven by deposition of Aeolian materials.

Figure 5.15 visualizes the differentiation among three regions: RRD, DM and NP in grain sizes (a), clay mineralogy (b), major elements (c) and minor elements (d) based on PCA treatment.

Different hydrodynamic processes are main driving forces for distribution of grain sizes, mirrored by one linear tendency of sediments in Dam Mon, other linear tendency in RRD and the intermediate behaviour of Nha Phu. Sediments in RRD, corresponding to deltaic source, have high freight of fine particles ($< 200 \mu\text{m}$). Distribution of particle sizes is principally driven by erosion process as discussed in Chapter 5.1. In opposite to RRD, sediments in Dam Mon correspond to mountainous coastline, composing mainly of coarse sedimentary materials and aeolian deposition as the principal driving force. Noticeable is the sediments in Nha Phu, which are composed of two groups as intermediate between grain size features of RRD and grain size features of Dam Mon. Distribution of grain sizes in Nha Phu has been demonstrated (Chapter 5.2.2) to be driven principally by hydrodynamic accumulation process.

Abundance of coarse sediments in Dam Mon links with high amount of quartz, and corresponding high SiO_2 concentration in this region (Figure 5.15c). Only exception is the surface muddy sediment sample in MF environment, which is more similar to chemical

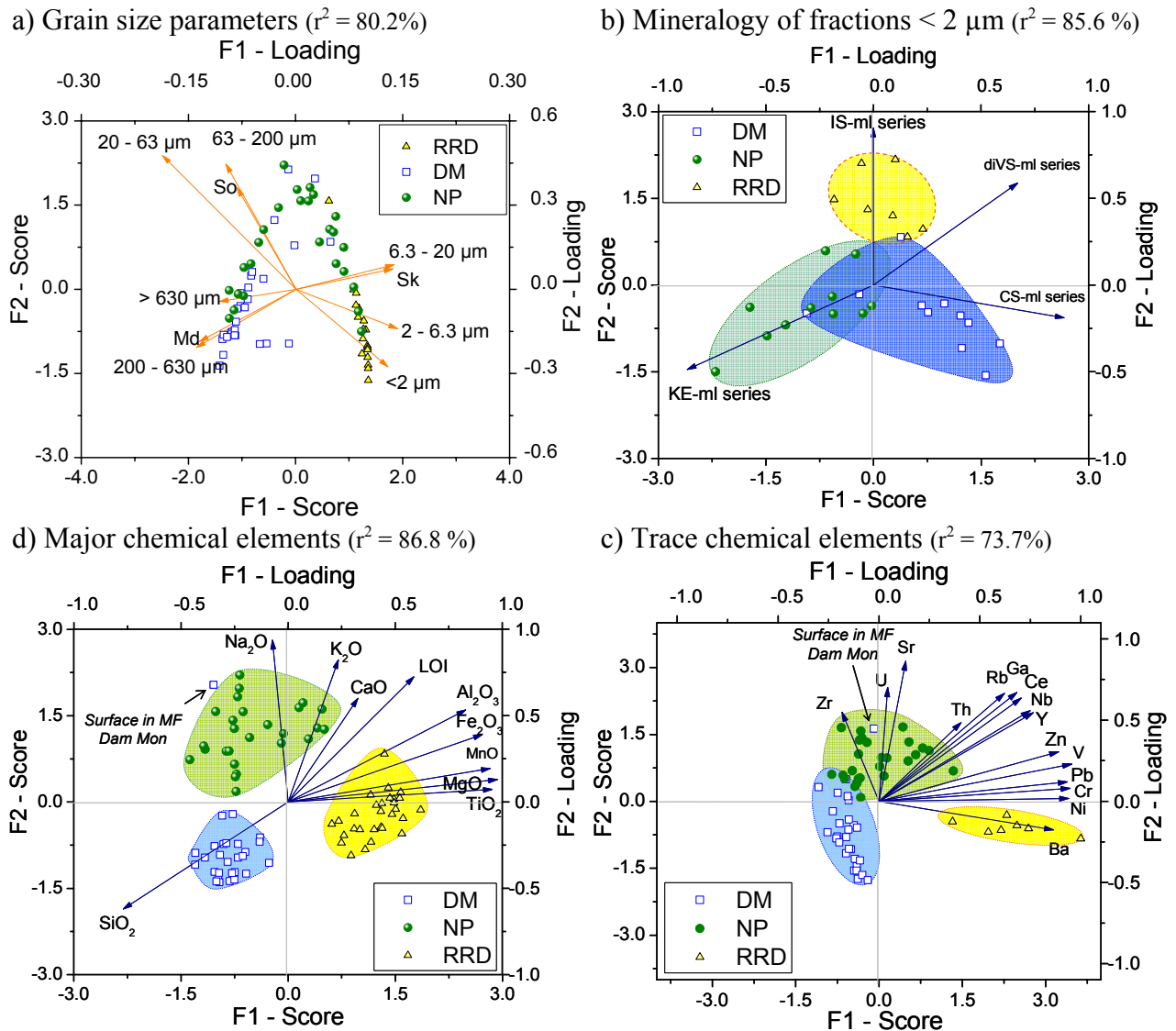


Figure 5.15. Differentiation in grain sizes, clay mineralogy, major and minor chemical elements between Red River Delta, Dam Mon and Nha Phu, as mirrors of sediment source

composition of mountainous deltaic sediments in Nha Phu. This suggests that origin of fine materials in Dam Mon could link with riverine alluvia. The only possible river to supply alluvia material to this region is Can river (see map of sampling sites in Dam Mon, Chapter 3.1.2). Deltaic sediments in RRD contain high amount of clay species, which register high amount of Al, Mn, Fe, Mg contents (Figure 5.15c). Sediments in Nha Phu also contain relative high amount of clay matters, as supplied from the coherent mountainous delta. However, these materials are characterized by high variation in concentrations of Ca, Na and K elements (Figure 5.15c), as interferences by sea factor and non-clay minerals from incongruent weathering products of mountainous materials.

Reveals from XRD of oriented mount for fraction < 2 μm and single particle analysis by TEM-EDX shows that the clay mineral assemblage in coastal sediments containing essentially of mixed layer series rather than being a simple suit of chlorite, kaolinite, illite and

montmorillonite as documented by several pre-researches (e.g. Chamley 1989; Parra & Pujos 1998; Marchand et al. 2004; Nghi 1988, Bach et al. 1998; Jagodziński 2005), which mainly based solely on XRD investigation of bulk samples. The mixed layer series included: IS-ml, diVS-ml, CS-ml and KE-ml, and dominated by diVS-ml structures.

In each mixed layer series, the proportional contribution of end-member varies in a wide range, mostly from 0 % to 100 %. Because of this complexity, it is difficult to quantify the mineral composition in these coastal sediments based on the current approaches such as XRD and chemistry combination (Moore & Reynolds 1997), Rietveld Refinement (Rietveld 1969). Semi-quantification is based on the frequency of appearance in TEM images with consideration of particle sizes. Proportion of these groups in the mineral assemblages varies depending on the region, which is different from each other in rock source, distance from the rock source as well as influences of biota, human activities. In all three regions: RRD, DM and NP, diVS-ml is the most abundant series, account for 68 – 72 % of total particle frequency. The sediment in estuary of the Red River Delta is more abundant in IS-ml whereas the sediments in mountainous coastline of Dam Mon and Nha Phu are more abundant in CS-ml and KE-ml, respectively.

In the Red River Delta Pb, Cu, Zn, Cr are largely reported to be detritus in origin and connected to industrial activities such as zinc smelt, steel works in the surrounding regions and industrial zones along the Red River catchment (e.g. Quyen et al. 1995; Kasbohm et al. 1998; Lai et al. 2005). These heavy metals Pb, Cu, Zn, Cr, Co, Ni and Cd are popularly described as important contaminants.

Investigation on heavy metals concentration of in coastal sediments of Vietnam indicates a regional variation, from RRD, via NP to DM. With high quantity of clay matters in bulk samples, sediments in RRD register the highest amount of heavy metals and other minor elements. Total concentrations of heavy metals in coastal muddy sediments of the Red River Delta are relatively high, particularly with enrichments ratios of Pb, Cu and Zn to the average world mud (Wedepohl 1960) are 5.2, 2.4 and 1.3, respectively (Table 5.4). Comparable data have been reported for the same region by Cu (1998). High accumulation of minor elements in coastal sediments of RRD could be caused by their richness in source materials and/or trapping by high amount of clay matters in this region. Unlike RRD, Dam Mon sediments exhibits very low concentrations of minor elements, of 1 – 8 times lower than the average world mud (Wedepohl 1960). This mirrors their poorness in source materials as well as the low retention capacity of sandy materials. Although similar chemistry of source sediments are suggested for Dam Mon and Nha Phu, higher concentrations of minor elements in Nha Phu, where more abundant of clay matters occur, could be indicative for adsorption and trapping function of clay minerals. Indeed, urbanisation level as well as density of industrial zones in these regions of the south central coast is much less than that in the Red River Delta.

González and Vargas (2004) claimed also that high metals levels may be attributed to local contamination instead of regional lithologic or pedogenic processes. In comparison to other tropical mangrove sediments, such as South Australian gulfs (Harbison 1986), Vembanad estuary, India (Bararudeen et al. 1996), French Guiana (Marchand et al. 2006) and to effect levels TEL and PEL (CCME 2002), the coastal sediments in DM and NP transects are considered to be poor in heavy metals and generally far under the levels of risk, but it is noteworthy that estuarine sediments in RRD is enriched to reach to pollution levels.

In sum, differentiations in grain sizes, mineralogy and chemistry among three case study regions: RRD, DM, SP are mirrors of source sediments, length of river as well as river freight.

Pollution potential in RRD transect

Most of the heavy metals, except for Cd, accumulated in RRD coastal muddy sediments to the levels higher than TEL (Threshold Effect Level), the level that sediments should be considered for possible hazards to aquatic organisms (CCME 2002). The coefficient pollution C / C_{TEL} for Pb, Cu, Zn, Cr, and Ni of these sediments are 3.4, 6.2, 1.0, 1.7 and 3.0, respectively (Table 5.4), reflecting moderately contamination level. In surface layer of mangrove forest profile and layer of 60 cm depth in low tidal mudflat profile, concentration of Cu, Pb and Ni were even 1 – 1.7 times higher than PEL (Probable Effect Level) - the level indicating an association with adverse biological effects (CCME 2002) (Table 5.4). Pollution by heavy metals in sediments of mangrove forest has been largely reported for several estuarine areas, where received industrial, livestock and domestic sewage from big cities, such as Cu, Pb, Zn, Mn contamination in Hong Kong mangrove sediments (Tam and Wong 2000), Cu, Pb, Zn, Ni in Brisbane River estuary, Australia (Mackey and Hodgkinson 1995). Highly accumulation of heavy metals in coastal mudflat sediments is great risk to coastal biota such as bivalves, fish, crab, alga, seaweed (Bou-Olayan et al. 1995; de Mora et al. 2004) that consume organic matters from mudflats.

Table 5.4 Enrichment ratios of heavy metals in coastal sediments of Vietnam

Env.	Pb	Cu	Zn	Cr	Ni	Cd
Enrichment ratio to average near-shore mud (Wedepohl 1960) ($C/C_{world-mud}$)						
RRD	5.2	2.4	1.3	0.9	0.9	
DM	0.8	< 1	0.2	0.2	0.1	
NP	1.5	< 1	0.6	0.3	0.2	
Ratios between average concentration to TEL (C/C_{TEL}), PEL (C/C_{PEL}) and average concentrations in suspended matters of Red River (Lai 1995) (C/C_{river})						
C/C_{TEL} (RRD)	3.4	6.2	1.0	1.7	3.0	0.4
C/C_{PEL} (RRD)	0.9	1.1	0.4	0.6	1.1	0.1
C/C_{river} (RRD)	1.2	3.5	0.7	0.9	1.0	
RRD sediments: Coefficient of potential contamination (C/C_{TEL})						
C/C_{TEL} (RRD-LM)	2.3 - 4.6	4.4 - 9.7	0.7 - 1.4	1.6 - 2.1	2.6 - 3.7	0.4 - 0.5
C/C_{TEL} (RRD-MF)	2.0 - 4.0	3.6 - 7.7	0.7 - 1.3	1.5 - 1.8	2.3 - 3.3	0.2 - 0.4
C/C_{TEL} (RRD-SP)	2.0 - 3.6	4.7 - 4.9	0.7 - 0.8	1.4 - 1.7	2.5 - 2.9	0.3 - 0.4
RRD sediments: Coefficient of contamination (C/C_{PEL})						
C/C_{PEL} (RRD-LM)	0.6 - 1.2	0.8 - 1.7	0.3 - 0.6	0.5 - 0.7	1.0 - 1.4	0.1 - 0.1
C/C_{PEL} (RRD-MF)	0.5 - 1.1	0.6 - 1.3	0.3 - 0.6	0.5 - 0.6	0.9 - 1.2	0.0 - 0.1
C/C_{PEL} (RRD-SP)	0.5 - 1.0	0.8 - 0.8	0.3 - 0.4	0.5 - 0.5	0.9 - 1.1	0.0 - 0.1

5.2.4. Summary on syn-sedimentary processes

(1) Distributions of clay matter and elemental in the coastal sediments in Vietnam are strongly influenced by texture of sediments. The finer materials register higher amount of clay species, clay-forming elements (Al, Mg, Fe, Ti, Mn, K) and higher concentration of minor elements. The coarser materials register higher amount of non-clay minerals such as quartz, feldspars and zircon and corresponding elements: Si, Ca, Na and Zr.

(2) Signals of influences by the principal hydrodynamic processes (i.e. accumulation in the sense of grain size separation, syn-sedimentary erosion and deposition by aeolian materials) can be recognized in coastal sediments of Vietnam, specifically in the profiles under limited influences by biota and human activities. In Nha Phu, influences of accumulation factor result in higher concentration of clay species, clay-forming elements (Al, Mg, Fe, Mn, Ti) and minor elements, indicating an offshore transportation of these matters with fine sizes to deposit in the deeper-water zones. In Dam Mon and Red River Delta, influences of accumulation factor can only be detected in LM profiles.

Erosion process caused strongly leaching of clay species out of in surface layer in LM and SP profiles. Whereas, aeolian influences in Dam Mon is the fundamental process to distribute elemental distribution, causing abundance amount of quartz and corresponding Si concentration in this region.

In MF and SP sediments, the original influences by syn-sedimentary hydrodynamic processes on elemental distribution tend to be interfered with syn-sedimentary chemical modification by mangrove biota, human impact and/or also post-sedimentary processes.

(3) A balance pH/Eh system is to be established as a mixture between river-born sediment and saline water, acting as buffer condition for chemical processes. In RRD, the narrow variation in pH/Eh values is linked with high sedimentation rate that limiting formation of reductive, acidic organic matter-rich layers. In south central coast, these narrow ranges are mainly linked with high permeability that facilitates the water exchange.

(4) The most obvious chemical modification during syn-sedimentary hydrodynamic process is desorption/ re-adsorption. Heavy metals and other minor elements are desorbed from river-born clay minerals and re-adsorbed by coastal organic matters, resulting in the intensive accumulation in organic- rich surface layer of mangrove sediments.

(5) Contamination of the heavy metals: Cu, Pb, Zn and Ni in coastal sediments of RRD is defined in medium levels, in comparison to Canadian standards for aquatic sediments. High supply of these contaminants from diversified industrial activities in the RRD catchment and the adsorption by clay species and organic matters in coastal mudflats could be the reason for this pollution potential.

(6) Mangrove forest is revealed to be the principal source of nutrients for the coastal sediments. Amount of organic supply mirrors the biomass as well as maturing of mangrove

forest. Burrier rate of organic matter sedimentation is function of sedimentation. RRD sediments with young mangrove forest and rapid vertical sedimentation retain low quantity of organic carbon. Dam Mon sediments with century-age mangrove forest and very low sedimentation rate retain the highest quantity of organic carbon. Sediments in Nha Phu (young mangrove, low sedimentation rate) exhibit medium organic carbon quantity as intermediate character between RRD and Dam Mon.

(7) Differentiations in grain sizes, mineralogy and chemistry among three case study regions: RRD, DM, SP are mirrors of source sediments, length of river as well as river freight. RRD sediments are characterized by high accumulation of fine materials, clay matters, clay-forming elements, minor elements and IS-ml series to follow the most abundance frequency diVS-ml series in clay fraction. In converse, Dam Mon sediments are characterized by high quantity of quartz, SiO_2 concentration but very low quantity of minor elements. Following diVS-ml series, the CS-ml series in fractions $< 2\mu\text{m}$ characterize for this peninsular sandy sediments. The intermediate characters on grain sizes, clay matters and minor elements between RRD and DM exhibit in Nha Phu. Sediments in this region shows readable interference of sea factor and non-clay minerals, those register main composition of Ca, Na and K elements. Together with diVS-ml series, KE-ml series are typically for clay mineralogy of Nha Phu.

5.3. Post-sedimentary processes - mirroring in elemental distribution and mineral matters

5.3.1. Geochemical mirror of post-sedimentary processes

Chemical results of the studied sediments exhibit different behaviours of K along depth profile, relatively to Al and other clay-forming elements (Figure 5.17a). With assumption that Al is the conservative element in sediments, enrichment of other elements can be determined by concentrative ratio to Al_2O_3 . In similar way, enrichment or relative abundance of feldspar and clay phases are determined by ratios of their XRD peak areas to peak area of quartz reflection (i.e. 1.82 \AA in bulk sample, powder specimen and 3.34 \AA in fractions $< 2 \mu\text{m}$, oriented mount specimen).

High correlation between enrichment of K and relative quantity of feldspar in bulk samples indicates the role of feldspar as fundamental host for the quantity of potassium along the core. However, the exception in surface sample, with very low enrichment of K versus high quantity of feldspar suggests a mobilization of this element by some leaching process.

Mobilization of K, Mg and Fe, if there is, could link with dissolution process and re-absorption by clay minerals, organic matters or biota-induced processes. The inverse correlation between K enrichment and expandable phase (Figure 5.17a) responds to a depletion in potassium in smectitic species. In other words, it refers to leaching of K out of expandable phase during the post-sedimentary process. Whilst, the direct correlations between enrichment of Fe (Figure 5.17b) and Mg (Figure 5.17c) and expandable phases indicate the incorporation of these elements

into lattice of smectitic species. Indeed, TEM investigations on chemical formulae of diVS-ml series revealed commonly the increase of Fe and Mg in octahedral layer in particles with higher smectitic proportion (Figure 4.32, Figure 4.40). These tendencies are most obvious in LM profile but rather interfering by other processes in MF and SP profiles.

In detrital clay matters, heavy metals are expected to associate with smectites – the expandable phase with the highest capacity of absorption, due to high specific surface area (Borchardt 1989). However in the coastal

sediments, only a very weak trend between amount of expandable phase and heavy metal are generally to see (Figure 5.18). It looks more likely, that distribution of heavy metals LM is linked with smectites directly, and the older sediments (MF and SP profiles) could be linked more tightly with organic material by mangroves and remains of organic matters in SP (notice the highest heavy metals values for lowest values for expandable phase). That means we have a rearrangement of heavy metals from detrital situation (clay matters) to post-sedimentary situation (organic matters). These evidences are furtherly supportive for the above discussion on desorption/re-adsorption processes in coastal zone (Chapter 5.2.2).

Additionally, surface sediment of LM and SP have depletion of heavy metals concentration. Erosion effects (Chapter 5.2.3) could be the reason for these depletions in LM surface layer but a leaching process could link directly to depletions of heavy metals in SP surface sediments (Chapter 5.5.1).

The minor element Rb shows also similar behaviour to heavy metals (Figure 5.18d) that correlate directly with expandable phase. However, as mentioned above for Figure 5.17a, concentration of K decreases in samples containing higher expandable phases. It has been discussed that Rb and K, due to similar chemical nature, both have tendency to concentrate in clay fractions (Figure 5.5 & Figure 5.6, Chapter 5.2.1). Therefore, these different trends between Rb and K in coastal sediments indicate that they are hosted by different clay species. Rb tend to be adsorbed on surface of smectitic species like heavy metals and other minor elements, whereas, K remains only in mica-like clay phase but can be leached away from lattice structure of expandable phase.

The exception is Rb enrichment in surface sediment of MF in Dam Mon (141 ppm), which is not plotted in Figure 5.18d for illustrating purpose. High accumulation of Rb in surface sediments of MF environment could be linked with abundance of organic matters, the substance with high absorption capacity.

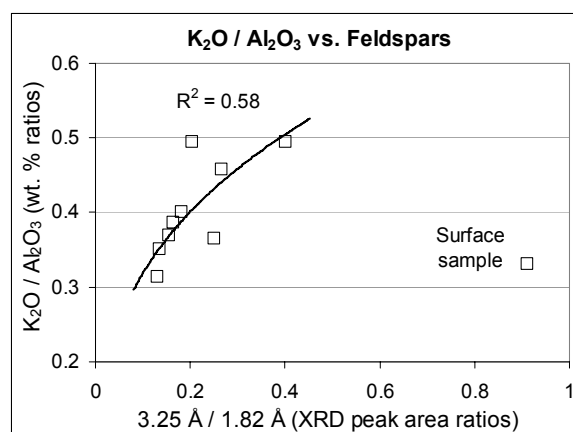
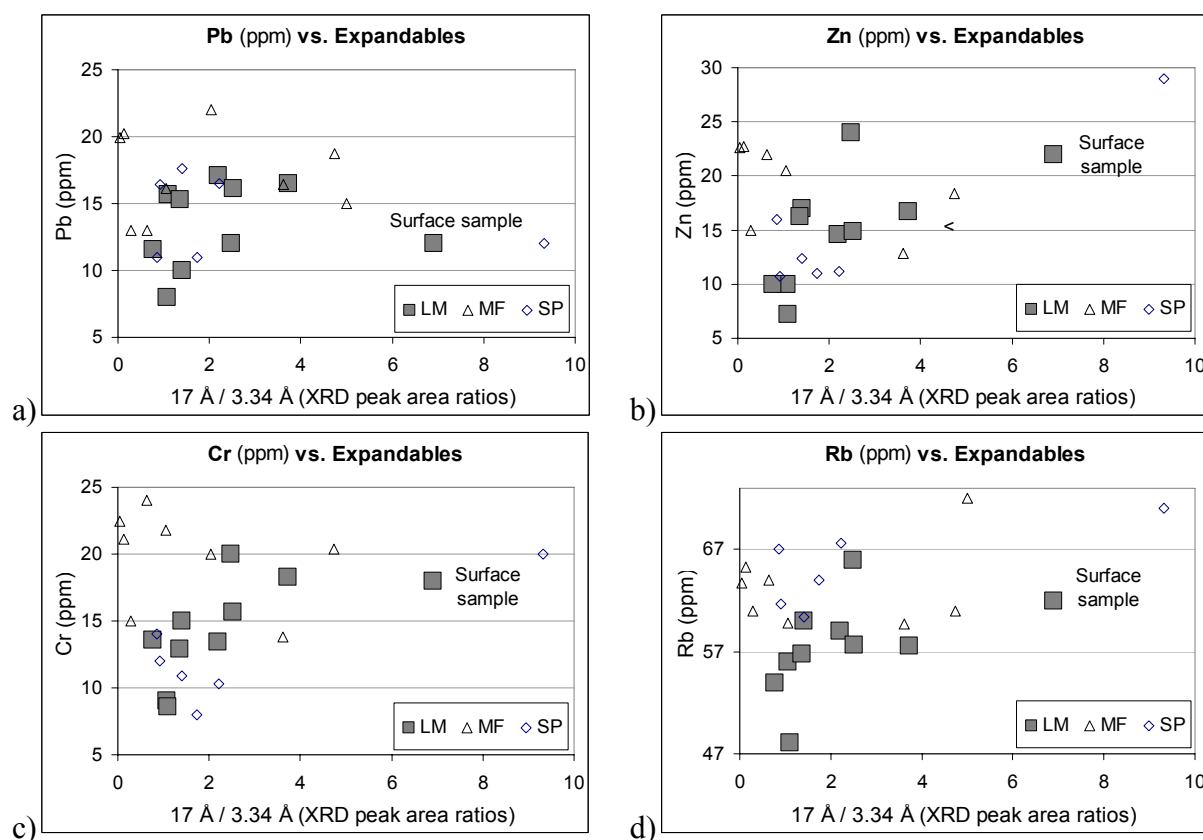
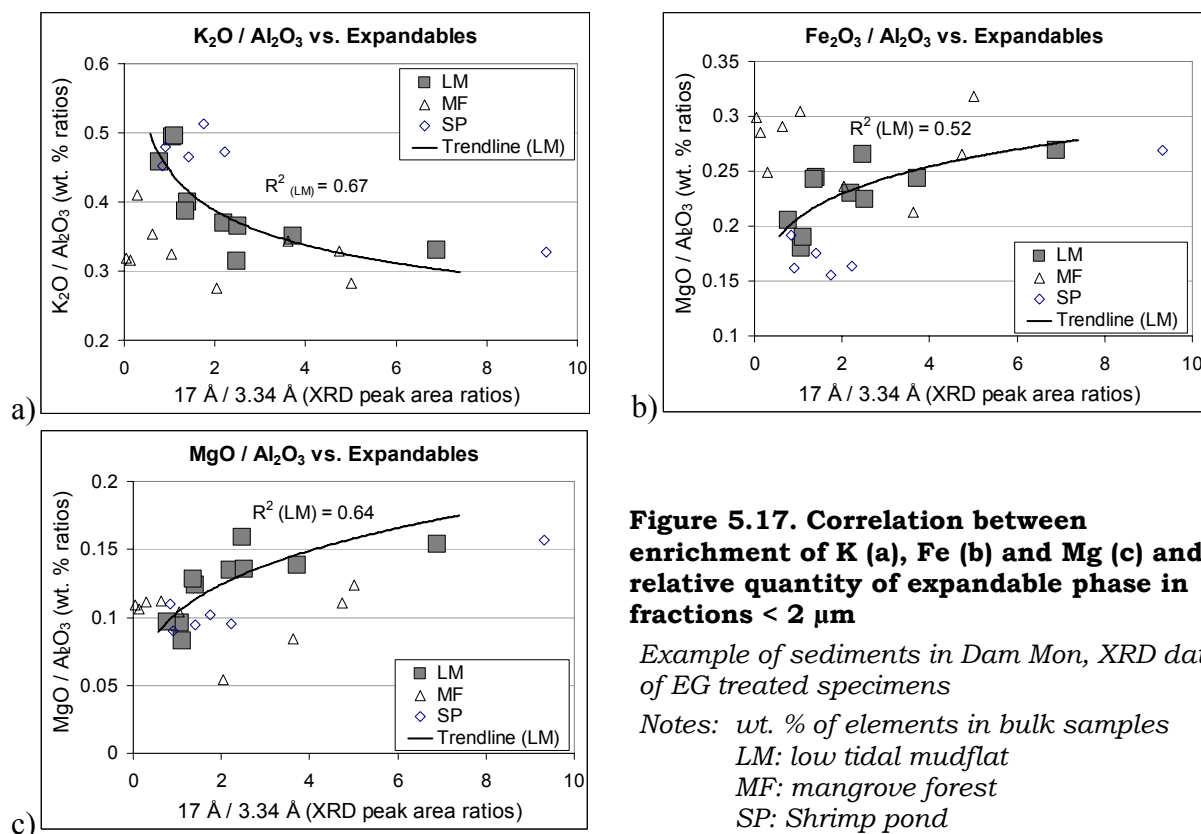


Figure 5.16. Correlation between enrichment of K and feldspar in bulk samples of LM profile in Dam Mon



5.3.2. Mineralogical mirror of post-sedimentation

The chapter 5.2 has shown that detrital sediments can be selectively distributed by hydrodynamic processes and also have some properties modified chemically. During settling, these materials can also be susceptible to diagenetic changes, such as chemical modification as a function of time or adaptation with a buried condition. Maturing order of sediments follows two sequences: younger to older from top to down along profiles and lateral aging of younger to older from LM, via MF to SP environment.

Because distribution of mineral assemblage is fundamentally driven by grain size distribution (Chapter 5.2), signals of mineralogical and chemical modifications can hardly be unravelled from the bulk samples. However, imprints of these processes are obviously recorded in sediments $< 2 \mu\text{m}$, the fractions which are richest in clay phases and thus most sensitive to chemical modifications. Analysis by XRD and TEM has revealed changes in relative quantity of clay phases (14 \AA , 10 \AA and 7 \AA), frequency as well as in chemistry of mixed layer series from the younger sediments in comparison to the older sediments. In the older sediments, relative amounts of clay phases are generally lower, structures of clay minerals are more disordered, and mixed layer series contain higher ratios of smectitic and kaolinitic components versus mica-like component. Main chemical variations along the profiles and assumed driving processes are summarized in the Table 5.5 and Figure 5.19, illustrating by samples in Dam Mon profiles. Corresponding evidences in Red River Delta and Nha Phu are shown in Table 8.13, Table 8.14 and Figure 8.35 to Figure 8.39 in Appendix. These Figures and Tables are used through out this chapter, to discuss which processes are to present and also how their influences are recored in mineral matters and chemical distribution of coastal sedimentary environment.

The assumed principal processes during post-sedimentary period are

- 1) Dissolution of clay phases
 - a. Dissolution in saline water as a function of time (abbreviated as Dt)
 - b. Re-suspension under surficial erosion (abbreviated as Ds)
 - c. Biota-induced dissolution (abbreviated as Db)
- 2) Smectitization
 - a. Pore water - induced smectitization (abbreviated as W_{diVS})
 - b. Biota- induced smectitization (abbreviated as B_{diVS})
- 3) Kaolinitization
 - a. Pore water - induced kaolinitization (abbreviated as W_{KE})
 - b. Biota- induced kaolinitization (abbreviated as B_{KE})
- 4) Upward streaming of Si (basin process) ((abbreviated as F_{Si})

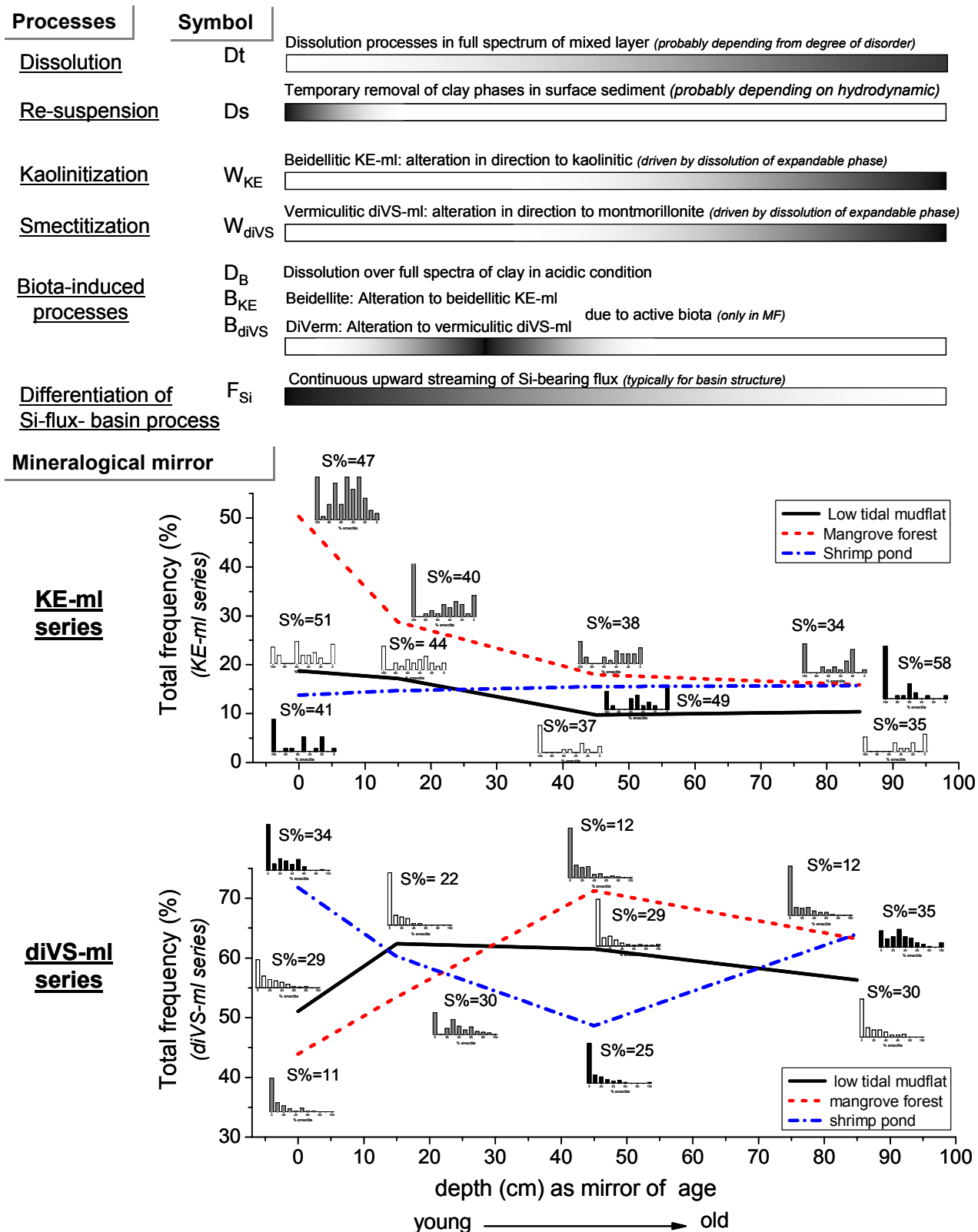


Figure 5.19. Mineralogical features as mirror of interactions among post-sedimentary processes in coastal environment

Example with the LM, MF and SP core of Dam Mon transect. S% expresses average smectitic percentage in series. Distribution curves of KE-ml display decreasing % smectite from right (beidellite, 100%) to left (kaolinite: 0%). Distribution curves of diVS-ml display increasing % smectite from right (diVerm: 0%) to left (montmorillonite, 100%)

Table 5.5. Principal mineral modification during post-sedimentation and assumed processes

Example in Dam Mon profiles

Profile	Depth (cm)	Ambient	Mirror in diVS	Mirror in KE	Dominant process
Low tidal mudflat (LM)	0 – 10	Low permeability, Low organic carbon	XRD: peak area of 10 Å and 14 Å phases decreases intensively phase decreases TEM: Original materials (like in MF) + decrease of diVS diVerm decreased	XRD: peak area of 7 Å phase decreases TEM: Beidellite dissolve total clay decrease, relatively to MF (original material)	Ds
	10 – 20	High permeability Intensive leaching Very low C _{org} , Low Eh	XRD: peak area of 10 Å and 14 Å phases decreases intensively TEM: Neoformation of diVerm by vermiculitic diVS -> diVerm Smectitic diVS decreased	XRD: peak area of 7 Å and 14 Å phases decreases intensively TEM: Neoformation of beidellite by beidellitic rich KE -> beidellite Total KE dissolve	Former Ds F _{Si}
	40-50	High permeability Medium organic	XRD: peak area of 10 Å and 14 Å phases is most like original material. TEM: Dissolution of diVerm Vermiculitic diVS to smectitic diVS	XRD: peak area of 7 Å phases is most like original material. TEM: Unchanged Beid/Kaol KE disappearing (TEM) Total KE increase (XRD)	Dt W _{diVS}
	80-90	Low & high permeability intermix Medium organic Slightly leaching	XRD: peak area of 10 Å and 14 Å phases decreases TEM: Dissolution of diVerm Vermiculitic diVS to smectitic diVS	XRD: peak area of 7 Å phases decreases TEM: More Kaol. by KE -> Kaol Beidellitic KE -> Kaolinitic KE	W _{diVS} W _{KE}
Mangrove forest (MF)	0 – 10	Low permeability High organic	Original materials	Original materials	Original state
	10 – 20	Root layer: High permeability Lower pH, starting root attack to K-rich minerals () Intensive leaching	XRD: peak area of 10 Å and 14 Å phases decreases intensively TEM: diVerm decrease Vermiculitic diVS to smectitic diVS	XRD: peak area of 7 Å phases decreases intensively TEM: KE disappearing Beid/Kaol = original materials diVerm decrease, diVS increase	Dt W _{KE} B _{diVS} (begin with diVerm end-member)
	20-40	Root layer Low permeability High organic	Assumption: Most intensive attack of diVerm to form diVS-ml	Assumption: Most intensive attack of Beidellite to form KE-ml	B _{diVS} B _{KE}
	40-50	Below root layer High permeability Lower pH, Starting root attack to interlayer cations	XRD: peak area of 10 Å and 14 Å phases decreases less intensively TEM: Formation of diVerm due to the dissolution of diVS	XRD: peak area of 7 Å phases decreases less intensively TEM: Destroying of beidellite (Beid/Kaol = constant)	B _{diVS} (no more with diVerm but with diVS) B _{KE}
	80-90	Never MF High permeability Intensive leaching	XRD: peak area of 10 Å and 14 Å phases decreases TEM: diVerm = constant Vermiculitic diVS to smectitic diVS	XRD: peak area of 7 Å phases decreases TEM: Beid/Kaol = constant KE disappearing Decrease of total clay	F _{Si} Dt
Shrimp pond (SP)	0-10	Was former MF, now addition by SP	XRD: peak area of 10 Å and 14 Å phases = MF TEM: smectitic diVS are more abundant Beid/Kaol = constant	XRD: peak area of 7 Å phases = MF TEM: KE disappearing Beid/Kaol = constant	Dt
	40-50	Used to be attacked by root (last 20 years), but no more active since then	XRD: peak area of 10 Å and 14 Å phases decreases TEM: Distribution spectra of diVS-ml is similar to MF (40-50) Slightly increase of diVerm	XRD: peak area of 7 Å phases decreases TEM: Dissolution of beidellite Neoformation of KE	See MF 40-50 Former B _{KE} and B _{diVS} but no more F _{Si}
	80-90	Never MF	XRD: peak area of 10 Å and 14 Å phases decreases TEM: diVerm decrease smectitic diVS increase	XRD: peak area of 7 Å phases decreases TEM: KE -> beidellite	F _{Si} Dt

5.3.3. Dissolution of clay minerals in saline water

When clay particle are transported to the coastal sea, partially they are supposed to dissolution processes under alkaline condition. Because distribution of mineral assemblage is fundamentally driven by grain size distribution, the signals of dissolution process can hardly be unravelled from chemistry and mineralogy of the bulk samples. However, imprints of dissolution process are obviously recorded in sediments $< 2 \mu\text{m}$, the fractions which are richest in clay phases and thus most sensitive to chemical modifications. Detected imprints include decrease in PA^5 of clay phases, CSD (XRD data) as well as modifications in particle morphology and frequency spectra of mixed layer series (TEM-EDX data). Degree of dissolution is estimated by the coefficient D_{CM} as mirror of relative quantity of clay phases:

$$D_{\text{CM}} = \text{PA}_{7\text{\AA}} + \text{PA}_{10\text{\AA}} + \text{PA}_{14\text{\AA}}$$

and the coefficient $D_{\text{CM}/\text{Q}}$ as mirroring of ratios of clay phases versus Quartz:

$$D_{\text{CM}/\text{Q}} = (\text{PA}_{7\text{\AA}} + \text{PA}_{10\text{\AA}} + \text{PA}_{14\text{\AA}}) / \text{PA}_{3.34\text{\AA}}$$

with PA = peak area in XRD-diffractogram of air-dried treated, oriented mount specimens.

From the imprints, three sub-processes can be separated: (1) dissolution as function of time (D_t) and (2) dissolution related to surficial erosion (D_s) and (3) dissolution related to acidic microenvironment surrounding root systems of mangroves (D_B).

Firstly, for the dissolution as function of time (D_t), the D_{CM} and $D_{\text{CM}/\text{Q}}$ parameters are mirroring the variations in clay phase from the top to down along profiles. The relative content of clay minerals in the deeper sediments is decreasing and the crystallinity of older smectites is reduced in comparison to the recent ones (considering CSD values – XRD data), and finally the depletion in frequency of mixed layer phases (TEM data) is also to note.

Secondly, for the dissolution related to surficial erosion (D_s), D_{CM} and $D_{\text{CM}/\text{Q}}$ are mirroring the leaching of clay phases in surface sediments of LM and SP profiles, where are under intensive influences of erosion by tide, wave (LM) and water discharge (SP).

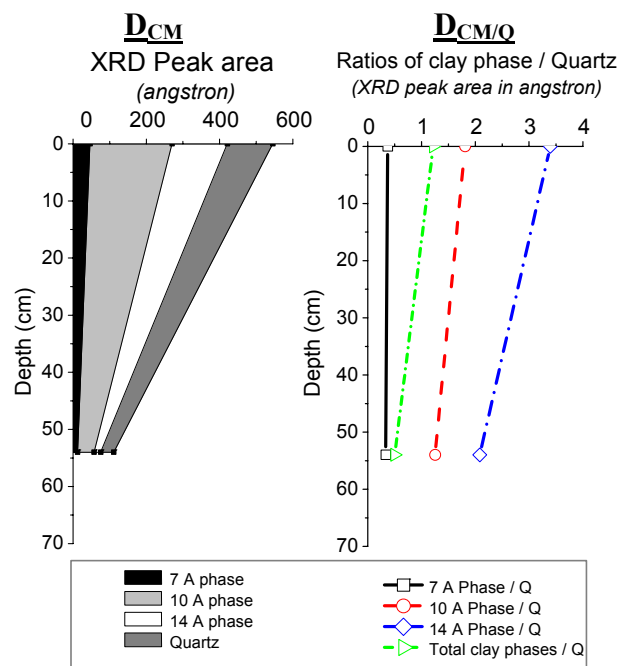


Figure 5.20. Decrease of D_{CM} and $D_{\text{CM}/\text{Q}}$ indicating dissolution of clay phases in the older sediments

Example of LM profile in RRD, Data from XRD patterns of air-dried, oriented mount specimens; the 3.34 \AA peak represents Quartz

⁵ PA = peak area in XRD-diffractogram of air-dried treated, oriented mount specimens

And for the dissolution related to acidic microenvironment surrounding root systems of mangroves (D_B), D_{CM} and $D_{CM/Q}$ are mirroring the depletion of clay phases in the rhizosphere layer of mangrove profiles. This sub-process will be further discussed in the chapter 5.4.1.

Dissolution in full spectra of clay phases as function of time

Investigation on XRD patterns of fractions $< 2 \mu m$ shows clearly that the deeper parts of the studied profiles contain lower amounts of all clay phases, as reflected by smaller values D_{CM} , $D_{CM/Q}$ for total clay phases and also for every single mineral phase (14 Å, 10 Å and 7 Å) (Figure 5.20). D_{CM} of the investigated profiles decreases approximately 1- 5 times from the top to the 100 cm depth. In addition, the calculated coherent scattering domain sizes (CSD) of clay phases based on these XRD peaks decrease from the top to down in all profiles (see Table 4.12 and Table 4.21 for 10 Å phases, Table 4.14 and Table 4.18 for 7 Å phase and Table 4.17 for 14 Å phase).

For example, kaolinite phases (peak 7.2 Å) along MF profile has decreasing CSD from 100 Å in surface layer to 60- 70 Å in the depth of 75 cm, corresponding to a decrease from average particle of 15 layers to 10 layers.

Similarly to XRD evidences for this dissolution process, investigations by TEM-EDX reveal also the tendency that frequency of mixed layer structures decrease significantly with depth (see example with KE-ml series in Figure 5.19 and all profiles in Appendix). This indicates that the older sediments (in the deeper part of profiles) have suffered from longer time of dissolution, under which, clay phases are most accessible to be dissolved.

This tendency is most obviously observed in RRD, where hydrodynamic variation is not intensive and permeability is almost unchanged along sediment profiles.

Exceptions are surface sediments in low tidal mudflat of NP and DM, SP in DM and the 10 – 20 cm depth intervals in NP and DM, which exhibit quantitative decrease of clay minerals intensively (XRD data, see D_{CM} and $D_{CM/Q}$ in Figure 8.37 & Figure 8.39, Appendix), with emphasis on mixed layer structures (TEM data, see Figure 5.19).

In sum, the dissolution over full spectra of clay phases can be addressed in clay size fractions of sediments, with decrease in amount as well as particle size of clay structures as a function of post-sedimentation time.

Resuspension under influence of surficial erosion

In addition to the dissolution in full clay mineral matter, signals of reduced clay mineral matter are also highlighted in the samples under intensive influences of erosion, such as surface layer of LM and SP profiles. The intensive decrease in amount of clay phases (see XRD peak area in Figure 5.20) in LM profile of Dam Mon and in both LM and SP profiles in Nha Phu is indicative for a re-suspension process (Ds). Re-suspension of clay size particles is

mirrored also by the depletion in frequency of beidellite end-member, diVerm end-member as well as full spectra of KE-ml and diVS-ml in the surface sediments of LM profiles in Dam Mon (Figure 5.19). For low tidal mudflat profile and shrimp pond, the clay matter can be re-suspended under influences of wave dynamic, rework and re-deposit during the lowering of tide level. Depletion of clay minerals only in surface sample indicates a post-sedimentary re-suspension process temporarily.

The resuspension are not to detect in mangrove forest, although this environment is also intensively influenced by erosion process, concerning the turbulent currents in between prop roots. For specific features of sedimentation in mangroves, this exception (for this case on resuspension process) will be discussed in more detail in Chapter 5.4, concerning the trapping function.

Dissolution rate of clay minerals depending from chemical composition

In the above discussions, XRD and TEM evidences reveal occurrence of dissolution process over full spectra of clay phases. However, different clay species can dissolve in different dissolution rate, as a function of chemical structure. The resistance of clay species as well as the different dissolution intensity mirrored in clay matter are discussed now in this chapter, based on TEM results.

Preferential dissolution of mixed layer structures relatively to 2:1 end-member mineral

Considering the dissolution of diVS-ml and KE-ml series, it is obvious that the mixed layer structures are more rapidly dissolved than the end-member minerals of these series. For example in Dam Mon low tidal mudflat profile (Figure 5.8), the ratios of frequency between total KE-ml : end-member beidellite decreases with depth, from 3.8 (top) to 1.6 (80 – 90 cm depth). The low tidal mudflat profile in Dam Mon (Figure 5.8), is also another example. Ratios between total diVS-ml : end-member diVerm decreases from 1.4 (top layer) to 0.5 – 0.9 in the lower parts. These evidences indicate that diVS-ml and KE-ml structures are more easily dissolved than the end-members diVerm and beidellite, respectively.

Such a preferential dissolution of interlayered materials relatively to 2:1 end-member minerals have also been widely observed in the surface horizons of acidic forest soils (Ross and Mortland 1966, Bouma et al. 1969, Gjems 1970, Hirai et al. 1989 and Funakawa et al. 1992)

Preferential dissolution of smectite versus dioctahedral vermiculite

In all studied low tidal mudflat profiles, frequency spectra of diVS-ml in subsurface sediments shows obvious faster dissolution of smectitic diVS-ml relatively to vermiculitic diVS-ml (Figure 5.19 and Figure 8.35, Figure 8.38 in Appendix). This tendency makes the spectra slightly bias toward vermiculitic end-member.

It also corresponds to decreases of the average smectitic proportion S% of diVS-ml series from 27 % (surface layer) to 26 % (~ 50 cm depth) in RRD, from 29 % (surface layer) to 22 % (10 – 20 cm depth) in Dam Mon and 26 % (surface layer) to 22 % (10 – 20 cm depth). Additionally, in clay-size fractions, smectite particles were observed more commonly in very small sizes (<0.5 μm) whereas diVerm and diVS ml particles were dominant in coarser sizes, from 0.4 – 1.5 μm . These indications infer to a preferential smectitic component versus dioctahedral vermiculitic component in diVS-ml structures in contact with saline water.

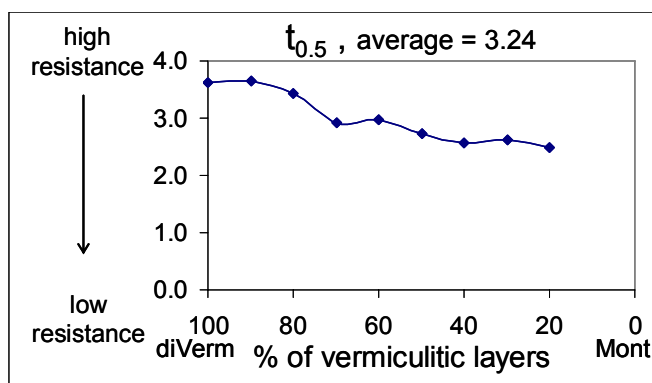


Figure 5.21. Dissolution resistance of diVS-ml structures, based on half-time-dissolution coefficient $t_{0.5}$

Example of samples: DM-MF (40-50 cm). Similar tendencies are determined for all investigated samples and shown in Fig (Appendix)

The main supporting arguments for this statement are the results on chemical composition of diVS-ml series, with emphasis on octahedral occupations. Analysis by TEM-EDX for all studied samples revealed that the occupation of Fe^{3+} and Mg^{2+} in octahedral layer increases with proportion of smectitic layers in diVS-ml structures (Figure 5.21). It infers that smectitic end-member in the mixed layer structures has higher octahedral substitutions by Fe^{3+} and Mg^{2+} . Besides, in experiments of bentonite Novák & Čížel (1976 1978) determined an empirical relationship between resistance of these mixed layer mineral against dissolution and octahedral substitution. The half-time-dissolution coefficient $t_{0.5}$ was developed based on the formula: $t_{0.5} = 3.95 - 1.96 \times \text{Fe}^{3+} - 2.3 \times \text{Mg}^{2+}$, visualizing the time which 50 % of the central atoms from octahedral layer of clay structure of bentonite samples structure can be leached out in contact with HCl (Novák & Čížel 1976, 1978). Because in this study, dioctahedral vermiculite end-member is defined for the K-deficient illitic species, it is reasonable to use $t_{0.5}$ coefficient for evaluating dissolution resistance of diVS-ml series. Figure 5.21 illustrates the continuous decrease of dissolution resistance in diVS-ml phase with higher smectitic proportion, corresponding to lower value of $t_{0.5}$.

Hence, the smectitic layers, characterized by higher octahedral substitution, are more accessible to dissolution processes.

In literature, among the clay minerals transported to the coastal sea, smectites constitute the group the most frequently quoted as possibly subject to post sedimentary modifications. This interpretation results from the sensitivity of smectitic minerals to cations-rich environment (Chamley 1989; Golubev et al. 2006).

Dissolution as driving force for mineral transformation

In alkaline condition of the studied environment, the dissolution of clay species is facilitated by abundance of hydroxyl ions. It is expected to involve with removal of tetrahedral layer (SiO_4) and octahedral cations (Al, Fe, Mg), consequently. Experiments by Golubev et al. (2006) on smectite dissolution over a wide range of pH at 25 also indicate that in alkaline condition, hydroxyl ions facilitate the release of Si. It is unclear on the leaching mechanism of interlayer cations.

Additionally, in contact with sea water, the edges of clay minerals tend to dissolve faster than the basal planes, as it is mirrored by morphologic features of clay particles in fractions $< 2 \mu\text{m}$, those exhibits commonly the ragged edges. The preferential dissolution in margin of particles is also widely reported for kaolinite and 2:1 clay minerals (Wieland and Stumm 1992; Ganor et al. 1995; Bosbach et al. 2000; Bickmoore et al. 2001).

Considering the lower resistance to dissolution of smectitic layer versus vermiculitic layer, once smectitic layers present in margin of diVS-ml particles, dissolution can result in slightly increase of vermiculitic proportion (Figure 5.22). Some diVS-ml particles with very low smectitic proportion ($\text{S}\% \sim 5 - 10 \%$) thus can be transformed to diVerm particles. This explains for the slightly increase in frequency of vermiculite end-member in some intervals, which are under intensive influences of dissolution process (e.g. 10- 20 cm depth layer in LM profile of Dam Mon).

However, this modification does not proceed as progressive vermiculization but rather being a marginal process. More detail discussions are shown in chapter 5.3.5.

In vice versa, vermiculitic layers, once presenting in margin of diVS-ml particles are supposed from leaching of interlayer cation facilitated from dissolution process. These influences can even facilitate the weathering sequence from mica-like species to smectite, with the sequent removal of SiO_4 and replacement of octahedral Al by dissolved Mg and Fe. Signals of the alteration were recorded with appearance of more smectitic phases in frequency spectra of diVS-ml series in the more matured materials (Figure 5.22). Further evidences for presence of smectitization process as well as its alteration mechanism will be discussed in the following section (Chapter 5.3.4).

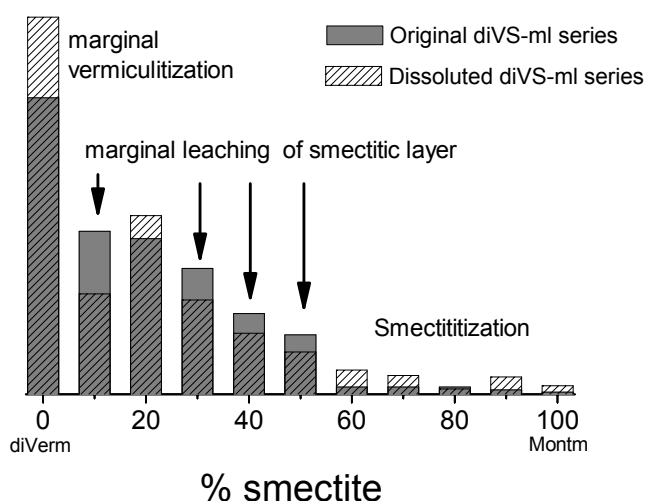


Figure 5.22. Typical modification in frequency spectra of diVS-ml during the dissolution process

Considering the effects of dissolution process on modification of KE-ml series, it is to notice that, the removal of SiO_4 layer and attack of OH to the exposed octahedral layer can results in structures which are more likely kaolinitic. This will be discussed in more detail in the following section (Chapter 5.3.5).

5.3.4. Smectitization

As discussed above, in contact with saline water, smectitic components are more easily dissolved than vermiculitic component and thus faster dissolved. With longer time of dissolution, the vermiculitic layers in diVS-ml particles are also to dissolve. TEM investigations on frequency distribution, particle morphology, polytype and chemical structure of diVS-ml series, the dominant clay phase in fractions $< 2 \mu\text{m}$, reveals that dissolution of vermiculitic layer can lead to progressive smectitization of diVS-ml series.

Evidences of smectitization mirroring in diVS-ml series

Red River Delta (RRD) data of clay phases along sedimentary profiles have revealed the common tendency that expandable 17 \AA phase has high reflection in surface sediments, depletion in the subsurface layer and then again increasing with depth, whereas the reflections

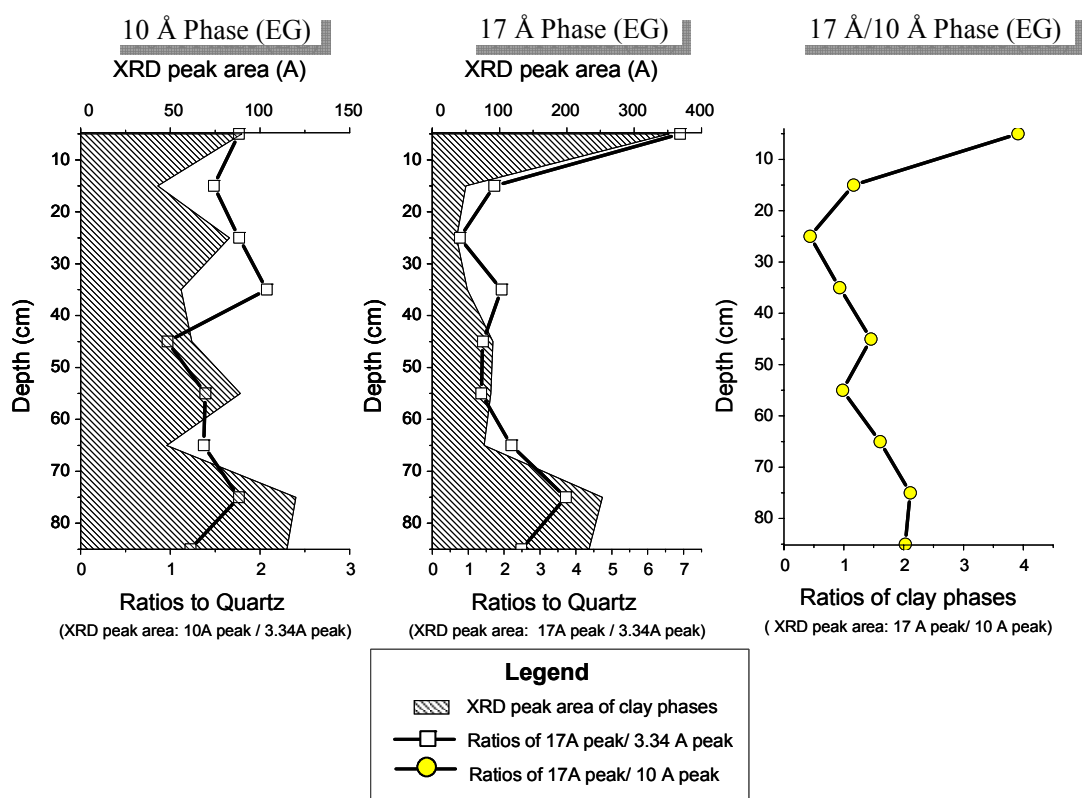


Figure 5.23. XRD evidences for smectitization (example of LM profile in Dam Mon, XRD for oriented mount, EG specimens)

Neoformation of smectitic phases is noticed with increase with depth of 17 \AA phase versus slightly decrease of 10 \AA phase.

of non-expandable 17 Å phase are more or less unchanged. Figure 5.23 visualize the variation of XRD peak area obtained from ethylene glycolated samples along depth profile, with illustrative example of low tidal mudflat in Dam Mon. As discussed in the above section, the smectitic phases, originated from river budget, are subjected to the dissolution process immediately in early stage of post-sedimentation. This explains for the decrease in peak areas of 17 Å in subsurface layer (i.e. 0-10 cm depth), relatively to the surface layer. However, it is noticeable that the increase with depth of 17 Å peak area versus the relative stability of 10 Å peak area could indicate for a neo-formation of clay phase with higher expandability. In other words, it could refer to a neo-formation of smectitic species.

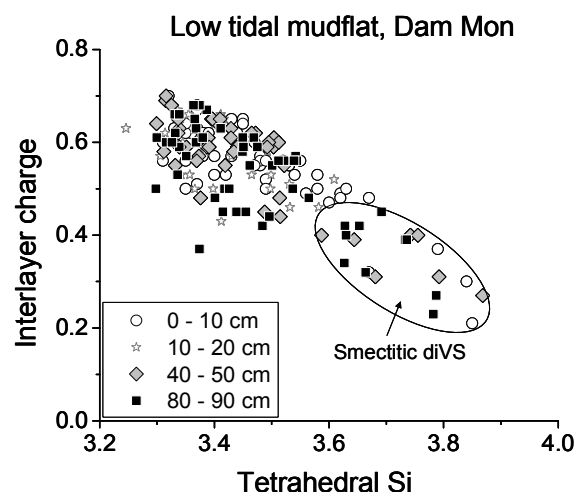


Figure 5.24. Abundance of smectitic diVS-ml in the deeper part of the core

On example of low tidal mudflat profile in Dam Mon

The abundance of smectitic species in deeper sediments is confirmed by TEM investigations. In comparison to the upper sediments, diVS-ml series in the deeper parts contain higher frequency of smectitic particles, exhibiting in frequency spectra as peaks in range of smectitic diVS-ml (Figure 5.19). This increase of smectitic diVS-ml species corresponds to structures with lower interlayer charge and higher tetrahedral Si (Figure 5.24).

Additionally, observations on morphology by TEM investigations also addressed modification signals of diVS-ml particles. In comparison to dioctahedral vermiculite crystals, with commonly well shapes, clear-cut edges and ordering polytypes (1M and 2M₁), the diVS-ml particles have more popularly ragged edges as well as turbostratic ordering. These features are not only signals of modifications by dissolution process, but also suggest a direction of modification: from dioctahedral vermiculite toward diVS-ml structures.

These evidences together demonstrate for the smectitization process during the maturing of coastal sediment profiles. The process is mirrored with increasing S% in diVS-ml series, most obviously in subsurface sediments in low tidal mudflat profile in DM (Figure 5.19) and NP (Figure 8.38). In mangrove forest and shrimp pond profiles, except for the mineral assemblage in rhizosphere layer (~ 30 – 60 cm depth intervals), the imprints of smectitization is also recorded by movement of diVS-ml frequency spectra toward smectitic end-member and corresponding increase of S%. In rhizosphere layer, the enrichment of smectitic species is much more intensively. It could be an indication for occurrence of some other biota-induced processes.

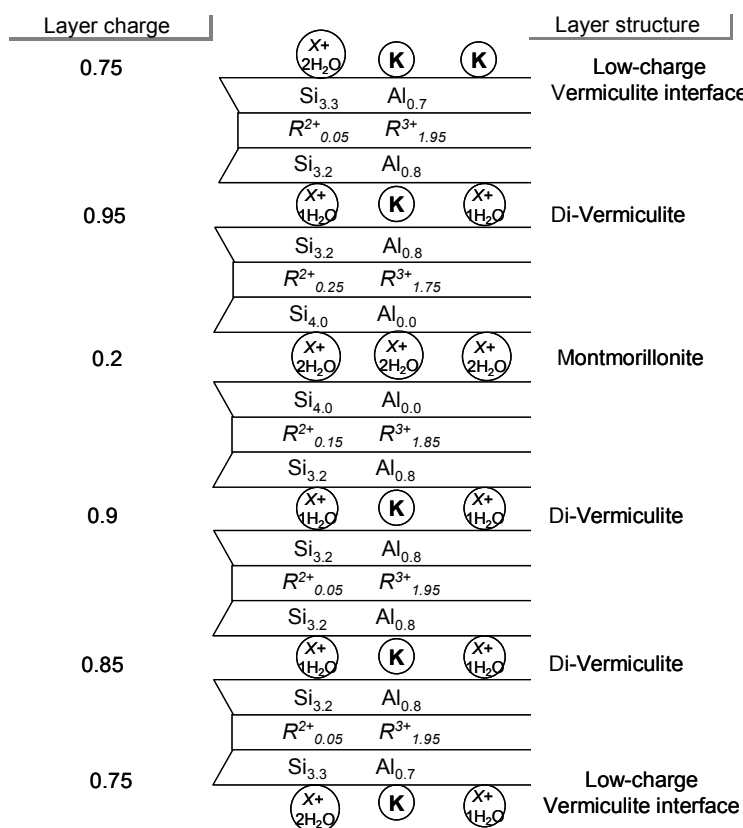


Figure 5.25. Schematic representation of the distribution of charges in a diVS-ml crystal (half unit-cell, Mac Evan crystallites)

The whole stacking gives average chemical composition.

The smectitization in soil environments has also been documented since 1937 by Bray. Lippmann (1979) has developed the thermodynamic conceptual pathway of mineral alteration (see Fig. 3, chapter 2), where addresses the transform direction from mica-like clay minerals to kaolinite in conditions of K-leaching and soluble Si availability. However the evidences offered by soil studies remains unclear to address the nature of intermediate products (mixed layering or dioctahedral vermiculite) as well as the transforming mechanism proposed by Srodon (1999).

Mechanism of smectitization

Figure 5.25 visualizes the distribution of charge and chemical composition of a diVS-ml particle. Because smectitic layers are more accessible to dissolution by saline water, the smectitization process can be assumed to occur on diVS-ml particle with vermiculitic layer at the edges. Attack on the interlayer cations of these vermiculitic layers results in low charged feature. The mechanism of transformation from vermiculitic diVS-ml structure to smectitic diVS-ml structures is to be revealed based TEM-EDX data of charge behaviors and octahedral occupations.

The Figure 5.26 illustrated charge behaviours of tetrahedral layer (IV), octahedral layer interlayer (VI), interlayer charge (XII) and content of potassium in the interlayer (K) with the ranking from high value (left) to low value of tetrahedral charge (example with sample NP-LM, 10 – 20 cm). In continuous series from vermiculitic structures to smectitic structures,

four corresponding tendencies were observed: (1) decrease of IV-charge was regular step-wise; (2) VI-charge arranged in a series of gauss-like distributions, each corresponded to each step of IV-charge, VI increased from negative in vermiculitic range (VI-charge > 6) turning to positive in smectitic range (VI-charge < 6 = deficient charge); (3) XII-charge showed a similarity to VI-charge with gauss-like distribution series but a parallel decrease with IV-charge; (4) Content of interlayer K varied high and low alternatively, high values were more sequently observed to go with high values of XII-charge and VI-charge (i.e. top of the gauss-like distribution).

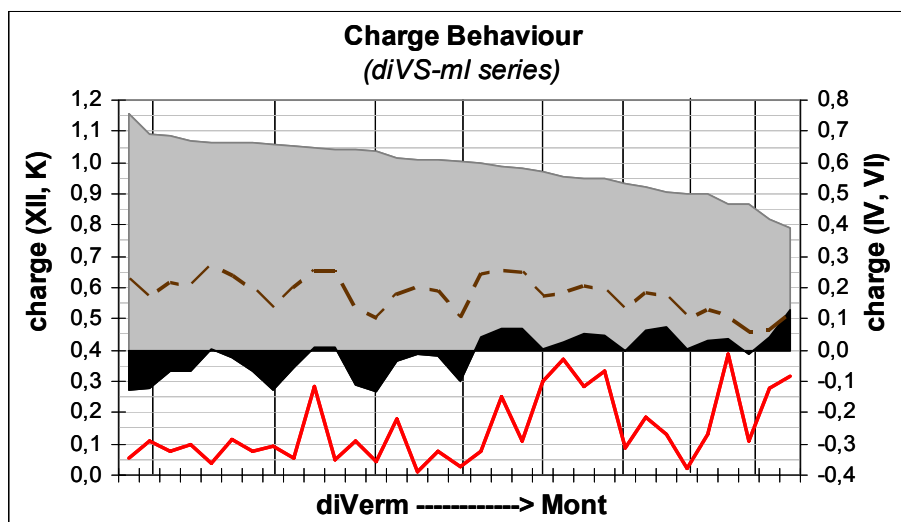


Figure 5.26. Charge behaviour of diVS-ml series (on example of sample DM-LM, 10 – 20 cm depth)

A stepwise arrangement in charges of IV- (grey area), VI-(black area), XII- (brown dash line) and interlayer K (red solid line) are to be noticed.

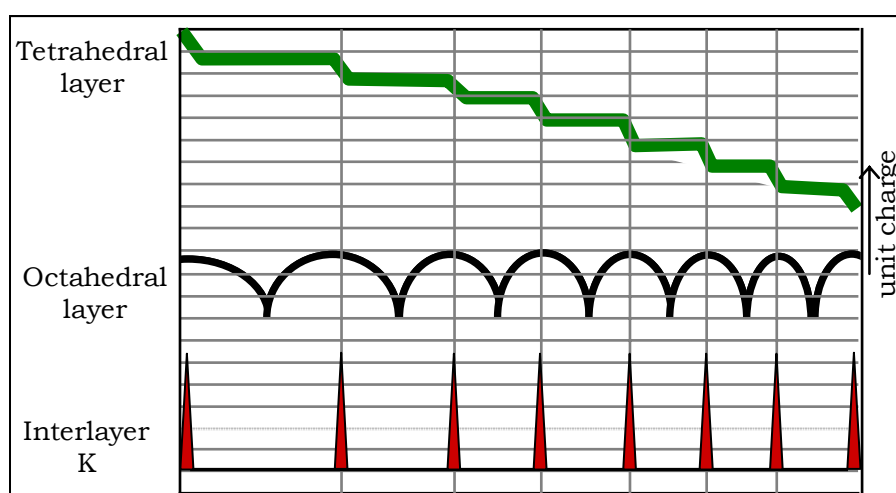


Figure 5.27. Model of step-wise arrangement in charges of IV- (green stepped line), VI- (grey gauss-like curve) and interlayer K (red solid bar)

A model of step-wise arrangement in chemical composition of diVS-ml particles (Figure 5.27) has been developed based on measured behaviors of layer charges (Figure 5.26), in order to reveal the smectitisation mechanism.

- In tetrahedral layers: each step of smectitisation responds to a group-wise replacement of vermiculitic layers by smectitic layers
- Formation of meta-stable plateau between group-wise replacements because of gauss-like minimizing of VI-charge (temporary Al + Fe³⁺ replacement)
- K shows commonly maximum amount in case of group-wise replacement of IV-layers

The behaviour of K in the interlayer space during the smectitization suggests that this cation may play the trigger function of the alteration process. Thus, when a potassium cation is leached out of the interlayer space of vermiculitic layer in diVS-ml particle, a smectitization can proceed consequently. It is expected that the leaching of interlayer cation is more intensive in dynamic condition of high energy (e.g. erosion by wave and tide in surface sediments). Therefore, an active environment with influences of erosion could result in higher speed of smectitization. This explains for the more abundance of smectitic species in surface sediments of low tidal mudflat in the investigated regions.

Besides, the roles of mangrove roots to uptake K from sediments, as discussed in the chapter 5.4, can also be an important factor to promote the smectitization process.

5.3.5. Kaolinitization

As discussed in chapter 5.3.1, the preferential dissolution of smectitic layer versus end-member has been suggested to be a possible driving force for kaolinitization of KE-ml particles. In this part, the occurrence of kaolinitization process as well as its mechanism is to discuss based on XRD and TEM investigation of fractions < 2 µm.

Evidences of kaolinitization mirroring in KE-ml series

XRD investigations on mineralogy of grain size fractions (Figure 4.29 of chapter 4.4.1) indicates that the 1.49 Å reflection, with narrow FWHM and high intensity characterized for fractions < 2 µm, which is distinctively from all coarser fractions. Additionally, the coherent scattering domain size (CSD) of kaolinite particles (7 Å phase) and KE-ml particles (7.2 – 7.8 Å phases) in the deepest parts of sediment profiles showed also higher values, in comparison to the uppermost parts (Table 4.14 and Table 4.20). These phenomena infer to a neo-formation of kaolinitic species during the maturing of sediment materials.

TEM evidences on particle morphology as well as frequency spectra of KE-ml series also support the assumption on neoformation of kaolinitic species. In sediments, occurrence of KE-ml particles in both typical shape of beidellite (xenomorphic) and kaolinite (pseudo-hexagonal), with more commonly signals of modification like diffused edges, turbostratic ordering than the end-member minerals (well shapes, 1M polytype) (Figure 4.33

and Figure 4.41) suggests for a transformation process over KE-ml series. In which, KE-mls could be intermediate products of transformation from beidellite end-member to kaolinite end-member. Besides, frequency spectra of KE-ml series along depth profile shows clearly the moving of frequency distribution curve toward kaolinitic component (see KE-ml series in Figure 5.19), resulting in a decrease of S% (e.g. from 51% to 35% in LM profile and from 47% to 34% in MF profile of

Dam Mon). This kaolinitization process is also mirrored by an increase in Kaol/Beid ratios, from 1.3:4.5 (10-20cm) to 3.3:2.7 (80 – 90 cm) as seen in LM profile of Dam Mon. Exception is high frequency of kaolinite particles in surface layer of LM profile in Dam Mon, where sediment matter is intensively influenced by erosion by wave dynamic.

Imprints of kaolinitization process are obvious in subsurface parts of all profiles. In root layer of MF, these imprints become suddenly intensified, but could respond to some other biota-induced processes. More details on these phenomena are discussed in the chapter 5.4.6.

Typical modification of KE-ml frequency spectra in the more matured materials is presented in Figure 5.28. Kaolinitization process could be linked with the dissolution process with preferential leaching of smectitic component. Dissolution of tetrahedral layer (SiO_4) promotes the expose of octahedral layer to ambient with abundance of hydroxyl cations. This contact can facilitate the progression of kaolinitization as discussed in the following part.

Mechanism of kaolinitization

Two mechanisms are usually proposed for transformation from smectite to kaolinite via mixed layer phases: (1) solid-state layer by layer transformation by atom rearrangement (Altschuler et al. 1963, Amouric & Olives 1991, Hughes et al. 1993); (2) dissolution of smectite phase and re-crystallization of kaolinite structures (Środoń 1980, Delvaux et al. 1989). Researches from Schultz et al. (1971) and Brindley et al. (1983a) documented that the layer transformation coming along with an inversion of one of the tetrahedral sheets in Al-hydroxy interlayered smectite. However, hydroxy-interlayered smectite has not been observed in association with natural soil K/S (Hughes et al. 1993), but rather in hydrothermal conditions (Środoń 1980, Delvaux et al. 1989). Altschuler et al. (1963) and Hughes et al. (1993) discussed that in weathering environments, this layer transformation tend to proceed via stripping of one of the tetrahedral sheets of the 2:1 layer.

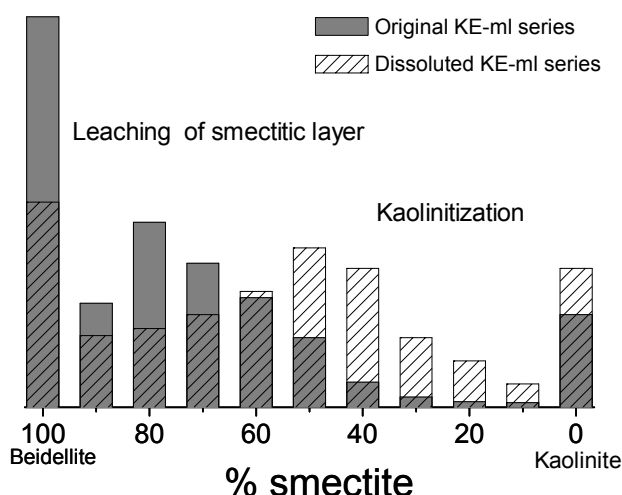


Figure 5.28. Typical modification in frequency spectra of KE-ml during the dissolution with preferential leaching of smectitic layer

Based on data revealed from XRD, thermogravimetry, chemical analysis and ^{29}Si MAS nuclear magnetic resonance on hydrothermal originated KS samples, Dudek et al. (2006) simulated the solid-state transformation from smectite to kaolinite that proceeding through several non-simultaneous stages: (1) formation of kaolinite-like patches by partly removal of tetrahedral sheet; (2) layer collapsed to 7 Å structures where the kaolinite-like patches are sufficiently large; (3) substitution: Al for Mg in octahedral layer, parallel to charge decrease and loss of interlayer cations; (4) Si for Al substitution in tetrahedral layer, parallel to further loss of interlayer cations.

In this contribution, additional evidences from TEM-EDX data on surface wetland sediments have been revealed to support that assumption on kaolinitization mechanism.

Non-linear correlation between % Kaol. vs % OH group

From TEM-EDX data, percentage of kaolinitic layers in KE-ml has been calculated based on an assumption that it is linearly correlated to number of OH-group (from 2 for beidellite to 8 for kaolinite). However, research results from Dudek et al (2006) showed that during the smectite kaolinitisation, the number of OH groups (determined by weight loss in DTA-TG patterns) in KE-ml do not increase proportionally to the relative amount of kaolinite layers as measured by XRD.

This non-linear relation divides into stages and can be mathematically simulated by polynomial curve. Figure 5.30 shows comparison between % of kaolinitic layers calculated from hypothetical linear function of % OH and % kaolinite calculated according to non-linear polynomial function mentioned by Dudek et al. (2006). Good agreements are obvious for the structures with kaolinitic percentage ranging from 40 to 90 % (bold marked number in Table 5.6). In comparison to the non-linear system, the linear system overestimated about 10 % kaolinitic percentage for the structures containing less than 30% kaolinitic layer and 7-8 % for structures containing more than 90% kaolinitic layer. In order to get agreement with evidence obtained from other methods, correction for the value of kaolinitic percentage according to non-linear system has been adopted (Figure 5.30).

Transformation from 2:1 to 1:1 structure

Figure 5.30 shows the relationship between the number of hydroxyl groups in the octahedral sheet and corrected percentage of kaolinitic layers for the muddy sediments in the Red River Delta (LM+MF+SP), in comparison with samples from Dudek et al. (2006). The trend of relation is obvious with three stages: three stages can be recognized: (1) 0 – 20 % Kaol.- a sharp increase in the number of OH groups; (2) 20 – 70 % Kaol.- very little OH increase; (3) 70 -100 % Kaol. – a sharp increase in the number of OH groups. Model of Dudek et al. (2006) refers this behaviour to a solid-state transformation that does not occur with simply continuous replacement but through a group-wise adding of OH-groups. In other words, the alteration proceeds with development of patches within smectite layers, where part of the

tetrahedral layer is stripped off, releasing Si and some Al, and protons are attached to the O ions in the octahedral sheet, forming OH-group (Figure 5.29).

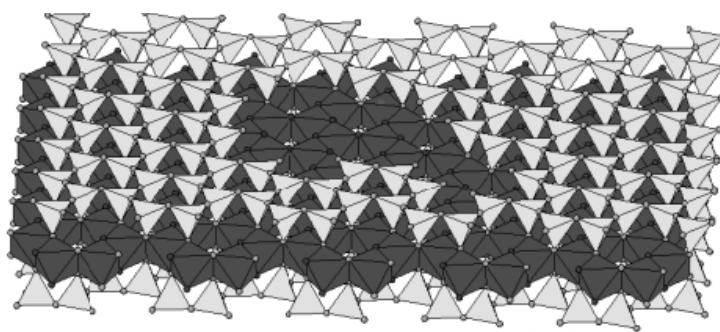


Figure 5.29. Sketch of a smectite 2:1 layer during kaolinitization

Some tetrahedral ions have been removed and a kaolinite-like patch forms and growth (see central area of the layer) (Dudek et al. 2006)

The patches have 1:1 structure, characterizing kaolinitic structure. During stages with sharp increase (stages 1 and 3), the size of kaolinitic patches grows larger, forming 7 Å domains or kaolinitic

layers. In the alternating stages with slight increase (stages 2), layer collapsed with a little exchange of tetrahedral ions by OH-groups. When a layer is totally removed, a new patch begins to develop on the next smectite layer and the number of OH-group increase again sharply.

The model developed above is sensitive to the number of layers per crystallite. For the samples in the Red River Delta, good fit as obtained in Figure 5.30 is valid for the crystals with averagely about 5 layers. The average size of coherent scattering domain (CSD) of KE-ml structures (based on 001 reflection (~ 7.4 Å) in XRD patterns of air-dried specimens, see Table 5.6) shows values of 34 – 129 Å, corresponding to 5 – 20 layers averagely. These values are 1 – 4 times higher than the simulated values above.

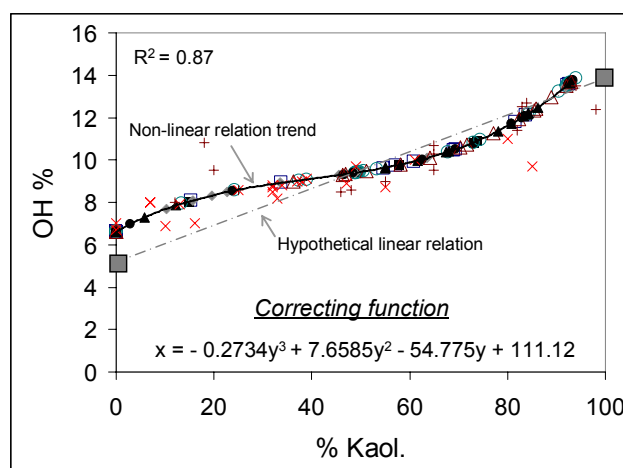


Figure 5.30. Percentage of OH-groups of the octahedral sheet vs. %K in KE-ml

The measured data has been corrected to of non-linear correlation between % Kaol & %OH according to model of Dudek et al. 2006
KE-series in samples Δ: RRD-LM (0-3cm); ▲: RRD-LM (53-56 cm); ○: RRD-MF (0-3cm); ◆: RRD-MF (53-56 cm); ●: RRD-MF (71-73 cm); □: RRD-SP (0-3cm); ■: RRD-SP (71-73 cm); +: Dudek et al. 2006; ×: Brindley 1983; ■: theoretical values of end-members (beidellite and kaolinite)

Table 5.6. Comparison between the % Kaol estimated by linear system & non-linear system of %(OH) vs. (% Kaol.)

Name	% OH	% of Kaolinitic layers in KE	
		Lineal system ⁽¹⁾	Non-linear system ⁽²⁾
Beidellite	4.6 - 5	0-5	0
KE10	5.3-6.1	7-13	0
KE20	6.7-7.1	17-23	3-10
KE30	7.2-8.1	25-33	12-24
KE40	8.7-8.9	39-42	34-37
KE50	9.0-9.8	45-53	39-53
KE60	9.9-10.5	55-63	55-64
KE70	10.7-11.4	67-74	68-77
KE80	11.5-11.8	78-84	81-85
KE90	12.1-12.5	87-88	86-89
Kaolinite	12.9-13	100	92-93

⁽¹⁾: Assumption in calculation system in this dissertation

⁽²⁾: Assumption by Dudek et al. 2006 based on XRD and DTA-TG data

It has been mentioned by Dudek et al. (2006) that the internal layers contribute their total surface to both removal of tetrahedra/adding of OH-groups and layer collapse whereas, the external layers contribute in terms of removal of tetrahedra/adding of OH-groups but not to the layer collapse. It is suggested that during stages which contain sharp increase, the transformation from smectite to kaolinite occurs not only in internal but also in external layers. During the stages with slight increase/plateaus, the layer collapse happens only on internal layers. The data in RRD samples in this contribution allow the assumption that the kaolinitization does occur essentially in external sides of crystals.

Study on morphology of individual particles brings more evidences to verify the above mentioned mechanism (Altschuler et al. 1963). The un-altered beidellite particles are commonly xenomorphic with diffuse edges. With initial kaolinitization, the edges of beidellite are discontinuously modified by regular outline and hexagonal outgrowths. Thus the observed development of regular, pseudo-hexagonal at edges of KE-ml series during the transformation from beidellite to kaolinite (see Fig. 9 in RRD-result part & Fig. 10 in KH-result parts for examples) is evidence of the lateral epitaxy, and implies the prior stripping of a silica layer to create a 1:1 kaolinite-like domain for some distance in from the edges. The similar phenomena have been observed in TEM-investigations on kaolinitization of montmorillonite via mixed layer series under weathering condition (Altschuler et al. 1963).

Nevertheless it has to be mentioned that the chemical structures of kaolinite or KE-ml may be modified to some extent by the electronic beams during the TEM-EDX investigations, resulting in slightly overestimation on obtained formulae of the mixed layer series. However, it is possible to assume that the defects are systematically and does not alter the essential shape of the plot in Figure 5.30.

Evolution of octahedral occupations during the smectite kaolinitization

Based on the chemical analysis by TEM-EDX, variation of octahedral occupations by Mg and trivalent Fe of KE-ml series during the kaolinitization are determined and presented in Figure 5.33 and Figure 5.34, respectively. Although the replacement of Mg by Al has been documented as one principal step in transformation process from beidellite to kaolinite (Dudek et al. 2006), the behaviour of octahedral Mg versus octahedral Al is underestimated because the smectite end-member (i.e. beidellite) in this contribution is Al-rich and contains regardless amount of Mg (Figure 5.33).

The lack of a trend in the plot of % Fe^{3+} versus % kaolinitic layers (Figure 5.34) implies that Fe remains in the 1:1 structures or it releases much slower than the rate of layer collapse. It is also indicative for the fact that the transformation from smectite to kaolinite proceeds through the inheritance of structures. Evenly, the concentration of octahedral Fe tends to increase slightly, indicating that the kaolinitic structures, due to poorer ordering, may absorb some Fe ions from ambient, where there is abundant of soluble Fe. This assumption needs further investigation to define.

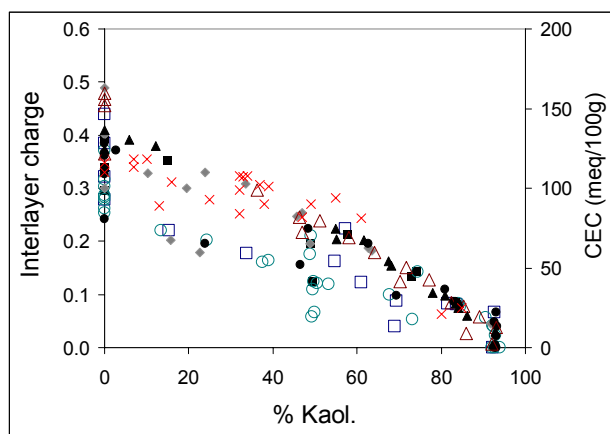


Figure 5.31. Interlayer charge of KE-ml series as a function of kaolinitic layer percentage

Symbol and samples as in Figure 5.30. Samples from Dudek et al. (2006) (x) are presented in values of CEC (right axis) – a mirror of interlayer charge

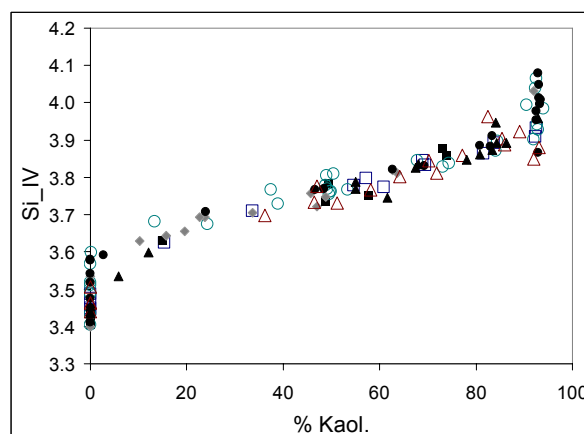


Figure 5.32. Tetrahedral Si of KE-ml series as a function of kaolinitic layer percentage

Symbol and samples as in Figure 5.30

The remains of Fe in kaolinitic products also reported in several studies (e.g. Hughes et al. 1993; Dudek et al. 2006) those stating that octahedral Fe in KE-ml is structurally bonded. Researches by Newman & Brown (1986), Weaver (1989), Schroeder & Pruett (1996) documented Fe-rich kaolinite species with the amount of Fe as high as 1.7 %. These values are presented as a bar in the Figure 5.34 as reference.

Evolution of layer-charge

Figure 5.31 shows that the correlation between interlayer charge and % of kaolinitic layers seems to be linearly, but better fits with a regression line, which is demonstrating unification on group-wise transformation, in terms of layer charge. This trend indicates that the depletion of interlayer charge happens in the same time with the stripping of tetrahedral and forming of kaolinite-like patches, but remains stable during the collapse of the whole layer. Some kaolinite layer, thus still contain some layer charge and resembles smectite. The charge perhaps resulted from small residual Mg occupation in the octahedral layer. Evidences for the kaolinite that bears some characteristics of smectite have been also given by Ma & Eggleton (1999) from HRTEM and CEC data. Also, the stable phase of interlayer charge may reflect appearance of a negative charge amount which is possibly resulted from residual Al for Si substitution in tetrahedral sheet.

Different from hydrothermally originated KE-ml series from Dudek et al. (2006), the KE-ml series in this contribution are characterized by Mg- poorness but Fe- richness. Therefore, the highlighted variations are not involved in substitution in octahedral layer (both kaolinite and beidellite are Al-rich in octahedral layer), but rather involved in substitution in tetrahedral sheet. The substitution of Si for Al in the tetrahedral layer is obviously in group-wise trend as shown in Figure 5.32. The stages determined are in agreement with those defined for OH-group, octahedral Al and interlayer charges.

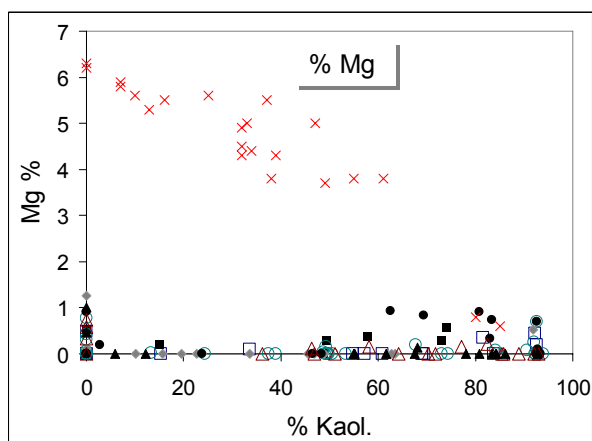


Figure 5.33. Octahedral Mg in KE-ml series as a function of kaolinitic layer percentage

Symbol and samples as in Figure 5.30

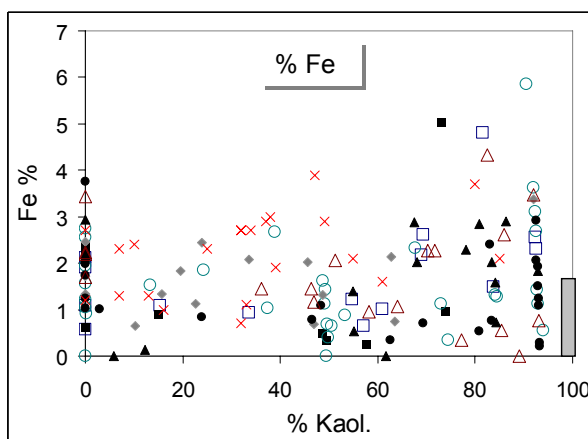


Figure 5.34. Octahedral Fe in KE-ml series as a function of kaolinitic layer percentage

Symbol and samples as in Figure 5.30. Vertical bar is the range of octahedral Fe in kaolinite from literatures (e.g. Weaver 1989; Newman & Brown 1987; Schroeder & Pruett 1996)

Conclusion on transformation mechanism

From the above named evidences, the following pattern of beidellite kaolinitization in solid-state is proposed:

- (1) Leaching of interlayer cations and synchronous or intermediately subsequent hydration and stripping of silica layer
- (2) Replacement of vacant tetrahedral oxygen sites by hydroxyl groups to form a kaolinite-like domain (patches)
- (3) Si for Al substitution in tetrahedral layer (however Fe tends to remain in octahedral occupations)
- (4) Extension of kaolinite-like domain and the development of regular hexagonal outgrowths at the edges of smectitic particles.

5.3.6. Meta-stable neoformed phases during post-sedimentary processes

Marginal vermiculization of vermiculitic diVS-ml

Although the smectitization process has been revealed as the principal process during the post-sedimentary maturing of sediment profiles, slightly increase of vermiculite frequency was still observed in subsurface sediments. Discussion in section 5.3.2 explains this abundance by the influences of dissolution process on diVS-ml particles with less than 5-10 % smectitic layers. The question is how to distinguish between those are strictly neo-formed and those which could be considered as resulting from an incongruent dissolution. In case the smectitic layers occur in margin of diVS particle, dissolution away of smectitic layer in margin of particle can make the particle becoming more vermiculitic. The typical modification of frequency spectra of diVS under dissolution process is visualized in Figure 5.22. The slightly increase in ratios of vermiculitic layer versus smectitic layers, facilitated

by the faster dissolution of smectitic layer versus vermiculitic layer, explains for the observed slightly increase frequency of vermiculite in some intervals (e.g. 10 – 20 cm depth in LM profiles of DM and NP).

However, this dissolution is more or less only a marginal modification when smectitic layer exposed to particle edges, but will not lead to progressive vermiculization of diVS-ml series. Because, a real vermiculization of smectitic layer need at least two requisitions: (1) introduction of more cations to interlayer space to raise the charge and (2) abundance of dissolved Si to introduce the tetrahedral space. Indeed, the microenvironment of porewater could be abundance in dissolved Si, which is derived from dissolution of smectite species, and also abundance in alkaline cations from seawater. But it is hardly possible for soluted potassium, with large cation size, from sea water to introduce the interlayer space of internal smectitic layer.

Meta-stable neoformation of beidellite from beidellitic KE-ml

Discussion in chapter 5.3.3 has demonstrated obvious occurrence of alteration process in direction from beidellite to kaolinite. However, in interaction with the other processes like dissolution and smectitization, imprints for the neo-formation of beidellite are also detected in LM profile and deeper parts of MF and SP profiles as a pseudo-stable phase. This was recorded by slightly increase in appearance frequency. For example in LM profile in Dam Mon, the 10 – 20 cm depth interval has frequency of beidellite equal to 4 %, which is slightly higher than frequency of beidellite in younger materials in surface sediment (3 %). Also, MF and SP profiles have beidellite frequency increasing with depth: from 4 % and 3 % (40 – 50 cm depth) to 5 % and 10 % (80 – 90 cm depth), respectively. Similar evidences were also found in profiles of Red River Delta and Nha Phu, most commonly in all length of LM profiles and the deepest part of MF and SP, where significant interferences by biota-induced processes are lack.

It is to notice that, increase in beidellite frequency occurs also in the intervals that smectitization exhibits readily. For beidellite neoformation from beidellitic KE-ml particle, a introduction of Si to tetrahedral space is required. This process, then could be linked with the abundance of Si in the surround microenvironment, which is leached from vermiculitic layer during smectitization process and also partly from dissolution in full spectra of mixed layer series.

Another motivation for this process can also links with distribution of dissolved Si by Si-streaming flux – the basinal process. This process is characterized by higher accumulation of Si flux in the margin of sea basin. This is also observed commonly in the basin of Baltic sea.

5.3.7. Summary on post-sedimentary processes

XRD and TEM evidences indicate that the three mineralogical processes: dissolution, smectitization and kaolinitization govern principally the mineralogical and geochemical features during the maturing process of coastal sediment profiles in Vietnam (Table 5.7). Locally formations of vermiculite or beidellite as meta-stable phases are only modification in margin of mixed layer particles, and resulted from incongruent dissolution process.

Table 5.7. Main chemical variations along sedimentary profiles and assumed driving processes

Abb	Process	Signals of influences	Main chemical variations	Data
Dt	Dissolution (function of time)	Increase: from younger sediments to older sediments	Amount of all clay minerals decrease from top to down Frequency of mixed layer particles decrease from top to down	XRD: peak area of 14 A, 10 A and 7 A phases of fractions < 2 μ m. TEM: frequency of KE - ml particles
Ds	Re-suspension (surficial erosion)	Only in surface layer of zones under intensive hydrodynamic influences (LM and SP)	Amount of all clay minerals decrease in top of LM profiles	XRD peak area of 14 A, 10 A and 7 A phases TEM: frequency of KE - ml particles
W _{KE}	Kaolinitization	Increase: from younger sediments to older sediments	Movement of frequency distribution from beidellitic KE toward kaolinitic KE	TEM: frequency distribution curve of KE series
*B _{KE}	Biota-induced kaolinitization	Increase in root layer of MF, inheritance in former root layer of SP	Beidellite layers alter to beidellitic KE	TEM: frequency distribution curve of KE series
*B _{diVS}	Biota-induced smectitization	Increase in root layer of MF, inheritance in former root layer of SP	Vermiculitic layers alter to smectitic diVS	TEM: frequency distribution curve of diVS series
W _{diVS}	Smectitization	Increase: from younger sediments to older sediments	Movement of frequency distribution from vermiculitic diVS toward smectitic diVS	TEM: frequency distribution curve of diVS series

Notes : directions of younger to older sediments: LM -> MF -> SP, from top to down along profile

*: The processes are discussed following in chapter 5.4.4 and 5.4.5, respectively.

(1) The dissolution process occurs in full spectra of clay minerals as a function of diagenetic time, leading to decrease in relative amount of clay phases versus quartz and release of Si, Al, Fe, Mg and alkali cations to the ambient. Smectitic diVS-ml structures are more accessible to dissolution, in comparison to the parent end-member dioctahedral vermiculite. Dissolution process is intensified by hydraulic erosion in surface sediment of low tidal mudflat and water discharge in shrimp pond, acidic micro-environment in rhizosphere layer of mangrove profile.

(2) The smectitization of diVS-ml series is evidently in clay size matters of the studied profiles with the increase of expandable phase with depth, migration of frequency spectra from vermiculitic to montmorillonitic structures as well as morphological modification of particles. This alteration process can be intensified under intensive surficial dissolution as well as under influence of mangrove root in rhizosphere layer. The smectitization in diVS-ml structures occurs in group-wise layer by layer transforming mechanism. Each step is indicated by a gauss-like distribution of the octahedral layer charge. K seems to have a trigger function with commonly maximum occurrence in the interlayer in between two neighboured tetrahedral levels.

Formation of expandable phase in clay size responds chemically to the leaching of potassium but absorption of Fe and Mg to octahedral spaces. Also, expandable phase possess higher retention capacity of heavy metals and other minor elements.

(3) The kaolinitization of KE-ml series can also be addressed based on the increase of CSD, 060-hkl reflection (XRD-data evidences) as well as particle morphology, polytype and increase of kaolinitic KE-ml in frequency spectra (TEM evidences). Similarly to smectitization process, kaolinitization occurs as a function of time, with more obvious imprints in the more matured materials at the bottom of sedimentary cores. Kaolinitization occurs following the smectitization process and is observed with lower intensity. Solid transformation with dissolution of interlayer and silica layer, then with attachment of hydroxyl groups on octahedral layer to form kaolinite-like domain could be the principal mechanism for this process.

The three processes occurred continuously (see Figure 5.35), characterizing short-term alteration sequence of clay mineral assemblage in weathering condition of coastal sediments. The transformation from smectite to kaolinite modifies wetland soils by substituting smectite (high capacity of retaining and exchanging nutrients, trace elements) by kaolinite, an inert soil component. In the view of using the wetland soil for agriculture, it is advantage point as the substitution impoverishes the soil materials (Dudek et al. 2006). However, in the view of using mangrove soils for shrimp cultivation, it is important to notice that the bottom sediments in pond may release toxic element to harm the shrimps. Chemical investigation showed the leaching of heavy metals out of surface sediments together with clayey species (Chapter 5.5.1), further emphasizing the disadvantage caused by kaolinitization. Additionally, although mangrove forest sediments with high amount of mud have long been known as a trap of toxic elements to prevent marine environment from pollution (e.g. Harbison 1986; Larcada 1993), the kaolinitization under surface weathering condition is going to decrease the effect of this function.

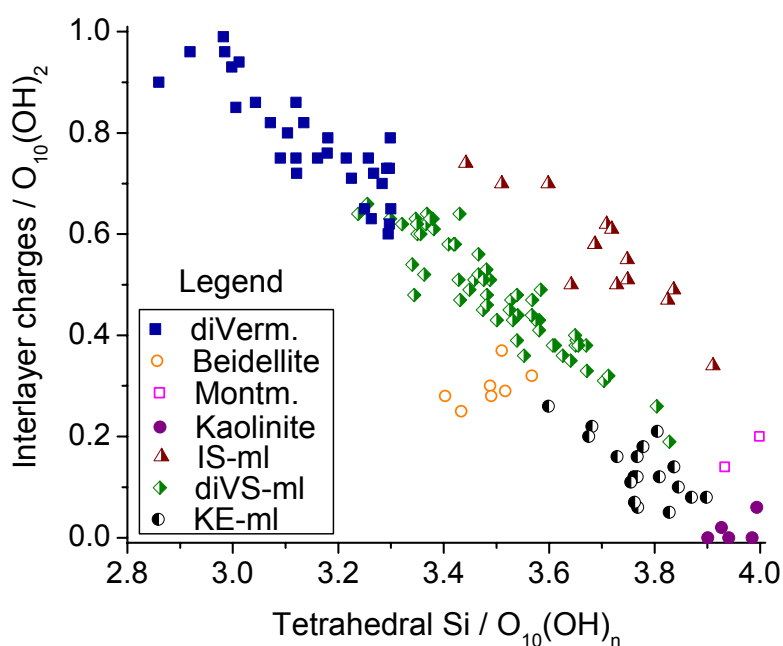


Figure 5.35. Continuous adaptation of interlayer charge during the development from structures with lower Si^{IV} to structures with higher Si^{IV} values in the determined mixed layer series

On example of sample RRD-MF (0 - 5 cm)

5.4. Post-sedimentary processes with involvement of mangrove biota – mirroring by elemental distribution and mineral matter

Chapter 5.1 discusses on the effective trapping of silty materials by root systems of mangrove forest, in the linkage with sedimentation in turbulent environment. Besides, Chapter 5.2 reveals the association of clay phases and corresponding clay-forming elements with fine materials, those possess also high capacity of heavy metal retention. The Chapter 5.2 also emphasizes roles of mangrove forest as principal nutrient supply, mirroring by high concentration of organic carbon in surface sediments of mangrove forest profiles. In this chapter, biota-induced processes in the view of geochemistry and mineralogy are to discuss.

Because the sediments in mangrove forest environments are influenced by mangroves in two main features: (1) supply of nutrients from surface and (2) bioturbation by the active roots at rhizosphere layers which locate at about 20 to 60 cm depth, depending on profiles. Surface layers and rhizosphere layer of mangrove forest profiles, as well as the former rhizosphere layer remained in nowadays shrimp pond profiles are to consider for studying post-sedimentary modifications.

5.4.1. Diagenetic process of nutrients

Chapter 5.2.2 has discussed on the role of mangrove as source of organic matter to the sediments, and also the correlation between C_{org} concentration and sedimentation rates. However, different from distribution of C_{org} , which is driven by syn-sedimentation process, presence of sulphur tends to link with post-sedimentary processes.

Indeed, when organic matters settle with mineral matters and decompose, reduction processes can transform SO_4^- from sea water to reductive forms and maintain sulphurs in fine sediments, of 0.11 – 0.28 % as seen in coastal sediments of Vietnam. The origin and reduction pathway of sulphurs species have been described in estuarine sediments of several tropical mangrove forest (e.g. Cu 1993; Marchand et al. 2004). Along profiles in young mangrove forest of RRD and Nha Phu, the higher amount of sulphur, occurs in the deeper part and corresponds to lower amount of organic carbon. It indicates that the organic matters from MF are limited and consumed by formation of sulphurs. However, in century old mangrove forest in Dam Mon as well as SP profiles in all three regions (i.e. RRD, DM, NP), amount of organic matters is abundant due to much longer time supplying by MF organic matters, that facilitating reduction process to form and maintain sulphurs. It explained for high correlation between sulphur and organic carbon in these profiles. Tight correlation between content of total sulphur and pyrite sulphur indicates that the formation of pyrite in these sedimentary environments is possible occurring.

It is to notice that, the measured concentration of sulphur in the sediments of south central coast is 1- 3 times higher than that in sediments of RRD. This could be a mirror of linkage between vertical sedimentation rate and the rate of sulphur burrier, similarly to the determined distribution behaviour of C_{org} . Both regions Dam Mon and Nha Phu have high amount of sulphur, corresponding to low vertical sedimentation rate. However, that the Dam Mon sediments with lower measured concentration of sulphur and intensive smelling of H_2S (field observations) in comparison to Nha Phu, can impress the reduction process of sulphur in this matured mangrove area.

The organic matters presenting in shrimp ponds were inherited from the former mangrove forest environments and maintained in fine materials. Depletion of organic carbon content in surface layers is linked with leaching of fine materials by water discharge, which sequenced in decrease in capacity of trapping nutrients. In low tidal mudflat, the depletions of C_{org} content in top profile is linked with strong surficial erosion without adding of new organic matters as observed in MF environments.

High accumulation of organic matters as well as the abundance of prop root system facilitate the trapping processes. Trapping of mud is also determined earlier by geomorphological study by Wolanski & Ridd (1986) that depend strongly on variation of tide dynamic.

5.4.2. pH/Eh zoning along depth profile in MF sediments

Results on physico-chemical parameters of coastal sediments in the south central coast of Vietnam (Chapter 4.3.1) have revealed the sudden decrease of pH and Eh values in some intervals of mangrove forest profiles. These intervals are 10 – 40 cm depth in DM-MF, 10 – 60 cm depth in NP-MF and 10 – 20 cm depth in NP-SP (highlighted bars in Table 4.2 and also in Figure 5.36). These variations make mangrove forest profiles different from low tidal mudflat and shrimp pond, where pH and Eh along the profiles remain in balance status as mixing between river-born sediments and sea water as discussed in Chapter 5.2.2

To interpret these physico-chemical modifications during the post-sedimentation in mangrove forest profiles, two possible factors are to consider: (i) supply of organic matters from surface sediments and (ii) bioturbation in rhizosphere layer.

Notice that in surface sediments of the investigated profiles, the decreases of Eh values are corresponding to the enhanced concentrations of organic matters (see Eh and TOC profiles in Figure 5.36). It infers that the reductive environment in these layers, mirrored by lower Eh, could be linked with abundance of reductive agents derived from organic matters. In earlier studies, the roles of organic matter and associated decomposition processes in water condition to favour production of reductive agents have been well documented (e.g. Clark 1997; Marchand et al. 2003). These evidences indicate presence of a reductive zone in upper profile.

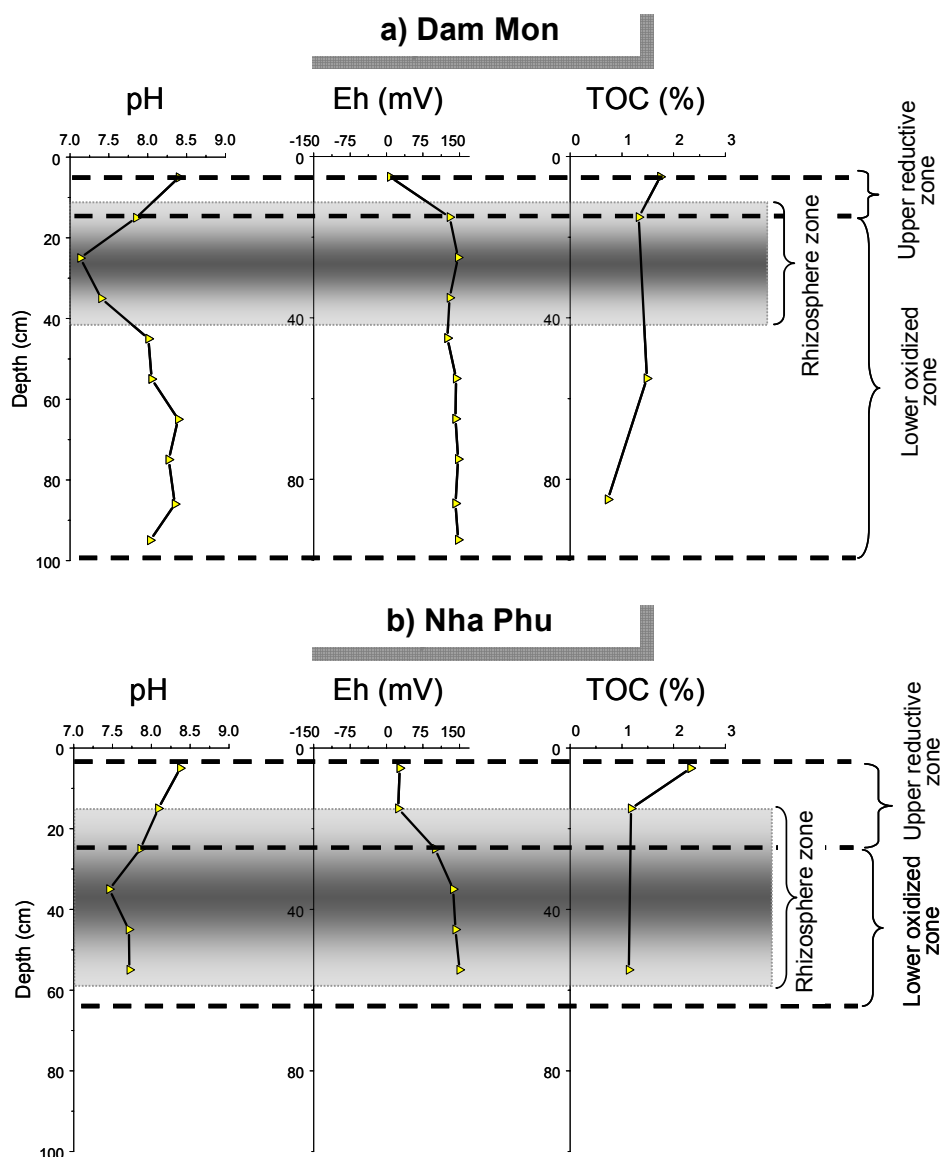


Figure 5.36. Zoning of pH/Eh system along mangrove forest sediment profiles in Dam Mon (a) and Nha Phu (b)

The lower parts of profiles exhibited depletion of organic matters, mirrored by lower TOC concentration (Figure 5.36). Values of Eh were slightly higher than surface layer, correspondingly. These evidences indicate presence of an oxidized zone in lower profile.

On the boundary between upper reductive zone and lower oxidized zone, there occurs a zone that pH values decreased intensively. In this zone, Eh increased slightly comparing to surface layer but the values were still lower than the deeper part. Because the rhizosphere of mangrove forest were commonly known to the depth of 20 – 70 cm in underlying sediments (Hong & San 1993, Tri et al. 1998), roles of active roots could be expected also in these layers.

Based on the above characterization and interpretation, a scheme can be developed on zoning of pH, Eh, TOC in mangrove forest sediments during the post-sedimentation period. The physico-chemical scheme is presented in Figure 5.36, allowing to distinguish three zones: (1) upper reduction zone and (2) lower oxidation zone and (3) rhizosphere layer.

Upper reduction zone (URZ)

The upper reduction zones (URZ) locate within 10 cm surface layer in RRD and Dam Mon but within 20 cm in Nha Phu, characterized by low values of Eh. Sediments in these zones are significantly influenced by high amount of decaying organic matter from mangrove falling leaves or sulphate reduction. The Eh values determined for these zones in central coast of Vietnam are 7 mV (within 10 cm) in Dam Mon, 27 to 37 mV in (within 20 cm) in Nha Phu, respectively. Eh values of these zones were also reported by Cu (1998) for RRD with -19 to -43 mV in 10 cm upper of MF sediments.

In the Eh stratigraphical model of mangrove sediments in Wynnum (Australia), Clark et al. (1998) mentioned presence of an thin upper oxidized zone lying above the upper reductive zone, which links with oxygen diffusion from the expose to the air. In this investigation for coastal MF sediments in Vietnam, presence of this thin upper oxidized zone is not determined. It is unclear if this layer does not exist, because the air expose periods are so short (few hours per day), or exists but mixed in the uppermost 10 cm sampling intervals.

Lower oxidation zone (LOZ)

Having higher Eh values in comparison to the upper reduction zone, the lower oxidation zones locate right below the URZ, from about 20 cm depth to the bottom of the core, so far in the investigated depth. Sediments in these zones related to flushing root biomass or sulphide oxidation. The determined Eh values of lower oxidation zones in Dam Mon and Nha Phu are, respectively.

Clark et al. (1997) suggested that a presence of a LRZ could be expected in deeper parts of profiles, where no more supply by dissolved oxygen or flushing root present. In the investigated profiles, location of such a zone, in case of appearance, should be at deeper than 100 cm.

The zoning of Eh values along profiles has also observed in SP, as inheritance of former MF, however the signals are much more fading.

Rhizosphere layer

Whereas the URZ and LOZ are distinguished based on the differentiation of Eh values, the presence of rhizosphere layer is defined based on variation of pH values. Along MF profiles, locations of these zones are marked with the depletion of pH values (Figure 5.36), indicating the acidification in the micro-environment surrounding mangrove roots. In Dam Mon, rhizosphere layer locates at 20 – 40 cm depth interval but in Nha Phu, this layer

locates at 15 – 60 cm depth interval. Similar observation and determination of this pH state are also widely reported in several investigations on root layer of mangrove forest (e.g. Larceda et al. 1993, Marchand et al. 2003).

To summary, the variations of pH and Eh along mangrove forest profiles respond to three main zones: (1) the upper reduction zone (URZ) in surface zone link with high amount of organic matter and decomposition processes (2) the lower oxidation zone (LOZ) in the deeper part of the core link with dissolved oxygen and flushing root, which supply oxygen and (3) the rhizosphere locating between URZ and LOZ, link with acidic microenvironment surrounding root systems.

5.4.3. Trapping processes in mangrove forest

In Chapter 5.1, it has been mentioned that MF profiles are rather strongly affected by syn-sedimentary erosion process, which involve with turbulent currents induced in prop root system. It could be expected also high re-suspension process directly in syn-sedimentary time. However, the depletion of the very fine size clay minerals is not to detect in this environment, How to interpret that? It is known that in the turbulent environment between prop root system of mangroves, not only the clay-sized grains but also sand-sized and silt-sized grains can be resuspended. Mechanical facing among particles can motivate the attachment of vary fine clay grain on surface of coarser particles. Therefore, clay minerals of fine size can be assumed to be attached on surface of coarser particles. Considering the grain size distribution shape of erosion end-member factor (Figure 5.1, discussing on shapes of hydrodynamic end-member and its meaning), the association of small clay peak with the large fine sand peak are obvious. This evidence demonstrates for the above mentioned assumption. Meaning of erosion factor in mangrove forest, thus points to distribution of particles in tuburlent environment between mangrove roots, which can bring away the suspended silt-sized grain but remain the very fine clay minerals on surface of coarser grains. This discussion is in agreement with the conluded tendency of erosion factor, based solely on grain size data (Chapter 5.1). Therefore, due to specific character of sedimentation process in mangroves – linked with the tuburlent environment between prof roots, enable for the trapping of very fine sized clay ($< 2\mu\text{m}$)

It is to note also that sedimentary environment in mangrove forest contained high amount of organic matters, which produced from mangroves, possibility that clay species can cooperate with organic matters is expected. Figure 5.11 and Figure 5.12 shows high concentration of Al_2O_3 as well as high enrichment of Pb in surface layer, but depletion in the deeper layer of mangrove forest sediment profile – the tendency make it different from LM and SP. Besides, the high correlations among Al and other elements in clay-forming element groups (Mg, Fe, Mn, K), Pb with other heavy metals (see Table 8.5) are to noticed.

Taken altogether, a conclusion can be drawn out: the trapping process do present in mangrove forest specifically. It is mirrored by high accumulation of clay minerals, Al and other clay-forming elements as well, heavy metals.

Trapping functions of mangrove forest are also widely determined for estuaries in tropical countries, e.g. by the studies of Padmala et al. (1997), Marchand et al. (2004).

5.4.4. Intensification of dissolution process under effects of root system

As mentioned in chapter 5.2.1, values of pH along the depth profile exhibits decrease in the rhizosphere layer of all mangrove forest profile, mirroring an occurrence of acidic microenvironment surrounding the roots. Acidic microenvironment is favourable condition for dissolution of clay minerals (Golubev et al. 2006).

Indeed, XRD results shows intensive decrease in peak area of clay phases in rhizosphere layer of mangrove profiles (see 20 – 40 cm interval in MF profile, Figure 8.36). These evidences, found in rhizosphere of MF profiles in RRD, Dam Mon and Nha Phu (Figure 8.36, Figure 8.37, Figure 8.39 - Appendix) demonstrate that dissolution of clay minerals is intensified under effects of root system in mangrove profiles, in connection with occurrences of acidic microenvironments.

Experiments by Golubev et al. (2006) on smectite dissolution over a wide range of pH at 25 ° indicated similar behaviours to other sheet silicates: in acidic to neutral solutions, Si-release rate increases with decrease of pH. High concentrations of most organic ligands (0.01–0.1 M) are also supportive for faster dissolution.

5.4.5. Intensification of smectitization under effects of root system

Although the dissolution process tend to be intensified in rhizosphere layer of MF profile, imprints of transformation process in direction from vermiculite to smectite are also clearly observed.

Under TEM investigations, SAEDs shows the conversion from $2M_1$ structure to turbostratic order when diVS 90 (with 90% of smectitic layers) was smectitized to diVS50 (with 50% of smectitic layers).

This transformation is recorded in frequency spectra (TEM-data), with the decrease in the abundance of diVerm and diVS-ml particles but increase of smectitic diVS-ml particles. In MF in Dam Mon, frequency spectra of diVS-ml showed at first the decrease of diVerm particles (see 10 – 20 cm depth interval of MF profile, Figure 5.19), making S% increase to 30 % relatively to the upper part (11 %). An intensive increase in frequency smectitic diVS particles is corresponding to the decrease of diVerm, also obviously in this layer. In the layer below rhizosphere layer (40 – 50 cm depth in MF of DM), frequency spectra of diVS

layer below rhizosphere layer (40 – 50 cm depth in MF of DM), frequency spectra of diVS shows no more decrease of diVerm. It indicates that the most intensive smectitization process should happen in the middle of rhizosphere layer (i.e. 20 – 40 cm interval), where pH values also indicate strongest acidic microenvironment.

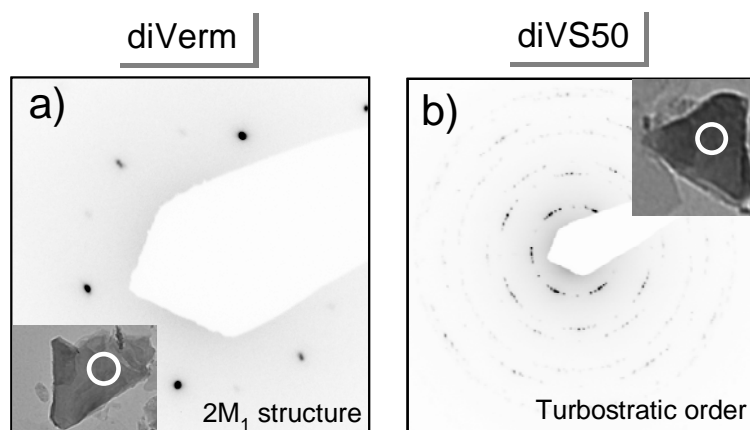


Figure 5.37. SAEDs shows the conversion from 2M₁ structure to turbostratic order when diVerm was smectitized to diVS50 (with 50% of smectitic layers)

On example of sample DM-MF (40-50 cm depth)

Similarly to MF profile in Dam Mon, the intensive decrease in diVerm frequency and corresponding intensive increase of smectitic diVS-ml abundance can also addressed in rhizosphere layer of RRD and Nha Phu. In RRD, S% of diVS-ml in rhizosphere layer (~ 50 cm depth) increase to 30 %, relatively to value of 24 % in surface layer. In Nha Phu, S% of diVS-ml series in rhizosphere layer is 30 %, also higher than that in surface layer (23 – 24 %)

How to explain for the roles of mangrove roots to motivate the smectitization? The discussion on mechanism of smectitization (Chapter 5.3.4) has impressed the function of interlayer K as trigger for this alteration process. In environment without influences of biota, dissolution could be the reason for the leaching of K out of interlayer space. Considering behaviour of K in rhizosphere of mangrove profile, it is widely reported that the root of fauna can uptake alkaline cations such as K, Na and Ca and bring them up to the shoot (). Study of Rains and Epsteins (1965) on the *Avicenia* species also confirmed the uptake of K and Na by these mangroves. In this sense, the uptake of K by mangrove roots can be interpreted as fundamental reason for removal of K out of interlayer space in diVerm particles and dioctahedral vermiculitic layer in diVS-ml particles. This removal of K, in turn, can intensify the smectitization process in rhizosphere layer.

Charge behaviours of diVS-ml in Figure 5.38 revealed also the occurrence of K-leached diVerm particles (zone II) with more similarity to diVS10 (zone III) (smectitic diVS-ml with approximately 10 % smectitic component) in terms of tetrahedral charge (IV). Formation of this K-leached diVerm from diVerm (zone I) mirrors the early stage of biota-induced smectitization.

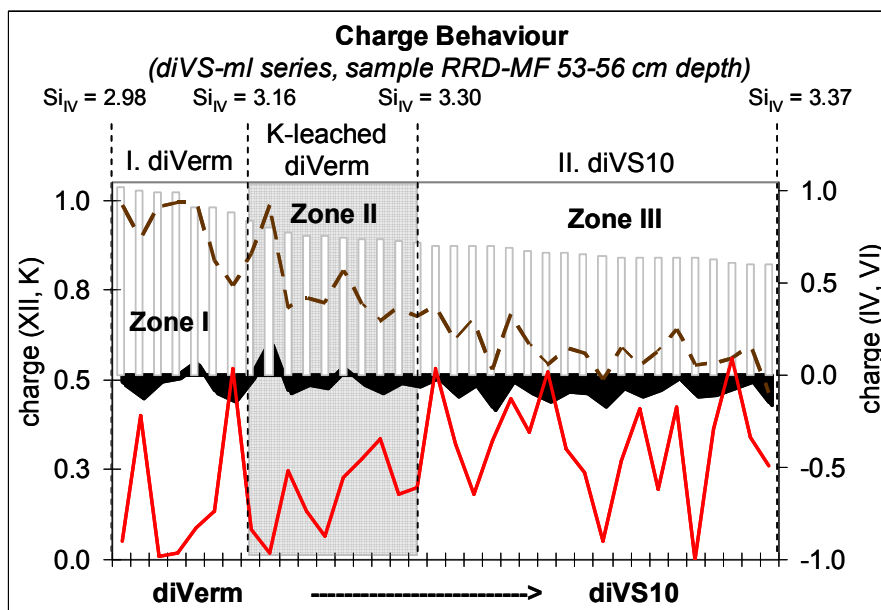


Figure 5.38. Layer charge behaviours of diVerm, K-leached diVerm and diVS10 in diVS-ml series in rhizosphere layer, MF profile in Red River Delta

Notes: charges of IV- (grey bar), VI- (black area), XII- (brown dash line) and interlayer K (red solid line); diVS10 is the vermiculitic diVS structure with 10% of smectitic proportion

It is to notice the similarity in IV-charge and interlayer K between the K-leached diVerm (zone II) and diVS10 (zone III), as indication for early stage of biota-induced smectitization

Uptake of K by mangrove roots, conclusively, is the main driving force for the biota-induced smectitization of mica-like clay minerals.

The effects of root layers to accelerate rates of secondary mineral formation in soil profile were also well addressed by several researches (e.g. Drever 1994).

5.4.6. Intensification of kaolinitization under effects of root system

Similarly to smectitization process, the kaolinitization process can also be revealed to enhance in rhizosphere layer of mangrove forest profile. Frequency spectra of KE-ml series in rhizosphere layer showed highly decrease of beidellite and corresponding movement of frequency spectra from beidellitic KE-ml toward kaolinitic KE-ml particles (see example of MF profile in Dam Mon, Figure 5.19). This process is mirrored also by decrease of average smectitic ratios S%. Surface layer of mangrove in Dam Mon has S% = 47 but the rhizosphere layers: interval of 10 – 20 cm depth has S% = 40 and interval of 40 – 50 cm depth has S% = 38 (Figure 5.19). Depletion of beidellite frequency and increasing of kaolinitic KE-ml particles frequency are also addressed in rhizosphere layer of mangrove sediments in RRD (Figure 8.35) and Nha Phu (Figure 8.38).

Discussion on mechanism of kaolinitization during the maturing of sediment profile has mentioned the roles of dissolution of interlayer cations, tetrahedral layer and attachment of hydroxyl group from ambient saline water as driving force. In rhizosphere layer, the

presence of acidic microenvironment makes it favorable for further dissolution of clay species (Chapter 5.4.3). Also, leaching of interlayer cations from beidellite can be more intensively, considering the roles to mangrove roots to uptake also Ca and Na (Rain & Epsteins 1965).

It is to notice that, the decrease of beidellite frequency is most intensive in the below part of rhizosphere layer, corresponding to interval of 40 – 50 cm in mangrove forest profile of Dam Mon. It is unlike the imprint of biota-induced smectitization, which makes highest deletion of the parent end-member diVerm in the upper part of rhizosphere layer (i.e. interval of 10 – 20 cm). This signal indicates that biota-induced smectitization begins earlier than the biota-induced kaolinitization. Or in other words, mangrove roots firstly attack to the K-rich minerals (i.e. diVerm) to promote smectitization, then later remove also to the other interlayer cations (i.e. Na, Ca, Mg) of the K-poor minerals – beidellite to promote kaolinitization.

To summary, in rhizosphere layer of MF profile, the kaolinitization is facilitated by the faster dissolution in acidic condition and removal of interlayer cations from beidellitic layer of KE-ml structure by root uptake. The biota-induced kaolinitization happen latterly, following the biota-induced smectitization.

5.4.7. Summary on biota-induced post-sedimentary processes

(1) Mangrove forest is the principal source of organic matter in the coastal sediments. Whereas C_{org} deposit during the syn-sedimentary process, sulphurs tend to be post-sedimentary formed by reduction of SO_4^- from sea water in occurrence of organic matter. Though low sedimentation rate facilitate accumulation of sulphurs, abundance supply of organic matter by century old mangrove in Dam Mon can motivate the transformation of sulphur to evaporable sulfides.

(2) In the submarine condition with influences of organic matter from surface to down, the values of Eh and pH can create three distinctive zones: (i) the upper reduction zone (URZ) in surface zone link with high amount of organic matter and decomposition processes (ii) the lower oxidation zone (LOZ) in the deeper part of the core link with dissolved oxygen and flushing root, which supply oxygen and (iii) the rhizosphere locating between URZ and LOZ, link with acidic microenvironment surrounding root systems.

(3) Presence of mangrove biota accelerates rates of dissolution and secondary mineral formation, as revealed from both XRD and TEM data. Acidic micro-environment surrounding the root could be the driving force for intensification of dissolution in rhizosphere layer. The root system, with function to uptake K, Na, can remove interlayer cations from vermiculitic layer of diVS-ml structures as well as from beidellitic layer of KE-ml structures. In turn, these attacks trigger for the smectitization and kaolinitization processes.

5.3. Post-sedimentary processes influenced by human activities (e.g. shrimp pond cultivation)

In order to recognize any mineralogical and geochemical imprints of human-induced post-sedimentary processes, all influence factors that define significantly the composition as well as the maturity of sediments in the studied shrimp pond environment should be considered. There are three principal influence factors: (i) syn-sedimentation position of shrimp pond profile, considering the effect of hydrodynamic accumulation factor (EMMA treatment), (ii) time of maturing process or lateral aging of SP sedimentary profile, and (iii) human-induced post-sedimentary modifications.

Chapter 5.2 has discussed on influences of hydrodynamic accumulation factor and erosion factor on distribution of grain sizes, major elements and minor elements of shrimp pond profiles. Conclusively, the more matured sediments with higher accumulation factor register higher clay minerals, clay-forming elements and heavy metals. Meanwhile, the erosion occurs intensively in surface layer can results in dispersion of clay matter and heavy metals.

Sediments in shrimp pond are the most matured sediments relatively to MF and LM in the lateral aging sequence of coastal sediments. In RRD, the estimated age of shrimp pond sediments is 40 year older than neo-sedimentation in mangrove forest. Correspondingly, these materials have higher kaolinitic proportion in KE-ml series (S% in SP = 42 – 45 %, S% in MF = 47 – 58 %). In Dam Mon and Nha Phu, due to low sedimentation and short distance between SP and MF profiles, the age of SP sediments can be suggested only few years older than MF sediments. Therefore, differentiation in maturity of KE-ml series can hardly be detected. However, the higher maturity of sediments in SP sediments is mirrored readily in composition of diVS-ml with higher smectitic proportion. The average S% in shrimp pond sediments (Dam Mon: S% = 25 – 35 %; Nha Phu S% = 24 – 38 %) is correspondingly higher than S% in mangrove forest sediments (Dam Mon: S% = 26 – 30%, Nha Phu: S% = 24 - 28%). These evidences support further for the assumption that the smectitization occurs earlier than kaolinitization process.

Only one exception that is not included in this example here is diVS-ml series in the 10 – 20 cm depth interval of DM, with the value S% = 44 %. This high smectitization level is caused by presence of active mangrove roots as discussed above in chapter 5.4.5.

Different from sediment profiles in low tidal mudflat and mangrove forest, sediments in shrimp pond is inherited from the former mangrove sediments without neo-sedimentation since then. Therefore, beside the characteristics induced from hydrodynamic processes and time effects, any further variation in mineralogy and geochemistry could be interpreted as human-induced post-sedimentary processes.

5.5.1. Dispersion in surface sediments

Results on distribution along the depth profile of grain sizes (Chapter 4.1), major and minor elements (Chapter 4.2), nutrients (Chapter 4.2) and clay mineralogy (Chapter 4.3) revealed the intensive depletion of clay matters and minor elements in surface layer of shrimp pond profiles. It seems to be more intensive than the depletion tendencies in LM profiles and both are completely different from the accumulation tendencies of these components in MF profiles.

Table 5.8 compares the sediment features between surface layer and the nearby subsurface layer, in terms of hydrodynamic erosion influences, nutrients content, mineral composition, major chemical elements and heavy metals. Discussion in Chapter 5.1 has impressed the high influence of erosion factor, in comparison to this former environment – mangrove forest. It is mirrored by higher values of erosion factor in SP (Table 5.8a). It should notice that, whereas the intensive influence of erosion in LM (Table 5.8a) is caused by wave or tide dynamic, influences of erosion in SP is linked with water discharge as man-made regulation for living condition in SP. Correspondingly, the higher erosion results in higher relative quantity of quartz (Table 5.8c), SiO₂ content (Table 5.8e) but much intensive decrease of expandable phases (Table 5.8c), Al₂O₃ and K₂O. These infer to a leaching of expandable clay matter out of the surface layer during human induced water discharge. However, the enrichment of CaO in shrimp pond sediments in surface layer is higher than in LM and MF environments (Table 5.8e). This high content can be a mirror of the residual Ca, which was added by human during the pH regulation. Enrichment of heavy metals is

Table 5.8. Ratios of key parameters between surface layer and the nearby subsurface layer
(on example of sediments in Red River Delta)

Group	Parameters	LM	MF	SP
a) Hydrodynamic	Erosion influence ⁽¹⁾	2.39	1.77	1.92
b) Nutrients	C _{org} (%)	0.52	1.62	0.58
	S _{Total} (%)	0.88	0.69	1.04
c) Mineralogy	XRD peak area (Å) of Quartz (3.34 Å)	132	149	200
	Expandables ⁽²⁾	0.63	0.92	0.12
e) Major elements	SiO ₂	1.02	0.94	1.01
	Al ₂ O ₃	0.99	1.17	0.92
	CaO	0.94	0.94	1.21
	K ₂ O	1.01	1.18	0.93
f) Minor elements	Cu	0.92	1.27	1.00
	Pb	0.96	1.02	0.66
	Zn	0.89	1.41	0.92
	Co	0.96	1.10	0.85
	Cr	0.98	1.25	0.83
	Ni	0.95	1.18	0.96
	Cd	0.83	1.38	1.00

⁽¹⁾: influence value of erosion factor (EMMA treatment, Chapter 5.1)

⁽²⁾: Relative quantity of expandable phases, determined by ratios between peak areas of 17 Å reflection relatively to 3.34 Å reflection (XRD, ethylene glycolated samples)

intensively depleted in SP sediments, in corresponding with the depletion of expandable accumulation. The high retention capacity to maintain heavy metals of expandable phases has been further discussed in chapter 5.3.1.

5.5.2. Removal of mangroves and effects from remains of decaying roots

Shrimp ponds are constructed from former mangrove forest, therefore sedimentary materials are inherited. Chapter 5.4 has revealed significant interference of organic matters from mangroves as well as active influences of rhizosphere layer on geochemical and mineralogical maturing sequence. In shrimp pond, because the former mangroves have been cut off and mostly removed before the construction, no more addition of new organic matters as well as active influences of root should be available.

Although the shrimp pond sediments in RRD exhibit higher maturity as mirroring by higher kaolinitic proportion in KE-ml series, imprints of influences from the former rhizosphere layer are much fading than the currently mangrove forest profile. Comparing the frequency ratios of end-members Kaol /Beid and Montm/diVerm in the former rhizosphere layer in SP with the active rhizosphere layer in MF can reveal a considerable decrease (SP sediments: Kaol /Beid = 1.2/1; Montm/diVerm = 1/67 comparing to MF sediments: Kaol /Beid = 3/1; Montm/diVerm = 1/20) (Figure 8.35). In former rhizosphere layer in SP, the dissolution as function of time (Dt) tends to be dominant. These evidences thus impress the fact that, whereas presence of mangrove rhizosphere motivates the dissolution, smectitization and kaolinitization processes, the human-induced removal of mangroves in SP profiles limits these intensifications.

Similar evidences could be found also in sediments of SP profiles of the south central coast. In Dam Mon, imprints of the former rhizosphere layer can be seen in the 40 – 50 cm depth interval of SP profile, where KE-ml series contains high frequency of KE and corresponding low frequency of beidellite, in comparison to the surface sediments. However, the Montm/diVerm ratio of this former rhizosphere layer in SP (= 0/4.2) is less than the Montm/diVerm of the active rhizosphere layer (20 – 40 cm depth interval) in the current mangrove forest (= 0.2/7.6). Also S% of the former rhizosphere layer in SP (= 25 %) is less than that in active rhizosphere layer of MF (= 44%), suggesting a depletion of smectitization. In Nha Phu, imprints of the former rhizosphere layer remains in the 10 – 20 cm depth and 40 – 50 cm depth intervals, where showed higher smectitization and also kaolinitization than both surface layer and the deeper part. However, in comparison to active rhizosphere layer, intensity of these alterations is less. The average smectitic percentage of KE-ml-series in former rhizosphere layer of SP (S% = 48 – 62 %) is higher than that in active rhizosphere layer of MF (S% = 43 – 55%), indicating lower kaolinitization intensity.

These evidences, similarly to RRD, infer that the active influences of former rhizosphere layer (Chapter 5.4) have been depleted by human-induced removal of mangroves in SP.

5.5.3. Summary of human-induced effects on post-sedimentary processes

Influences of erosion in SP occur in surface layer (0-10 cm), linked with water discharge as man-made regulation for living condition in SP. These result in a higher relative quantity of quartz, SiO₂ content but much intensive decrease of expandable phases, Al₂O₃, K₂O and heavy metals (Cu, Pb, Zn, Ni, Cd), in comparison to LM and MF profiles. Decrease in heavy metal retentions of surface sediments in shrimp pond mirror dispersion to the ambient, which make these toxic elements more accessible to consumption by shrimps.

These dispersion processes in pond sediments explain also for the high concentrations of antibiotic (Le & Munekage 2004) as well as nutrients (Trott & Alongi 2000) in effluence from shrimp pond, which are causing pollution and eutrophication in littoral areas.

Considering the influence of shrimp pond construction on natural mineralogical processes, it is to notice the removal of mangroves that in turn limits biota-induced processes of former rhizosphere layers. Consequently, imprints of biota-induced dissolution, smectitization and kaolinitization are diminished and progressively return to the dominance of diagenetic processes without mangroves.

6 CONCLUSION & SUMMARY

Coastal areas are developed and intensive exploited regions on the one side (GESAMP et al. 1997), but on the other side these areas are very sensitive ecological zones. High population and intensive human activities like cutting mangroves, aqua-farming etc. in recent decades lead to severe deterioration of environment quality, limiting sustainable development. Beside, coastal processes are a real complex interaction between land – sea – mangrove biota – human activities. Imprints of these environmental variations can be recorded in clay minerals of sediment background. It is interesting white field for study of geochemical, mineralogical processes as mirror of early diagenesis as well as environmental variations there in recent decades, which are until now inadequately understood.

Studies were based on three case environments with different features on coastline types, source rock, distance between river mouth and location of sedimentation, sedimentation rate, mangrove maturity, and intensity of human activities: Red River Delta in North Vietnam and Dam Mon, Nha Phu in the South Central Coast. For all studied region, it should be investigated the upper 1 m only to recognize especially processes in the youngest past. The background for this limitation of sampling is to get a better knowledge, what is happened during the sedimentation and in the early diagenesis to consider better these processes better also for investigations in deeper horizons of a basin development. For grain size distribution data, End-member Modelling Algorithim was used to address principal hydrodynamic factors, solving the problem of mixing sedimentary environment. For clay minerals in fractions < 2 μm , TEM-EDX was used for analyzing morphological features and chemical structure of single particle, to distinguish mixed layer series

Integrated results on grain sizes, nutrients, geochemistry and clay mineral matter in the three case studies of Vietnam coastal sediments (low tidal mudflat – LM; mangrove forest – MF. shrimp ponds - SP) can reveal not only regional characteristics but also principal synsedimentary and postsedimentary (diagenetic) processes. Additionally, effects of mangrove biota and human-induced activities on alteration processes can be clarified.

1) Mirroring of regional patterns by distribution of grain sizes, mineral matter and chemical elements

Accumulation and distribution of grain sizes, mineral composition, major and minor chemical elements in coastal zone of Vietnam mirror the regional features like source rock, distance between river mouth and position of sedimentation, sedimentation rate, mangrove biota and human activities.

- RRD sediments are characterized by rather homogeneous detrital muddy materials, low organic matter and high enrichment of heavy metals, *as mirroring of mega-delta*, long river with high freight, rapid progradating and vertical sedimentation, accumulation/

erosion as dominant hydrodynamic, young mangrove forest (<30 years old) and intensive human-induced influences. Slightly pollution states (reference to Canadian standards – CCME 1992) have been addressed for Cu, Pb, Zn, Cr and Ni, with highest potential threats in surface sediments in MF profile.

- Nha Phu sediments exhibits interlayering between sandy and silty materials along profiles, due to even-like moving of neighbor sand bar. High variation of Ca, Na, high organic matters and medium concentrations of heavy metals *mirror* conditions in mountainous coastline, with short - slope rivers with low freight, low sedimentation rate (< 1cm/year), young mangrove forest (<30 years old) and not so intensive human-activities.
- Dam Mon sediments are linked with sandy materials, quartz dominant, SiO₂ -rich, high C_{org} accumulation and sulphur reduction, and depletion of heavy metals, as mirroring of peninsular coastline, low sedimentation rate (< 1cm/year), aeolian dynamic dominance, century-old mangrove forest and only human impacts by shrimp farming.

2) Principal hydrodynamic processes in coastal muddy environment

Three principal hydrodynamic factors can be revealed based on End-Member Modeling Algorithm (EMMA) for data of the polymodal grain-size distribution patterns, those driving granulometric distributions of all depth profiles in Red River Delta, Dam Mon and Nha Phu:

- **Accumulation factor:** accumulation of terrigenous sediments in sense of grain size separation
(*distance dependence*)
- **Erosion factor:** synsedimentary erosion by wave activities
- **Aeolian factor:** deposition from neighbour sand bar by wind
(*typically only for low sedimentation rates, like in South Central Coast but missing in RRD*)

These determined principal hydrodynamic factors and literature data (i.e. sedimentation rates, core length, and distance between profiles) are basis to reconstruct paleogeographical situation for the studied sediment profiles in RRD, Dam Mon and Nha Phu. Age and distance between sedimentation position and syn-sedimentary coastline of studied profiles decrease from shrimp pond > mangrove profile > low tidal mudflat.

3) Mirroring of hydrodynamic processes by elemental distribution and mineral matters

Distributions of clay matter and elemental in the coastal sediments in Vietnam are strongly influenced by texture of sediments. The determined enrichment of clay matters, heavy metals in fine sediments, especially in < 2µm fraction, agrees with literatures (e.g. Chamley 1989).

Influences of hydrodynamic factors on elemental distribution and clay amount vary upon profiles: erosion is responsible for distribution in RRD profiles *but* aeolian for Dam Mon profiles *and* accumulation are for Nha Phu profiles. Geochemical and mineralogical mirrors of hydrodynamic influences in mangrove forest and shrimp pond sediments are overprinted by other processes.

4) Syn-sedimentary chemical modification

When the river-born sediments reach saline water and temporary settle down, beside the establishment of balance pH/Eh system, desorption process of heavy metals from detrital clay minerals and re-absorption by organic matters can be detected. These modifications are recognized from strong correlations with mangrove – induced organic matters. Possibility of heavy metals desorption make it more easily uptaken by coastal ecosystem and become more harmful (Habison et al. 1986, Bou-Olayan et al. 1995).

5) Early diagenetic processes of clay matters (*decadal time-scale*)

For investigation of clay size materials, TEM-EDX – methodology of particle-wise analysis for mixed layer structures is a very suitable and sensitive tool. It is possible to distinguish between different ml-series, and also in the typical case for mixtures of ml-series. Clay mineralogical composition is diverse with *predominance of four mixed layers series*: IS-ml, diVS-ml, CS-ml & KE-ml. Of the four series, diVS-ml series exhibits dominant particle frequency in the fractions < 2 μ m (68 – 72% of total frequency), following by KE-ml series.

Integrated results of XRD (e.g. XRD-peak area, CSD) and TEM-EDX (frequency spectra of mixed layer series, particle morphology, crystallite structures and chemical structures) enable recognition of post-sedimentary geochemical-mineralogical alterations. The determined principal diagenetic processes are: dissolution, smectitization and kaolinitization.

Dissolution process in the coastal alkaline condition is a function of diagenetic time, leading to decrease in full frequency spectra of clay phases in fractions < 2 μ m. It can be intensified by intensive hydrodynamic process (e.g. surficial erosion in LM and SP profiles) and also in contact with acidic microenvironment (e.g. rhizosphere layer in MF profiles). In diVS-ml series, smectitic structure is more easily dissolved in comparison to dioctahedral vermiculitic structure, as a linkage higher octahedral substitution in chemical structures.

The smectitization of diVS-ml series is evidently in clay size matters of the studied profiles with the increase of expandable phase with depth, migration of frequency spectra from vermiculitic to montmorillonitic structures as well as morphological modification of particles. This alteration process can be intensified under intensive surficial dissolution as well as under influence of mangrove root in rhizosphere layer. The smectitization in diVS-ml structures occurs in *group-wise layer by layer transforming mechanism*. Each step is indicated by a gauss-like distribution of the octahedral layer charge. K seems to have a trigger function with commonly maximum occurrence in interlayers between two neighboured tetrahedral levels.

The kaolinitization of KE-ml series occur also as function of time, parallel to smectitization and dissolution processes. This alteration process can be intensified under intensive surficial dissolution as well as under influence of mangrove root in rhizosphere layer. When interlayer cations and tetrahedral layer of beidellitic component are released by dissolution process, attachment of hydroxyl group from sea water to the octahedral layer facilitates formation and growth of kaolinite patch. This solid transformation of KE-ml series is comparable to kaolinitization mechanism discussed by Dudek et al. (2006).

6) Influences of biota on geochemical and clay mineralogical processes

Mangrove forest is determined as the principal source of organic matter in the coastal sediments. Though low sedimentation rate facilitate accumulation of sulfurs, abundance supply of organic matter by century old mangrove in Dam Mon can motivate the transformation of sulfur to evaporable sulfides.

With presence of mangroves as reductive-matters supply and root system, the variations of pH and Eh along mangrove forest profiles respond to three main zones: (1) the upper reduction zone (URZ) in surface zone link with high amount of organic matter and decomposition processes (2) the lower oxidation zone (LOZ) in the deeper part of the core link with dissolved oxygen and flushing root, which supply oxygen and (3) the rhizosphere locating between URZ and LOZ, link with acidic microenvironment surrounding root systems.

Presence of mangrove biota accelerates rates of dissolution and secondary mineral formation, as revealed from both XRD and TEM data. Acidic micro-environment surrounding the root could be the driving force for intensification of dissolution in rhizosphere layer. The root system, with function to uptake K, Na, can remove interlayer cations from vermiculitic layer of diVS-ml structures as well as from beidellitic layer of KE-ml structures. In turn, these attacks trigger for the smectitization and kaolinitization processes.

7) Influences of human activities on geochemical and clay mineralogical processes

Influences of erosion in SP occur in surface layer (0-10 cm), linked with water discharge as man-made regulation for living condition in SP. These result in a higher relative quantity of quartz, SiO₂ content but much intensive decrease of expandable phases, Al₂O₃, K₂O and heavy metals (Cu, Pb, Zn, Ni, Cd), in comparison to LM and MF profiles. Decrease in heavy metal retentions of surface sediments in shrimp pond mirror dispersion to the ambient, which make these toxic elements more accessible to consumption by shrimps.

Additionally, because SP sediments inherited from former MF environment after removing mangroves, remains of the above mentioned biota-induced effects on intensification of mineralogical processes can also be addressed, but with less intensity.

7 REFERENCES

- Alongi D.M., Tirendi F. and Trott L. A. 1999. Rates and pathways of benthic mineralization in extensive shrimp ponds of the Mekong delta, Vietnam. *Aquaculture* 175/3-4: 269-292.
- ACIAR 1999. Annual report: Regional Water and Soil Assessment for Managing Sustainable Agriculture 1997 - 2001. *Project: LWR1/95/07*.
- Adger W. N. 1999. Evolution of economy and environment: an application to land use in lowland Vietnam. *Ecological Economics* 31/ 3: 365-379.
- Adger W.N., Kelly, P.M. and Nguyen Huu Ninh. 2001 "Environment, society and precipitous change." *In: Living with Environmental Change: Social Vulnerability, Adaptation and Resilience in Vietnam (Eds.), pp.3-18 Routledge, London.*
- Allen J. R. L. 2000. Morphodynamics of Holocene salt marshes: a review sketch from the Atlantic and Southern North Sea coasts of Europe. *Quaternary Science Reviews* 19/12: 1155-1231.
- Alloway (ed.) 1990. Heavy Metals in Soils. *Glasgow, Scotland: Blackie, 62 p.*
- Alongi D. M. 1996. The dynamics of benthic nutrient pools and fluxes in tropical mangrove forests . *Journal of Marine Research* 54/1: 123-148 (26)
- Alongi D. M., Tirendi F. and Clough B. F. 2000. Below-ground decomposition of organic matter in forests of the mangroves *Rhizophora stylosa* and *Avicennia marina* along the arid coast of Western Australia. *Aquatic Botany* 68/2: 97-122.
- Alongi D.M., WattayakorG. n, Pfitzner J., Tirendi F., Zagorskis I., Brunskill G.J., Davidson A. and Clough B.F. 2001.Organic carbon accumulation and metabolic pathways in sediments of mangrove forests in southern Thailand. *Marine Geology* 179: 85–103.
- Altschuler ZS, Dwornik EJ, Kramer H. 1963. Transformation of montmorillonite to kaolinite during weathering. *Science* 141: 148– 52.
- Amouric M, Olives J. 1991. Illitization of smectite as seen by high-resolution electron microscopy. *Eur. J. Mineral.* 3: 831– 35.
- Andersen T. J. 1999Suspended sediment transport and sediment reworking at an intertidal mudflat, the Danish wadden sea. *København Geografisk Institut, Meddelelser fra Skalling-Laboratoriet* 37. 72pp.
- Andrew D. Miall 2006. How do we identify big rivers? And how big is big?, *Sedimentary Geology, In Press, Corrected Proof, Available online 20 December 2005*
- Arrhenus G. 1963. Pelagic sediments. *In Hill M.N. Ed. The sea, ideas and observations on progress in the study of the seas. 3. The earth beneath the sea. Interscience, New York. Pp. 655-727.*
- Bach N. V. and Phuc N. H. 1999. Characteristic and deposition from the Red River alluvia. *Journal of Geology No 255 (11-12)/1999. In Vietnamese with English abstract.*
- Bach N.V., Hai N.T., Phuc N.H. 1998. Mineral composition and genesis of clays in the delta of the Red River. *Journal of Geosciences: 211 – 214. In Vietnamese with English abstract.*
- Badarudeen A., Damodaran K. T., Sajan K., Padmalal D. 1996. Texture and geochemistry of the sediments of a tropical mangrove ecosystem, southwest coast of India. *Environmental Geology* Volume 27/3: 164-169.
- Bailey S.W., Lister JS. 1989. Structures, Compositions, and X-ray Diffraction Identification of Dioctahedral Chlorites. *Clays and Clay Minerals* 37:193-202.
- Bardgett R.D., Anderson J.M., Behan-Pelletier V., Brussaard L., Coleman D.C., Ettema C., Moldenke A., Schimel J.P. and Wall D.H. 2001. The influence of soil biodiversity on

- hydrological pathways and the transfer of materials between terrestrial and aquatic ecosystems. *Ecosystems* 4: 421–429.
- Barker W. W. and Banfield, J.F. 1998. Zones of chemical and physical interaction at interfaces between microbial communities and minerals. *Geomicrobiology Journal* 15: 223–244.
- Beierle B.D., Lamoureux S.F., Cockburn J.M.H., Spooner I. 2002. A new method for visualizing sediment particle size distributions. *Journal of Paleolimnology* 27/2: 279–283.
- Berner R.A. 1971. Principles of chemical sedimentology. *McGraw-Hill, New York*. 240p
- Bickmore B., Bosbach D., Hochella M.F., Charlet L. and Rufe E. 2001. In situ atomic force microscopy study of hectorite and nontronite dissolution Implications for phyllosilicate edge surface structures and dissolution mechanisms. *American Mineralogist* 86: 411–423.
- Bieu N., Nghi T. 1998. Lithodynamic evolution of surface sediments in Tonkin Bay. *Proceeding, 4th National Conference on marine science and technology, Hanoi*, pp. 847–853 (in Vietnamese)
- Borchardt G. 1989. Smectites. pp. 675–727. In J.B. Dixon and S.B. Weed (eds.) *Minerals in soil environments*. 2nd ed. SSSA Book Ser. No. 1. SSSA, Madison, WI.
- Bosbach D., Charlet L., Bickmore B. and Hochella M.F. 2000. The dissolution of hectorite In-situ, real-time observations using atomic force microscopy. *American Mineralogist* 85: 1209–1216.
- Bouma J., Hoeks J., van der Plas L. and van Scherrenburg B. 1969. Genesis and morphology of some Alpine podzol profiles. *Journal of Soil Science* 20: 384–398.
- Bou-Olayan A. H., Al-Mattar S., Al-Yakoob S. and Al-Hazeem S. 1995. Accumulation of lead, cadmium, copper and nickel by pearl oyster, *Pinctada radiata*, from Kuwait marine environment. *Marine Pollution Bulletin* 30/3: 211–214.
- Bray RH. 1937. Chemical and physical changes in soil colloids with advancing development in Illinois soils. *Soil Science* 43: 1– 14.
- Brindley GW, Zalba PA, Bethke CM. 1983b. Hydrobiotite, a regular 1:1 interstratification in biotite and vermiculite layers. *American Mineralogist* 68: 420– 25.
- Brouder S. M. and Cassman K. G. 1990. Root development of two cotton cultivars in relation to potassium uptake and plant growth in a vermiculitic soil. *Field Crops Research* 23/ 3-4: 187–203.
- Canfield D. E., Thamdrup B. and Hansen W. J. 1993. The anaerobic degradation of organic matter in Danish coastal sediments: Iron reduction, manganese reduction, and sulfate reduction. *Geochimica et Cosmochimica Acta* 57/16: 3867–3883.
- Caroll D., Starkey H.C. 1958. Effect of sea-water on clay minerals. *Clays and Clay minerals*, 7th Natl. Conf. Pergamon, Oxford., pp. 80–101.
- CCME 2002. Canadian Sediment Quality Guidelines for the Protection of Aquatic Life. *Canadian Council of Ministers of the Environment 2001 Except from Publication No. 1299. Update in 2002*.
- Chamley H. 1989. Clay Sedimentology: *Berlin (Springer-Verlag)*. 623 p.
- Christiansen C. and Hartmann D. 1991. The hyperbolic distribution. In: Syvitski JPM (ed) *Principle, methods, and applications of particle size analysis*. Cambridge University Press, pp 237–248.
- Clark M. W., McConchie D., Lewis D. W. and Saenger P. 1998. Redox stratification and heavy metal partitioning in Avicennia-dominated mangrove sediments: a geochemical model. *Chemical Geology* 149/ 3-4: 147–171.
- Clark M.W., McConchie, D., Saenger, P. and Pillsworth, M. 1997. Hydrological controls on copper, cadmium, lead and zinc concentrations in an anthropogenically polluted mangrove ecosystem Wynnum, Brisbane. *Journal of Coastal Research* 13: 1050–1058

- Cliff G., Lorimer G. W. 1975. The quantitative analysis of thin specimens. *Journal for Microscopy* 103: 203-207
- Colin C., Turpin, L., Bertaux, J., Desprairies, A., Kissel, C. 1998. Erosional history of the Himalayan and Burman ranges during the last two glacial interglacial cycles. *Earth Planet. Sci. Lett.* 171, pp. 647-660.
- Con T.H., Viet P.H., Chuyen N.T., Berg M., Giger W., Schertenleib R. 2000 Arsenic contamination in sediment and ground water of Red river delta. *Report in 26th WEDC Conference, Dhaka.*
- Cu N.D 1996. Geochemical distribution of sulphurs in tidal mudflat sediments of Bachdang river mouth. (in Vietnamese). *In Resource and Marine Environment III, Hanoi 1996.*
- Cu N.D 1998. Geochemical sedimentary changes under human impact in Bachdang River Mouth, (in Vietnamese). *In Resource and Marine Environment V, Hanoi 1998.*
- Cu N.D 2000. Investigation on geochemical environmental properties of some estuarine regions of Vietnam.(in Vietnamese). *In Resource and Marine Environment VII, Hanoi.*
- Cu N.D. 1993. Geochemical sedimentary characteristics of estuarine region of Hai Phong - Quang Yen. *Ph. D. Thesis, Hanoi University of Science. 183 p.(in Vietnamese).*
- Cu N.D. (ed.) 1993. Inventory of the tidal wetlands in the inshore zone of the Red River Delta. *Archives at the Hai Phong Institute of Oceanology. (in Vietnamese)*
- Cuadros J. and Dudek T. 2006 Fourier investigation of the evolution of the octahedral sheet of kaolinite-smectite with progressive kaolinization. *Clays and clay minerals* 54/ 1: 1-11.
- de Lange G.J., Rispens F.B. 1986. Indication of a diagenetically induced precipitation of a Fe-Si mineral in sediment from the Nares abyssal plain, Western North Atlantic. *Marine Geology* 73: 85-97.
- de Mora S, Fowler SW, Wyse E, Azemard S. 2004. Distribution of heavy metals in marine bivalves, fish and coastal sediments in the Gulf and Gulf of Oman. *Marine Pollution Bulletin* 49/ 5-6: 410-424.
- de Souza C. M. M., Pestana M. H. D. and Lacerda L. D. 1986. Geochemical partitioning of heavy metals in sediments of three estuaries along the coast of Rio de Janeiro (Brazil) *The Science of The Total Environment, Volume 58/1-2: 63-72.*
- Dao P. T. A. 2004. Report on shrimp pond aquaculture in Giao Thuy districts, Nam Dinh provinces (*unpublished data*).
- Delvaux B, Mestdagh MM, Vielvoye L, Herbillon AJ. 1989. XRD, IR and ESR study of experimental alteration of Al-nonttronite into mixed-layer kaolinite/smectite. *Clay Minerals* 24: 617– 30
- Dill K., Rao C.N. 1982. A note on burial diagenesis of clay minerals in the Bengal fan. *Geo. Soc. India*, 23: 561-566
- Douglas L. A. (1989) Vermiculites. *In Minerals in Soil Environments (eds. J. B. Dixon and S. B. Weed), pp. 635–728. Soil Science Society of America, Madison, WI.*
- Drever I.J. 1994. The effect of land plants on weathering rates of silicate minerals. *Geochimica et Cosmochimica Acta* 58/10: 2325-2332.
- Dudek T., Cuadros J., and Fiore S. 2006. Interstratified kaolinite-smectite: Nature of the layers and mechanism of smectite kaolinization. *American Mineralogist* 91: 159 - 170.
- Dyer K.R. 1997. Estuaries, a Physical Introduction. *Second Ed. Wiley, Chichester, 195 p.*
- Eberl D.D., Drits V., Środoń J. 1998. Deducing growth mechanisms for minerals from the shapes of crystal size distributions. *American Journal of Science* 298: 499 - 533
- Evans D. W. and Cutshall, N. H. 1973. Effects of ocean water on the soluble-suspended distribution of Columbia River radionuclides. *In Radioactive Contamination of the Marine Environment: 125-140.*

- Flemming B.W. 1988. Process and pattern of sediment mixing in a microtidal coastal lagoon along the west coast of South Africa. In: *de Boer, P.L., van Gelder, A. & Nio, S.D. (eds), Tide-influenced Sedimentary Environments and Facies. D. Reidel Publ. Co., Dordrecht, p. 275-288.*
- Folk RL, Ward WC .1957. Brazos River bar: a study in the significance of grain size parameters. *Journal of Sedimentary Petrology* 27: 3-26.
- Fried M. and Shaphiro R.E. 1961. Soil-plant relationship in ion uptake. *Annual review of plant physiology* 12: 91- 112.
- Funakawa S., Nambu K., Hirai H. and Kyuma K. 1992. Pedogenic acidification process of forest soils in northern Kyoto. *Soil Science and Plant Nutrition* 39: 677–690.
- Furukawa K., Wolanski E. and Mueller H. 1997. Currents and Sediment Transport in Mangrove Forests. *Estuarine. Coastal and Shelf Science* 44/3: 301-310.
- Ganor J., Mogollon J.L. and Lasaga A.C. 1995. The effect of pH on kaolinite dissolution rates and on activation energy. *Geochimica et Cosmochimica Acta* 59: 1037–1052.
- General Statistics Office of Vietnam 2004. <http://www.gso.gov.vn/> Accessed 24.02.2006.
- GESAMP ET AL., IMO, FAO, UNESCO-IOC, WMO. 1997. "Opportunistic Settlers and the Problem of the Ctenophore Mnemiopsis leidyi Invasion in the Black Sea." *Url: http://gesamp.imo.org/no58/*. [Accessed May 1, 2006]
- Gibbs R.J. 1977b. Clay mineral segregations in the marine environment. *Journal of sedimentary petrology* 47: 237 – 243.
- Gier S. and Johns W.D. 2000. Heavy metal-adsorption on micas and clay minerals studied by X-ray photoelectron spectroscopy. *Applied Clay Science* 16/5-6:289-299.
- Gieskes J.M. 1983. The chemistry of interstitial waters of deep sea sediments: interpretation of the Deep Sea Drilling data. In: *Riley J.P., Chester R., Eds., Chemical oceanography. Academic Press, New York, London, 8. pp: 222-269.*
- Gingele F.X., Deckker, P.D., Hillenbrand, C.-D. 2001. Clay mineral distribution in surface sediments between Indonesia and NW Australia source and transport by ocean currents. *Marine Geology* 179: 135– 146.
- Gjems O. 1970. Mineralogical composition and pedogenic weathering of the clay fraction in podzol soil profiles in Zalesine, Yugoslavia. *Soil Science* 110: 237–243.
- Goldhaber M.B. 2005. Sulphur-rich sediments. In *Elservier's Treatise on Geochemistry. Vol 7.10: 257-284.*
- Golubev S. V., Bauer A. and Pokrovsky O. S. 2006. Effect of pH and organic ligands on the kinetics of smectite dissolution at 25 °C. *Geochimica et Cosmochimica Acta*.70/17: 4436-4451.
- Grim R.E., Johns W.D. 1954. Clay mineral investigations of sediments in the northern Gulf of Mexico. *Clays and Clay minerals, 2nd Natl. Conf. Pergamon, New York. Pp. 81-103.*
- Grim R.E., Loughnan F.C. 1962. Clay minerals in sediments from Sydney Harbour, *Australian Journal of Sedimentary Petrology* 32: 240-248.
- Harbison P. 1986. Mangrove muds—A sink and a source for trace metals. *Marine Pollution Bulletin* 17/6: 246-250
- Hatje V., Payne T. E., Hill D. M., McOrist G., Birch G. F. and Szymczak R. 2003. Kinetics of trace element uptake and release by particles in estuarine waters: effects of pH, salinity, and particle loading. *Environment International* 29/5: 619-629
- Henning K.-H., Störr M. 1986. Electron micrographs (TEM, SEM) of clays and clay minerals. *Akademie-Verlag Berlin (Schriftenreihe für geologische Wissenschaften, Bd. 25): 352 p.*

- Herbert H. J., Kasbohm J., Moog H. C. and Henning K. H. 2004. Long-term behaviour of the Wyoming bentonite MX-80 in high saline solutions. *Applied Clay Science*, 26/ 1-4: *Clays in Natural and Engineered Barriers for Radioactive Waste Confinement*: 275-291.
- Hirai H., Araki S. and Kyuma K. 1989. Clay mineralogical properties of brown forest soils in northern Kyoto with special reference to their pedogenetic process. *Soil Science and Plant Nutrition* 35: 585–596.
- Hirst D. M. 1962a. The geochemistry of modern sediments from the Gulf of Paria—I The relationship between the mineralogy and the distribution of major elements. *Geochimica et Cosmochimica Acta* 26/2: 309-334.
- Hirst D. M. 1962b. The geochemistry of modern sediments from the Gulf of Paria—II The location and distribution of trace elements. *Geochimica et Cosmochimica Acta* 26/11: 1147-1187.
- Hoa N.X. 2001. Investigation on mangrove forest ecosystem in Tuan Le hamlet (Dam Mon) and Nha Phu lagoon (*unpublished data*).
- Hoffman J.C. 1979. An evaluation of potassium uptake by Mississippi river borne clays following deposition in the Gulf of Mexico. *Ph.D. Diss. Case Western*
- Hong P.N. and San H.T. 1993. Mangroves of Vietnam. *International Union for the Conservation of Nature, Bangkok, Thailand*.
- Hori K., Tanabe S., Saito Y., Haruyama S., Nguyen V. and Kitamura A. 2004. Delta initiation and Holocene sea-level change: example from the Song Hong (Red River) delta, Vietnam. *Sedimentary Geology* 164: 237–249.
- Hughes RE, Moore DM, Reynolds RCJr. 1993. The nature, detection, occurrence, and origin of kaolinite/smectite. In *Kaolin Genesis and Utilization*, ed. H Murray, W Bundy, C Harvey, pp. 291– 323. Boulder, CO: Clay Mineral. Soc.
- Hughes R. E., D. M. Moore, Glass, H. D. 1994. Qualitative and Quantitative Analysis of Clay Minerals in Soils: 330-359. In *Amonette J. E. and Zelazny L. W (Eds) Quantitative Methods in Soil Mineralogy. Soil Science Society of America Miscellaneous Publication*.
- Institute of Mechanics. 2000. Report of National project KHCN. 06-10 on Climatology and Oceanography of Vietnam. *Hanoi. In Vietnamese*.
- Jaffé R., Boyer J. N., Lu X., Maie N., Yang C., Scully N. M. and Mock S., 2004. Source characterization of dissolved organic matter in a subtropical mangrove-dominated estuary by fluorescence analysis. *Marine Chemistry, Volume 84, Issues 3-4, Pp.195-210*.
- Jagodziński R. 2005. Petrography and geochemistry of surface sediments from Sunda nad Vietnamese shelves (South China Sea). *Wydawnictwo Naukowe Uniwersytetu Im.Adama Mickiewicza. Seria Geologa Nr 16. 143p*.
- JCPDS International Center for Diffraction Data. 1978. ASTM - set 28 & 29 of the power diffraction file, *USA*.
- JCPDS International Center for Diffraction Data. 1979. Power diffraction file: alphabetical index inorganic materials, *USA*.
- Jeans C.V. 1971. The neoformation of clay minerals in brackish and marine environments. *Clay Minerals* 9: 209-217.
- Jefferson D. A., Tricker M. J. and Winterbottom A. P. 1975. Electron microscopic and Mossbauer spectroscopic studies of iron-stained kaolinite minerals. *Clays and Clay Minerals* 23: 355-360.
- Jokic A., Cutler J. N., Ponomarenko E., van der Kamp G. and Anderson D. W. 2003. Organic carbon and sulphur compounds in wetland soils: insights on structure and

- transformation processes using K-edge XANES and NMR spectroscopy. *Geochemica et Cosmochimica Acta* 67/ 14: 2585-2597.
- Joussein E.; Petit, S.; Churchman, J.; Theng, B.; Righi, D.; Delvaux, B. 2005. Halloysite clay minerals – a review. *Clay Minerals* 40: 383-426.
- Kasbohm J., Lai L.T, Schafmeister M.-T., Hue T. T., Henning K. H. 2003. Mineralogical investigation of soils in selected settlements of the Nam Dinh region, Viet Nam. *Journal of Geology, Series B, No.21*.
- Kasbohm J., Henning, K.H., Herbert, H.-J. 1998. Transmissionselektronenmikro-skopische Untersuchungen am Bentonit MX80. *Ber. Deutsche Ton- und Tonmineralgruppe, Bd. 6, Greifswald*: 228-236.
- Kastner M. 1981. Authigenic silicates in deep-sea sediments: formation and diagenesis. pp. 915-980. *In: Emilliani C., Ed., The sea. Wiley & Sons, New York, 7*.
- Keil R.G., Montlucon D.B., Prahl F.G. and Hedges J.I. 1994. Sorptive preservation of labile organic-matter in marine sediments. *Nature* 370 (6490): 549-552.
- Kemp A.L.W. 1976. Cultural impacts on the geochemistry of sediments in Lake Erie. *Journal of Fishery Research. Board Can.* 33: 440-462.
- Kharkar D.P., Turekian K.K., and Bertine K.K.1968. Stream supply of dissolved silver, molybdenum, antimony, selenium, chromium, cobalt, rubidium and cesium to the oceans. *Geochim Cosmochim Acta* 32 : 285/298.
- Kloprogge J.T., Jansen, J.B.H. Geus, J.W. 1990. Characterization of synthetic Na-beidellite. *Clays and Clay Minerals* 38(4): 409-414.
- Köster H. M. 1977. Die Berechnung kristallchemischer Strukturformeln von 2:1-Schichtsilikaten unter Berücksichtigung der gemessenen Zwischenschichtladungen und Kationenaustauschkapazitäten, sowie die Darstellung der Ladungsverteilung in der Struktur mittels Dreieckskoordinaten. *Clay Minerals* 12: 45-54.
- Krögel F., Flemming B. W. 1998. Evidence for temperature-adjusted sediment distributions in the back-barrier tidal flats of the East Frisian Wadden Sea (southern North Sea). *In: Alexander CR, Davis RA, Henry VJ (eds) Tidalites: processes and products. SEPM Spec Publ* 61: 31-41.
- Krumm S. (1994): WINFIT 1.0 - A Computer Program for X-ray Diffraction Line Profile Analysis. *Acta Universitatis Carolinae Geologica*, 38, XIIIth Conference on Clay Mineralogy and Petrology, Praha, 253-261.
- Lacerda L. D., Carvalho C. E. V., Rezende C. E. and Pfeiffer W. C. 1993. Mercury in sediments from the Paraíba do Sul River continental shelf, S.E. Brazil. *Marine Pollution Bulletin* 26/ 4: 220-222.
- Lai L.T, Kasbohm J., Hue T. T., Quy D. H., Schafmeister M.-T. 2003. Geochemical characterization pathways "production site - water - sediment - soil - food – residents" as basis for an in-situ treatment system in the craft-settlements of Nam Dinh province, *Journal of geology, Series B, No.21/2003*
- Lai.L.T. 2005. Element distribution in suspended matter and bed load sediments of the Red River. *Journal of geology. Series b. Nr. 26*.
- Lanson R. and Champion D. 1991. The IIS-to-illite reaction in the late stage diagenesis. *American Journal of Science* 291: 473-506.
- Larsen G., Chilingar G.V. 1979, 1983. Diagenesis in sediments and sedimentary rocks. *Elsevier, Dev. Sediment.*, 25A: 579p. 25B: 572 p.
- Li Y.H., Burkhardt L. and Teraoka H. 1984. Desorption and coagulation of trace elements during estuarine mixing. *Geochimica et Cosmochimica Acta* 48/0:1879-1884.

- Li Z., Saito Y., Matsumoto E., Wang Y., Tanabe S. and Lan V. Q. 2006. Climate change and human impact on the Song Hong (Red River) Delta, Vietnam, during the Holocene. *Quaternary International* 144/1: 4-28.
- Lippmann F. 1979. Stabilitätsbeziehungen der Tonminerale (Stability diagrams involving clay minerals). 8th Conference of Clay Mineralogy and Petrology, Teplice. N. Jb. Miner. Abh. 136: 287-309.
- Ma C. and Eggleton, R.A. 1999. Surface layer types of kaolinite: A high-resolution transmission electron microscope study. *Clays and Clay Minerals* 47: 181-191.
- Machado W. and Larceda L.D. 2004. Overview of the biogeochemical controls and concerns with trace metal accumulation in mangrove sediments. Pp. 319 – 334. In *Environmental geochemistry in tropical and subtropical environments*. Larceda et al. (eds). Springer.
- Machado W., Silva-Filho E. V., Oliveira R. R. and Lacerda L. D. 2002. Trace metal retention in mangrove ecosystems in Guanabara Bay, SE Brazil. *Marine Pollution Bulletin* 44/11: 1277-1280.
- Mackenzie, F. T., and R. M. Garrels. 1966a. Chemical mass balance between rivers and oceans. *American Journal of Sciences* 264: 507– 525.
- Mackenzie, F. T., and R. M. Garrels. 1966b. Silica-bicarbonate balance in the ocean and early diagenesis. *Journal of Sedimentary Researches*, 36(4). pp. 1075–1084.
- Mackey A. P. and Hodgkinson M. C. 1995. Concentrations and spatial distribution of trace metals in mangrove sediments from the Brisbane River, Australia. *Environmental Pollution* 90/ 2: 181-186.
- Mackey A.P. & Hodgkinson, M. 1996 Assesment of the impact of Naphthalene contamination on mangrove fauna using behavioral bioassays. *Bulletin of Environmental Contamination and Toxicology* 56: 279–286.
- Mackin J.E. Control of dissolved Al distributions in marine sediments by clay reconstitution reactions: experimental evidence leading to a unified theory. *Geochim. Cosmochim. Acta*, 50. pp. 207-214.
- Mackin J.E., Aller R.I. 1984. Dissolved Al in sediment waters of the East China Sea: implications for authigenic mineral formation. *Geochim. Cosmochim. Acta*, 48. pp. 281-297.
- Malla P.B. and Douglas, L.A. 1987a. Identification of expanding layer silicates: Charge density vs. expansion properties. In *8th International Clay Conference* (eds. L. G. Schultz, H. van Olphen, and F. A. Mumpton), pp. 277–283.
- Malla P.B. and Douglas, L.A. 1987b. Problems in identification of montmorillonite and beidellite. *Clays and Clay Minerals* 35(3): 232-236.
- Manjunatha B. R., Shankar R. 1997. The influence of rivers on the geochemistry of shelf sediments, southwestern coast of India. *Environmental Geology* 31/1-2: 107-116.
- Marchand C., Baltzer F., Lallier-Vergès E. and Albéric P. 2004. Pore-water chemistry in mangrove sediments: relationship with species composition and developmental stages (French Guiana). *Marine Geology* 208/2-4: 361-381.
- Marchand C., Lallier-Vergès E., Baltzer F. 2003. The composition of sedimentary organic matter in relation to the dynamic features of a mangrove-fringed coast in French Guiana. *Estuarine, Coastal and Shelf Science* 56/ 1: 119-130.
- Marchand C., Lallier-Vergès E., Baltzer F., Albéric P., Cossa D. and Baillif P. 2006. Heavy metals distribution in mangrove sediments along the mobile coastline of French Guiana. *Marine Chemistry* 98/ 1, 2: 1-17.
- Mathers S., Zalasiewicz, J. 1999. Holocene Sedimentary Architecture of the Red River Delta, Vietnam. *J. Coast. Res.* 15: 314– 325.

- Mathers, S.J., Davies, J., McDonald, A., Zalasiewicz, J.A., Marsh, S. 1996. The Red River Delta of Vietnam. *British Geological Survey Technical Report WC/96/02*, 41 pp. *Change and Asia Pacific Coasts. Proceedings of APN/LOICZ Joint.*
- McLaren P (1981) An interpretation of trends in grain size measures. *Journal of Sedimentary Petrology* 51: 611-624.
- McLaren P, Bowles D. 1985. The effects of sediment transport on grain size distribution. *Journal of Sedimentary Petrology* 55: 457-470.
- Mehra, O.D. and Jackson M.L. 1960. Iron oxide removal from soils and clays by a dithionite-citrate system buffered with sodium bicarbonate. *Clays and Clay Minerals* 5:317-327.
- Meunier A. and Velde B. 1989. Solid solutions in I/S mixed-layer minerals and illite. *American Mineralogist* 74: 1106 – 12.
- Meunier A., Lanson B., and Beaufort D. 2000. Vermiculitization of smectite interfaces and illite layer growth as a possible dual model for illite-smectite illitization in diagenetic environments: a synthesis. *Clay Minerals* 35(3):573-586
- Middleburg, J.J., J. Nieuwenhuize, F.J. Slim and B. Ohowa 1996. Sediment biogeochemistry in an East African mangrove forest (Gazi Bay, Kenya). *Biogeochemistry* 34: 133-155.
- Milliman J.D. and Syvitski J.P.M. 1992. Geomorphic/ tectonic control of sediment discharge to the ocean; the importance of small mountainous rivers. *Journal of Geology* 100: 525–544.
- Millot G. 1970. Geology of Clays: weathering, sedimentology, geochemistry. *Springer, Berlin*. 425 p. *Translated from the French by W.R. Farand and H. Paquet.*
- Millward G. E. and Liu Y. P. 2003. Modelling metal desorption kinetics in estuaries. *The Science of the total environment* 314-316: 613-23.
- Montalto A. Franco and Steenhuis S. Tammo 2004. The link between hydrology and restoration of tidal marshes in the New York/New Jersey estuary. *Wetlands* 24/2: 414-425
- Moore D. E., & Reynolds, R. C., Jr. 1997. X-Ray Diffraction and the Identification and Analysis of Clay Minerals. 2nd Edition, *Oxford University Press*, 378 p
- Moreira-Turcq P., Jouanneau J.M., Turcq B., Seyler P., Weber O. and Guyot J.L. 2004. Carbon sedimentation at Lago Grande de Curuai, a floodplain lake in the low Amazon region: insights into sedimentation rates. *Palaeogeography, Palaeoclimatology, Palaeoecology* 214/1-2: 27-40.
- Morton R.A. 1972. Clay mineralogy of Holocene and Pleistocene sediment. Guadalupe delta of Texas. *Journal of Sedimentary Petrology* , 56. pp. 228-236.
- National report of Viet Nam 2003. On the formulation of a transboundary diagnostic analysis and preliminary framework of a strategic action programme for the south china sea. United nations environment programme - East Asian Areas regional coordinating unit.
- Nesbitt, H.W., and Young, G.M. 1984, Prediction of some weathering trends of plutonic and volcanic rocks based on thermodynamic and kinetic consideration: *Geochimica et Cosmochimica Acta* 48: 1523-1534.
- Newman A.C.D. 1987. Chemistry of Clays and Clay Minerals. *Longman Scientific and Technical, Harlow, Essex, UK*. 480 pp.
- Newman A.C.D. and Brown, G. 1987. The chemical constitution of clays. In A.C.D. Newman (Ed.), *Chemistry of Clays and Clay Minerals*, Mineralogical Society, London. p. 1.128.
- Nghi T. 1989. Evaluation of maturity of unconsolidation sediments and detritic sedimentary rocks based on quantitative method (in Vietnamese). *Journal of Earth's Sciences. Hanoi*.
- Nghi T. 1988. Evolution of coastal sediments of the Red River Delta (in Vietnamese). *Journal of Earth's Sciences. Hanoi*

- Nghi T., Toan N.Q., Thanh D. T., V, Minh N.D. and Vuong N.V. 1991. Quaternary sedimentation of the principal deltas of Vietnam. *Journal of Southeast Asian Earth Sciences* 6/2: 103 - 110
- Ngoi C.V., Nghi T., Nhuan M.T.m Luyen D.V., Duc D.M. 2000. Geodynamics characteristics in Red River delta. *Journal Geology, additional number*, pp 40 - 45
- Nhuan M.T., Ngoc N.T.M., Luyen D.V., Viet P.H., Son V.T., Tien D.M. 2003. Application of organochlorine pesticides and polychlorinated biphenyls as molecular marker for assessment of sediment source, quality and sedimentation rate in Vietnam coast. *VNU Journal of Science. Nat., Sci., & Tech., T.XIX No 2*: 37-45.
- Nhuan M.T., Ninh N.H, Huy L.Q, Sam D.D., Ha T.H., Thanh N.C, Oanh B.K, Nga D.T., Son N.N., Du N.Q. 2003. Report on economic valuation of demonstration wetland sites in Vietnam. *Vietnam wetland component. UNEP/SCS/GEF*. 63 p.
- Nhuan, M.T., Ngoc N.T.M., Luyen D.V. 2002. Geochemical sedimentary evolution of the progress of formation, development and deradation of mangrove forest in the Red River mouth (on example of Namdinh province). *Proceeding of WOTRO conference*. 2002.
- Nolting R. F., Sundby B. and Duinker J. C. 1990. Behaviour of minor and major elements in suspended matter in the Rhine and Meuse rivers and estuary. *The Science of The Total Environment* 97-98: 169-183.
- Novák I., Čičel, B. 1978. Dissolution of smectites in hydrochloric acid: II. dissolution rate as a function of crystallochemical composition. *Clays and Clay Minerals* 26: 431-434.
- Olorunfemi B. N., Fyfe W. S., Etu-Efeotor J. O. and Kronberg B., 1987. Environmental and diagenetic implications for the rare earth element geochemistry of sediments of the Niger Delta. *Journal of African Earth Sciences* 6/6: 861-868.
- Owens J. P.; Stefannson, Karl; and Sirkin, L. A. 1974. Chemical, mineralogic, and palynologic character of the Upper Wisconsinan-Lower Holocene fill in parts of Hudson, Delaware, and Chesapeake estuaries. *Journal of Sedimentary Petrology*, v. 44, no. 2, p. 390-408.
- Padmala D., Maya K., Seralathan P. 1997. Geochemistry of Cu, Co, Ni, Zn, Cd and Cr in the surficial sediments of a tropical estuary, southwest coast of India: a granulometric approach. *Environmental Geology* 31 (1/2): 85 – 93.
- Padmalal D. 1993. Mineralogy and geochemistry of the sediments of Muvattupuzha river and Central Vembanad estuary, Kerala, India. *PhD Thesis (unpublished), Cochin University of Science and Technology, Cochin*, 122 p.
- Padmalal D. and Seralathan P. 1995. Geochemistry of Fe and Mn in the surficial sediments of a tropical river and estuary, India – a granulometric approach. *Environmental Geology* 25/4: 270–276.
- Padmalal D., Maya K., Seralathan P. 1997. Geochemistry of Cu, Co, Ni, Zn, Cd and Cr in the surficial sediments of a tropical estuary, southwest coast of India: a granulometric approach. *Environmental Geology* 31/1-2: 85-93.
- Parra M., Pujos, M. 1998. Origin of late Holocene fine grained sediments on the French Guiana shelf. *Cont. Shelf Res* 18: 1613– 1629.
- Pernetta J. C. and J. D. Milliman. 1995. Land-Ocean Interactions in the Coastal Zone Implementation Plan. *IGBP Report No. 33. Stockholm, IGBP*: 215.
- Pfeiffer E.W. 1984. The conservation of nature in Viet Nam. *Environmental Conservation* 11: 217-221.
- Phai V. V. et al. 1998. Study on morphological changes of river mouths and coastal area of the Red River Delta. *Report of scientific study, Hanoi*, 48 pp. *In Vietnamese*.
- Phai V. V., Hoan N., Truong N.X, Kha N.D. 1997. Topographic changes of river mouths of the Red River Delta and related heavy minerals. *Journal of Science, No6, Vol. XIII, VNU, Hanoi*, p.25-31 (in Vietnamese with English abstract).

- Power M.C. 1954. Clay diagenesis in the Chesapeake bay area. *Clays and Clay minerals*, 2nd Natl. Conf. Pergamon, Oxford, New York. Pp. 68-80.
- Power M.C. 1957. Adjustment of land-derived clays to marine environment. *Journal of Sedimentary Petrology* 27: 355-372.
- Power M.C. 1959. Adjustment of clays to chemical change and the concept of the equivalence level. *Clays and Clay minerals*, 6nd Natl. Conf. Pergamon, Oxford, New York. Pp. 309-326.
- Price N.B. 1976. Chemical diagenesis in sediments. In Riley J.P., Chester R. Eds., *Chemical oceanography* 6: 30: 1-58.
- Prins M.A., Postma, G., Cleveringa, J., Cramp, A., Kenyon, N.H., 2000a. Controls on terrigenous sediment supply to the Arabian Sea during the late Quaternary: the Indus Fan. *Marine Geology* 169: 327– 349.
- Prins, M.A., Postma, G., Weltje, G.J. 2000b. Controls on terrigenous sediment supply to the Arabian Sea during the late Quaternary: the Makran continental slope. *Marine Geology* 169: 351– 371.
- Pruszek Z., Szmytkiewicz M. Hung N.M., and Ninh P.V. 2002. Coastal processes in the Red River Delta area, Vietnam. *Coastal Engineering Journal* 44/ 2: 97 – 126.
- Purkait.B. 2002. Patterns of grain-size distribution in some point bars of the usri river, india. *Journal of sedimentary research* 72/3: 367–375.
- Quyen P.B., Nhan D. D. and San N.V. 1995. Environmental pollution in Vietnam: analytical estimation and environmental priorities. *TrAC Trends in Analytical Chemistry* 14/8: 383-388.
- Rains D. W., Epstein, E. 1967. Preferential absorption of potassium by leaf tissue of the mangrove *Avicennia marina*: an aspect of halophytic competence in coping with salt. *Australian Journal of Biological Sciences*: 20, 847-857.
- Ramsar Wetland Classification System. 1996. Url: <http://www.ramsar.org/> . [Accessed 24.02.2006].
- Rhigi D., Meunier A. 1995. Origin of clays by rock weathering and soil formation. In Velde B. (Ed.) *Origin and mineralogy of clays: New York, Springer-Verlag*, p. 8–42
- Rieder M., Cavazzini, G., D'yakonov, Y.S. et al. 1998. Nomenclature of the micas. *Clay and Clay Minerals* 46: 586-595.
- Rietveld H. M. 1969. A profile refinement method for nuclear and magnetic structures. *J. Appl. Cryst.* 2: 65-71.
- Roberson, H.F. (1974): Early diagenesis; Expansible soil clay sea water reactions. *Journal of Sedimentary Petrology* 44: 441–449.
- Ross R.J. and Mortland M.M. 1966. A soil beidellite. *Proceedings-Soil Science Society of America* 30: 337–343.
- Saad S., Lokman Husain M., Yaacob R. and Asano T. 1999. Sediment accretion and variability of sedimentological characteristics of a tropical estuarine mangrove: Kemaman, Terengganu, Malaysia. *Mangroves and Salt Marshes* 3: 51–58.
- Sato T, Fujii M, Watanabe T, Otsuka R. 1990. Properties of expandable layer in illitization of smectite. *Journal of Mineral society of Japan. Special Issue* 19: 17-22.
- Schimanski A. and Stattegger, K. 2005. Deglacial and Holocene evolution of the Vietnam shelf: stratigraphy, sediments and sea-level change. *Marine Geology* 214: 365–387
- Schroeder P. A. and R. J. Pruett. 1996. Fe ordering in kaolinite: Insights from ²⁹Si and ²⁷Al MAS NMR spectroscopy. *American Mineralogist* 81: 26-38.

- Schultz LG, Shepard AO, Blackmon PD, Starkey HC. 1971. Mixed-layer kaolinite-montmorillonite from the Yucatan Peninsula, Mexico. *Clays and Clay minerals* 19: 137–50.
- Sekhar N. U. 2005. Integrated coastal zone management in Vietnam: Present potentials and future challenges. *Ocean & Coastal Management* 48/9-10: 813-827.
- Sholkovitz E. 1979. Chemical and physical processes controlling the chemical composition of suspended material in the River Tay Estuary. *Estuarine and Coastal Marine Science* 8/6: 523-545.
- Soil Survey Staff 1998. Keys to Soil Taxonomy., 8th ed. Natural Resources Conservation Service., United States Department of Agriculture. *Url: <http://soils.usda.gov/classification/keys>. [Accessed 17 February 2006]*.
- Soil Survey Staff, Official Soil Series Descriptions 2006. Natural Resources Conservation Service, nited States Department of Agriculture. *Url: <http://soils.usda.gov/technical/classification/osd/index.html>" [Accessed 17 February 2006]*.
- Środoń J. 1999a. Nature of mixed-layer clays and mechanisms of their formation and alteration. *Annual Review of Earth and Planetary Sciences* 27: 19-53.
- Środoń J. 1999b. Use of clay minerals in reconstructing geological processes: recent advances and some perspectives. *Clay Minerals* 34: 27-37.
- Środoń J., Elsass F., Mchardy W. J., Morgan D. J. (1992) Chemistry of illite-smectite inferred from TEM measurements of fundamental particles. *Clay Minerals* 27: 137-158.
- Starkey H.C., Blackmon, P.D., & Hauff, P.L. (1984): The routine mineralogical analysis of clay-bearing samples. *Washington, DC, US Geological Survey, 32 p. (US Geological Survey Bulletin 1563)*.
- Talley D.M., North E.W., Juhl A.R., Timothy D.A., Conde D., de Brouwer J.F.C., Brown C.A., Campbell L.M., Garstecki T., Hal C.J. I, Meysman F.J.R., Nemerson D.M., Filho P.W.S. and Wood R.J. 2003. **Research challenges at the land–sea interface, Estuar. Coast. Shelf 58: 699–702.**
- Tam N.D. 1992. Coastal erosion in Vietnam, role of geoscience and CCOP. *Journal of Southeast Asian Earth Sciences* 7/1:82-83
- Tanabe S., Hori K., Saito Y., Haruyama S., Vu V.P. and Kitamura A. 2003. Song Hong (Red River) delta evolution related to millennium-scale Holocene sea-level changes. *Quaternary Science Reviews* 22: 2345–2361.
- Tanabe S., Saito Y., Lan V.Q., Hanebuth J.J.T., Lan N.Q. and Kitamura A. 2006. Holocene evolution of the Song Hong (Red River) delta system, northern Vietnam. *Sedimentary Geology, In Press, Corrected Proof, Available online 19 January 2006*.
- Tang V.T. 1994. Ecosystems in Vietnam estuaries. *Science and Technology Publisher. Vietnam. (In Vietnamese)*
- Thang N.V. (Eds.) 2000. Weathering Crust and Quaternary Sediments Map of Vietnam. *Department of Geology and Minerals of Vietnam, Hanoi. 269 pp. (In Vietnamese)*
- Thanh T. D., Lan T. D. and Huy D. V. 1997. Natural and Human Impact on the Coastal Development of the Red River Delta. *Proc. LOICZ Open Science Meeting, Hanoi.*
- Thanh T. D., Lan, T. D., Huy, D. V. 1997. Natural and Human Impact on the Coastal Development of the Red River Delta. *Proc. LOICZ Open Science Meeting, Hanoi.*
- Thanh T.D., Huy D.V. 2000. Coastal development of the modern Red River delta. *Bulletin of the Geological Survey of Japan* 51, 276.
- Thanh N.H., and Egashira, K. 2000. Clay Mineralogical Composition of Some Fluvisols in Vietnam. *Clay Science* 11: 205-217.
- Thibodeau FR & Nickerson NH 1986. Differential oxidation of mangrove substrate by *Avicennia germinans* and *Rhizophora mangle*. *Amer. J. Bot.* 73: 512–516.

- Thon Nguyen The. 1994. Neotectonic and modern movements in coastal and marginal belt from Mong Cai to Cua Hoi areas. *Journal of Geology A No 223*. pp 1-6. (In Vietnamese).
- Thornton C., Shanahan M., Williams J. 2003. From Wetlands to Wastelands: Impacts of Shrimp Farming. *The Society of Wetland Scientists Bulletin 20/1*: 48-53.
- Thorsten Dittmar, Rubén José Lara and Gerhard Kattner 2001. River or mangrove? Tracing major organic matter sources in tropical Brazilian coastal waters. *Marine Chemistry 73/3-4*: 253-271.
- Tra, H.T.L., Thanh, N.H., and Egashira, K. 2000. Clay Mineralogical Composition of Vietnam Soils Derived from Different Parent Rocks. *Clay Science 11*: 285-297.
- Tri N.H., Adger W.N. and Kelly P.M. 1998. Natural resource management in mitigating climate impacts: the example of mangrove restoration in Vietnam. *Global Environmental Change 8/1*: 49-61.
- Trott L. A. and Alongi D. M. 2000. The Impact of Shrimp Pond Effluent on Water Quality and Phytoplankton Biomass in a Tropical Mangrove Estuary. *Marine Pollution Bulletin 40/11*: 947-951.
- Tuan L.X. and Munekage Y. 2004. Residues of selected antibiotics in water and mud from shrimp ponds in mangrove areas in Viet Nam. *Marine Pollution Bulletin 49/11-12*: 922-929.
- Tuan L.X., Yukihiro M., Dao Q. T. Q., Tho N. H., Dao P. T. A. 2003. Environmental Management in Mangrove Areas. *Environmental Informatics Archives, ISEIS Publication Vol 1*: 38-52.
- Tuyen L.H., Viet P.H., Hung N.V., Hoi N.C., and Dieu L.V. 2001. Research on Hydrochemical Characters and Water Quality in the Coastal Region from Quangninh to Haiphong. *The 3rd UNU-ORI Joint International Workshop for Marine Environment*.
- UNEP 1999. Report of the UNEP Meeting on Early Warning of Emerging Environmental Threats. *UNEP Publication*.
- UNEP 2003. Annual national report on Wetland of Vietnam in 2003.
- van den Bergh G.D., Boer W., Schaapveld M.A.S., Duc D.M. and van Weering Tj.C.E. 2006. Recent sedimentation and sediment accumulation rates of the Ba Lat prodelta (Red River, Vietnam). *Journal of Asian Earth Sciences, In Press, Corrected Proof, Available online 22 May 2006*.
- van der Weijden C. H., Arnoldus M. J. H. L. and Meurs C. J. 1977. Desorption of metals from suspended material in the Rhine estuary. *Netherlands Journal of Sea Research 11/2*: 130-145.
- van Maren D. S., Hoekstra P. 2004. Seasonal variation of hydrodynamics and sediment dynamics in a shallow subtropical estuary: the Ba Lat River, Vietnam. *Estuarine, Coastal and Shelf Science 60/3*: 529-540.
- van Maren D.S. 2006. Water and sediment dynamics in the Red River mouth and adjacent coastal zone. *Journal of Asian Earth Sciences, In Press, Corrected Proof, Available online 30 June 2006*.
- van Maren, D.S. 2005. Barrier formation on an actively prograding delta system: The Red River Delta, Vietnam. *Marine Geology 224*: 123– 143.
- van Maren, D.S., Hoekstra, P., Hoitink, J.F. 2004. Tidal flow asymmetry in the diurnal regime: bed load transport and morphologic changes around the Red River Delta. *Ocean Dynamics 3-4*: 424– 434.
- Veizer J. and Mackenzie F. T. 2005. Evolution of sedimentary rock. *In Elsevier's Treatise on Geochemistry 7-15*: 370-403.
- Velde B. & Brusewitz A. M. 1986. Compositional variation in component layers in natural illite/smectite. *Clays and Clay Minerals 34/6*: 651-657.

- Velde B. 1995. Composition and mineralogy of clay minerals. In Velde, B. (ed.) 1995. *Origin and mineralogy of clays*. New York, Springer-Verlag, p. 8–42.
- Vicente M. A.; Elsass, F.; Molina, E.; Robert, M. 1997. Palaeoweathering in slates from the Iberian Hercynian Massif (Spain): investigation by TEM of clay mineral signatures. *Clay Minerals* 32: 435-451.
- Vietnam Institute of Forest Inventory and Management. 2002. *National investigation on mangrove forest of Vietnam*. Ha Noi. 106p.
- Vietnam Ministry of Fishery. 2000, 2001. Annual statistic investigation.
- Wasserman J. C., Figueiredo A. M. G., Pellegatti F. and Silva-Filho E. V. 2001. Elemental composition of sediment cores from a mangrove environment using neutron activation analysis. *Journal of Geochemical Exploration* 72/ 2: 129-146.
- Weaver C.E. 1989. Clays, muds, and shales. *Developments in sedimentology* 44. Elsevier, Amsterdam, 819 p.
- Wedepohl, K.H. 1960. Spurenanalytische Untersuchungen an Tiefseetonen aus dem Atlantik. *Geochimica et Cosmochimica Acta* 18: 200–231.
- Weltje G. J., Prins M. A. 2003. Muddled or mixed? Inferring palaeoclimate from size distributions of deep-sea clastics. *Sedimentary Geology* 162: 39–62.
- Weltje G.J. 1997. End-member modeling of compositional data: numerical– statistical algorithms for solving the explicit mixing problem. *Journal of Mathematical Geology* 29: 503–549.
- Whitehouse U.G., Jeffrey L.M., Debrecht J.D. 1960. Differential settling tendencies of clay minerals in saline waters. *Clays and Clay Mineral*, 7th Natl. Conf. pp. 1-80.
- Whitehouse UG, McCarter RS (1958) Diagenetic modifications of clay minerals types in artificial sea water. *Proc 5th National Conference on Clays and clay minerals*. Natl Res Council Publ 566. National Academy of Science, Washington, DC, pp 81-119.
- Wieland E. and Stumm W. 1992. Dissolution kinetics of kaolinite in acidic aqueous solutions at 25°C. *Geochimica et Cosmochimica Acta* 56/ 3339–3355.
- Woesten J.H.M., de Willigen P., Tri N.H., Lien T.V., Smith S.V. 2003. Nutrient dynamics in mangrove areas of the Red River Estuary in Vietnam. *Estuarine, Coastal and Shelf Science* 57: 65–72
- Wolanski E. and Ridd P. 1986. Tidal mixing and trapping in mangrove swamps. *Estuarine, Coastal and Shelf Science* 23/6: 759-771
- Worldbank 1996. The World Bank Annual Report. *Washington D.C.*
- World Conservation Monitoring Center 1992. National Biodiversity Profile. *The Socialist Republic of Vietnam, Fevrier*. World Conservation Monitoring Center, Cambridge, UK.
- WOTRO 2000. Annual report 2000 for WOTRO Multidisciplinary Program: Social and environmental implications of Global Change in the Red River Delta. *The Netherland Foundation for Tropical Research*.
- Yang C., Yang L., Yang Y. and Ouyang Z. 2004. Rice root growth and nutrient uptake as influenced by organic manure in continuously and alternately flooded paddy soils, *Agricultural Water Management* 70/1: 67-81.
- Yong N. Raymond and Mulligan N. Catherine 2004. Natural attenuation of contaminants in Soils. *Lewis publishers*. 319 p.
- Zöller M. H. 1993. Charakterisierung von Illitkristallen durch konvergente Elektronenbeugung. In: *Berichte der Deutschen Ton- und Tonmineralgruppe e.V.: 211-220 [Beiträge zur Jahrestagung der DTTG 1992]*.

8 APPENDICES

8.1 Methods

XRF

Table 8.1. Results obtained for the reference material Miramichi River Estuary Sediment (MESS-1) and Baie des Chaleurs (BCSS-1) and real samples in coastline of Vietnam

Element	MESS-1 certificate d value* ($\mu\text{g g}^{-1}$)	MESS-1 measured value ($\mu\text{g g}^{-1}$)	BCSS-1 certificate d value* ($\mu\text{g g}^{-1}$)	BCSS-1 measured value ($\mu\text{g g}^{-1}$)	RRD 1 st ($\mu\text{g g}^{-1}$)	RRD Measurement 2 nd ($\mu\text{g g}^{-1}$)	KH 1 st	KH 2 nd	DL** ($\mu\text{g g}^{-1}$)
Ce	60	79.4	70	46.8	89	78.1	40.8	47.2	
Co	14 ± 1.9	9.9	18 ± 2.1	9.6	13	14	< 5	< 5	< 5
Cr	60 ± 11	56.8	90 ± 14	110.7	85	75.8	17.1	13.4	
La	30	47.6	33	30.8	50	51.2	< 20	22.4	< 20
Nd	40	33.6	30	23.8	37	38.6	27.4	< 20	
Ni	50 ± 2.7	21.23	70 ± 3.6	55.3	37	34.2	< 5	< 5	< 5
Pb	40 ± 6.1	38.802	28 ± 3.4	23.1	72	70.2	27.6	24.5	
V	100 ± 17	72.2	110 ± 4.9	93.5	89	93.2	33.6	33.9	
Zn	200 ± 17	164.3	140 ± 12	93.2	111	107.2	37.4	39.5	
Y	35	37.6	50	26.6	42	44.8	17	21.5	

*: According to NRC (1990)

DL : detection limits of equipment

PCA & EMMA

Notations used in PCA:

Following notations are used for PCA-approach:

Variables: variables were assigned for analyzed parameters. Principal components will be extracted from vectors of variables (Q-mode).

Observations: observations were assigned for analyzed samples. All the observations and components are expressed in standardized form with a mean of zero and a standard deviation of 1.

Principal components: are computed factors from Eigenvectors by PCA, which explained the main trends or characteristics of the original datasets.

Total explained variance: the total variance is explained by each one has to be considered in order to decide how many components are needed to represent the data structure. The total variance is the sum of the variance of each variable. Thus, a model with the 1st components may be adequate to represent the data since it contains components that account for variances greater than 1 (either value greater than 1). These variances are generally attributable to an association of variables.

Number of principal components (f): \leq number of variables (m) and number of observations (n). This number was determined based on the slope of screen plot (Eigenvalues vs. PCs) and the cumulative values of total variables explained, to assure that PCs can explain at least 85% of characteristics and trends caused by the original datasets. This number was also adapted to the assumed number of main factors reveals from other methods (e.g. number of sediment sources or hydraulic modes influencing on grain size data which may be observed in field work, or number of minerals or mineral aggregations influencing on geochemical and mineralogical data which may be determined by XRD, DTA-TG and TEM-EDX methods)

Score matrix and loading matrix: are products of PCA for the original datasets (Figure 8.1)

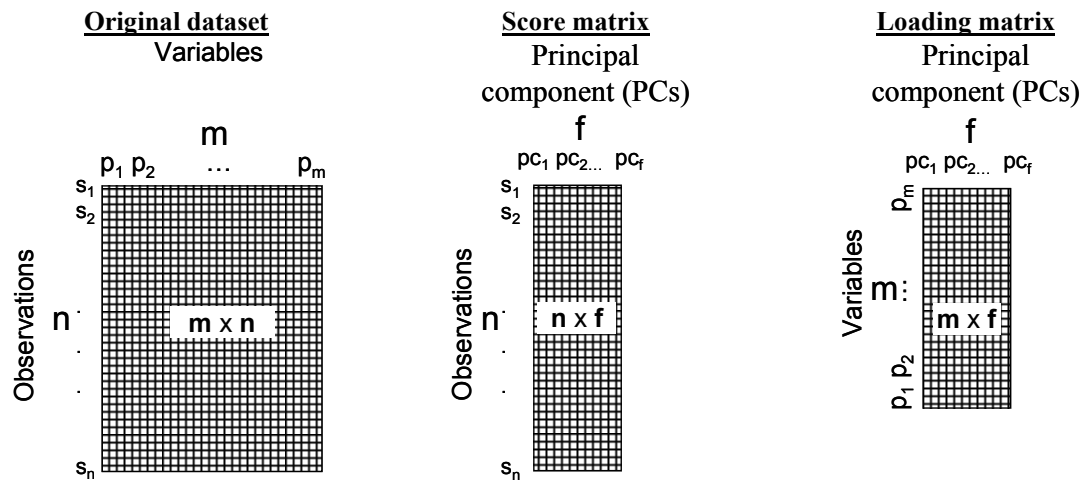


Figure 8.1. Simulation of original dataset and products of PCA –score and loading matrixes

Score matrix: displays the weightings (so-called score) of PCs contributing in the original observations

(samples). A Score Plot allows to see the relative influence of PCs (or underlying processes) on the sample. In a score plot, weightings of samples are presented in spots.

Loading matrix: displays the constituent elements (so-called loading) of the computed PCs. Loadings can be interpreted as the derived relative weightings of the original 'variables' (analyzed parameters) in the derived linear combination that constitutes each PC. A Loading Plot allows to see the relative influence of parameters on the PCs. In loading plot, weightings of variables (analyzed parameters) are presented in vectors.

Biplots of 2 main principal components: is the combination of loading plot (presented in vector) and score plot (presented in spot) which were projected on 2 main principal components (**Figure 8.2**) which allows searching for correlations among samples and analyzed parameters as well as their tendency.

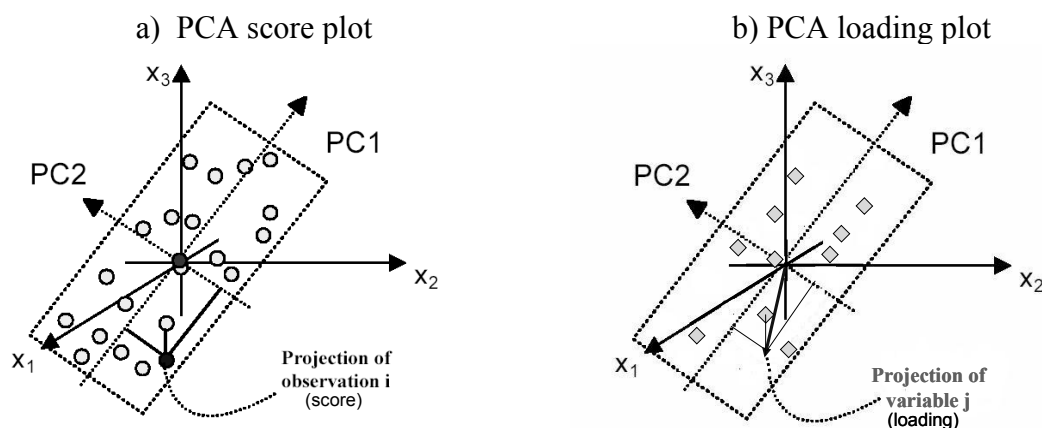


Figure 8.2. PCA score plot (a) and loading plot (b) projected on the two main principal components

Biplots of PCA are a combination of these score and loading plots in one graphic

Table 8.2. Summary on protocol and established commands of PCA and EMMA**a) Protocol of PCA (pca and pcach commands established in MATLAB 7.0.1)**

Step 1: Data scaling (normalisation: values of variables minus average values, afterwards dividing to standard deviation). This step is to give balance for the weightings of variables.

Step 2: Calculation of Eigenvectors

Step 3: Calculation of PCs (loading matrix and score matrix), based on Eigenvectors

Step 4: Based on slope of Scree plot (Eigenvalues vs. PCs) and calculation of total variables explained, chose the number of factors, which could explain at least 80 % of tendencies and characteristics of the dataset for the next steps.

Step 5: Interpretation of loading matrix, searching for prevalent specific events with each PC.

Step 6: Interpretation of biplots (loading and score) to reveal main features or tendency of the datasets

b) Protocol of EMMA (Modeling commands established in MATLAB 7.0.1)

Step 1: Data scaling

Command:

scaled_data = data_scaling(data, option:[scaling_type, centering_shift, total])

There are several types of scaling data (i.e. normalisation to STDV value of 1, normalisation by minus STDV after dividing to average value, etc.). In the measured datasets, the most suitable scaling type was determined by normalisation to value of 1 for STDV of the first loading vector.

Step 2: Data selection

Based on the plot of “scaled_data matrix” irregular data were identified and excluded from the original datasets to obtain “selected-data-matrix”. Scaling this “selected-data-matrix” (step 1) obtains the new “scaled_data matrix” as input positive matrix (V) for step 3.

Step 3: PCA to determine p - optimum number of principal components (factor)

Step 4: Ordinary Least Square Non-negative Matrix Factorization

Command: **[score loading] = posifact (V, p, maxiter, error)**

Input parameters:

- (1) V: input positive matrix of size m-by-n;
- (2) p: number of factors, p normally should be less than m and n;
- (3) maxiter: maximum iteration step;
- (4) error: tolerance of the factorization .

Output:

Two matrices score (m-by-p) and loading (p-by-n) with non-negative elements;

Step 5: Rescaling loading matrix

Command: **loading-matrix = loading*diag(scale))**

The loading matrix displays the contribution of observations in each end member (principal components of EMMA model) whereas the score matrix displays the contribution of end members in each observation (sample).

Step 6: Normalisation of score matrix to total percentage of end-members = 100 %.

Step 7: Interpretation

Principal components in the obtained loading matrix is interpreted as the end-members of the dataset, corresponding to every (or group of coherent members) principal, distinctive feature or principal process which were underlying and governing the dataset through analytical parameters.

Scores of end members, when having been normalised to total percentage of end-members = 100 %, express their proportional contribution in each sample.

Table 8.3. Rotated principal component matrix – reveals from PCA for chemical parameters of sediments in Dam Mon and Nha Phu

Total variance explained	Dam Mon				Nha Phu			
	PC1	PC2	PC3	PC4	PC1	PC2	PC3	PC4
	61.7%	15.8%	9.4%	4.1%	67.3%	10.9%	10.0%	5.2%
SiO ₂	-0.71	-0.41	-0.26	-0.39	-0.69	-0.47	-0.26	-0.47
TiO ₂	0.89	0.13	0.37	0.05	0.48	0.58	0.59	0.23
Al ₂ O ₃	0.58	0.79	-0.11	0.07	0.64	0.54	0.32	0.36
Fe ₂ O ₃	0.69	0.67	0.15	0.14	0.66	0.63	0.29	0.21
MnO	0.84	0.30	0.41	0.06	0.35	0.76	0.43	0.23
MgO	0.19	0.93	0.18	0.09	0.56	0.69	0.32	0.30
CaO	0.02	0.30	0.81	-0.30	0.05	0.92	-0.06	-0.14
Na ₂ O	0.39	0.48	-0.14	0.70	0.93	0.07	-0.05	-0.01
K ₂ O	-0.16	0.08	-0.90	-0.15	-0.08	-0.09	-0.95	-0.16
P ₂ O ₅	0.32	0.76	0.11	0.40	0.77	0.56	0.18	0.08
LOI	0.85	0.39	-0.06	0.26	0.86	0.15	0.23	0.24
H ₂ O	0.84	0.25	-0.21	0.20	0.15	0.01	0.18	0.95

*High correlation coefficients of element with principal component (PC) were marked in **bold***

Table 8.4. Rotated principal component matrix – reveals from PCA for chemical parameters of sediments in Dam Mon and Nha Phu

Total variance explained	Dam Mon			Nha Phu		
	F1	F2	F3	F1	F2	F3
	62.6%	15.4%	6.9%	61.5%	10.8%	8.6%
Pb	0.93*	0.16	0.08	0.79	0.36	0.23
Zn	0.87	0.34	0.14	0.93	0.25	0.23
Cr	0.95	0.1	0.1	0.92	0.11	0.19
Ni	0.94	0.1	-0.01	0.84	0.13	0.28
Rb	0.56	0.72	0.16	0.41	0.49	0.47
Sr	0.07	0.85	0.28	0.39	0.59	-0.56
Ba	0.87	-0.03	-0.18	0.42	0.81	0.1
Y	0.72	0.56	0.23	0.87	0.28	0.16
Zr	-0.18	0.11	0.86	-0.37	-0.25	-0.76
Nb	0.72	0.46	0.42	0.93	0.01	0.13
V	0.94	0.26	0.13	0.92	0.14	0.23
Ga	0.62	0.74	0.15	0.9	0.14	0.34
Ce	0.67	0.56	0.38	0.9	0.11	0.11
U	-0.03	0.83	-0.02	0.24	0.02	0.55
Th	0.4	0.21	0.64	0.51	-0.67	-0.25

*High correlation coefficients of element with principal component (F) were marked in **bold***

8.2 Results

Table 8.5. Correlation matrix of the major and minor elements in the coastline of Vietnam

	SiO ₂	TiO ₂	Al ₂ O ₃	Fe ₂ O ₃	MnO	MgO	CaO	Na ₂ O	K ₂ O	P ₂ O ₅	LOI	H ₂ O	Pb	Cr	Zn	Ni	Rb	Sr	Ba	Y	Zr	Nb	V	Ga	Ce	U	Th
SiO ₂	1.00																										
TiO ₂	-0.69	1.00																									
Al ₂ O ₃	-0.98	0.69	1.00																								
Fe ₂ O ₃	-0.94	0.80	0.96	1.00																							
MnO	-0.89	0.88	0.91	0.96	1.00																						
MgO	-0.78	0.83	0.81	0.91	0.90	1.00																					
CaO	-0.69	0.47	0.68	0.67	0.67	0.54	1.00																				
Na ₂ O	-0.81	0.35	0.77	0.66	0.56	0.42	0.55	1.00																			
K ₂ O	-0.73	0.29	0.76	0.67	0.59	0.39	0.55	0.74	1.00																		
P ₂ O ₅	-0.66	0.82	0.69	0.83	0.83	0.90	0.42	0.33	0.44	1.00																	
LOI	-0.89	0.54	0.85	0.78	0.68	0.55	0.55	0.87	0.63	0.43	1.00																
H ₂ O	-0.59	0.29	0.52	0.42	0.40	0.37	0.22	0.42	0.26	0.19	0.53	1.00															
Pb	-0.74	0.76	0.78	0.86	0.87	0.86	0.40	0.35	0.52	0.87	0.50	0.37	1.00														
Cr	-0.62	0.85	0.64	0.80	0.82	0.91	0.33	0.21	0.32	0.95	0.35	0.27	0.85	1.00													
Zn	-0.89	0.81	0.92	0.97	0.94	0.92	0.59	0.57	0.63	0.89	0.68	0.39	0.91	0.85	1.00												
Ni	-0.56	0.76	0.59	0.74	0.75	0.86	0.28	0.18	0.33	0.94	0.26	0.23	0.84	0.96	0.83	1.00											
Rb	-0.87	0.52	0.90	0.85	0.78	0.64	0.63	0.78	0.94	0.63	0.73	0.36	0.69	0.54	0.83	0.54	1.00										
Sr	-0.76	0.32	0.75	0.67	0.61	0.42	0.87	0.77	0.77	0.29	0.72	0.30	0.35	0.18	0.57	0.14	0.78	1.00									
Ba	-0.36	0.48	0.44	0.54	0.54	0.63	0.17	0.03	0.38	0.70	0.11	0.07	0.73	0.72	0.61	0.76	0.46	0.05	1.00								
Y	-0.90	0.79	0.91	0.95	0.93	0.87	0.60	0.63	0.64	0.81	0.74	0.39	0.85	0.78	0.94	0.72	0.81	0.59	0.53	1.00							
Zr	-0.14	0.41	0.08	0.12	0.22	-0.05	0.28	0.24	0.19	0.07	0.23	-0.13	-0.03	0.02	0.07	-0.06	0.17	0.29	-0.17	0.13	1.00						
Nb	-0.84	0.88	0.85	0.89	0.91	0.82	0.61	0.57	0.55	0.79	0.69	0.34	0.77	0.78	0.90	0.71	0.75	0.56	0.47	0.89	0.34	1.00					
V	-0.76	0.85	0.79	0.90	0.89	0.92	0.45	0.39	0.50	0.96	0.52	0.32	0.92	0.96	0.94	0.93	0.70	0.36	0.72	0.88	0.04	0.85	1.00				
Ga	-0.96	0.67	0.98	0.95	0.89	0.81	0.65	0.77	0.74	0.71	0.82	0.48	0.75	0.66	0.92	0.63	0.90	0.73	0.41	0.90	0.07	0.86	0.80	1.00			
Ce	-0.92	0.83	0.91	0.93	0.91	0.82	0.60	0.72	0.61	0.74	0.82	0.44	0.77	0.71	0.90	0.64	0.79	0.64	0.39	0.91	0.30	0.89	0.81	0.89	1.00		
U	-0.53	0.24	0.51	0.44	0.36	0.27	0.32	0.62	0.46	0.19	0.57	0.19	0.18	0.16	0.42	0.15	0.54	0.50	0.02	0.41	0.18	0.40	0.27	0.58	0.47	1.00	
Th	-0.55	0.50	0.53	0.51	0.56	0.41	0.42	0.50	0.35	0.35	0.50	0.32	0.37	0.33	0.46	0.23	0.46	0.41	0.03	0.50	0.33	0.54	0.40	0.52	0.56	0.18	1.00

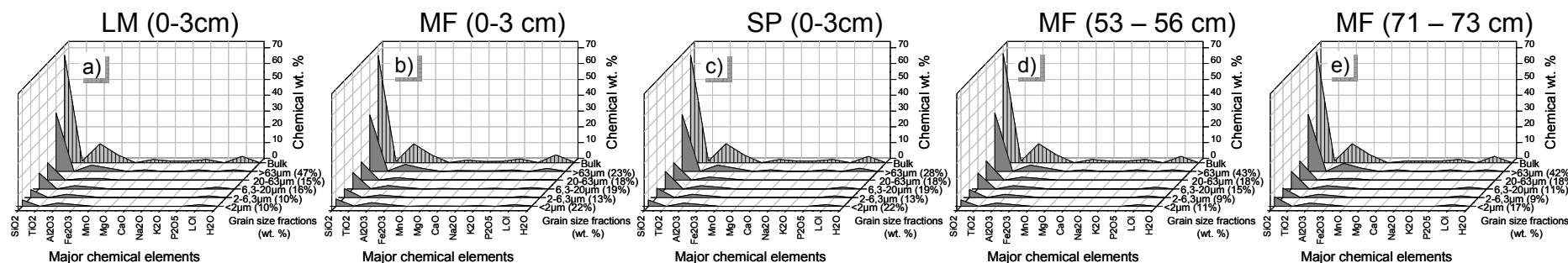


Figure 8.3. Concentrative contribution of major elements from grain size fractions to the bulk of mudflat sediments in the Red River Delta

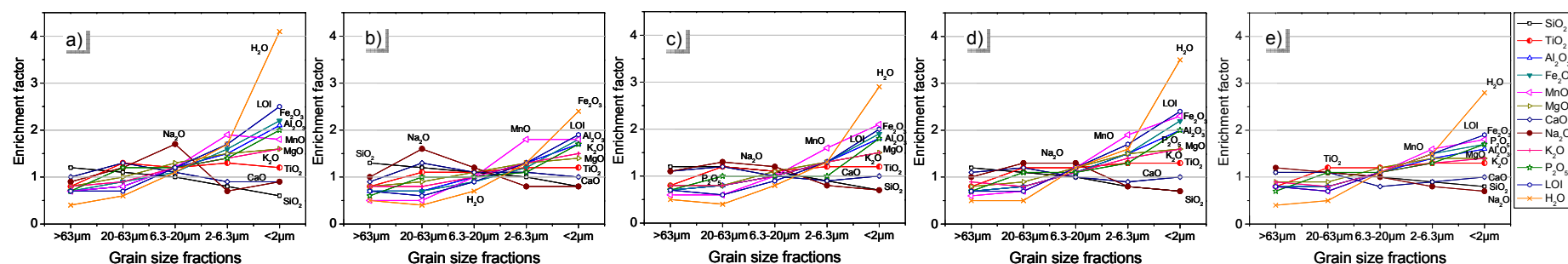


Figure 8.4. Concentrative enrichments major elements in grain size fractions in comparison to the bulk of mudflat sediments in RRD

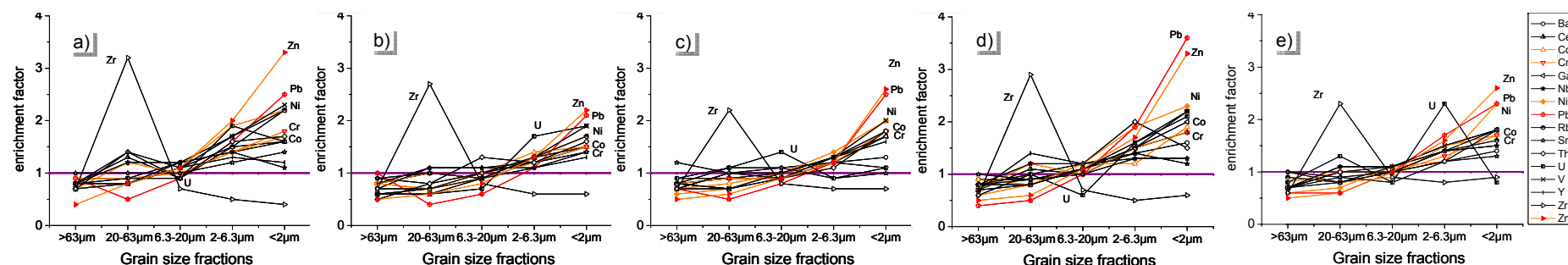


Figure 8.5. Concentrative enrichments minor elements in grain size fractions in comparison to the bulk of mudflat sediments in RRD

Remark: a) Surface of low tidal mudflat (LM) profile (0-3 cm); b) Surface of mangrove forest (MF) profile (0-3 cm); c) Surface of shrimp pond (SP) profile (0-3 cm); d) interval of 53 – 56 cm depth in mangrove forest profiles; e) interval of 71 – 73 cm depth in mangrove forest profiles

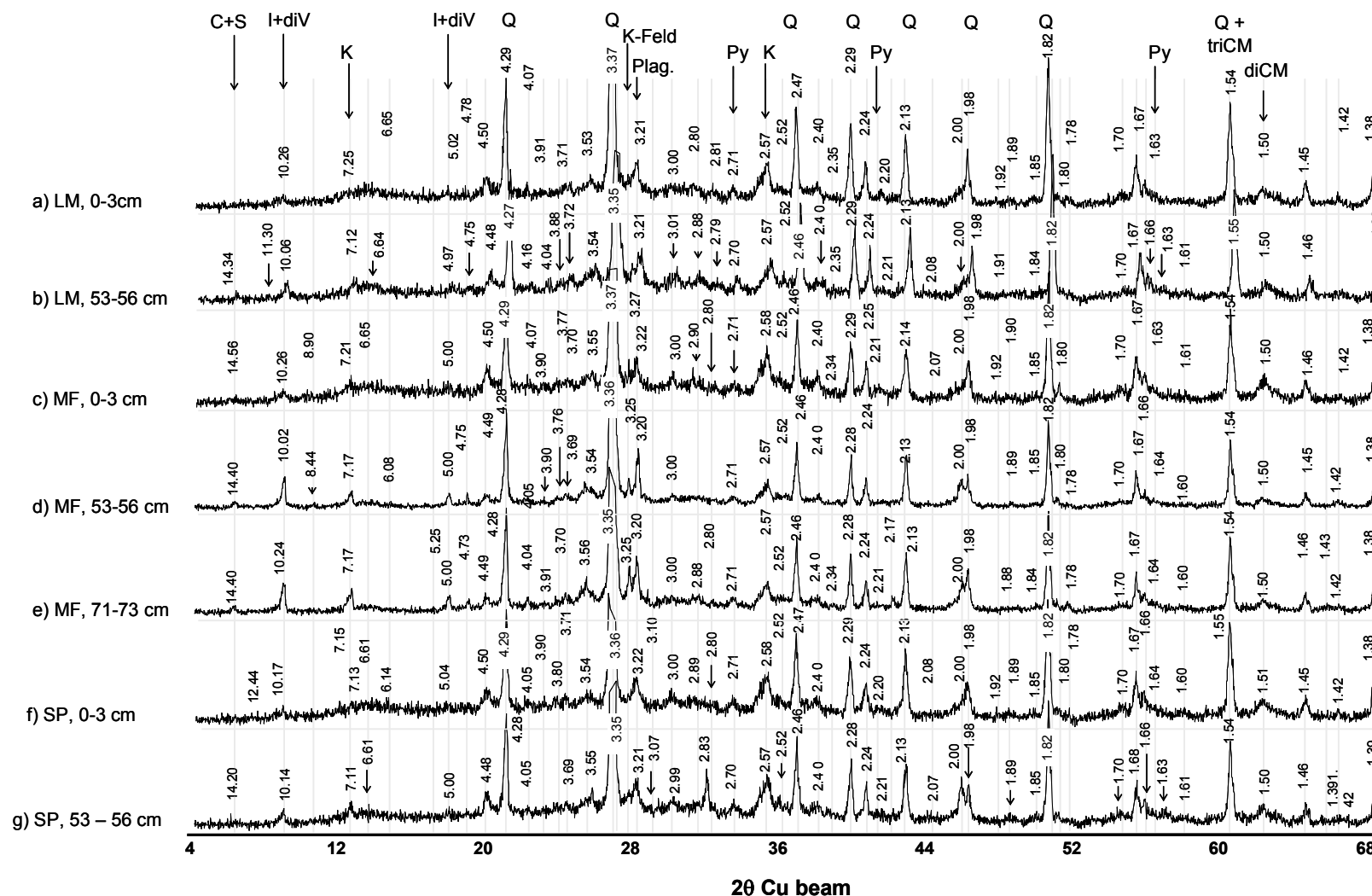


Figure 8.6. XRD patterns of powder, random oriented mount specimen of bulk sample from muddy sediment profiles in the estuary of the Red River Delta

Measurement by SIEMENS D-5000.C: Chlorite; S: Smectite; K: Kaolinite; I: illite; diV: dioctahedral vermiculite; Q: quartz; K-Feld: K-Feldspar; Plag: Plagioclase; Py: Pyrite; triCM: trioctahedral clay mineral; diCM: dioctahedral clay mineral

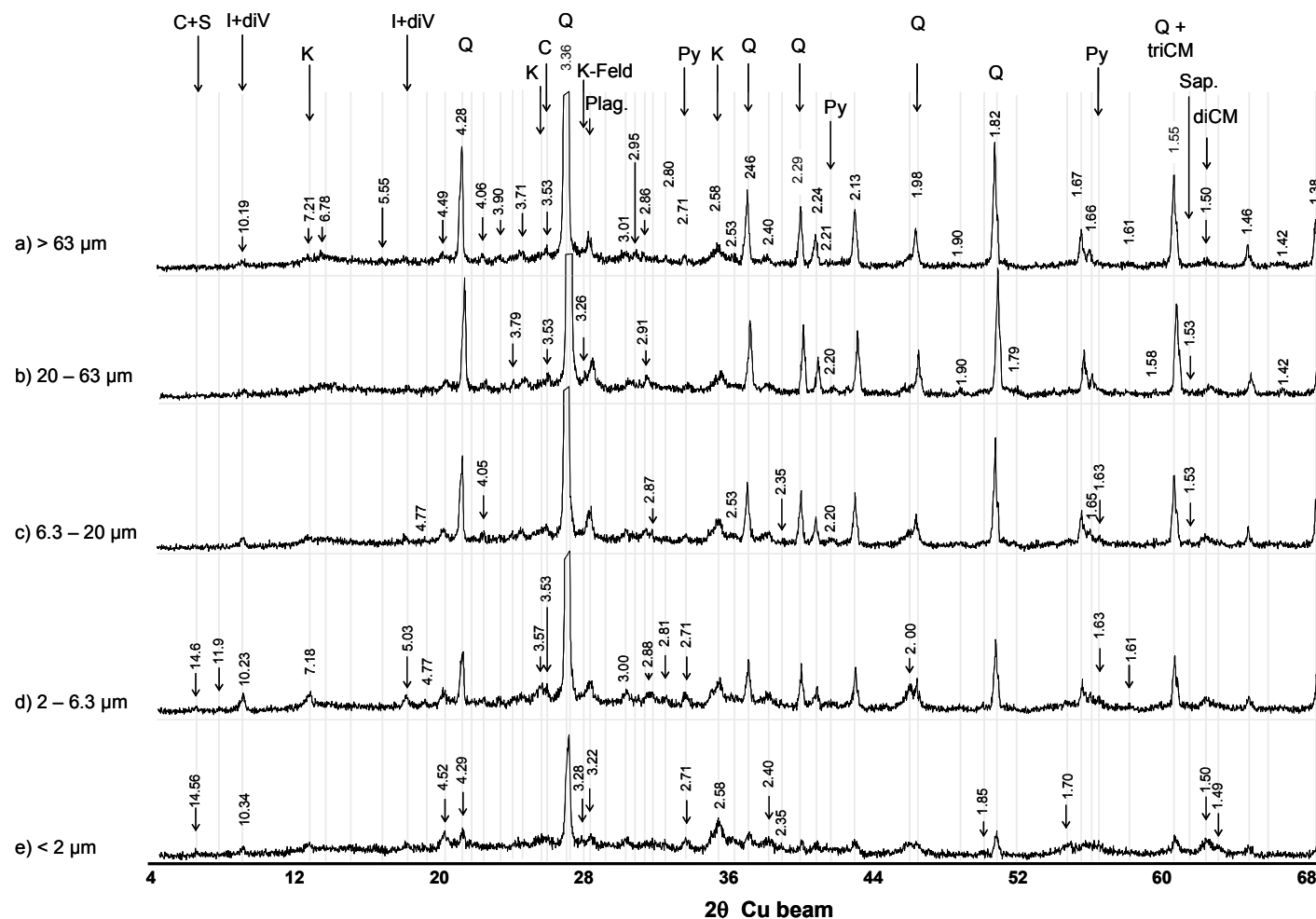


Figure 8.7. XRD- powder, random oriented mount patterns of grain-size fractions separated from bulk, surface sediment (0-3cm) in mangrove forest of the Red River Delta

Separation by Atterberg sedimentation method; Measurement by SIEMENS D-5000.; a) > 63 μm fraction (22.5 % weight of bulk); b) 20 -63 μm fraction (18.3 % weight of bulk); c) 6.3 -20 μm fraction (25.0 % weight of bulk); d) 2 – 6.3 μm fraction (12.5 % weight of bulk); e) <2 μm fraction (21.5 % weight of bulk); C: Chlorite; S: Smectite; K: Kaolinite; I: illite; diV: dioctahedral vermiculite; Q: quartz; K-Feld: K-Feldspar; Plag: Plagioclase; Py: Pyrite; triCM: trioctahedral clay mineral; diCM: dioctahedral clay mineral; Sap: Saponite

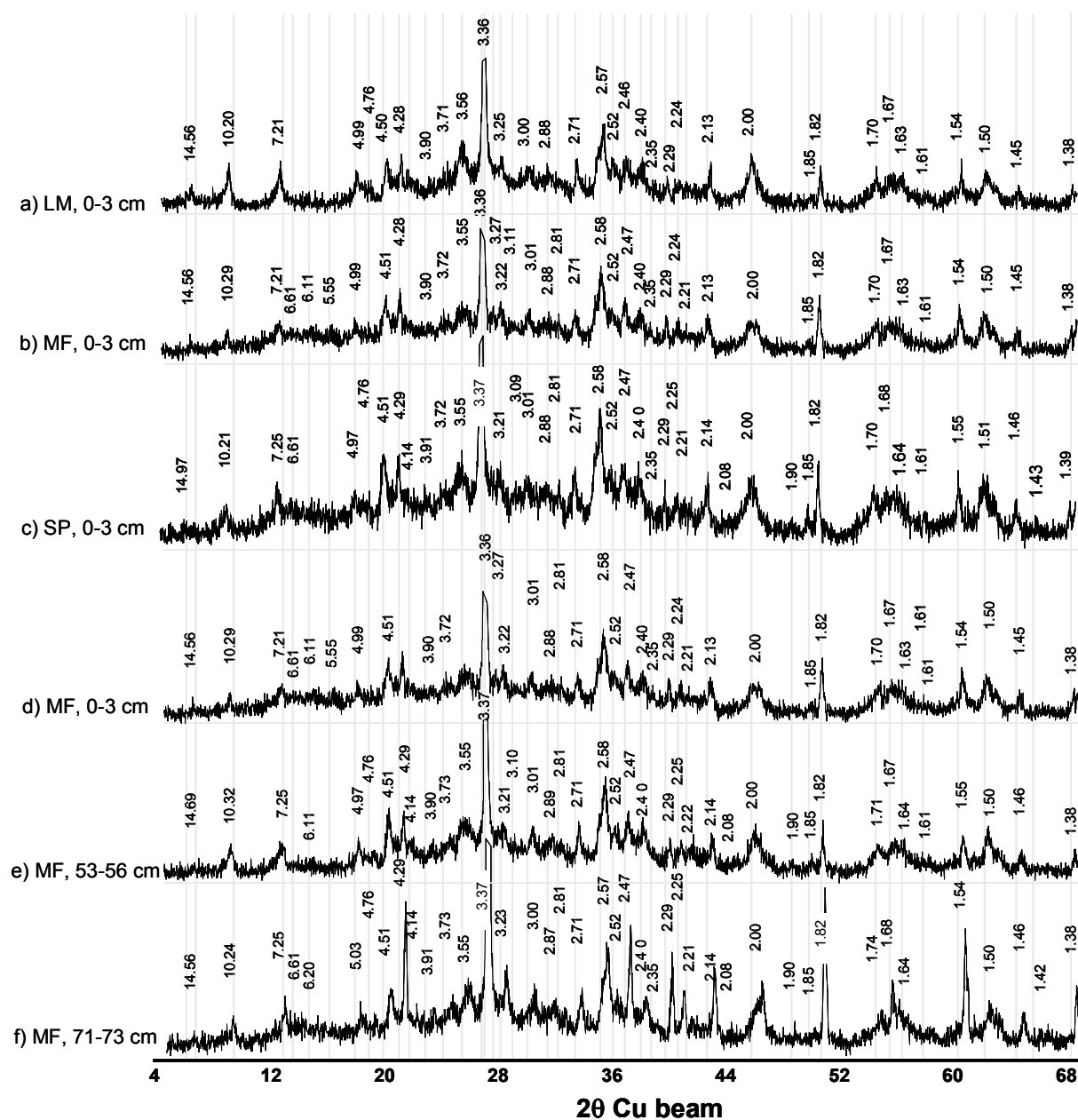


Figure 8.8. XRD patterns of powder, random oriented mount specimen of clay fractions (<2 μ m) dispersed from muddy sediment profiles in the estuary of the Red River Delta

Measurement by SIEMENS D-5000; a, b, c: Surface sediments in low tidal mudflat, mangrove forest and shrimp pond, respectively; d, e, f: Intervals along the depth in mangrove forest sediment profile

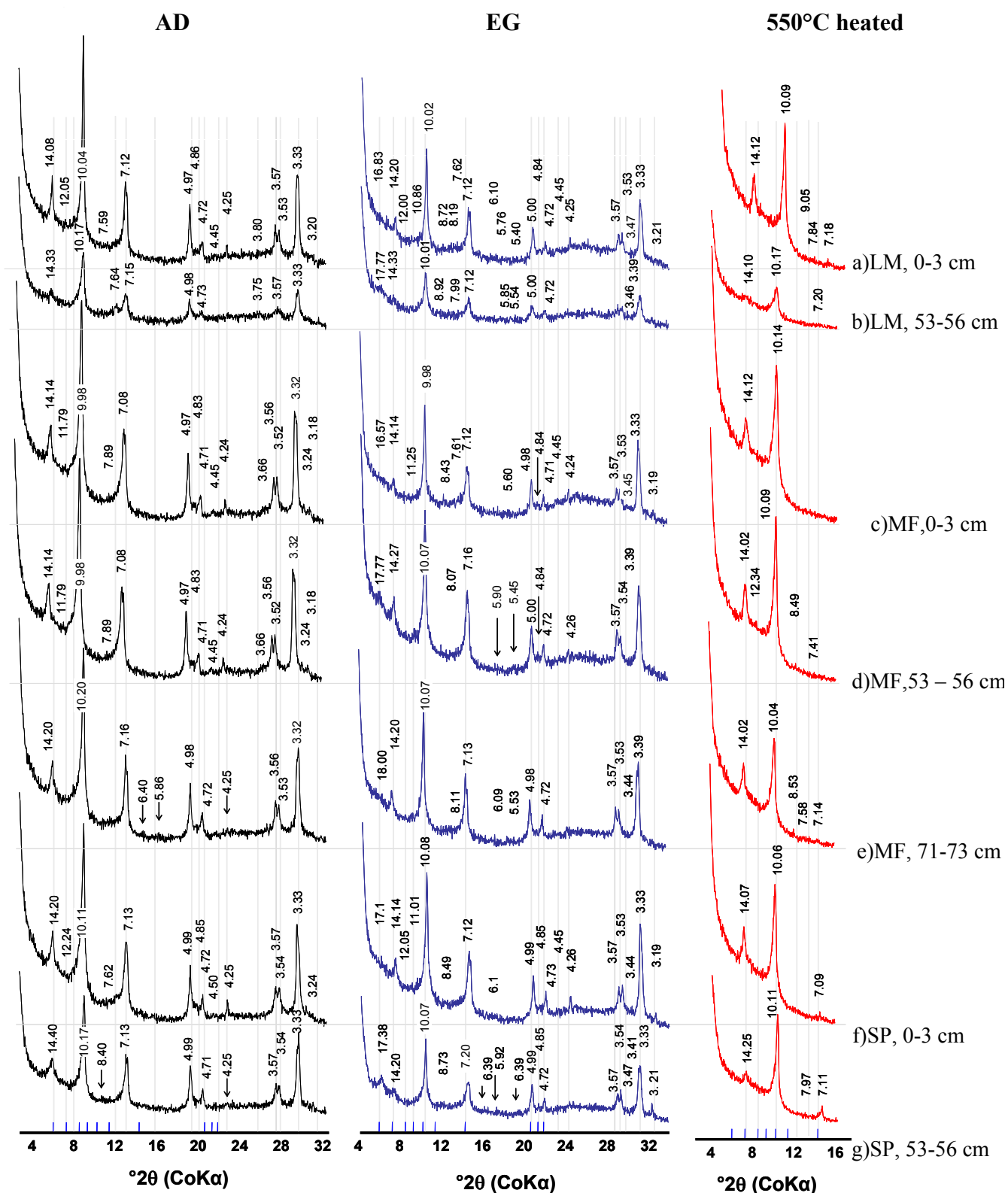


Figure 8.9. XRD patterns of oriented mount specimens of clay fractions (<2μm) dispersed from muddy sediment profiles in estuary of the Red River Delta

Measurement by HZG4/Seifert C3000.; a, b) Low tidal mudflat profile (LM); c,d,e) Mangrove forest profile (MF); f,g) Shrimp pond profile (SP)

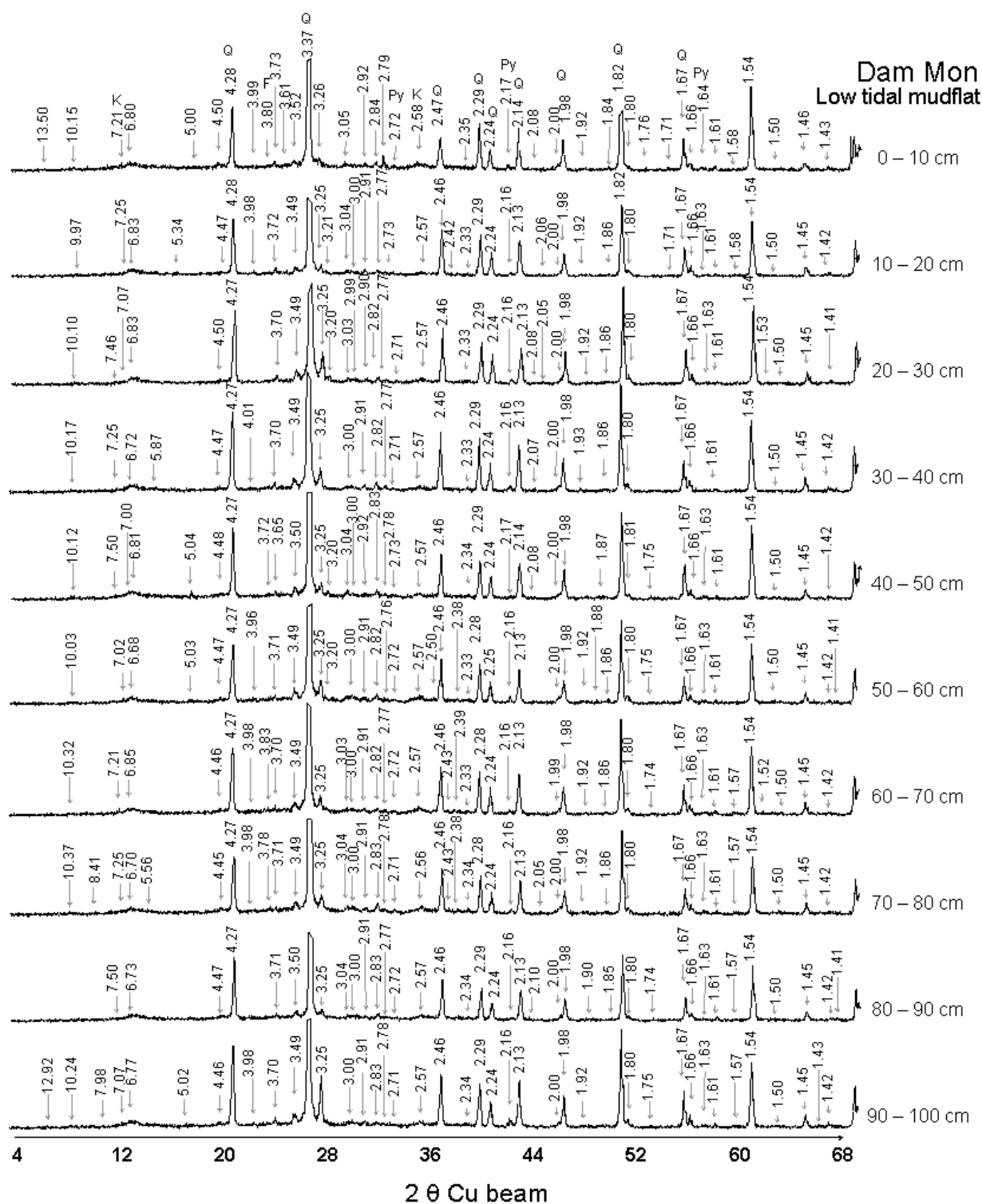


Figure 8.10. XRD patterns of powder, random oriented mount specimen of clay fractions (<2 μ m) dispersed from muddy sediment in low tidal mudflat profile in Dam Mon

Measurement by SIEMENS D-5000

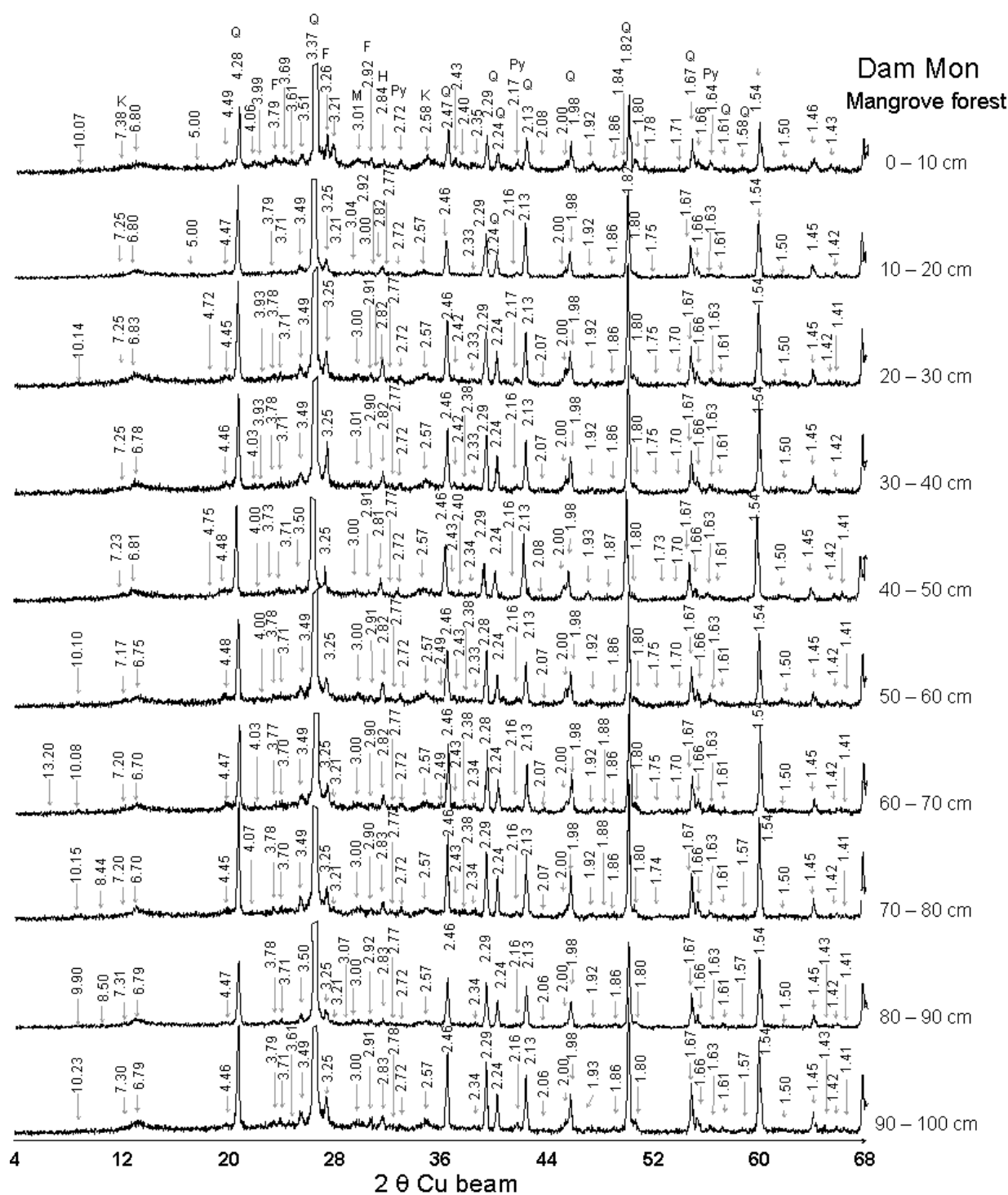


Figure 8.11. XRD patterns of powder, random oriented mount specimen of clay fractions (<2 μ m) dispersed from muddy sediment in mangrove forest profile in Dam Mon

Measurement by SIEMENS D-5000

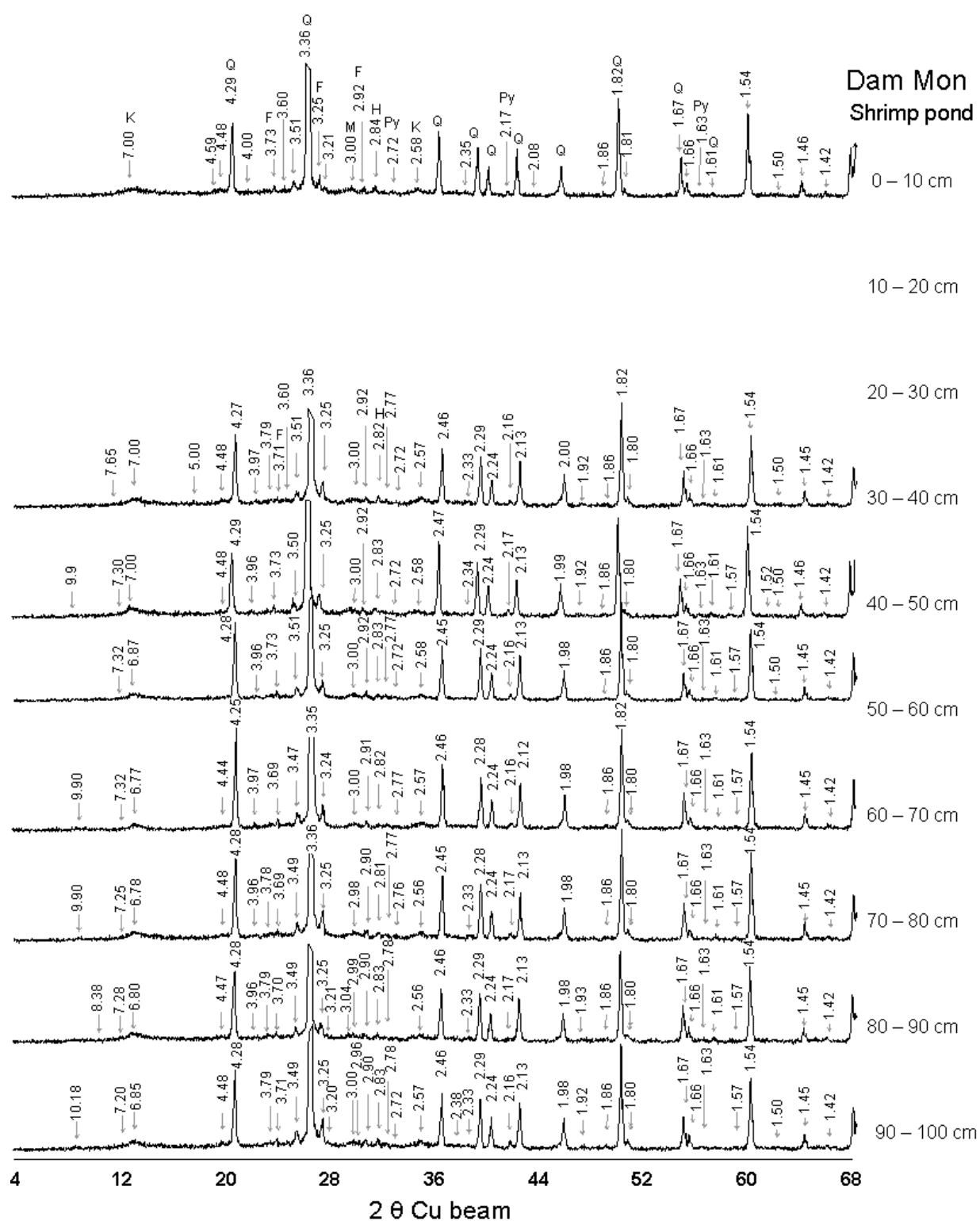


Figure 8.12. XRD patterns of powder, random oriented mount specimen of clay fractions (<2 μ m) dispersed from muddy sediment in shrimp pond profile in Dam Mon

Measurement by SIEMENS D-5000

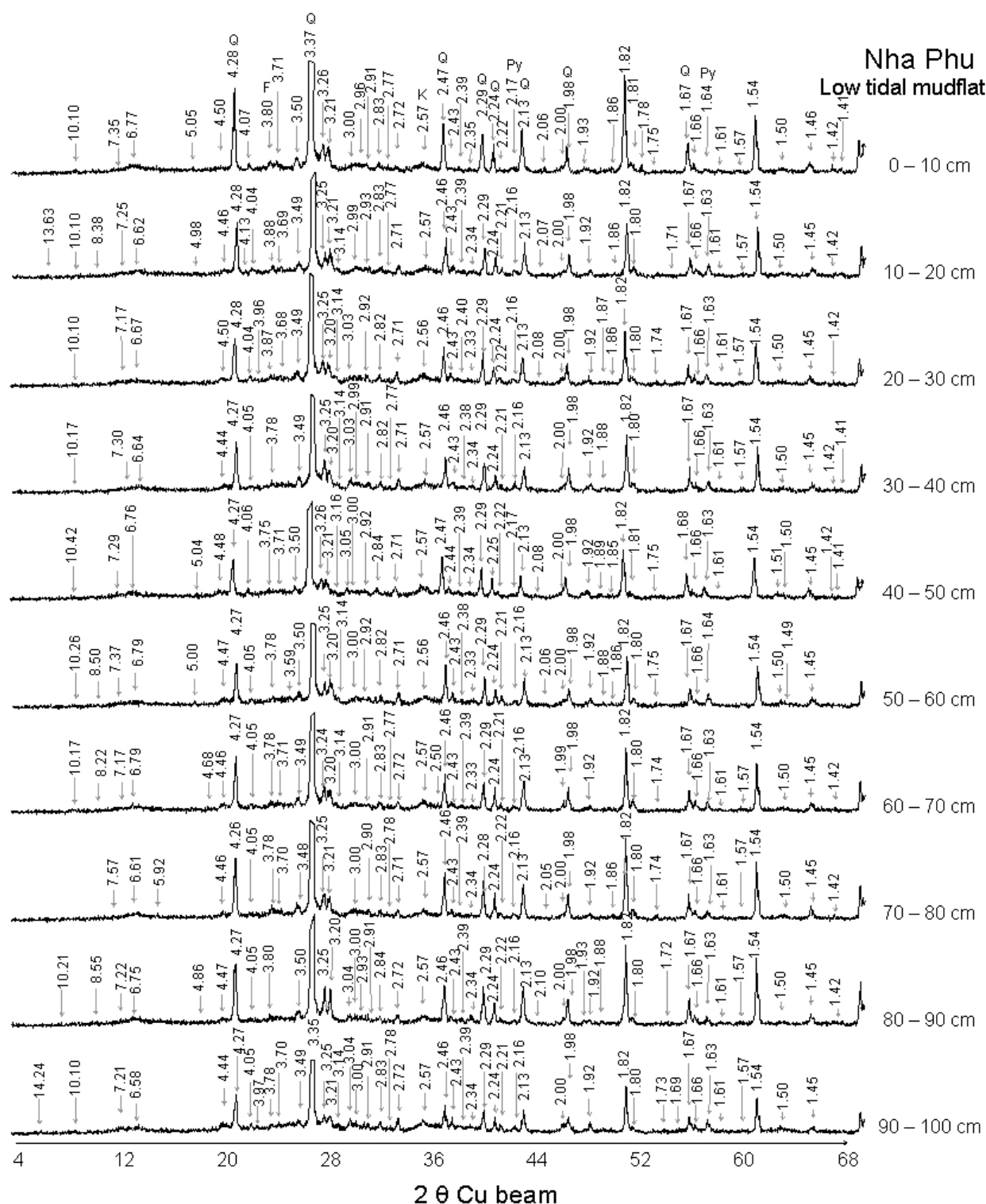


Figure 8.13. XRD patterns of powder, random oriented mount specimen of clay fractions (<2 μ m) dispersed from muddy sediment in low tidal mudflat profile in Nha Phu

Measurement by SIEMENS D-5000

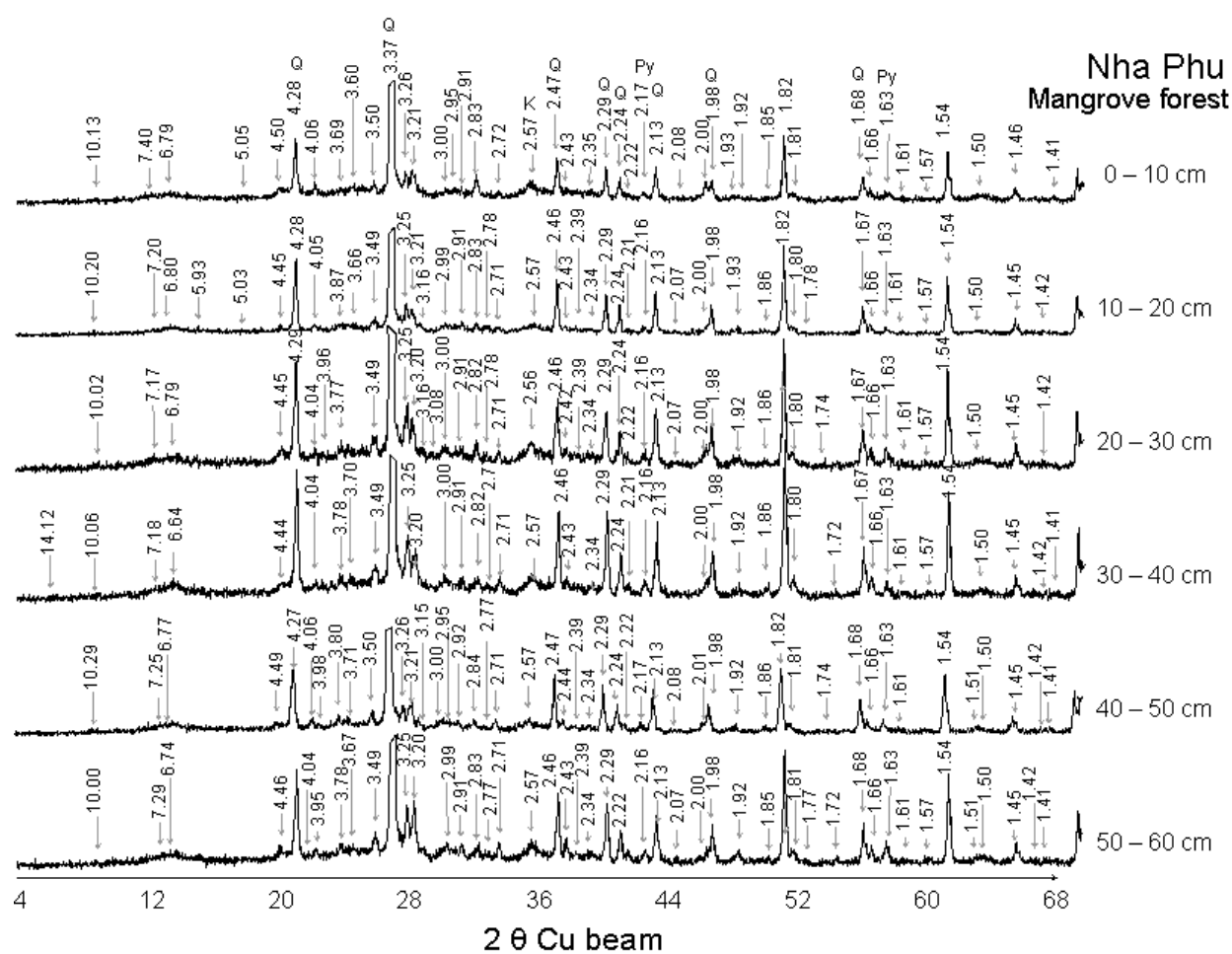


Figure 8.14. XRD patterns of powder, random oriented mount specimen of clay fractions (<2 μ m) dispersed from muddy sediment in mangrove forest profile in Nha Phu

Measurement by SIEMENS D-5000

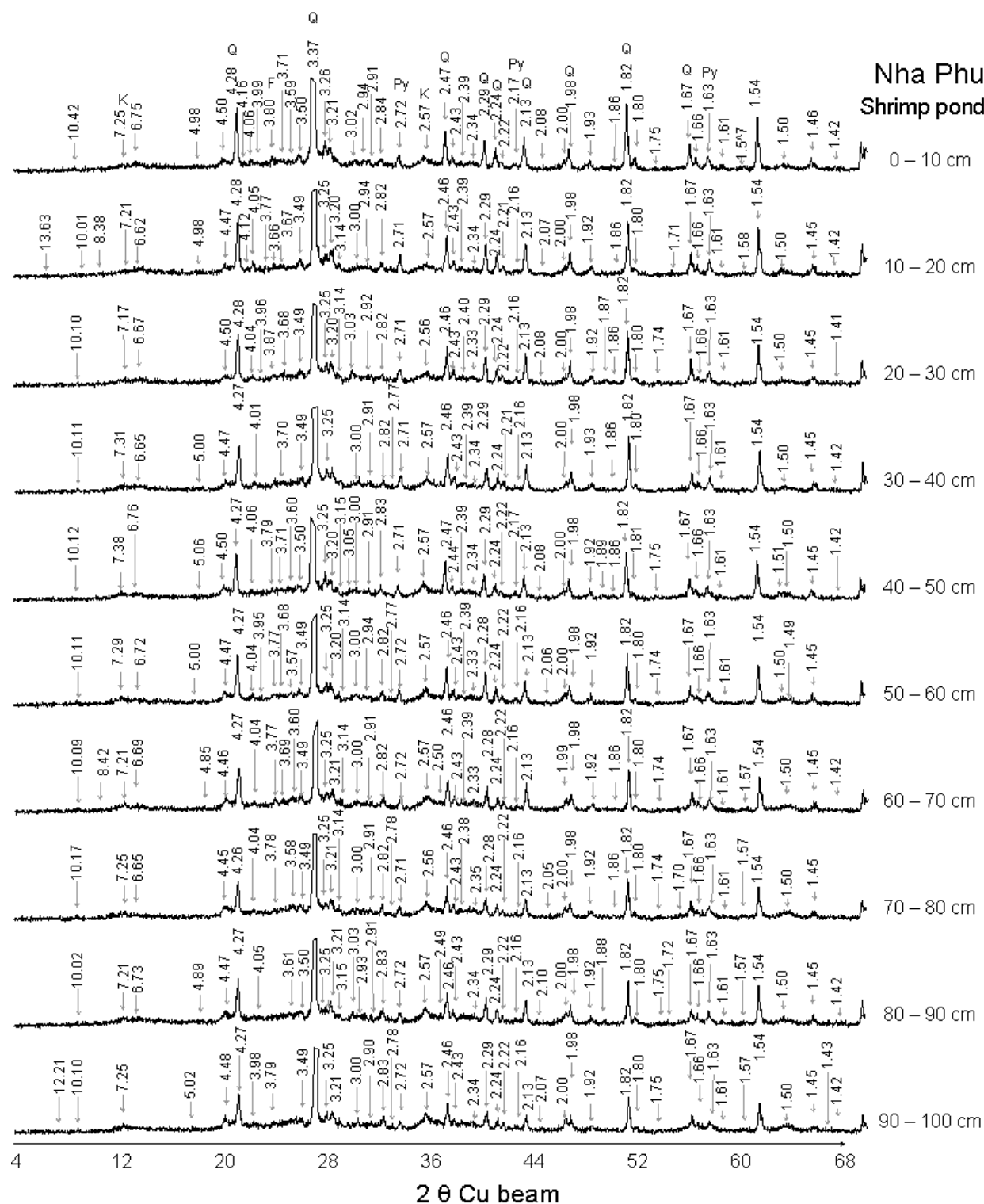


Figure 8.15. XRD patterns of powder, random oriented mount specimen of clay fractions (<2 μ m) dispersed from muddy sediment in shrimp pond profile in Nha Phu

Measurement by SIEMENS D-5000

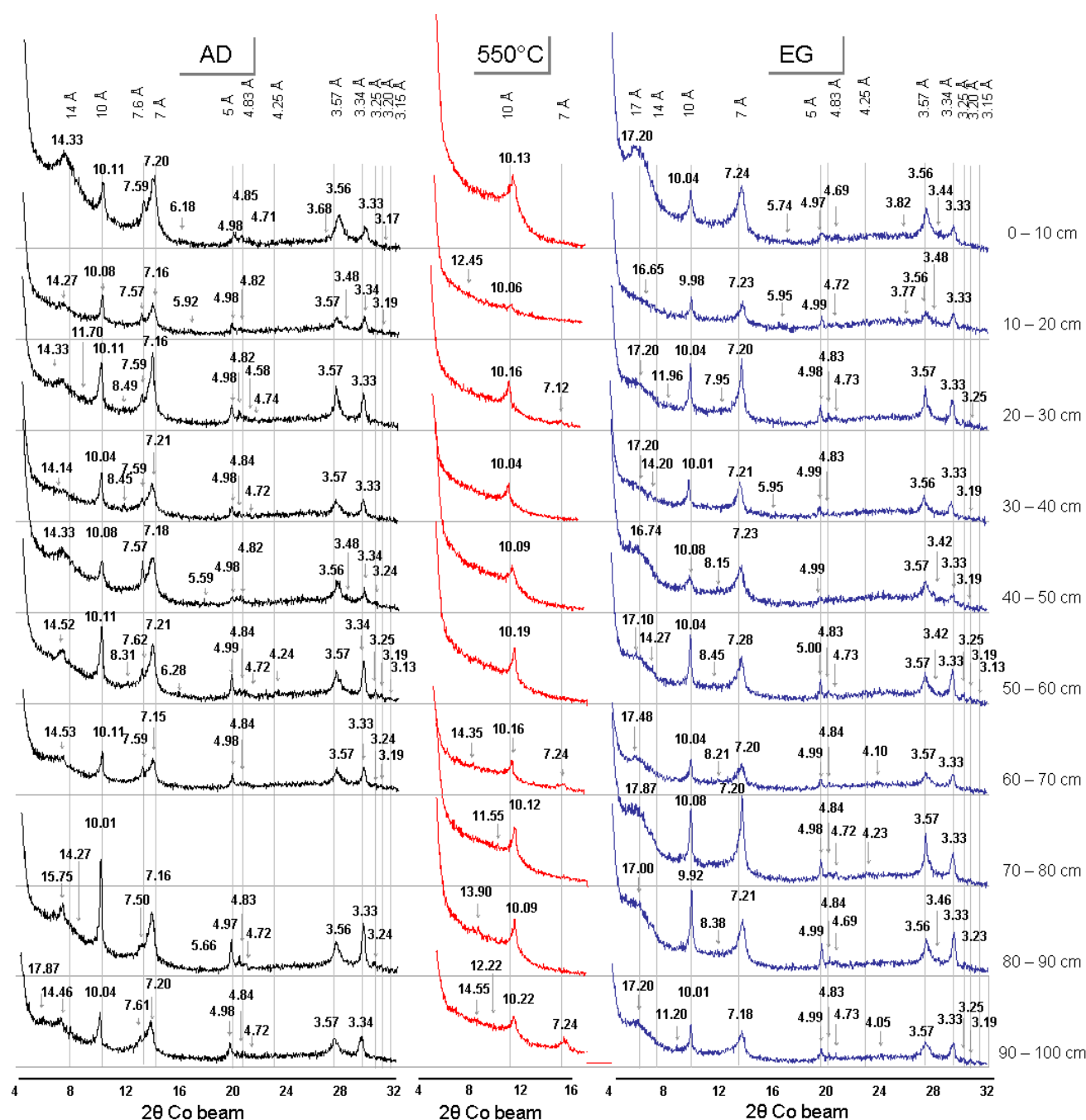


Figure 8.16. XRD pattern of oriented mount specimens for sediment samples in low tidal mudflat profile of Dam Mon

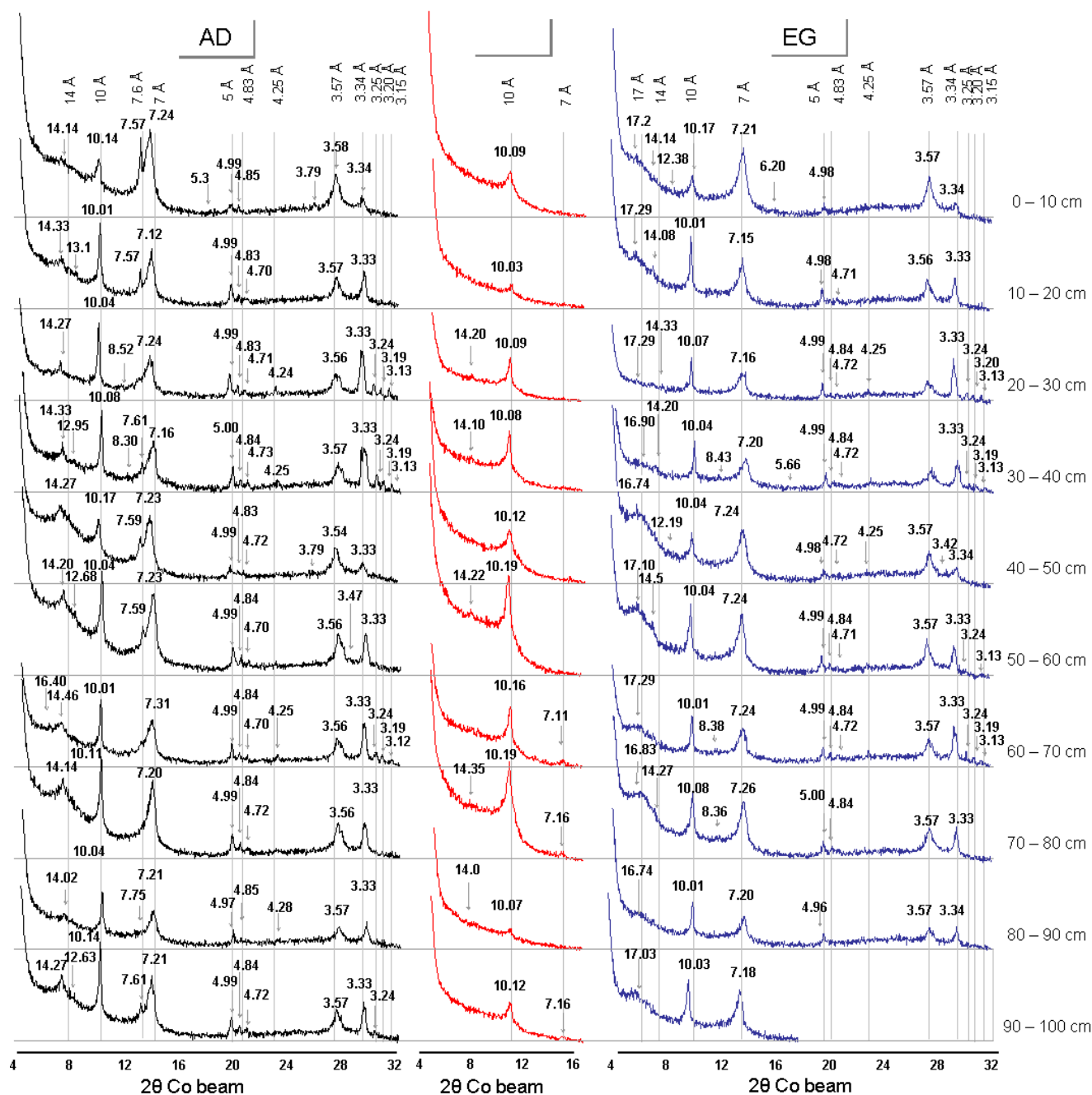


Figure 8.17. XRD pattern of oriented mount specimens for sediment samples in mangrove forest profile of Dam Mon

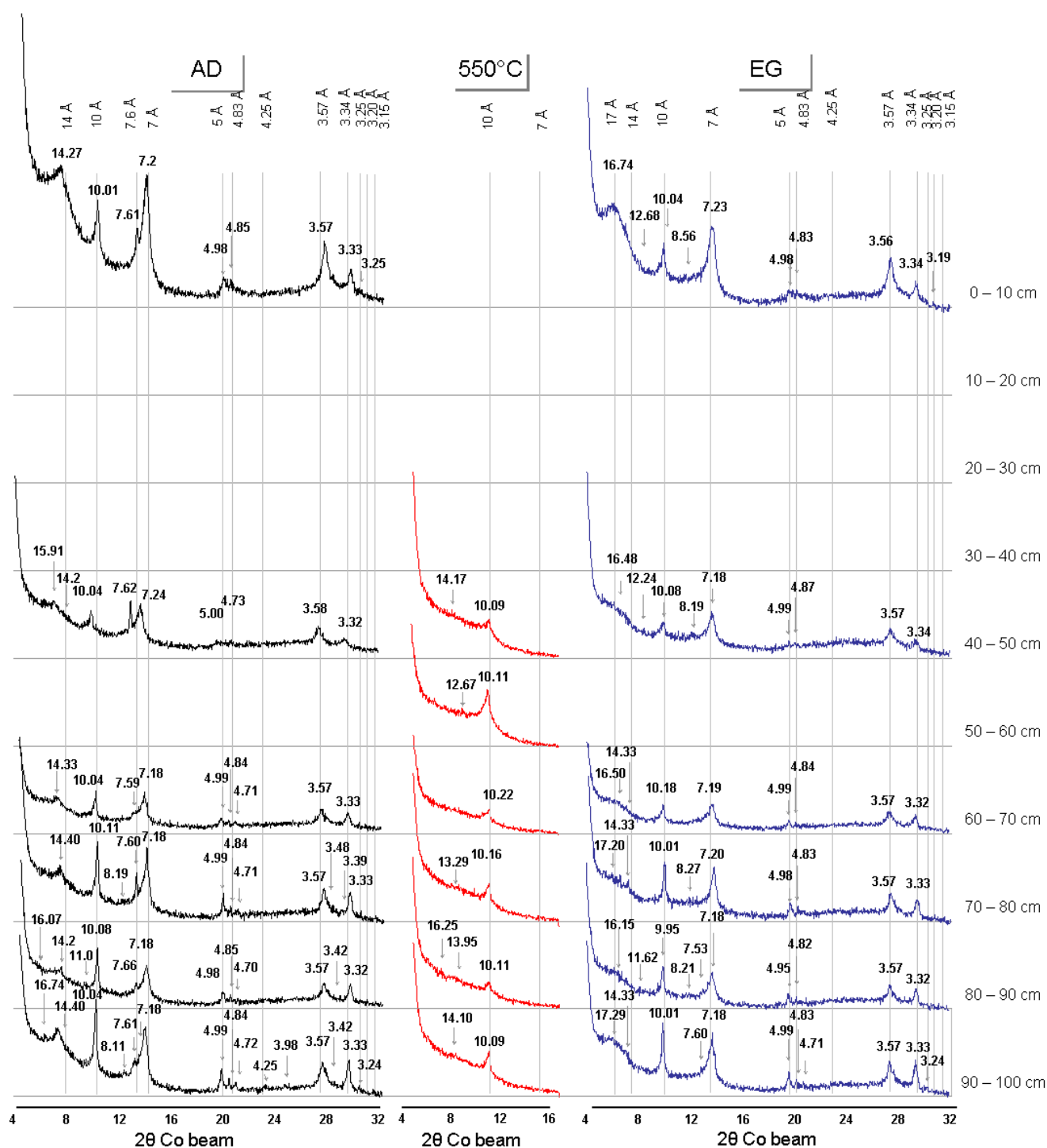


Figure 8.18. XRD pattern of oriented mount specimens for sediment samples in shrimp pond profile of Dam Mon

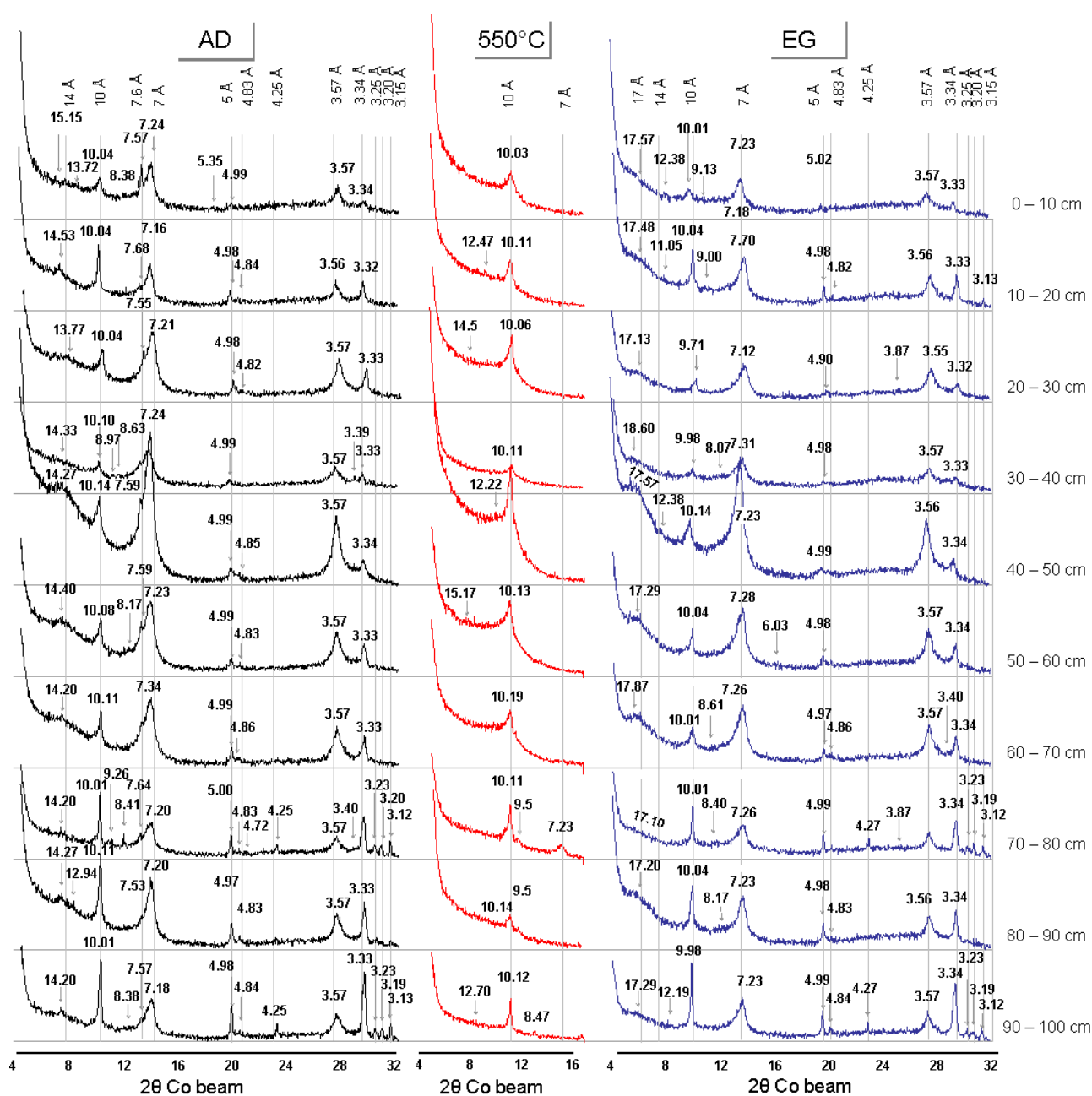


Figure 8.19. XRD pattern of oriented mount specimens for sediment samples in low tidal mudflat profile of Nha Phu

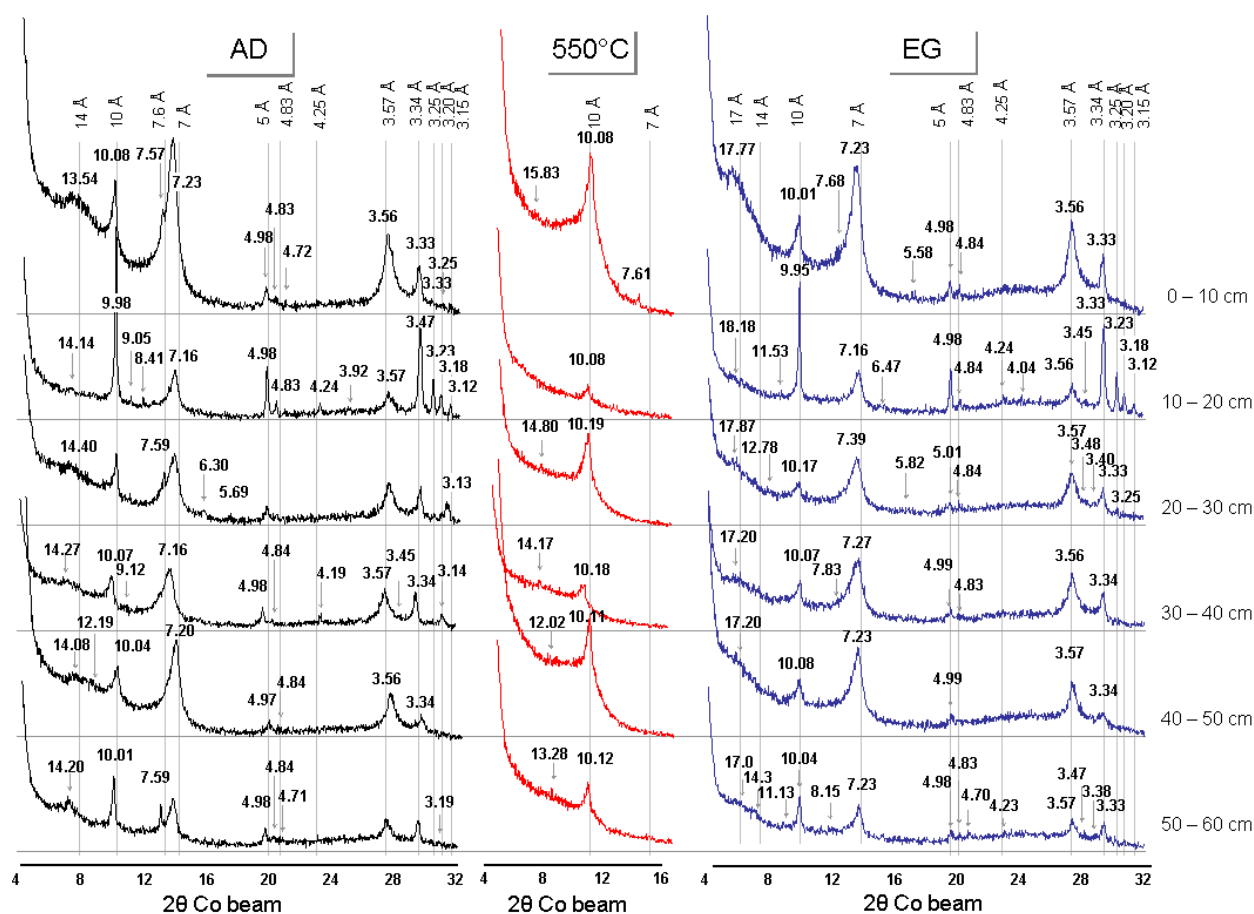


Figure 8.20. XRD pattern of oriented mount specimens for sediment samples in mangrove forest profile of Nha Phu

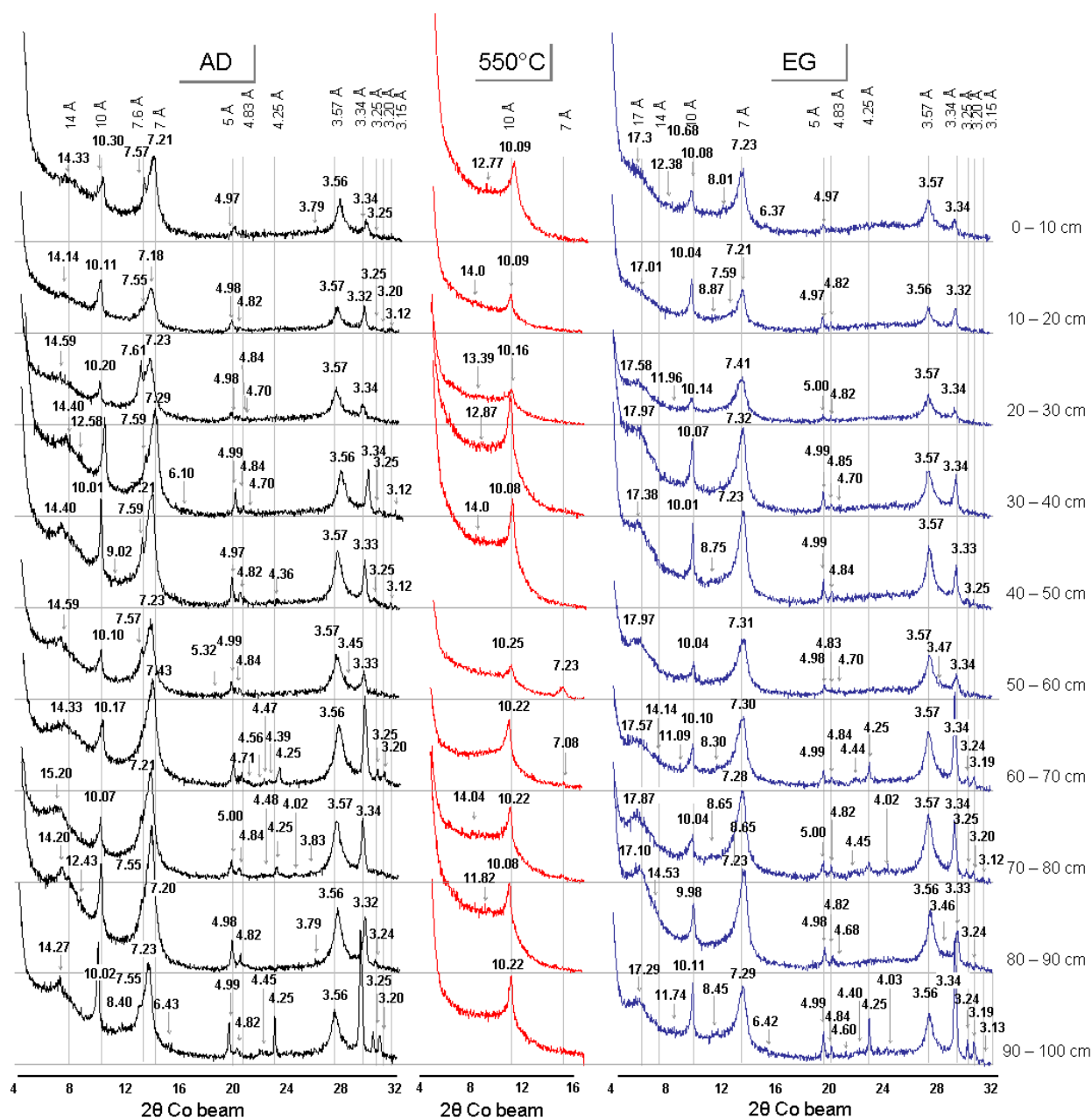


Figure 8.21. XRD pattern of oriented mount specimens for sediment samples in shrimp pond profile of Nha Phu

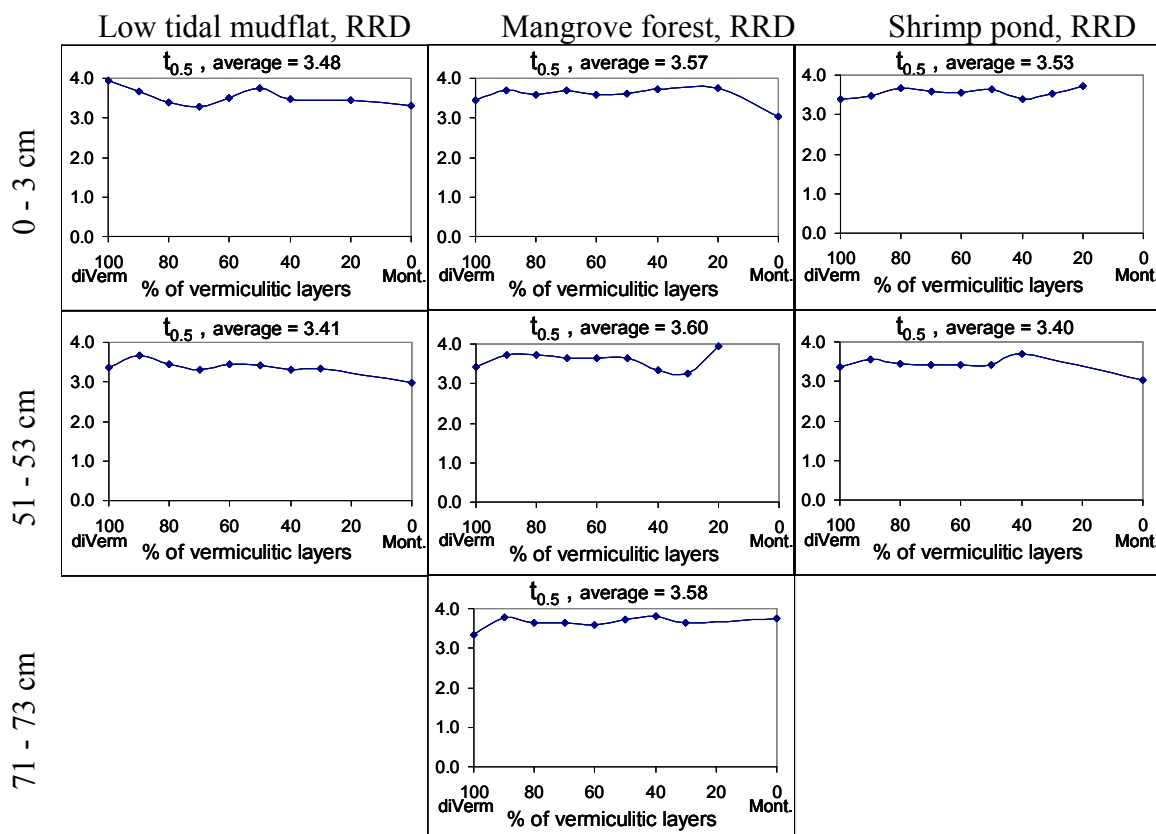


Figure 8.22. Haft time of dissolution ($t_{0.5}$) of dioctahedral vermiculite/smectite mixed layer series (diVS-ml series) of clay fractions (<2 μ m) dispersed from sediment profiles in estuary of the Red River Delta

($t_{0.5}$ expresses the time which 50% of the central atoms from octahedral are leached out in contact with HCl, according to I. Novák & B. Čičel 1978). Calculation based on TEM-EDX data, Jeol JEM-1210. Solid line displays average value calculated from formulae of particles; diVerm: diVermiculite; Mont: Montmorillonite

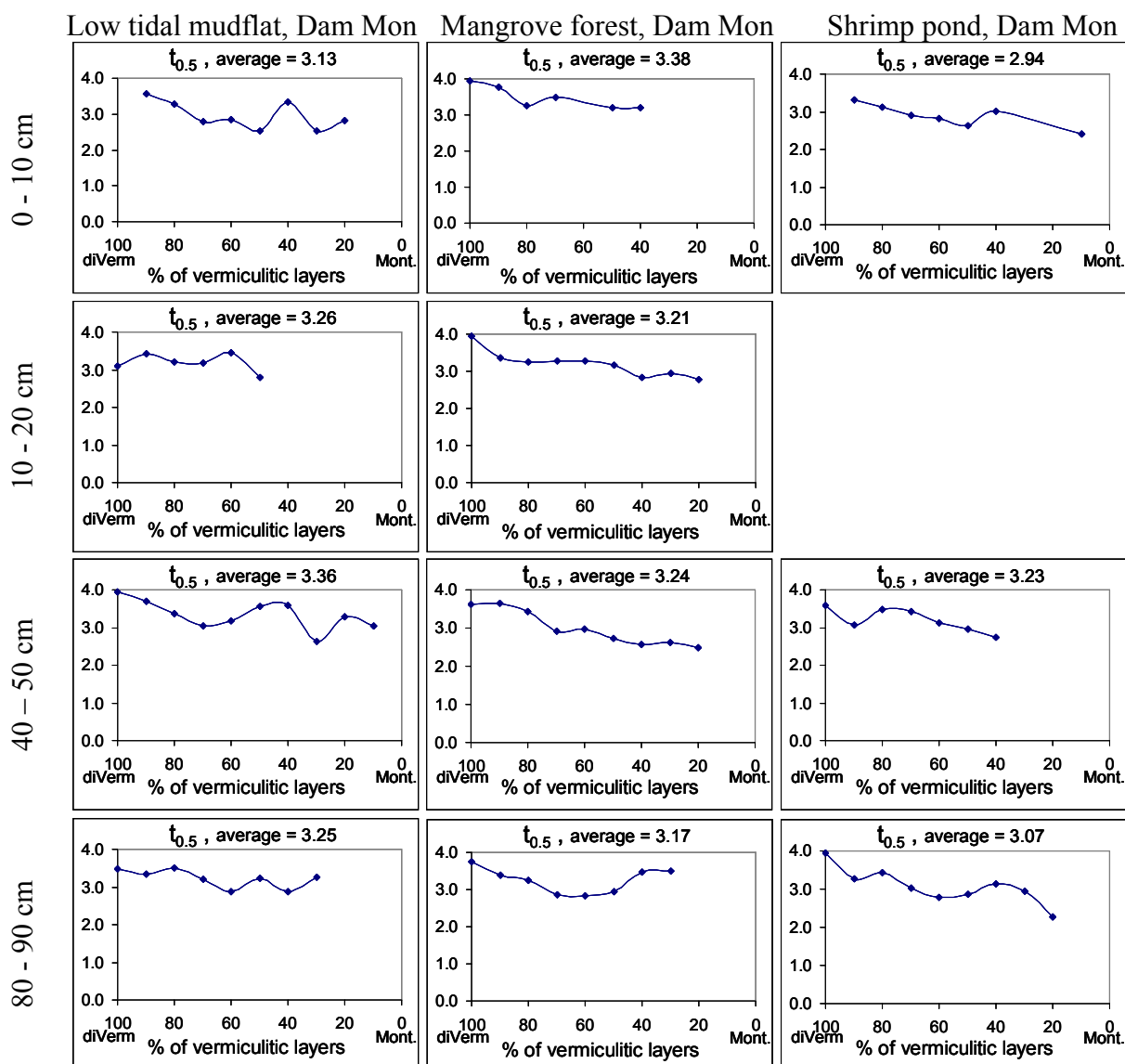


Figure 8.23. Haft time of dissolution ($t_{0.5}$) of dioctahedral vermiculite/smectite mixed layer series of clay fractions ($<2\mu\text{m}$) dispersed from sediment profiles in estuary of the Dam Mon

($t_{0.5}$ expresses the time which 50% of the central atoms from octahedra are leached out in contact with HCl, according to I. Novák & B. Čížel 1978). Calculation based on TEM-EDX data, Jeol JEM-1210; diVerm: diVermiculite; Mont: Montmorillonite

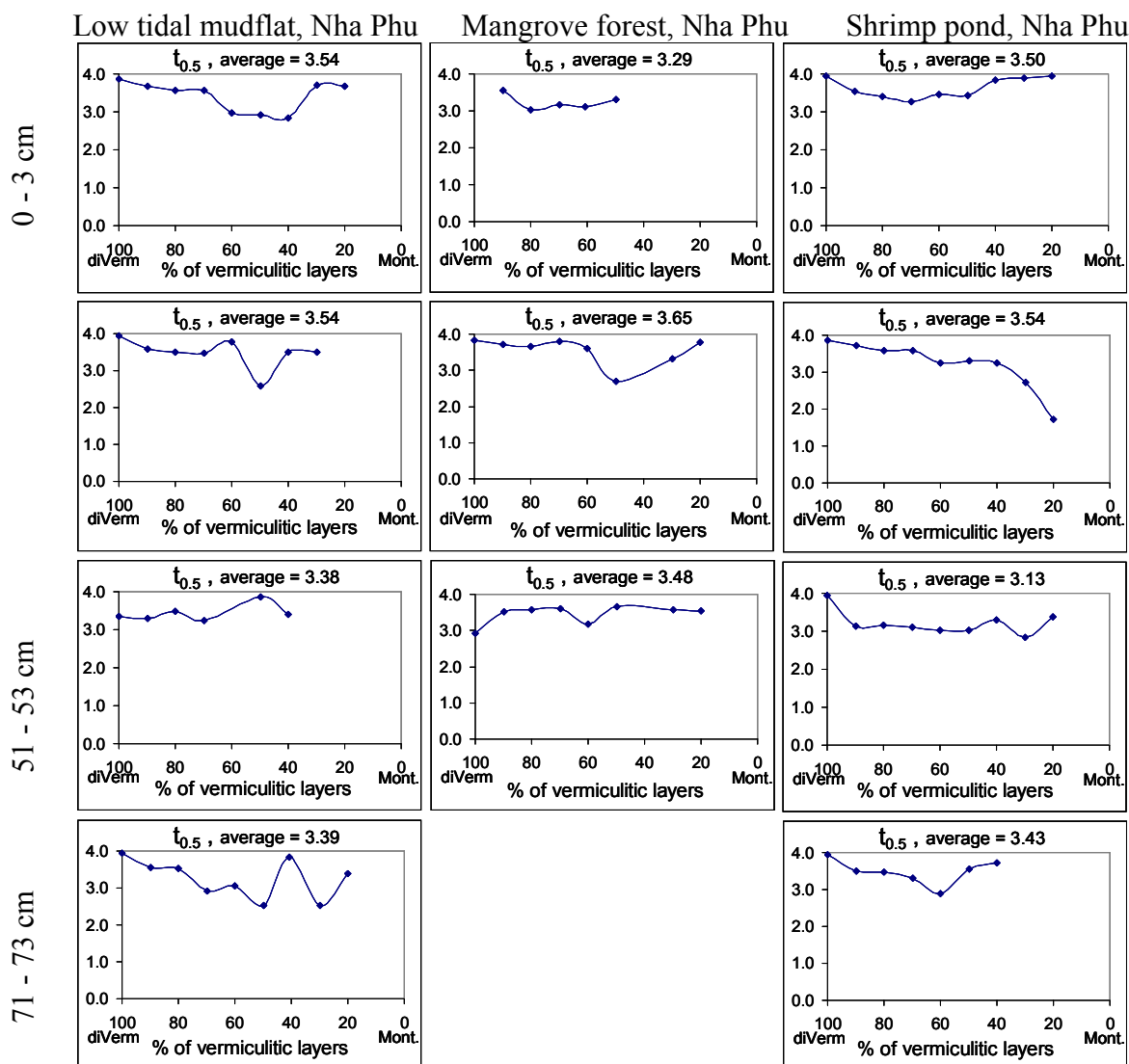


Figure 8.24. Haft time of dissolution ($t_{0.5}$) of dioctahedral vermiculite/smectite mixed layer series of clay fractions ($<2\mu\text{m}$) dispersed from sediment profiles in estuary of the Nha Phu

($t_{0.5}$ expresses the time which 50% of the central atoms from octahedra are leached out in contact with HCl, according to I. Novák & B. Čičel 1978). Calculation based on TEM-EDX data, Jeol JEM-1210; diVerm: diVermiculite; Mont: Montmorillonite

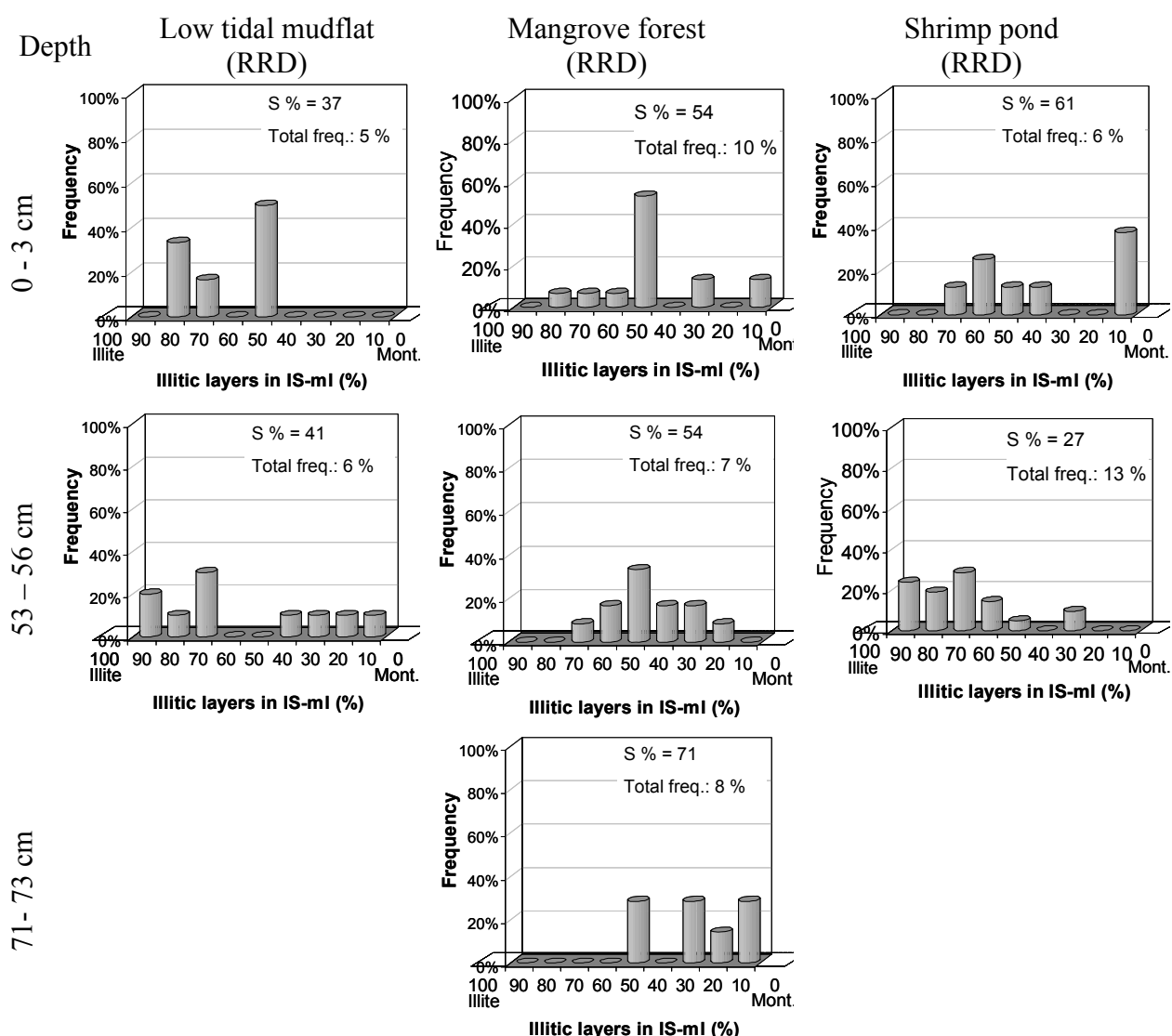


Figure 8.25. Frequency distribution of IS-ml series in sediment profiles of Red River delta
Reveals from TEM-EDX analyses (Jeol JEM-1210); Mont: Montmorillonite; S% displayed weighted average proportion of montmorillonitic layers in all particles. This figure is to observe with consideration that the frequency of IS-ml series were relatively low

Table 8.6. Mineral formulae [O₁₀(OH)₂] of clay minerals from fraction < 2 µm, dispersed from sediment profiles in estuary of Red River Delta*Average values calculated based on TEM-EDX analyses (Jeol JEM-1210)*

Sediment profile	Depth (cm)	No of particles	Interlayer					Octahedral layer				Tetrahedral layer				n ^{VI}
			Ca	Mg	Na	K	Fe ²⁺	Al	Fe ³⁺	Fe ²⁺	Mg	Ti	Al	Si	XII	
Illite		4	0.01	0.07	0.26	0.53	0.00	1.70	0.21	0.00	0.10	0.01	0.94	3.06	0.96	2.01
LM	53-56	1	0.04	0.00	0.21	0.64	0.00	1.66	0.23	0.00	0.08	0.03	0.88	3.12	0.93	1.97
MF	71-73	1	0.00	0.07	0.15	0.72	0.00	1.92	0.01	0.00	0.08	0.00	0.93	3.07	1.00	2.00
SP	53-56	2	0.01	0.11	0.34	0.38	0.00	1.62	0.29	0.00	0.12	0.01	0.97	3.03	0.96	2.03
Montmorillonite		12	0.00	0.02	0.01	0.12	0.01	1.62	0.16	0.04	0.15	0.01	0.02	3.98	0.19	1.97
LM	0-3	3	0.01	0.07	0.00	0.06	0.00	1.36	0.33	0.00	0.29	0.03	0.02	3.98	0.22	1.98
LM	53-56	1	0.00	0.07	0.00	0.09	0.00	1.54	0.25	0.00	0.21	0.00	0.00	4.00	0.22	2.00
MF	0-3	2	0.00	0.00	0.05	0.11	0.00	1.50	0.25	0.00	0.17	0.03	0.03	3.97	0.17	1.91
MF	71-73	5	0.00	0.00	0.00	0.13	0.01	1.86	0.03	0.09	0.00	0.01	0.02	3.98	0.16	1.97
SP	53-56	1	0.00	0.00	0.00	0.30	0.00	1.59	0.08	0.00	0.33	0.00	0.00	4.00	0.30	2.00
IS-mi		86	0.01	0.03	0.06	0.40	0.02	1.67	0.14	0.00	0.11	0.01	0.35	3.65	0.60	1.92
LM	0-3	6	0.01	0.05	0.00	0.55	0.01	1.71	0.16	0.00	0.05	0.00	0.43	3.57	0.69	1.92
LM	53-56	10	0.02	0.00	0.03	0.59	0.00	1.64	0.21	0.00	0.06	0.02	0.41	3.59	0.67	1.90
MF	0-3	14	0.01	0.04	0.00	0.40	0.03	1.70	0.12	0.00	0.11	0.01	0.30	3.70	0.56	1.93
MF	53-56	13	0.01	0.04	0.00	0.42	0.01	1.68	0.16	0.00	0.07	0.02	0.28	3.72	0.54	1.90
MF	71-73	14	0.02	0.04	0.03	0.23	0.06	1.72	0.10	0.00	0.10	0.01	0.20	3.80	0.50	1.92
SP	0-3	8	0.02	0.03	0.04	0.32	0.04	1.72	0.11	0.00	0.08	0.01	0.27	3.73	0.53	1.91
SP	53-56	21	0.01	0.03	0.21	0.41	0.00	1.61	0.16	0.00	0.19	0.01	0.49	3.51	0.72	1.96

Notes: Particles of Illite and Montmorillonite were not detected in the other samples

Table 8.7. Crystallite parameters of chlorite & CS-ml structures of RRD sediments based on 7 Å, 14 Å and 14.2 Å reflection*Data extraction by WinFit, XRD patterns for oriented mount specimen*

Profile	Depth (cm)	Air-dried				Ethylene Glycolation			
		D-value (Å)	CSD (Å)	Int. max	FWHM (Å)	D-value (Å)	CSD (Å)	Int. max	FWHM (Å)
Chlorite									
LM	0 – 3	7.05	> 400	95	0.089	7.07	330 - 350	99	0.186
LM	53 – 56	7.06	> 400	28	0.107	7.06	180 - 190	25	0.287
MF	0 - 3	7.08	160 - 170	260	0.371	7.04	> 400	46	0.097
MF	53 – 56	7.11	220 – 230	196	0.306	7.05	> 400	58	0.036
MF	71 – 73	7.12	200 - 210	196	0.33	7.05	> 400	94	0.129
SP	0 – 3	7.10	210 - 220	141	0.29	7.08	210 - 230	103	0.273
SP	53 – 56	7.06	> 400	73	0.056	7.08	> 400	25	0.134
Chlorite									
LM	0 – 3	14.09	150 – 170	134	0.185	14.12	280 - 390	46	0.188
LM	53 – 56	nd				14.11	380 – 400	21	0.144
MF	0 - 3	nd				14.11	270 – 290	40	0.226
MF	53 – 56	14.09	110 - 120	40	0.55	14.14	310 - 350	50	0.168
MF	71 – 73	14.13	> 400	52	0.133	14.15	200 – 210	67	0.264
SP	0 – 3	14.13	120 - 130	118	0.268	14.15	140 - 150	73	0.252
SP	53 – 56	14.24	70 - 80	67	0.464	14.18	180 - 190	19	0.26
CS-ml structure									
LM	0 – 3	14.39	270 – 280	23	0.23	15.17	110 - 120	5	0.544
LM	53 – 56	14.27	220 – 230	25	0.292	14.59	> 400	11	0.128
MF	0 - 3	14.28	130 - 150	54	0.224	nd			
MF	53 – 56	14.13	270 – 280	67	0.218	nd			
MF	71 – 73	14.16	130 - 140	66	0.459	14.35	130 - 140	26	0.481
SP	0 – 3	14.58	~ 180	18	0.362	14.73	> 400	22	0.068
SP	53 – 56	14.92	90 - 100	11	0.672	nd			

Table 8.8. Crystallite parameters of CS-ml structures in SCC sediments based on reflections in 14 Å peaks in XRD patterns of AD specimen

Dam Mon						Nha Phu					
Profile	Depth (cm)	d-value (Å)	CSD (Å)	Int.Max	FWHM (Å)	Profile	Depth (cm)	d-value (Å)	CSD (Å)	Int.Max	FWHM (Å)
LM	0 - 10	13.74	100 - 110	29	0.727	LM	0 - 10	14.04	40 – 50	127	1.468
LM	10 - 20	13.91	170 - 200	24	0.185	LM	10 - 20	14.07	50 - 60	23	0.824
LM	40 - 50	13.72	30 – 40	72	1.88	LM	40 - 50	14.30	~ 70	38	0.975
LM	80 - 90	14.16	100 – 110	33	0.514	LM	80 - 90	14.13	~ 90	82	0.442
MF	0 - 10					MF	0 - 10	13.97	~ 60	31	0.712
MF	10 - 20	14.08	230 – 240	15	0.31	MF	10 - 20	14.11	50 – 60	52	0.835
MF	40 - 50	14.13	200 – 210	17	0.36	MF	40 - 50	14.20	210 - 220	35	0.354
MF	80 - 90	14.09	200 – 280	23	0.126						
SP	0 - 10	13.83	~ 180	14	0.384	SP	0 - 10	13.99	110 – 120	30	0.316
						SP	10 - 20	14.18	~ 40	149	1.574
SP	40 - 50	14.28	~ 50	72	0.908	SP	40 - 50	14.16	30 – 40	51	1.458
SP	80 - 90	14.27	80 - 90	64	0.47	SP	80 - 90	14.24	50 - 60	34	0.806

Table 8.9. Mineral formulae [O₁₀(OH)_n] of clay minerals from fraction < 2 µm, dispersed from sediment profiles in estuary of Red River Delta

Average values calculated based on TEM-EDX analyses (Jeol JEM-1210)

Sediment profile	Depth (cm)	No of particles	Interlayer					Octahedral layer				Tetrahedral layer				n ^{VI}
			Ca	Mg	Na	K	Fe ²⁺	Al	Fe ³⁺	Fe ²⁺	Mg	Ti	Al	Si	XII	
Chlorite		10	0.00	0.00	0.00	0.02	0.00	1.50	0.00	3.03	1.08	0.06	1.05	2.95	0.03	5.62
LM	0-3	3	0.00	0.00	0.00	0.01	0.00	1.46	0.00	3.30	0.87	0.02	0.85	3.15	0.01	5.62
LM	53-56	2	0.02	0.00	0.00	0.03	0.00	0.97	0.00	2.92	1.89	0.15	1.19	2.81	0.06	5.78
MF	71-73	1	0.00	0.00	0.00	0.05	0.00	1.44	0.00	4.39	0.01	0.00	1.18	2.82	0.05	5.85
SP	53-56	4	0.00	0.00	0.00	0.01	0.00	1.82	0.00	2.55	1.10	0.05	1.09	2.91	0.01	5.47
CS-mi		59	0.01	0.02	0.01	0.07	0.00	1.64	0.00	1.14	1.17	0.03	0.83	3.17	0.16	3.96
LM	0-3	5	0.00	0.05	0.00	0.03	0.00	2.07	0.00	0.49	1.18	0.02	0.85	3.15	0.14	3.74
LM	53-56	13	0.02	0.00	0.03	0.09	0.00	1.80	0.00	1.11	1.12	0.05	0.89	3.11	0.17	4.03
MF	0-3	6	0.01	0.04	0.00	0.11	0.00	1.59	0.00	1.16	0.90	0.02	0.70	3.30	0.20	3.65
MF	53-56	13	0.01	0.02	0.00	0.07	0.00	1.47	0.00	1.30	1.36	0.02	0.85	3.15	0.12	4.12
MF	71-73	9	0.01	0.04	0.00	0.06	0.01	1.60	0.00	1.49	0.76	0.03	0.77	3.23	0.17	3.85
SP	0-3	2	0.00	0.02	0.04	0.12	0.00	1.74	0.00	1.75	0.72	0.05	1.02	2.98	0.20	4.21
LM	53-56	11	0.01	0.03	0.01	0.06	0.00	1.51	0.00	0.89	1.60	0.03	0.81	3.19	0.14	4.00

*: n_(chlorite) = 8; n_(saponite) = 2; and n_(CS) were assumed to be linearly proportional intermediate

Table 8.10. Mineral formulae [O₁₀(OH)₂] of CS-mI series from fractions < 2 µm, dispersed from sediment profiles in Nha Phu*Average values based on TEM-EDX (Jeol JEM-1210)*

Average values based on 12M EDX (see EDX 12-0)																
Sediment profile		Depth (cm)	No of particles	Interlayer				Octahedral layer				Tetrahedral layer				n ^{VI}
				Ca	Mg	Na	K	Fe ²⁺	Al	Fe ³⁺	Fe ²⁺	Mg	Ti	Al	Si	XII
Profiles in Dam Mon																
Saponite			57	0.04	0.02	0.07	0.09	0.00	0.83	0.00	0.72	1.06	0.02	0.45	3.55	0.27
LM	0 - 10	5		0.06	0.01	0.11	0.09	0.00	0.64	0.00	0.79	1.22	0.01	0.36	3.64	0.34
LM	10 - 20	2		0.02	0.00	0.15	0.11	0.00	0.84	0.00	0.77	1.04	0.00	0.45	3.55	0.29
LM	40 - 50	1		0.04	0.00	0.15	0.09	0.00	0.59	0.00	1.05	1.01	0.02	0.28	3.72	0.32
LM	80 - 90	8		0.04	0.05	0.08	0.04	0.00	0.73	0.00	0.77	1.17	0.01	0.41	3.59	0.28
MF	10 - 20	2		0.02	0.11	0.00	0.10	0.00	0.61	0.00	0.99	1.02	0.00	0.31	3.69	0.35
MF	80 - 90	17		0.03	0.01	0.07	0.10	0.00	0.95	0.00	0.68	0.96	0.01	0.49	3.51	0.26
SP	0 - 10	8		0.04	0.03	0.00	0.08	0.00	0.94	0.00	0.80	0.82	0.04	0.51	3.49	0.21
SP	40 - 50	4		0.05	0.05	0.03	0.06	0.00	0.91	0.00	0.59	1.10	0.02	0.49	3.51	0.29
SP	80 - 90	10		0.03	0.01	0.07	0.11	0.00	0.77	0.00	0.60	1.26	0.03	0.46	3.54	0.27
CS-mI			88	0.04	0.03	0.04	0.08	0.00	1.25	0.03	0.84	1.13	0.03	0.65	3.58	0.30
LM	0 - 10	10		0.05	0.02	0.04	0.07	0.00	1.10	0.00	0.97	1.38	0.01	0.62	3.38	0.25
LM	10 - 20	7		0.03	0.05	0.05	0.07	0.00	1.03	0.00	0.92	1.16	0.03	0.64	3.36	0.29
LM	40 - 50	8		0.07	0.00	0.03	0.08	0.00	0.95	0.00	1.09	1.44	0.01	0.57	3.43	0.26
LM	80 - 90	14		0.02	0.03	0.03	0.12	0.00	1.01	0.00	0.85	1.16	0.06	0.57	3.43	0.26
MF	0 - 10	1		0.11	0.00	0.00	0.22	0.00	0.92	0.00	1.17	0.81	0.01	0.61	3.39	0.43
MF	10 - 20	4		0.02	0.03	0.00	0.06	0.00	1.34	0.00	1.64	1.18	0.03	0.83	3.17	0.16
MF	40 - 50	3		0.13	0.00	0.00	0.05	0.00	1.17	0.00	0.97	0.94	0.01	0.63	3.37	0.30
MF	80 - 90	9		0.04	0.00	0.09	0.13	0.00	0.99	0.00	0.81	1.22	0.03	0.60	3.40	0.31
SP	0 - 10	12		0.03	0.04	0.01	0.07	0.00	1.32	0.00	0.71	1.07	0.02	0.59	3.41	0.23
SP	40 - 50	14		0.04	0.02	0.03	0.08	0.00	1.05	0.00	0.80	1.33	0.03	0.64	3.36	0.24
SP	80 - 90	6		0.02	0.09	0.11	0.07	0.00	1.05	0.13	0.61	1.00	0.01	0.57	3.43	0.41
Profiles in Nha Phu																
Saponite			7	0.02	0.02	0.04	0.08	0.00	0.94	0.00	0.96	0.68	0.00	0.35	3.65	0.20
LM	0 - 10	1		0.04	0.00	0.13	0.14	0.00	0.59	0.00	1.12	0.92	0.00	0.25	3.75	0.36
LM	10 - 20	1		0.01	0.00	0.05	0.00	0.00	1.06	0.00	1.00	0.54	0.02	0.44	3.56	0.06
LM	80 - 90	3		0.03	0.01	0.00	0.13	0.00	0.91	0.00	0.92	0.75	0.00	0.34	3.66	0.21
SP	10 - 20	1		0.00	0.13	0.00	0.00	0.00	1.06	0.00	0.97	0.50	0.00	0.37	3.63	0.25
SP	80 - 90	1		0.02	0.00	0.07	0.01	0.00	1.13	0.00	0.87	0.56	0.00	0.38	3.62	0.12
CS-mI			48	0.03	0.01	0.05	0.12	0.00	1.06	0.03	1.33	0.94	0.03	0.62	3.38	0.26
LM	0 - 10	6		0.05	0.00	0.04	0.15	0.00	1.06	0.00	1.31	0.90	0.05	0.64	3.36	0.30
LM	10 - 20	10		0.02	0.02	0.07	0.03	0.00	1.32	0.00	1.41	0.84	0.02	0.65	3.35	0.19
LM	40 - 50	4		0.02	0.00	0.11	0.10	0.00	0.83	0.00	1.60	1.06	0.02	0.56	3.44	0.25
LM	80 - 90	6		0.03	0.02	0.03	0.25	0.00	0.84	0.00	1.31	0.97	0.07	0.64	3.36	0.37
MF	0 - 10	1		0.00	0.00	0.21	0.01	0.00	0.74	0.00	1.85	1.18	0.01	0.63	3.37	0.22
MF	10 - 20	1		0.00	0.00	0.00	0.44	0.00	0.87	0.00	1.33	0.85	0.05	0.72	3.28	0.44
MF	40 - 50	1		0.02	0.03	0.00	0.05	0.00	0.66	0.00	1.64	1.52	0.02	0.63	3.37	0.15
SP	0 - 10	1		0.00	0.00	0.00	0.39	0.00	0.44	1.19	1.19	0.84	0.00	0.97	3.03	0.40
SP	10 - 20	2		0.00	0.00	0.01	0.32	0.00	0.95	0.00	0.91	0.94	0.07	0.61	3.39	0.33
SP	40 - 50	4		0.05	0.00	0.00	0.09	0.00	1.04	0.00	1.46	1.00	0.01	0.63	3.37	0.19
SP	80 - 90	12		0.03	0.03	0.05	0.06	0.00	1.09	0.00	1.31	1.02	0.01	0.59	3.41	0.24

LM: Low tidal mudflat; MF: Mangrove forest; SP: Shrimp pond;

XII: interlayer charge; n^{IV}: number of octahedral cations

Table 8.11. Mineral formulae [O₁₀(OH)₂] of IS-ml series from fractions < 2 µm, dispersed from sediment profiles in South Central Coast*Average values calculated based on TEM-EDX analyses (Jeol JEM-1210)*

Sediment profile	Depth (cm)	No of particles	Ca	Mg	Interlayer		Fe ²⁺	Octahedral layer				Tetrahedral layer				n ^{VI}
					Na	K		Al	Fe ³⁺	Fe ²⁺	Mg	Ti	Al	Si	XII	
Profiles in Dam Mon																
Illite		Low frequency														
Montmorillonite		9	0.05	0.04	0.07	0.06	0.00	1.34	0.32	0.00	0.33	0.01	0.02	3.98	0.32	1.99
LM	40 - 50	2	0.08	0.00	0.12	0.06	0.00	1.29	0.33	0.00	0.38	0.01	0.01	3.99	0.33	2.00
SP	40 - 50	1	0.00	0.19	0.00	0.04	0.00	0.88	0.53	0.00	0.55	0.06	0.01	3.99	0.43	1.96
SP	80 - 90	6	0.05	0.03	0.06	0.06	0.00	1.44	0.28	0.00	0.28	0.00	0.02	3.98	0.29	1.99
IS-ml		21	0.02	0.09	0.03	0.32	0.01	1.47	0.28	0.00	0.19	0.02	0.30	3.70	0.58	1.94
LM	0 - 10	1	0.01	0.24	0.00	0.10	0.05	1.67	0.30	0.00	0.01	0.02	0.73	3.27	0.70	1.98
LM	80 - 90	2	0.00	0.06	0.00	0.49	0.02	1.68	0.15	0.00	0.10	0.00	0.37	3.63	0.65	1.94
MF	10 - 20	3	0.03	0.07	0.02	0.43	0.00	1.76	0.05	0.00	0.11	0.01	0.36	3.64	0.65	1.92
MF	40 - 50	2	0.00	0.09	0.01	0.46	0.00	1.14	0.58	0.00	0.23	0.00	0.36	3.64	0.65	1.94
SP	0 - 10	2	0.02	0.13	0.00	0.29	0.00	1.47	0.29	0.00	0.14	0.04	0.29	3.71	0.59	1.90
SP	40 - 50	1	0.00	0.00	0.00	0.67	0.00	1.83	0.10	0.00	0.00	0.01	0.54	3.46	0.67	1.92
SP	80 - 90	10	0.02	0.09	0.06	0.21	0.00	1.35	0.32	0.01	0.28	0.02	0.19	3.81	0.51	1.96
Profiles in Nha Phu																
Illite		5	0.01	0.00	0.50	0.36	0.01	1.55	0.31	0.00	0.10	0.06	0.91	3.09	0.89	1.96
LM	40 - 50	2	0.00	0.00	0.63	0.22	0.02	1.54	0.28	0.00	0.07	0.08	0.85	3.15	0.88	1.90
SP	0 - 10	2	0.00	0.00	0.62	0.28	0.00	1.56	0.39	0.00	0.01	0.02	0.89	3.11	0.90	1.96
SP	80 - 90	1	0.05	0.00	0.00	0.80	0.00	1.53	0.19	0.00	0.33	0.08	1.07	2.93	0.90	2.06
Montmorillonite		Low frequency														
IS-ml		21	0.02	0.06	0.19	0.27	0.00	1.36	0.41	0.01	0.15	0.02	0.37	3.63	0.62	1.93
LM	40 - 50	2	0.00	0.15	0.06	0.08	0.00	1.53	0.15	0.10	0.13	0.03	0.12	3.88	0.45	1.92
LM	80 - 90	1	0.02	0.00	0.09	0.65	0.00	1.79	0.14	0.00	0.02	0.00	0.58	3.42	0.77	1.94
MF	0 - 10	7	0.03	0.02	0.37	0.22	0.00	1.25	0.40	0.00	0.30	0.03	0.40	3.60	0.67	1.96
MF	10 - 20	1	0.07	0.23	0.19	0.01	0.00	1.22	0.70	0.00	0.07	0.01	0.74	3.26	0.79	1.99
MF	40 - 50	1	0.01	0.01	0.00	0.35	0.09	0.66	1.25	0.00	0.00	0.00	0.27	3.73	0.56	1.90
SP	0 - 10	3	0.00	0.03	0.19	0.44	0.00	1.53	0.30	0.00	0.10	0.01	0.52	3.48	0.69	1.93
SP	40 - 50	3	0.04	0.04	0.03	0.37	0.00	1.71	0.12	0.00	0.08	0.01	0.24	3.76	0.54	1.91
SP	80 - 90	3	0.00	0.13	0.11	0.18	0.00	1.10	0.74	0.00	0.07	0.00	0.26	3.74	0.55	1.91

LM: Low tidal mudflat; MF: Mangrove forest; SP: Shrimp pond; XII: interlayer charge; n^{VI}: number of cations in octahedral layer; CS-ml: Chlorite/Saponite mixed layers; IS-ml: Illite/Smectite mixed layer; diVS: dioctahedral vermiculite/smectite mixed layers; KE: Kaolinite/ Expandable mixed layers

Table 8.12. Mineral formulae [O₁₀(OH)₂] of clay minerals from fractions < 2 µm, dispersed from sediment profiles in Nha Phu*Average values calculated based on TEM-EDX analyses (Jeol JEM-1210)*

Sediment profile	Depth (cm)	No of particles	Interlayer				Octahedral layer				Tetrahedral layer				n ^{VI}	
			Ca	Mg	Na	K	Fe ²⁺	Al	Fe ³⁺	Fe ²⁺	Mg	Ti	Al	Si		XII
Profiles in Dam Mon																
Trioct. Vermiculite		13	0.07	0.14	0.11	0.15	0.00	0.45	0.07	1.03	1.27	0.03	1.01	2.99	0.69	2.82
LM	0 – 10	2	0.06	0.00	0.00	0.53	0.00	0.52	0.00	0.92	1.25	0.10	1.00	3.00	0.65	2.70
LM	10 – 20	3	0.08	0.10	0.29	0.12	0.00	0.26	0.00	1.38	1.28	0.00	0.98	3.02	0.77	2.93
LM	40 – 50	1	0.27	0.00	0.17	0.00	0.00	0.41	0.00	1.36	1.22	0.00	1.19	2.81	0.72	2.99
MF	40 – 50	1	0.05	0.25	0.00	0.00	0.00	0.76	0.00	1.27	0.76	0.00	1.07	2.93	0.61	2.80
MF	80 – 90	2	0.04	0.25	0.04	0.03	0.00	0.42	0.48	0.47	1.28	0.03	1.03	2.97	0.64	2.65
SP	0 – 10	1	0.00	0.30	0.00	0.03	0.00	0.45	0.00	0.95	1.50	0.02	0.98	3.02	0.63	2.90
SP	80 – 90	3	0.05	0.17	0.09	0.15	0.00	0.50	0.00	0.94	1.39	0.02	0.95	3.05	0.68	2.83
Low charge Saponite		40	0.03	0.00	0.04	0.10	0.00	0.96	0.00	0.68	0.91	0.01	0.37	3.63	0.21	2.55
LM	0 - 10	6	0.06	0.00	0.06	0.09	0.00	0.90	0.00	0.69	0.97	0.01	0.36	3.64	0.27	2.56
LM	10 - 20	6	0.03	0.00	0.04	0.15	0.00	0.95	0.00	0.73	0.89	0.00	0.38	3.62	0.26	2.56
LM	40 - 50	5	0.05	0.00	0.03	0.09	0.00	0.96	0.00	0.70	0.92	0.00	0.34	3.66	0.20	2.57
LM	80 - 90	10	0.03	0.01	0.05	0.08	0.00	1.00	0.00	0.67	0.88	0.02	0.40	3.60	0.21	2.54
MF	0 - 10	1	0.00	0.00	0.11	0.10	0.00	0.98	0.00	0.85	0.67	0.00	0.26	3.74	0.20	2.51
MF	10 - 20	1	0.01	0.00	0.00	0.04	0.00	0.91	0.00	1.01	0.69	0.00	0.23	3.77	0.06	2.61
MF	40 - 50	1	0.00	0.00	0.08	0.04	0.00	1.08	0.00	0.65	0.76	0.00	0.27	3.73	0.12	2.49
MF	80 - 90	1	0.00	0.00	0.00	0.17	0.00	0.87	0.00	0.75	0.83	0.01	0.20	3.80	0.17	2.45
SP	0 - 10	1	0.00	0.00	0.00	0.10	0.00	1.31	0.00	0.33	0.86	0.00	0.43	3.57	0.10	2.51
SP	40 - 50	4	0.03	0.02	0.02	0.07	0.00	0.92	0.00	0.71	0.97	0.02	0.42	3.58	0.19	2.61
SP	80 - 90	4	0.00	0.00	0.05	0.17	0.00	0.95	0.00	0.54	1.03	0.02	0.36	3.64	0.22	2.51
di-triVerm		54	0.11	0.06	0.15	0.00	0.84	0.59	0.05	0.80	0.04	0.88	3.12	0.69	2.28	
LM	0 - 10	7	0.08	0.12	0.18	0.14	0.00	0.82	0.54	0.05	0.91	0.01	0.81	3.19	0.71	2.31
LM	10 - 20	3	0.06	0.11	0.11	0.24	0.00	0.93	0.58	0.00	0.82	0.01	0.90	3.10	0.70	2.33
LM	40 - 50	16	0.27	0.01	0.07	0.08	0.00	0.79	0.54	0.04	0.92	0.03	0.80	3.20	0.71	2.29
LM	80 - 90	6	0.05	0.17	0.02	0.22	0.00	0.82	0.67	0.00	0.74	0.07	0.94	3.06	0.66	2.23
MF	0 - 10	3	0.11	0.16	0.00	0.23	0.00	0.88	0.58	0.35	0.36	0.10	1.04	2.96	0.78	2.17
MF	10 - 20	2	0.04	0.18	0.00	0.24	0.00	0.84	0.83	0.00	0.58	0.03	1.01	2.99	0.69	2.25
MF	80 - 90	1	0.07	0.00	0.40	0.22	0.00	0.58	0.55	0.55	0.61	0.08	0.80	3.20	0.75	2.28
SP	40 - 50	16	0.05	0.18	0.02	0.16	0.00	0.90	0.60	0.00	0.77	0.04	0.91	3.09	0.64	2.27
High charge diVS-mi		105	0.04	0.22	0.03	0.13	0.00	1.18	0.50	0.00	0.34	0.01	0.49	3.51	0.69	2.02
LM	0 - 10	22	0.03	0.26	0.05	0.11	0.00	1.20	0.48	0.00	0.34	0.01	0.52	3.48	0.74	2.02
LM	10 - 20	10	0.04	0.17	0.07	0.22	0.00	1.15	0.50	0.00	0.36	0.03	0.55	3.45	0.73	2.00
LM	40 - 50	19	0.09	0.18	0.02	0.07	0.00	1.12	0.53	0.00	0.37	0.01	0.40	3.60	0.63	2.02
LM	80 - 90	20	0.02	0.24	0.02	0.11	0.00	1.19	0.48	0.00	0.34	0.02	0.45	3.55	0.66	2.01
MF	0 - 10	17	0.02	0.24	0.00	0.14	0.00	1.18	0.53	0.00	0.31	0.01	0.49	3.51	0.66	2.02
MF	10 - 20	1	0.22	0.12	0.01	0.10	0.00	1.15	0.51	0.00	0.35	0.02	0.54	3.46	0.78	2.01
MF	40 - 50	7	0.05	0.28	0.06	0.10	0.00	1.12	0.54	0.00	0.35	0.01	0.56	3.44	0.81	2.01
SP	40 - 50	9	0.03	0.21	0.02	0.21	0.00	1.32	0.38	0.00	0.31	0.01	0.52	3.48	0.71	2.02

LM: Low tidal mudflat; MF: Mangrove forest; SP: Shrimp pond; XII: interlayer charge; n^{IV}: number of octahedral cations

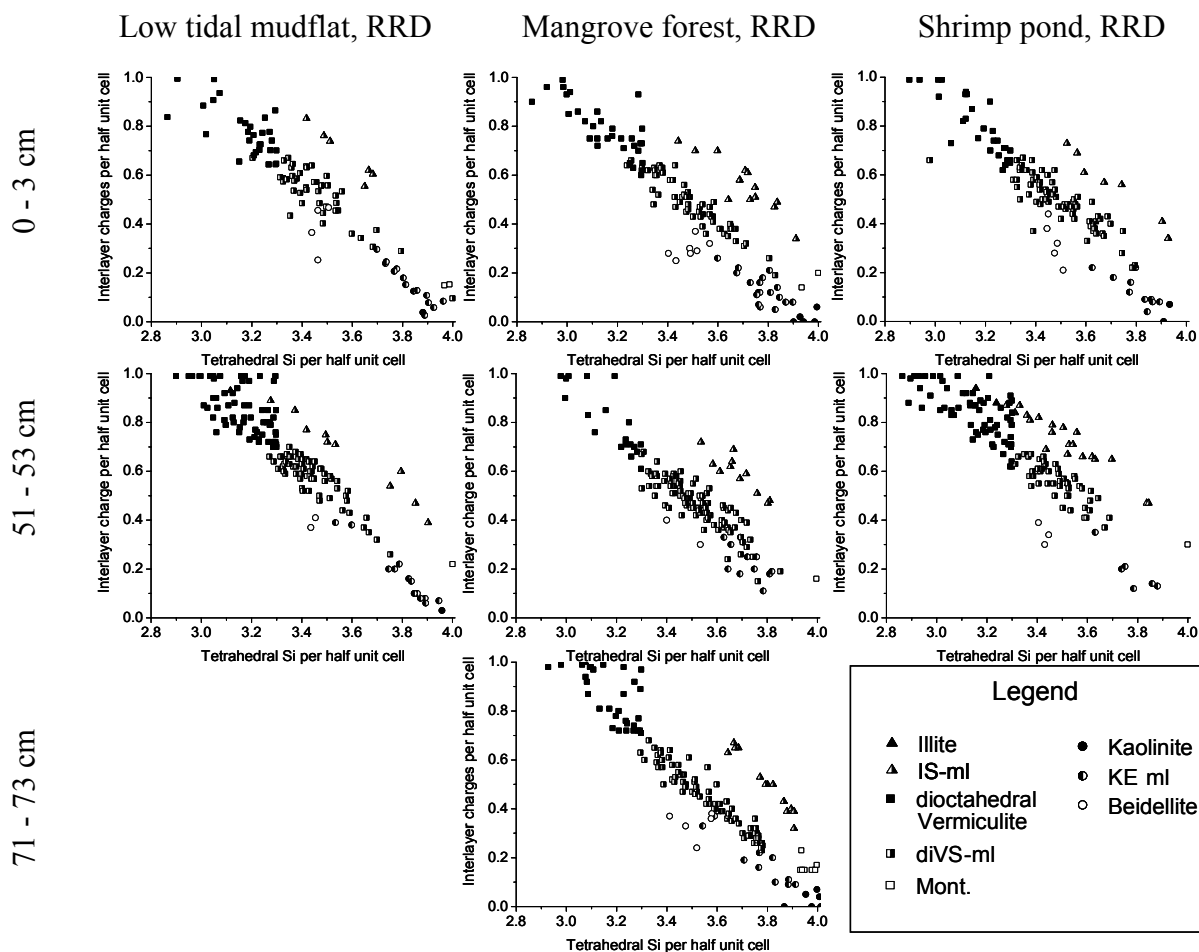


Figure 8.26. Interlayer charge versus tetrahedral Si in mixed layer series of clay fractions (<2 μ m) dispersed from sediment profiles in estuary of the Red River Delta

Calculation based on TEM-EDX data, Jeol JEM-1210. IS-ml: Illite/Smectite mixed layer; diVS-ml: dioctahedral vermiculite/smectite mixed layer; Mont: Montmorillonite; KE-ml: Kaolinite/Beidellite mixed layer.

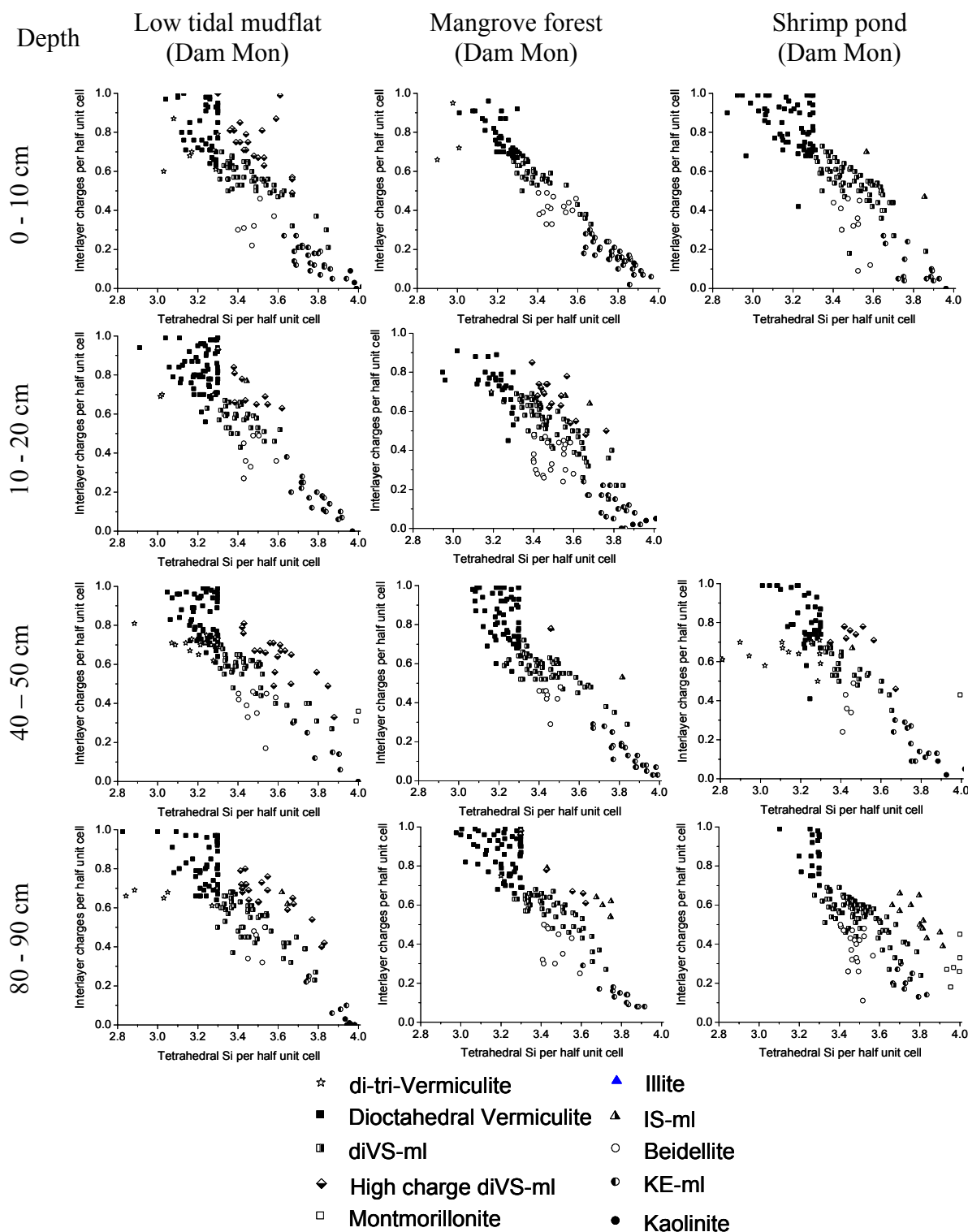


Figure 8.27. Interlayer charge versus tetrahedral Si in mixed layer series of clay fractions (<2μm) dispersed from sediment profiles in estuary of the Red River Delta

Calculation based on TEM-EDX data, Jeol JEM-1210. IS-ml: Illite/Smectite mixed layer; diVS-ml: dioctahedral vermiculite/smectite mixed layer; Mont: Montmorillonite; KE-ml: Kaolinite/Beidellite mixed layer.

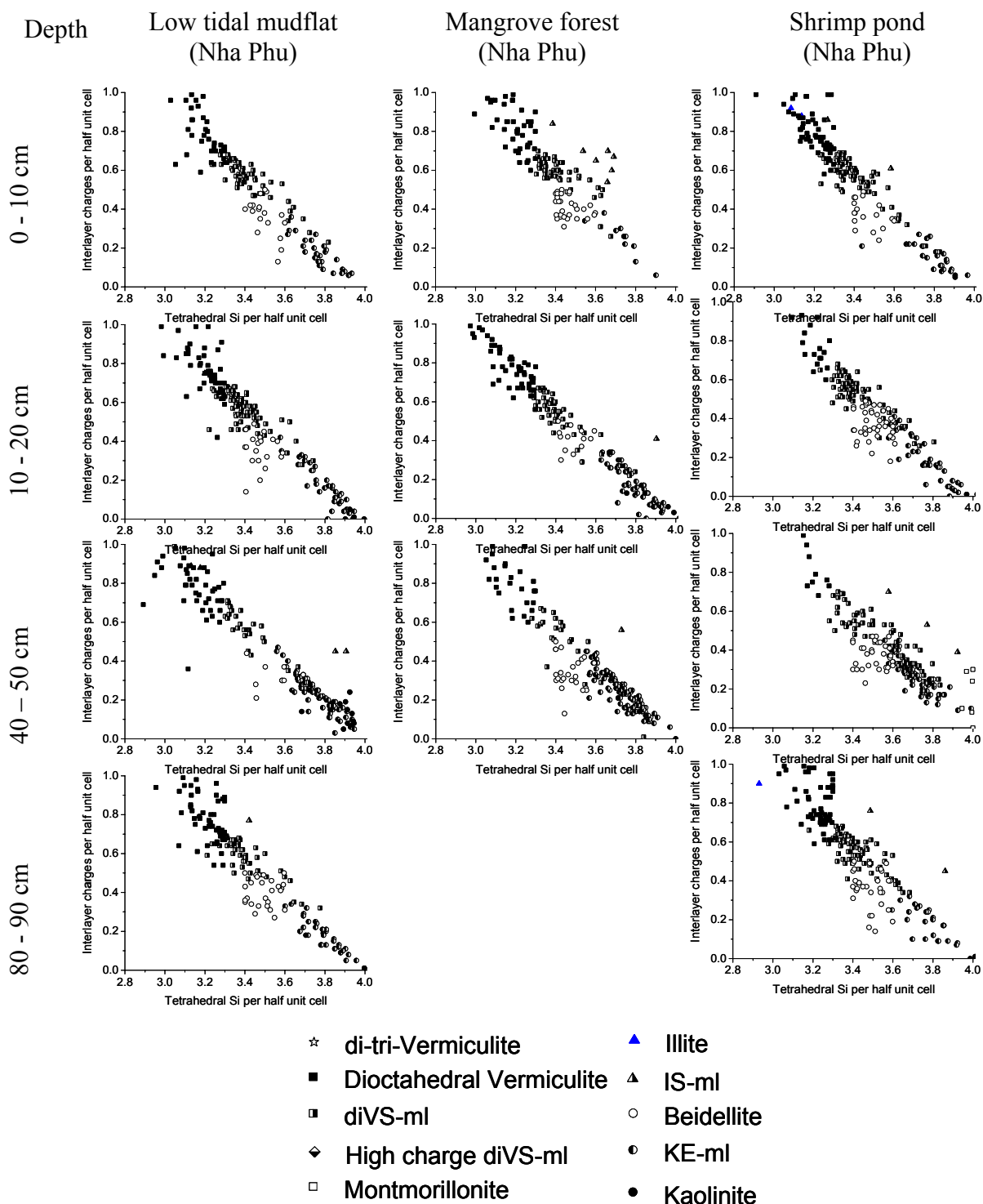


Figure 8.28. Interlayer charge versus tetrahedral Si in mixed layer series of clay fractions (<2μm) dispersed from sediment profiles in estuary of the Red River Delta

Calculation based on TEM-EDX data, Jeol JEM-1210. IS-ml: Illite/Smectite mixed layer; diVS-ml: dioctahedral vermiculite/smectite mixed layer; Mont: Montmorillonite; KE-ml: Kaolinite/Beidellite mixed layer.

8.3 Discussion

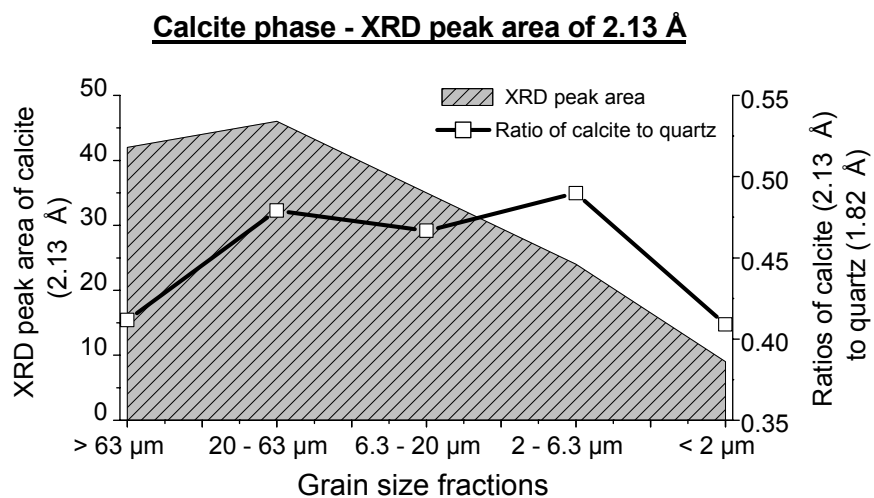


Figure 8.29. XRD peak area of calcite (2.13 Å) and ratios to quartz peak (1.82 Å) indicates the abundance of calcite in coarse and medium sizes

*On example of XRD patterns of grain size separates of sample RRD-MF (0 - 3 cm);
The intensive depletion of calcite amount in fractions < 2 μm can enable discussion on
meaning of LOI (Chapter 5.2.1)*

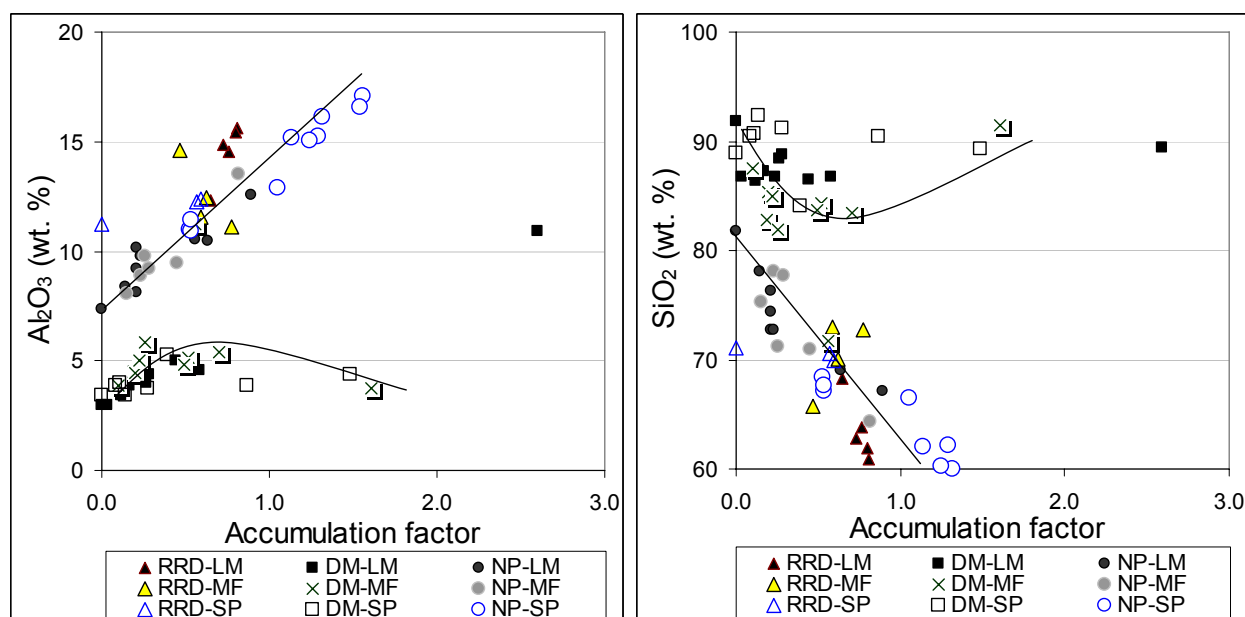


Figure 8.31. Influences of accumulation factor on major elemental distribution in coastal sedimentary sites along Vietnam

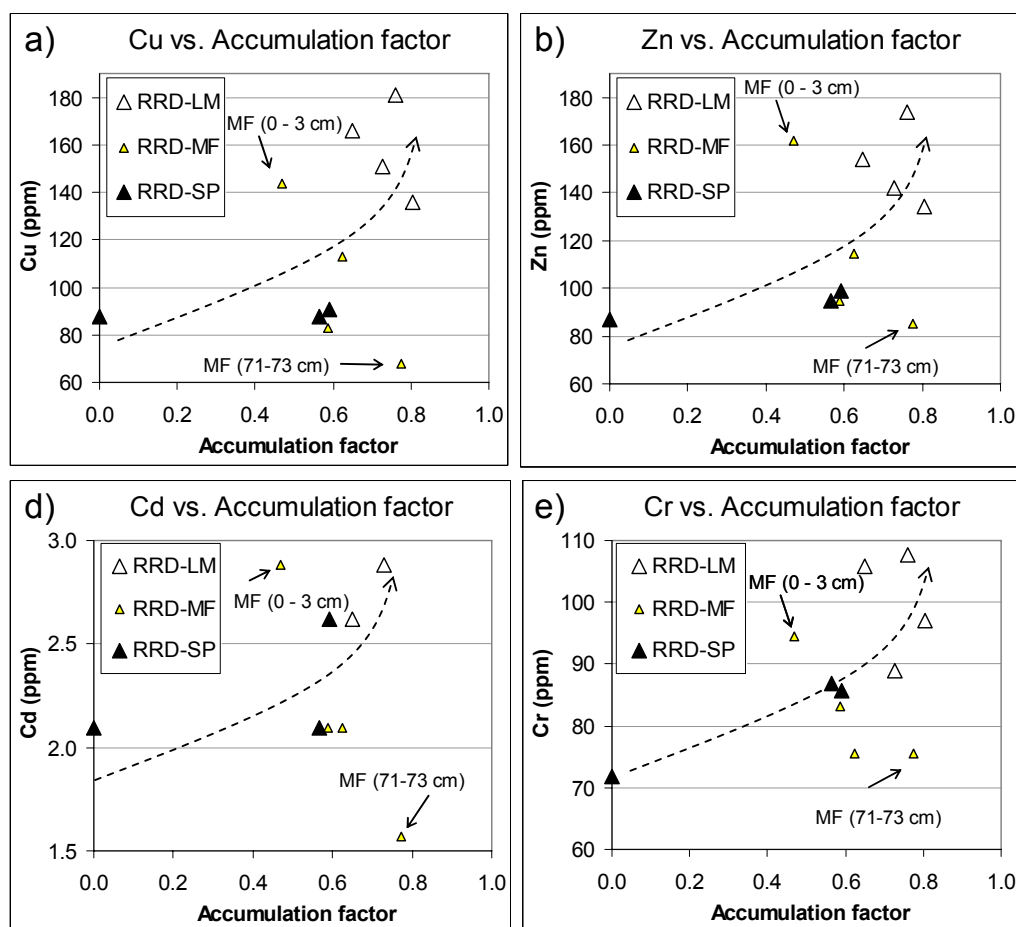
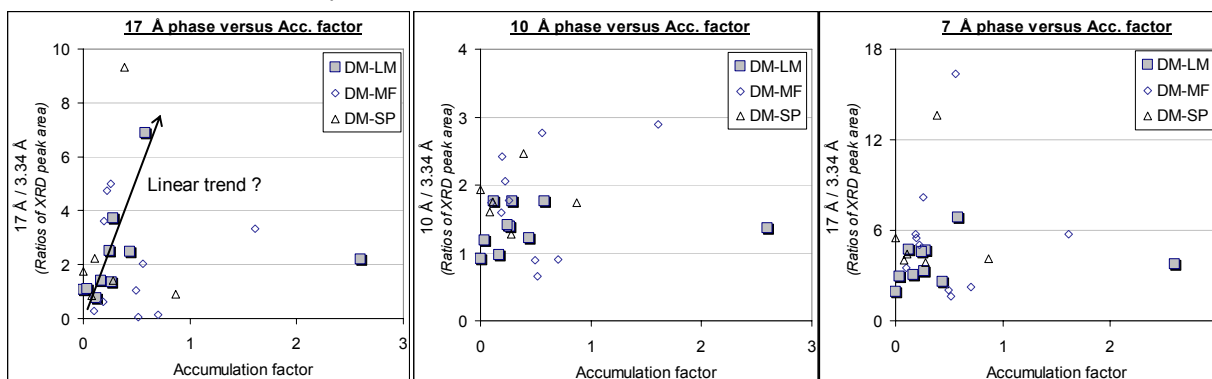
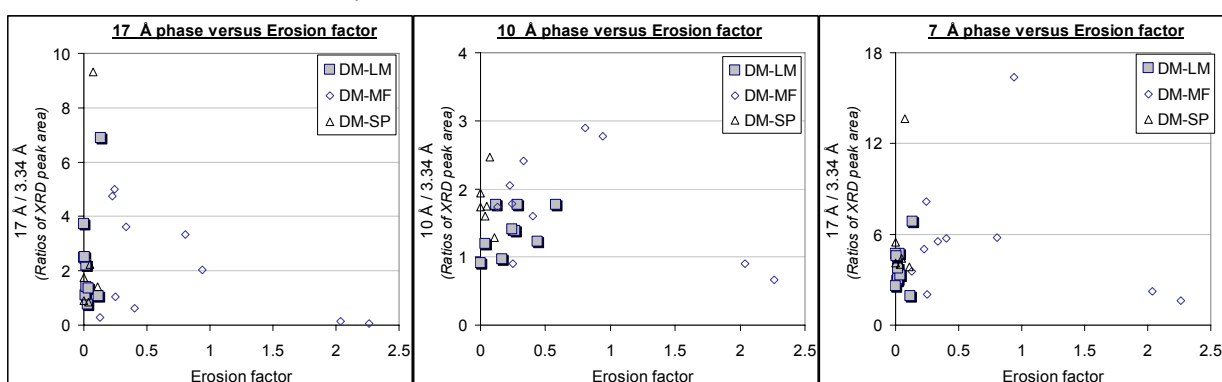


Figure 8.30. Influences of accumulation factor on distribution of heavy metals in RRD

a) Clay phases in fractions < 2 versus accumulation factor



b) Clay phases in fractions < 2 versus erosion factor



c) Clay phases in fractions < 2 versus aeolian factor

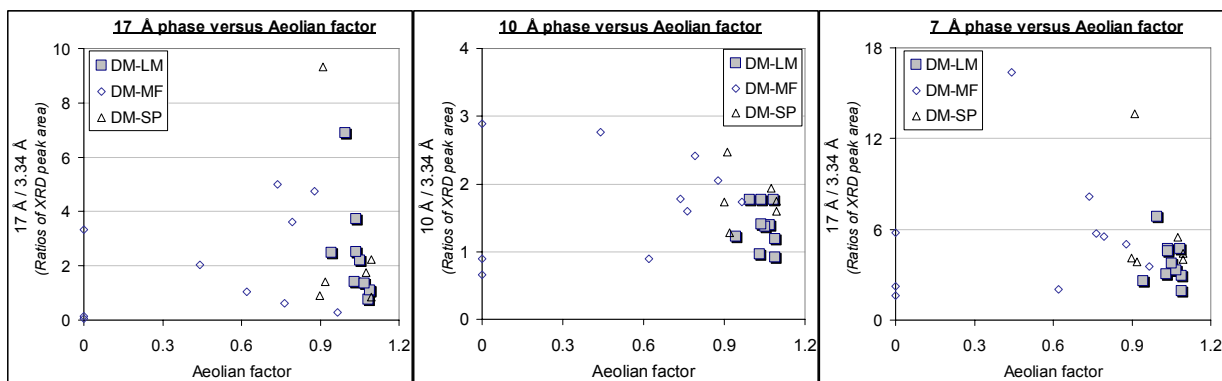


Figure 8.32. Influences of hydrodynamic factors on clay mineral composition in fractions < 2 μ m

Illustrating for sediment samples in Dam Mon profiles; Relative quantification of clay phases was based on ratios of XRD peak area versus the 3.34 Å peak of quartz (EG-treated samples)

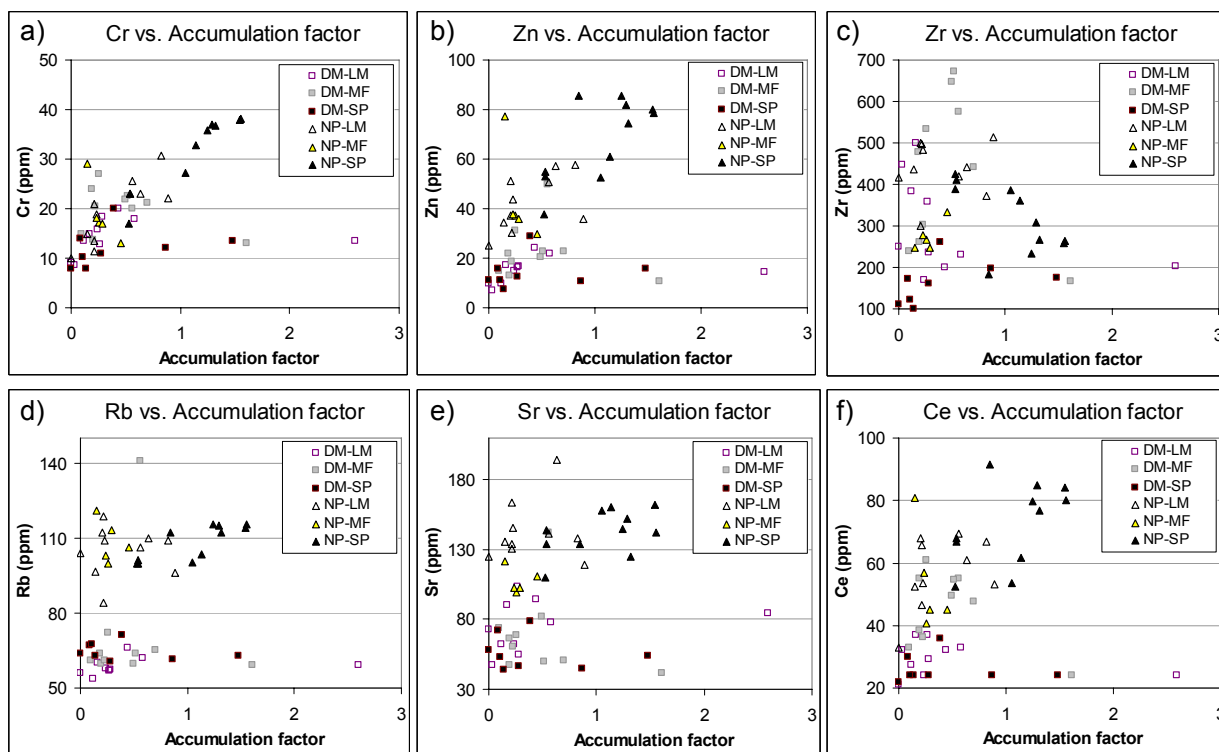


Figure 8.33. Influences of accumulation factor on distribution of heavy metals and minor elements in Dam Mon and Nha Phu

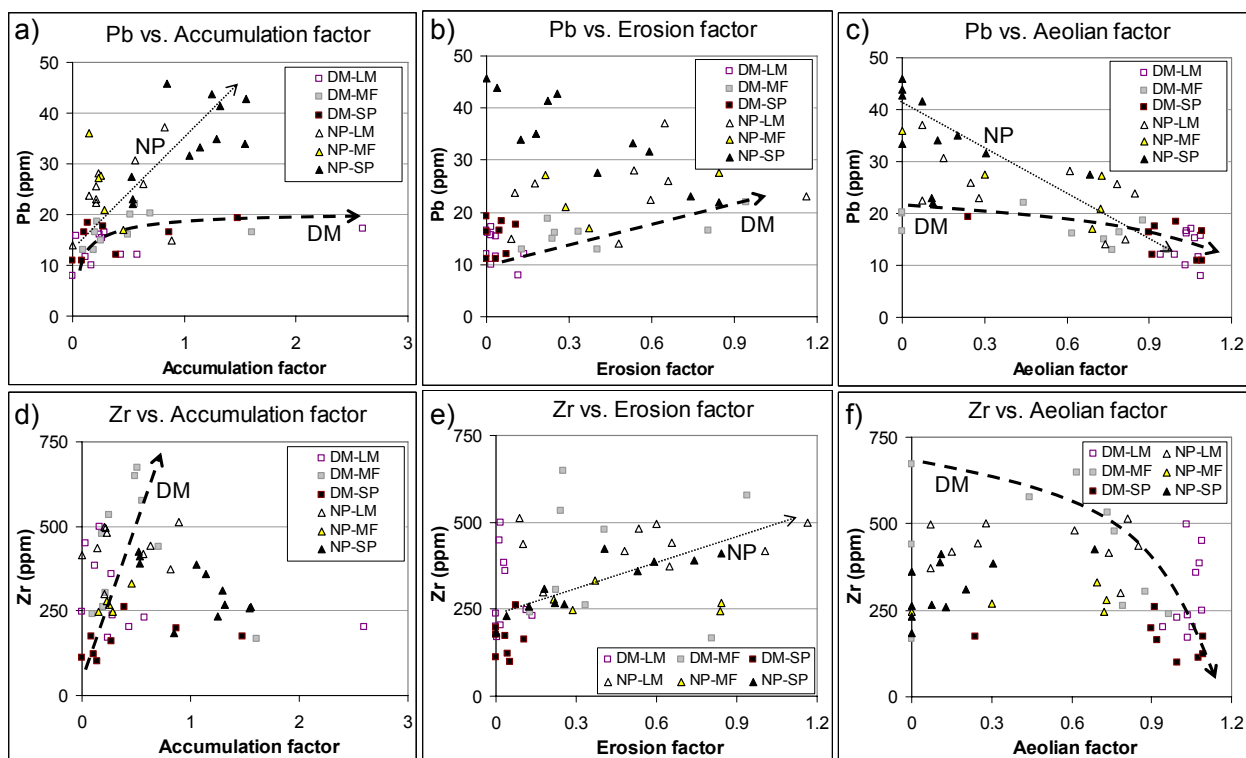


Figure 8.34. Influences of accumulation factor on distribution of heavy metals and minor elements in Dam Mon and Nha Phu

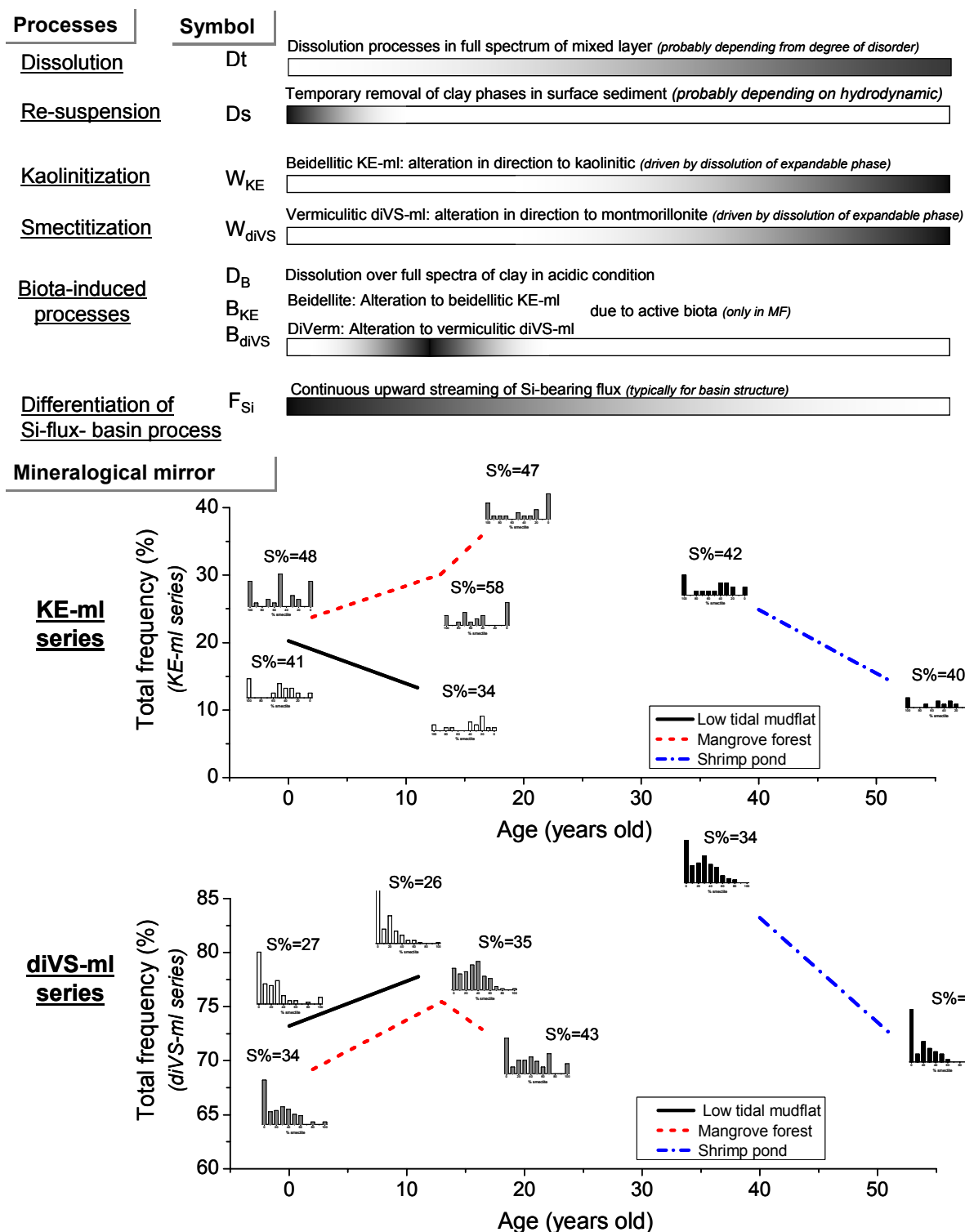


Figure 8.35. Mineralogical features as mirror of interactions among post-sedimentary processes in coastal environment of Red River Delta

S% expresses average smectitic percentage in series. Distribution curves of KE-ml display decreasing % smectite from right (beidellite, 100%) to left (kaolinite: 0%). Distribution curves of diVS-ml display increasing % smectite from right (diVerm: 0%) to left (montmorillonite, 100%)

Red River Delta

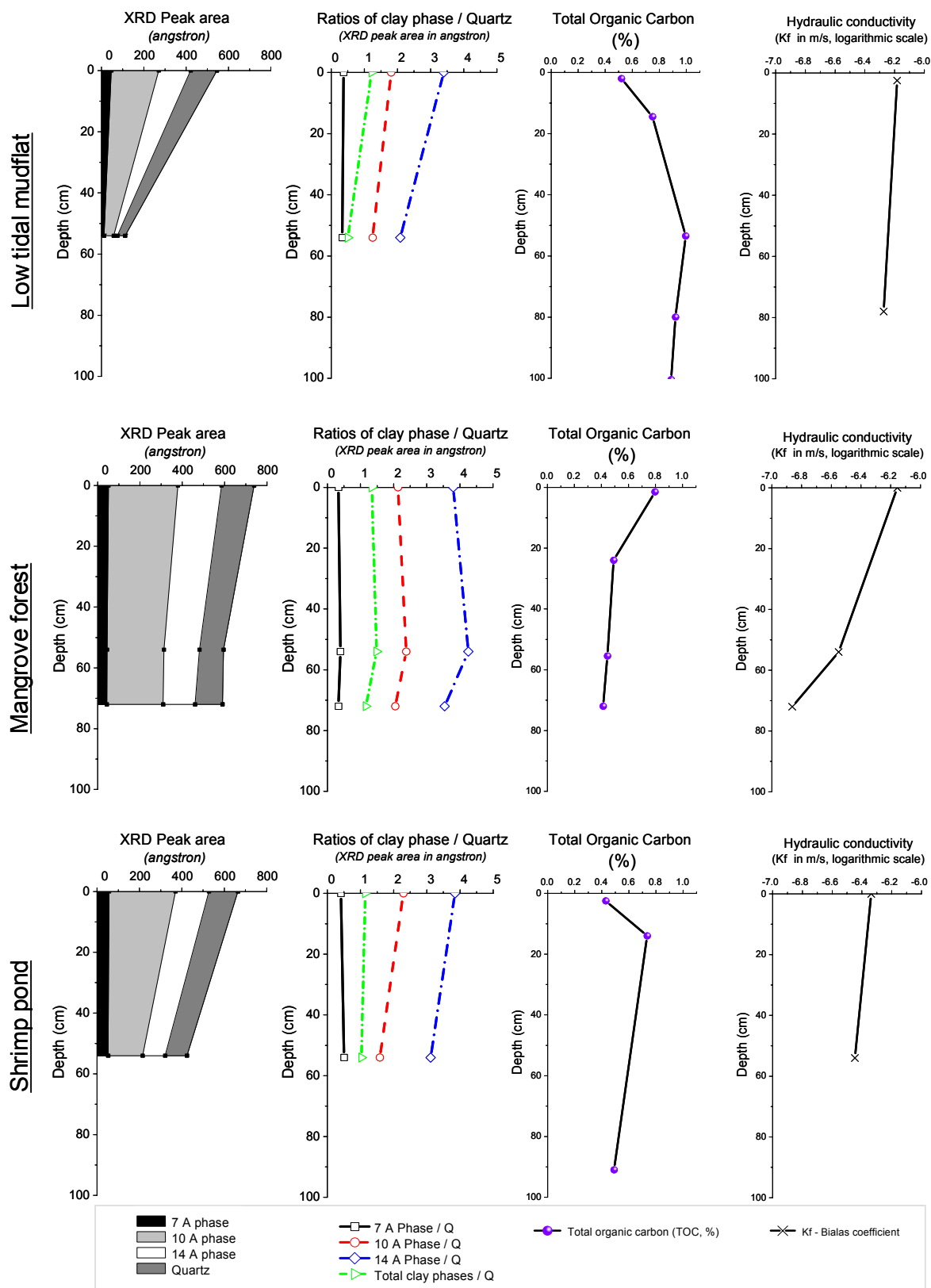


Figure 8.36. Variation of XRD peak area along profiles in RRD in connection with TOC, and hydraulic permeability

Table 8.13. Principal mineral modification during post-sedimentation and assumed processes in Red River Delta

Profile	Depth (cm)	Ambient	Mirror in diVS	Mirror in KE	Dominant process
Low tidal mudflat (LM)	0	Low permeability High organic	Original materials	Original materials	Original state
	50	Low permeability High organic	XRD: peak area of 10 Å and 14 Å phases decreases TEM: diVerm increases slightly parallel to decrease of vermiculitic diVS Smectitic diVS increases slightly	XRD: peak area of 7 Å phases decreases TEM: Beidellite begins to disappear More kaolinitic KE KE-ml dissolve	D_t W_{diVS} W_{KE}
Mangrove forest (MF)	0	Low permeability High organic	TEM: diVerm begins to decrease, smectitic diVS increase	TEM: Beidellite begins to disappear	Missing D_s & F_{Si} W_{diVS} W_{KE}
	50	Very low permeability Low organic	XRD: peak area of 10 Å and 14 Å phases decreases TEM: diVerm decrease Vermiculitic diVS to smectitic diVS	XRD: peak area of 7 Å phases decreases TEM: Beidellite to KE	$B_{diVS} + W_{diVS}$ $B_{KE} + W_{KE}$ D_t : slightly
	75	Very low permeability Low organic	XRD: peak area of 10 Å and 14 Å phases decreases TEM: diVerm increase due to dissolution of vermiculitic diVS diVS is more dissolved No more influence of active root	XRD: peak area of 7 Å phases decreases TEM: KE is more dissolved No more influence of active root	D_t B_{diVS} and B_{KE} decrease W_{diVS}
Shrimp pond (SP)	0	Low permeability Low organic	XRD: peak area of 10 Å and 14 Å phases decreases TEM: Spectra similar to original materials, like MF but more smectitic diVS	XRD: peak area of 7 Å phases decreases TEM: Spectra similar to original materials	Remains of W_{diVS}
	50	Very low permeability High organic No more influence of active root	XRD: peak area of 10 Å and 14 Å phases decreases TEM: diVerm increase due to dissolution of vermiculitic diVS diVS is more dissolved	Former root horizon Beidellitic KE - > Kaolinitic KE Kaolinitic KE -> Kaol.	D_t Remains of former B_{diVS} and B_{KE}

Dam Mon

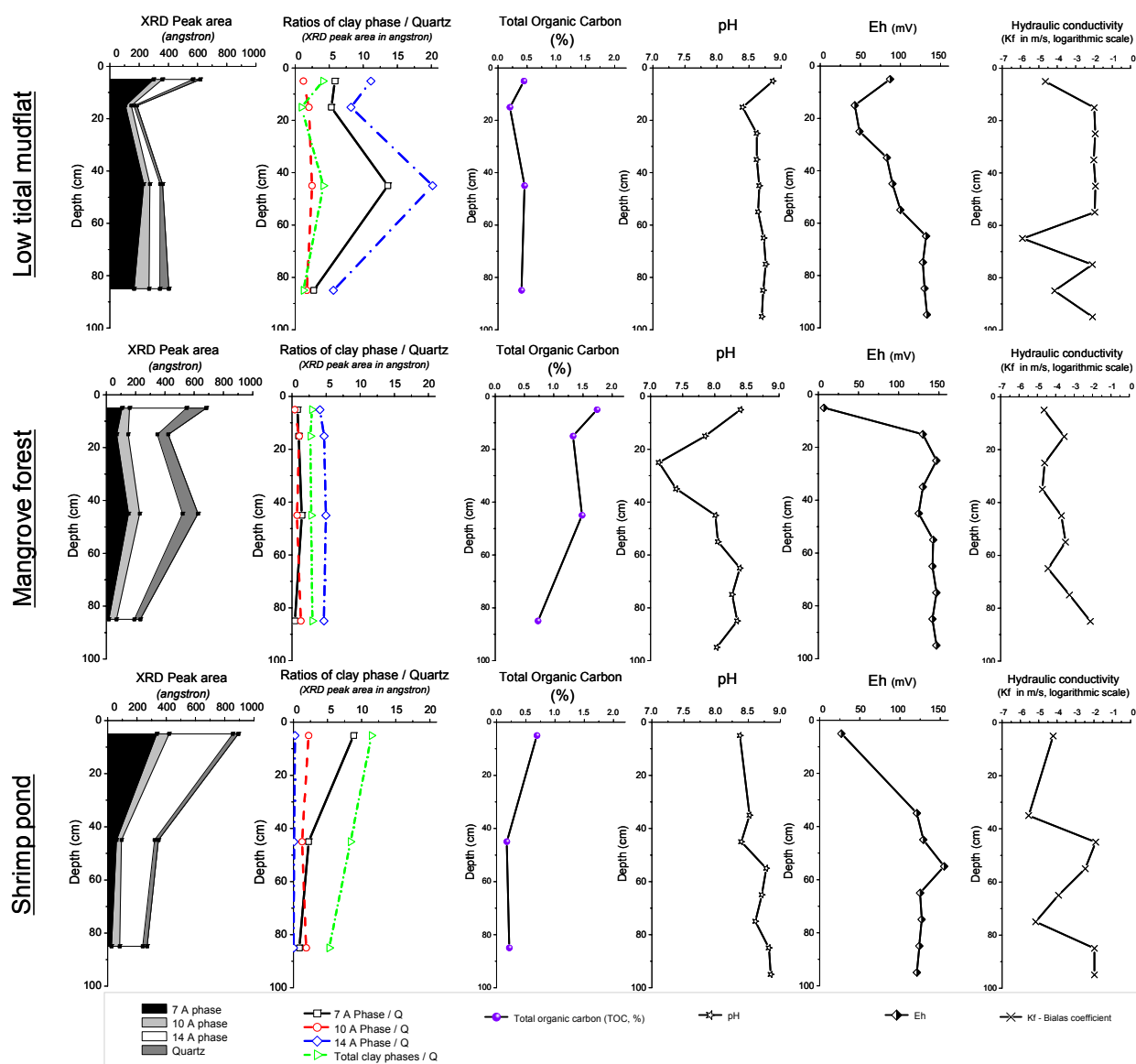


Figure 8.37. Variation of XRD peak area along profiles in Dam Mon in connection with TOC, pH, Eh and hydraulic permeability

Processes	Symbol	
<u>Dissolution</u>	Dt	Dissolution processes in full spectrum of mixed layer (<i>probably depending from degree of disorder</i>)
<u>Re-suspension</u>	Ds	Temporary removal of clay phases in surface sediment (<i>probably depending on hydrodynamic</i>)
<u>Kaolinitization</u>	W_{KE}	Beidellitic KE-ml: alteration in direction to kaolinitic (<i>driven by dissolution of expandable phase</i>)
<u>Smectitization</u>	W_{diVS}	Vermiculitic diVS-ml: alteration in direction to montmorillonite (<i>driven by dissolution of expandable phase</i>)
<u>Biota-induced processes</u>	D_B	Dissolution over full spectra of clay in acidic condition
	B_{KE}	Beidellite: Alteration to beidellitic KE-ml
	B_{diVS}	DiVerm: Alteration to vermiculitic diVS-ml
<u>Differentiation of Si-flux- basin process</u>	F_{Si}	Continuous upward streaming of Si-bearing flux (<i>typically for basin structure</i>)

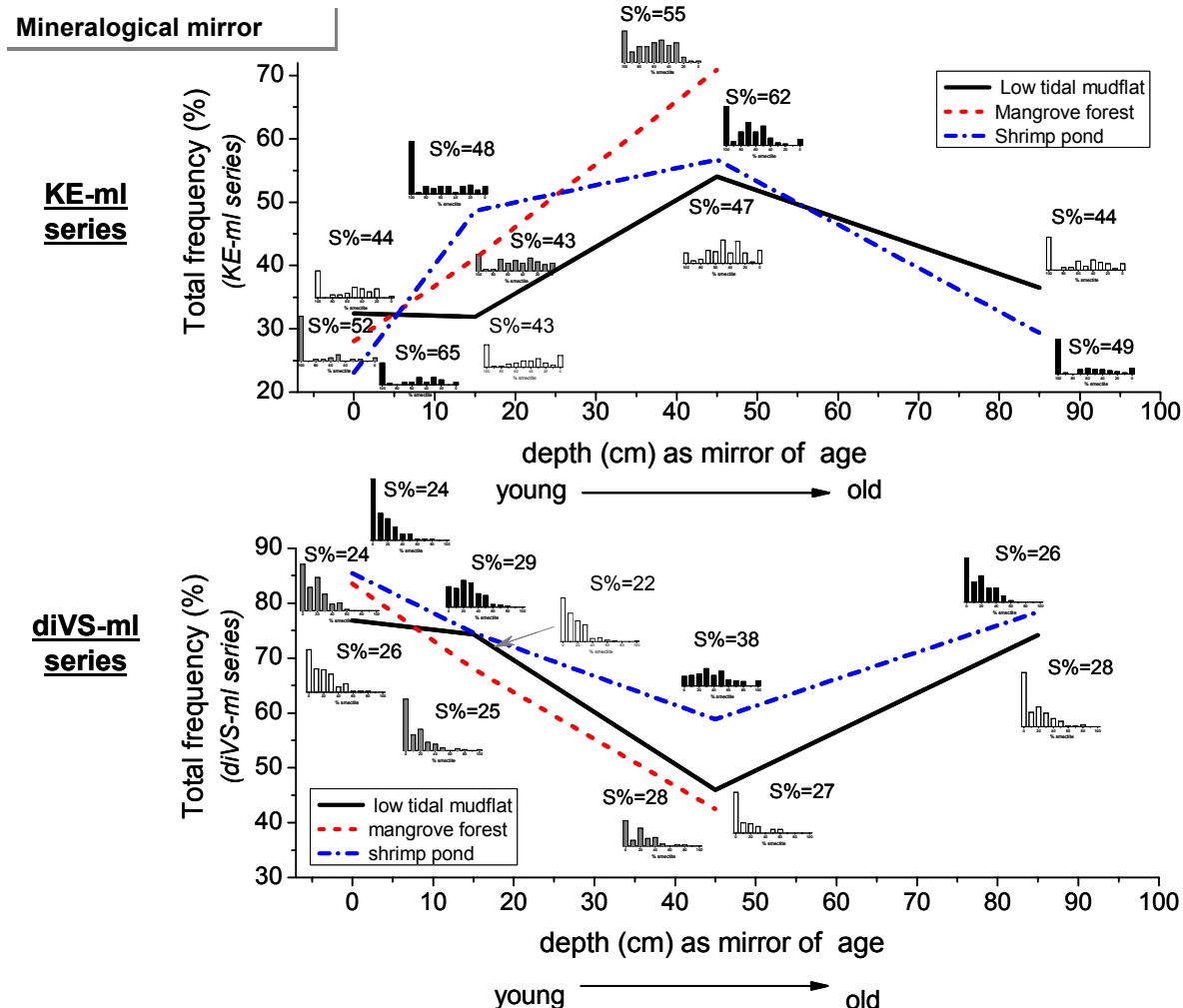


Figure 8.38. Mineralogical features as mirror of interactions among post-sedimentary processes in coastal environment of Nha Phu

S% expresses average smectitic percentage in series. Distribution curves of KE-ml display decreasing % smectite from right (beidellite, 100%) to left (kaolinite: 0%). Distribution curves of diVS-ml display increasing % smectite from right (diVerm: 0%) to left (montmorillonite, 100%)

Nha Phu

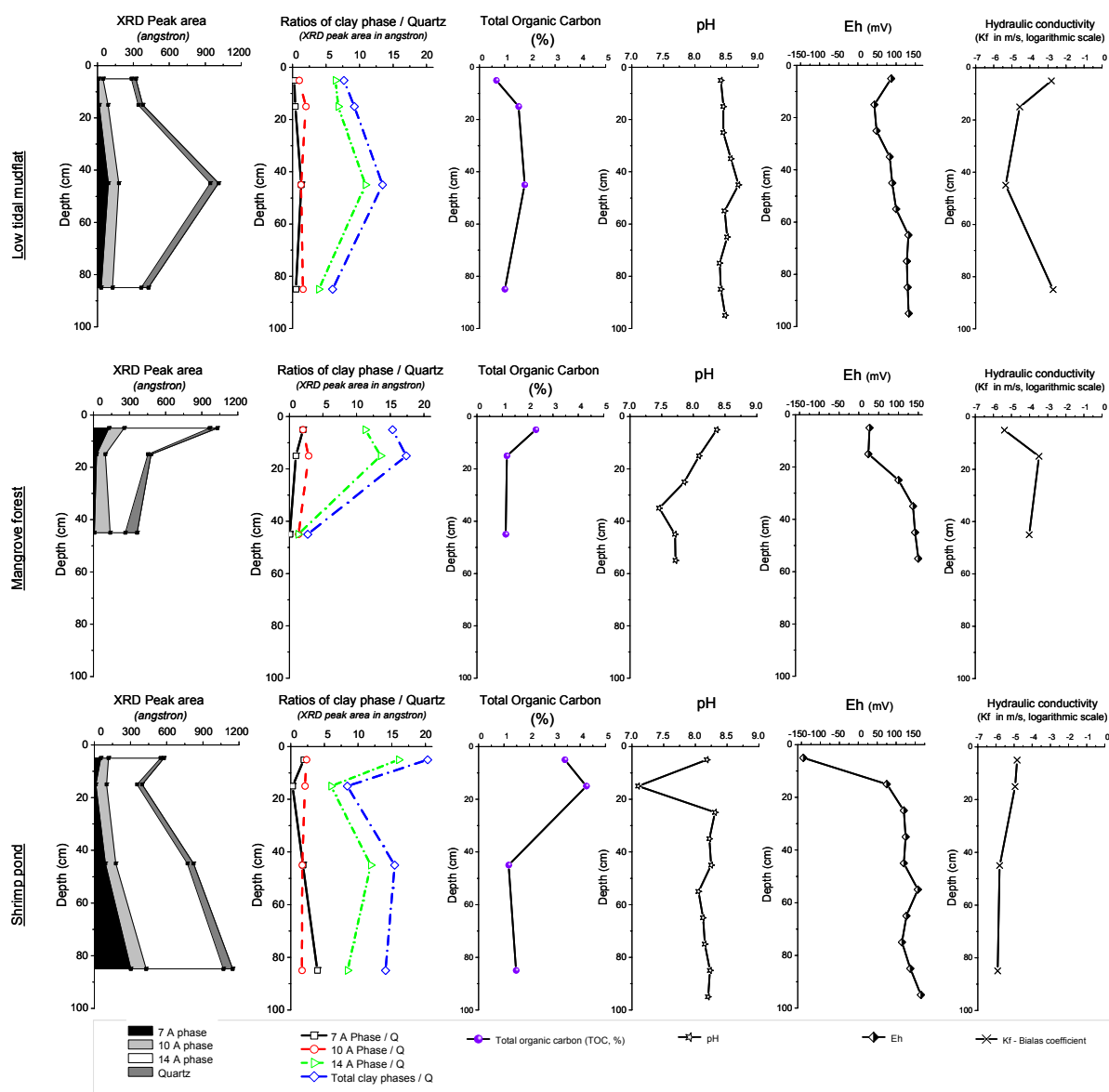


Figure 8.39. Variation of XRD peak area along profiles in Nha Phu in connection with TOC, pH, Eh and hydraulic permeability

Table 8.14. Principal mineral modification during post-sedimentary processes in Nha Phu

Pro file	Depth (cm)	Ambient	Mirror in diVS	Mirror in KE	Dominant process
Low tidal mudflat (LM)	0-10	High permeability Low organic matter	XRD: peak area of 10 Å and 14 Å phases decreases intensively TEM: Dissolution of diVS << KE	XRD: peak area of 7 Å phases decreases intensively TEM: Intensive lost of KE	D _s
	10-20	Lower permeability Higher organic	XRD: peak area of 10 Å and 14 Å phases decreases intensively TEM: Smectitic diVS decreases	XRD: peak area of 7 Å phases decreases intensively TEM: Transformation: Beidellitic KE to Kaolinitic KE and to Kaolinitization	D _s D _t + W _{KE}
	40-50	Low permeability Higher organic	XRD: peak area of 10 Å and 14 Å phases is most like the original materials TEM: transformation from vermiculitic diVS to smectitic total diVS decreases	XRD: peak area of 7 Å phases is most like the original materials TEM: B-KE->K-KE->B Kaolinitization > Smectitization Accumulation of KE & diVS,	W _{diVS} W _{KE} D _s disappears D _t begins
	80-90	High permeability Low organic	XRD: peak area of 10 Å and 14 Å phases decreases intensively TEM: transformation from vermiculitic diVS to smectitic total diVS decreases	XRD: peak area of 7 Å phases decreases intensively TEM: Lost of KE, high Beid + high diVerm Leaching of KE & diVS (XRD)	D _t W _{diVS} W _{KE}
Mangrove forest (MF)	0 - 10	Low permeability Higher organic	XRD+TEM: Original material	XRD+TEM: Original material	Original state
	10 - 20	Root layer High permeability Low organic	XRD: peak area of 10 Å and 14 Å phases decreases TEM: vermiculitic diVS -> smectitic diVS (slightly) Total diVS decrease	XRD: peak area of 7 Å phases decreases TEM: Beidellite -> Beidellitic KE	B _{diVS} B _{KE} slightly D _t
	40 - 50	Root layer High permeability Low organic Low pH	XRD: peak area of 10 Å and 14 Å phases decreases intensively TEM: diVerm -> vermiculitic diVS-> smectitic diVS	XRD: peak area of 7 Å phases decreases intensively TEM: Beid.-> beidellitic KE -> Kaolinitic KE-ml (intensive) Kaolinitization > Smectitization (=> reducing diVS, increasing KE, both are leached)	B _{diVS} slightly B _{KE} D _t W _{diVS}
Shrimp pond (SP)	0-10	High permeability High organic	XRD: peak area of 10 Å and 14 Å phases decreases TEM: decrease in frequency of diVS-ml < KE-ml	XRD: peak area of 7 Å phases decreases TEM: Total frequency of KE decreases Beidellite decreases	Intensive D _s
	10-20	Former root layer Low permeability High organic Low pH	XRD: peak area of 10 Å and 14 Å phases decreases intensively TEM: diVerm -> vermiculitic diVS-> smectitic diVS S% increases	XRD: peak area of 7 Å phases decreases intensively TEM: beidellitic KE -> Kaolinitic KE-ml High beidellite => remains from former MF	D _s Remains of former (B _{diVS} + B _{KE}) W _{diVS} W _{KE}
	40-50	Former root layer Very low permeability Very low organic	XRD: peak area of 10 Å and 14 Å phases higher than the surface TEM: diVerm -> vermiculitic diVS-> smectitic diVS, S% increases	XRD: peak area of 7 Å phases higher than the surface TEM: Beid.-> B KE-ml -> K KE-ml S% decreases	No more D _s Remains of former (B _{diVS} + B _{KE}) W _{diVS} W _{KE}
	80-90	Very low permeability Very low organic	XRD: peak area of 10 Å and 14 Å phases higher than the surface TEM: diVerm is high S% increases	XRD: peak area of 7 Å phases higher than the surface TEM: Increase of total KE-ml S% decreases	No more D _s D _t

Table 8.15. Ratios of key parameters between surface layer and the nearby subsurface layer in sediments of Dam Mon and Nha Phu

Group	Parameters	Dam Mon			Nha Phu		
		LM	MF	SP	LM	MF	SP
a) Hydrodynamic	Erosion influence ⁽¹⁾	3.64	1.23	1.98	0.88	1.70	2.39
b) Nutrients	C _{org} (%)	2.17	1.31	3.96	0.43	1.98	0.80
	S _{Total} (%)	3.45	2.45	1.42	0.26	1.08	1.01
c) Mineralogy	XRD peak area (Å) of Quartz (3.34 Å)	51	26	32	15	50	29
	Expandables ⁽²⁾	4.00	3.23	3.62	0.77	65.34	6.15
e) Major elements	SiO ₂	0.94	0.87	0.94	1.12	0.85	1.02
	Al ₂ O ₃	1.52	2.50	1.20	0.72	1.67	1.01
	CaO	1.12	5.67	1.40	0.86	1.01	0.87
	K ₂ O	1.02	1.95	1.01	0.99	0.96	1.00
f) Minor elements	Pb	1.50	1.69	0.62	0.61	2.12	0.96
	Cr	2.00	0.83	1.49	0.48	2.23	1.00
	Zn	2.20	2.27	1.86	0.49	2.57	1.04

⁽¹⁾: influence value of erosion factor (EMMA treatment, Chapter 5.1)
⁽²⁾: Relative quantity of expandable phases, determined by ratios between peak areas of 17 Å reflection relatively to 3.34 Å reflection (XRD, ethylene glycolated samples)

PUBLICATIONS

1. MAI Trong Nhuan, **NGUYEN Thi Minh Ngoc**, LUONG Xuan Huan, 2000. Mineralogogeochemical method for evaluation of weathering and erosion rate in tropical conditions (On example of South Vietnam)". *Journal of Geology, series A, special issue/2000*: . In Vietnamese
2. DAO Manh Tien, MAI Trong Nhuan, VU Truong Son, DAO Chi Bien, PHAM Hung Thanh, NGUYEN Ngoc Son, **NGUYEN Thi Minh Ngoc**, 2001. Distribution of arsenic in sea water and sediment (0-30m water) of the Hau river mouth (South Vietnam). In *Current situation or Arsenic pollution in Vietnam. Scientific technical communication on Geology. Department of Geology and Minerals of Vietnam. Hanoi. Pp. 35-46. In Vietnamese.*
3. MAI Trong Nhuan, **NGUYEN Thi Minh Ngoc**, DANG Van Luyen, PHAM Hung Viet, VU Truong Son, DAO Manh Tien, 2003. Application of organochlorine pesticides and polychlorinated biphenyls as molecular marker for assessment of sediment source, quality and sedimentation rate in Vietnam coast. *VNU Journal of Science. Nat., Sci., & Tech., T.XIX No2. 37-45.*

PROCEEDINGS AND ABSTRACTS

1. **NGUYỄN Thị Minh Ngọc**, 2000. Mineralogo-geochemical method for evaluation of weathering and erosion rate in tropical conditions (On example of South Vietnam). Vietnam National University. *University Contest of Student's Scientific Researches, 2000, Hanoi, Vietnam; Proceedings, Vol.5, p.142 (in Vietnamese).*
2. **NGUYỄN Thị Minh Ngọc**, 2001. Geochemical sedimentary evolution of the progress of formation, development and deradation of mangrove forest in Red River mouth (on example of Namdinh province). *Vietnam National University. University Contest of Student's ScientificResearches, 2001, Hanoi, Vietnam; Proceedings, Vol.6 p.121-122 (in Vietnamese).*
3. **NGUYEN Thi Minh Ngoc**, MAI Trong Nhuan, Jörn KASBOHM, 2004. Mineralogical - geochemical characterization of sediments below mangrove forests at the Red River Mouth (an example from Nam Dinh province, Vietnam). *The Clay Minerals Society; Gorges, Clays, and Coulees - 41st Annual Meeting, June 19-24, 2004, Richland, USA; Abstracts, p. 73.*
4. **NGUYEN Thi Minh Ngoc**, MAI Trong Nhuan, Jörn KASBOHM, 2004: *Mineralogical - geochemical characterization of sediments in mangrove forests in Red River Mouth (an example from Nam Dinh province, Vietnam)* Deutschen Mineralogischen Gesellschaft und der Deutschen Ton- und Tonmineralgruppe e.V.; DMG 2004 Tagung, Karlsruhe 19.-22. September 2004; Berichte der Deutschen Mineralogischen Ges., Beih. Z. Eur. J. Mineral. Vol. 16 (2004), No. 1, p.97
5. **NGUYEN Thi Minh Ngoc**, Jörn KASBOHM, MAI Trong Nhuan, 2005: *Geochemical and Mineral characteristics of sediments in mangrove forest, the Red River Delta, Vietnam.* Association Internationale Pour l'Etude des Argiles; The 13th International Clay Conference -

Claysphere: past, present and future and 49th Annual Meeting of the Clay Science Society of Japan, August 21-27, 2005, Waseda University, Tokyo, Japan; Program with Abstracts, p. 56.

6. NGUYEN Thi Minh Ngoc, Jörn KASBOHM, MAI Trong Nhuan, 2006: *Geochemical and Mineral characteristics of sediments in mangrove forest, the Red River Delta, Vietnam*. Groupe Français des Argiles & The Clay Minerals Society. Bridging Clays - Joint Meeting of The Clay Minerals Society and the French Clay Group: 43rd Annual meeting of the CMS - 4^{ème} Colloque du GFA, June 3-7, 2006, France; Program & Abstracts, p. 125

CURRICULUM VITAE

Personal information:

Name	NGUYEN, Thi Minh Ngoc
Sex	Female
Date of birth	17.7.1979
Place of birth	Phu Tho, Vietnam
Parents	NGUYEN Vinh Tuyen & PHAM Thi Thu
Nationality	Vietnamese
Marital status	Single
Religion	None
E-mail	ngoc.nguyen@uni-greifswald.de

Education:

1985-1994	Primary and secondary school in Phu Tho province, Vietnam
1994-1997	High school in Ha Noi, Vietnam
1997-2001	B.Sc. in Geology - Honors Program, Hanoi National University, Vietnam
2001-2003	Researcher and Teaching Assistance Faculty of Geology, Hanoi University of Science, Hanoi National University, Vietnam
2002-2003	Diploma of Equivalent in Geosciences and Environment “Joint Educational Training Center Hanoi-Greifswald” program
2003-2006	Ph.D. student in Geology - Institute of Geography and Geology, Ernst-Moritz-Arndt University of Greifswald, Germany

Work experience:

- Participate in Sub-subject: “Sediment characteristics in Delta and Mangrove system”, in Red River Delta Program, a part of Global Change Program, cooperation between Netherlands Institute for Sea Research (NIOZ) and National University of Vietnam (VNU).
- Participate in project: “Geoenvironmental mapping of Vietnam shallow sea (0 –30 m water depth), in scale 1: 500.000 ”, 1991 - 2001.
- Participate in project “Geoenvironmental mapping of south middle Vietnam shallow sea (0 –30 m water depth), in scale 1: 100.000 ”, 2001 - 2005.
- Participate in project “Training of trainers on Integrated Coastal Management” – CDG, Germany.
- Participate in project “Regressing the degradation of the South China Sea” – UNEP, Vietnam

Scholarships and honors:

- Honors Program Scholarship, Hanoi University of Science, annually 1997- 2001.
- “First Award” at the “University Contest of Student’s Scientific Researches, 2001”, Faculty of Geology, Hanoi University of Science, May 2001.
- “Outstanding Award for top talent graduated students”, Hanoi University of Science, June 2001.
- 3-years-scholarship supporting Ph.D. study by “Project on Training Scientific and Technical Cadres in educational institutions abroad by the State budget” (322 Project), Ministry of Education and Training of Vietnam.
- “Second Award” for best poster presentations at the “Bridging Clays conference”, Groupe Français des Argiles & The Clay Minerals Society, France, June 2006.

ERKLÄRUNG

Hiermit erkläre ich, Nguyen Thi Minh Ngoc, dass diese Arbeit bisher von mir weder an der Mathematisch- Naturwissenschaftlichen Fakultät der Ernst-Moritz-Arndt-Universität Greifswald noch einer anderen wissenschaftlichen Einrichtung zum Zwecke der Promotion eingereicht wurde.

Ferner erkläre ich, dass ich diese Arbeit selbständig verfasst und keine anderen als die darin angegebenen Hilfsmittel benutzt habe.

NGUYEN Thi Minh Ngoc

STATEMENT OF ORIGINAL AUTHORSHIP

I, Nguyen Thi Minh Ngoc, hereby state that the work contained in this assignment has not previously been submitted for assessment, either in whole or in part, by either myself or any other student at either Faculty of Mathematics and Sciences, Ernst-Moritz-Arndt-University of Greifswald or at any other tertiary institution except where explicitly acknowledged.

To the best of my knowledge and belief, the assignment contains no material which has been previously published or written by another person except where due reference is made.
